



City Research Online

City, University of London Institutional Repository

Citation: Abrahams, I. (1986). Mössbauer spectroscopic and structural studies of tin materials.. (Unpublished Doctoral thesis, The City University)

This is the accepted version of the paper.

This version of the publication may differ from the final published version.

Permanent repository link: <https://openaccess.city.ac.uk/id/eprint/34278/>

Link to published version:

Copyright: City Research Online aims to make research outputs of City, University of London available to a wider audience. Copyright and Moral Rights remain with the author(s) and/or copyright holders. URLs from City Research Online may be freely distributed and linked to.

Reuse: Copies of full items can be used for personal research or study, educational, or not-for-profit purposes without prior permission or charge. Provided that the authors, title and full bibliographic details are credited, a hyperlink and/or URL is given for the original metadata page and the content is not changed in any way.

MÖSSBAUER SPECTROSCOPIC
AND STRUCTURAL STUDIES
OF TIN MATERIALS

A THESIS

SUBMITTED FOR THE DEGREE OF
DOCTOR OF PHILOSOPHY
IN THE FACULTY OF SCIENCE OF
THE CITY UNIVERSITY, LONDON

BY

ISAAC ABRAHAMS

Department of Chemistry,
The City University,
London.

September 1986

IMAGING SERVICES NORTH

Boston Spa, Wetherby

West Yorkshire, LS23 7BQ

www.bl.uk

**BEST COPY AVAILABLE.
VARIABLE PRINT QUALITY**

IMAGING SERVICES NORTH

Boston Spa, Wetherby
West Yorkshire, LS23 7BQ
www.bl.uk

**PAGE NUMBERS ARE CUT
OFF IN THE ORIGINAL**

WARRANTY OF MERCHANTABILITY
AND STATUTE OF LIMITS
IN THE STATE OF

To my wife [REDACTED]

Department of Commerce
The State of [REDACTED]
[REDACTED]

September 1971

MÖSSBAUER SPECTROSCOPIC AND STRUCTURAL STUDIES
OF TIN COMPOUNDS.

CONTENTS

	Page
ABSTRACT	5
CHAPTER ONE	Introduction. 6
CHAPTER TWO	Preparations of tin(II) complexes in solution. 57
CHAPTER THREE	Thermoanalytical studies on the KBr : SnX ₂ system (where X = Br, Cl, F). 122
CHAPTER FOUR	Mössbauer spectroscopic studies on tin materials. 166
CHAPTER FIVE	Structure determination of tin(II) complexes. 248
CHAPTER SIX	Conclusions. 330
APPENDIX ONE	Computer programs. 343
APPENDIX TWO	Structure factor data. 370

ACKNOWLEDGEMENTS

I would like to thank Professor John Donaldson for his help and guidance throughout the course of this project and for offering me the opportunity of doing post graduate research. I am indebted to Dr.Sue Grimes for advice and constructive criticism concerning this work. My thanks to Dr.S.J.Clark for his day to day advice and assistance.

I would also like to thank the SERC and the International Tin Research Institute for a CASE award studentship. My special thanks to Dr.P.J.Smith, Dr.P.A.Cussack, Mrs.D.Searle and Dr.M.Warwick for numerous Mössbauer samples.

For Single crystal X-ray data collection I would like to thank Professor S.Calogero and Dr.G.Valle at Padua University Italy; Dr.M.Hursthouse at Queen Mary College London and Dr.E.M.McPartlin and Dr.K.Hendrick at the Polytechnic of North London.

My gratitude to The City University for research facilities. I would very much like to thank colleagues and staff in the Chemistry and Physics departments of The City University especially [REDACTED] for microanalytical work and [REDACTED] for running numerous X-ray diffractograms. My thanks also to The City University Computer Unit and to The University of London Computer Centre especially Dr.A.Quick.

Finally I would like to thank my family and friends for their encouragement and support, especially, my wife Anne, for all her help and patience over this course of study.

I declare that single copies of this thesis may be made, in whole or in part, without further reference to me, for the purpose of study, subject to the normal conditions of acknowledgement, at the discretion of the University Librarian.



Isaac Abrahams

ABSTRACT

X-ray crystallography and Mössbauer spectroscopy have been used to study some tin(II) materials. Some alkali metal and ammonium halostannates have been prepared both from aqueous solutions and from solid state melts.

The crystal structures of 3 materials have been determined viz. RbSn_2Br_5 , $\text{CsSn}_3\text{Br}_{1.5}\text{F}_{5.5}$ and $\text{KBr.KSnBr}_2\text{Cl.H}_2\text{O}$; and the structures of $\text{KCl.KSnCl}_3.\text{H}_2\text{O}$ and Sn_3BrF_5 have been refined. The structure of RbSn_2Br_5 is stabilised by overlap of the 5s orbital on tin and empty 4d orbitals on the bromine atoms, resulting in partial delocalisation of the non-bonding electron pairs on tin. This is part of a range of interactions shown by the lone pairs on tin atoms ranging from dimer formation to the population of solid state conduction bands.

Preparations in solution and in the solid state have confirmed the existence of mixed halide complexes of tin(II). Evidence from the structure determination of $\text{KBr.KSnBr}_2\text{Cl.H}_2\text{O}$ suggests two halogen atom sites on the $[\text{SnX}_3]^-$ anion are interchangeable between bromine and chlorine. The expansion of the lattice in accommodating the larger halide in salts of the type $\text{KSnBr}_n\text{Cl}_{3-n}.\text{xH}_2\text{O}$ has been monitored using X-ray powder diffraction.

Thermal analysis has been used in the construction of phase diagrams and together with X-ray powder diffraction is used to identify new phases in the system KBr:SnX_2 , where $\text{X} = \text{Br, Cl, F}$.

The conversion electron Mössbauer (CEM) spectra for some normal tin(II) compounds are reported and have been compared with transmission Mössbauer data. Some applications of CEMS, in commercially important materials, are discussed and results on several examples are reported, including ceramic tiles and glazes, tinplates and alloys, fabrics, glass coatings and biocides.

CHAPTER ONE

INTRODUCTION

	Page
1.1 Introduction.	7
1.2 Tin, the element.	8
1.3 Bonding in tin.	8
1.4 Bonding in tin(IV) compounds.	9
1.5 Bonding in tin(II) compounds.	14
1.6 Introduction to X-ray crystallography.	22
1.7 Single crystal data collection.	31
1.8 Structure determination.	36
1.9 Computer programs used in X-ray crystallography.	45
References.	53

CHAPTER ONE

1.1 Introduction

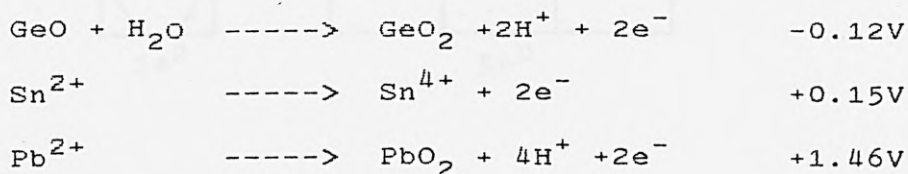
The aim of this work has been to achieve a greater understanding of certain aspects of tin(II) chemistry, in particular the environment and nature of the tin(II) species in various halogen complexes and to examine applications of conversion electron Mössbauer spectroscopy (CEMS), in the study of surface environments of tin containing materials.

The project has been divided into different areas of research reflected in the organisation of the various chapters. This introductory chapter serves as a brief account of bonding in tin materials and as an introduction to the technique of X-ray crystallography. Chapter 2 describes the results of investigations into tin(II) products isolated from solutions containing mixtures of alkali metal and stannous halides, while the third chapter deals with some of these systems in the solid state. Chapter 4 examines the uses of CEMS in the study of tin environments and compares the results with those obtained by conventional transmission experiments. Chapter 5 describes the structure determinations of various tin(II) complexes carried out during this work, while the conclusions and recommendations for future work are included in the final chapter.

1.2 Tin, the element.

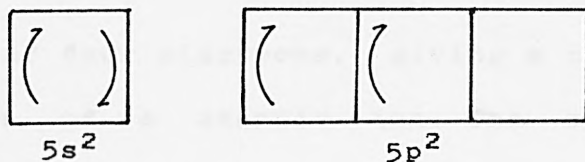
Tin, atomic number 50, is a silver-white lustrous element exhibiting various metallic properties such as conductivity and ductility. It exists in two allotropic forms, stable in defined temperature ranges; α - or grey tin up to 13.2 °C and β - or white tin above 13.2 °C.

Tin is the fourth member of the main group IV and like the other heavier members it forms compounds in the oxidation states 4+ and 2+. The stability of the lower oxidation state within the group, increases with atomic number which can be seen on comparison of the oxidation potentials [1,2].



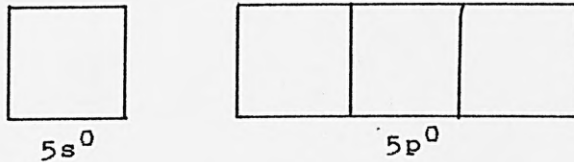
1.3 Bonding in tin.

Tin has the ground state outer shell electronic configuration of $5s^2 5p^2$ as shown below:

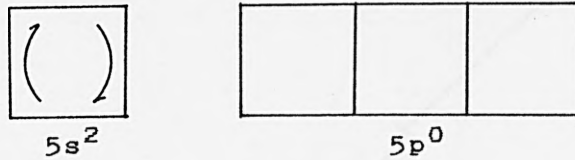


(Note, unless stated otherwise, in all subsequent examples, the outer electronic configuration only, is represented.)

Fig.1.1 [2] shows the successive ionization energies of tin, these favour the loss of four electrons to give a closed shell resulting in the spherical stannic ion Sn^{4+} .



The loss or use in bond formation, of only two electrons may also occur and results in a Sn(II) species with the formal outer shell configuration of $5s^2 - 5p^0$ as seen below:



1.4 Bonding in tin(IV) compounds.

In compounds where the formal oxidation state of tin is 4+ bonding is actually achieved in three different ways as follows:

(1) By loss of four electrons, giving a closed 4d shell, in formation of a stannic ion. The stannic ion is spherical with respect to charge distribution and has a radius of approximately 0.71Å [2]. Fig.1.2 shows the structures of SnO_2 [3,4] and BaSnO_3 [5] which, have the typically ionic rutile and perovskite structures

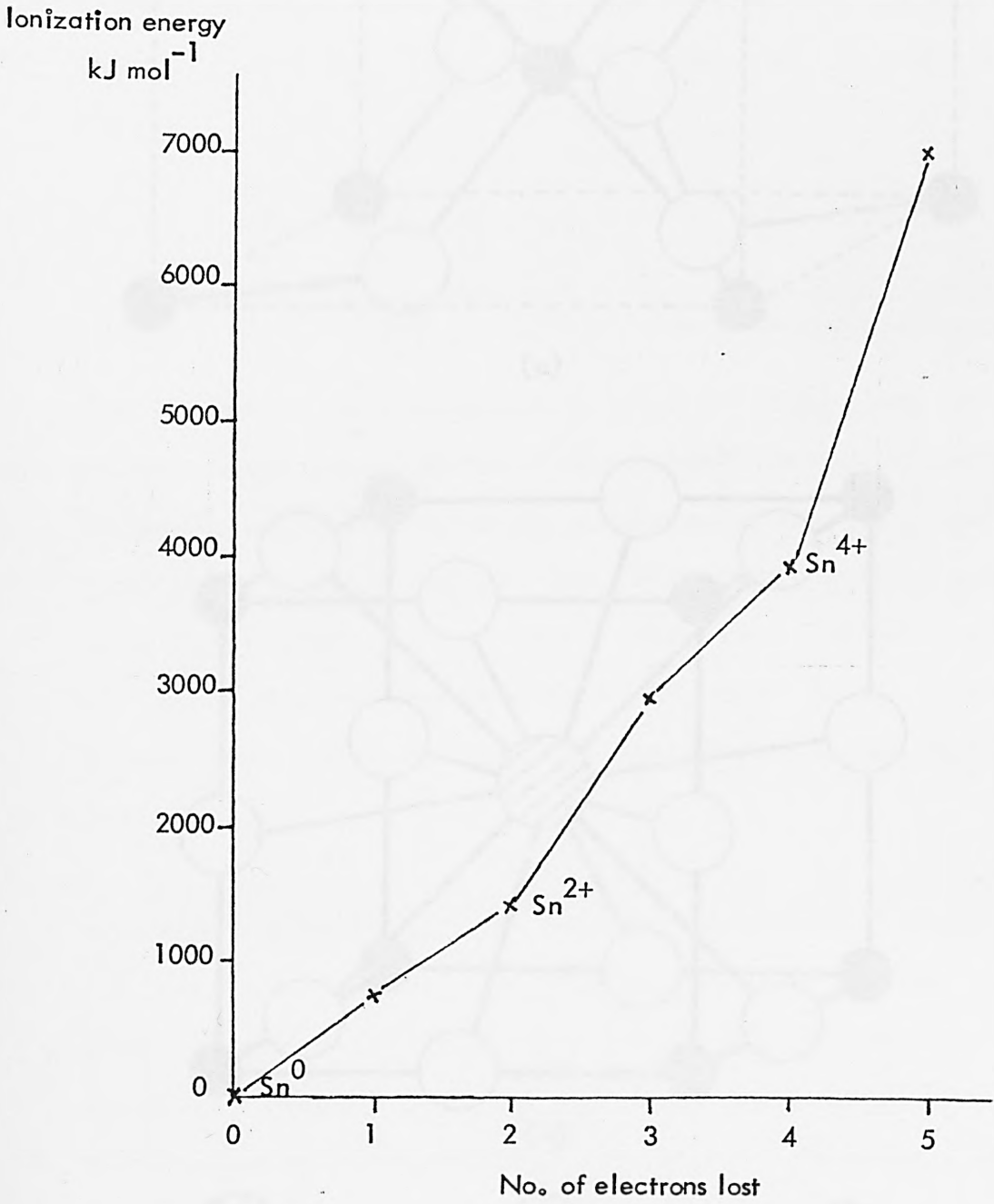
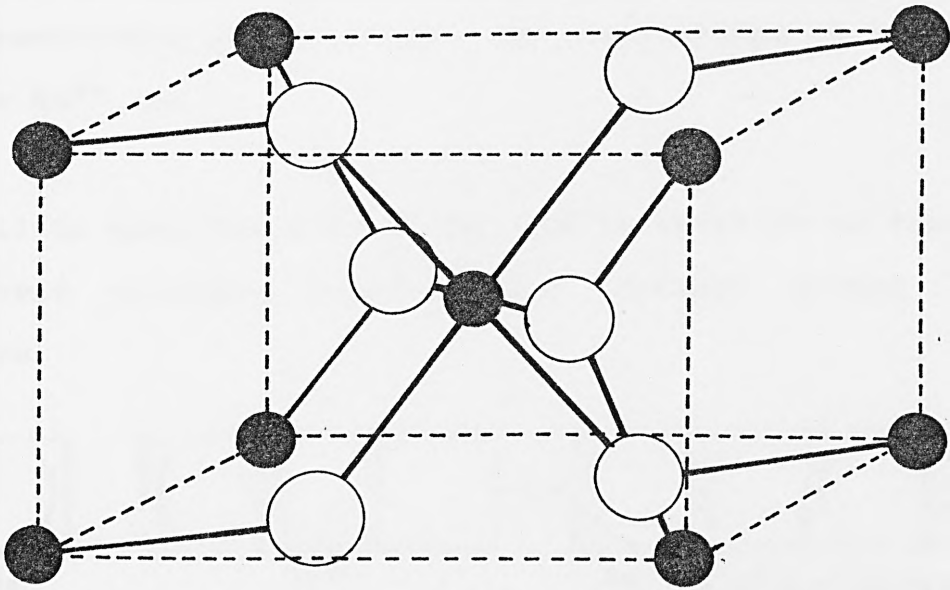
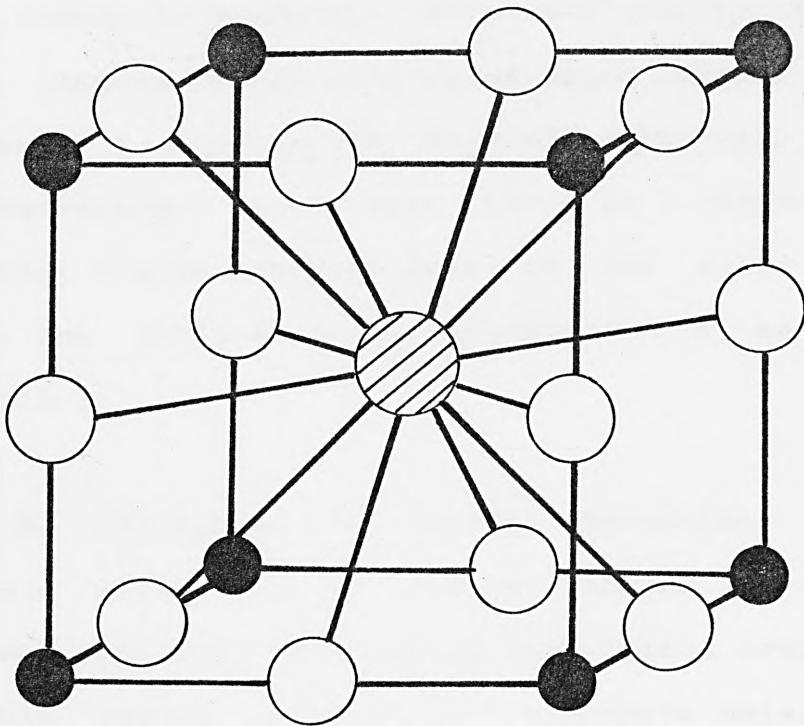


Fig. 1.1

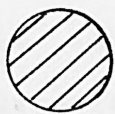
Successive ionization energies for tin.



(a)



(b)



Ba



O



Sn

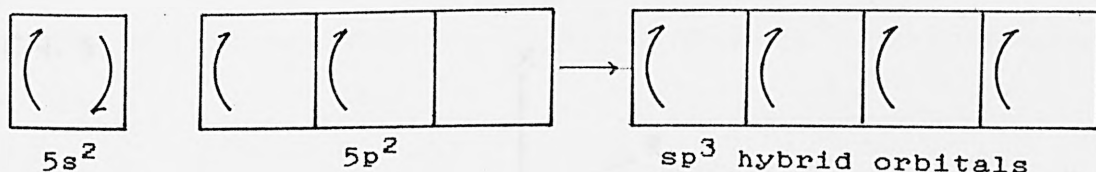
Fig.1.2

Ionic tin(IV) structures:

(a) SnO_2 (rutile), (b) BaSnO_3 (perovskite)

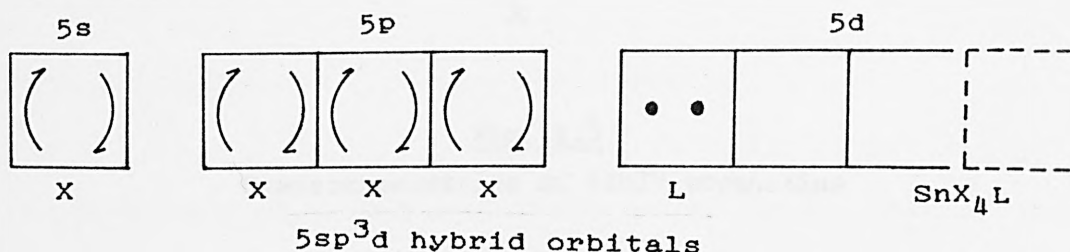
respectively and which can be represented as containing the Sn^{4+} ion.

(ii) By hybridisation of 5s and 5p orbitals to form four hybrid orbitals tetrahedrally arranged around the tin core.

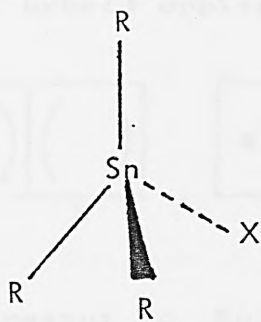


The situation is analogous to that in carbon and is known to be common in organotin compounds [6,7]. for example Ph_4Sn . However X-ray crystallographic studies have shown that in several organotin compounds originally thought to have tetrahedral structures there is a tendency for tin to adopt higher coordinations in the solid state by inter- and intra-molecular association [8] as summarised in fig.1.3.

(iii) By utilising, in complex formation, empty 5d orbitals which are of similar energy to the valence electron orbitals. This occurs when filled orbitals on a suitable ligand overlap with the empty metal orbitals. The trigonal bipyramidal structure of $(\text{CH}_3)_3\text{SnCl}\cdot\text{Py}$ [9] is achieved in this way formally by sp^3d hybridisation:

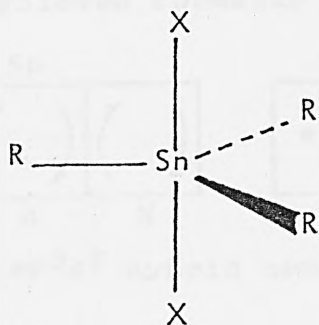


CN. 4



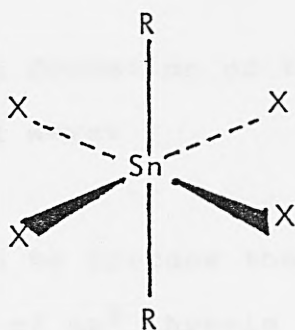
eg. Ph_2SnCl_2

CN. 5



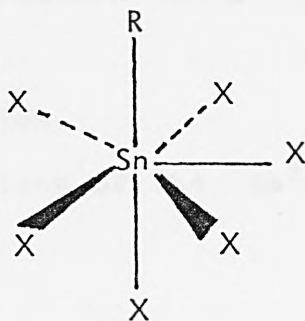
eg. Me_3SnOH

CN. 6



eg. Me_2SnF_2

CN. 7

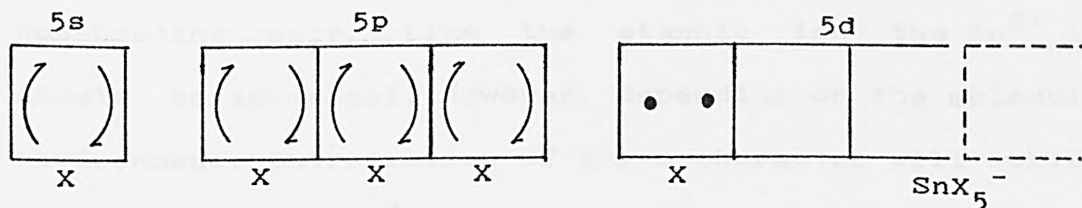


eg. $\text{MeSn}(\text{NO}_3)_3$

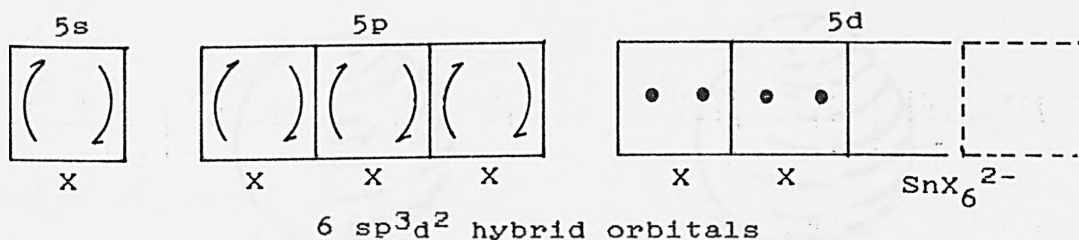
Fig. 1.3

Stereochemistries of tinIV organotins

5sp³d hybrid orbitals



While in [SnF₆]²⁻ (present in Sn₃F₈ where tin exists in both oxidation states [10]), an octahedral environment about Sn(IV) is achieved formally by sp³d² hybridisation.



6 sp³d² hybrid orbitals

1.5 Bonding in tin(II) compounds.

As with tin(IV) the formation of tin(II) materials can be achieved in several ways:

- (i) By ionisation to produce the stannous ion.
- (ii) By formation of sp² hybrid orbitals in covalent bonding.
- (iii) By complex formation using the 5p and possibly 5d orbitals.
- (iv) By σ - donation.
- (v) By delocalisation of the 5s² electron pair in the solid state.

Each of these will now be discussed.

- (i) The loss of only two electrons by ionisation forms

the stannous ion Sn^{2+} and leaves the $5s^2$ electrons as a non-bonding pair. Like the stannic ion the Sn^{2+} ion should be spherical, however, depending on the molecular environment, introduction of any p character will subject the non-bonding $5s^2$ electrons to a degree of s-p mixing, thus inducing a directional effect resulting in a non-spherical charge distribution on Sn^{2+} (see fig.1.4).

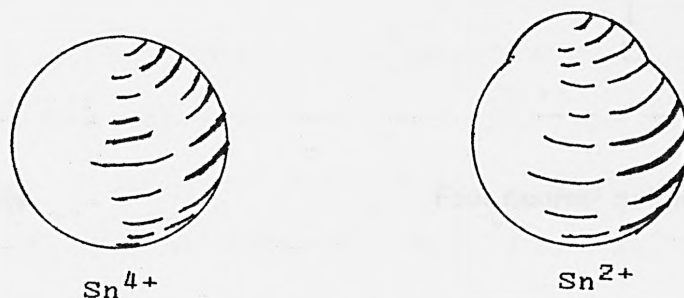
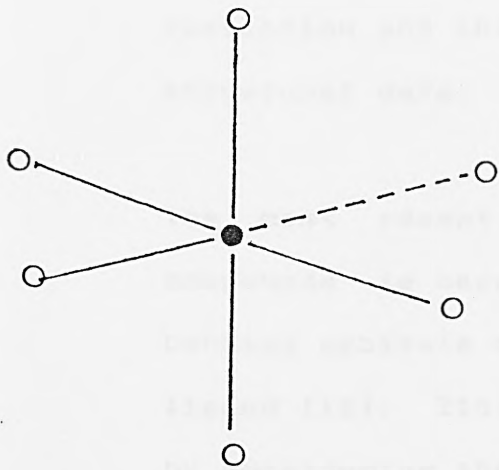


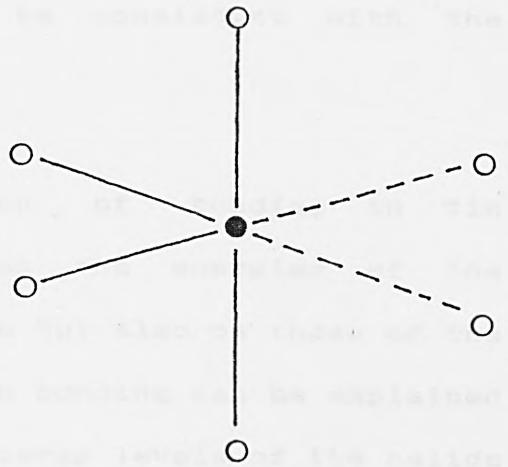
Fig.1.4 Electron density around tin ions.

The effect of the bulge of electron density in the solid state is to prevent the close approach of anions along the direction in which it points, and is known as the 'lone pair effect'.

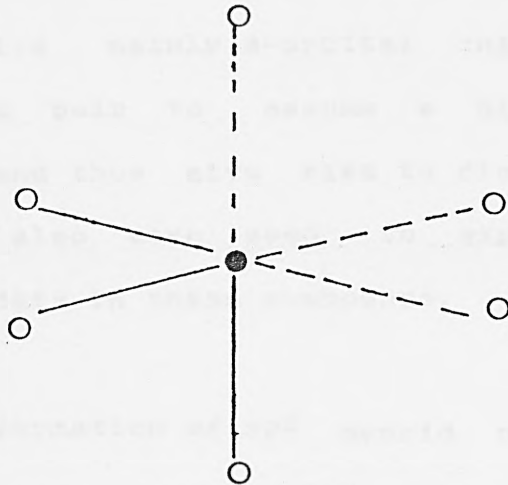
Orgel [11] has noted that the presence of low lying excited energy levels often leads to distortion from a symmetrical coordination and that in the event of s and p orbitals being degenerate, the distortion would be significant. In the stannous ion the first excited state $5s^1 5p^1$ is separated by only 6.64 eV from the groundstate, this comparatively small energy separation means that the s-p mixing will be significant enough to cause distortion. The three simplest unsymmetrical distortions are shown in fig.1.5. The crystal field



Five nearest neighbours



Four nearest neighbours



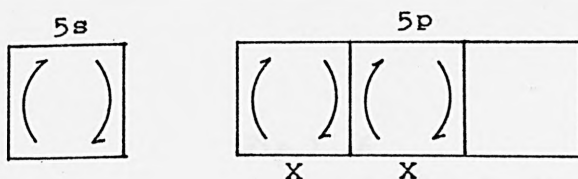
Three nearest neighbours

Fig.1.5.
Unsymmetrical distortions in octahedral environments

energy, however, decreases rapidly with ligand bond distance. Thus, small anions should give the greatest distortion and this appears to be consistent with the structural data.

The most recent interpretation of bonding in tin compounds is based not only on the energies of the bonding orbitals of the tin atom but also on those of the ligand [12]. Tin(II) to halogen bonding can be explained by considering the relative energy levels of the halide series which are shown in fig.1.6. Bonding with chlorine will involve a fair degree of s and p character, however bonding in tin iodide compounds will involve much p and little s character leaving the non-bonding pair with much s character resulting in a near-spherical tin atom in an octahedral environment. In contrast bonds with fluorine will involve mainly s-orbital character leaving the non-bonding pair to assume a directional p-orbital character and thus give rise to distorted environments. This has also been used to explain the anomalous Mössbauer data in these compounds.

(ii) The formation of sp^2 hybrid orbitals result in covalent bonding as in SnX_2 eg. $SnCl_2$ in the vapour phase.



The symmetry of the resulting molecule depends on the

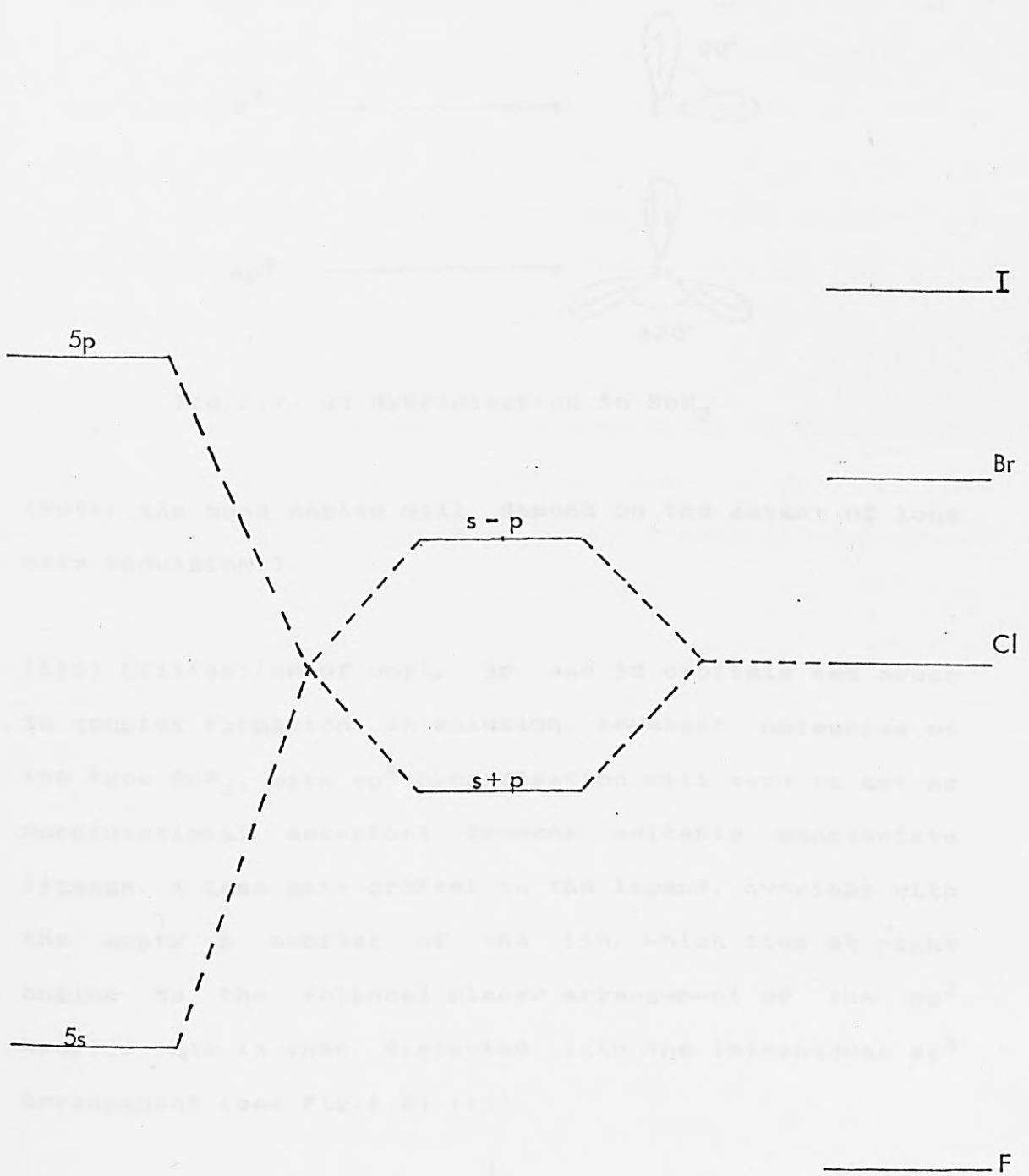


Fig.1. 6
Approximate relative energy levels for bonding in tin
halide series

hybridisation in the valence shell i.e. on the inclusion of the 5s electrons in hybridisation (see fig.1.7).

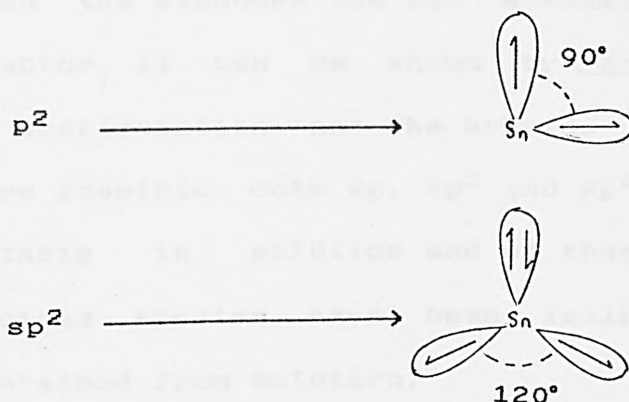


Fig.1.7. Sn Hybridisation in SnX_2

(Note: the bond angles will depend on the extent of lone pair repulsion.)

(iii) Utilisation of empty 5p and 5d orbitals can occur in complex formation. In solution, covalent molecules of the type SnX_2 , with sp^2 hybridisation will tend to act as monofunctional acceptors towards suitable monodentate ligands. A lone pair orbital on the ligand, overlaps with the empty p orbital of the tin, which lies at right angles to the trigonal planar arrangement of the sp^2 hybrid. This is then distorted into the tetrahedral sp^3 arrangement (see fig.1.8) [13].

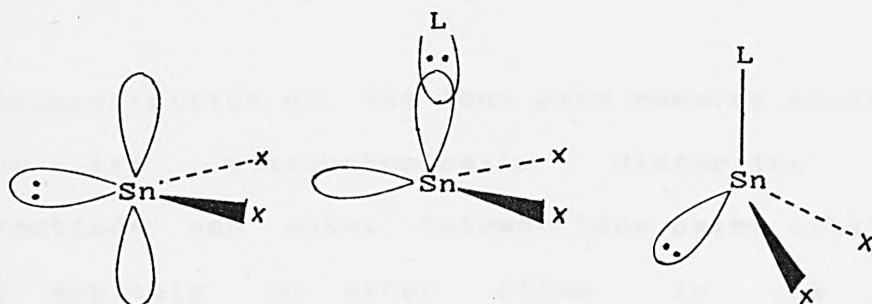


Fig.1.8 $sp^2 \rightarrow sp^3$ hybridisation in complex formation.

In solution the stannous ion can similarly act as a ligand acceptor. It can be shown by consideration of electronic configuration that the hybrids illustrated in fig.1.9 are possible. Only sp , sp^3 and sp^2 hybridisation are detectable in solution and of these only sp^3 and sp^2 hybridised species have been isolated in solid products obtained from solution.

(iv) σ - donation can be achieved by electron pair overlap with a suitable acceptor species and has been used to explain the unusual trigonal bipyramidal coordination of the platinum atom in $Pt(SnCl_3)_5^{3-}$ [14]. Similarly the ions $Cl_3SnBF_3^-$ and $Cl_3SnBCl_3^-$ have been explained by σ - donation [15] (see fig.1.10). In these materials tin is essentially in a tin(IV) state because it is using all four valence shell electrons in bonding.

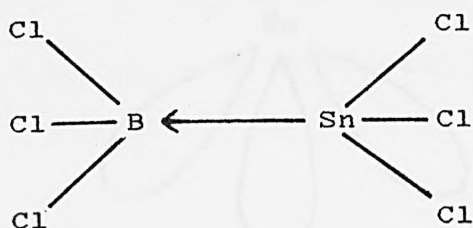


Fig.1.10 σ - donation by $SnCl_3^-$

(v) Delocalisation of the lone pair removes partially or wholly its stereochemically distorting effect. Interactions can occur between lone pair orbitals and empty orbitals on other atoms. In the case of $Sn[CH(SiMe_3)_2]_2$ [16] stability is achieved by the lone pair on one tin atom overlapping with the empty orbital

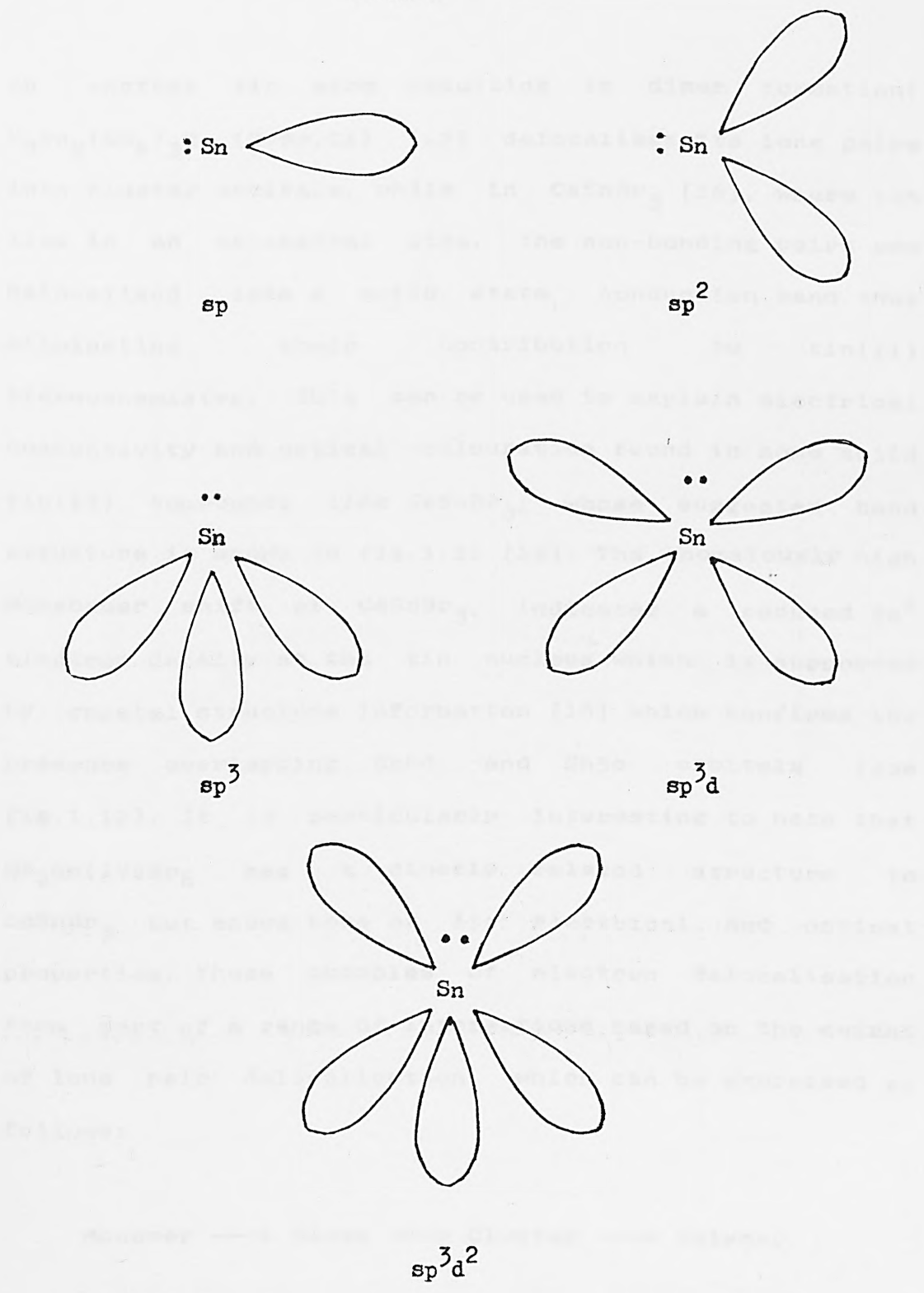
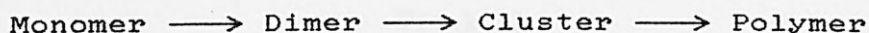


Fig.1.9

Possible stannous hybrids

on another tin atom resulting in dimer formation; $K_3Sn_2(SO_4)_3X$ ($X=Br,Cl$) [17] delocalises its lone pairs into cluster orbitals, while in $CsSnBr_3$ [18], where tin lies in an octahedral site, the non-bonding pairs are delocalised into a solid state conduction band thus eliminating their contribution to tin(II) stereochemistry. This can be used to explain electrical conductivity and optical colouration found in some solid tin(II) compounds like $CsSnBr_3$, whose suggested band structure is shown in fig.1.11 [19]. The anomalously high Mössbauer shift of $CsSnBr_3$, indicates a reduced $5s^2$ electron density at the tin nucleus which is supported by crystal structure information [18] which confirms the presence overlapping $Br4d$ and $Sn5s$ orbitals (see fig.1.12). It is particularly interesting to note that $Cs_2Sn(IV)Br_6$ has a closely related structure to $CsSnBr_3$ but shows none of its electrical and optical properties. These examples of electron delocalisation form part of a range of interactions based on the extent of lone pair delocalisation, which can be expressed as follows:



The environments of tin atoms in tin(II) derivatives are summarised in fig.1.13.

1.6 Introduction to X-ray diffraction

This section is an introduction into the techniques of

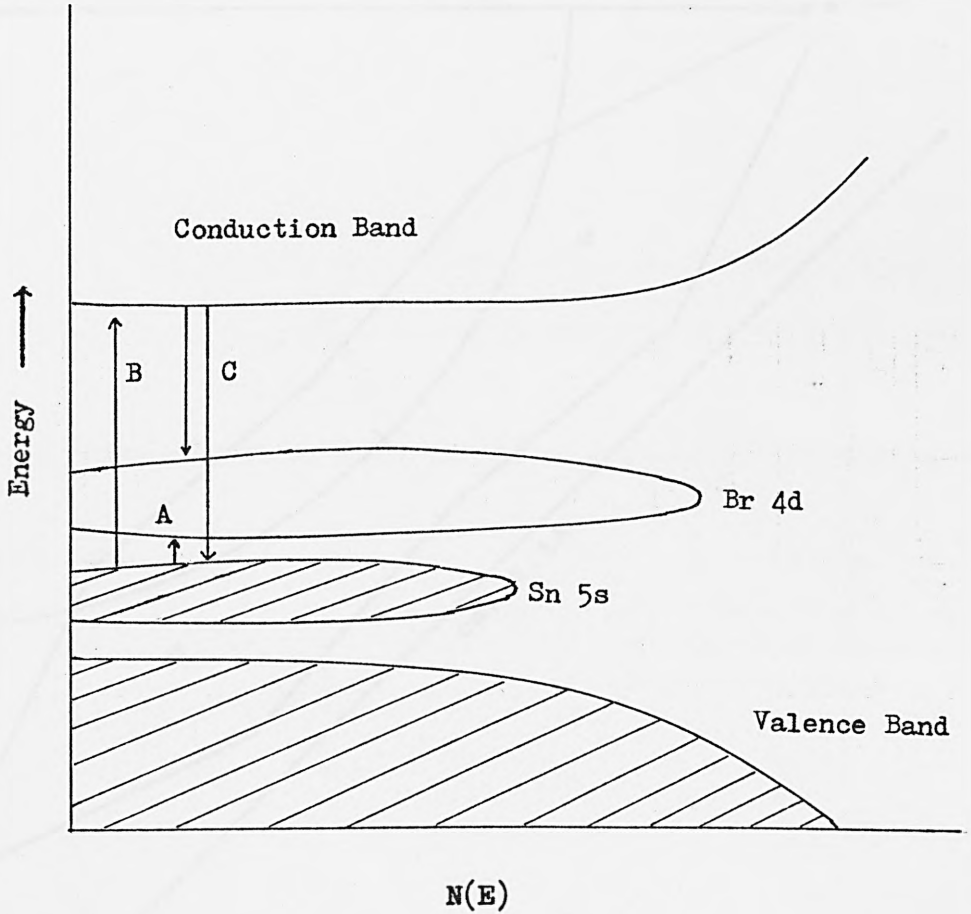


Fig.1.11

Suggested band structure for CsSnBr₃ showing thermal population (A), optical absorption (B), and emission (C).

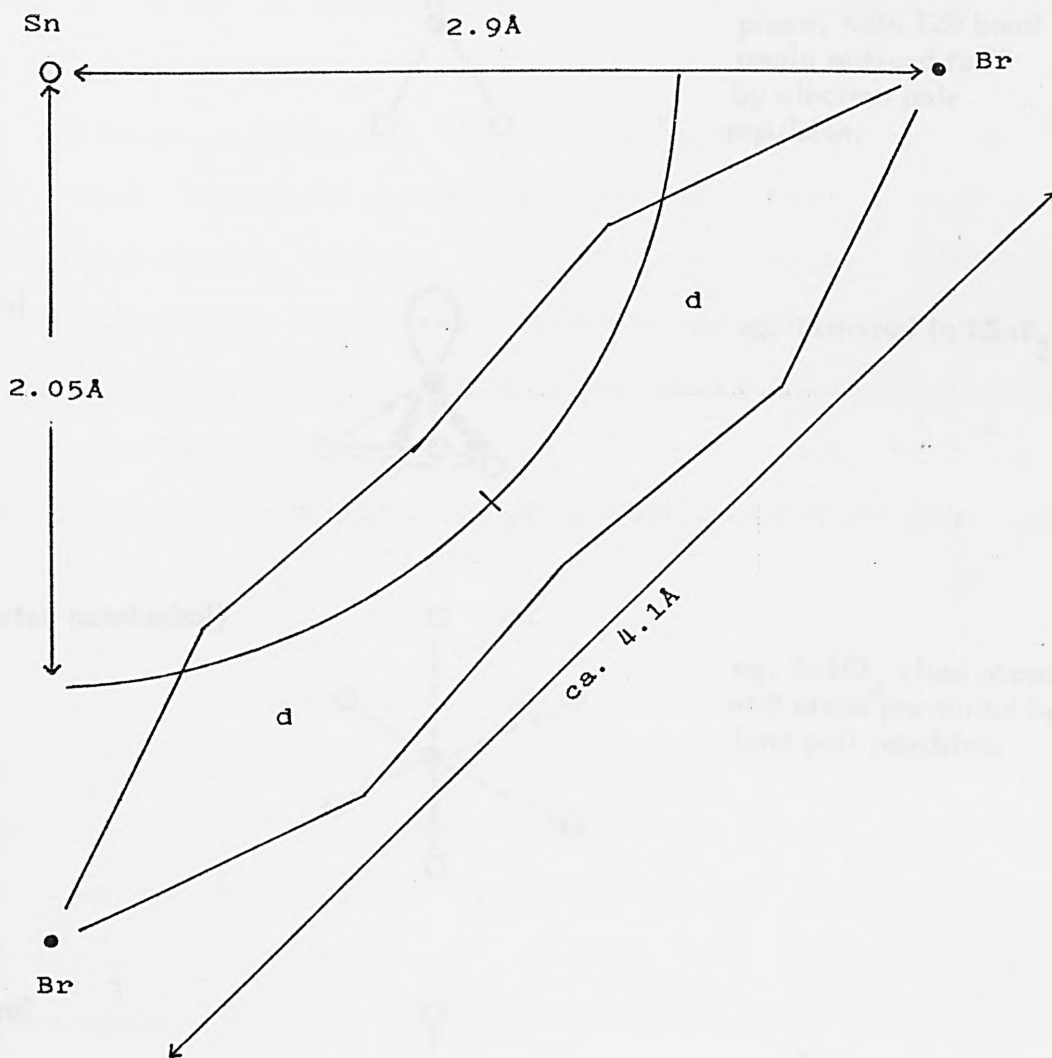


Fig.1.12

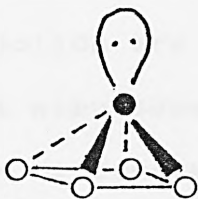
Orbital overlap between Sn 5s and Br 4d
orbitals in CsSnBr₃

Angular



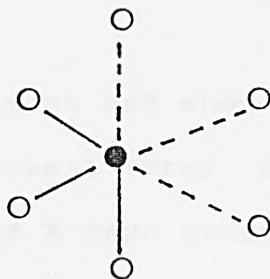
eg. SnX_2 in vapour phase, note 120 bond angle reduced to 95 by electron pair repulsion.

Square pyramidal



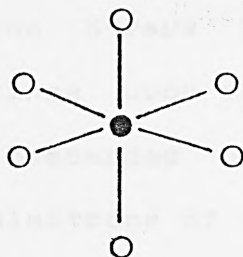
eg. distorted in $\text{KSnF}_3 \cdot \frac{1}{2}\text{H}_2\text{O}$

Pyramidal (distorted octahedral)



eg. SnSO_4 close approach of 3 atoms prevented by lone pair repulsion.

Regular octahedral



eg. SnSe

Fig.1.13

Environments of tin(II)

X-ray powder and single crystal diffraction.

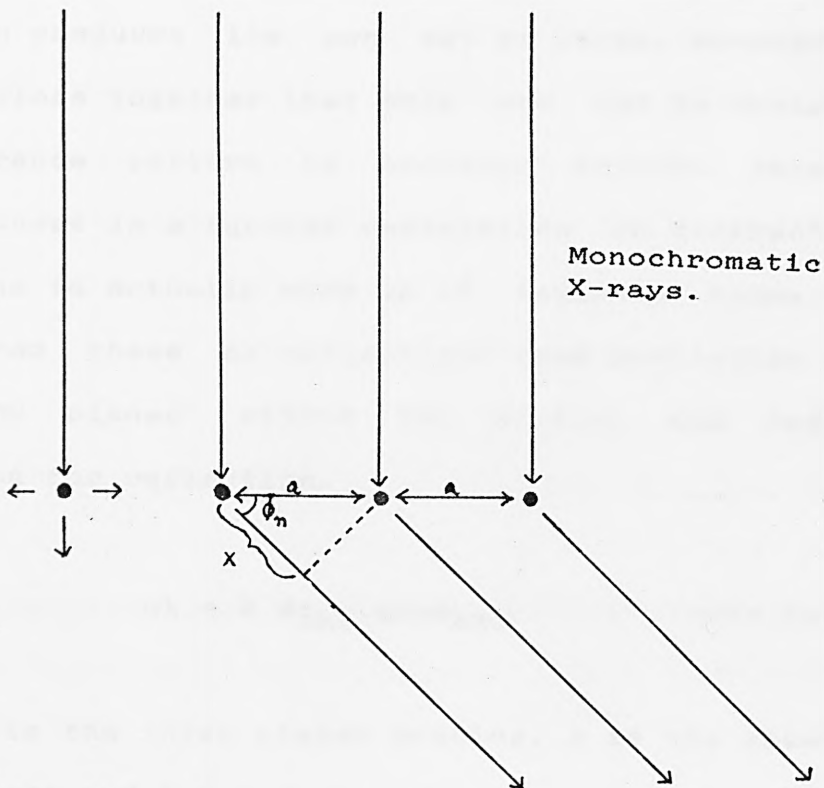
X-rays were discovered by Wilhelm Konrad Rontgen in 1895 for which he was awarded the first Nobel prize in 1901. The name X-ray - X for unknown - was adopted as, originally, little was known about their physical nature. By 1912 Max von Laue had proved that X-rays were electromagnetic waves [20]. Von Laue's experiment had also shown that solids are made up of atoms in a regular three dimensional structure. A detailed interpretation of X-ray diffraction by crystals was soon given by Bragg in 1913 [21], and the development of X-ray crystallography followed.

Von Laue's experiment had shown that a crystal is made up of a three dimensional array of regularly spaced atoms. The wavelengths of X-rays range from 0.1 to 100 Å lying between gamma and U.V. radiation, thus they are comparable to the atom spacings in crystals. Hence, crystals act upon X-rays in a similar fashion to diffraction gratings upon visible light. Consider a row of atoms being bombarded by X-rays in a particular direction. The electrons of the atoms scatter the X-rays as shown in fig.1.14.

Now $n\lambda = x$ where $x = a \cos \phi_n$. Therefore for diffraction,

$$n\lambda = a \cos \phi_n$$

Where $n = 0, 1, 2, 3, \dots$



$$n\lambda = x, \text{ where } x = a \cos \phi_n \text{ (} n = 0, 1, 2, 3 \dots \text{)}$$

$$n\lambda = a \cos \phi_n$$

Fig.1.14

Geometry of X-ray diffraction by regularly spaced atoms.

This results in concentric cones of radiation of $1/2\phi_n$. Each row produces its own set of cones, however, atoms are so close together that only one set is observed. An interference pattern is produced between cones, as a result there is a further restriction on diffraction and each cone is actually made up of isolated beams. Bragg considered these as reflections from particular sets of imaginary planes within the crystal and defined a condition for reflection.

$$n\lambda = 2 d_{hkl} \sin\theta_{hkl} \quad \text{---- (1.1)}$$

Where d is the inter planar spacing, θ is the glancing or Bragg angle and h, k and l are indices used to describe different planes. This has become known as the Bragg law.

If a crystal is rotated about the axis of the X-ray beam, the diffracted rays form a cone. This property can be observed in a Weissenberg camera in the oscillation mode. The same effect can be obtained by dividing the crystal into smaller segments and orientating them around the beam axis. As a result of the random positioning of each particle, several sets of indices will be in a diffracting position resulting in several cones of X-rays being formed. The finer the powder the more continuous the cone, therefore bulky crystals would diffract X-rays as spots on a cone rather than a continuous line. In the Debye-Scherrer method of powder diffraction a beam of monochromatic X-rays enter a closed camera, at the

centre of which is mounted a powdered sample in a Lindermann tube. The deflected beams form cones and are recorded as arcs on photographic film. The diameter of the cone is related to 4θ (see figs.1.15 and 1.16) and hence the Bragg angle can be calculated with a knowledge of the camera radius.

$$\theta(\text{in radians}) = D/4R$$

Where R is the camera radius and D is the distance between the centres of arcs on the same cone as measured across the backplate hole, on the photographic film. 'd' spacings can then be calculated using the Bragg law (equation 1.1).

In this work X-ray powder diffraction was used for the identification of new phases in prepared samples. The data were collected on a Phillips PW1051 diffractometer using $\text{CuK}\alpha$ radiation. Data were read electrically as opposed to photographically and output was in the form of a graphical trace of intensity verses 2θ . In order to assist in the interpretation and comparison of X-ray powder traces a Basic program was developed to run on the BBC and Acorn Electron microcomputers, a full listing of the program is given in Appendix 1. The program requires peak heights and 2θ values to be input and will output data in easily comparable forms. Another advantage of this type of interpretation is that a permanent computer record of each trace can be stored on disc.

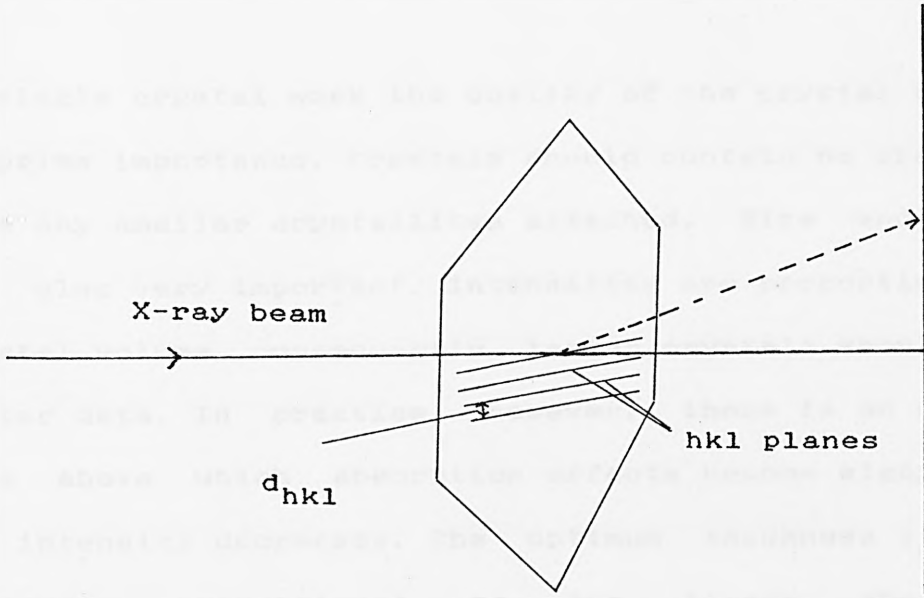


Fig.1.15

Diffraction by hkl planes in a single crystal

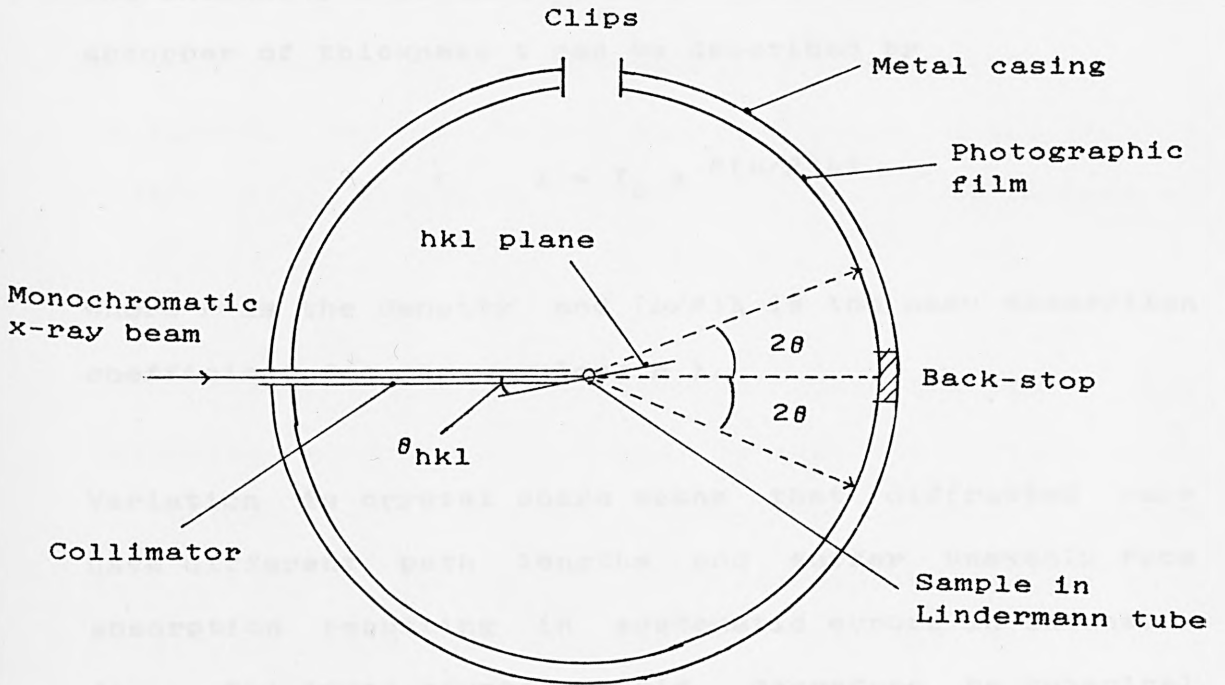


Fig.1.16

Cross section through powder camera

1.7 Single Crystal data collection.

In single crystal work the quality of the crystal used is of prime importance. Crystals should contain no cracks or have any smaller crystallites attached. Size and shape are also very important. Intensities are proportional to crystal volume, consequently, larger crystals should give better data. In practice, however, there is an optimum size above which absorption effects become significant and intensity decreases. The optimum thickness t_{opt} is inversely proportional to the linear absorption coefficient μ which itself is dependent on wavelength λ .

$$t_{opt} = 2/\mu$$

The intensity I of an X-ray beam after passing through an absorber of thickness t can be described by

$$I = I_0 e^{-\rho(\mu/\rho)\lambda t}$$

Where ρ is the density and $(\mu/\rho)\lambda$ is the mass absorption coefficient for the wavelength λ .

Variation in crystal shape means that diffracted rays have different path lengths and suffer unevenly from absorption resulting in systematic errors in intensity data. The ideal crystal would, therefore, be spherical with an average diameter of around 0.5mm. In practice, in order to overcome these disadvantages, small crystals were used along with penetrating $\text{MoK}\alpha$ radiation,

thus reducing the need for absorption corrections.

Crystals once selected were mounted. Two methods were employed; either in Linderman tubes using grease to prevent movement or on the end of quartz or glass needles using 'Araldite' as an adhesive. The former was more suitable for samples that were likely to deteriorate in atmospheric conditions.

All X-ray single crystal data, included in this work were obtained on Phillips PW1100 four circle diffractometers located at The Polytechnic of North London; Queen Mary College, London and Padua University, Italy. As an example of data collection, that of benzyl ammonium hexachlorostannate(IV) is now described.

The crystals were found to be long needles. A small crystal mounted on a quartz needle which was placed on a goniometer and the crystal centred to ensure the correct diffraction of X-rays. The crystal had to be central to four circles; ϕ , ω , χ and 2θ (see fig.1.17 [22]).

After centering, the background radiation level was determined and this value used as a discriminating level in the peak hunt which then commenced. During the peak hunt, optimum values for the four angle settings at a particular peak were measured and recorded for twenty five low angle reflections and from these, the orientation matrix was calculated. This matrix (UB) represents the orientation of the crystal and therefore,

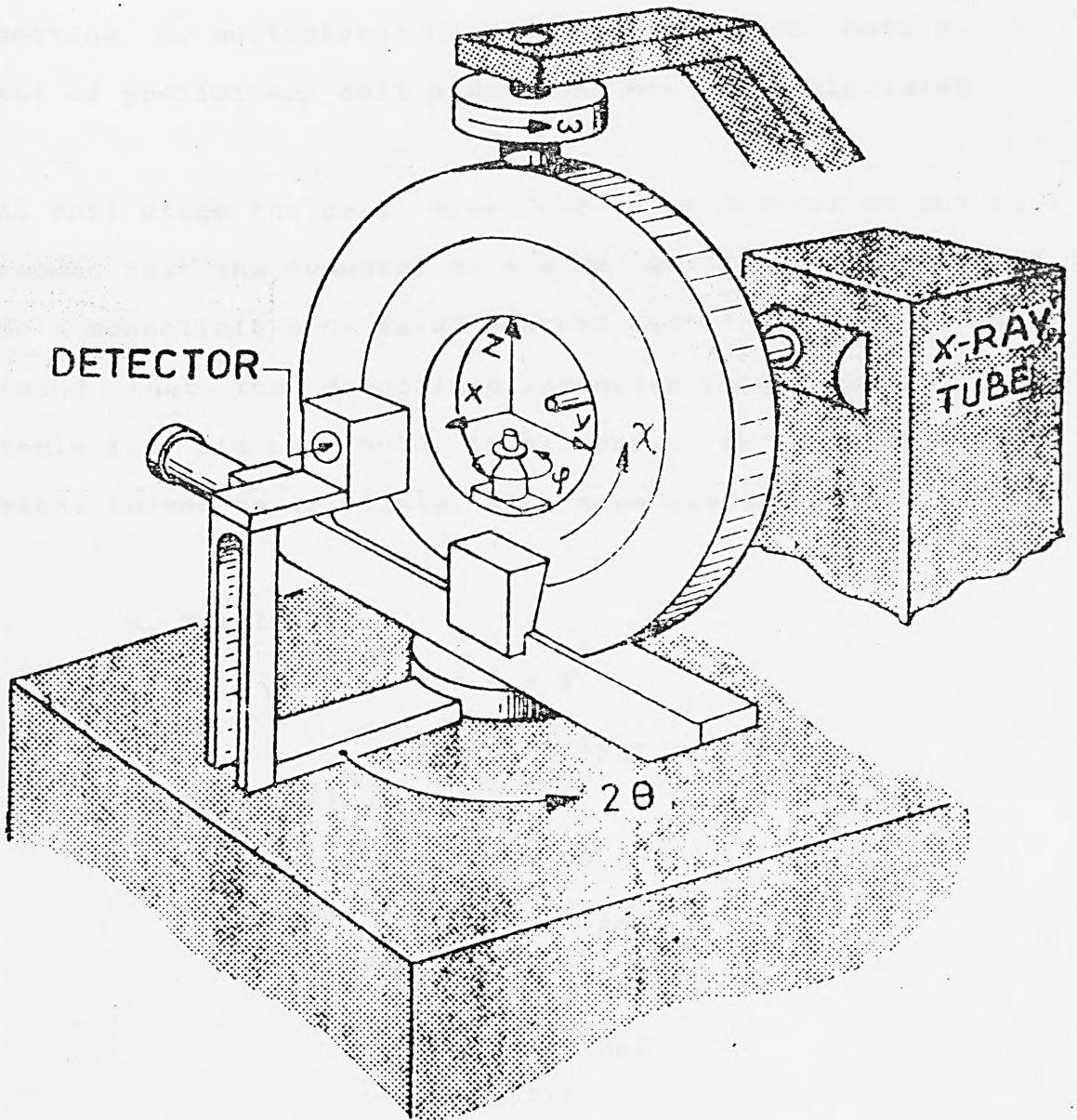


Fig. 1.17: Definition of angles and coordinates on four circle diffractometers.

changes every time a crystal is put on. A second matrix (MX) gives information on the size, shape and symmetry of the unit cell, i.e., it is directly related to the cell constants; a, b, c, α , β and γ .

Subsequently the diffractometer manual was consulted and the unit cell re-defined to correspond to a standard setting by multiplying UB by a reorientation matrix. A set of preliminary cell dimensions was also calculated.

At this stage the cell type had to be decided on and it seemed that the symmetry of the MX matrix resembled that of a monoclinic a C- faced centred cell. However, it was found that the monoclinic intensity relationships (see table 1.1) did not hold in all cases, and that the cell might indeed be triclinic, with some pseudosymmetry.

a. Triclinic.

$$\alpha = \beta = \gamma$$

$$I_{hkl} = I_{\bar{h}\bar{k}\bar{l}}$$

b. Monoclinic.

$$\alpha = \gamma = 90^\circ$$

$$I_{hkl} = I_{\bar{h}\bar{k}\bar{l}}$$

$$= I_{h\bar{k}l}$$

$$= I_{\bar{h}kl}$$

Table 1.1

Triclinic and monoclinic Intensity and unit cell angle relationships.

Unlike higher symmetries, in order to solve triclinic

cell structures, all the information in the unit cell must be collected, therefore, data collection covered the whole unit cell.

Values for h , k and l were input into the diffractometer, which then drove to the point at which the set of planes defined by h, k and l were in a reflecting position, and the detector arm in the correct position to measure the intensities. The diffractometer then re-measured the four angles for the peak. A set of twenty five peaks were recorded which had over 1000 counts for intensity, and θ angles greater than 10° . The orientation matrix and cell constants were then redetermined.

Data collection then began within a set range for θ . Maximum h, k and l values were also put in and these acted as a halt for the collection. The diffractometer was set to collect all positive values for h, k and l , but also negative values in h . Three peaks of high intensity taken from the original peak hunt data were used as references to see if the crystal had moved or decomposed, these were remeasured every three hours. If any difference was found when checking the references, the twenty five high angle reflections, used in calculating the orientation matrix, were remeasured and the matrix recalculated. The diffractometer drove to peaks within the ranges given, for each peak, a background level of radiation was determined both before and after the peak and then the total radiation intensity measured in a scan of 2° width. All this was recorded automatically on magnetic tape over

a period of 5 days.

After data collection the magnetic tape was read into the main frame computer where it underwent data reduction. In this, data were first simplified by subtracting background radiation levels from total peak intensities. The intensities were then corrected for geometric factors by multiplying by the reciprocal of the Lorentz polarisation factor (L_p) ie.

$$(I)_{\text{corr}} = I(1/L_p)$$

The reduced data were read onto magnetic tape once again and transferred onto the University of London Computer Centre (ULCC) where structure determination proceeded.

1.8 Structure determination

The basic principles involved in structure determination will now be discussed. Fig.1.18 is a flow chart summarising the procedure followed during structure determination.

The scattering of X-rays by a single electron is described by the amplitude E of the scattered wave at a distance r and is given by, [23,24]

$$E = E_0 \frac{e^2}{mc^2} \frac{1}{r} \sin\chi$$

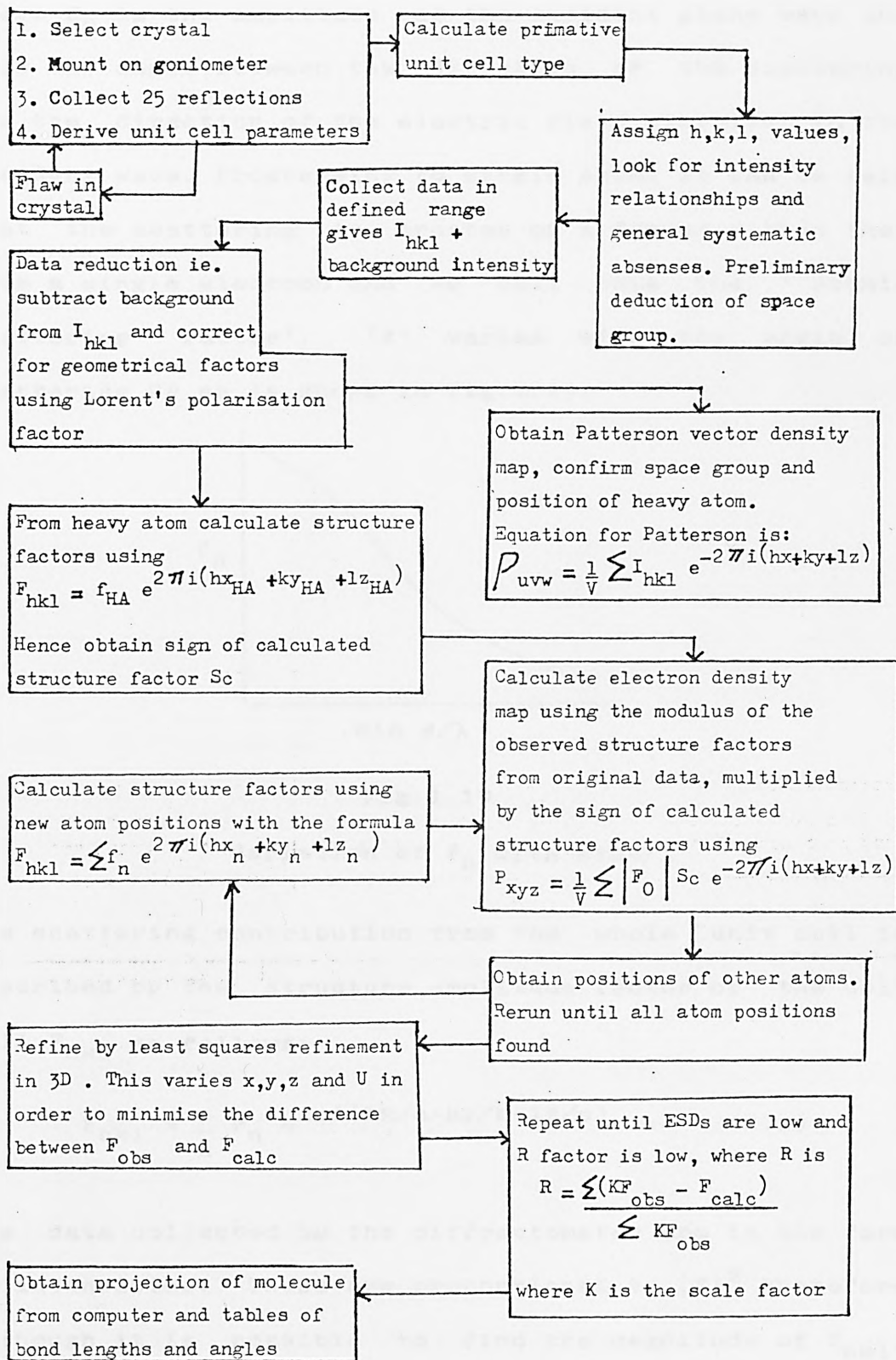


Fig.1.18

Flow chart showing procedure followed during structure determination

Where E_0 is the amplitude of the incident plane wave and χ is the angle between the direction of the scattering and the direction of the electric field vibration in the incident wave. Progressing to single atoms it can be said that the scattering is greater by a factor f than that from a single electron and we call this the 'atomic scattering factor'. ' f ' varies with the angle of scattering 2θ as is shown in fig.1.19.

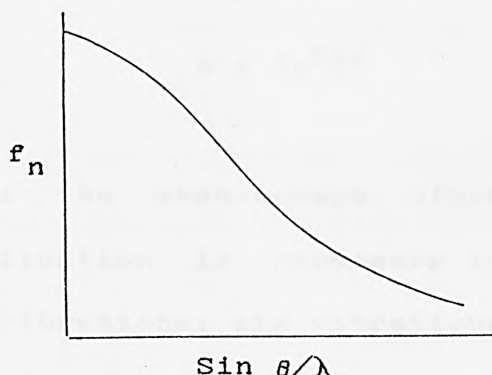


Fig.1.19

Variation of f_n with $\sin\theta/\lambda$

The scattering contribution from the whole unit cell is described by the structure amplitude factor of the unit cell F_{hkl} as follows:

$$F_{hkl} = \sum_n f_n e^{2\pi i(hx/a+ky/b+lz/c)} \quad \text{---- (1.2)}$$

The data collected by the diffractometer are in the form of intensities. These are proportional to $|F|^2$ therefore although it is possible to find the magnitude of F_{hkl} , its phase is indeterminate, this is known as the phase problem.

Equation 1.2 assumes that atoms are spherical and stationary. In real crystals, however, atoms vibrate and scattering power is reduced because of the increased electron cloud distribution. For isotropic vibrations atomic scattering is modified by,

$$e^{-B(\sin\theta)/\lambda^2} \quad \text{--- (1.3)}$$

B, the the isotropic temperature factor is given by,

$$B = 8\pi^2\bar{u}^2$$

Where \bar{u}^2 is the mean-square vibrational amplitude. Further modification is necessary in order to describe anisotropic vibrations; six vibrational parameters are needed to describe a thermal ellipsoid and are incorporated into the following modification [25].

$$\exp [-2\pi i^2(U_{11}h^2a^{*2} + U_{22}k^2b^{*2} + U_{33}l^2c^{*2} + 2U_{12}hka^{*}b^{*} + 2U_{13}hla^{*}c^{*} + 2U_{23}klb^{*}c^{*})]$$

Calculated structure factors (F_C) are determined for each reflection using the modified equation 1.2. Initially the coordinates of a heavy atom are input (x_{ha}, y_{ha}, z_{ha}) thus equation 1.2 becomes:

$$F_C = f_{ha} e^{2\pi i(hx_{ha} + ky_{ha} + lz_{ha})} \quad \text{---- (1.4)}$$

With only one atom input the magnitude of F_C is approximate, the phase, however, is correct. We can then

use the calculated phases S_C and the observed structure factor F_O with all the reflections to calculate an electron density map using a 3-dimensional Fourier summation.

$$\rho_{xyz} = 1/V \sum_h \sum_k \sum_l S_C F_O e^{-2\pi i(hx+ky+lz)} \quad \text{--- (1.5)}$$

Where ρ_{xyz} is the electron density at a particular point, V is the volume of the unit cell and F_O is given by:

$$F_O = \sqrt{I_{hkl}}$$

Very often a difference Fourier summation is used after the heavy atoms have been located in order to find the lighter atoms.

$$\Delta\rho_{xyz} = 1/V \sum_h \sum_k \sum_l (F_O - F_C) e^{-2\pi i(hx + ky + lz)} \quad - (1.6)$$

The resultant E-map shows only the residual electron density.

Computers are used to locate maxima in electron density over a grid of points in the unit cell. These maxima are output as coordinates in order of electron density and are accompanied by possible bonding distances to other maxima. It is possible to assign atoms to many of these maxima and using these positions recalculate structure factors. More of the calculated phases will now be correct and hence a more accurate electron density map can be obtained from which further atoms may be located and the process repeated. After all the atom positions are located the three position parameters x_n , y_n , z_n , and

the thermal parameter U_n , are refined for each atom along with the overall scale factor K . Refinement takes the form of an iterative, 3-dimensional, least squares calculation in which $((F_O - F_C)/K)^2$ is minimised. K is given by,

$$K = \frac{\sum F_C}{\sum F_O}$$

The matrix relating all the components in the least squares procedure is inverted to give the standard errors on the refined parameters. A successful structure determination is gauged by two things; the estimated standard deviations on the final parameters and a reliability (or residual) factor R which is given by,

$$R = \frac{\sum (K F_O - F_C)}{\sum K F_O}$$

In general for a well refined structure, an R factor of between 0.02 - 0.06 is the norm. However this varies with the quality of the data and the atoms present; for example structures containing Br atoms tend to give higher R factors than those without.

Two methods were employed in the solution of the phase problem; a Patterson synthesis was used to locate heavy atom positions for input into equation 1.2, alternatively direct methods calculations were used when Patterson synthesis failed to distinguish single heavy atom sites. Each of these will be discussed in turn.

(i) Patterson synthesis. [26]

Patterson maps are produced after data correction and prior to structure determination in order to locate heavy atoms. They are vector density maps generated using a Fourier summation:

$$\rho_{uvw} = 1/V \sum_h \sum_k \sum_l I_{hkl} e^{-2\pi i(hu+kv+lw)}$$

Where ρ_{uvw} is the vector density at point uvw in the vector map. Every peak in the vector map corresponds to a pair of peaks in the real unit cell and peak height is proportional to the product of the atomic numbers of the two atoms. Each Patterson maximum is located at a distance and in a direction from the origin $(0,0,0)$ corresponding to the vector between a pair of atoms in the real unit cell (see fig.1.20)

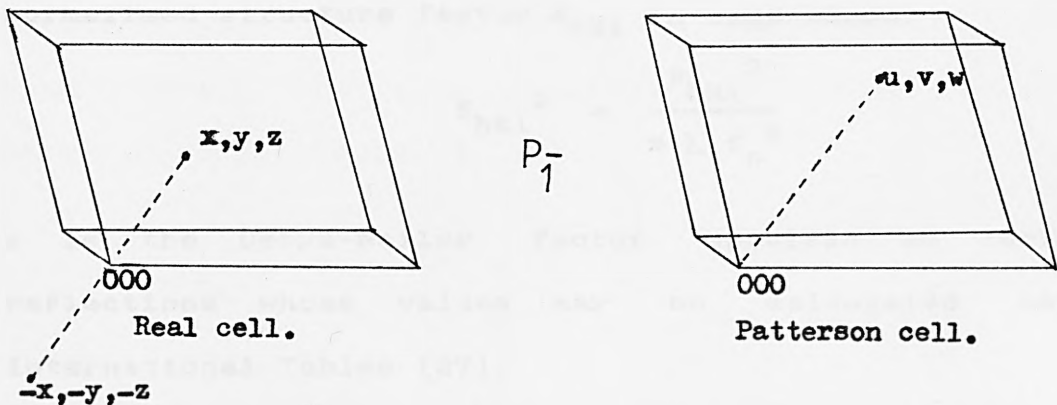


Fig.1.20

Relationship between Patterson and real unit cells
in P_1 symmetry.

Summarising, every pair of atoms at points x,y,z and x_1,y_1,z_1 give rise to a Patterson peak at u,v,w where,

$$u = x_1 - x$$

$$v = y_1 - y$$

$$w = z_1 - z$$

Since peak heights are proportional to the atomic numbers of atoms contributing to the vectors, if there is an atom particularly heavier than the rest its vectors will show at the top of the list and hence its coordinates may be calculated and input into a Fourier synthesis to get an electron density map.

(ii) Direct methods

Direct methods were used in structures where no single heavy atom was distinguishable in the Patterson map. In direct methods the $|F|$ quantity is unsuitable for use in phase determination as it declines with $\sin\theta$, so a normalised structure factor E_{hkl} is used where,

$$E_{hkl}^2 = \frac{F_{hkl}^2}{x \sum f_n^2}$$

x is the Debye-Waller factor specific to certain reflections whose values may be calculated using International Tables [27].

Tentative phases for selected E_{hkl} values are determined by the magnitude of the structure factors. A series of phase relationships are then set up using stronger reflections. The relationships are of the form:

$$\phi_{-H} + \phi_{H'} + \phi_{H-H'} = \phi_{H,H'}$$

Where ϕ_H is the phase of E_H and $Q_{H,H'}$ is an estimated weighted phase.

An elimination process based on structure information reduces the number of relationships to be used in phase determination. This process, known as convergence, uses space group information to determine which reflections are structure semi-invariants and how many are needed to define the origin. The best reflections for origin definition are selected as well as several other starting points for phase determination. These alternative starting points are based on the strongest phase relationships and are selected using the algorithm described by Germain et. al [28]. The initially unknown phases of the selected reflections are assigned using a 'magic integer' sequence [29,30] resulting in a multiple starting point for the tangent formula in phase determination. Phases are eventually determined using a weighted tangent formula [31]:

$$\tan\phi_H = \frac{\sum W_H W_{H'-H} E_H E_{H'-H} \sin(\phi_H + \phi_{H'-H})}{\sum W_H W_{H'-H} E_H E_{H'-H} \cos(\phi_H + \phi_{H'-H})}$$

Where W is a weighting factor. Electron density maps can now be calculated as previously described.

Modern direct methods programs are designed for the automatic and complete solution of structures with atoms of approximately equal atomic number. In practice it is often convenient to use direct methods to locate heavy atoms only, ie as an alternative to the Patterson

synthesis, and then use normal Fourier techniques to achieve full structure determination.

1.9 Computer programs used in X-ray crystallography

The following computer programs were used in the present work in connection with X-ray structure determination:

'SHELX-76' [32]

An easy to use integrated program for computing crystallographic calculations on X-ray and neutron diffraction data. The calculations are valid for all space groups and facilities include:

- (i) Data reduction and absorption corrections.
- (ii) Rejection of systematic absences and averaging of equivalent reflections.
- (iii) Fast automatic centrosymmetric direct methods.
- (iv) Multisolution tangent refinement including convergence mapping.
- (v) Full-matrix, accelerated full-matrix and blocked full-matrix least squares calculations.
- (vi) Constrained refinement of hydrogen atoms, rigid groups and bond lengths.
- (vii) Refinement of isotropic extinction and crystal size.
- (viii) Analysis of variance and automatic optimisation of weighting scheme.
- (ix) Various Fourier syntheses, with peak searches.
- (x) Lists of structure factors.

'MULTAN-80' [33]

A powerful set of programs designed to perform all the necessary calculations for the complete solution of a structure by direct methods. The package consists of 4 separate programs that communicate via data sets. The programs are summarised as follows: 'NORMAL' computes normalised structure factors and prepares a file for use with 'MULTAN'. 'MULTAN' consists of two logical sections: 'FIRST' finds sets of 3 strong reflections whose indices are related as H, H' and $H-H'$. It then uses convergence to find starting reflections for the tangent formula. As phase values are initially unknown, selected phases are assigned by 'magic integers' producing a multiple starting point. Convergence is used to reject certain reflections. Sets of 3 reflections are found such that E_H is small and $E_{H'}$ and $E_{H-H'}$ are large. 'LAST' determines phases for all reflections from each starting set produced by convergence using a weighted tangent formula. 'EXFFT' computes an electron density map (E-map) from a set of normalised structure factors. 'SEARCH' searches for the highest peaks in the E-map and for molecular structure and fragments and computes bond lengths and angles.

'PLUTO' and 'PLUTO-78' [34,35]

These programs are used for the plotting of molecular and crystal structures on microfilm. Their main features include:

- (i) Plotting of single molecules or assemblies.
- (ii) Stick, solid ball and spoke or space filling

representations.

(iii) Automatic labelling.

(iv) Stereo or mono views with or without perspective.

(v) Flexible view direction.

Additional features of 'PLUTO-78' are:

(vi) Calculation of inter and intra molecular distances.

(vii) Compatibility with entries in the Cambridge Crystallographic Data Base.

'MOLPLOT'

In order to assist in the interpretation of refined X-ray structure parameters, a BASIC computer program was written in BBC BASIC to run on a BBC or Acorn Electron microcomputer fitted with a disc filling system. To save space which is limited in the standard microcomputer, the final version which is listed in Appendix 1 consists of a main program 'MOLPLOT' with 7 overlays, 'MOL 1-7'. A simple flow chart explaining the program layout is shown in fig.1.21. The contents of the program are discussed below:

'MOLPLOT'

Contains the main menu and common procedures and functions. The arrays are dimensioned at the beginning with the number of atoms N% set to 100. This may be increased to 150 with few problems but any further increase must be accompanied with more memory space, for example by the fitting of a second processor.

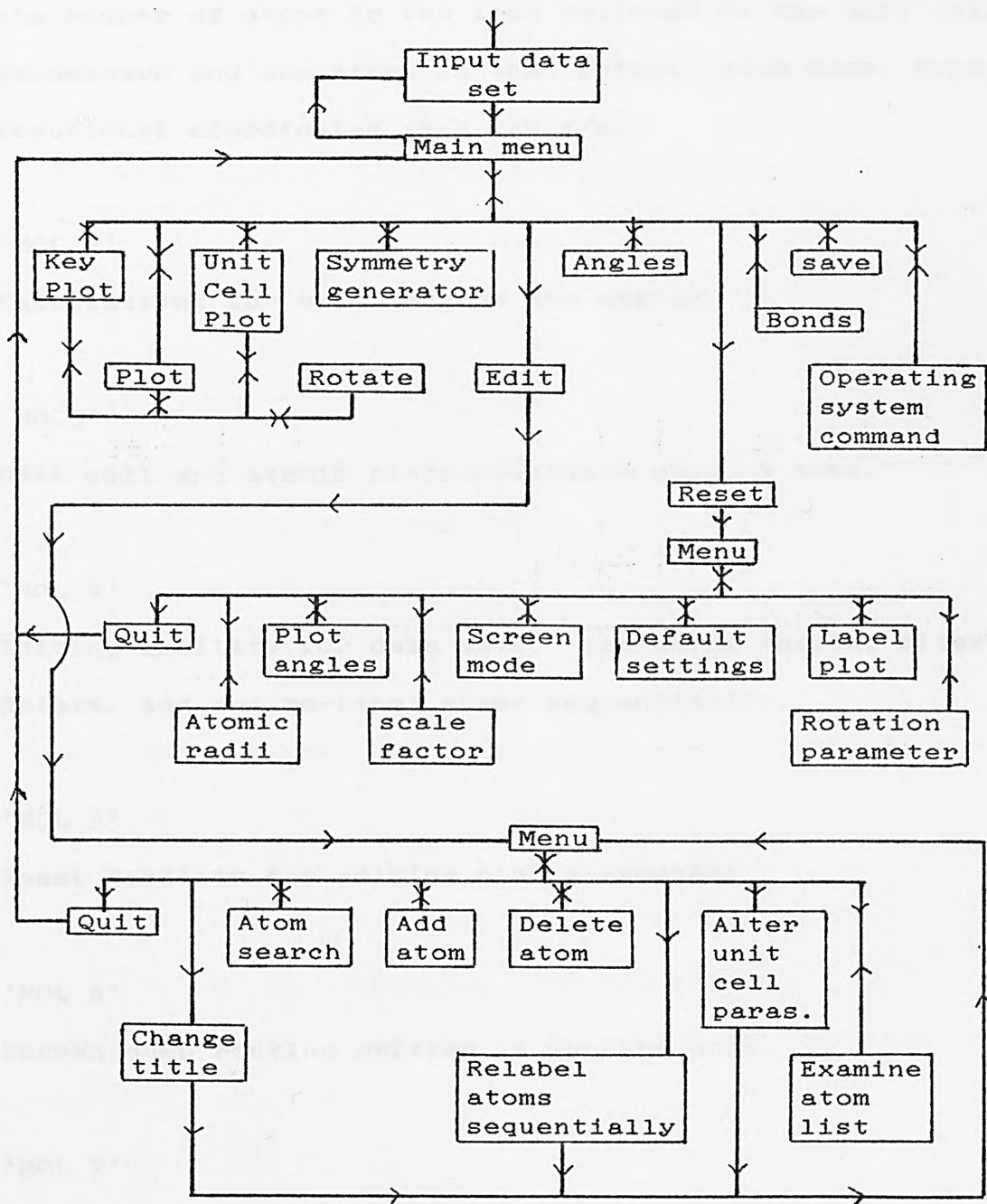


Fig.1.21

'MOLPLOT' program layout

'MOL 1'

Input and output of data sets. Each data set consists of the number of atoms in the list followed by the unit cell parameters and the atoms in the format: atom name, type, fractional coordinates (x/a,y/b,z/c).

'MOL 2'

Calculations for bond lengths and angles.

'MOL3'

Unit cell and atomic plots rotatable about 3 axes.

'MOL 4'

Editing facility for data sets, including search, alter, delete, add and re-label atoms sequentially.

'MOL 5'

Reset facility for editing plot parameters.

'MOL 6'

Screen dump routine written in machine code.

'MOL 7'

Symmetry generating routine. Data sets are expanded to include positions generated by centered lattices centers of symmetry and symmetry relations. Care must be taken not to exceed the maximum no. of atoms.

For the plotting, bond length and bond angle routines it was necessary to re-define the atomic coordinates with

respect to fixed three dimensional space. This was achieved in Cartesian coordinates as follows:

$$X = a.(x/a) + \cos\beta.(z/c).c + \cos\gamma.(y/b).b$$

$$Y = b.(y/b).\sin\gamma.\sin\alpha$$

$$Z = c.(z/c).\sin\beta + b.(y/b).\cos\alpha$$

Where a,b,c,α,β and γ are the unit cell parameters.

With the coordinates thus defined it is possible to calculate the distance between two points (X,Y,Z) and (X₁,Y₁,Z₁), using equation 1.7.

$$D = \sqrt{\{(X-X_1)^2 + (Y-Y_1)^2 + (Z-Z_1)^2\}} \quad \text{---- (1.7)}$$

The distances between 3 atoms A, B and C can now be defined as follows:

d = distance between A and B

d₁ = distance between A and C

d₂ = distance between B and C

Using these, the three angles generated can now be computed using equations 1.8.

$$\left. \begin{aligned} \text{Angle ABC} &= \frac{(d_2^2 + d^2 - d_1^2)}{2 \cdot d_3 \cdot d} \\ \text{Angle BAC} &= \frac{(d^2 + d_1^2 - d_2^2)}{2 \cdot d \cdot d_1} \\ \text{Angle ACB} &= \frac{(d_1^2 + d_2^2 - d^2)}{2 \cdot d_1 \cdot d_3} \end{aligned} \right\} \quad \text{---- (1.8)}$$

Rotating in three dimensions requires the setting up of a

rotation matrix. The overall rotation may be broken down into three constituent rotations. If we take three perpendicular axes X,Y,Z rotation about these axes may be described in terms of three angles θ , ψ and ϕ respectively. Rotation about the X axis is described by the transformation matrix shown below.

$$A = \begin{pmatrix} 1 & 0 & 0 \\ 0 & \cos \theta & \sin \theta \\ 0 & -\sin \theta & \cos \theta \end{pmatrix}$$

Similarly, rotations about the Y and Z axes can be described by the following matrices: About Y

$$B = \begin{pmatrix} \cos \psi & 0 & \sin \psi \\ 0 & 1 & 0 \\ -\sin \psi & 0 & \cos \psi \end{pmatrix}$$

and about Z

$$C = \begin{pmatrix} \cos \phi & \sin \phi & 0 \\ -\sin \phi & \cos \phi & 0 \\ 0 & 0 & 1 \end{pmatrix}$$

The complete rotation is therefore defined as the product of the 3 component matrices ie. $R = ABC$. Thus,

$$R = \begin{pmatrix} a(11) & a(12) & a(13) \\ a(21) & a(22) & a(23) \\ a(31) & a(32) & a(33) \end{pmatrix}$$

Where,

$$a(11) = \cos\psi$$

$$a(12) = \cos\psi \cdot \sin\phi$$

$$a(13) = \sin\psi$$

$$\begin{aligned} a(21) &= -\cos\theta.\sin\phi - \sin\theta.\sin\psi.\cos\phi \\ a(22) &= \cos\theta.\cos\phi - \sin\theta.\sin\psi.\sin\phi \\ a(23) &= \sin\theta.\cos\psi \\ a(31) &= \sin\theta.\sin\phi - \cos\theta.\sin\psi.\cos\phi \\ a(32) &= -\sin\theta.\cos\phi - \sin\psi.\sin\phi.\cos\theta \\ a(33) &= \cos\theta.\cos\psi \end{aligned}$$

[1] C. R. D. Srinivasan, *Journal of Chemical and Physical Data*, 1970, 1(1), 1-10.

[2] H. K. Sauer, *Acta Cryst.*, 1950, 3, 531.

[3] W. B. Brown and A. R. Shull, *Acta Cryst.*, 1975, 10, 1070.

[4]

[5] G. Wright and P. Shuman, *J. Chem. Phys.*, 1952, 17, 716.

[6]

[7] R. S. Ingber, *J. Polym. Sci. Polym. Chem. Ed.*, 1970, 8, 375.

[8]

[9] R. C. Fuller, *J. Organometal. Chem.*, 1953, 3, 207.

[10] P. Smith and L. Smith, *Chemistry of Metals*, 1979, 11, 208.

[11]

[12] A. Nijm, *J. Chem. Soc.*, 1953, 3528.

[13] H. F. A. Dove, W. King and Y. J. King, *Chem. Comm.*, 1973, 13, 940.

[14]

REFERENCES, CHAPTER ONE

- (1) A.J.Baird, R.Parsons and J.Jordan, 'Standard Potentials in Aqueous Solution', I.U.P.A.C., (Marcell Dekker, Inc.), New York and Basel, 1985.
- (2) 'C.R.C Handbook of Chemistry and Physics' 61st edition (1980-81). C.R.C. Press.
- (3) W.H.Bauer, Acta Cryst., (1956), 9, 515.
- (4) W.H.Bauer and A.A.Khan, Acta Cryst., B27, (1970), 2133.
- (5) G.Wagner and H.Binder, Z.Anorg.Chem., (1959), 298, 12.
- (6) R.K.Ingham, S.D.Rosenberg and H.Gilman, Chem.Rev., (1960), 60, 459.
- (7) R.C.Poller, J.Organometal.Chem., (1965), 3, 321.
- (8) P.Smith and L.Smith, Chemistry in Britain, (1975), 11, 208.
- (9) R.Hulme, J.Chem.Soc., (1963), 1524.
- (10) M.F.A.Dove, R.king and T.J.King, Chem.Comm., (1973), 11, 944.

(11) L.E.Orgel, J.Chem.Soc., (1959), 3815.

(12) J.D.Donaldson and S.M.Grimes, Reviews of Silicon, Germanium Tin and Lead Compounds, (1984), 8 (1), 1-132.

(13) J.D.Donaldson, Progress Inorganic Chem., (1967), 8, 287.

(14) R.D.Cromer, R.V.Lindsey, C.T.Prewitt and U.G.Stolberg, J.Am.Chem.Soc., (1965), 87, 658.

(15) M.P.Johnson, D.F.Shriver and S.A.Shriver, J.Am.Chem.Soc., (1966), 88, 1568.

(16) J.D.Cotton, P.J.Davidson, M.F.Lappert, J.D.Donaldson and J.Silver, J.Chem.Soc. Dalton Trans., (1976), 2286.

(17) J.D.Donaldson and S.M.Grimes, J.Chem.Soc. Dalton Trans., (1984), 1301.

(18) J.D.Donaldson, J.Silver, S.Hadjiminolis and S.D.Ross, J.Chem.Soc. Dalton Trans., (1975), 1500.

(19) S.J.Clark, C.D.Flint and J.D.Donaldson, J.Phys.Chem.Solids, (1981), 42, 133.

(20) W.Friedrich, P.Knippling and M.Laue, Proc.Bavarian Acad.Science, (1912), 303.

- (21) W.L.Bragg, Proc.Camb.Phil.Soc., (1913), 17, 43.
- (22) Philips PW1100 instruction manual.
- (23) G.E.Bacon, 'X-ray and Neutron Diffraction', Pergamon Press, 1966.
- (24) A.H.Compton and S.K.Allison, 'X-rays in Theory and Experiment', Van Nostrand, New York, p.56.
- (25) G.H.Stout and L.H.Jensen, 'X-Ray Structure Determination' Macmillan 1968.
- (26) A.L.Patterson, Z.Krist., A90, (1935), 517.
- (27) 'International Tables for X-ray crystallography' Kynoch Press, Birmingham, 1962.
- (28) G.Germain, P.Main and M.M.Woolfson, Acta Cryst., A26, (1970), 274.
- (29) P.Main, Acta Cryst., A33, (1977), 750.
- (30) P.Main, Acta Cryst., A34, (1978), 31.
- (31) G.Germain, P.Main and M.M.Woolfson, Acta Cryst., A27, (1971), 368.
- (32) G.M.Sheldrick, 'Program for Crystal Structure determination', University of Cambridge, 1975.

(33) P.Main, S.J.Fiske, S.E.Hull, L.Lessinger, G.Germain, J.P.Declercq, M.M.Woolfson, 'MULTAN-80 - A system of computer programs for the automatic solution of crystal structures from X-ray diffraction data.' 1980, Universities of York, England and Louvain, Belgium.

(34) W.D.S.Motherwell, 'PLUTO - A Program for Plotting Molecular and Crystal Structures', University of Cambridge 1976.

(35) W.D.S.Motherwell, 'Program for Plotting Molecular and Crystal Structures - PLUTO78', University of Cambridge 1978.

CHAPTER TWO

PREPARATIONS OF TIN(II) COMPLEXES IN SOLUTION

	Page
2.1 Introduction.	59
2.2 General preparative and analytical methods.	60
(i) Sn analysis.	61
(ii) Br and Cl analyses.	61
(iii) K ⁺ analysis.	65
(iv) Cs and Rb analyses.	65
(v) Water analysis.	66
(vi) N and H analysis.	66
2.3 The aqueous systems $xMX:ySnY_2 + HZ$ (where M = Cs, Rb, NH ₄ , K; X and Y = Cl, Br, F; Z = Br, Cl, OH, HSO ₄).	68
MSnX ₃ .nH ₂ O	69
MSn ₂ X ₅ .nH ₂ O	74

$M\text{Sn}_3\text{X}_7 \cdot n\text{H}_2\text{O}$ 103

$KX \cdot K\text{SnX}_3 \cdot \text{H}_2\text{O}$ 109

Materials containing sulphate. 119

References. 120

CHAPTER TWO

2.1 Introduction

The present work has concentrated on the fate of tin(II) halides in solutions, containing mixtures of the general composition $xMX + ySnY_2$ (where $X, Y = Br, Cl, F$ and $M = K, Rb, Cs, NH_4$). Studies [1-3] have shown that in solutions of tin(II) halides the stable and predominant species is the trihalostannate(II) anion $[SnX_3]^-$ and this is reflected in the products isolated from solution eg $CsSnCl_3$ [4] and $KCl.KSnCl_3.H_2O$ (see section 5.5 and [5]). In solutions that contain high concentrations of SnY_2 , with respect to MX , the resulting lack of sufficient halides to complex all the tin as $[SnX_3]^-$, results in the formation of polyatomic anions $[Sn_2X_5]^-$ [6-9].

Four types of solid products have previously been obtained from solutions of the type $xMX:ySnY_2$ [9,10] as follows:

- (i) $MSnX_3$
- (ii) $MX.MSnX_3$
- (iii) MSn_2X_5
- (iv) MSn_3X_7

The complexes that crystallise from solution depend upon the relative concentration of MX to SnY_2 in solution and on the relative lattice energies of the complex lattices.

Bird [9] carried out a systematic study on solutions of this type but restricted himself to single halide systems. The present work has involved both single and mixed halide systems.

2.2 General preparative and analytical methods.

Most of the products used in the present work were synthesised using the general preparative method: Appropriate molar quantities of MX and SnY₂ (where M = K, Cs, Rb, NH₄; and X,Y = F, Cl, Br) were dissolved separately in the minimum amounts of boiling water. In the case of SnY₂ the solution also contained a small piece of tin metal and a few drops of HZ (where Z = Br, Cl, HSO₄) to minimise oxidation and hydrolysis respectively. The solutions were then mixed and evaporated to give a clear solution. Crystals formed in the cooled solutions and were collected by vacuum filtration and dried *in vacuo* over silica gel. The whole process was carried out under N₂ to minimise oxidation.

Products were analysed for Sn, Br, Cl, K, N, H, Cs and H₂O, depending on starting materials used, and products were characterised by X-ray powder diffraction and differential thermal analysis (DTA). In most cases, where new phases were judged to have been formed Mössbauer spectra were collected. The methods used for chemical analysis were as follows:

(i) Sn(II) analysis

Samples were analysed for tin(II) using a modification of the method described by Donaldson and Moser [11]. A small amount (ca. 0.01g) of the sample being analysed was accurately weighed into a 100ml conical flask. To this was added 2M HCl (10ml) and acidified 0.2M FeCl_3 (10ml). The material was allowed to dissolve and 3 drops of phenanthroline indicator were added. The solution was then titrated with 0.1M CeSO_4 solution from a 10ml burette, the end point being detected by a red to green colour change. Standardisation was with ammonium ferrous sulphate to which was added the FeCl_3 (10ml) and HCl (10ml) solutions. A blank determination was also carried out under identical conditions to sample titrations using a 1ml burette. All titrations were performed in triplicate.

(ii) Bromine and chlorine analysis.

Samples were analysed for bromine and chlorine using a potentiometric titration involving the precipitation of the respective silver halide. This technique was particularly useful for analysing mixed halide samples. The apparatus used is shown in fig.2.1. An aliquot (25ml) of a sample solution, containing ca. 0.1g/100ml of sample in water, acidified with dilute H_2SO_4 , was placed in a 250ml beaker. The volume was increased by adding water (50ml) and the potential difference between silver and calomel reference electrodes, dipping into the solution, was measured. 0.01M silver nitrate solution (1ml) was

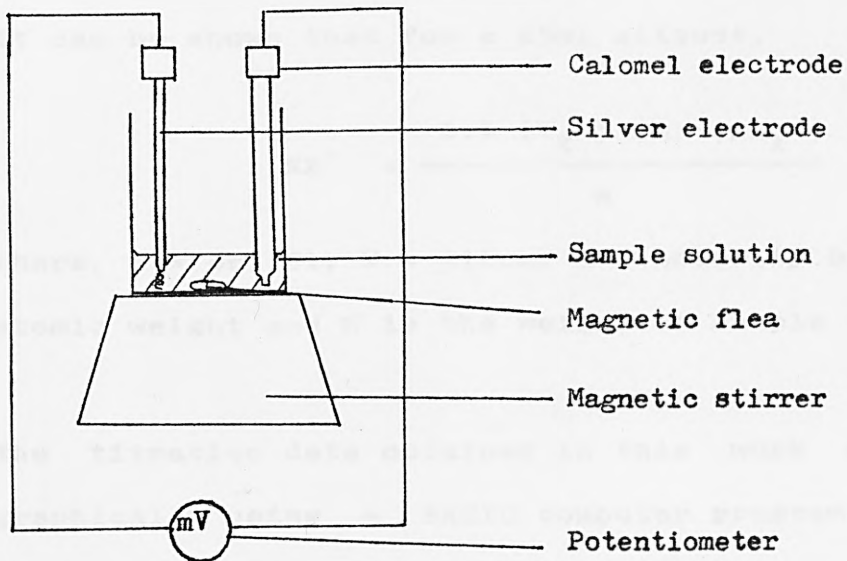
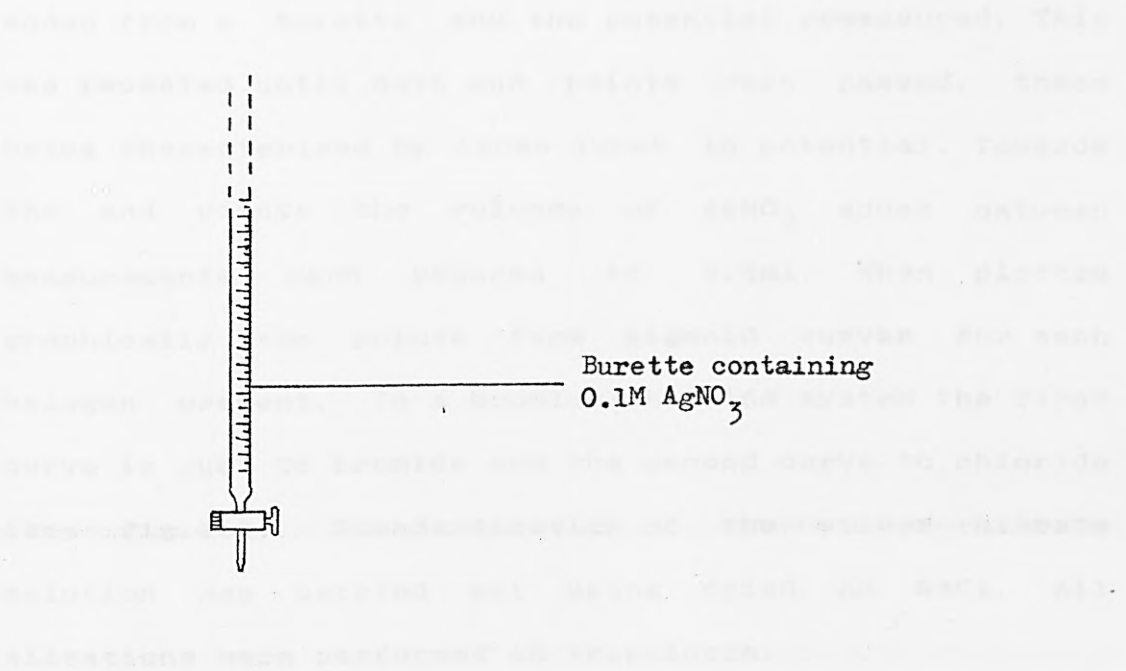


Fig.2.1

Apparatus for potentiometric halide determination

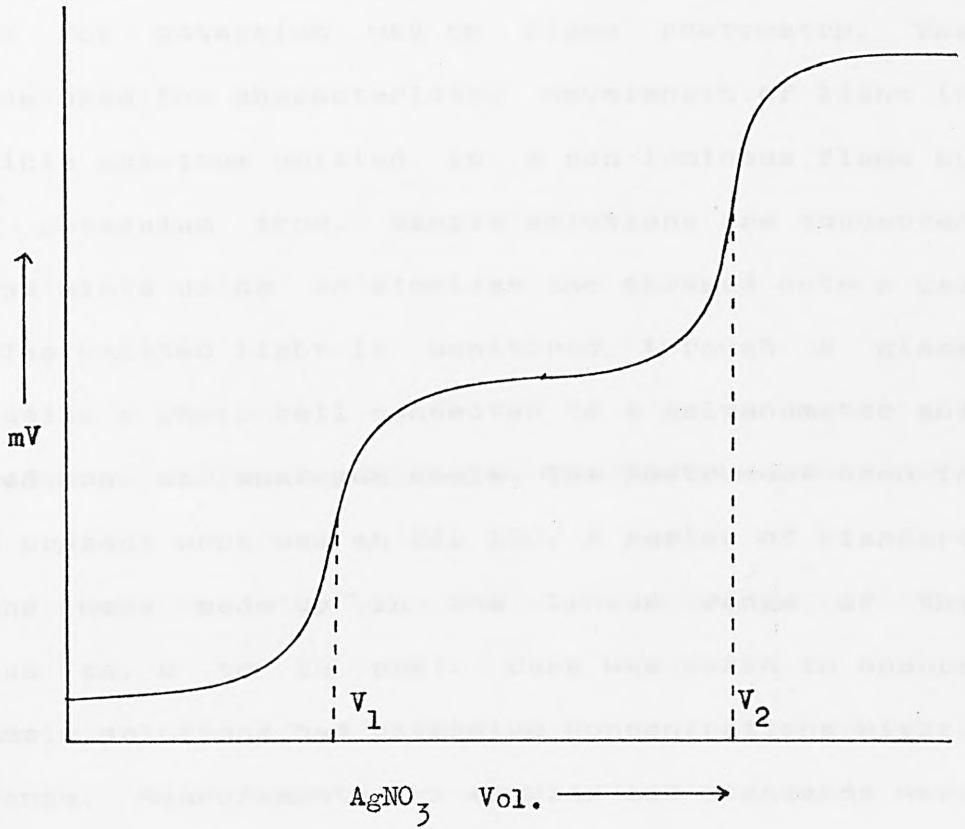
added from a burette and the potential remeasured. This was repeated until both end points were passed, these being characterised by large jumps in potential. Towards the end points the volumes of AgNO_3 added between measurements were reduced to 0.5ml. When plotted graphically the points form sigmoid curves for each halogen present. In a bromide-chloride system the first curve is due to bromide and the second curve to chloride (see fig.2.2). Standardisation of the silver nitrate solution was carried out using dried AR NaCl. All titrations were performed in triplicate.

It can be shown that for a 25ml aliquot.

$$\%X^- = \frac{0.4 (V_{X^-}) (M) (Aw_{X^-})}{W} \quad \text{---- (2.1)}$$

where, X = Br, Cl; V = titre; M = molarity of AgNO_3 ; Aw = atomic weight and W is the weight of sample in 100ml.

The titration data obtained in this work were plotted graphically using a BASIC computer program "TPLOT" [12] (see Appendix 1) running on a BBC microcomputer. The points of inflection on the graphs were calculated by plotting the second differential and calculating the point at which this cut the x - axis. As a result very precise results were obtained. The program also contained a routine for automatically calculating Br and Cl percentages using equation 2.1.



$V_1 = \text{titre for Br}$

$V_2 - V_1 = \text{titre for Cl}$

Fig.2.2

Idealised potentiometric curves for Br and Cl determination

(iii) K^+ analysis.

Analysis for potassium was by flame photometry. The technique used the characteristic wavelength of light in the visible spectrum emitted in a non-luminous flame by excited potassium ions. Sample solutions are converted into fine mists using an atomiser and sprayed onto a gas flame. The emitted light is monitored through a glass filter using a photo cell connected to a galvanometer and displayed on an analogue scale. The instrument used in all the present work was an EEL 100. A series of standard solutions were made up in the linear range of the technique (ca. 0 to 20 ppm). Care was taken to ensure that sample solutions had potassium concentrations within this range. Measurements on samples and standards were conducted at the same time and repeated. Results of the standard solutions were plotted by computer on a calibration graph and fitted by least squares to a straight line. Results for the samples were computed automatically using the fitted parameters.

(iv) Cs and Rb analysis.

Analysis of caesium proved very difficult. Gravimetric methods involving precipitation using sodium borohydride [13] proved inaccurate because of the small amounts of sample in use. Cs was finally analysed by ion exchange chromatography on a DIONEX 2010i ion exchange chromatograph. The technique involves separation of cations in a resin based column. The reaction of

monovalent cations with the column resin is summarised below.

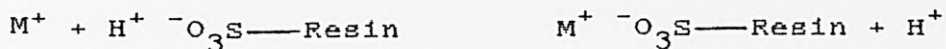


Fig.2.3 is a schematic representation of the chromatographic system used [14]. The retention times of different cations vary with size, thus, Na^+ and K^+ ions were detected more rapidly than Cs^+ ions. Peak heights were measured from recorded traces. A set of standard solutions in the concentration range 0 to 30 ppm Cs^+ were used in the construction of a calibration graph which was fitted by least squares as for K^+ analysis. Sample solutions were made up in this range and Cs percentages calculated automatically using the fitted line parameters. Rubidium was also analysed in this way.

(v) Water analysis.

Water assays were obtained by weight loss on heating under N_2 by thermogravimetry (TG). A TG trace was recorded with a simultaneous DTA trace on a Stanton Redcroft STA-780 simultaneous thermal analyser that is described in more detail in section 3.1.

(vi) N and H analysis.

Nitrogen and hydrogen were analysed by standard microanalytical techniques using The City University Microanalysis service.

Samples were further characterised by X-ray powder

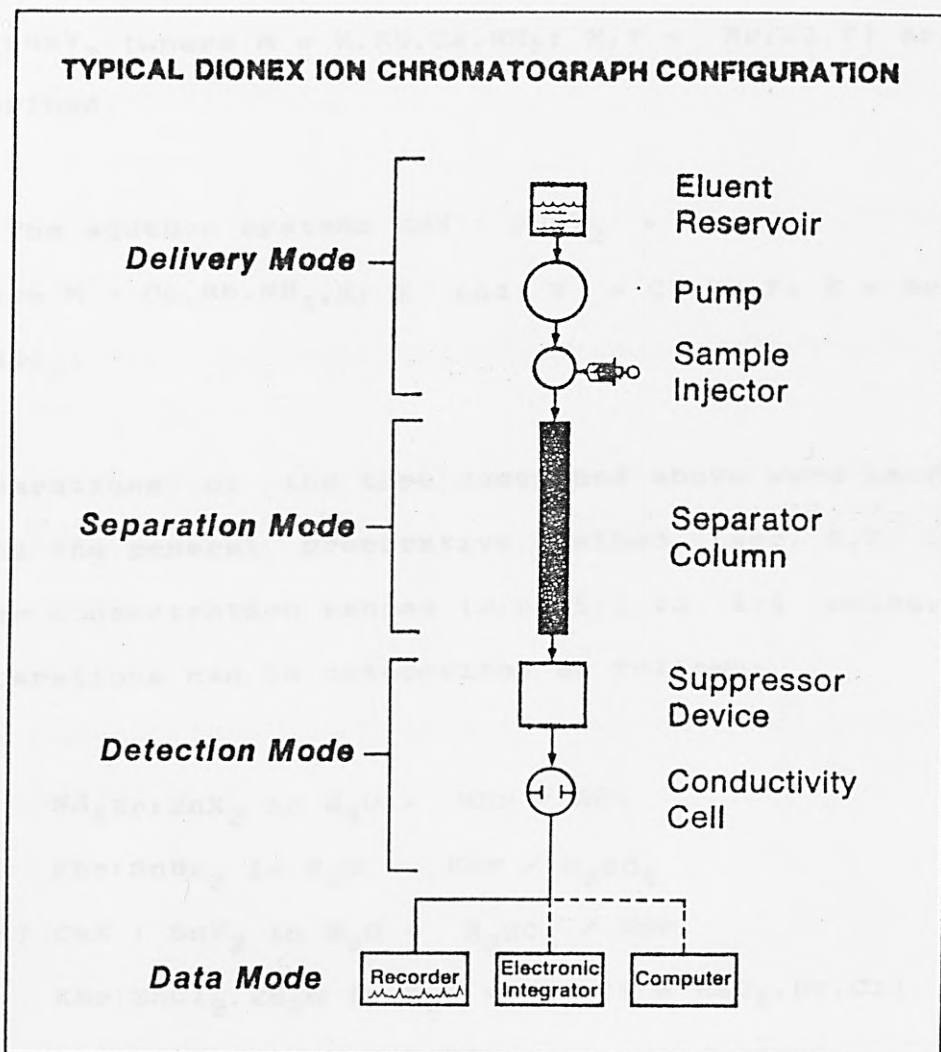


Fig.2.3

Schematic representation of Dionex 2010i ion chromatograph

diffraction and Mössbauer spectroscopy. These techniques are detailed in sections 1.6 and 4.1 respectively.

The preparations and results of various mixtures of $xMX:ySnY_2$ (where $M = K, Rb, Cs, NH_4$; $X, Y = Br, Cl, F$) are now described.

2.3 The aqueous systems $xMX : ySnY_2 + HZ$

(where $M = Cs, Rb, NH_4, K$; X and $Y = Cl, Br, F$; $Z = Br, Cl, OH, HSO_4$)

Preparations of the type described above were performed using the general preparative method (sec. 2.2) in the molar concentration ranges ($x:y$) 5:1 to 1:5 moles. The preparations can be categorised as follows:

- (i) $NH_4Br:SnX_2$ in $H_2O + HBr / HCl$
- (ii) $KBr:SnBr_2$ in $H_2O + HBr / H_2SO_4$
- (iii) $CsX : SnY_2$ in $H_2O + H_2SO_4 / HBr$
- (iv) $KBr:SnCl_2 \cdot 2H_2O$ in $H_2O + HZ$ ($Z = HSO_4, Br, Cl$)
- (v) $RbBr:SnBr_2$ in $H_2O + HBr$

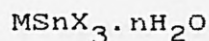
The products from many of these preparations were identified as mixtures in the DTA traces and could only be characterised by X-ray powder diffraction. No exact formulae could be calculated for these products. In general the products isolated reflected the $MX:SnX_2$ ratio in solution. Pure distinct products have however been isolated from some of the preparations and several new phases have been identified. These have been

characterised and identified using DTA, X-ray powder diffraction and elemental analysis as detailed in the previous section. Mössbauer results are reported on most of the new materials and in some cases where suitable crystals have been obtained, single crystal X-ray data have been collected.

The new phases can be categorised into types of complexes as follows:

- (i) $MSnX_3 \cdot xH_2O$
- (ii) $MSn_2X_5 \cdot xH_2O$
- (iii) $MSn_3X_7 \cdot xH_2O$
- (iv) $MX \cdot MSnX_3 \cdot H_2O$

These categories and the systems that produce them are detailed below:



Mixed halide caesium halostannates have been observed in molten systems [15] but little work has been done on materials prepared from solution [10]. Evidence from the structure determination of $KBr \cdot KSnBr_2Cl \cdot H_2O$ (see section 5.4) indicates that at least two halogen sites on the trihalostannate(II) anion are interchangeable between Br and Cl. It is, therefore, reasonable to argue that in the $KSnX_3$ system, where the trihalostannate species is believed to exist, the Br/Cl ratio in products isolated in the solid state, will, to a certain extent, reflect

that in solution providing lattice energies are favourable. Thus, by adjusting the Br/Cl ratio in solution it was possible to isolate various materials of the general formula $\text{KSnBr}_n\text{Cl}_{3-n}\cdot x\text{H}_2\text{O}$. The products isolated and their preparations are summarised in table 2.1 and the analytical data are given in table 2.2. Decomposition temperatures are given in table 2.3.

The Br/Cl ratio in solution was adjusted using HBr and HCl which also served to suppress hydrolysis. This was preferred to altering the mole ratios of starting materials as this usually resulted in the formation of the $\text{MX}\cdot\text{MSnX}_3\cdot\text{H}_2\text{O}$ species in excess KX and of KSn_2X_5 in excess SnX_2 and often a mixture of products.

The materials $\text{KSnCl}_3\cdot\text{H}_2\text{O}$ and $\text{KSnBr}_3\cdot 2\text{H}_2\text{O}$ were isolated and characterised by Bird [9]. In the present work $\text{KSnBr}_3\cdot 2\text{H}_2\text{O}$ was re-synthesised several times in order to prepare crystals suitable for crystallography. Crystals of $\text{KSnBr}_3\cdot 2\text{H}_2\text{O}$ are white fibres mainly present in bundles which were unsuitable for single crystal X-ray data collection. The fibres however, are aligned in parallel and rotate plane polarised light with four points of extinction in 360 degrees. A single cell dimension of 8.74 Å was obtained, from a zero layer Weissenberg photograph, by rotation about the fibre axis. This compares with the values of $a = 18.81$, $b = c = 8.81\text{Å}$ observed by Bird for $\text{KSnCl}_3\cdot\text{H}_2\text{O}$.

The X-ray powder data for these materials are all similar

Table 2.1

Preparations from solution of Phases
of the type $\text{KSnBr}_n\text{Cl}_{3-n}\cdot x\text{H}_2\text{O}$.

Formula	MX:SnY ₂	Acid content	M, X, Y
$\text{KSnBr}_3\cdot 2\text{H}_2\text{O}$	1:1	ca. 1cm ³ conc HBr	K, Br, Br
$\text{KSnBr}_{2.5}\text{Cl}_{0.5}\cdot \text{H}_2\text{O}$	1:1	ca. 3cm ³ dil HCl	K, Br, Br
$\text{KSnBr}_2\text{Cl}\cdot 2\text{H}_2\text{O}$	1:1	ca. 3cm ³ dil HCl	K, Cl, Br
$\text{KSnBr}_{1.3}\text{Cl}_{1.7}\cdot \text{H}_2\text{O}$	1:1	ca. 1cm ³ conc HBr	K, Br, Cl
$\text{KSnBrCl}_2\cdot \text{H}_2\text{O}$	1:1	none	K, Br, Cl
$\text{KSnBr}_{0.7}\text{Cl}_{2.3}\cdot \text{H}_2\text{O}$	1:1	ca. 3cm ³ dil HCl	K, Br, Cl
$\text{KSnBr}_{0.3}\text{Cl}_{2.7}\cdot 2\text{H}_2\text{O}$	1:2	ca. 10cm ³ dil HCl	K, Br, Cl

Table 2.2

Analytical results for phases

of the type $\text{KSnBr}_n\text{Cl}_{3-n}\cdot x\text{H}_2\text{O}$

(calculated values are given in brackets)

Formula	%K	%Sn	%Br	%Cl	%H ₂ O
$\text{KSnBr}_3\cdot 2\text{H}_2\text{O}$	9.0 (9.0)	27.8 (27.4)	57.4 (55.3)	0.00 (0.00)	8.0 (8.3)
$\text{KSnBr}_{2.5}\text{Cl}_{0.5}\cdot \text{H}_2\text{O}$	10.3 (9.9)	27.5 (30.2)	50.4 (50.8)	4.3 (4.5)	3.0 (4.6)
$\text{KSnBr}_2\text{Cl}\cdot 2\text{H}_2\text{O}$	12.8 (10.1)	30.4 (30.5)	40.3 (41.1)	10.8 (9.1)	10.0 (9.3)
$\text{KSnBr}_{1.3}\text{Cl}_{1.7}\cdot \text{H}_2\text{O}$	11.9 (11.5)	33.5 (34.9)	31.4 (30.6)	17.5 (17.7)	5.8 (5.3)
$\text{KSnBrCl}_2\cdot \text{H}_2\text{O}$	13.1 (12.0)	33.7 (36.3)	25.7 (24.5)	20.8 (21.7)	5.3 (5.5)
$\text{KSnBr}_{0.7}\text{Cl}_{2.3}\cdot \text{H}_2\text{O}$	14.0 (12.5)	36.8 (37.9)	18.2 (17.9)	25.4 (26.0)	4.5 (5.8)
$\text{KSnBr}_{0.3}\text{Cl}_{2.7}\cdot 2\text{H}_2\text{O}$	11.3 (12.5)	36.2 (37.9)	7.4 (7.7)	31.0 (30.5)	11.0 (11.5)

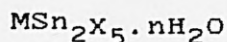
Table 2.3

Decomposition points for phases
of the type $\text{KSnBr}_n\text{Cl}_{3-n}\cdot x\text{H}_2\text{O}$

Formula	Decomposition pt. °C
$\text{KSnBr}_3\cdot 2\text{H}_2\text{O}$	243
$\text{KSnBr}_{2.5}\text{Cl}_{0.5}\cdot \text{H}_2\text{O}$	232
$\text{KSnBr}_2\text{Cl}\cdot 2\text{H}_2\text{O}$	224
$\text{KSnBr}_{1.3}\text{Cl}_{1.7}\cdot \text{H}_2\text{O}$	206
$\text{KSnBrCl}_2\cdot \text{H}_2\text{O}$	206
$\text{KSnBr}_{0.7}\text{Cl}_{2.3}\cdot \text{H}_2\text{O}$	206
$\text{KSnBr}_{0.3}\text{Cl}_{2.7}\cdot 2\text{H}_2\text{O}$	186

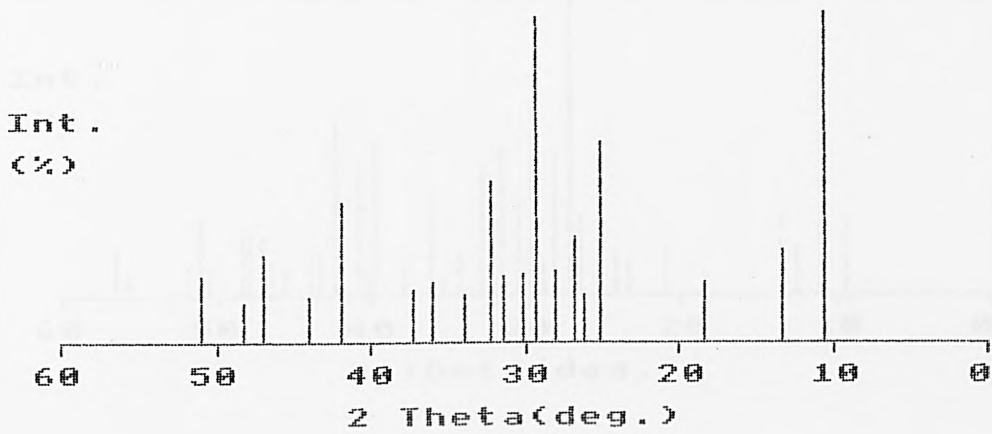
and are given in figs.2.4-11. The relative intensities of the reflections vary not only from material to material, but often from sample to sample of the same material. Common to all the data, however, was an intense line corresponding to a d spacing of ca. 8.0Å. which was assigned to the 101 reflection using the program POWREF [16] By careful measurement of 2 theta on an expanded scale and calibrating using the 002 line of RbSn_2Br_5 , it was possible to calculate accurate d-spacings and these are shown in table 2.4. A correlation exists between Br content and variation in the $d_{(101)}$ spacings and this is illustrated in fig.2.12. This supports the idea of replacement of Cl by Br in the lattice with a resulting lattice expansion.

The Mössbauer data for some of these materials are given in table 2.5. No real trend is observed in the chemical shifts measured in the present work, as these all lie within experimental error of each other. The quadrupole splittings, however, do show a trend - there is a decrease in splitting with an increase in Br content. This is consistent with data on the $\text{CsSn}_2\text{Br}_n\text{Cl}_{5-n}$ system [15] prepared from molten mixtures. These data indicate that the electronic environment around the tin shows greater symmetry in the presence of bromine atoms.



Complexes of the type $\text{MSn}_2\text{X}_5 \cdot n\text{H}_2\text{O}$ were prepared from solutions containing an excess of SnBr_2 . Very often the

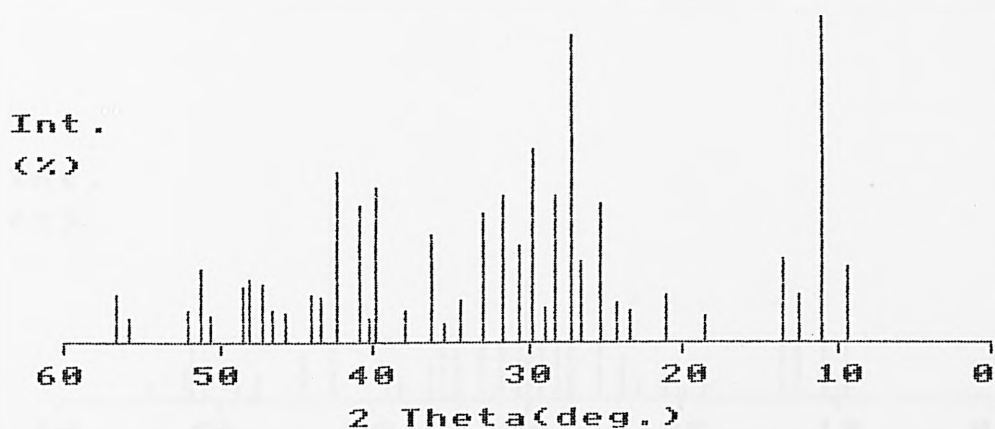
Fig.2.4
X-ray Powder Diffraction Pattern
KSnBr \cdot 3.2H $_2$ O



Rel. Int. (%)	d(hkl)Å
100	8.346
29	6.657
20	4.848
61	3.562
16	3.401
32	3.326
22	3.187
100	3.048
21	2.969
20	2.849
50	2.771
16	2.637
20	2.495
17	2.417
43	2.151
14	2.062
28	1.937
12	1.884
20	1.791

Fig.2.5

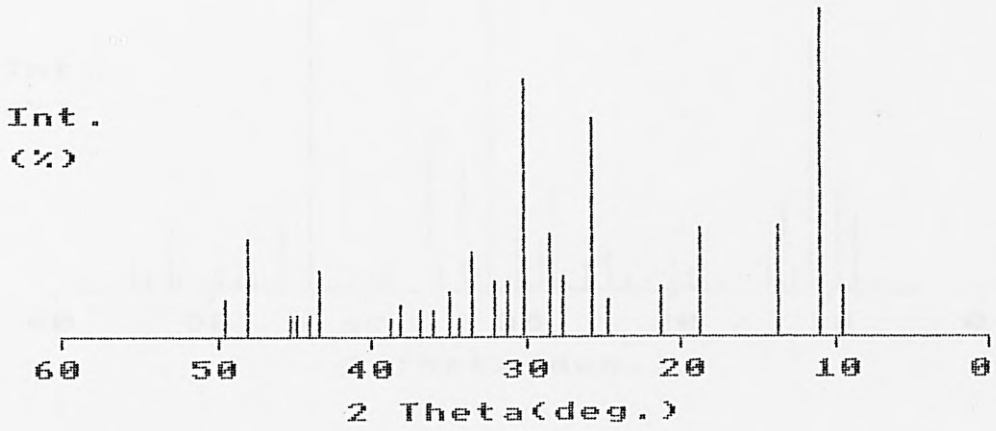
X-ray Powder Diffraction Pattern
KSnBr_{2.5}Cl_{0.5}.H₂O



Rel. Int. (%)	d(hkl)Å
23	9.509
100	8.117
16	7.138
27	6.559
8	4.770
16	4.230
10	3.802
12	3.663
43	3.520
26	3.363
96	3.290
46	3.164
10	3.089
60	3.008
30	2.931
44	2.831
40	2.730
13	2.614
6	2.543
33	2.475
10	2.380
48	2.270
7	2.243
41	2.206
52	2.137
13	2.090
16	2.053
10	1.985
10	1.953
19	1.929
20	1.899
17	1.877
8	1.807
22	1.784
10	1.762
7	1.647
16	1.623

Fig.2.8

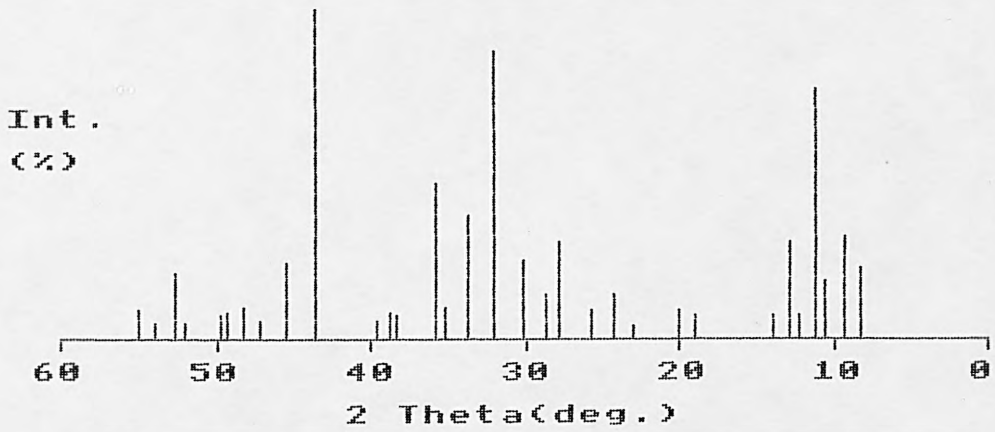
X-ray Powder Diffraction Pattern
KSnBrCl₂.H₂O



Rel. Int. (%)	d(hkl)Å
15	9.408
100	8.043
34	6.463
33	4.720
15	4.171
11	3.619
67	3.466
19	3.232
31	3.132
79	2.959
18	2.876
18	2.797
25	2.675
6	2.607
15	2.571
9	2.501
9	2.442
10	2.356
6	2.327
20	2.090
7	2.053
7	2.019
7	2.002
30	1.892
11	1.841

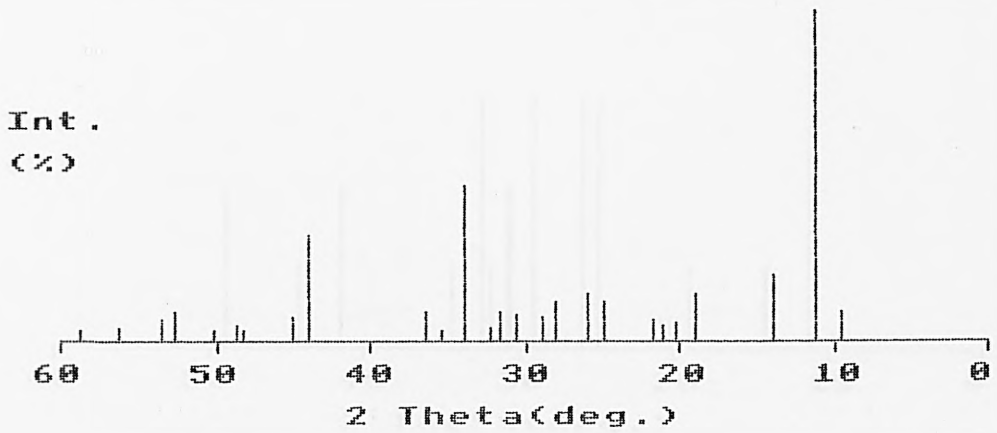
Fig.2.9

X-ray Powder Diffraction Pattern
KSnBr_{0.7}Cl_{2.3}.H₂O



Rel. Int. (%)	d(hkl)Å
21	10.782
31	9.509
18	8.346
77	7.971
8	7.196
30	6.916
8	6.417
8	4.695
9	4.418
5	3.867
13	3.663
10	3.466
30	3.220
14	3.110
24	2.969
88	2.788
38	2.659
11	2.557
48	2.508
8	2.344
8	2.321
7	2.276
100	2.080
23	1.993
7	1.926
11	1.888
8	1.848
8	1.834
6	1.759
20	1.737
6	1.704
9	1.670

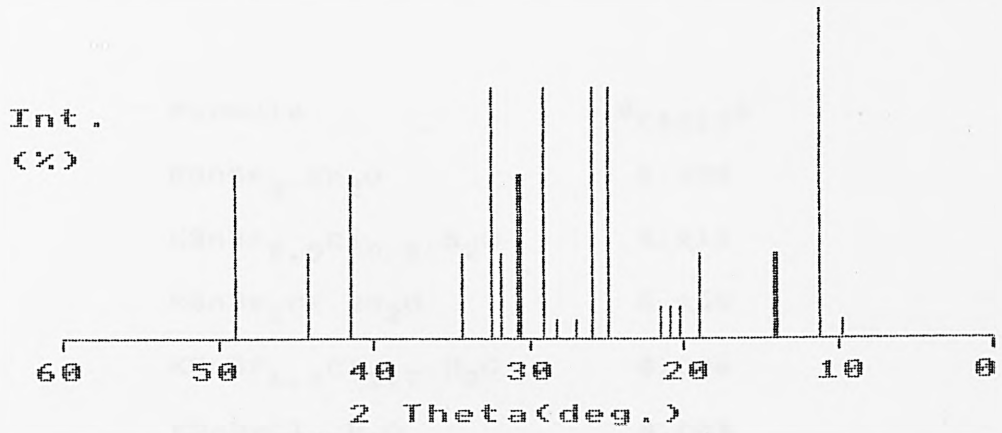
Fig.2.10
X-ray Powder Diffraction Pattern
KSnBr_{0.3}Cl_{2.7}·2H₂O



Rel. Int. (%)	d(hkl)Å
10	9.408
100	7.900
20	6.371
16	4.671
7	4.375
6	4.230
7	4.114
13	3.576
15	3.427
13	3.187
8	3.100
9	2.931
10	2.831
4	2.780
48	2.637
4	2.536
10	2.468
33	2.062
8	2.010
4	1.884
6	1.870
4	1.817
10	1.740
8	1.716
4	1.637
4	1.570

Fig.2.11

X-ray Powder Diffraction Pattern
KSnCl₃.H₂O



Rel. Int. (%)	d(hkl)Å	h	k	l
6	9.212	0	0	2
100	7.900	1	0	1
26	6.417	1	0	2
26	6.281	0	0	7
26	4.671	0	0	4
10	4.374	0	2	0
10	4.269	2	0	1
10	4.133	1	0	4
76	3.590	0	2	3
76	3.453	1	0	5
6	3.302	2	1	3
6	3.164	0	0	6
76	3.069	2	2	1
50	2.922	0	3	0
50	2.903	3	0	1
26	2.823	0	3	2
76	2.756	1	1	6
26	2.615	2	2	4
50	2.181	4	0	1
26	2.044	3	2	5
50	1.863	4	1	5

Table 2.4

$d_{(101)}$ spacings in $\text{KSnBr}_n\text{Cl}_{3-n}\cdot x\text{H}_2\text{O}$

Formula	$d_{(101)}^A$	
$\text{KSnBr}_3\cdot 2\text{H}_2\text{O}$	8.236	
$\text{KSnBr}_{2.5}\text{Cl}_{0.5}\cdot \text{H}_2\text{O}$	8.217	
$\text{KSnBr}_2\text{Cl}\cdot 2\text{H}_2\text{O}$	8.160	
$\text{KSnBr}_{1.3}\text{Cl}_{1.7}\cdot \text{H}_2\text{O}$	8.096	
$\text{KSnBrCl}_2\cdot \text{H}_2\text{O}$	8.048	
$\text{KSnBr}_{0.7}\text{Cl}_{2.3}\cdot \text{H}_2\text{O}$	7.994	
$\text{KSnBr}_{0.3}\text{Cl}_{2.7}\cdot 2\text{H}_2\text{O}$	7.940	
$\text{KSnCl}_3\cdot \text{H}_2\text{O}$	7.900	[9]

Fig.2.12 Lattice expansion in KSnBrnC13-n.xH2O

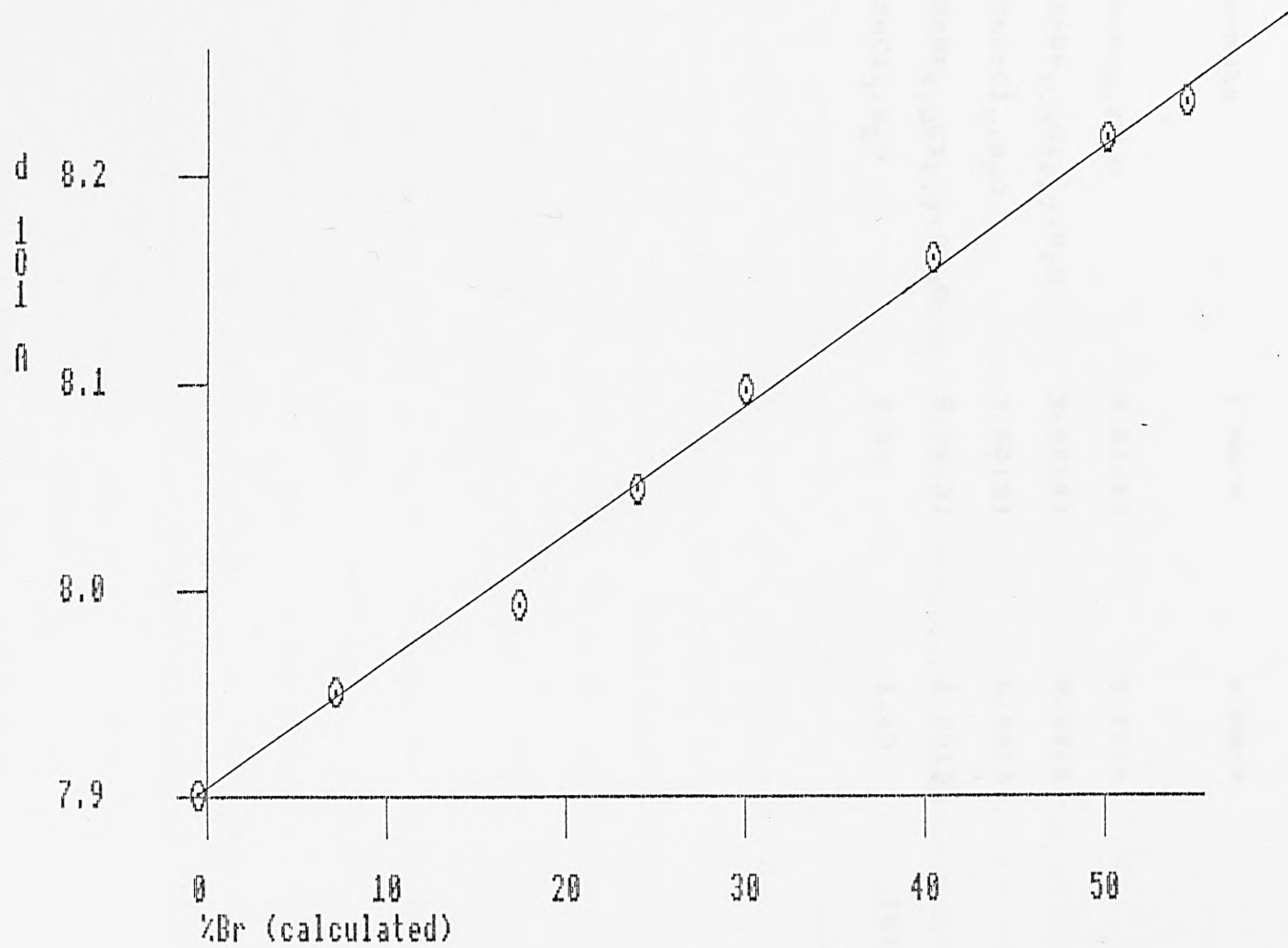


Table 2.5

Mössbauer parameters for some
phases of the type $\text{KSnBr}_n\text{Cl}_{3-n}\cdot x\text{H}_2\text{O}$

Formula	δ mm/s	Δ mm/s	
$\text{KSnBr}_3\cdot 2\text{H}_2\text{O}$	3.61(4)	0.79(4)	
$\text{KSnBr}_{1.3}\text{Cl}_{2.7}\cdot \text{H}_2\text{O}$	3.58(4)	0.94(4)	
$\text{KSnBrCl}_2\cdot \text{H}_2\text{O}$	3.60(3)	0.95(3)	
$\text{KSnBr}_{0.3}\text{Cl}_{2.7}\cdot 2\text{H}_2\text{O}$	3.58(3)	1.00(3)	
$\text{KSnCl}_3\cdot \text{H}_2\text{O}$	3.49	1.10	[9]

products prepared were mixtures and the exact formulae were not calculable but the X-ray patterns resembled that of $\text{KSn}_2\text{Cl}_5 \cdot \text{H}_2\text{O}$. In a systematic study Bird [9] prepared the following materials:

- (1) $\text{KSn}_2\text{Cl}_5 \cdot \text{H}_2\text{O}$
- (2) $\text{RbSn}_2\text{Cl}_5 \cdot \text{H}_2\text{O}$
- (3) $\text{NH}_4\text{Sn}_2\text{Cl}_5$
- (4) CsSn_2Br_5

In the present study both the rubidium and potassium pentabromodistannates have been isolated and the structure of RbSn_2Br_5 has been determined (see section 5.2) by X-ray crystallography. A number of mixed halide phases have also been isolated. The preparations are summarised in table 2.6 and the analytical data and decomposition temperatures are given in tables 2.7 and 2.8 respectively. The Mössbauer data for these materials are shown in table 2.9.

The X-ray powder patterns for the phases isolated are in Figs. 2.13-23. The phases RbSn_2Br_5 , KSn_2Br_5 and $\text{NH}_4\text{Sn}_2\text{Br}_4\text{Cl}$ appear to be isostructural. From a knowledge of the cell dimensions of RbSn_2Br_5 it was possible to index several of the reflections as follows:

d_{obs} Å	$d_{\text{calc.}}$	h k l
7.437	7.377	0 0 2
3.678	3.689	0 0 4
2.468	2.459	0 0 6
2.127	2.111	0 4 0

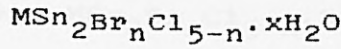
Table 2.6

Preparations from solution of
 Phases of the type $M\text{Sn}_2\text{Br}_n\text{Cl}_{5-n}\cdot x\text{H}_2\text{O}$.

Formula	MX:SnY ₂	Acid content	M, X, Y
RbSn ₂ Br ₅	1:2	ca. 1cm ³ conc HBr	Rb, Br, Br
KSn ₂ Br ₅	1:2	ca. 5cm ³ dil H ₂ SO ₄	K, Br, Br
NH ₄ Sn ₂ Br ₄ Cl	1:1	ca. 5cm ³ dil HCl	NH ₄ , Br, Br
NH ₄ Sn ₂ Br _{2.5} Cl _{2.5} .0.5H ₂ O	1:1	ca. 5cm ³ dil H ₂ SO ₄	NH ₄ , Br, Cl
KSn ₂ Br _{0.4} Cl _{4.6} ·H ₂ O	1:5	ca. 5cm ³ dil HCl	K, Br, Cl
CsSn ₂ Br ₄ Cl _{1.2.5} H ₂ O	1:1	ca. 5cm ³ dil H ₂ SO ₄	Cs, Cl, Br

Table 2.7

Analytical results for phases of the type



Formula	%M	%Sn	%Br	%Cl	%H ₂ O
RbSn ₂ Br ₅	11.2 (11.8)	32.7 (32.8)	55.3 (55.3)	0.0 (0.0)	0.0 (0.0)
KSn ₂ Br ₅	5.0 (5.7)	35.1 (35.1)	55.8 (58.5)	0.0 (0.0)	0.0 (0.0)
KSn ₂ Br _{0.4} Cl _{4.6} ·H ₂ O	8.3 (8.0)	48.6 (48.5)	6.9 (6.5)	35.6 (33.3)	2.0 (3.7)
CsSn ₂ Br ₄ Cl _{1.2.5} H ₂ O		27.8 (17.3)	41.5 (30.8)	4.2 (41.5)	5.2 (4.6)
	%N	%H	%Sn	%Br	%Cl
NH ₄ Sn ₂ Br ₄ Cl	2.39 (2.29)	0.56 (0.66)	35.3 (38.9)	52.9 (52.4)	4.6 (5.8)
NH ₄ Sn ₂ Br _{2.5} Cl _{2.5} ·0.5H ₂ O	2.39 (2.53)	0.84 (0.91)	42.1 (42.9)	35.2 (36.1)	15.8 (16.0)

Table 2.8
Decomposition points for phases
of the type $M\text{Sn}_2\text{Br}_n\text{Cl}_{5-n}\cdot x\text{H}_2\text{O}$

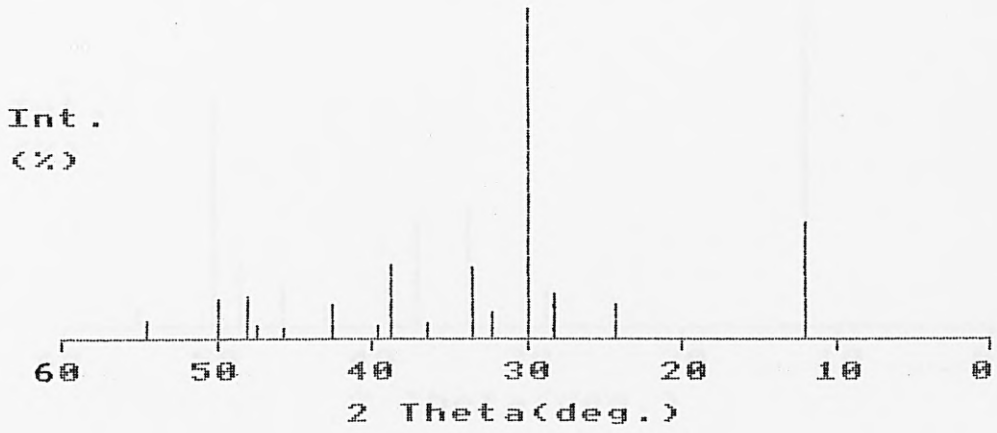
Formula	Decomposition pt. °C
RbSn_2Br_5	290
KSn_2Br_5	263
$\text{NH}_4\text{Sn}_2\text{Br}_4\text{Cl}$	257
$\text{NH}_4\text{Sn}_2\text{Br}_{2.5}\text{Cl}_{2.5}$ $\cdot 0.5\text{H}_2\text{O}$	237
$\text{KSn}_2\text{Br}_{0.4}\text{Cl}_{2.5}\cdot\text{H}_2\text{O}$	189
$\text{CsSn}_2\text{Br}_4\text{Cl}_{1.2.5}\text{H}_2\text{O}$	261

Table 2.9
Mössbauer parameters for some
phases of the type $M\text{Sn}_2\text{Br}_n\text{Cl}_{5-n}\cdot x\text{H}_2\text{O}$

Formula	δ mm/s	Δ mm/s
RbSn_2Br_5	3.91(6)	0.89(5)
KSn_2Br_5	3.83(3)	0.88(3)
$\text{NH}_4\text{Sn}_2\text{Br}_4\text{Cl}$	3.84(7)	0.96(7)
$\text{NH}_4\text{Sn}_2\text{Br}_{2.5}\text{Cl}_{2.5}$ $\cdot 0.5\text{H}_2\text{O}$	3.93(4)	0.92(4)
$\text{KSn}_2\text{Br}_{0.4}\text{Cl}_{4.6}\cdot\text{H}_2\text{O}$	3.87(2)	1.03(2)
$\text{CsSn}_2\text{Br}_4\text{Cl}_{1.2.5}\text{H}_2\text{O}$	3.80(3)	0.95(3)

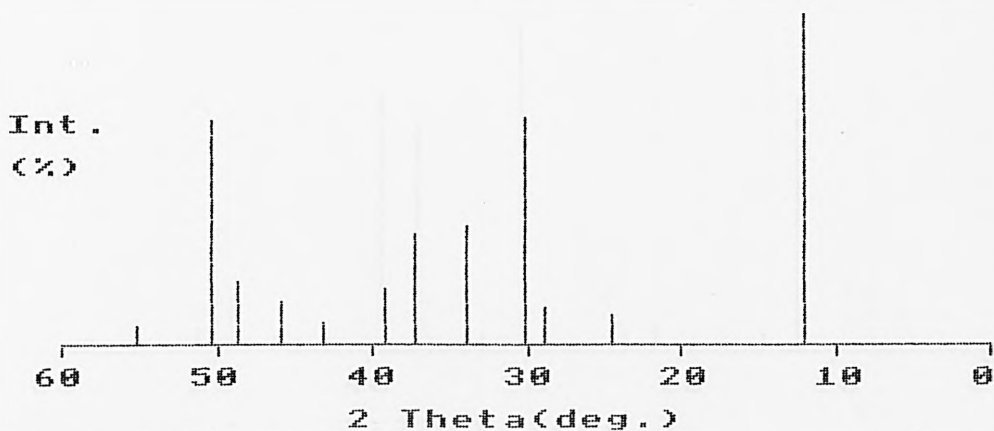
Fig.2.13

X-ray Powder Diffraction Pattern
RbSn₂Br₅



Rel. Int. (%)	d(hkl)Å	h	k	l
36	7.437	0	0	2
11	3.678	0	0	4
14	3.143	1	1	4
100	2.998	2	1	3
9	2.780	2	0	4
22	2.675	3	1	0
6	2.468	0	0	6
23	2.327	2	1	5
4	2.276	1	1	6
11	2.127	2	0	6
3	1.989	3	3	0
4	1.922	3	3	2
13	1.892	1	4	3
13	1.831	0	4	4
7	1.684	1	4	5

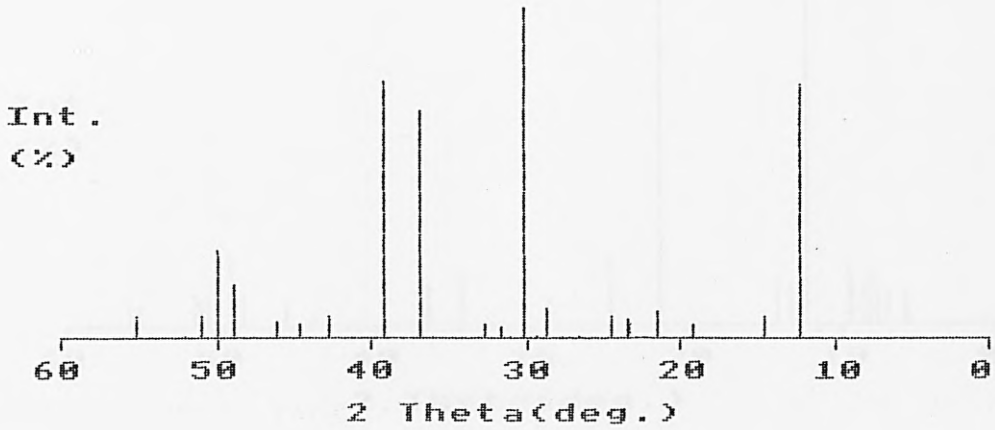
Fig.2.14
X-ray Powder Diffraction Pattern
KSn₂Br₅



Rel. Int. (%)	d(hkl)Å	h	k	l
100	7.314	0	0	2
9	3.633	0	0	4
12	3.100	1	1	4
69	2.969	2	1	3
36	2.652	3	1	0
33	2.417	0	0	6
17	2.298	2	1	5
6	2.094	2	0	6
14	1.977	3	3	0
19	1.873	1	4	3
69	1.811	0	4	4
6	1.664	1	4	5

Fig.2.15

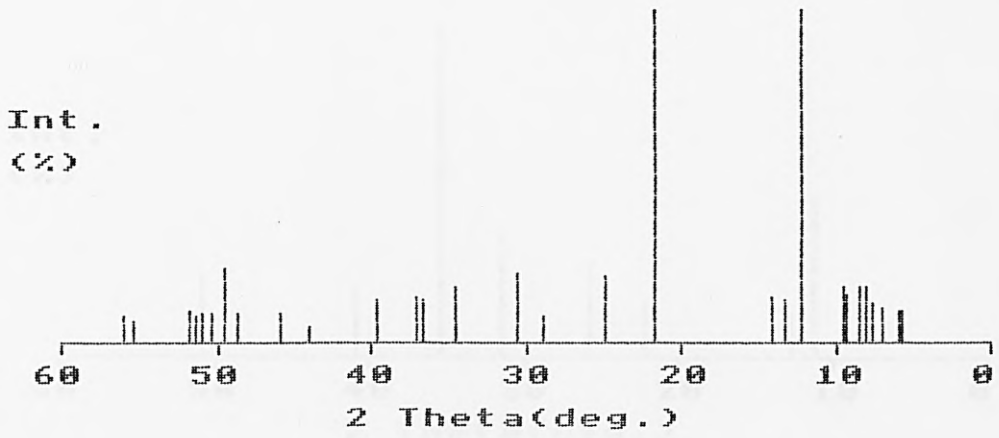
X-ray Powder Diffraction Pattern
NH₄Sn₂Br₄Cl



Rel. Int. (%)	d(hkl)Å	h	k	l
77	7.255	0	0	2
7	6.109	1	1	0
5	4.647	1	1	2
9	4.152	2	0	0
5	3.802	2	1	0
7	3.633	0	0	4
10	3.121	1	1	4
100	2.959	2	1	3
4	2.831	3	0	0
5	2.747	1	0	5
70	2.436	3	0	3
79	2.304	2	1	5
6	2.113	4	0	0
5	2.032	4	1	1
27	1.831	4	2	2
7	1.794	3	1	6
6	1.667	2	0	8

Fig.2.16

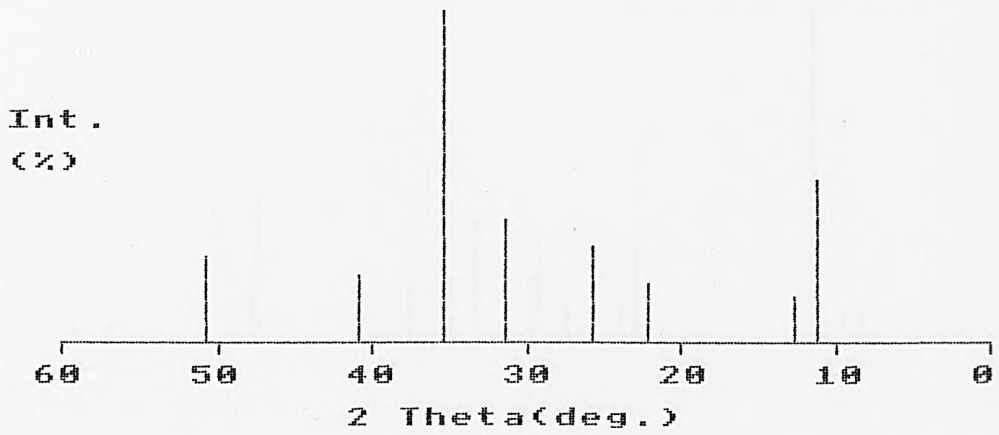
X-ray Powder Diffraction Pattern
NH₄Sn₂Br_{2.5}Cl_{2.5}O₅H₂O



Rel. Int. (%)	d(hkl)A
10	15.781
10	14.730
11	12.628
12	11.632
18	10.915
18	10.526
16	9.612
18	9.408
100	7.255
13	6.707
14	6.281
100	4.114
20	3.590
9	3.089
21	2.931
18	2.600
13	2.449
14	2.423
13	2.276
6	2.058
10	1.977
10	1.873
23	1.845
10	1.811
10	1.791
9	1.781
10	1.768
8	1.658
9	1.645

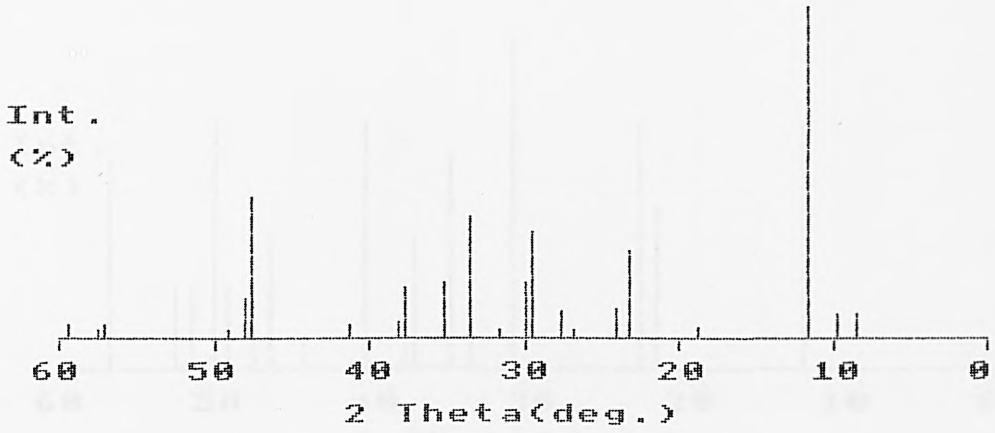
Fig.2.17

X-ray Powder Diffraction Pattern
KSn₂Br_{0.4}Cl_{14.6}.H₂O



Rel. Int. (%)	d(hkl)A
49	7.900
13	7.025
19	4.022
30	3.480
38	2.849
100	2.543
21	2.206
26	1.797

Fig.2.18
X-ray Powder Diffraction Pattern
CsSn2Br4Cl.2.5H2O

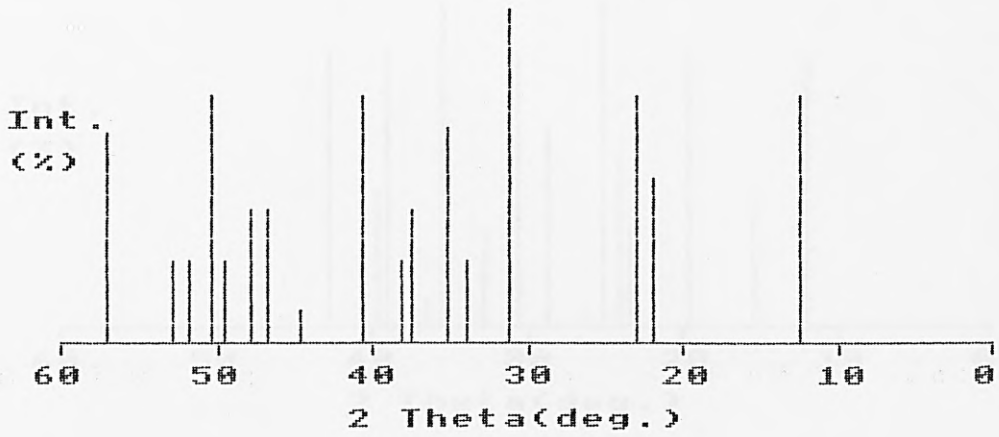


Rel. Int. (%)	d(hkl)Å
8	10.526
8	9.213
100	7.695
4	4.745
28	3.850
10	3.708
3	3.326
9	3.232
32	3.038
18	2.988
3	2.840
38	2.675
18	2.557
16	2.386
6	2.356
5	2.191
43	1.914
13	1.899
3	1.859
4	1.616
3	1.605
4	1.556

Fig.2.19

X-ray Powder Diffraction Pattern
NH₄Sn₂C₁₅

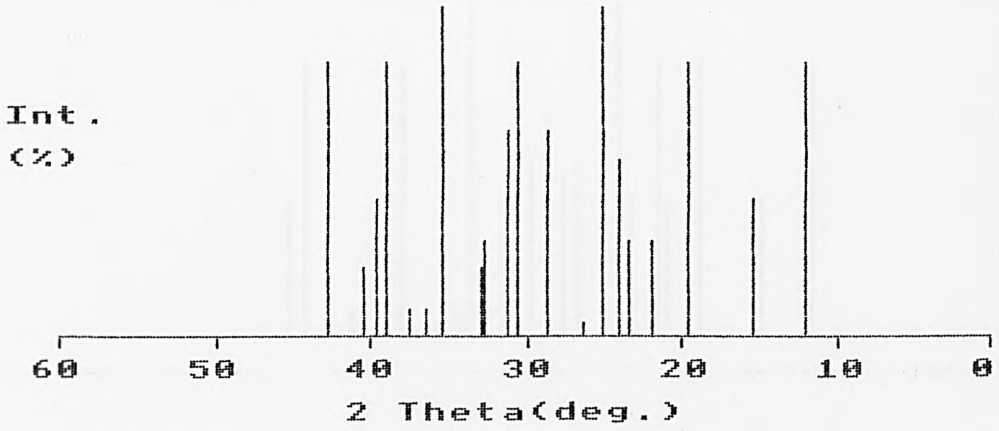
[9]



Rel. Int.(%)	d(hkl)Å
76	7.081
50	4.059
76	3.883
100	2.867
26	2.644
66	2.557
40	2.405
26	2.356
76	2.223
10	2.031
40	1.941
40	1.903
26	1.841
76	1.810
26	1.764
26	1.733
66	1.613

Fig.2.20

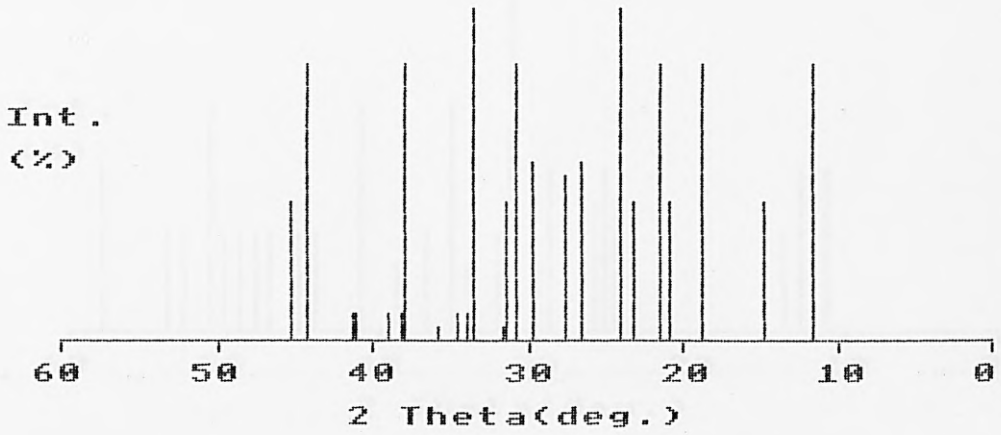
X-ray Powder Diffraction Pattern
CsSn₂C15 [15]



Rel. Int. (%)	d(hkl)Å
83	7.440
42	5.750
83	4.550
30	4.070
30	3.800
55	3.710
100	3.560
5	3.390
63	3.120
83	2.930
63	2.870
30	2.740
20	2.720
100	2.540
8	2.470
8	2.400
83	2.310
42	2.276
20	2.230
83	2.117

Fig.2.21

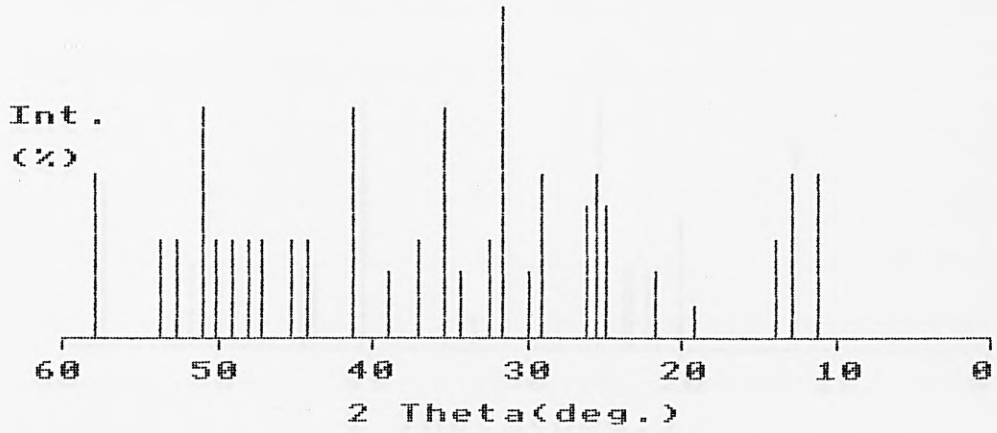
X-ray Powder Diffraction Pattern
CsSn₂Br₅ [9]



Rel. Int. (%)	d(hkl)Å
83	7.700
42	6.030
83	4.750
42	4.260
83	4.120
42	3.830
100	3.720
55	3.360
50	3.230
55	3.010
5	2.830
83	2.900
42	2.850
100	2.680
8	2.640
8	2.600
5	2.510
63	2.380
83	2.372
8	2.356
8	2.310
8	2.199
8	2.187
83	2.049
42	2.004

Fig.2.22

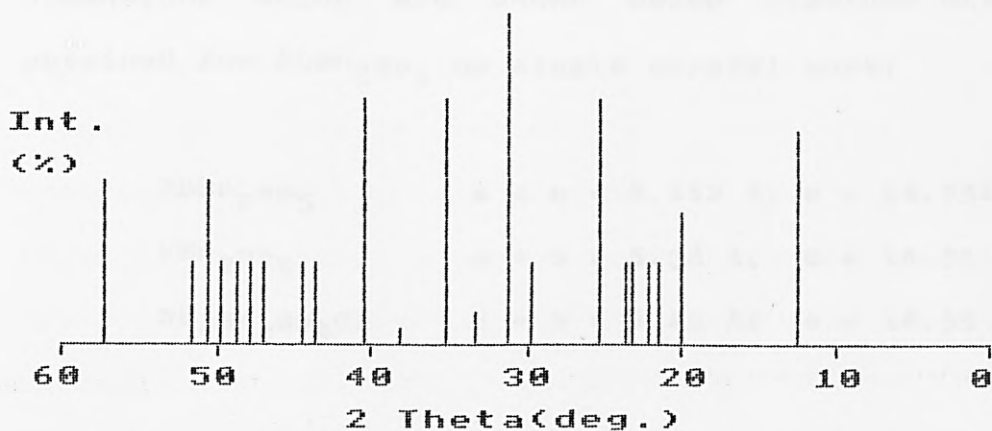
X-ray Powder Diffraction Pattern
KSn₂C₁₅.H₂O [9]



Rel. Int. (%)	d(hkl)Å
50	7.865
50	6.930
30	6.360
10	4.634
20	4.100
40	3.576
50	3.485
40	3.414
50	3.082
20	2.998
100	2.832
30	2.756
20	2.613
70	2.540
30	2.420
20	2.318
70	2.192
30	2.044
30	1.999
30	1.929
30	1.892
30	1.858
30	1.824
70	1.793
30	1.736
30	1.708
50	1.593

Fig.2.23

X-ray Powder Diffraction Pattern
RbSn2C15.H2O [9]



Rel. Int. (%)	d(hkl)Å
66	7.138
40	4.439
26	4.152
26	4.040
26	3.850
26	3.770
76	3.520
26	3.018
100	2.876
10	2.691
76	2.557
6	2.362
76	2.233
26	2.076
26	2.035
26	1.937
26	1.903
26	1.873
26	1.837
50	1.808
26	1.770
50	1.610

Identifying these lines in the powder patterns of KSn_2Br_5 and $\text{NH}_4\text{Sn}_2\text{Br}_4\text{Cl}$ enabled the calculation of cell dimensions which are shown below together with those obtained for RbSn_2Br_5 by single crystal work:

RbSn_2Br_5 $a = b = 8.442 \text{ \AA}; c = 14.754 \text{ \AA}$

KSn_2Br_5 $a = b = 8.38 \text{ \AA}; c = 14.51 \text{ \AA}$

$\text{NH}_4\text{Sn}_2\text{Br}_4\text{Cl}$ $a = b = 8.45 \text{ \AA}; c = 14.55 \text{ \AA}$

The a/b cell dimensions of the three materials are very similar. In contrast the c -axis is significantly shorter in KSn_2Br_5 and $\text{NH}_4\text{Sn}_2\text{Br}_4\text{Cl}$. This may be explained with a knowledge of the structure of these materials (see section 5.2). In RbSn_2Br_5 , tin and bromine form 2-dimensional polymeric layers running perpendicular to the c -axis separated by rubidium cations. Hence, in KSn_2Br_5 , little difference would be expected in the a/b cell dimensions as the Sn and Br sites should be unaffected, but the c -axis would be reduced in accomodating the smaller cation. The ammonium cation is of a similar size to K^+ and therefore, the c -axes in KSn_2Br_5 and $\text{NH}_4\text{Sn}_2\text{Br}_4\text{Cl}$ are expected to be approximately the same in the two materials. In the two dimensional polymeric network, in RbSn_2Br_5 , there is evidence of interaction between the non-bonding electrons on the Sn atoms and empty 4d orbitals on Br. One of the Br sites is not involved in this interaction and lies in a plane with Sn. It is likely that it is this Br, which has been replaced by Cl in $\text{NH}_4\text{Sn}_2\text{Br}_4\text{Cl}$, as the other halide sites

require the use of suitable d-orbitals to maintain their stereochemistry and these are unavailable on Cl. With Cl directly replacing Br in the a/b cell plane a slight lattice shrinkage might be expected, but this has not been observed. In the Mössbauer data the quadrupole splittings are similar in the all bromine materials, RbSn_2Br_5 and KSn_2Br_5 , but increases in $\text{NH}_4\text{Sn}_2\text{Br}_4\text{Cl}$, indicating a greater electronic asymmetry at the tin site in the Cl containing material.

The X-ray powder pattern of $\text{CsSn}_2\text{Br}_4\text{Cl} \cdot 2.5\text{H}_2\text{O}$ is similar to that of CsSn_2Br_5 [15]. Indexing some of the powder lines as for CsSn_2Br_5 as follows:

d Å	h k l
7.695	0 0 2
3.850	0 0 4
2.988	4 0 0
2.557	0 0 6

It is possible to derive a set of cell dimensions for $\text{CsSn}_2\text{Br}_4\text{Cl} \cdot 2.5\text{H}_2\text{O}$:

$$a = b = 11.95\text{Å}; \quad c = 15.39\text{Å}$$
$$a = b = c = 90^\circ$$

These dimensions lie between those of CsSn_2Br_5 (12.05, 15.40Å) and CsSn_2Cl_5 (11.497, 14.28Å) and are similar to the anhydrous $\text{CsSn}_2\text{Br}_4\text{Cl}$ (11.88 and 15.35Å). It is therefore likely that the water molecules fit

into lattice spaces without significantly distorting the lattice. the Mössbauer data seem to confirm this as parameters measured for the hydrated complex are similar to those of the anhydrous material at $\delta = 3.81(1)$ and $\Delta = 0.92$ mm/s.

The powder pattern of $\text{KSn}_2\text{Br}_{0.4}\text{Cl}_{4.6}\cdot\text{H}_2\text{O}$ is similar to that of $\text{KSn}_2\text{Cl}_5\cdot\text{H}_2\text{O}$ as determined by Bird [9], suggesting that these materials are isostructural. The Mössbauer data do differ significantly, however, with ($\delta = 3.88$, $\Delta = 0.88$ mm/s for $\text{KSn}_2\text{Cl}_5\cdot\text{H}_2\text{O}$). Both shift and splitting are larger in the mixed halide material. The X-ray powder pattern of $\text{NH}_4\text{Sn}_2\text{Br}_{2.5}\text{Cl}_{2.5}\cdot 0.5\text{H}_2\text{O}$ does not resemble that of any known phase.

$\text{MSn}_3\text{X}_7\cdot n\text{H}_2\text{O}$

Three phases of the general formula $\text{MSn}_3\text{X}_7\cdot n\text{H}_2\text{O}$ were isolated from aqueous systems. Preparations are summarised in table 2.10. Analytical data, Mössbauer parameters and decomposition temperatures are given in tables 2.11-13 respectively. X-ray powder patterns for these materials are recorded in figs.2.24-26.

Single crystal X-ray data had been collected for what was believed to be the material $\text{CsSn}_2\text{BrF}_4$ [17]. Attempts to resynthesise crystals of $\text{CsSn}_2\text{BrF}_4$ always resulted in the isolation of $\text{CsSn}_3\text{Br}_{1.5}\text{F}_{5.5}$, which has the same X-ray powder pattern as $\text{CsSn}_2\text{BrF}_4$, as observed by Grimes [10]. The crystal structure however would not

Table 2.10
Preparations in solution of
Phases of the type $MSn_3X_7 \cdot xH_2O$.

Formula	MX:SnY ₂	Acid used	M, X, Y
$CsSn_3Br_{1.5}F_{5.5}$	1:2	ca. 3cm ³ dil H ₂ SO ₄	Cs, Br, F
$KSn_3Br_2Cl_{15} \cdot 1.5H_2O$	1:5	ca. 1cm ³ conc HBr	K, Br, Cl
$KSn_3Br_{0.7}Cl_{16.3} \cdot 3H_2O$	1:5	none	K, Br, Cl

Table 2.11
Analytical data for phases of the
type $MSn_3X_7 \cdot xH_2O$

Formula	%M	%Sn	%Br	%Cl	%H ₂ O
$CsSn_3Br_{1.5}F_{5.5}$	19.4 (18.6)	50.1 (49.9)	16.5 (16.8)	0.0 (0.0)	0.0 (0.0)
$KSn_3Br_2Cl_{15} \cdot 1.5H_2O$	5.0 (5.1)	46.2 (46.9)	21.6 (21.0)	23.7 (23.3)	3.5 (3.6)
$KSn_3Br_{0.7}Cl_{16.3} \cdot 3H_2O$	5.2 (5.4)	47.2 (48.9)	7.1 (7.7)	29.2 (30.7)	8.0 (7.4)

Table 2.12

Mössbauer data for phases
of the type $M\text{Sn}_3\text{X}_7 \cdot x\text{H}_2\text{O}$

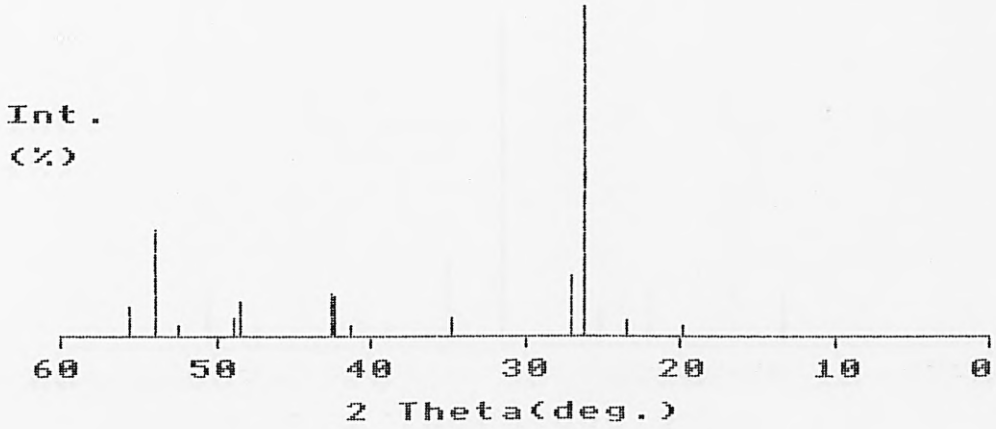
Formula	δ mm/s	Δ mm/s
$\text{CsSn}_3\text{Br}_{1.5}\text{F}_{5.5}$	3.50(1)	1.50(1)
$\text{KSn}_3\text{Br}_2\text{Cl}_5 \cdot 1.5\text{H}_2\text{O}$	3.88(2)	0.96(2)
$\text{KSn}_3\text{Br}_{0.7}\text{Cl}_{6.3} \cdot 3\text{H}_2\text{O}$	3.72(2)	1.19(1)

Table 2.13

Decomposition points for phases
of the type $M\text{Sn}_3\text{X}_7 \cdot x\text{H}_2\text{O}$

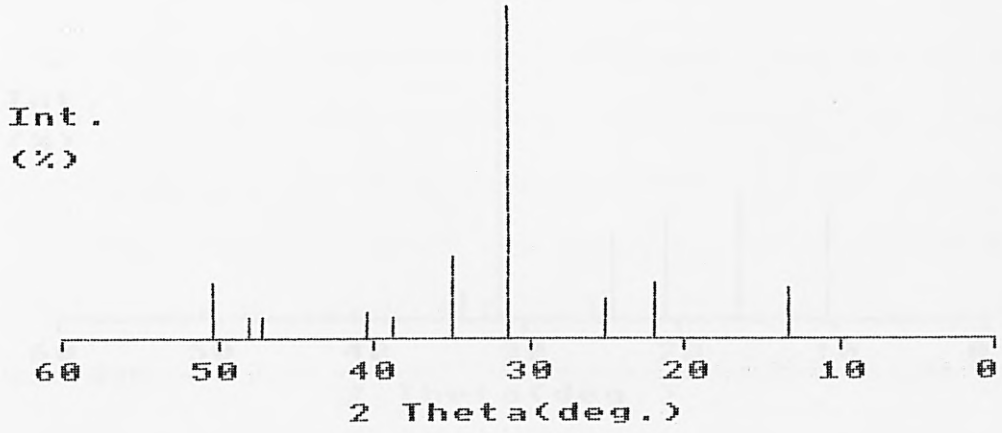
Formula	Decomposition pt. °C
$\text{CsSn}_3\text{Br}_{1.5}\text{F}_{5.5}$	225
$\text{KSn}_3\text{Br}_2\text{Cl}_5 \cdot 1.5\text{H}_2\text{O}$	210
$\text{KSn}_3\text{Br}_{0.7}\text{Cl}_{6.3} \cdot 3\text{H}_2\text{O}$	205

Fig.2.24
X-ray Powder Diffraction Pattern
CsSn₃Br_{1.5}F_{5.5}



Rel. Int. (%)	d(hkl)Å	h	k	l
4	4.484	2	0	1
6	3.802	6	0	-1
100	3.401	4	1	0
19	3.314	0	0	3
6	2.578	4	0	3
4	2.191	4	0	4
13	2.132	10	0	1
13	2.127	2	0	-5
11	1.877	6	2	0
6	1.863	6	0	4
4	1.743	12	0	1
30	1.701	4	0	-6
33	1.698	6	0	-6
8	1.656	4	2	3

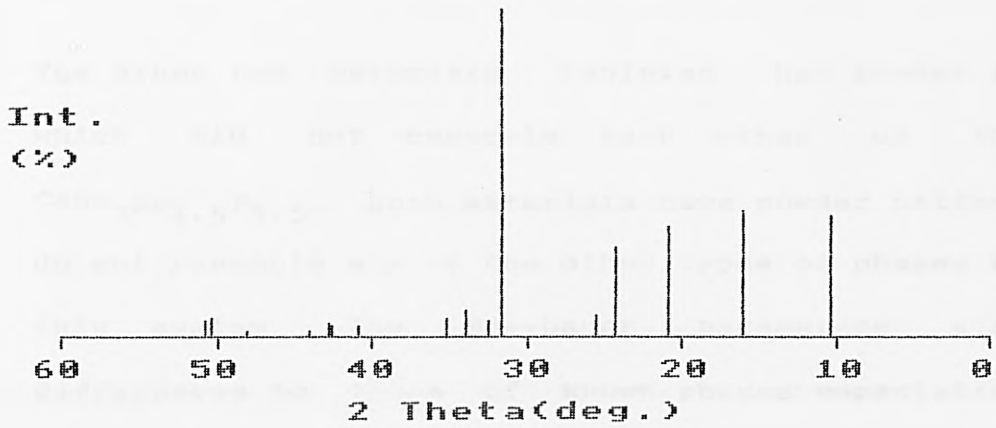
Fig.2.25
X-ray Powder Diffraction Pattern
KSn3Br2Cl5.1.5H2O



Rel. Int. (%)	d(hkl)A
16	6.657
17	4.058
12	3.548
100	2.858
26	2.571
6	2.321
8	2.227
6	1.926
6	1.899
17	1.811

Fig.2.26

X-ray Powder Diffraction Pattern
 $\text{KSn}_3\text{Br}_{0.7}\text{Cl}_{16.3}\cdot 3\text{H}_2\text{O}$



Rel. Int. (%)	d(hkl)Å
38	8.506
40	5.574
34	4.250
27	3.663
7	3.493
100	2.831
5	2.763
8	2.637
6	2.550
4	2.212
4	2.122
5	2.113
2	2.058
2	1.899
6	1.814
5	1.801

resolve as $\text{CsSn}_2\text{BrF}_4$ and a solution was eventually derived using the formula $\text{CsSn}_3\text{Br}_{1.5}\text{F}_{5.5}$ (see section 5.3).

The other two materials isolated had powder patterns which did not resemble each other or that of $\text{CsSn}_3\text{Br}_{1.5}\text{F}_{5.5}$. Both materials have powder patterns that do not resemble any of the other types of phases known in this system. The Mössbauer parameters also show differences to those of known phases especially in the quadrupole splitting of $\text{KSn}_3\text{Br}_{0.7}\text{Cl}_{6.3}\cdot 3\text{H}_2\text{O}$ which is unusually large.

KX.KSnX₃.H₂O

Several materials corresponding to the general formula $\text{M}_2\text{SnBr}_n\text{Cl}_{4-n}\cdot\text{H}_2\text{O}$ (where $\text{M} = \text{K}, \text{NH}_4$) have been isolated from solution. The preparations are summarised in table 2.14 and analytical data and decomposition temperatures are given in tables 2.15-16. X-ray powder patterns are recorded in figs.2.27-32, along with those of some related materials [9].

$\text{KBr}\cdot\text{KSnBr}_2\text{Cl}\cdot\text{H}_2\text{O}$ was prepared from a solution containing a 5:1 mole ratio of $\text{KBr} : \text{SnCl}_2$. Very often KBr itself crystallises out of solution when present in a large excess. Because of the high solubility of KBr (53.48g/l in cold water [18]) in water, crystallisation of KBr can be avoided, providing enough mother liquor is left. The structure of $\text{KBr}\cdot\text{KSnBr}_2\text{Cl}\cdot\text{H}_2\text{O}$ has been determined by

Table 2.14

Preparations from solution of
phases of the type $\text{MX.MSnX}_3.\text{H}_2\text{O}$

Formula	MX:SnY_2	Acid content	M, X, Y
$\text{K}_2\text{SnBr}_3\text{Cl}.\text{H}_2\text{O}$	5:1	ca. 1cm^3 conc. HBr	K, Br, Cl
$(\text{NH}_4)_2\text{SnBr}_{2.6}\text{Cl}_{1.4}.\text{H}_2\text{O}$	2:1	ca. 3cm^3 dil HCl	NH_4 , Br, Cl
$(\text{NH}_4)_2\text{SnBr}_{1.9}\text{Cl}_{2.1}.\text{H}_2\text{O}$	2:1	ca. 5cm^3 dil HCl	NH_4 , Br, Cl
$(\text{NH}_4)_2\text{SnBr}_{1.5}\text{Cl}_{2.5}.\text{H}_2\text{O}$	2:1	ca. 5cm^3 dil HCl	NH_4 , Br, Cl

Table 2.15

Analytical data for phases
of the type $\text{MX.MSnX}_3.\text{H}_2\text{O}$

Formula	%K	%Sn	%Br	%Cl	% H_2O
$\text{K}_2\text{SnBr}_3\text{Cl}.\text{H}_2\text{O}$	18.5 (15.9)	22.6 (24.2)	47.5 (48.9)	7.7 (7.2)	5.3 (3.7)
$(\text{NH}_4)_2\text{SnBr}_{2.6}\text{Cl}_{1.4}.\text{H}_2\text{O}$	6.34 (6.51)	2.20 (2.34)	27.6 (27.6)	48.7 (48.3)	10.9 (11.5)
$(\text{NH}_4)_2\text{SnBr}_{1.9}\text{Cl}_{2.1}.\text{H}_2\text{O}$	6.80 (7.02)	2.42 (2.53)	29.8 (29.7)	37.9 (38.0)	18.8 (18.7)
$(\text{NH}_4)_2\text{SnBr}_{1.5}\text{Cl}_{2.5}.\text{H}_2\text{O}$	7.26 (7.35)	2.42 (2.64)	30.2 (31.1)	31.9 (31.4)	22.7 (23.3)

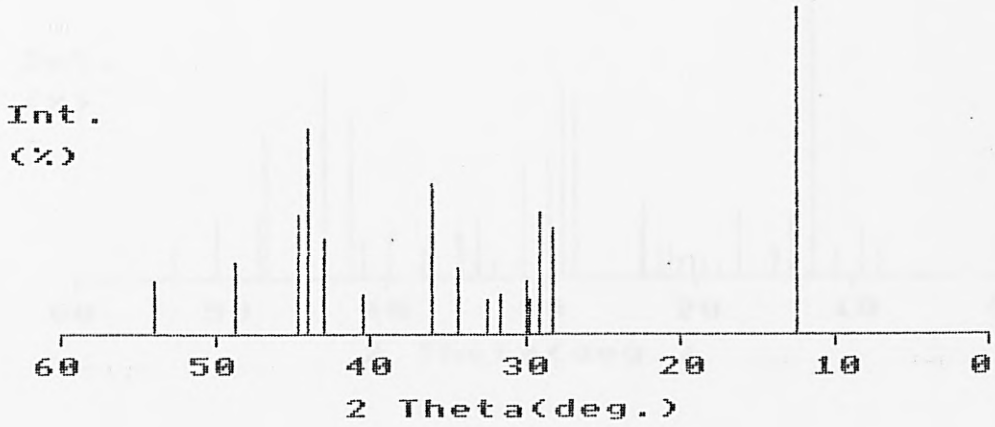
Table 2.16
Decomposition points for phases
of the type $\text{MX.MSnX}_3.\text{H}_2\text{O}$

Formula	Decomposition pt.	
	°C	
$\text{K}_2\text{SnBr}_3\text{Cl}.\text{H}_2\text{O}$	224	
$(\text{NH}_4)_2\text{SnBr}_{2.6}\text{Cl}_{1.4}.\text{H}_2\text{O}$	218	
$(\text{NH}_4)_2\text{SnBr}_{1.9}\text{Cl}_{2.1}.\text{H}_2\text{O}$	204	
$(\text{NH}_4)_2\text{SnBr}_{1.5}\text{Cl}_{2.5}.\text{H}_2\text{O}$	198	

Table 2.17
Mössbauer data for phases
of the type $\text{MX.MSnX}_3.\text{H}_2\text{O}$

Formula	δ mm/s	Δ mm/s	
$(\text{NH}_4)_2\text{SnBr}_{2.6}\text{Cl}_{1.4}.\text{H}_2\text{O}$	3.64(5)	0.96(4)	
$(\text{NH}_4)_2\text{SnBr}_{1.9}\text{Cl}_{2.1}.\text{H}_2\text{O}$	3.61(2)	0.95(4)	
$(\text{NH}_4)_2\text{SnBr}_{1.5}\text{Cl}_{2.5}.\text{H}_2\text{O}$	3.58(4)	0.94(4)	
$\text{NH}_4\text{Br}.\text{NH}_4\text{SnBr}_3.\text{H}_2\text{O}$	3.59	0.67	[9]
$\text{NH}_4\text{Cl}.\text{NH}_4\text{SnCl}_3.\text{H}_2\text{O}$	3.65	0.95	
$\text{K}_2\text{SnBr}_3\text{Cl}.\text{H}_2\text{O}$	3.77(5)	0.76(5)	
$\text{KCl}.\text{KSnCl}_3.\text{H}_2\text{O}$	3.41(4)	0.98(3)	
$\text{KBr}.\text{KSnBr}_3.\text{H}_2\text{O}$	3.63	0.76	[9]

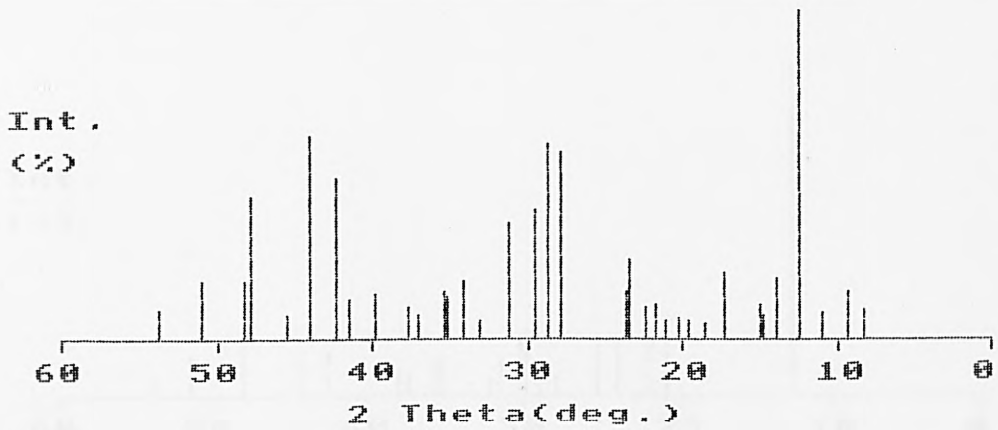
Fig.2.27
X-ray Powder Diffraction Pattern
KBr.KSnBr₂Cl.H₂O



Rel. Int. (%)	d(hkl)Å	h	k	l
100	7.138	0	1	1
20	3.164	2	2	0
32	3.153	0	0	4
38	3.079	2	2	1
11	3.008	0	2	3
20	2.607	0	3	2
47	2.495	1	3	2
12	2.227	4	1	1
30	2.108	0	3	4
63	2.058	1	3	4
37	2.032	1	0	6
22	1.870	1	4	3
17	1.704	5	2	1

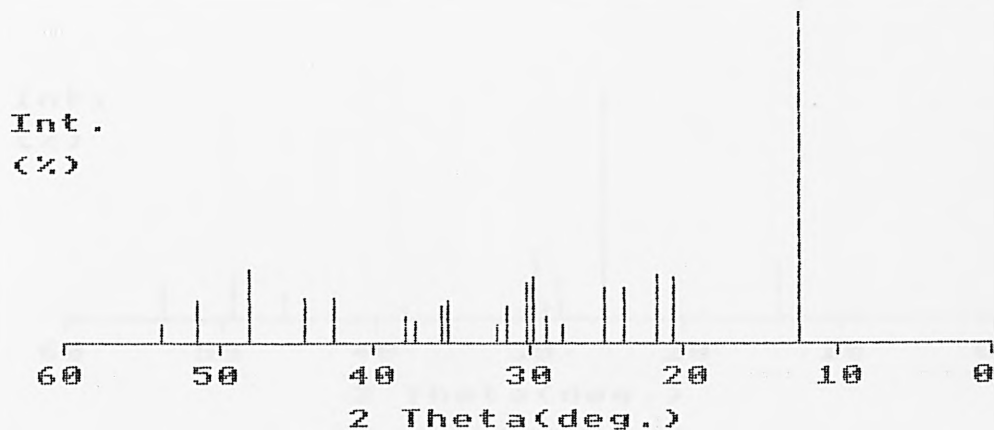
Fig.2.28

X-ray Powder Diffraction Pattern
 $(\text{NH}_4)_2\text{SnBr}_2 \cdot 6\text{Cl} \cdot 1.4 \cdot \text{H}_2\text{O}$



Rel. Int. (%)	d(hkl)Å
10	10.782
16	9.509
8	8.117
100	7.138
18	6.371
7	6.026
10	5.906
21	5.126
5	4.770
6	4.529
6	4.396
6	4.230
10	4.095
10	3.986
25	3.818
15	3.770
57	3.209
60	3.110
39	3.028
36	2.867
5	2.706
17	2.629
13	2.557
15	2.543
7	2.423
10	2.386
14	2.265
12	2.176
50	2.132
61	2.053
7	1.998
44	1.907
17	1.888
17	1.791
8	1.710

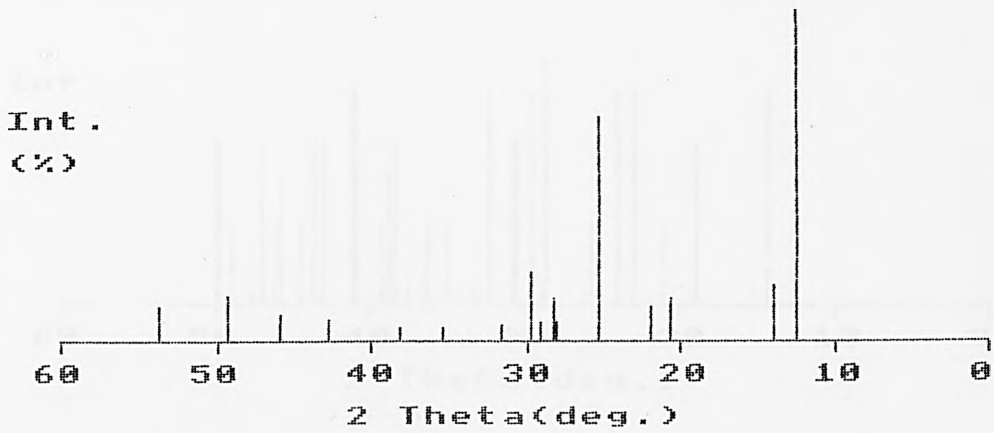
Fig.2.29
X-ray Powder Diffraction Pattern
(NH₄)₂SnBr_{1.9}Cl_{2.1}.H₂O



Rel. Int. (%)	d(hkl)Å
100	7.081
20	4.311
21	4.095
17	3.754
17	3.562
6	3.209
8	3.100
20	3.018
19	2.969
11	2.858
6	2.788
13	2.550
11	2.529
7	2.417
8	2.374
15	2.122
15	2.040
23	1.895
13	1.778
6	1.707

Fig.2.30

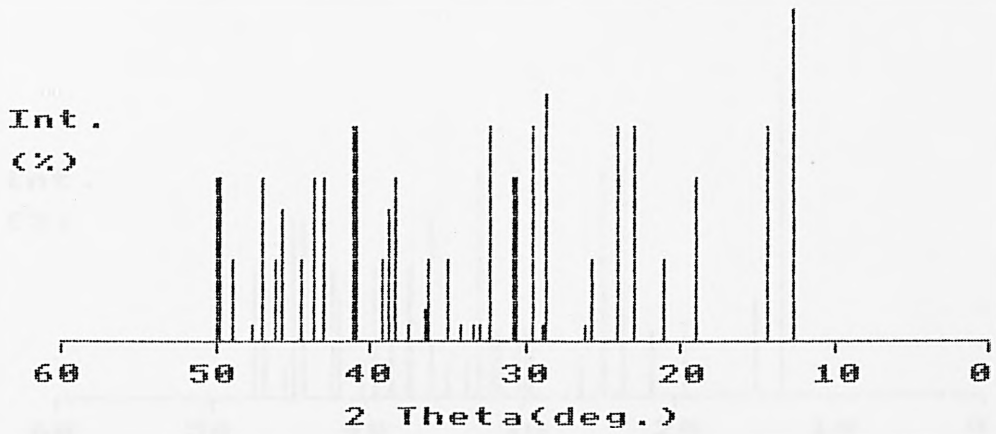
X-ray Powder Diffraction Pattern
 $(\text{NH}_4)_2\text{SnBr}_{1.5}\text{Cl}_{2.5}\cdot\text{H}_2\text{O}$



Rel. Int. (%)	d(hkl)Å
100	7.081
18	6.326
13	4.291
11	4.077
69	3.534
7	3.198
13	3.153
7	3.069
21	3.008
6	2.831
4	2.536
4	2.362
8	2.113
9	1.981
14	1.852
11	1.710

Fig.2.31

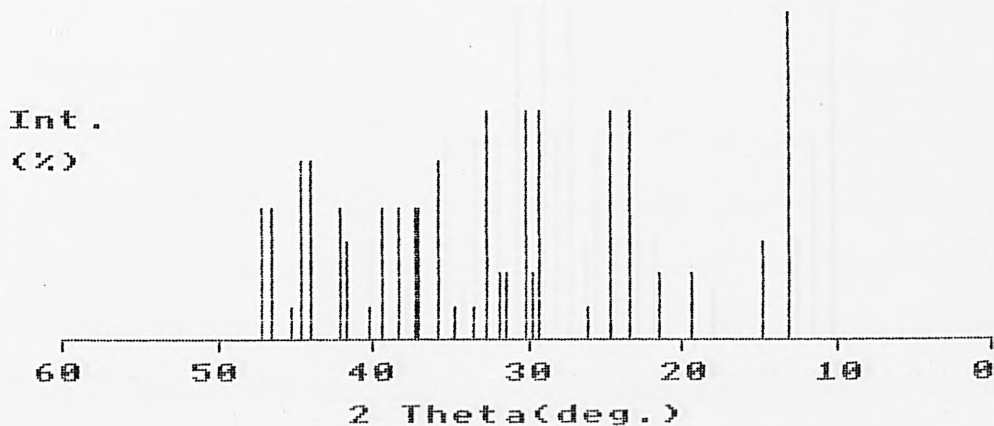
X-ray Powder Diffraction Pattern
NH4Cl.NH4SnCl3.H2O [9]



Rel. Int. (%)	d(hkl)Å
100	6.983
66	6.204
50	4.658
26	4.200
66	3.878
66	3.705
26	3.478
6	3.410
76	3.121
6	3.097
66	3.026
50	2.936
50	2.901
66	2.782
6	2.734
6	2.687
6	2.633
26	2.572
26	2.484
10	2.463
6	2.402
50	2.350
40	2.327
26	2.298
66	2.205
66	2.195
50	2.110
50	2.073
26	2.037
40	1.986
26	1.967
50	1.936
6	1.911
26	1.864
50	1.834
50	1.830

Fig.2.32

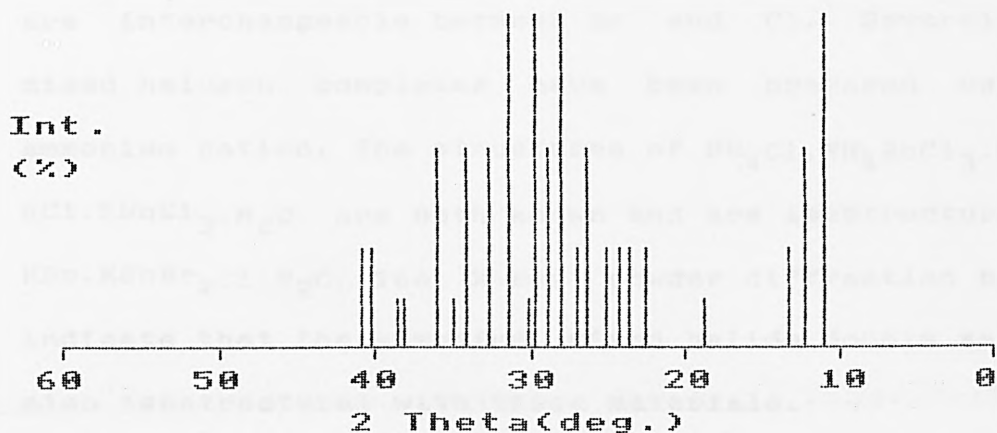
X-ray Powder Diffraction Pattern
KCl.KSnCl₃.H₂O [9]



Rel. Int. (%)	d(hkl)Å
100	6.834
30	6.046
20	4.581
20	4.152
70	3.802
70	3.619
10	3.418
70	3.051
20	3.016
70	2.968
20	2.859
20	2.823
70	2.736
10	2.679
10	2.575
56	2.515
40	2.429
40	2.409
40	2.346
40	2.286
10	2.245
30	2.162
40	2.143
56	2.061
56	2.031
10	2.000
40	1.952
40	1.929

Fig.2.33

X-ray Powder Diffraction Pattern
KBr.KSnBr3.2H2O [9]



Rel. Int. (%)	d(hkl)Å
100	8.116
60	7.196
30	6.657
16	4.745
30	3.952
30	3.786
30	3.679
30	3.548
60	3.375
30	3.302
100	3.175
60	3.089
100	3.018
16	2.978
100	2.849
60	2.740
60	2.630
16	2.564
60	2.488
16	2.362
16	2.338
30	2.248
30	2.206

X-ray crystallography and is discussed in section 5.4. Evidence from this determination indicates that at least two of the halide sites on the trihalostannate(II) anion are interchangeable between Br and Cl. Several other mixed halogen complexes have been prepared using the ammonium cation. The structures of $\text{NH}_4\text{Cl} \cdot \text{NH}_4\text{SnCl}_3 \cdot \text{H}_2\text{O}$ and $\text{KCl} \cdot \text{KSnCl}_3 \cdot \text{H}_2\text{O}$ are both known and are isostructural with $\text{KBr} \cdot \text{KSnBr}_2\text{Cl} \cdot \text{H}_2\text{O}$. The X-ray powder diffraction patterns indicate that the ammonium mixed halide double salts are also isostructural with these materials.

Table 2.17 shows the Mössbauer parameters for these related salts. The parameters of the ammonium salts all lie within experimental error of each other and hence no trends can be identified.

Materials containing sulphate

Many of the materials produced from solutions containing dilute sulphuric acid have analytical data that suggest that sulphate has been incorporated into the lattice. This is not unknown, the structure of $\text{K}_3\text{Sn}_2(\text{SO}_4)_3\text{Br}$ as determined by Donaldson and Grimes [19], was from a product isolated from a solution containing dilute H_2SO_4 . The presence of SO_4 in these materials has been confirmed using ir spectroscopy the SO_4 group showing an intense line at 1190 cm^{-1} . Unfortunately most of these products crystallised as mixtures and were not studied further in this work.

REFERENCES, CHAPTER TWO

- (1) C.E.Vanderzee and D.E.Rhodes, J.Amer.Chem.Soc., (1952), 74, 3552.
- (2) W.B.Schaap, J.A.Davis and W.H.Nebergall, J.Amer.Chem.Soc., (1954), 76, 5226.
- (3) J.D.Donaldson, Progress Inorganic Chem., (1967), 8, 287.
- (4) F.R.Poulsen and S.E.Rasmussen, Acta Chem.Scand., (1970), 24,150.
- (5) B.Kamenar and D.Grdenic, J.Inorg.Nucl.Chem., (1962), 24, 1039.
- (6) J.D.Donaldson and J.D.O'Donoghue, J.Chem.Soc., (1964), 271.
- (7) J.D.O'Donoghue Ph.D.Thesis, London 1965.
- (8) R.R.McDonald, A.C.Larson and D.T.Cromer, Acta Cryst., 17, (1964), 1104.
- (9) S.R.A.Bird, Ph.D. Thesis, London 1971.
- (10) S.M.Grimes, Ph.D. Thesis, The City University 1982.

- (11) J.D.Donaldson and W.Moser, *Analyst*, (1959), 84, 10.
- (12) S.J.Clark, Private communication.
- (13) A.I.Vogel. 'A Textbook of Quantitative Inorganic Analysis', 3rd edition, Longmans, London 1964.
- (14) Dionex 2010i Instruction Manual.
- (15) J.D.Donaldson, J.Silver, S.Hadjiminolis and S.D.Ross, *J.Chem.Soc. Dalton Trans.*, (1975), 1500.
- (16) D.C.Puxley, Ph.D. Thesis, London 1972.
- (17) J.D.Donaldson, Private communication.
- (18) 'C.R.C. Handbook of Chemistry and Physics' 61st edition (1980-81). C.R.C. Press.
- (19) J.D.Donaldson and S.M.Grimes, *J.Chem.Soc. Dalton trans.*, (1984), 1301.

CHAPTER THREE

THERMOANALYTICAL STUDIES ON THE KBr : SnX₂ SYSTEM

(WHERE X = Br, Cl, F).

	Page
3.1 Introduction to thermal analysis.	123
3.2 Phases, components and the phase rule.	133
3.3 Construction of phase diagrams.	136
3.4 Phase diagrams for the system KBr:SnX ₂ .	138
KBr : SnBr ₂	139
KBr : SnCl ₂	146
KBr : SnF ₂	154
References	165

CHAPTER THREE

3.1 Introduction to thermal analysis.

Thermal analysis is the general term given to analytical techniques which involve the measuring of a physical property as a function of temperature. For many thousands of years man has observed and utilised the effect of heat on materials, the smelting of iron and copper are early examples. At the end of the 18th century Josiah Wedgwood conducted one of the first recorded thermogravimetric experiments, involving gases evolved from china clays during heating. During the late 19th century, thermal analysis was pioneered with the first DTA results in 1899. The term 'thermal analysis' was eventually introduced in 1905 by Tammann. Work continued steadily throughout the beginning of this century, but, it was not until fairly recently, with the introduction of modern thermoanalytical instrumentation, that thermoanalysis became a common analytical tool.

Fundamental to thermoanalytical techniques is the second law of thermodynamics which, at constant pressure, may be expressed in terms of the change in free energy of a system (ΔG) by the Gibbs-Helmholtz expression [1]:

$$\Delta G = \Delta H - T \Delta S \quad \text{----- (3.1)}$$

Where ΔH and ΔS are the changes in enthalpy and entropy in the system, respectively, and T is the absolute

temperature. A reaction is stable when ΔG is positive, at equilibrium when $\Delta G = 0$, and is likely to proceed spontaneously when ΔG is negative. Thus, by adjusting temperature it is possible to make a reaction more likely to occur spontaneously, ie. make ΔG negative. Differentiating equation 3.1 with respect to T gives:

$$\frac{d(\Delta G)}{dT} = - \Delta S \quad \text{---- (3.2)}$$

Therefore, increase in temperature will make a reaction more likely to occur spontaneously when ΔS is positive and the situation is reversed when ΔS is negative.

Fig.3.1 shows the main categories and principal techniques used in thermal analysis. The most important of these techniques are differential scanning calorimetry (DSC), differential thermal analysis (DTA) and thermogravimetry (TG). In the present work only the latter two techniques have been used and are discussed below.

TG.

Thermogravimetry involves the measurement of mass as a function of temperature. The type of reactions observable are:

- (i) Reactants \longrightarrow Products + Gas
- (ii) Gas + Reactants \longrightarrow Products

Thus, reactions involving mass loss or mass gain can be

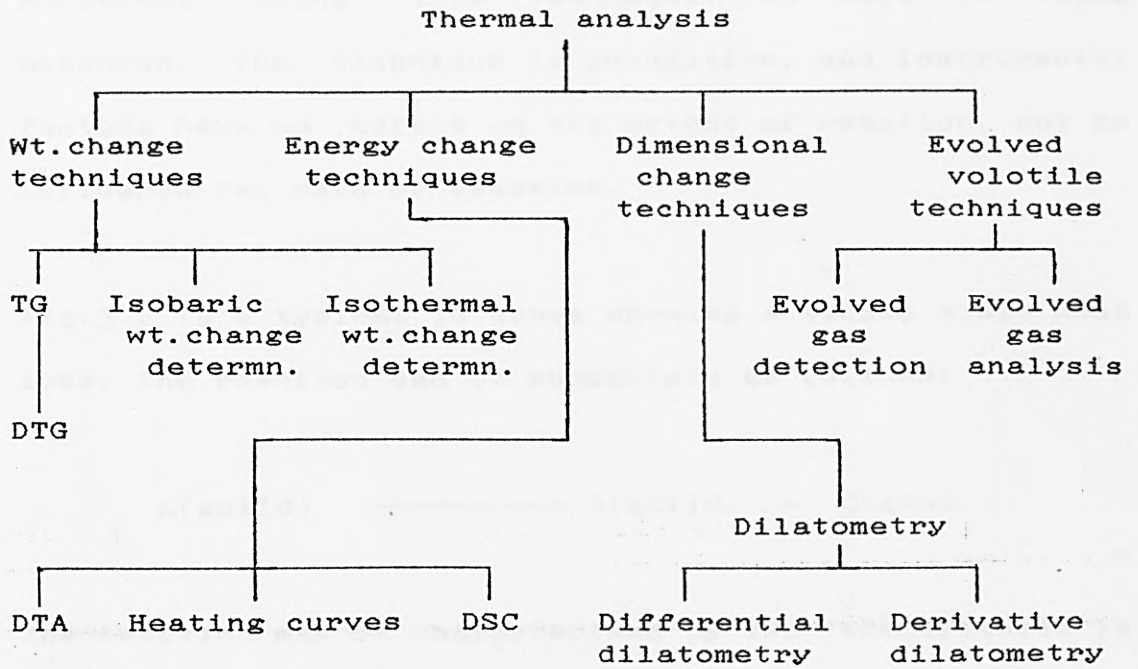
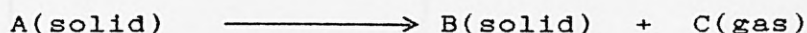


Fig.3.1

Important thermoanalytical techniques

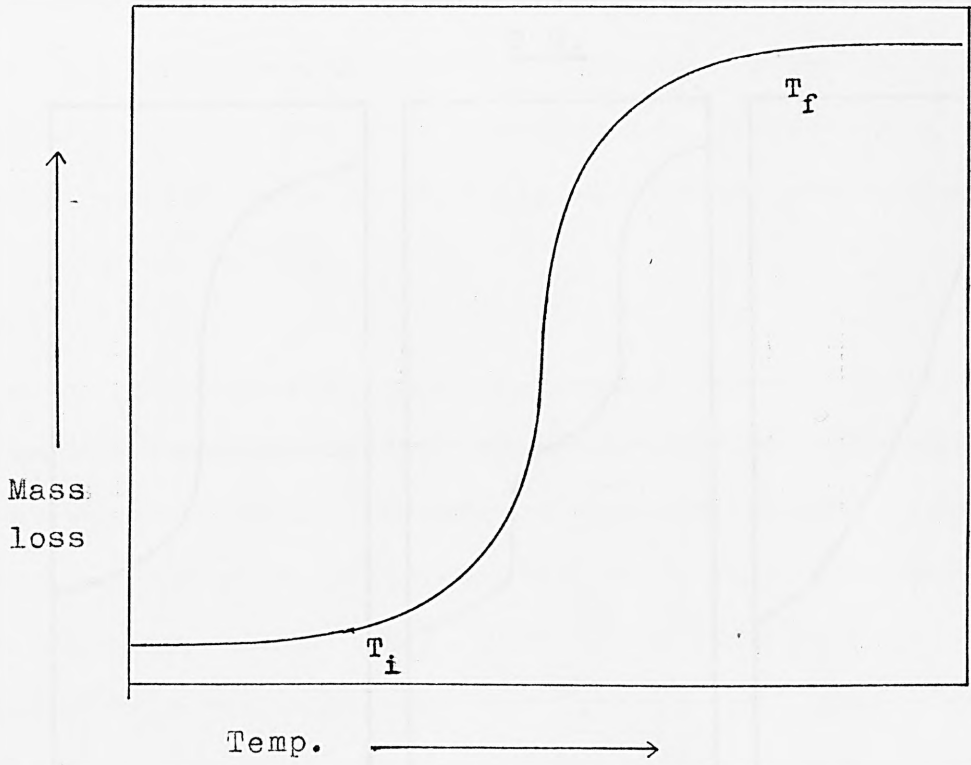
monitored using this technique. As mass is being measured, the technique is quantitative, and instrumental factors have no effect on the extent of reaction, but do influence the rate of reaction.

Fig.3.2 is a typical TG curve showing a single stage mass loss. The reaction can be summarised as follows:



The reaction may be characterised by two temperatures as marked in fig.3.2: T_1 , is the initial temperature at which cumulative mass change reaches an observable magnitude; T_p , the final temperature, is the temperature at which cumulative mass change is at a maximum. The difference $T_p - T_1$ is called the reaction interval. Thus quantitative measurements are possible by measuring the mass losses corresponding to particular reaction intervals.

In addition to TG curves differential thermogravimetric curves (DTG) were recorded, ie. the derivative of mass change with respect to time, as a function of temperature. In most cases no additional information is available by using DTG, however, in cases where overlapping mass changes occur, the sharp maxima of DTG can enable their separation. Some TG and corresponding DTG curves are shown in fig.3.3.

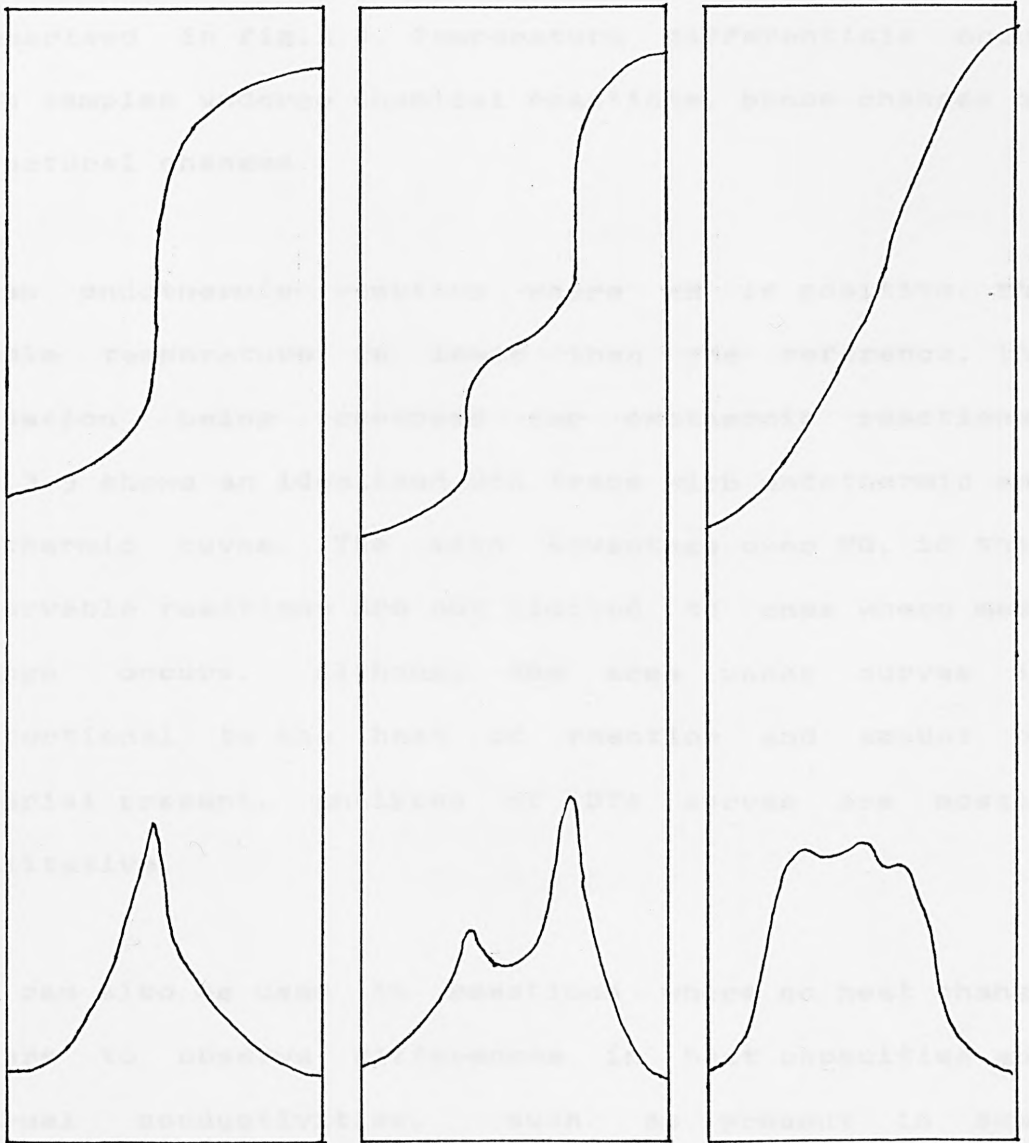


$$\text{Reaction interval} = T_f - T_i$$

Fig. 3.2

Typical T.G. curve showing single stage mass-loss.

T G.



D T G.

Fig. 3.3

Some T.G. curves and corresponding D.T.G. curves.

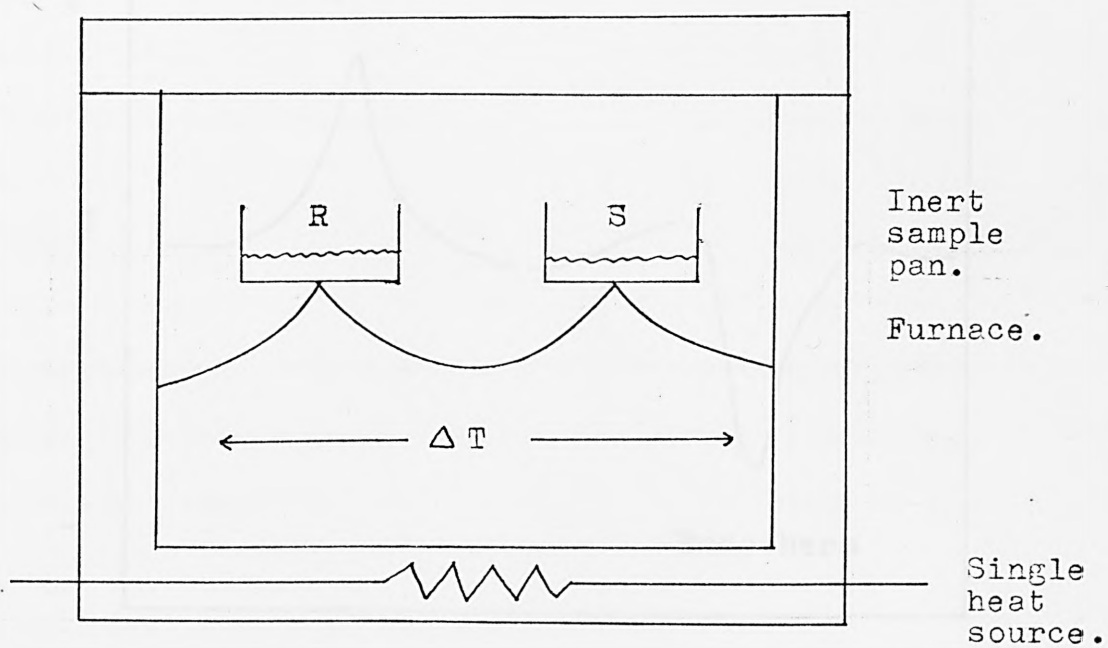
DTA.

Differential thermal analysis (DTA) involves the monitoring of temperature differences between a test sample and an inert reference under identical conditions. The difference in temperature is monitored by a thermocouple located beneath the sample holder as summarised in fig.3.4. Temperature differentials occur when samples undergo chemical reactions, phase changes or structural changes.

In an endothermic reaction where ΔH is positive, the sample temperature is lower than the reference, the situation being reversed for exothermic reactions. Fig.3.5 shows an idealised DTA trace with endothermic and exothermic curves. The main advantage over TG, is that observable reactions are not limited to ones where mass change occurs. Although the area under curves is proportional to the heat of reaction and amount of material present, analyses of DTA curves are mostly qualitative.

DTA can also be used in reactions where no heat change occurs to observe differences in heat capacities and thermal conductivities, such as present in some solid-solid phase transitions, providing allowances have been made for sample mass and packing density. A shift in the baseline position is characteristic of such a change.

A summary of the type of phenomena observable in TG and DTA experiments is shown in table 3.1.



R = Reference.

S = Sample.

T = Temperature.

Fig. 3.4

Schematic representation of DTA.

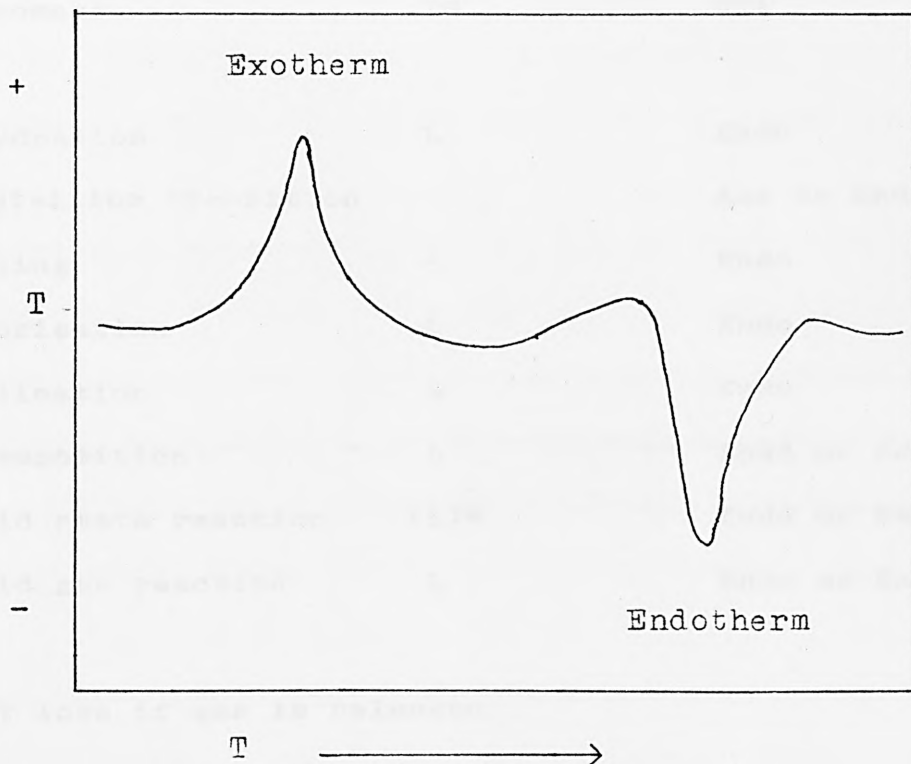


Fig. 3.5

Idealised DTA trace.

Table 3.1

Some observable phenomena in TG and DTA

Phenomena	TG	DTA
Dehydration	L	Endo
Crystalline transition	-	Exo or Endo
Melting	-	Endo
Vaporisation	L	Endo
Sublimation	L	Endo
Decomposition	L	Endo or Exo
Solid state reaction	(L)*	Endo or Exo
Solid gas reaction	L	Endo or Exo

* Wt loss if gas is released.

L = Weight loss

Endo = Endothermic peak observable

Exo = Exothermic peak observable

3.2 Phases, components and the phase rule.

Gibbs defined a phase as " a state of matter that is uniform throughout not only in chemical composition but also in physical state ". For example, ice is a single phase but a slurry of ice in water is a 2 phase system.

The number of components in a system is the minimum number of chemical species needed to define the composition of that system. For a simple mixture of two materials, that do not react with each other, the number of components is 2, however, this becomes more complicated in cases where equilibria occur.

Using these two definitions it is possible to describe a function defining the number of degrees of freedom (F) in a system as follows:

$$F = C - P + 2 \quad \text{----- (3.3)}$$

where, C is the number of components and P is the number of phases. Equation 3.3 is known as the phase rule. The degrees of freedom relate to the variation in pressure and temperature for example, in a one component system with one phase, $F = 2$, this means that pressure and temperature may be varied independently. With two phases in a one component system $F = 1$, consequently pressure and temperature cannot be varied independently and one of these variables must be fixed. With 3 phases $F = 0$, thus 3 phases can only coexist at a set value for

pressure and temperature. F cannot have a negative value so 3 phases is the maximum number in a 1 component system.

All of the present work has involved two component systems ie $F = 4 - P$. As pressure was kept constant during the experiments equation 3.3 may be further simplified to:

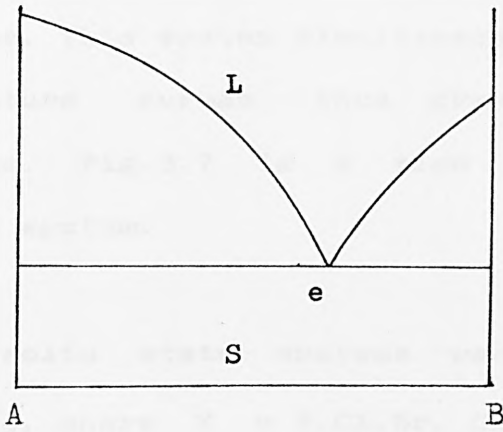
$$F = 3 - P$$

To examine the phases present in a mixture of two solids a two component phase diagram can be constructed. Fig.3.6 shows some simple two component phase diagrams and illustrates the type of features observable. In a simple two component mixture where no new phases are present on mixing, melting occurs at a lower temperature than the highest melting component and falls to a single low point known as a eutectic. At the eutectic the material composition is a mixture of both components. Towards the extremes of the diagram the compositions begin to resemble the pure phases. Thus, in more complex systems there is a eutectic for every pair of neighbouring phases on a phase diagram, even if these phases show no congruent melting point.

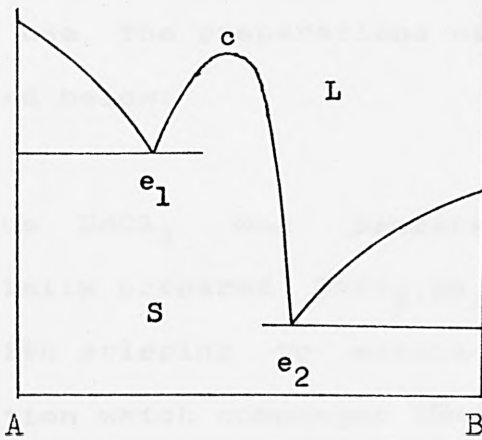
Phase diagrams have been constructed in the current work by measuring melting points and eutectic temperatures over a comprehensive composition range using DTA.

Fig. 3.6

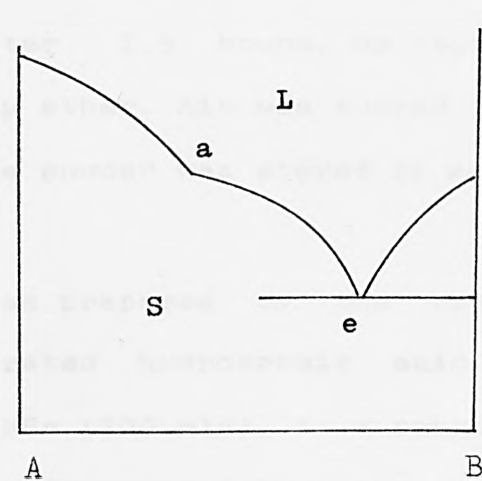
Some simple 2 component phase diagrams.



Simple mixture of two solids with eutectic e.



Congruently melting new phase formed at c, giving two eutectics e₁ & e₂.



Incongruently melting phase at a with a single eutectic e.

e = Eutectic.
L = Liquid phase.
S = Solid phase.

3.3 Construction of phase diagrams

In the present work all thermal analyses were carried out on a Stanton Redcroft STA-780 simultaneous thermal analyser. This system simultaneously ran TG, DTG, DTA and temperature curves thus overcoming any correlation problems. Fig.3.7 is a flow chart representing the STA-780 system.

Three solid state systems were examined of the type $\text{KBr}:\text{SnX}_2$, where $X = \text{F, Cl, Br}$. Commercially prepared SnF_2 and KBr were used. KBr was dried in an oven at 80°C before use. The preparations of SnBr_2 and of SnCl_2 are discussed below:

Anhydrous SnCl_2 was prepared by dehydration of commercially prepared $\text{SnCl}_2 \cdot 2\text{H}_2\text{O}$. $\text{SnCl}_2 \cdot 2\text{H}_2\text{O}$ (22.6g) was added with stirring to acetic anhydride (20.4g). The dehydration which commences immediately is accompanied by intense heat evolution. A fine white powder was filtered off after 1.5 hours, by vacuum filtration, and washed with dry ether. Air was sucked through the filtrate until dry. The powder was stored *in vacuo*, over silica gel.

SnBr_2 was prepared by the reaction of tin metal with concentrated hydrobromic acid. To tin metal (100g) was added HBr (200 mls), in a round bottomed flask. This was heated under reflux conditions in an atmosphere of N_2 . After much of the tin had dissolved the solution was decanted into a beaker and heated, under N_2 , to evaporate

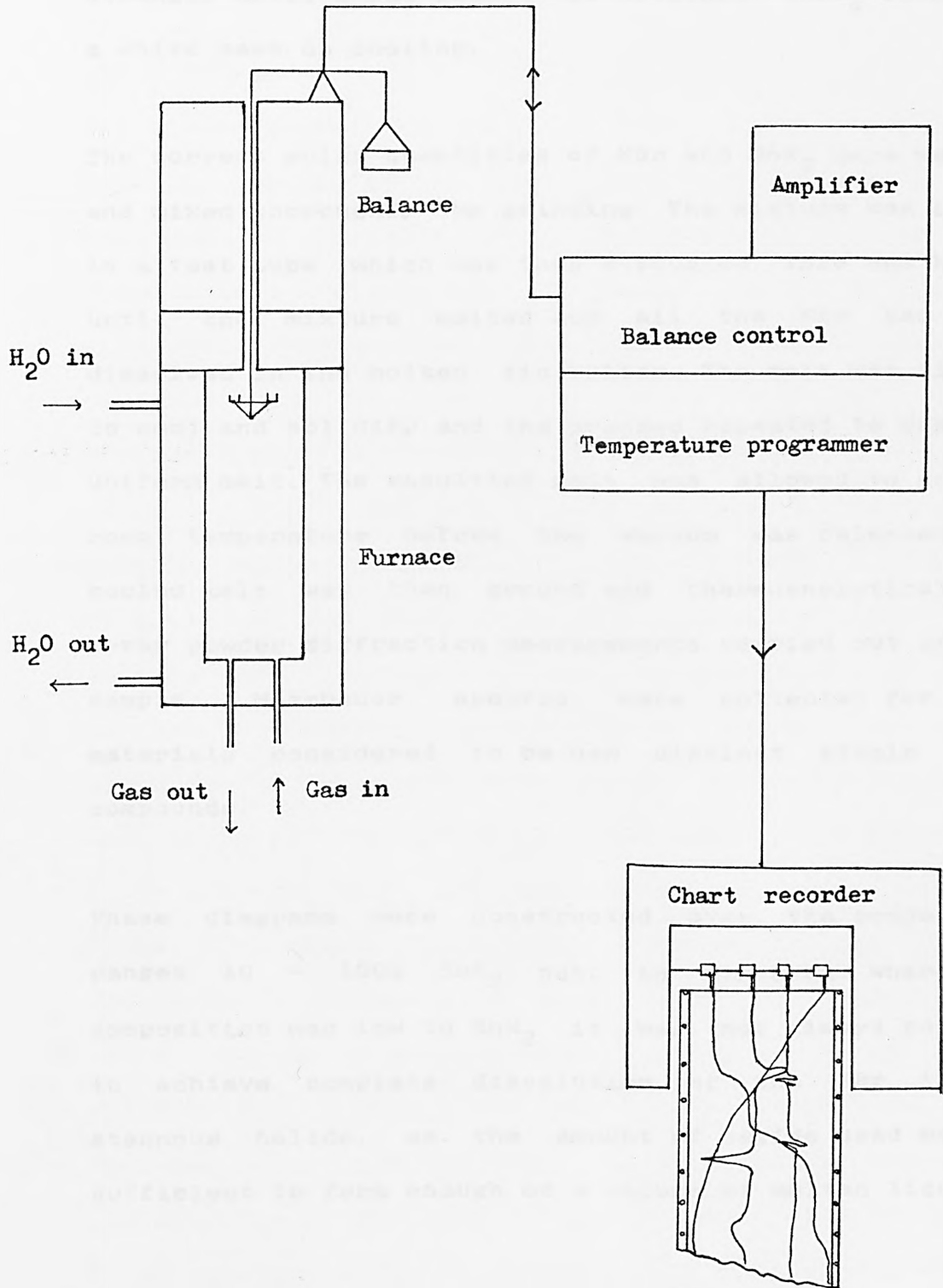


Fig.3.7

Schematic representation of STA-780 thermal analyser

excess HBr. The resulting yellow solid was heated strongly until a red liquid was obtained. SnBr_2 formed as a white mass on cooling.

The correct molar quantities of KBr and SnX_2 were weighed and mixed thoroughly by grinding. The mixture was placed in a test tube which was then evacuated. This was heated until the mixture melted and all the KBr had been dissolved in the molten tin halide. The melt was allowed to cool and solidify and the process repeated to ensure a uniform melt. The resulting melt was allowed to cool to room temperature before the vacuum was released. The cooled melt was then ground and thermoanalytical and X-ray powder diffraction measurements carried out on each sample. Mössbauer spectra were collected for those materials considered to be new distinct single phase compounds.

Phase diagrams were constructed over the composition ranges 10 - 100% SnX_2 but, in mixtures where the composition was low in SnX_2 it was not always possible to achieve complete dissolution of the KBr in the stannous halide, as the amount of halide used was not sufficient to form enough of a volume of molten liquid.

3.4 Phase diagrams for the systems KBr : SnX_2

Using the techniques described in section 3.3, phase diagrams were constructed for the 3 solid state systems KBr : SnX_2 where X = Br, Cl, F. These systems are

discussed below.

KBr : SnBr₂

The phase diagram for the KBr : SnBr₂ system is shown in fig.3.8. Melts in the composition range 10 - 90 % SnBr₂ were used in its construction. Melting point and eutectic temperatures are recorded in table 3.2. X-ray powder diffraction was used to characterise the cooled melts.

There are two new congruently melting phases centred at A (m.p. = 254° C at 50% SnBr₂) and B (m.p. = 264° C at 67% SnBr₂). Below 50% SnBr₂ no new phases could be isolated. In addition two eutectics are observable at 55% (230° C) and 90% (216° C) SnBr₂. In order to confirm the existence of two new distinct phases, X-ray powder diffraction measurements have been made on all samples and compared with those for the phases A and B (given in figs.3.9 and 3.10) and with SnBr₂ and KBr (given in figs.3.11 and 3.12). The X-ray powder data of the melts from 0% SnBr₂ upto phase A indicate a mixture of KBr and phase A. Melts between 50 and 67% show mixtures of phase A and phase B and above 67% the X-ray powder data are of mixtures of phase B and SnBr₂. No evidence was found of a new eutectic composition between phase A and KBr. The X-ray powder data, therefore, confirm the existence of the new phases A and B.

The molar compositions of the two congruently melting phases correspond to the formulae KSnBr₃ (calculated at 50% SnBr₂) for phase A and KSn₂Br₅ (calculated at 66.7%

Fig. 3.8. Phase diagram for KBr : SnBr₂ system

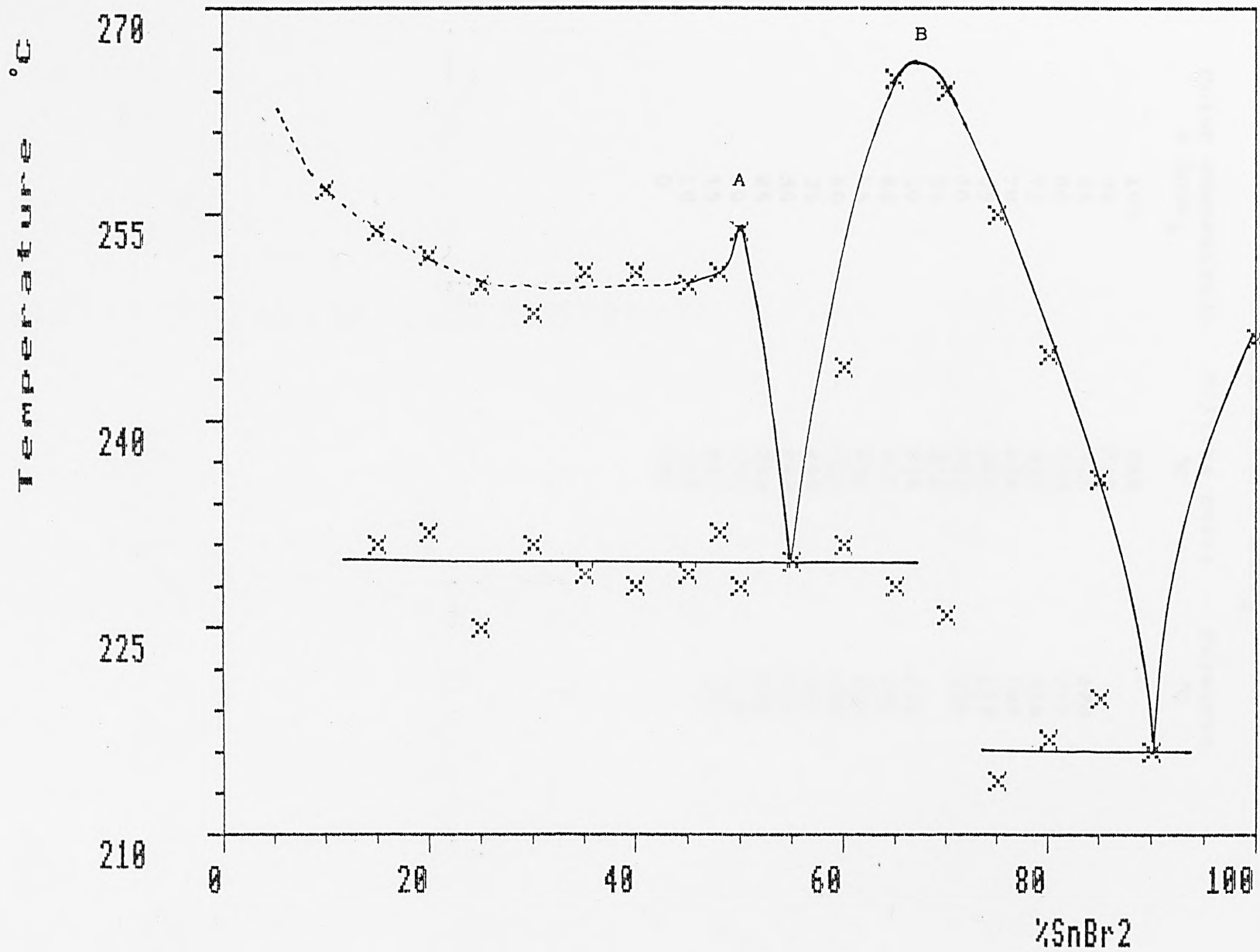
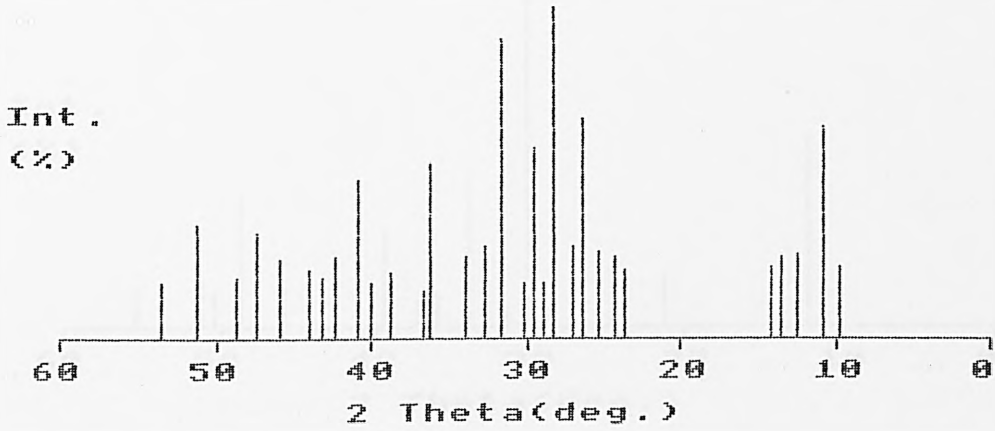


Table 3.2
Melting points and eutectics for
system KBr : SnBr₂

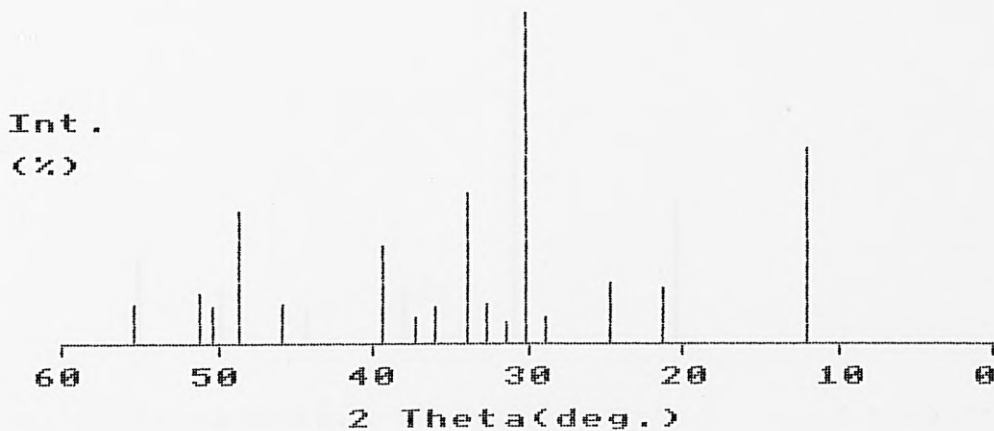
Molar composition % SnBr ₂	Melting point °C	Eutectic °C
100	246	
90	216	
85	236	220
80	245	217
75	255	214
70	264	226
65	265	228
60	244	231
55	230	
50	254	228
48	251	232
45	250	229
40	251	228
35	250	229
30	248	231
25	250	225
20	252	232
15	254	231
10	257	
0	734	

Fig.3.9
X-ray Powder Diffraction Pattern
KSnBr3



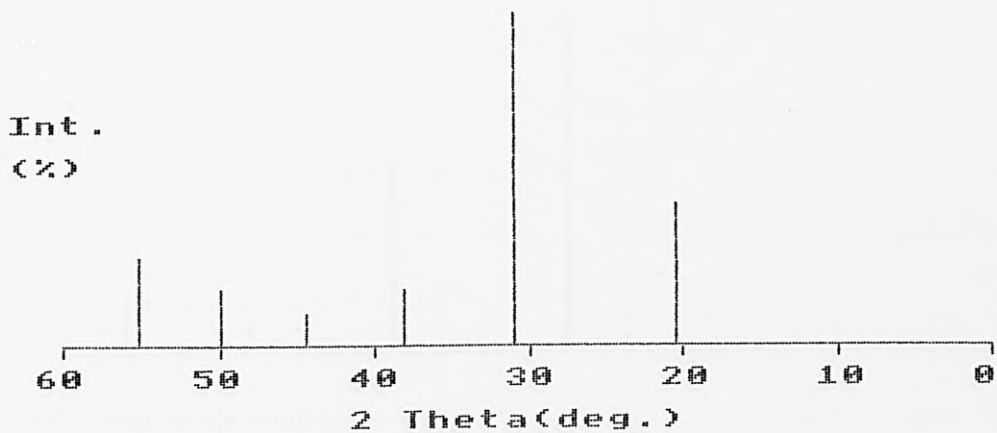
Rel. Int. (%)	d(hkl)Å
22	9.213
64	8.192
27	7.138
26	6.607
22	6.237
21	3.770
26	3.663
28	3.534
68	3.376
29	3.302
100	3.164
18	3.089
59	3.028
18	2.959
91	2.831
29	2.747
26	2.637
53	2.481
16	2.449
20	2.327
18	2.249
49	2.206
26	2.137
20	2.094
21	2.053
24	1.973
32	1.922
20	1.870
36	1.784
18	1.716

Fig.3.10
X-ray Powder Diffraction Pattern
KSn2Br5



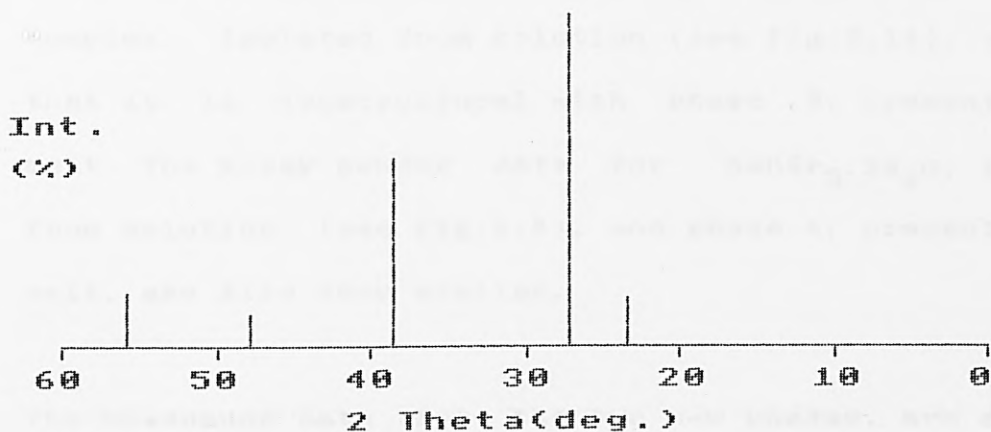
Rel. Int. (%)	d(hkl)A
60	7.314
17	4.191
20	3.619
9	3.089
100	2.959
7	2.849
12	2.747
46	2.652
11	2.488
9	2.417
30	2.292
12	1.973
40	1.873
11	1.811
16	1.784
12	1.661

Fig.3.11
X-ray Powder Diffraction Pattern
SnBr2



Rel. Int.(%)	d(hkl)A
43	4.353
100	2.885
18	2.362
10	2.036
18	1.824
28	1.667

Fig.3.12
X-ray Powder Diffraction Pattern
KBr



Rel. Int.(%)	d(hkl)Å
16	3.818
100	3.290
58	2.332
10	1.907
17	1.650
18	1.475

SnBr_2) for phase B. These compare with the complexes KSn_2Br_5 and $\text{KSnBr}_3 \cdot 2\text{H}_2\text{O}$ isolated from work in solution (see section 2.3). The X-ray powder data for the KSn_2Br_5 complex, isolated from solution (see fig.2.14), confirms that it is isostructural with phase B, present in the melt. The X-ray powder data for $\text{KSnBr}_3 \cdot 2\text{H}_2\text{O}$, isolated from solution (see fig.2.4), and phase A, present in the melt, are also very similar.

The Mössbauer data for the two new phases, are shown in table 3.3 along with those of SnBr_2 , $\text{KSnBr}_3 \cdot 2\text{H}_2\text{O}$ and KSn_2Br_5 isolated from solution. Not suprisingly as the the Sn/Br ratio increases from 0.33 in KSnBr_3 to 0.4 in KSn_2Br_5 there is an increase in chemical shift, which increases still further in SnBr_2 , the parent material, which has a Sn/Br ratio of 0.5. This change of shift is simply indicative of the way in which Sn is changing its use of bonding electrons from that in the parent material, SnBr_2 , to the complex tribromostannate, which has three relatively covalent Sn-Br bonds. The shifts of the new phases are similar to those observed in the corresponding phases isolated from solution. The quadrupole splittings of the two tribromostannates are approximately equal. There is a slight difference in the quadrupole splittings of the two potassium pentabromodistannate complexes, the difference, however, lies within fitting error of each other.

$\text{KBr} : \text{SnCl}_2$

The phase diagram for the $\text{KBr} : \text{SnCl}_2$ system is shown in

Table 3.3

Mössbauer data for new phases in the
solid state system $\text{KBr} : \text{SnBr}_2$

Phase	δ mm/s	Δ mm/s
KSnBr_3	3.59(7)	0.74(6)
KSn_2Br_5	3.84(9)	0.99(8)
$\text{KSnBr}_3 \cdot 2\text{H}_2\text{O}$	3.61(4)	0.79(4)
KSn_2Br_5 (from soln.)	3.83(3)	0.88(3)
SnBr_2	3.90(2)	0.00

fig.3.13. Melts in the composition range 10 - 90 % SnCl_2 were used in its construction. Melting point and eutectic temperatures are recorded in table 3.4.

There are two new congruently melting phases centred at A (m.p. = 235°C at 43% SnCl_2) and B (m.p. = 198°C at 71% SnCl_2). In addition four eutectics are observed in the phase diagram, with three at ca. 17% (mp. 205°C), 64% (mp. 183°C) and 77.5% (mp. 189°C) SnCl_2 ; The fourth eutectic is present between the molar composition range 50-60 % SnCl_2 (mp. 192°C), which is below an incongruently melting phase C. A fourth region centered at D may also represent an incongruently melting phase. In order to confirm the existence of two new distinct phases, X-ray powder diffraction measurements have been made on all samples and compared with those for the phases A and B (given in figs.3.14 and 3.15) and with SnCl_2 [2] and KBr (given in figs.3.16 and 3.12). The X-ray powder data do confirm these observations. The X-ray powder data of the melts from 0% upto 43% SnCl_2 indicate a mixture of KBr and phase A. Between 45 and 70 % SnCl_2 the X-ray powder data show mixtures of phase A and phase B. Above 75% SnCl_2 the X-ray powder data are those of a mixture of SnCl_2 and phase B.

The molar percentages of the two new congruently melting phases correspond to the formulae $\text{K}_2\text{Sn}_{1.5}\text{Cl}_3\text{Br}_2$ (calculated at 42.9% SnCl_2) for phase A and $\text{KSn}_{2.5}\text{BrCl}_5$ (calculated at 71.4% SnCl_2) for phase B. There are no similar phases isolated from solution (see section 2.3).

Fig. 3.13. Phase diagram for KBr : SnCl₂ system

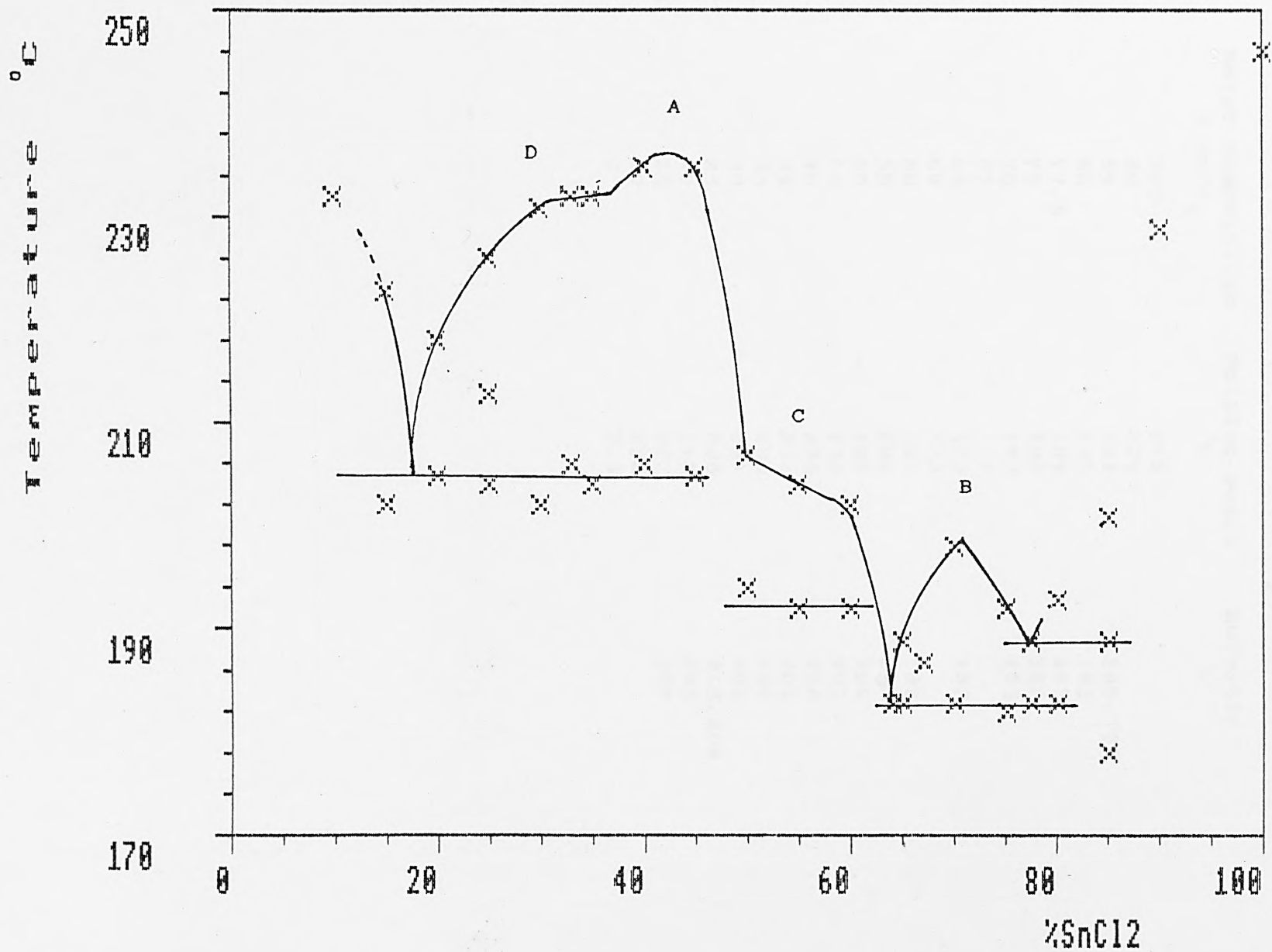
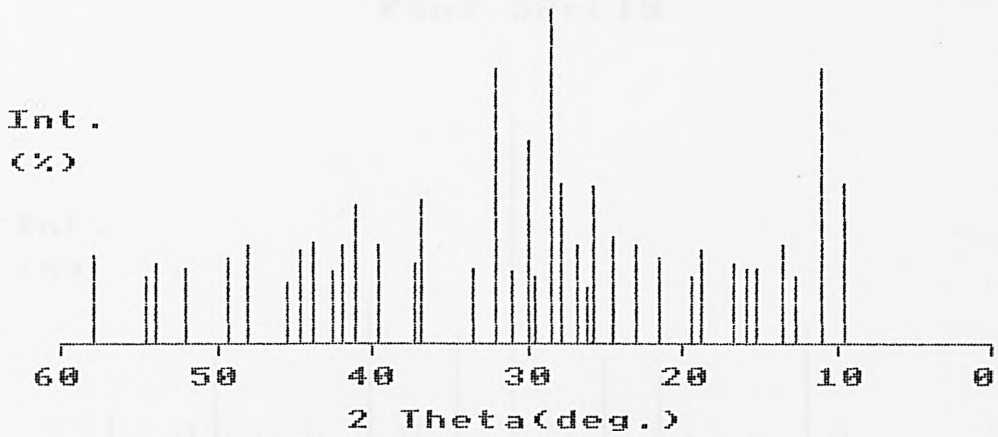


Table 3.4
Melting points and eutectics for
the system KBr : SnCl₂

Molar composition % SnCl ₂	Melting point °C	Eutectic °C
100	246	
90	229	
85	201	189, 178
80	193	183
77.5	189	183
75	192	182
70	198	183
67	187	
65	189	183
64	183	
60	202	192
55	204	192
50	207	194
45	235	205
40	235	206
35	232	204
33	232	206
30	231	202
25	226	213, 204
20	218	205
15	223	202
10	232	
0	734	

Fig.3.14

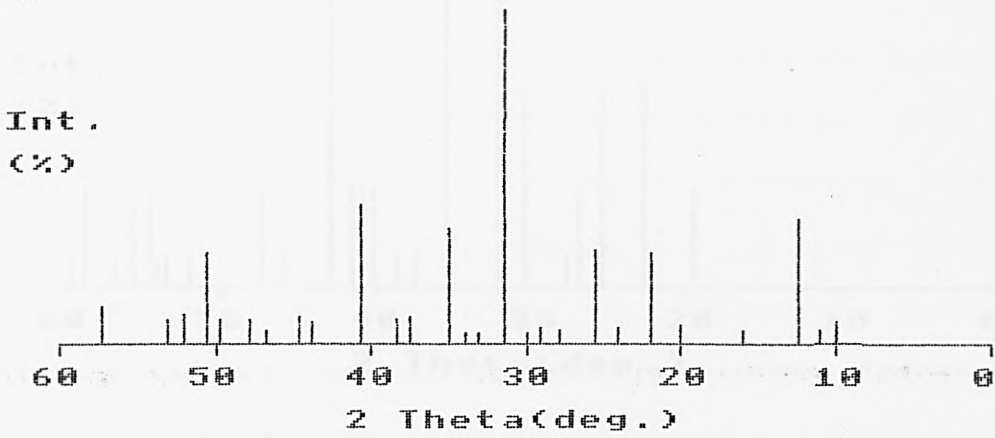
X-ray Powder Diffraction Pattern
K₂Sn_{1.5}Cl₃Br₂



Rel. Int. (%)	d(hkl)Å
49	9.309
82	8.117
21	7.025
29	6.559
23	5.867
23	5.644
24	5.340
29	4.745
21	4.599
26	4.152
29	3.883
32	3.633
47	3.480
18	3.401
29	3.339
49	3.220
100	3.132
21	3.038
61	2.979
21	2.885
82	2.805
23	2.683
44	2.442
24	2.417
29	2.276
42	2.201
21	2.122
29	2.151
32	2.067
29	2.027
18	1.998
29	1.895
26	1.848
23	1.762
24	1.704
21	1.681
27	1.595

Fig.3.15

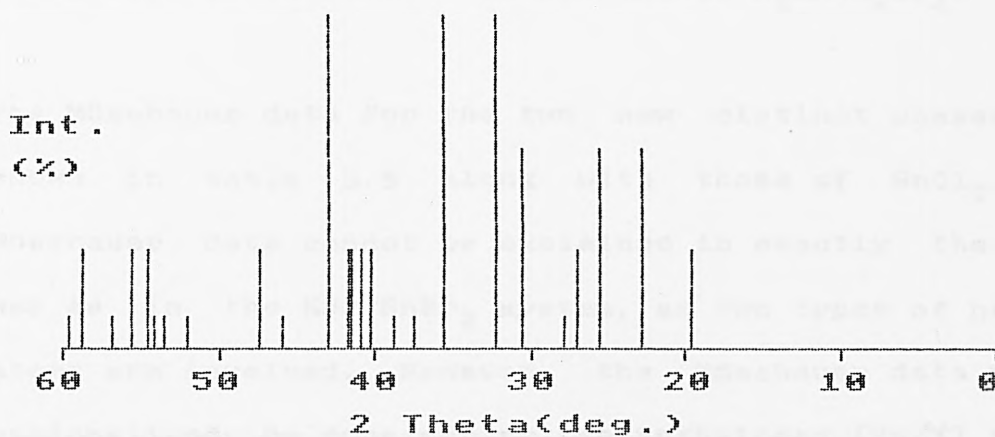
X-ray Powder Diffraction Pattern
KSn_{2.5}BrCl₅



Rel. Int. (%)	d(hkl)Å
6	9.025
4	8.117
38	7.081
4	5.574
6	4.462
28	4.058
4	3.708
29	3.507
4	3.209
4	3.079
4	2.998
100	2.858
3	2.706
3	2.644
35	2.564
9	2.404
8	2.344
42	2.222
7	2.067
8	2.027
5	1.945
7	1.907
8	1.838
27	1.807
8	1.755
8	1.728
11	1.610

Fig.3.16

X-ray Powder Diffraction Pattern
SnCl₂



Rel. Int. (%)	d(hkl)Å
30	4.520
60	3.910
60	3.510
30	3.320
10	3.210
60	2.936
100	2.775
100	2.525
10	2.405
10	2.327
30	2.243
30	2.206
30	2.181
30	2.166
100	2.103
10	1.979
30	1.916
10	1.757
10	1.711
10	1.693
30	1.682
30	1.654
10	1.621
30	1.573
10	1.554
30	1.528
10	1.469

The incongruently melting phase (C) at ca. 50% corresponds to a phase of formula of KSnCl_2Br and that at 33% (D) corresponds to a formula of $\text{K}_2\text{SnCl}_2\text{Br}_2$.

The Mössbauer data for the two new distinct phases, are shown in table 3.5 along with those of SnCl_2 . The Mössbauer data cannot be explained in exactly the same way as in the $\text{KBr}:\text{SnBr}_2$ system, as two types of halogen atoms are involved. However, the Mössbauer data may be rationalised by considering the Sn/halogen (Sn/X) ratio, which follows the same trend as observed in the $\text{KBr}:\text{SnBr}_2$ system, ie shift increases with increase in the Sn/X ratio. Thus, $\text{K}_2\text{Sn}_{1.5}\text{ClBr}_2$, which has a Sn/X ratio of 0.30, has the lowest shift at 3.53 mm/s which increases to 3.72 mm/s in $\text{KSn}_{2.5}\text{BrCl}_5$ which a Sn/X ratio of 0.42. Both shifts are considerably lower than that of the parent material SnCl_2 with a Sn/X ratio of 0.5, this is expected as complex formation reduces the s-electron density at the tin nucleus.

$\text{KBr}:\text{SnF}_2$

The phase diagram for the $\text{KBr} : \text{SnF}_2$ system is shown in fig.3.17. Melts in the composition range 10-90 % SnF_2 were used in the construction. The numerical values for melting points and eutectics are given in table 3.6.

There are two new congruently melting phases centred at A (m.p. = 250°C at 50% SnF_2) and B (m.p. = 262°C at 67% SnF_2). In addition six eutectics are observed in the phase diagram with three at ca. 42% (mp. 240°C), 53%

Table 3.5

Mössbauer data for new phases in the
solid state system $\text{KBr} : \text{SnCl}_2$

Phase	δ mm/s	Δ mm/s
$\text{K}_2\text{Sn}_{1.5}\text{Cl}_3\text{Br}_2$	3.53(7)	0.85(6)
$\text{KSn}_{2.5}\text{BrCl}_5$	3.72(3)	0.85(6)
SnCl_2	4.06(1)	0.00

Fig. 3.17. Phase diagram for KBr : SnF₂ system

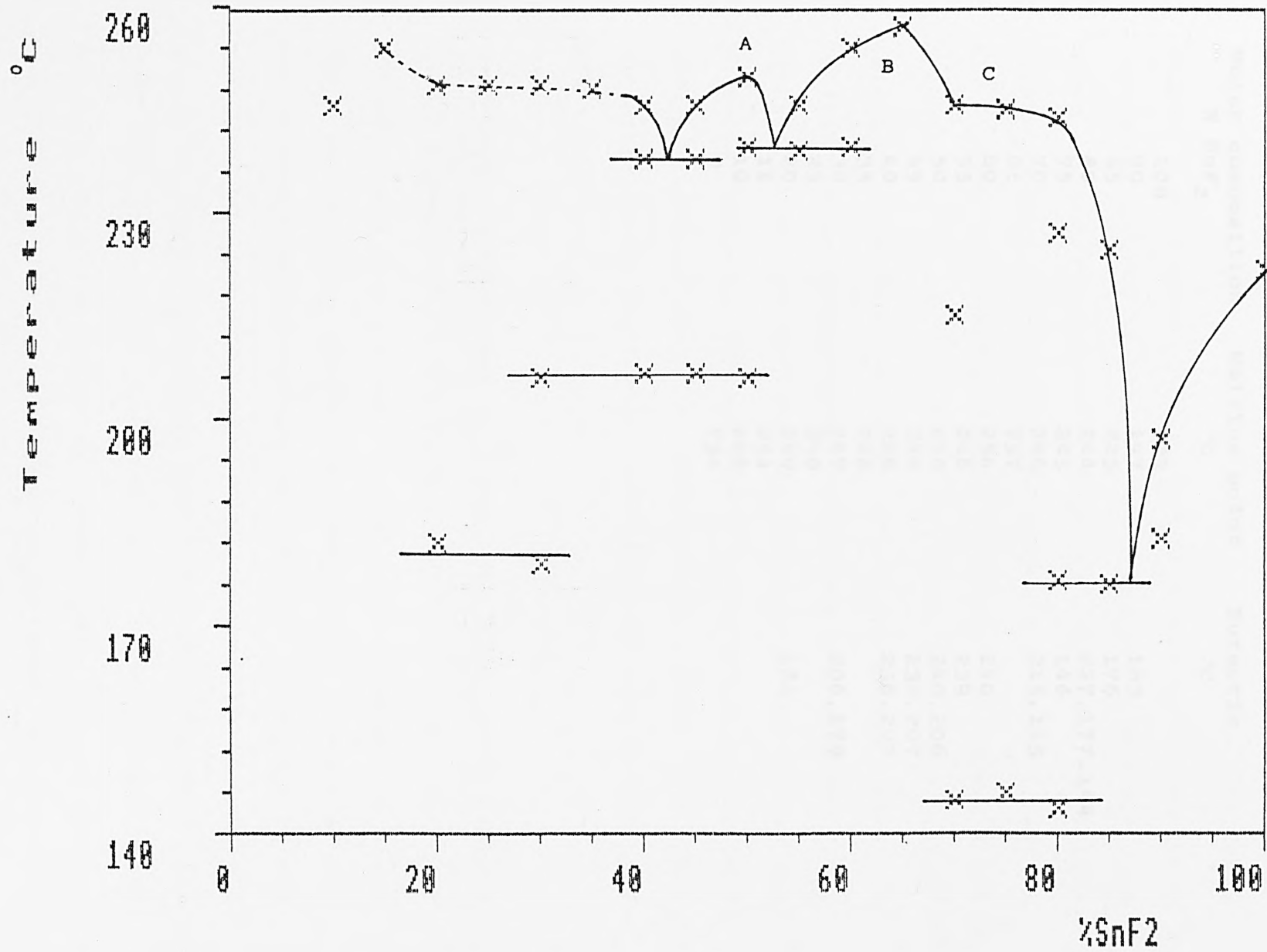


Table 3.6
Melting points and eutectics for
system KBr : SnF₂

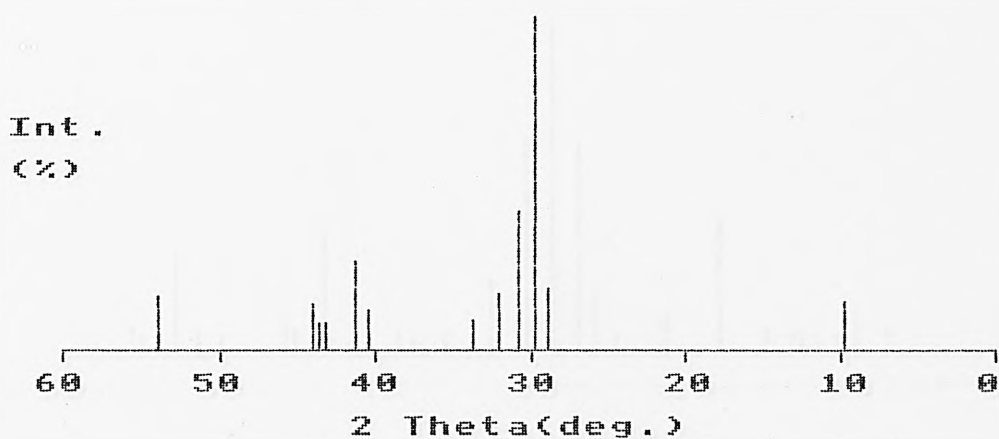
Molar composition % SnF ₂	Melting point °C	Eutectic °C
100	222	
90	197	183
85	225	176
80	244	227, 177, 144
75	245	146
70	246	215, 145
65	257	
60	254	240
55	246	239
50	250	240, 206
45	246	238, 207
40	246	238, 207
35	248	
30	249	206, 179
25	249	
20	249	182
15	254	
10	246	
0	734	

(mp. 240° C) and 87% (mp. 176° C) SnF₂; the fourth eutectic is present between the molar composition ranges of 70-80 %SnF₂ which is below an incongruently melting phase C. The fifth and sixth eutectics lie in the molar composition ranges 20-30% and 30-50% SnF₂ respectively but no new phases have been identified below 50% SnF₂. In order to confirm the existence of two new distinct phases, X-ray diffraction measurements have been made on all samples and compared with those for the phases A and B (given in figs. 3.18 and 3.19) and with SnF₂ and KBr (given in figs. 3.20 and 3.12). The X-ray powder data do confirm these observations. The X-ray powder data of the melts from 0% upto 50% SnF₂ indicate a mixture of KBr and phase A. Between 50% and 67% SnF₂ the X-ray powder data show mixtures of phase A and phase B. Above 67% SnF₂ the X-ray powder data are those of a mixture of SnF₂ and phase B.

The molar percentages of the two congruently melting phases correspond to the formulae KSnBrF₂ (calculated at 50% SnF₂) for phase A and KSn₂BrF₄ (calculated at 66.7% SnF₂) for phase B. The incongruent melting phase C at ca. 40% corresponds to a phase of formula K₂Sn₃Br₂F₆. Phases A and B at 50% and 67% SnF₂ are consistent with the phases A and B identified in the KBr:SnBr₂ system and like that system no new phases can be identified below 50% SnX₂ (X=Br, F). The X-ray powder data for the two 67% SnX₂ phases identified from the KBr:SnBr₂ and KBr:SnF₂ systems are dissimilar as are the two 50% SnX₂ phases. This is not surprising as the nature of the Sn-Br bond

Fig.3.18

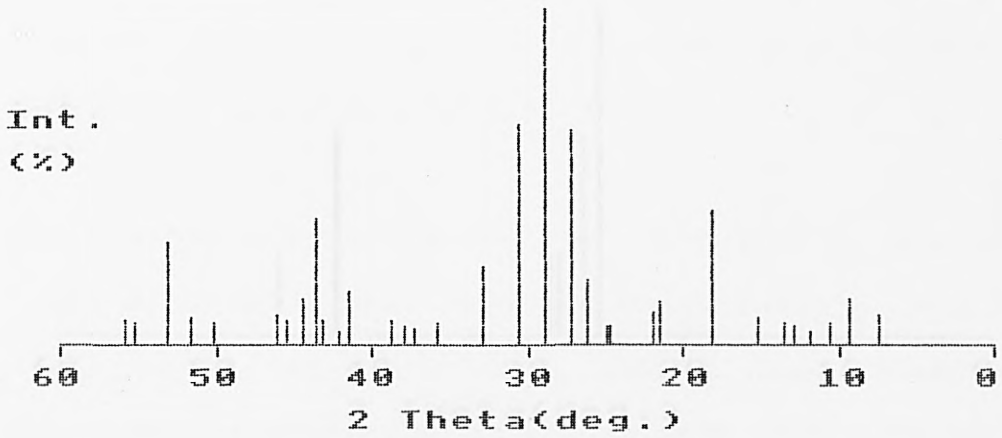
X-ray Powder Diffraction Pattern
KSnBrF₂



Rel. Int. (%)	d(hkl)Å
16	9.118
20	3.089
100	3.008
42	2.912
10	2.667
12	2.227
28	2.186
9	2.094
9	2.080
14	2.062
18	2.788
17	1.701

Fig.3.19

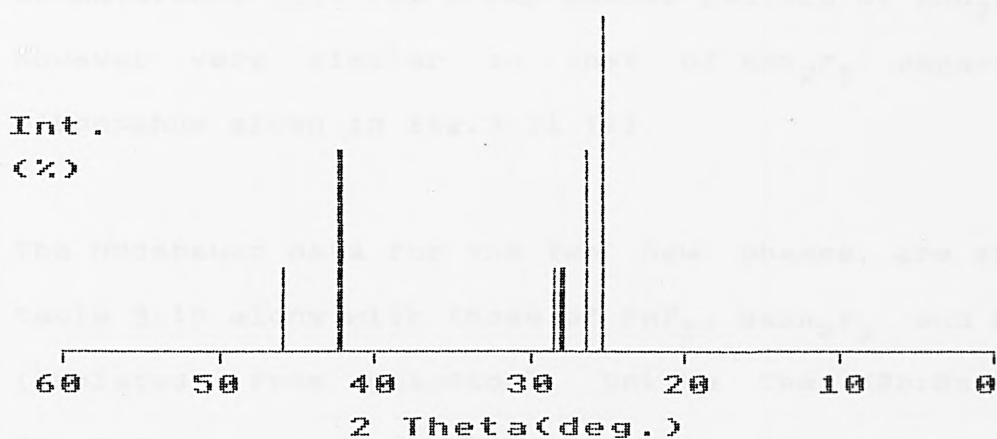
X-ray Powder Diffraction Pattern
KSn₂BrF₄



Rel. Int. (%)	d(hkl)Å
10	11.946
15	9.509
7	8.425
4	7.500
6	6.862
7	6.607
8	5.867
40	4.901
13	4.133
10	4.077
6	3.619
7	3.576
19	3.414
64	3.278
100	3.089
66	2.931
23	2.722
7	2.508
6	2.411
6	2.374
8	2.321
17	2.181
5	2.141
8	2.099
37	2.076
15	2.036
8	1.993
10	1.969
7	1.817
8	1.771
31	1.725
7	1.664
8	1.647

Fig.3.20

X-ray Powder Diffraction Pattern
SnF₂



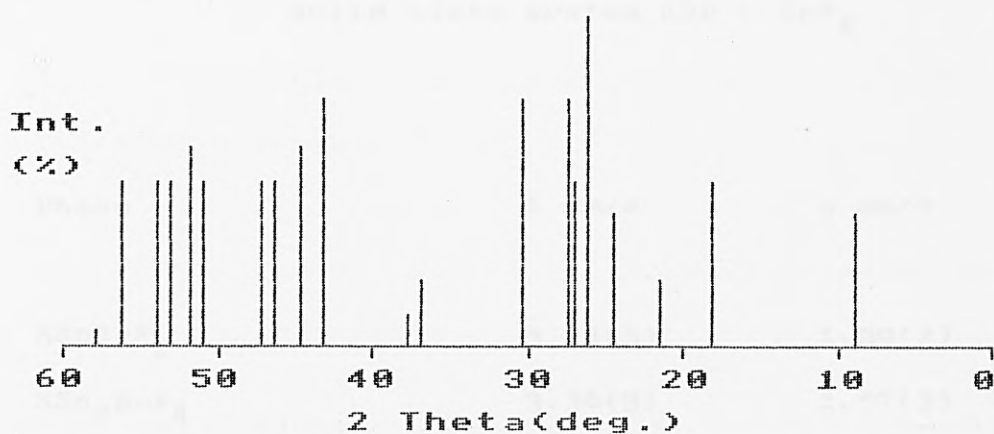
Rel. Int. (%)	d(hkl)Å
100	3.530
60	3.390
26	3.210
26	3.190
26	3.140
60	2.150
60	2.140
26	1.980

is very different to that of Sn-F and this is reflected in the type of crystal structures formed by the two types of materials [3]. The X-ray powder pattern of KSn_2BrF_4 is however very similar to that of KSn_2F_5 reported by O'Donoghue given in fig.3.21 [4].

The Mössbauer data for the two new phases, are shown in table 3.10 along with those of SnF_2 , NaSn_2F_5 and NH_4SnF_3 (isolated from solution). Unlike the $\text{KBr}:\text{SnCl}_2$ and $\text{KBr}:\text{SnBr}_2$ systems the Mössbauer data cannot be explained by simple consideration of the Sn/halogen (Sn/X) ratio. The KSn_2BrF_4 complex which has a Sn/X ratio of 0.4 has a lower shift than KSnBrF_2 which has a Sn/X ratio of 0.33. The reason for the discrepancy is as mentioned previously, the difference in nature between the Sn-F and Sn-Br bonds. The shifts of tin fluoride complexes are known to be anomalously low even on consideration of electronegativities [3]. Thus, the utilisation of the less electronegative Br^- anion in complex formation means that there is an increased electron density at the tin nucleus, on comparison with the all fluorine analogues, which is characterised by a higher shift. This is more significant where the Br/F ratio is high as in KSnBrF_2 , whose shift is very much higher than NH_4SnF_3 , but becomes less significant as the Sn/F ratio decreases, as in KSn_2BrF_4 , which has a shift close to that of $\text{Na}_2\text{Sn}_2\text{F}_5$. The quadrupole splittings also reflect the Br/F ratio and show a decrease with increase in the Br/F ratio.

Fig.3.21

X-ray Powder Diffraction Pattern
KSn₂F₅ [4]



Rel. Int. (%)	d(hkl)Å
40	9.940
50	4.910
20	4.130
40	3.630
100	3.410
50	3.300
76	3.270
76	2.940
20	2.440
10	2.390
76	2.100
60	2.030
50	1.961
50	1.929
50	1.791
60	1.767
50	1.728
50	1.701
50	1.634
6	1.595

Table 3.7

Mössbauer data for new phases in the
solid state system KBr : SnF₂

Phase	δ mm/s	Δ mm/s	
KSnBrF ₂	3.54(3)	1.30(2)	
KSn ₂ BrF ₄	3.36(3)	1.57(3)	
SnF ₂ (ortho)	3.20	2.20	[5]
SnF ₂ (mono)	3.60	1.80	[5]
NaSn ₂ F ₅	3.32	1.86	[6]
NH ₄ SnF ₃	3.18	1.88	[7]

REFERENCES, CHAPTER THREE

(1) P.W. Atkins, 'Physical Chemistry', 1978, Oxford University Press.

(2) X-ray Powder Data File (Inorganic), American Society for Testing Materials, Philadelphia 1967.

(3) J.D. Donaldson and S.M. Grimes, Reviews on Silicon, Germanium, Tin and Lead Compounds, (1984), 8 (1), 1-132.

(4) J.D. O'Donoghue, Ph.D. Thesis, London 1965.

(5) J.D. Donaldson, R. Oteng and B.J. Senior, Chem. Comm., (1965), 618.

(6) J.D. Donaldson, D.C. Puxley and M.J. Tricker, J. Inorg. Nucl. Chem., (1975), 37, 655.

(7) J.D. Donaldson and B.J. Senior, J. Chem. Soc., (A), (1966), 1798.

CHAPTER FOUR

MÖSSBAUER SPECTROSCOPIC STUDIES OF TIN MATERIALS

	Page
4.1 The Mössbauer effect and Mössbauer spectroscopy.	168
4.2 Conversion electron Mössbauer spectroscopy.	178
4.3 Instrumentation.	184
4.4 Fitting programs.	186
4.5 Instrumentation changes and calibration.	191
4.6 A comparison of transmission and conversion electron Mössbauer spectra of normal tin(II) compounds.	195
4.7 Applications of ^{119}Sn CEMS to Sn containing systems.	202
(i) An examination of tinfoil passivation and anodic oxide coatings.	202
(ii) An examination of tin oxide films on glass and quartz.	212

(iii) An examination of NiSn alloy.	220
(iv) An examination of the effects of air and light on $\text{CsSn}_3\text{Br}_{1.5}\text{F}_{5.5}$ using CEMS.	225
(v) An examination of flame resistant wool and cotton.	230
(vi) An examination of tin impregnated coal samples.	232
(vii) An examination of wood preservatives.	233
(viii) Tin(II) chloride films on white PVC.	234
(ix) Surface reactions.	234
(x) An examination of tin biocides on leaf samples.	237
(xi) An examination of tin in coloured ceramic tiles.	238
References.	243

CHAPTER FOUR

4.1 The Mössbauer Effect and Mössbauer Spectroscopy.

The recoilless emission and resonant absorption of γ -radiation, by an atomic nucleus, was first observed in 1957 by R.L. Mössbauer [1,2]. Since then the effect has been measured in many elements and the technique has emerged as a useful tool in structural chemistry. Most studies have been concerned with the ^{57}Fe and ^{119}Sn isotopes and their respective γ -ray transitions of 14.4 and 23.8 KeV. the present work involves the ^{119}Sn isotope only. The ^{119}Sn decay scheme is shown in fig.4.1.

γ -radiation results from the decay of an excited nuclear spin state to the ground state. In the decaying nucleus there is some loss of energy due to recoil (see fig.4.2). If we assign the energies of the two states as E_{ex} and E_{g} the energy of the γ -ray is given by,

$$E_{\gamma} = E_{\text{ex}} - E_{\text{g}} - (E_{\text{R}} + E_{\text{D}}) \quad \text{---- (4.1)}$$

E_{R} , the recoil energy and E_{D} a Döppler term can be calculated using equations 4.2 and 4.3 respectively.

$$E_{\text{R}} = \frac{E_{\gamma}^2}{2mc^2} \quad \text{---- (4.2)}$$

$$E_{\text{D}} = 2\sqrt{(E_{\text{R}} kT)} \quad \text{---- (4.3)}$$

Where T is the absolute temperature and k is Boltzman's constant.

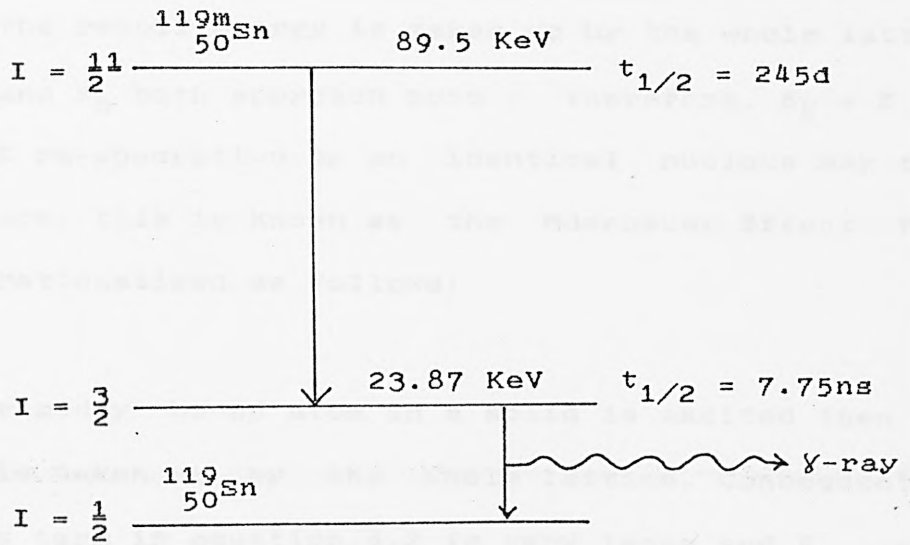
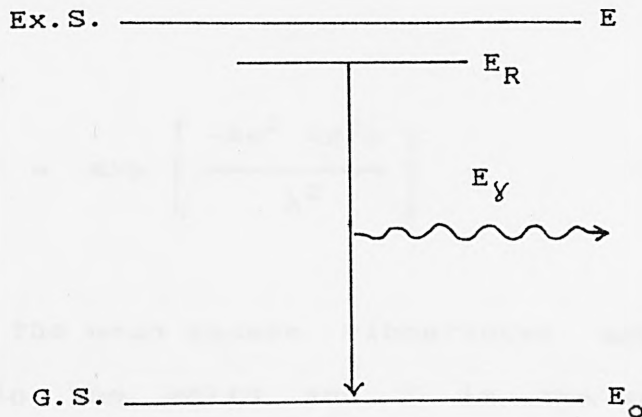


Fig.4.1

^{119}Sn decay scheme



$$E_\gamma = E - E_R - E_D$$

(E_D = Doppler term)

Fig.4.2

Energy loss due to recoil.

For certain low energy γ -ray transitions, in the solid state, the recoil energy is taken up by the whole lattice and E_R and E_D both approach zero. Therefore, $E_\gamma = E$ and resonant re-absorption by an identical nucleus may then take place, this is known as the Mössbauer Effect. This may be rationalised as follows:

If a rigidly bound atom in a solid is excited then the recoil is taken up by the whole lattice. Consequently, the mass term in equation.4.2 is very large and $E_R \rightarrow 0$. In practice, however, atoms are not rigidly bound and vibration occurs. If E_R is large enough it may be transferred to a quantised lattice vibration. However if E_R is less than the energy required to reach the lowest vibrational level, the lattice recoils as a whole and resonance is observed. In practice only a small fraction of these events take place, the quantity being known as the recoil free, or Mössbauer, fraction, f , and is given by,

$$f = \exp \left[\frac{-4\pi^2 \langle X^2 \rangle}{\lambda^2} \right] \quad \text{---- (4.4)}$$

$\langle X^2 \rangle$ is the mean square vibrational amplitude of the nucleus in the solid and λ is the wavelength of the γ -photon. 'f' varies from solid to solid and increases with decreasing temperature ie. as atoms become more rigidly bound in the lattice. Most Mössbauer spectra are, therefore, accumulated at reduced temperatures (typically

80K) in order to enhance the effect.

Mössbauer spectroscopy can give information on atoms and molecules in the solid state, from hyperfine interactions between nuclear and electronic properties (see fig.4.3), ie. between nuclear charge distribution and extranuclear electric and magnetic fields.

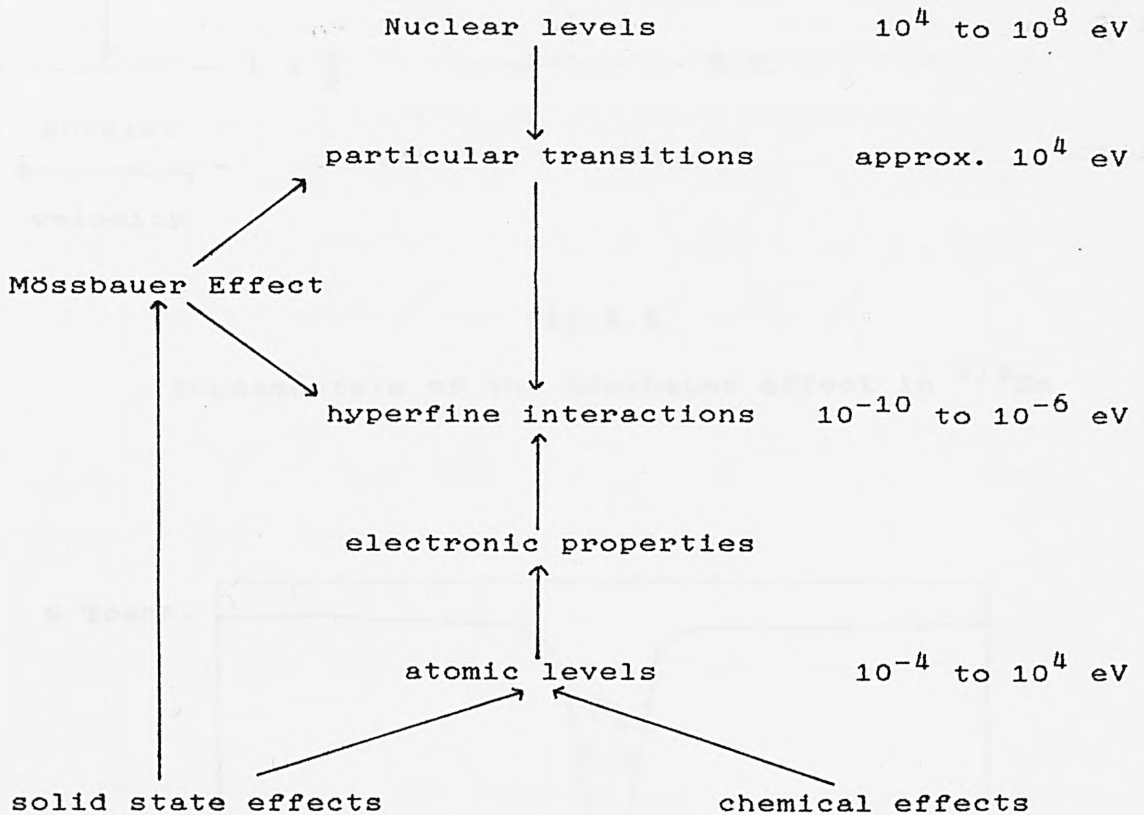


Fig.4.3: Scale of hyperfine interactions between nuclear energy levels and electronic properties.

Hyperfine interactions cause very small splittings in the nuclear energy levels (approx. 5×10^{-8} eV for ^{119}Sn). To observe this in Mössbauer spectroscopy a small relative motion is applied to the source. The energy of

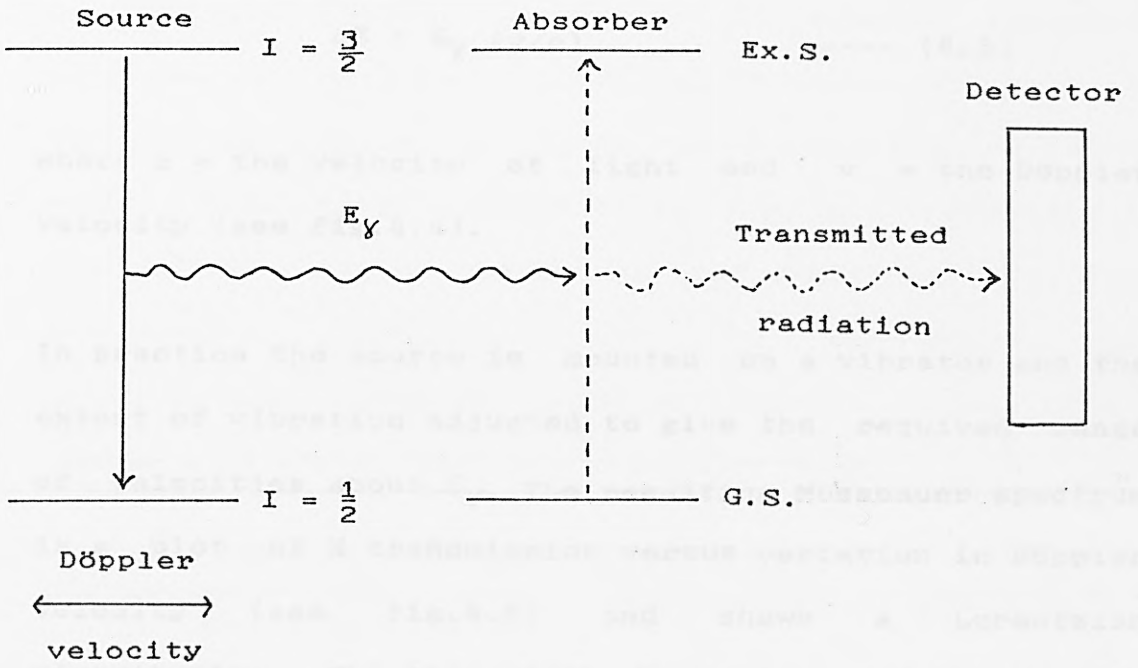


Fig.4.4

Fundamentals of the Mössbauer effect in ^{119}Sn

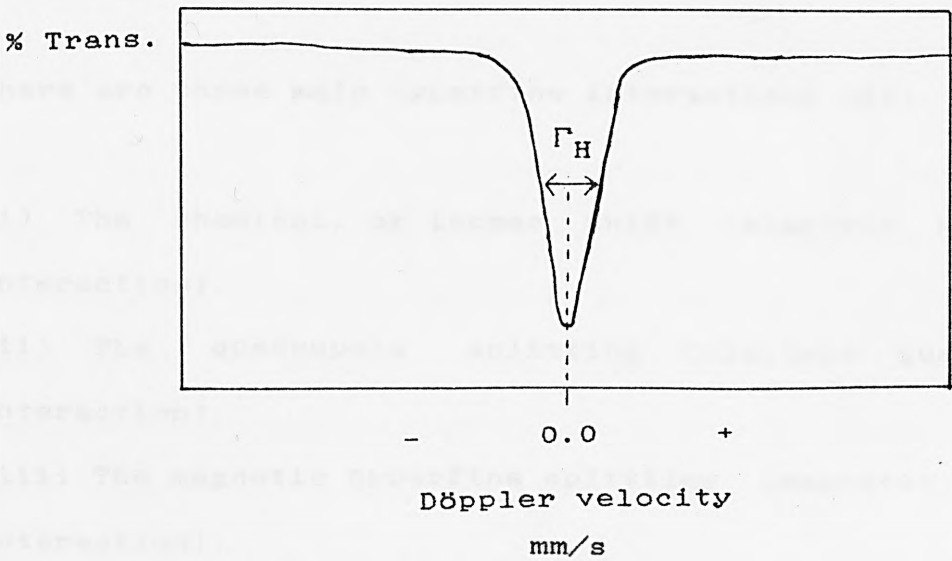


Fig.4.5

Mössbauer spectrum for identical source and absorber

the γ -ray is now Döppler shifted by an amount,

$$\Delta E = E_{\gamma} (v/c) \quad \text{---- (4.5)}$$

where c = the velocity of light and v = the Döppler velocity (see fig.4.4).

In practice the source is mounted on a vibrator and the extent of vibration adjusted to give the required range of velocities about E_{γ} . The resulting Mössbauer spectrum is a plot of % transmission versus variation in Döppler velocity (see fig.4.5) and shows a Lorentzian distribution. The line width Γ depends on the half life ($t_{1/2}$) of the excited state and is given by,

$$\Gamma_H = \frac{h}{2\pi} \frac{0.693}{t_{1/2}} \quad \text{---- (4.6)}$$

where h is Planks constant.

There are three main hyperfine interactions viz:

- (i) The chemical, or isomer shift (electric monopole interaction).
- (ii) The quadrupole splitting (electric quadrupole interaction).
- (iii) The magnetic hyperfine splitting (magnetic dipole interaction).

These are discussed below.

(i) Chemical shift.

Interaction between nuclear charge distribution and s-electronic charge results in an altered resonance position, the difference in energy between the source and absorber resonances is known as the chemical or isomer shift. This energy separation is due to a difference in the nuclear radii of the ground and excited states. Thus extranuclear factors must be considered when rationalising chemical shift and therefore equation 4.7 contains an atomic term and a nuclear term.

$$\delta = \underbrace{\frac{4 \pi Z e^2}{5} R^2 \frac{\Delta R}{R}}_{\text{nuclear term.}} \underbrace{\{ |\Psi_s(0)|_a^2 - |\Psi_s(0)|_s^2 \}}_{\text{atomic term.}}$$

Equation 4.7

where, $|\Psi_s(0)|^2$ is the total s-electron density at the nucleus for source (s) and absorber (a), $\Delta R/R$ is the change in nuclear radii and Ze is the nuclear charge.

For ^{119}Sn $\Delta R/R$ is positive, therefore, as the nuclear term is constant for any given transition, a positive chemical shift will indicate an increase in s-electron density at the nucleus. Thus chemical shift is used as a measure of nuclear s-electron density. By convention, in work with ^{119}Sn , α -tin has been taken as an arbitrary zero and all tin chemical shifts relate to it. Therefore by considering the occupancy of the 5s orbital, the chemical shift of a particular tin compound would be positive for a tin(II) compound or negative for a

tin(IV) material (see fig.4.6).

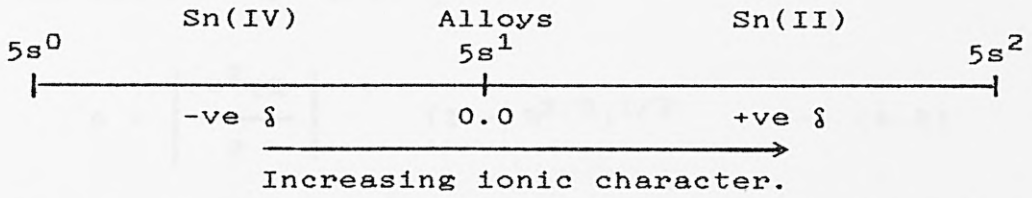


Fig.4.6: Variation of δ in Sn materials wrt α -Sn.

The degree of ionic character and, hence, nuclear s-electron density, increases with increase in positive chemical shift. For convenience the shifts quoted in this work are with respect to a CaSnO_3 source, these can easily be corrected with respect to α -tin by subtraction of 2.05 mm/s.

(ii) Quadrupole splitting.

Quadrupole splitting is a result of the coupling of the electric field gradient e_q with the nuclear quadrupole moment eQ . Any nucleus with $I > 1/2$ (where I is the spin quantum number) possesses a nuclear quadrupole moment as a direct result of the non-spherical charge distribution around the nucleus. In ^{119}Sn , application of a non symmetrical extra-nuclear field (eg. in Sn(II) materials), results in a splitting of the $I=3/2$ nuclear energy level into two possible spin states defined by the magnetic quantum number m_I ($m_I = +3/2, +-1/2$). The $I=1/2$ level does not split. Transitions between the 3 resulting nuclear levels causes a splitting in the resonance line and appears as a characteristic doublet in the Mössbauer spectrum. The difference between the two peaks in the spectrum is known as the quadrupole

splitting (Δ) (see figs. 4.7 and 4.8). The difference in energy can be expressed as:

$$\Delta = \left| \frac{e^2 q Q}{2} \right| (1 - \eta^2/3)^{1/2} \quad \text{---- (4.8)}$$

Where η is the asymmetry of the electric field gradient, Q is the quadrupole moment of the nucleus, q is the field gradient and e is the protonic charge.

Thus, the extent of quadrupole splitting provides valuable information on the asymmetry of the nuclear s-electron density. Therefore, in tin, an imbalance in p or d electron density distribution would cause an electric field gradient at the nucleus inducing asymmetry in the electronic environment around the metal. High symmetry compounds have low quadrupole splittings, eg. SnO_2 has a zero quadrupole splitting reflecting the high symmetry octahedral environment around the tin atom. Blue/black SnO , however, which has a square pyramidal environment around Sn, has a splitting of 1.45 mm/s [3]. This is a direct result of the asymmetry caused by the non bonding electron pair whose location prevents the close approach of 4 more oxygen atoms to complete octahedral symmetry. Where Δ is not resolved the Mössbauer line width Γ can give information on the symmetry about the tin nucleus, the broader the line the greater the asymmetry. It should be noted that line widths may be affected by other factors eg source to detector distance (cosine broadening) and sample depth (thickness broadening) and care should be taken when

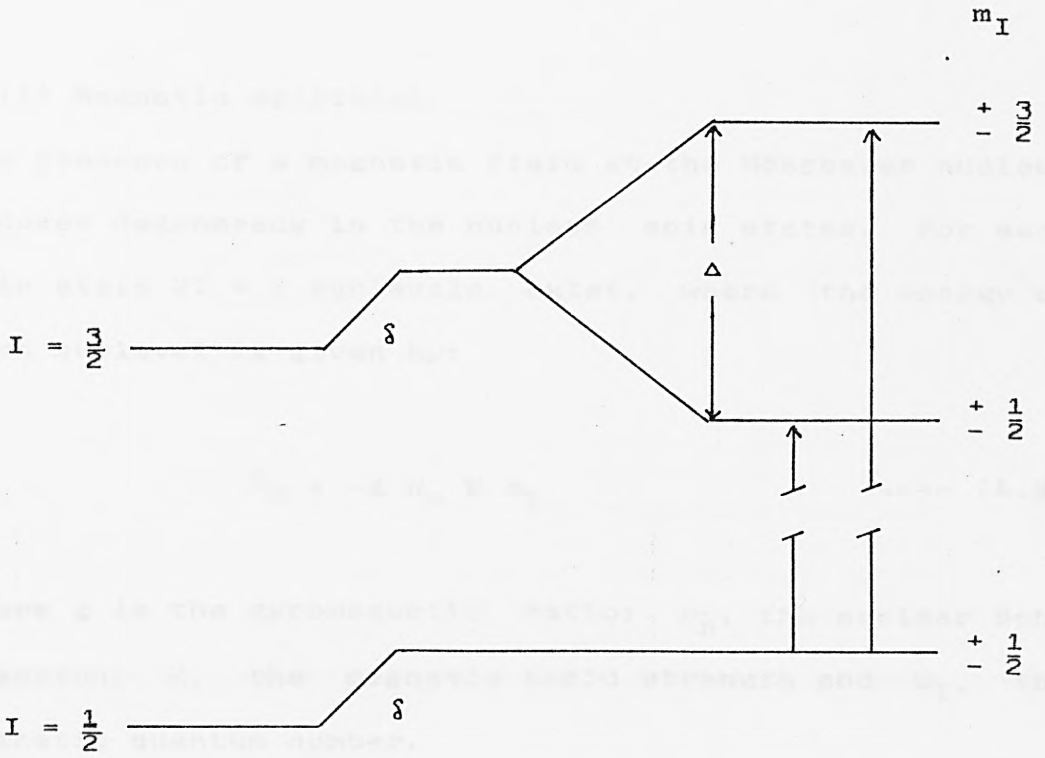


Fig.4.7

Absorber energy levels showing isomer shift δ
and quadrupole splitting Δ

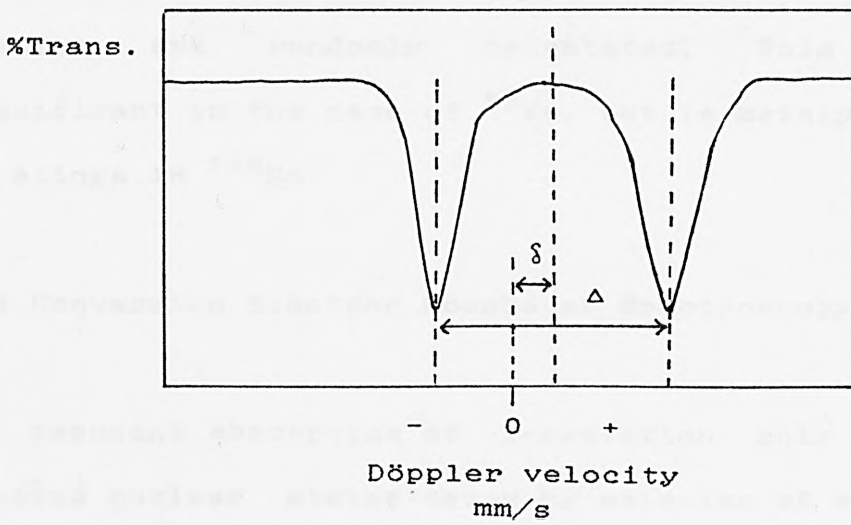


Fig.4.8

Mössbauer spectrum showing a quadrupole
split doublet

interpreting line width values.

(iii) Magnetic splitting.

The presence of a magnetic field at the Mössbauer nucleus induces degeneracy in the nuclear spin states. For each spin state $2I + 1$ sublevels exist, where the energy of each sublevel is given by:

$$E_m = -g \mu_n H m_I \quad \text{----- (4.9)}$$

Where g is the gyromagnetic ratio; μ_n , the nuclear Bohr magneton; H , the magnetic field strength and m_I , the magnetic quantum number.

In ^{57}Fe and ^{119}Sn a symmetric 6 line spectrum is observed reflecting the 6 allowed transitions (see figs 4.9 and 4.10). The intensities are in a calculatable ratio, typically 3:2:1:1:2:3 for a sample in which the magnetic domains are randomly orientated. This effect is significant in the case of ^{57}Fe , but is mainly restricted to alloys in ^{119}Sn .

4.2 Conversion Electron Mössbauer Spectroscopy.

On resonant absorption of γ -radiation only some of the excited nuclear states decay by emission of a γ -photon. In fact in ^{119}Sn , 85% of the $I=3/2$ excited states decay by internal conversion [4]. Internal conversion begins in the L-shell, resulting in the ejection of a 19.6 KeV conversion electron. An electron from the M-shell then

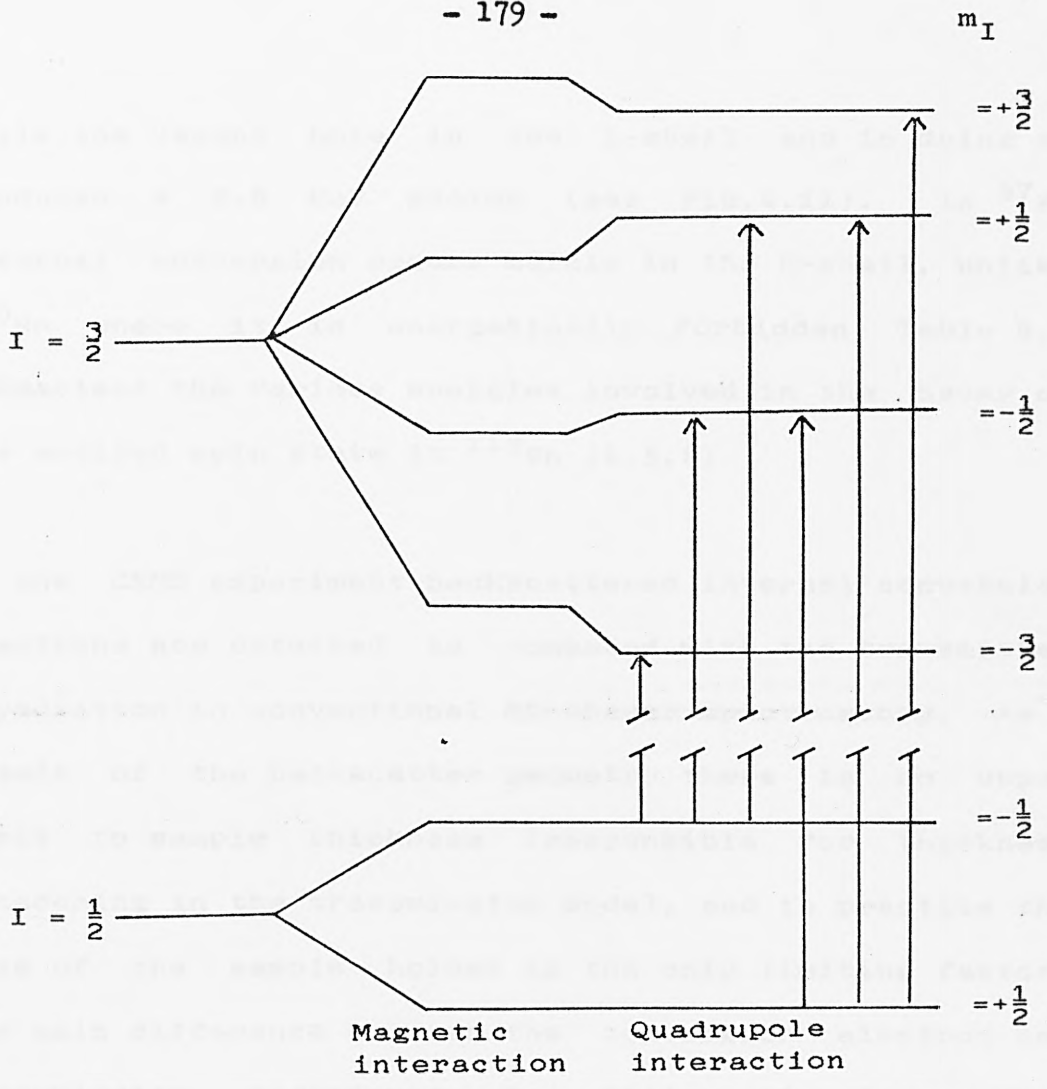


Fig. 4.9
Effects of quadrupole and magnetic interaction on absorber nuclear energy levels.

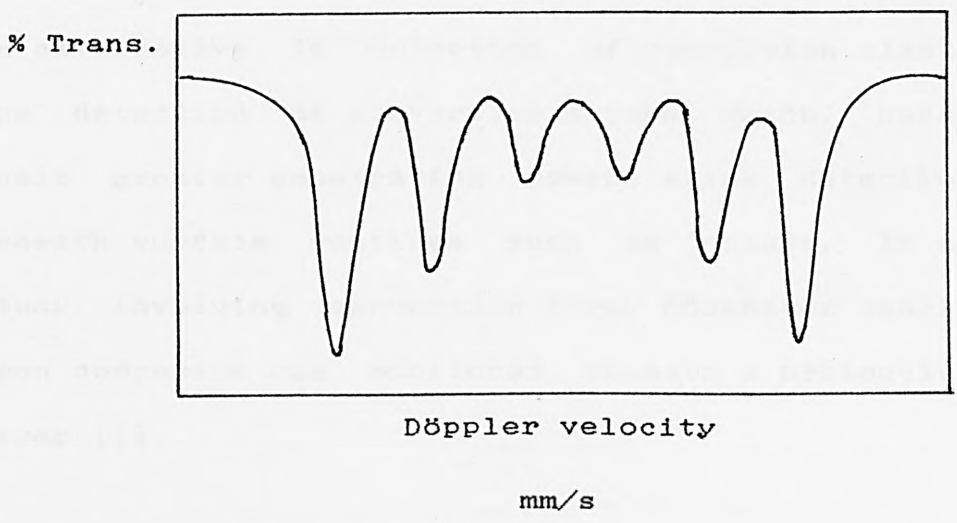


Fig. 4.10
Magnetically split Mössbauer spectrum

fills the vacant hole in the L-shell and in doing so produces a 2.8 KeV photon (see fig.4.11). In ^{57}Fe internal conversion occurs mainly in the K-shell, unlike ^{119}Sn where it is energetically forbidden. Table 4.1 summarises the various energies involved in the decay of the excited spin state in ^{119}Sn [4,5,6]

In the CEMS experiment backscattered internal conversion electrons are detected as compared with the transmitted γ -radiation in conventional Mössbauer spectroscopy. As a result of the backscatter geometry there is no upper limit to sample thickness (responsible for thickness broadening in the transmission mode), and in practice the size of the sample holder is the only limiting factor. The main difference between the conversion electron and transmission techniques is that only information pertaining to the surface is detected in the former technique as opposed to information from the bulk material in the latter. This is explained by the attenuation of electrons ejected from within the sample. An alternative to detection of conversion electrons is the detection of conversion X-rays which, because of their greater penetrating power allow detection from beneath surface coatings such as paints. In a recent study involving conversion X-ray Mössbauer spectroscopy iron corrosion was monitored beneath a protective paint layer [7].

Two basic CEMS experiments exist:

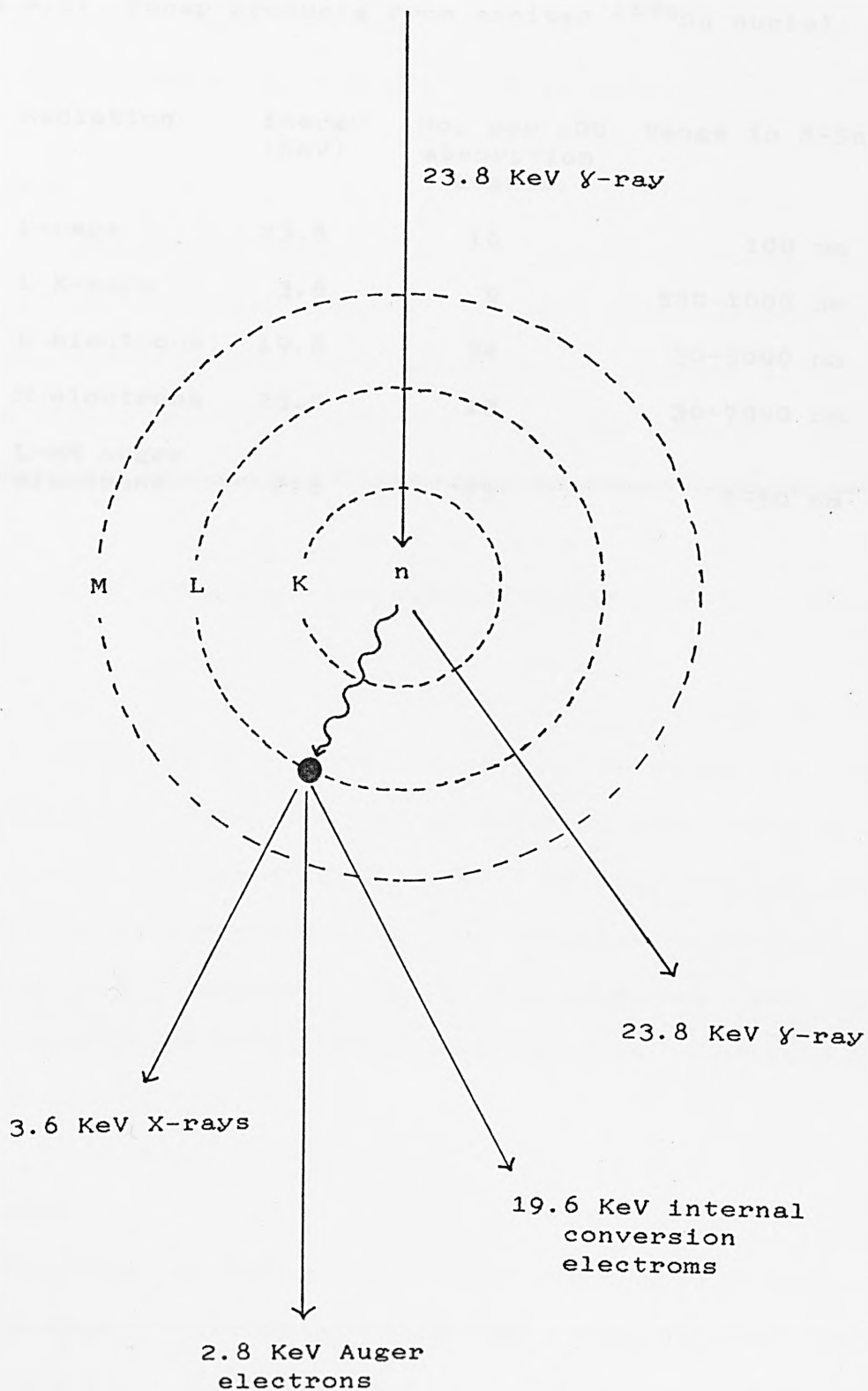


Fig.4.11

Decay of the excited nucleus in ^{119}Sn

Table 4.1: Decay products from excited ^{119m}Sn nuclei.

Radiation	Energy (KeV)	No. per 100 absorption events.	Range in β -Sn
γ -rays	23.8	16	100 nm
L X-rays	3.6	9	520-1000 nm
L electrons	19.8	84	30-5000 nm
M electrons	23.0	13	30-7000 nm
L-MM Auger electrons	2.8	75	5-50 nm

(i) Depth resolution CEMS (DCEMS)

(ii) Integral CEMS (ICEMS)

These techniques will be dealt with in turn.

(i) DCEMS

DCEMS hinges on the resolution of the total energy flux of the backscattered electrons into selected bands of energies corresponding to specific depth ranges within a sample. The number of counts in the n th channel of a Mössbauer spectrum can be expressed as [5,8]:

$$T(E)_n = \int_0^{\infty} w(E,x) P(x)_n dx$$

Where, $w(E,x)$ is a weighted function relating to the probability of detection of an electron from depth x at spectrometer setting E . $P(x)_n$ is the electron emission probability at depth x and at the velocity corresponding to the n th channel. Empirical methods for the interpretation of ^{119}Sn DCEMS data have been described by Bonchev et al [9,10,11].

(ii) ICEMS

ICEMS involves the detection of the total energy flux of backscattered electrons and in general, spectral interpretation is as for transmission Mössbauer spectroscopy. Several workers have tried to derive empirical formulae to describe layer thicknesses from ICEMS data [12,13,14] and have been reviewed by Tricker [5]. The most recent and detailed interpretation of

multilayer ICEMS spectra is by Salvat et al, [15,16,17] who describe a spectral function S_n as the probability of absorption of a gamma ray of specified energy to be absorbed in the nth layer and express this as follows:

$$S_n = PE_n + GCE_n + GPE_n + XPE_n - BD$$

Where PE = primary electron contribution

GCE = secondary electron contribution

GPE = secondary gamma ray contribution

XPE = secondary X-ray contribution

BD = resonant background.

All of the present work on CEMS has been carried out using the ICEMS technique and all further reference to CEMS is to this technique.

4.3 Instrumentation

The spectrometers used in the present work were Cryophysics MS-102 Mössbauer spectrometers running in a constant acceleration mode. Spectra were accumulated over 512 channels in a multi channel analyser. Earlier work was carried out on a teletype controlled spectrometer but this was later upgraded to a microcomputer controlled instrument. The computerised system is summarised in fig 4.12.

The detector used for the CEMS studies was a gas flow proportional counter designed by M.Tricker at the

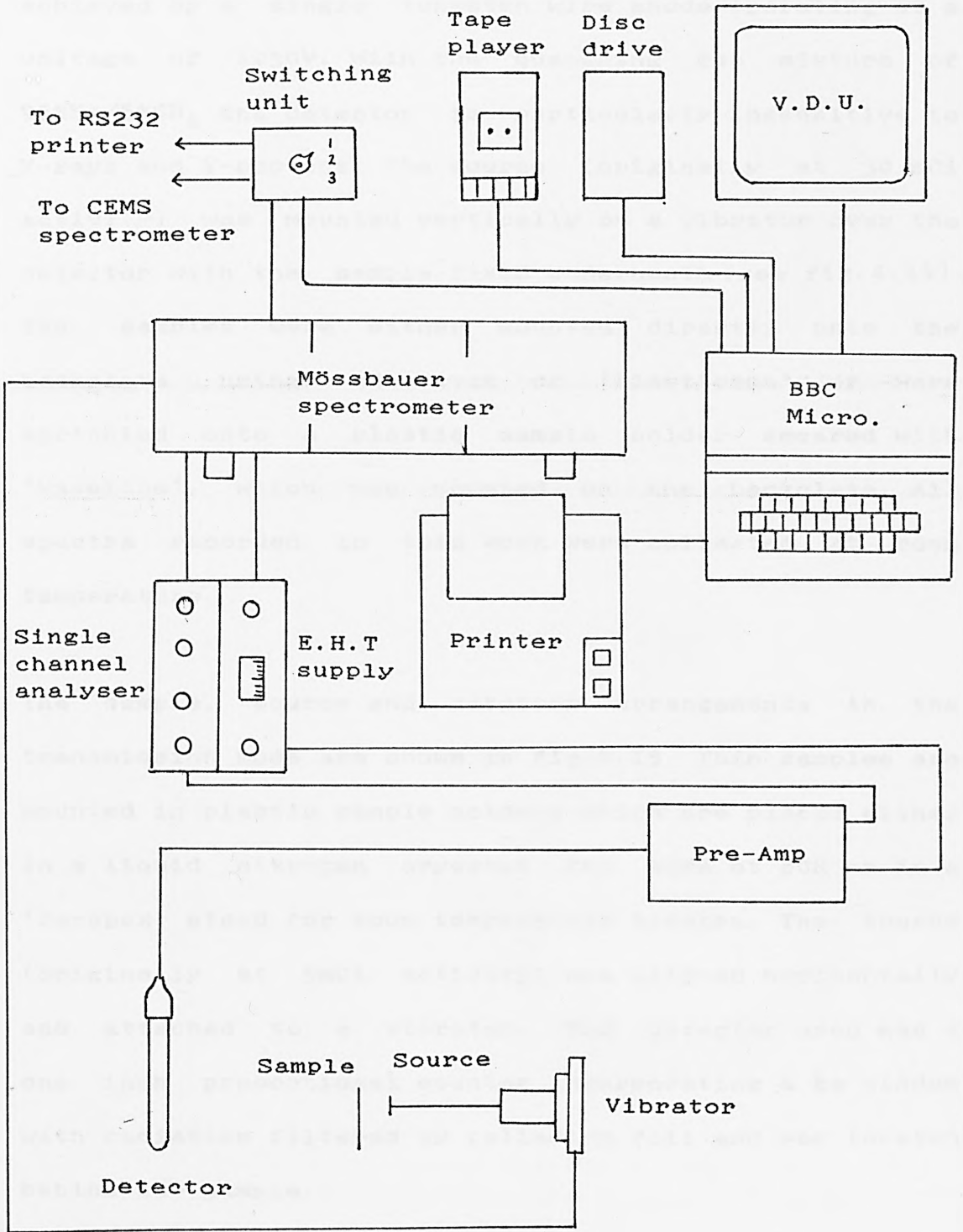


Fig. 4.12

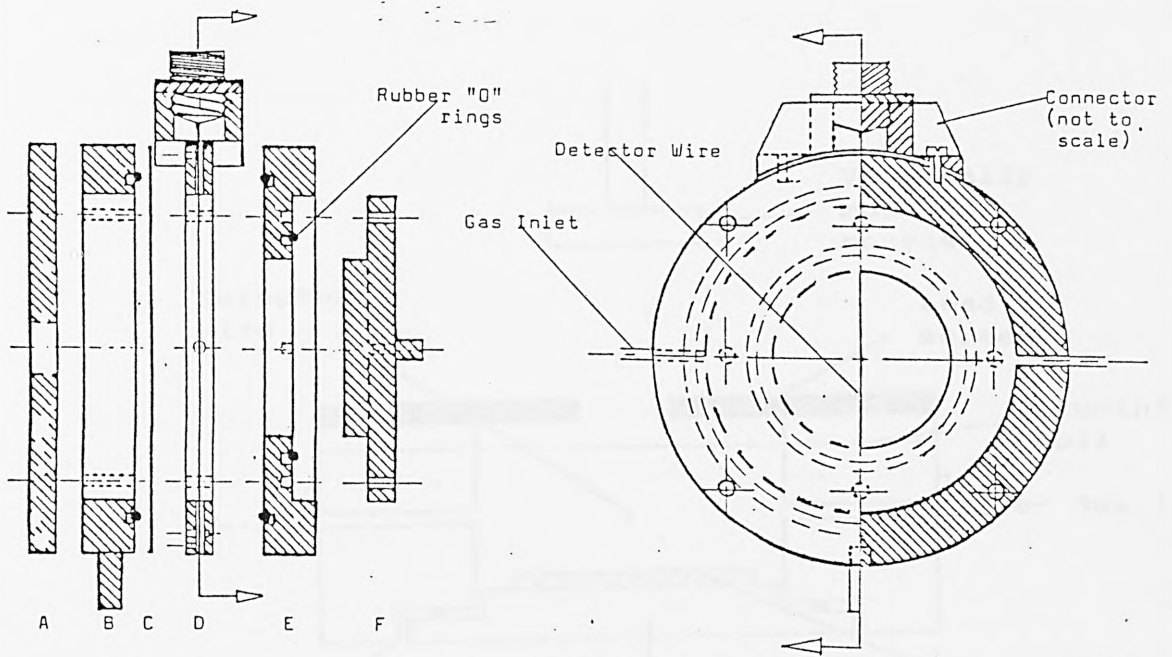
Schematic representation of a computer controlled Mössbauer system

Heriot-Watt University, Edinburgh. Sections through the detector are shown in figs.4.13 [6]. Detection is achieved by a single tungsten wire anode operating at a voltage of 1050V. With the quenching gas mixture of 95%He/5%CH₄ the detector is particularly insensitive to X-rays and γ -photons. The source (originally at 30 mCi activity) was mounted vertically on a vibrator over the detector with the sample fixed underneath (see fig.4.14). The samples were either mounted directly onto the backplate using adhesives or 'Plasticene' or were sprinkled onto a plastic sample holder smeared with 'Vaseline', which was mounted on the backplate. All spectra recorded in this work were collected at room temperature.

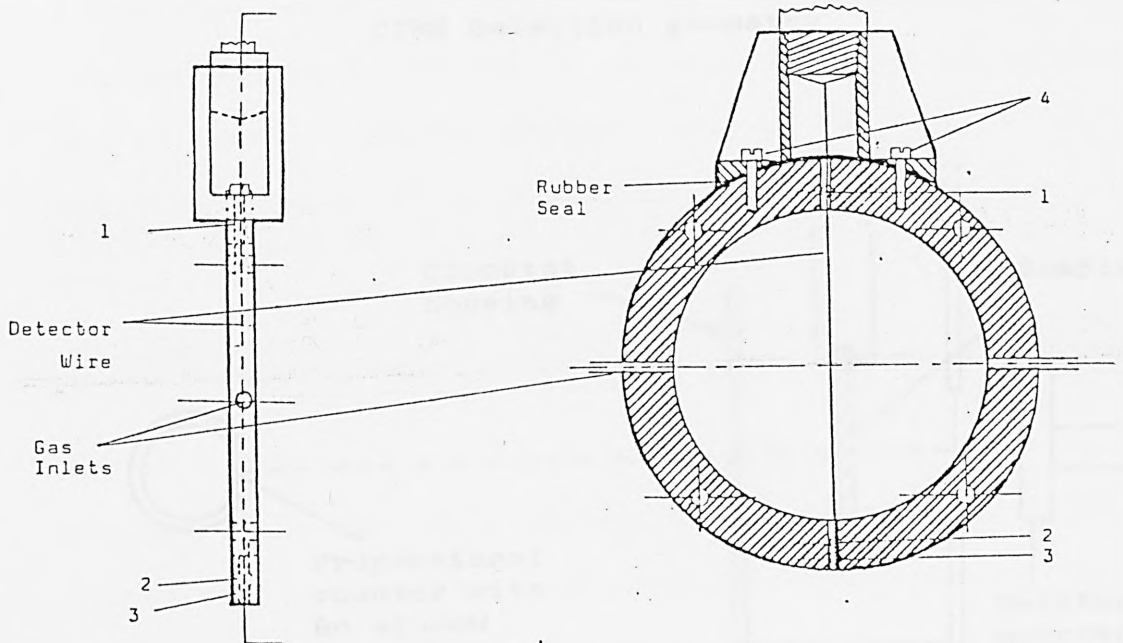
The sample, source and detector arrangements in the transmission mode are shown in fig.4.15. Thin samples are mounted in plastic sample holders which are placed either in a liquid nitrogen cryostat for work at 80K or in a 'Perspex' stand for room temperature spectra. The source (originally at 5mCi activity) was aligned horizontally and attached to a vibrator. The detector used was a one inch proportional counter incorporating a Be window with radiation filtered by palladium foil and was located behind the sample.

4.4 Fitting programs

As described in section 4.1 Mössbauer spectra consist of n points in an assumed Lorentzian distribution. The



Schematic representation of a CEMS detector: The detector is made up from a lead shield A, a front plate B, an aluminium window C, a wire assembly D, a backplate E and a sample holder F.



Details of the wire assembly: The wire is tensioned by means of screws 1, 2 and 3. The anode is fed through the guide channel and secured by screws 3 and 1 and then tensioned by turning screw 2. The anode is replaced by undoing screws 1, 2, 3 and 4, holding the connector to the main body.

Fig. 4.13

Sections through CEMS detector.

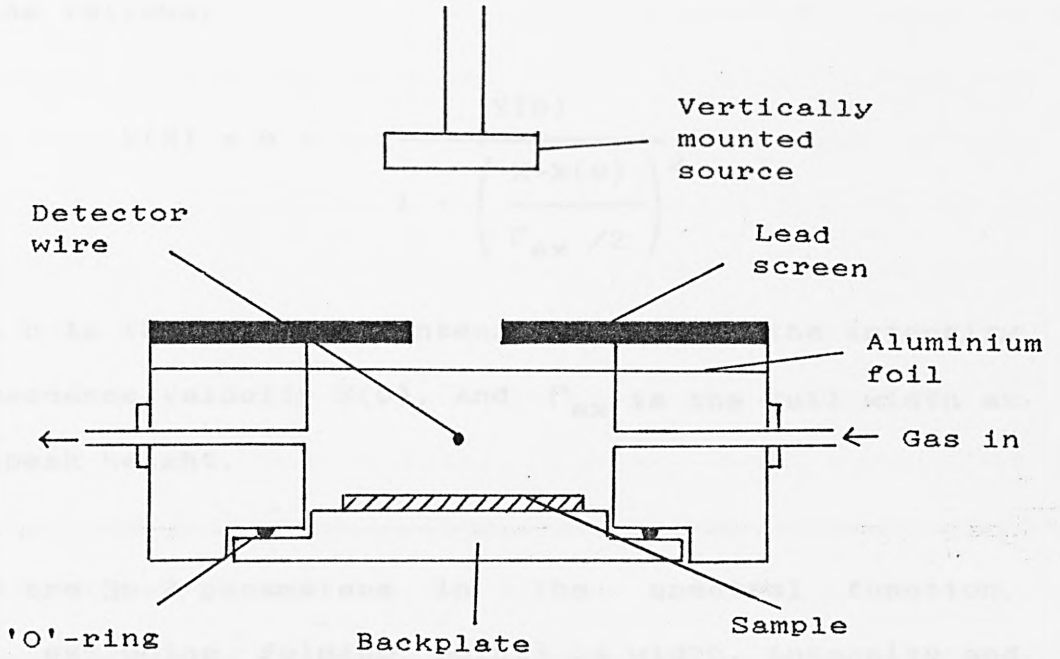


Fig. 4.14

CEMS Detection geometry

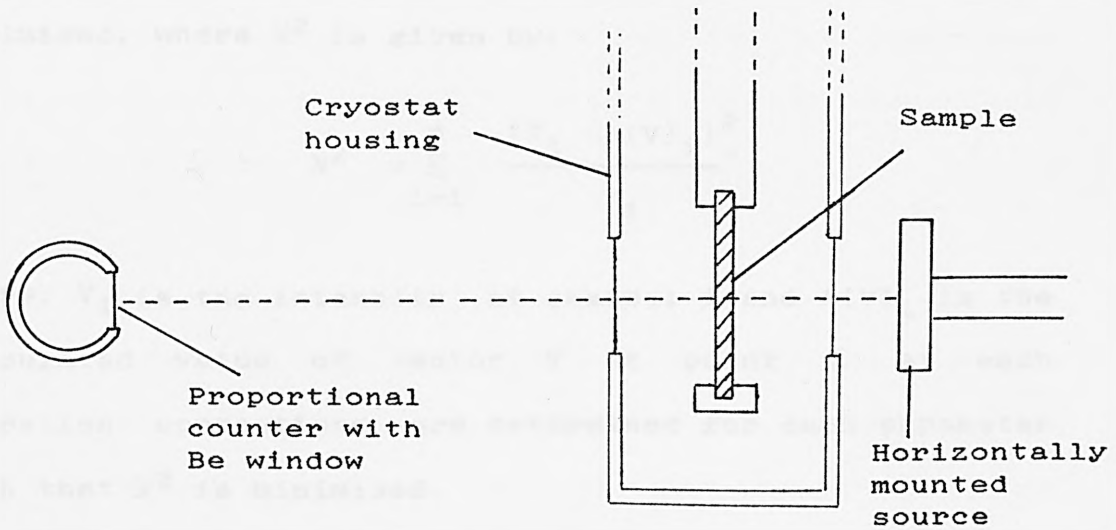


Fig. 4.15

Transmission Mössbauer detection geometry

Lorentzian line shape can be described by the function $Y(X)$ as follows:

$$Y(X) = b + \frac{Y(0)}{1 + \left(\frac{X-X(0)}{\Gamma_{ex}/2} \right)^2}$$

Where b is the baseline intensity, $Y(0)$ is the intensity at resonance velocity $X(0)$, and Γ_{ex} is the full width at half peak height.

There are $3n+2$ parameters in the spectral function, (N.B. excluding folding point) ie width, intensity and position for each line and a baseline and baseline correction value for the spectrum. These variables can be represented by a vector V . Fitting is normally achieved by a least squares method where the value χ^2 is minimised, where χ^2 is given by:

$$\chi^2 = \sum_{i=1}^n \frac{[Y_i - A(V)_i]^2}{Y_i}$$

Where, Y_i is the intensity at channel i and $A(V)_i$ is the calculated value of vector V at point i . At each iteration corrections are determined for each parameter such that χ^2 is minimised.

Several programs were used to fit Mössbauer spectra in this work and these are described below:

1 'MOSFIT'[18,19]

Two versions of this program were used. The most commonly

used fitting program in the present work was the PASCAL version of 'MOSFIT' (V9.1) which is permanently stored in the memory of the Spectrometer. This gave convenient and rapid fits at the time of collection, but the system would not allow spectra to be re-loaded for fitting after down-loading from the spectrometer. These fits, obtained at the time of collection were satisfactory for most of the spectra accumulated, but occasionally, spectra had to be fitted using other programs. A second BASIC version of 'MOSFIT' was also used in some cases, and ran on a BBC microcomputer. This program was used for checking alternative fits on stored spectra.

2 'MFIT' [20]

The FORTRAN program 'MFIT' was used when a satisfactory fit could not be attained using 'MOSFIT'. The program was particularly useful in resolving narrow quadrupole splittings and for calculating the field strength in magnetically split spectra.

3. 'MOSFUN' [21]

This program was used for fitting complicated spectra that could not be fitted by 'MOSFIT' or 'MFIT'. The program consisted of a set of routines and programs designed to fit data by any theoretical line fitting approach including:

- a) Simple correlated Lorentzian distributions
- b) Voigt approximations
- c) Convolution integral calculations.

Least squares fitting in 'MOSFUN' is by the Newton or Gradient methods. The advantage of this program is that even the most complicated spectra can be fitted. The main disadvantage, however, is that the input format is extremely complex and several input files are needed to fit a single spectrum.

In the current work, all fitted results subsequently reported have been fitted with one of the above programs, where more than one program has been used the best fit only, is reported.

4.5 Instrumentation changes and calibration.

The system used in the CEMS experiments is as described previously. Several changes were made to the system used by Grimes [6]. Data were collected by Grimes on a J&P Mössbauer spectrometer over 256 channels. In the present study, this was replaced by a Cryophysics MS-102 Mössbauer spectrometer accumulating data over 512 channels. The vibrator inherited was in poor condition with much noise accompanying the drive signal. This was overhauled and the vibrator carefully tuned in and the signal trimmed, however, some residual noise was still present. The CaSnO_3 Mössbauer source was replaced with a new source at a starting activity of 30mCi. For most of the spectra collected the detector had a backplate hole of ca. 1 cm. The backplate hole was later doubled to increase the count rate but this also had the effect of

slightly increasing linewidths by cosine broadening (see section 4.1).

The CEMS detector was calibrated using SnO_2 and $\beta\text{-Sn}$. Difficulty was encountered in trying to fit SnO_2 spectra as singlet lines. The fitted line often missed out data (see fig.4.16), indicating that the points were not in a single Lorentzian distribution. This was originally explained by the fact that SnO_2 picks up moisture very rapidly and the effect would be observed in the CEM spectrum as an unresolvable doublet. However, fitting as a symmetric doublet also proved very difficult and in general spectra had to be fitted as two separate lines (see fig.4.17) to achieve acceptable statistics. Subsequently the vibrator was again overhauled and on reassembly the signal was found to be much cleaner than had previously been obtained and the residual noise left after the first overhaul was eliminated. An SnO_2 calibration spectrum that had been accumulating previously was re-run after the second overhaul and gave a single Lorentzian peak as compared with a broad line obtained before. SnO_2 spectra run before and after the second vibrator overhaul are shown in figs.4.18 and 4.19. The distortion seems to have been limited to within ± 1.0 mm/s around the SnO_2 resonance, as materials with resonances outside this range seem to be unaffected.

A brief experiment was conducted to assess the feasibility of low temperature CEM experiments using this type of detector. To the detector base plate was

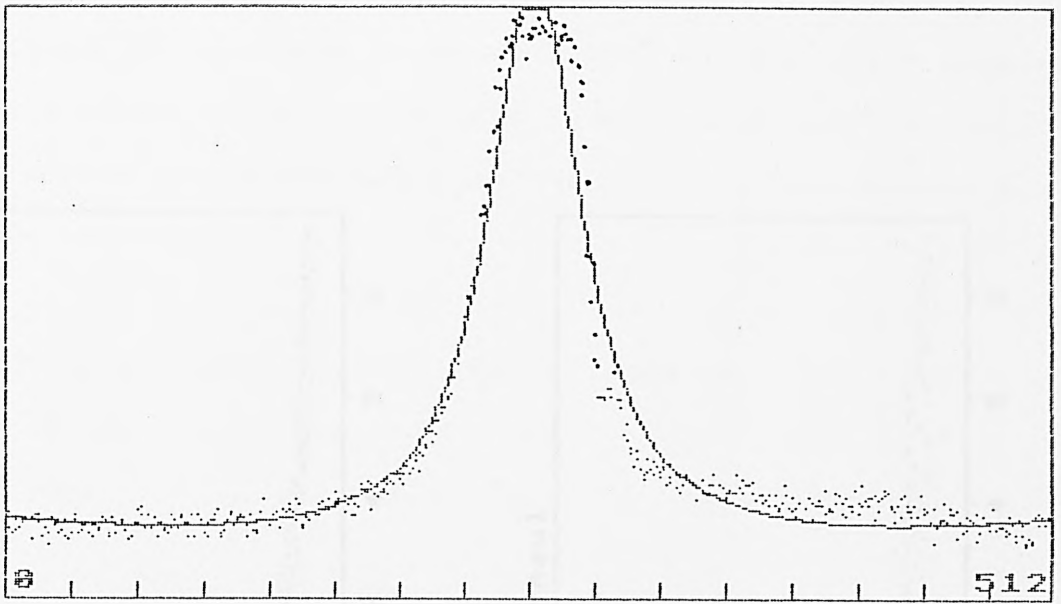


Fig.4.16: Single line fit to calibration spectrum

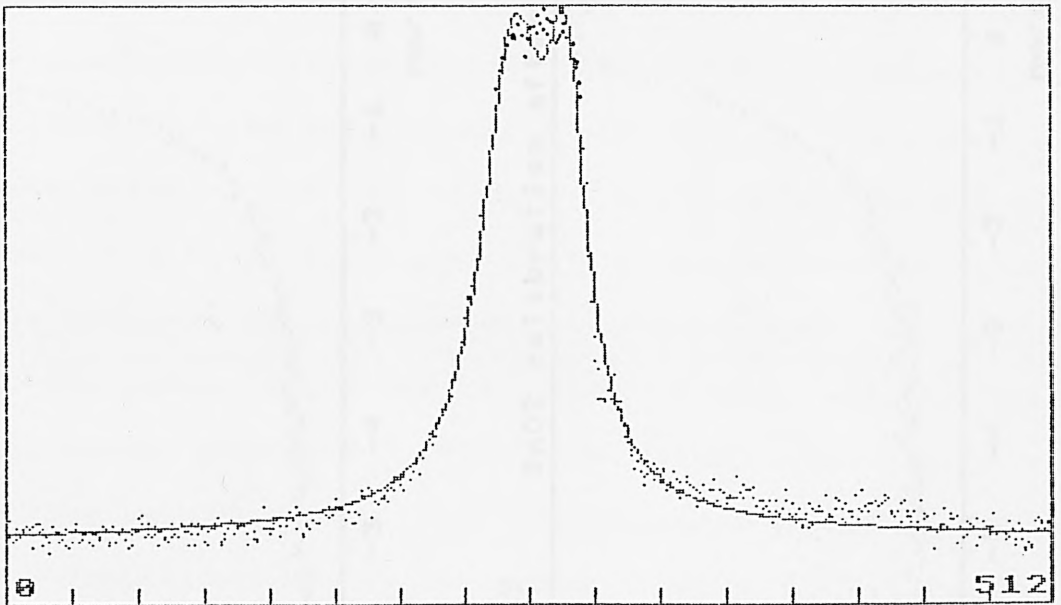


Fig.4.17: Doublet fit to calibration spectrum

Fig.4.18

SnO₂ calibration before detector overhaul

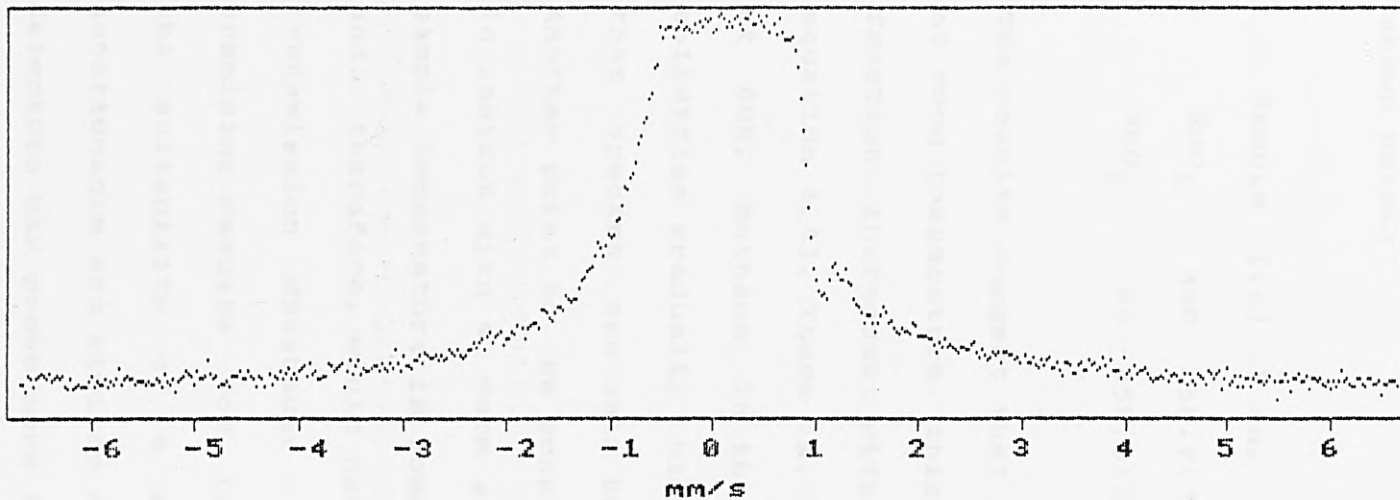
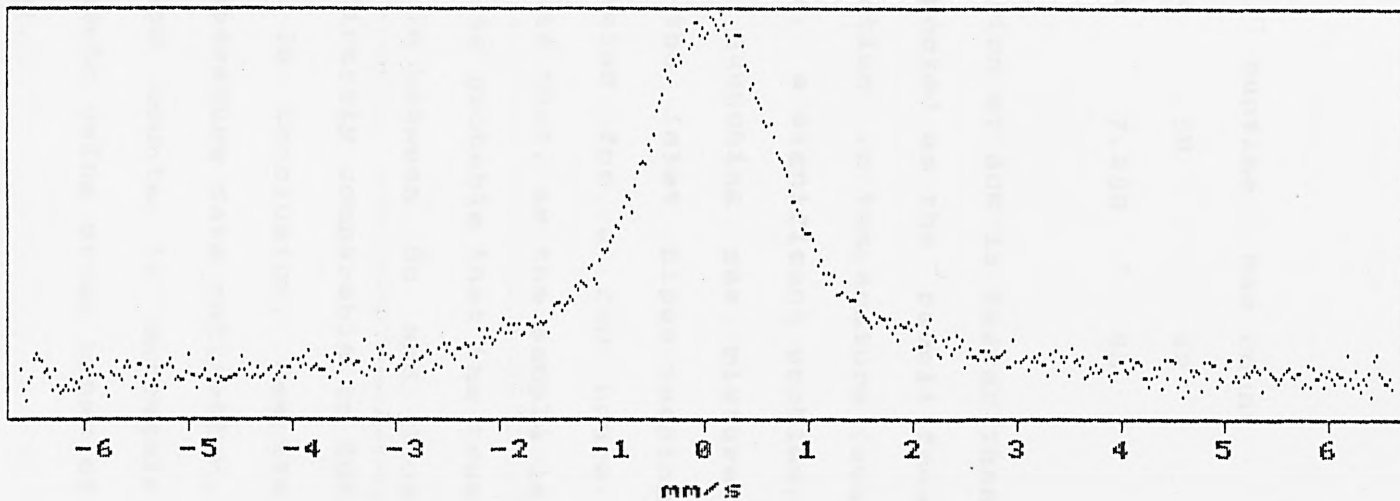


Fig.4.19

SnO₂ calibration after detector overhaul



attached a one inch diameter aluminium rod which dipped into a Dewar flask containing liquid nitrogen. Thermally conducting paste was used at the join. The results are shown below:

Sample	T(K)	δ ch.	%eff.	runtime	Max count
SnO ₂	300	258.7(3)	200	5H	42
SnO ₂	80	258.5(3)	260	7.25H	88

The results suggest that collection at 80K is faster than at room temperature, this is expected as the recoil free fraction increases with reduction in temperature (see equation 4.4). There is, however, a significant problem, at 80K, methane, in the He/Me quenching gas mixture, solidifies gradually blocking the inlet pipes meaning that spectra can only be collected for a few hours. Another point to be considered is that, as the sample is in contact with a warm gas, it is probable that the true sample temperature is somewhere in between 80 and 300K and, therefore, would not be directly comparable to 80K transmission Mössbauer data. In conclusion, despite promising results for low temperature data collection, the suitability of a gas flow counter is extremely questionable and similar experiments using other types of detectors may prove more fruitful.

4.6 A comparison of transmission and conversion electron Mössbauer spectra of normal tin(II) compounds.

The room temperature conversion electron and 80K and

room temperature transmission Mössbauer spectra of several normal tin(II) compounds were collected and the results compared. Samples have been divided into three groups; Sn(II) halides, Sn(II) materials containing chalcogen atoms, and Sn(II) carboxylates. The results from each of these groups are discussed below.

(1) Sn(II) halides

The compounds SnX_2 , where $X = \text{F}, \text{Cl}, \text{Br}, \text{I}$, were examined by CEMS and the results compared with transmission Mössbauer data. The fitted Mössbauer parameters of these materials, together with those of $\text{SnCl}_2 \cdot 2\text{H}_2\text{O}$ are shown in table.4.2. The SnF_2 and SnBr_2 spectra show no significant variation in shift between CEM and transmission modes. The parameters of SnCl_2 in the room temperature transmission spectrum are close to those of $\text{SnCl}_2 \cdot 2\text{H}_2\text{O}$ which suggest the Sn is using its bonding electrons in a similar way. It proved difficult to obtain spectra of SnBr_2 at room temperature. This is due to the relatively high degree of radiation absorption shown by bromine and the small recoil free fraction of SnBr_2 at room temperature. Both in the CEMS and transmission experiments, long collecting times were needed, on fresh samples, in order to obtain some tin (II) information. In SnI_2 , the small recoil free fraction and high degree of radiation absorption, in addition to rapid oxidation made it impossible to collect a CEM spectrum, despite several attempts. An increase in quadrupole splitting observed in the CEM spectra for SnF_2 and $\text{SnCl}_2 \cdot 2\text{H}_2\text{O}$

Table 4.2
 Fitted Mössbauer parameters
 for Sn(II) halides.

Compound	CEM data		R.t. trans. data		80K trans. data		80K Lit. value.		Reference
	§ mm/s	Δ mm/s	§ mm/s	Δ mm/s	§ mm/s	Δ mm/s	§ mm/s	Δ mm/s	
SnF ₂	3.33(3)	1.64(2)	3.38(2)	1.55(2)	3.50(3)	1.76(2)	3.60	1.8	[39]
SnCl ₂	4.21(3)	0.00	3.66(4)	0.83(3)	4.06(1)	0.00	4.07	0.0	[39]
SnBr ₂	3.90(4)	0.00	3.92(7)	0.00	3.90(2)	0.00	3.93	0.0	[39]
SnI ₂	-----	----	3.88(3)	0.00	3.88(2)	0.00	3.85	0.0	[39]
SnCl ₂ .2H ₂ O	3.60(4)	1.62(8)	3.62(3)	1.30(3)	3.63(2)	1.29(1)	3.63	1.21	[40]

indicates an increase in asymmetry at the surfaces of these materials compared to the bulk.

(ii) Sn(II) materials containing chalcogen atoms.

Table 4.3 shows the fitted Mössbauer parameters for some Sn(II) materials containing chalcogen atoms. Blue/black and red tin oxides show no significant variation in shift between CEM and room temperature transmission spectra. A decrease in quadrupole splitting occurs in the CEM spectrum for black SnO, indicating a higher symmetry around tin nuclei at the surface of the material than in the bulk. In red SnO there appears to be no significant difference between the bulk and surface tin environments. The rest of the Sn(II) chalcogenides all show an increase in shift in the CEM spectra indicating an increase in s electron density at the tin nucleus consistent with a reduction in the use of s-electrons in bond formation, but there does not appear to be any accompanying loss of symmetry at the surface. SnSe is present as a singlet in the CEM spectrum, contrary to that found earlier [6] where the spectrum showed an asymmetric doublet which was explained in terms of greater asymmetry about the tin atoms at the surface. The probable explanation for the asymmetry in the earlier reported data could be due to the poorer resolution of the former being collected over only 256 channels plus at the time of collection a weaker source was used.

There is little difference between surface and bulk

Table 4.3
 Fitted Mössbauer parameters
 for Sn(II) materials containing
 chalcogen atoms.

Compound	CEM data		R.t. trans. data		80K trans. data		80K Lit. value.		Reference
	δ mm/s	Δ mm/s	δ mm/s	Δ mm/s	δ mm/s	Δ mm/s	δ mm/s	Δ mm/s	
Black SnO	2.61(1)	1.24(1)	2.62(2)	1.35(1)	2.59(5)	1.46(5)	2.71	1.4	[39]
Red SnO	2.59(3)	1.99(2)	2.62(2)	1.97(1)	2.57(3)	2.14(3)	2.60	2.2	[39]
SnS	3.31(2)	0.90(1)	3.20(3)	0.92(3)	3.38(1)	1.09(1)	3.16	0.8	[39]
SnSe	3.51(3)	0.00	3.31(5)	0.00	3.34(9)	0.00	3.30	0.0	[39]
SnTe	3.50(1)	0.00	3.37(2)	0.00	3.51(1)	0.00	3.21	0.0	[39]
SnSO ₄	3.86(4)	0.93(3)	3.84(1)	0.93(1)	3.94(2)	1.03(1)	3.90	1.0	[39]
SnHPO ₄	3.70(2)	1.57(2)	3.61(1)	1.40(1)	3.70(2)	1.76(2)	3.25	1.74	[40]

measurements for SnSO_4 . In contrast, SnHPO_4 shows an increase in shift and quadrupole splitting in the CEM spectrum. The results indicate a different environment for tin atoms located at the surface of the material, with a greater asymmetry in s-electron density around the tin nuclei and a decrease in covalency in bonds to tin atoms located at the surface.

(iii) Sn(II) carboxylates.

Several Sn(II) carboxylates were examined in the present study. Fitted Mössbauer parameters for the Sn(II) carboxylates studied are shown in table 4.4. Sn(II) formate and Sn(II) malonate show no significant differences between CEM and room temperature transmission spectra. The remaining Sn(II) carboxylates all show increases in shift in the surface technique. In general this increase in shift is accompanied by a significant increase in quadrupole splitting except in the spectrum of Sn(II) succinate. These observations may be explained in terms of a weakening of the Sn-O bonds and subsequent breakdown at the surface of the polymeric networks that exist in the structures of these materials.

Comparison of room temperature and 80K transmission reveals two interesting trends. Quadrupole splitting is a temperature dependent quantity (see section 4.1, equation.4.8) and increases with decreasing temperature. In general this feature is apparent in the materials studied, although in a small number of samples there was

Table 4.4

Fitted Mössbauer parameters

for some Sn(II)carboxylates.

Compound	CEM data		R.t. trans. data		80K trans. data		80K Lit. value.		Reference
	δ mm/s	Δ mm/s	δ mm/s	Δ mm/s	δ mm/s	Δ mm/s	δ mm/s	Δ mm/s	
Sn formate	3.12(8)	1.75(7)	3.17(2)	1.72(2)	3.26(2)	1.75(1)	3.10	1.56	[41]
Sn acetate	3.40(8)	1.86(7)	3.20(5)	1.45(5)	3.34(1)	1.80(1)	3.26	1.77	[41]
Sn oxalate	3.60(4)	1.62(4)	3.46(2)	1.50(1)	3.56(2)	1.55(2)	3.75	1.52	[41]
Sn malonate	3.46(5)	1.67(4)	3.39(2)	1.65(1)	3.46(2)	1.76(1)			
Sn succinate	3.33(3)	1.91(3)	3.25(3)	1.89(2)	3.28(2)	1.94(1)			
Sn maleate	3.46(7)	1.78(7)	3.22(2)	1.45(2)	3.37(2)	1.69(1)			

no significant difference between room temperature and 80K Δ values. Little variation in shift with temperature is observed in the two tin oxides, SnBr_2 , SnI_2 and Sn(II)succinate , the remaining materials, however, all show an increase in shift at 80K. This suggests that there is an increase in s-electron density at the tin nuclei and consequently a weakening of the Sn-L bonds with decrease in temperature.

4.7 Applications of ^{119}Sn CEMS to Sn containing systems.

Several applications of ^{119}Sn CEMS to Sn containing systems were undertaken in the present work. Two types of surface reactions were outlined by Grimes [6] viz: those reactions at tin containing matrix surfaces and those reactions of tin compounds on matrix surfaces. Results from both of these areas are now described.

(i) An examination of tinplate passivation and anodic oxide, coatings.

During tinplate manufacture surface coatings are applied to ensure long term stability to oxidation. These passivation films, directly affect the surface properties of the tinplate; in particular, rust resistance, corrosion reactions, laquer wetting, adhesion and welding characteristics.

One of the conclusions reached, using other techniques [22,23,24,25], is that the film consists mainly of

chromium(III)oxide with a high degree of hydration in the outer layers. The film also consists of Cr metal and tin oxide. In a recent study involving X-ray photoelectron spectroscopy (X.P.S.) [25], the tin oxygen ratio, in samples where Cr had been extracted, indicated the presence of SnO and it was suggested that CEMS would be able to verify this.

The samples, used in this study, were commercially produced electrolytic tinplate with a nominal coating mass of 2.8g/m^2 . Results on six samples are discussed:

- a. As-received tinplate.
- b. Fully-extracted tinplate.
- c. Alkaline extracted tinplate.
- d. Stripped alloy layer.
- e. 'Detinned' tinplate.
- f. '300' passivated tinplate.

Two types of commercially available tinplates were examined. The as-received plate had undergone the conventional cathodic dichromate passivation, whilst a second plate had the '300' passivation treatment. Two chromium extracted plates had been placed in boiling NaOH in order to dissolve chromium from the surface. In addition the fully-extracted plate, had previously been anodically oxidised in a phosphate buffer electrolyte, to reduce the Cr metal concentration in the film by oxidation to Cr(VI). In order to further examine the alloy layer, two samples were prepared. In the first, the

alloy layer had been removed from tinned steel and in the second the surface of the tinplate had been stripped of tin metal using an acid wash.

A sample of anodised tinned steel was also examined. Anodic oxide coatings on tinned steel are used in baking ware to produce heat absorbing scratch resistant and adherent surfaces. By modifying the anodising solution a black matt tin oxide deposit is achieved [26], which may be of use in the construction of electronic machine frames.

The CEMS spectra of the 6 samples are shown in figs.4.20-25 and the fitted results in table 4.5. All the samples showed similar spectra, being fitted to 8 lines with two singlets at ca. 0.0 and 2.7 mm/s, corresponding to SnO_2 and Sn metal respectively, and a magnetic sextet resulting from the alloy FeSn_2 . The field at the Sn nucleus in the alloy is believed to result from the Sn atoms being particularly strongly associated with a ferromagnetic row of iron atoms [27]. Difficulty was experienced in fitting the two inner lines of the sextet as these were coincident with the tin metal line; thus the errors in the positions of these lines are greater than those of the other lines. A computer simulation of the component lines, based on the fitted results of the as-received spectrum, is shown in fig.4.26 and reflects the idealised section through tinplate shown in fig.4.27.

The only significantly different spectrum is that of the

Table 4.5.

CEM parameters for tinplate samples.

	δ_1 mm/s	δ_2 mm/s	Δ_2 mm/s	H_{eff} KOe	δ_3 mm/s
As-recieved	-0.17(3)	2.50(7)	0.07(7)	147.7	2.69(1)
Fully-extracted	-0.15(3)	2.42(12)	0.11(12)	146.7	2.68(1)
Alkali extracted	-0.13(4)	2.46(16)	0.08(16)	154.3	2.61(1)
Stripped alloy	-0.15(4)	2.34(6)	0.11(6)	157.8	2.62(1)
Detinned alloy	-0.13(3)	2.41(7)	0.09(7)	149.6	2.79(4)
300 passivated	-0.14(2)	2.45(4)	0.06(4)	148.8	2.73(1)

Table 4.6

CEM parameters for anodised
tinned steel.

	δ_1 mm/s	Δ_1 mm/s	δ_2 mm/s	δ_3 mm/s
Anodised steel	0.03(2)	0.70(2)	0.97(5)	2.63(9)

Fig.4.20

'As-received' tinplate

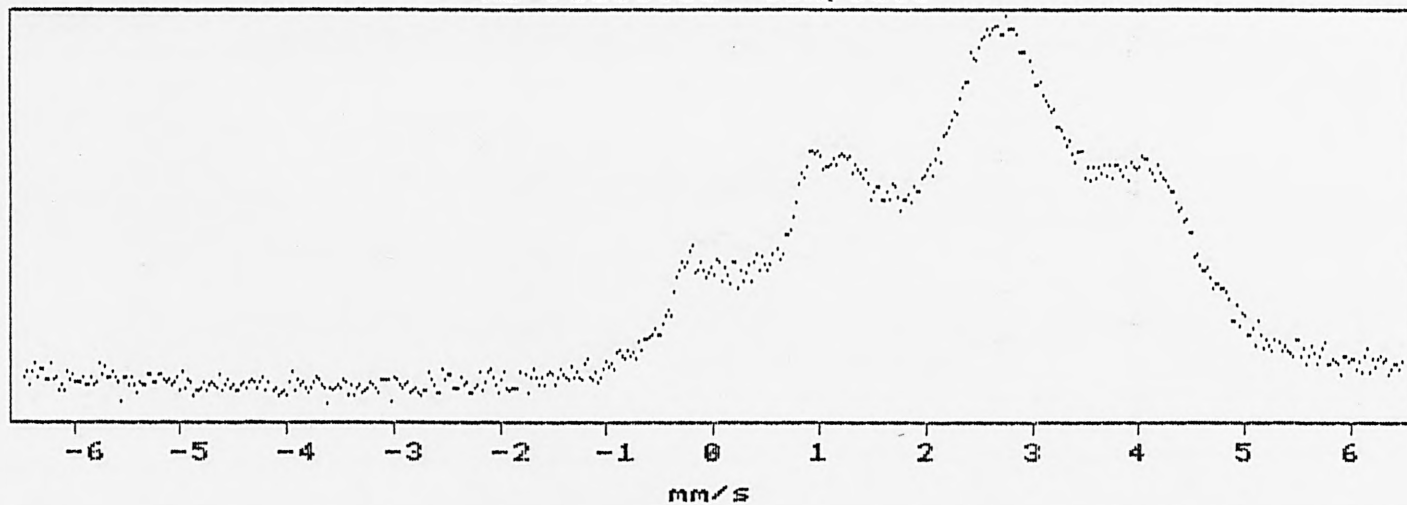


Fig.4.21

'300' passivated tinplate

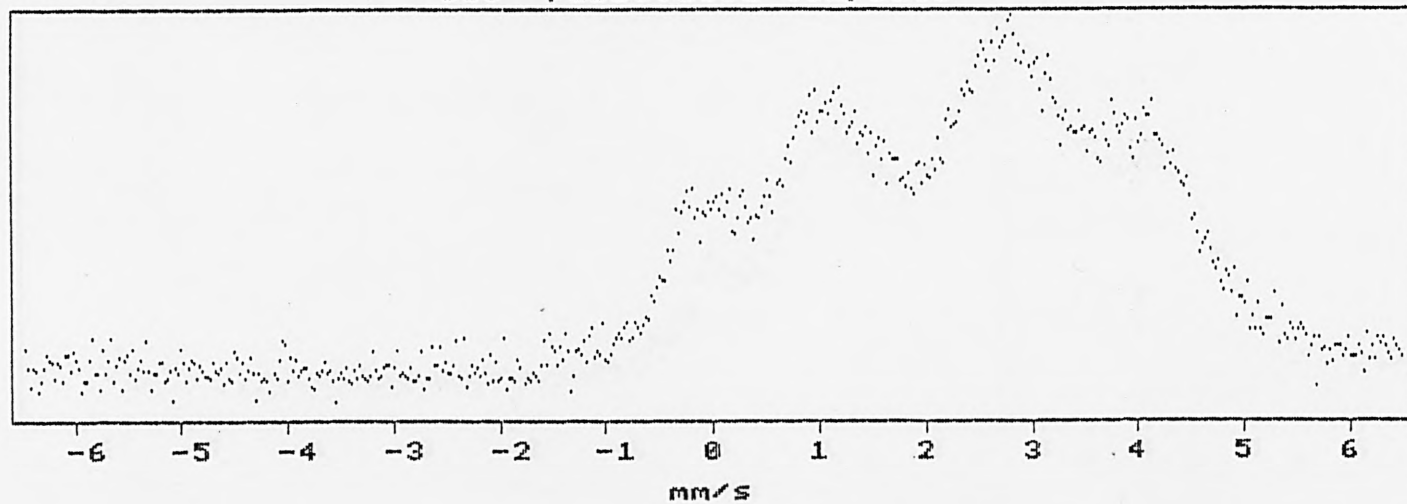


Fig.4.22

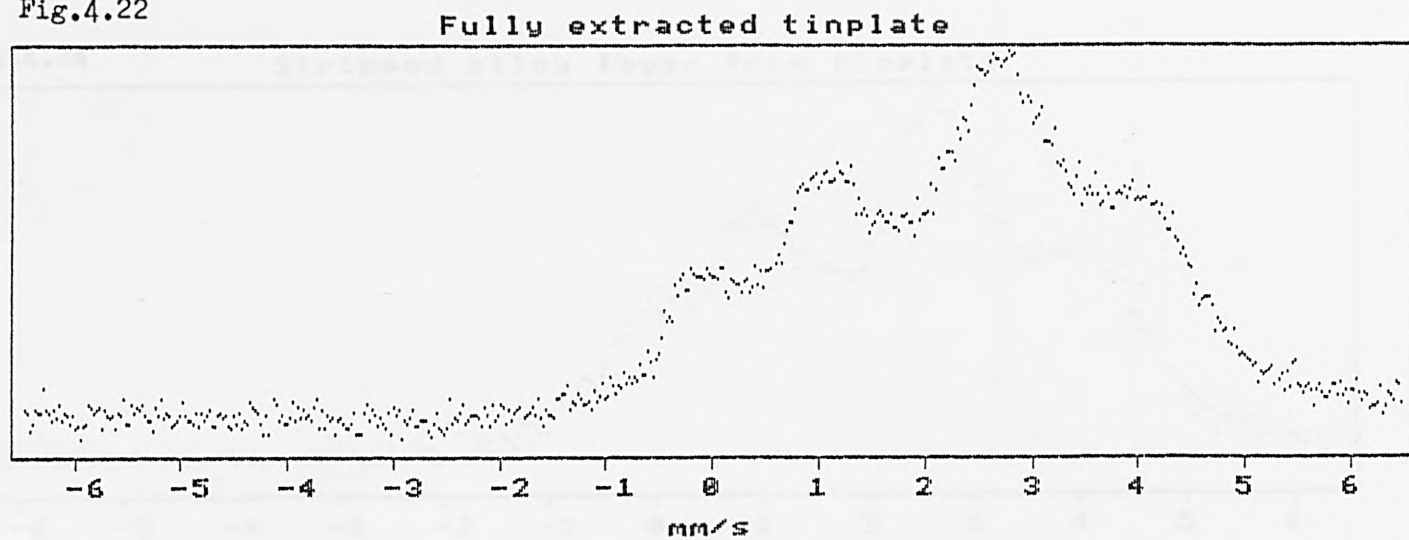


Fig.4.23

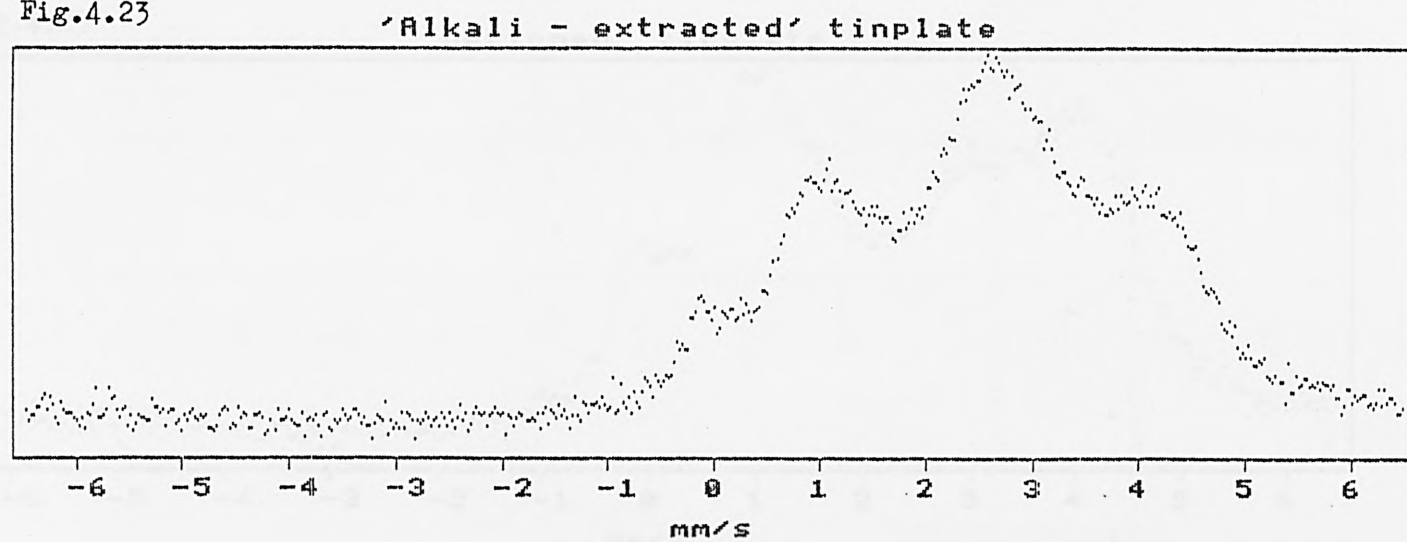


Fig.4.24

Stripped alloy layer from tinplate

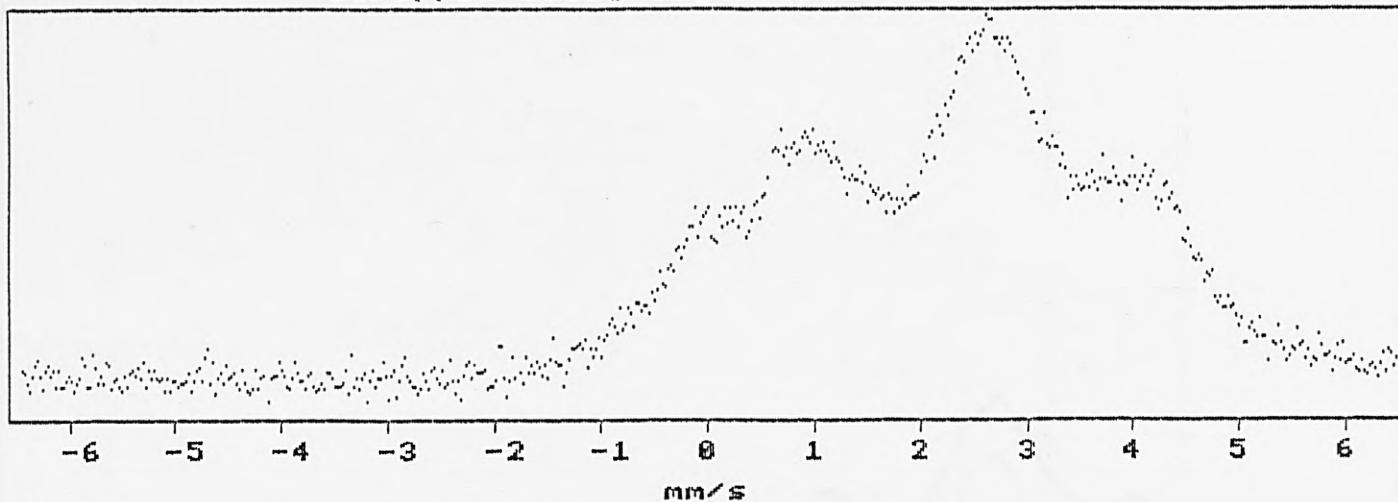
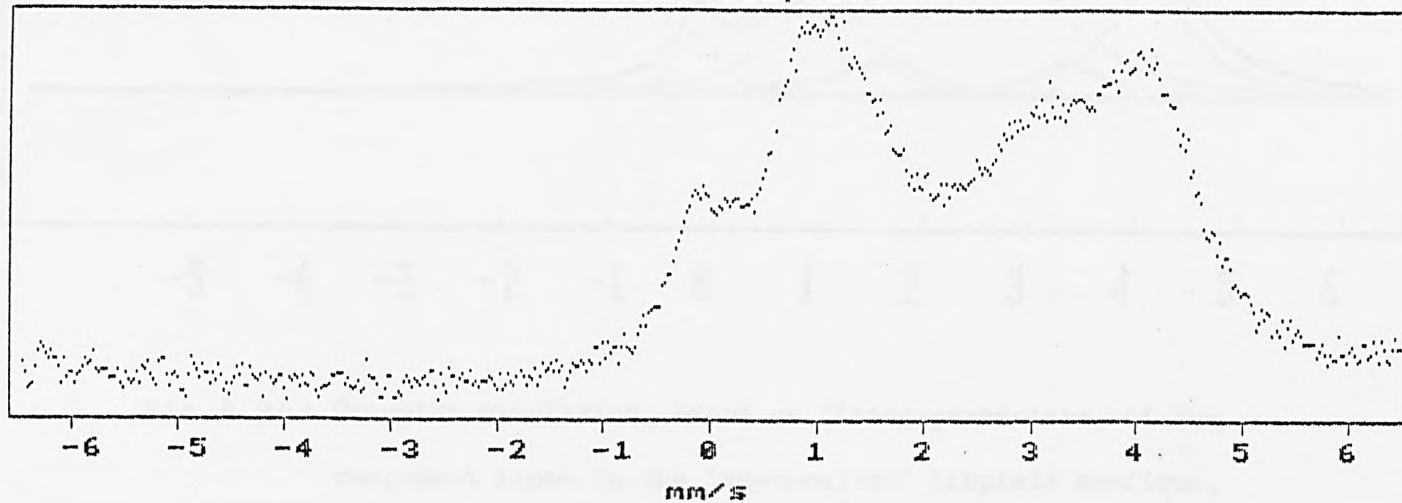


Fig.4.25

'Detinned' tinplate



As Recieved Tin Plate

% DIP

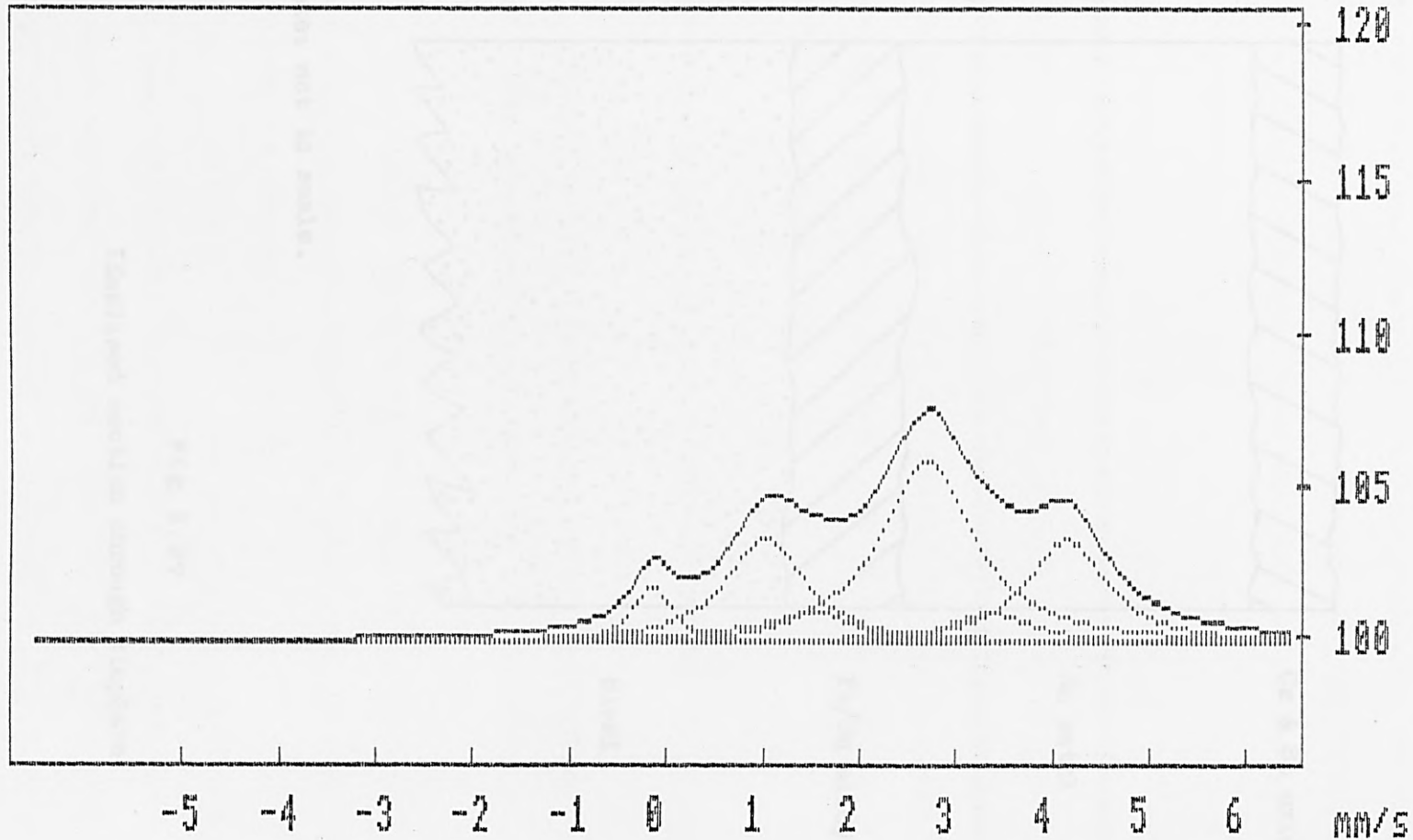
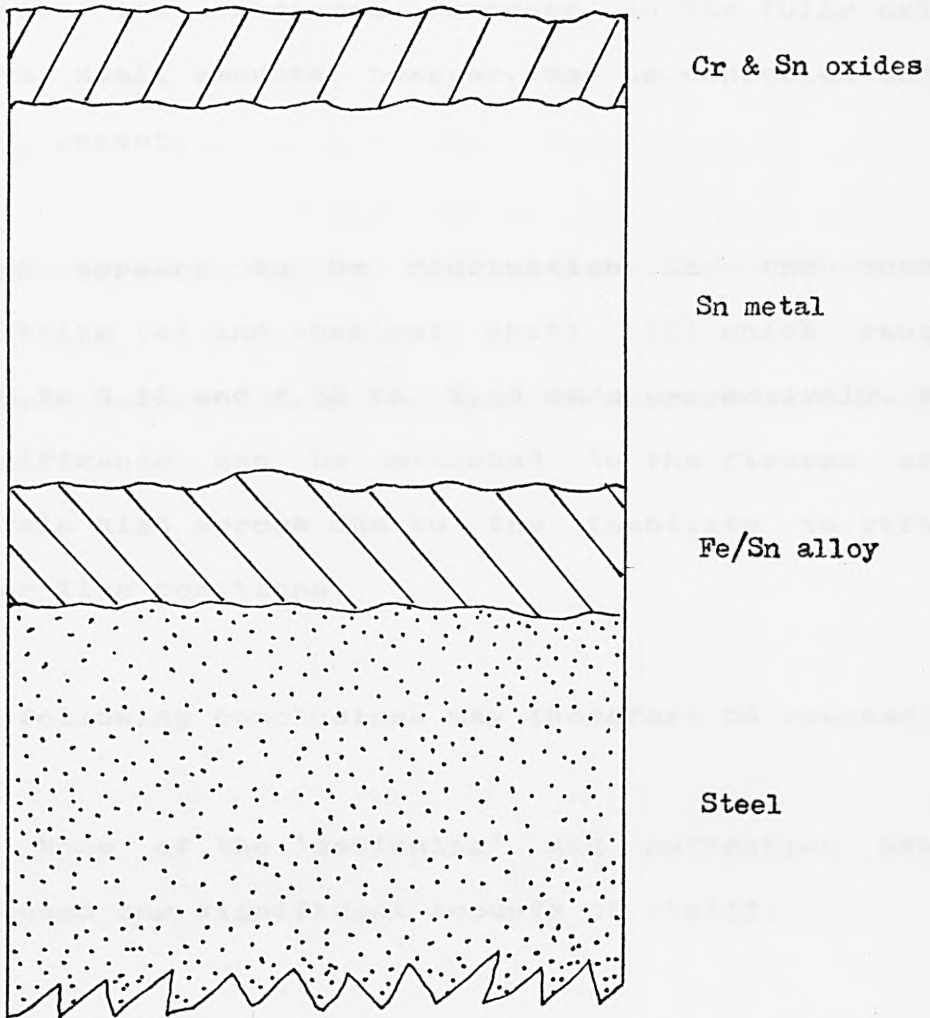


Fig.4.26: Computer simulation, based on fitted parameters, of the component lines in the 'as-received' tinplate spectrum.



Note: not to scale.

Fig.4.27

Idealised section through tinplate

'detinned' plate. The detinning is incomplete as Sn is certainly still present. The Sn metal peak is greatly reduced and the sextet is hence more prominent, however there are still high errors in the inner line positions. No evidence was seen of Sn(II)O, in any of the samples, despite its predicted presence in the fully-extracted plate. Small amounts, however, may be concealed under the FeSn₂ sextet.

There appears to be fluctuation in the quadrupole splitting (Δ) and chemical shift (δ) which range from 0.06 to 0.11 and 2.34 to 2.50 mm/s respectively. No real significance can be attached to the figures as they contain high errors due to the inability to refine the inner line positions.

The following conclusions may therefore be reached:

1. None of the 'detinning' and extraction processes produced any significant amounts of tin(II).
2. 'Detinning' with acid reduces Sn metal at the surface but SnO₂ is seen, suggesting that oxidation of the new surface is rapid.
3. No significant differences exist between the tin phases present in the as-received tinplate and the '300' passivated sample.

The CEMS spectrum of anodised tinned steel is shown in

fig.4.28 and the fitted results in table 4.6. The spectrum shows a broad SnO_2 peak centred at 0.03 and a second line due to Sn metal at 2.63 mm/s. A third line is also present at ca. 1.0 mm/s, and was originally attributed to a phase arising from the phosphate electrolyte used in the anodising process. On repeating this spectrum (see fig.4.29) after the vibrator had been overhauled (see sec.4.5) the broadness of the SnO_2 peak was eliminated and the line at ca. 1.0 mm/s disappeared. These effects must, therefore, be attributed to instrumentation factors and are not genuine surface features. The fitted parameters for the second spectrum are as follows:

δ_1 mm/s	δ_2 mm/s
0.05(1)	3.21(9)

Any suggestion that the black colour of the anodised coating could be due to tin(II)oxide cannot be correct, as no peaks were found in the tin(II) region of the spectrum.

(ii) An examination of tin oxide films on glass and quartz.

The uses of SnO_2 films are varied [28,29], and include use in the bottle industry for glass strengthening and as transparent electrodes in the electronics industry.

Several samples of commercially produced tin oxide films

Fig.4.28

Anodised tinned steel

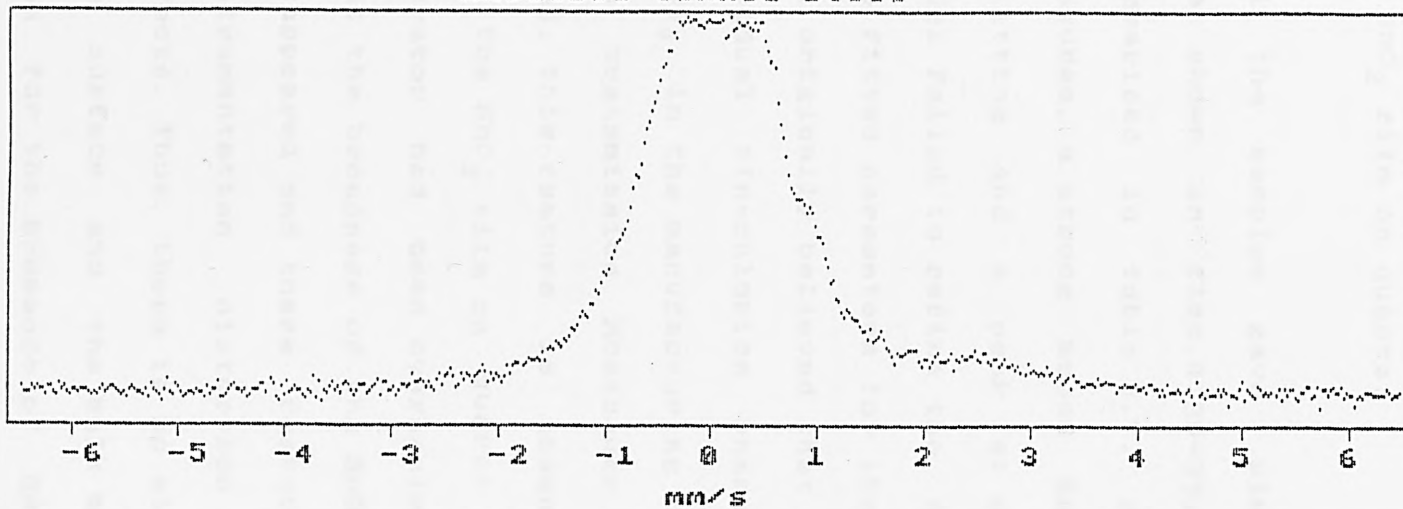
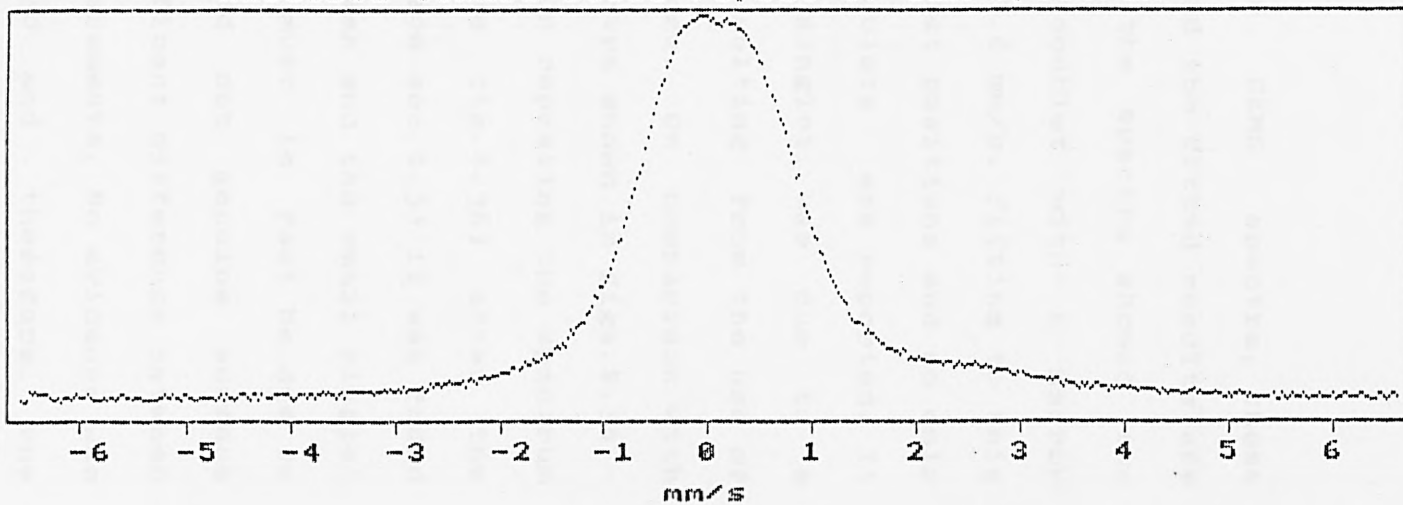


Fig.4.29

Anodised tinned steel repeat of CEM spectrum



on glass and quartz were examined, in the present study including:

- a. 500 Ω/cm^2 film on glass.
- b. 200 Ω/cm^2 black film on glass.
- c. 50 Ω/cm^2 film on glass.
- d. SnO_2 film on quartz.

All the samples gave similar CEMS spectra, these are shown in figs.4.30-33, and the fitted results are summarised in table 4.7. All the spectra showed two features, a strong broad SnO_2 doublet with a narrow splitting and a peak at ca. 0.8 mm/s. Fitting to this model failed to refine the singlet positions and so only the fitted parameters for the doublets are reported. It was originally believed that the singlet, was due to a residual tin-chloride phase resulting from the use of SnCl_4 in the manufacturing process. On comparison with the transmission Mössbauer spectra shown in figs.4.34 - 4.35, this feature is absent. On repeating the spectrum for the SnO_2 film on quartz (see fig.4.36) after the vibrator had been overhauled (see sec.4.5) it was found that the broadness of the SnO_2 peak and the small singlet disappeared and these features must in fact be due to instrumentation distortion and not genuine surface effects. Thus, there is no significant difference between the surface and the bulk measurements. No evidence was seen for the presence of Sn(II)O and therefore, the black colour of the 200 Ω/cm^2 film cannot be due to this phase.

Table 4.7a.

SnO₂ films on glass and quartz

Fitted CEM data.

Sample	δ (mm/s)	Δ (mm/s)	Γ (mm/s)
500 Ohm	0.04 +- 0.02	0.75 +- 0.02	0.72 +- 0.02
200 Ohm	0.08 +- 0.01	0.66 +- 0.01	0.90 +- 0.01
50 Ohm	0.08 +- 0.02	0.67 +- 0.02	0.78 +- 0.03
Quartz	0.04 +- 0.02	0.62 +- 0.02	0.78 +- 0.02

Table 4.7b.

SnO₂ films on glass and quartz

Fitted transmission Mössbauer data

Sample	δ (mm/s)	Γ (mm/s)
500 Ohm	-0.05 +- 0.02	0.65 +- 0.04
200 Ohm	-0.01 +- 0.01	0.70 +- 0.01
Quartz	-0.05 +- 0.02	0.67 +- 0.02

Fig. 4.30 500 Ω/cm^2 SnO₂ film on glass CEM spectrum

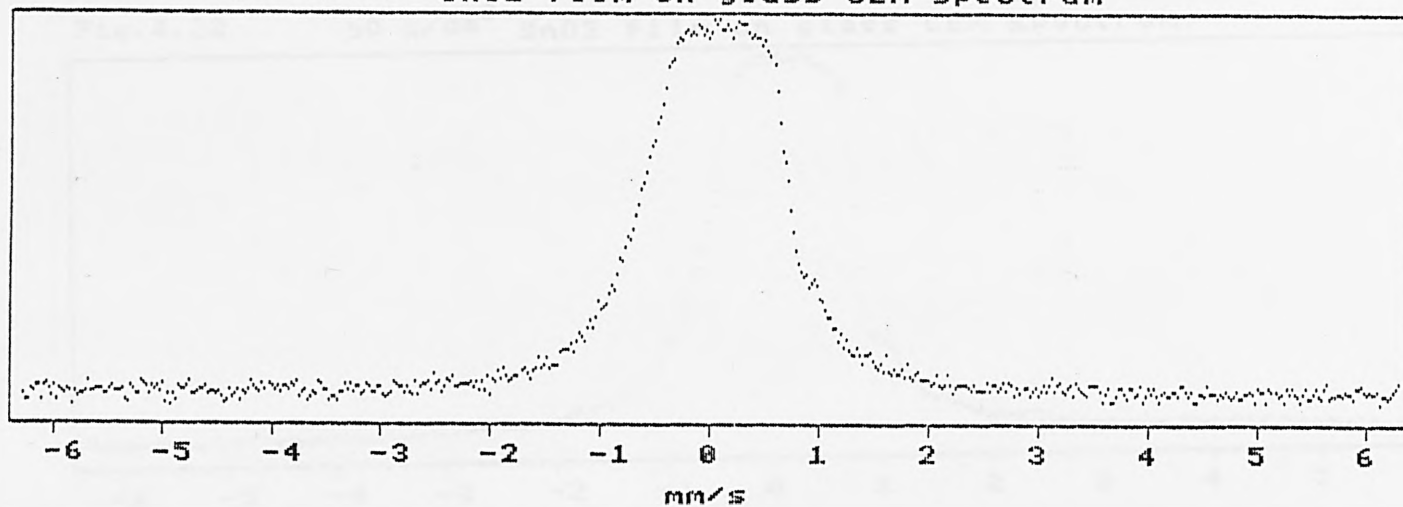


Fig. 4.31 200 Ω/cm^2 SnO₂ film on glass CEM spectrum

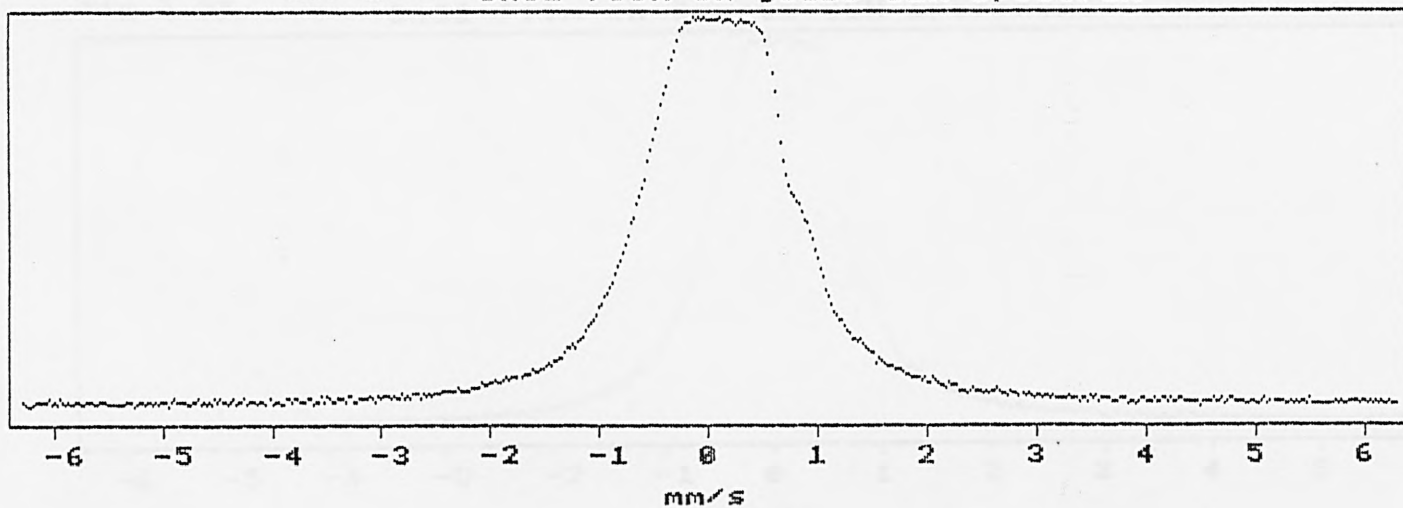


Fig.4.32 $50 \Omega/\text{cm}^2$ SnO₂ film on glass CEM spectrum.

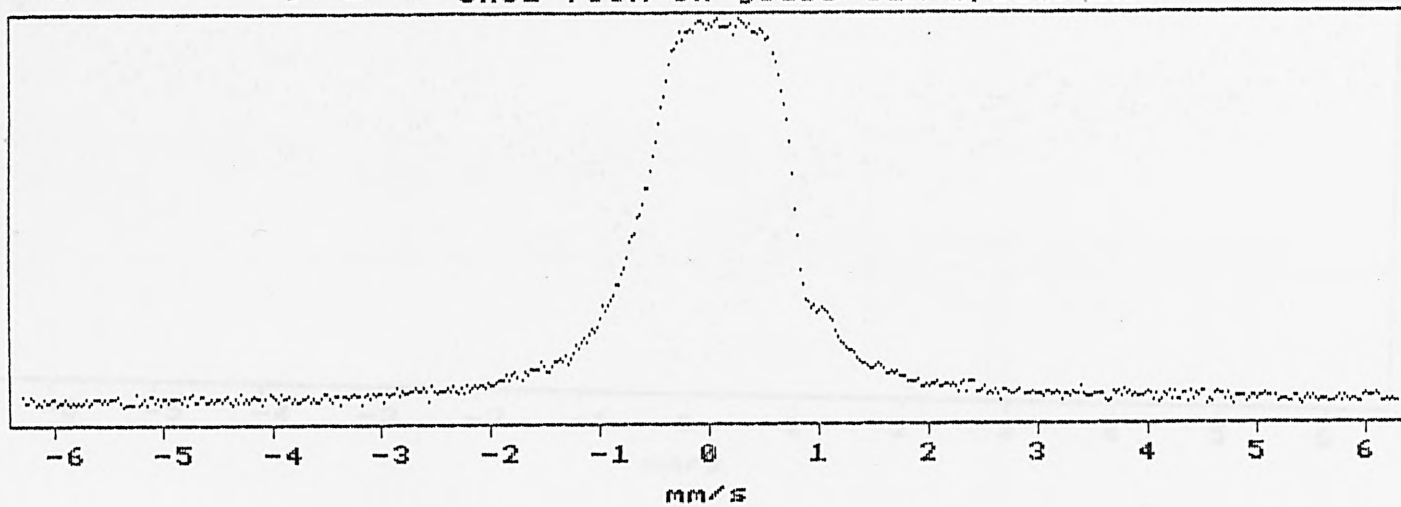


Fig.4.33 SnO₂ film on Quartz CEM spectrum.

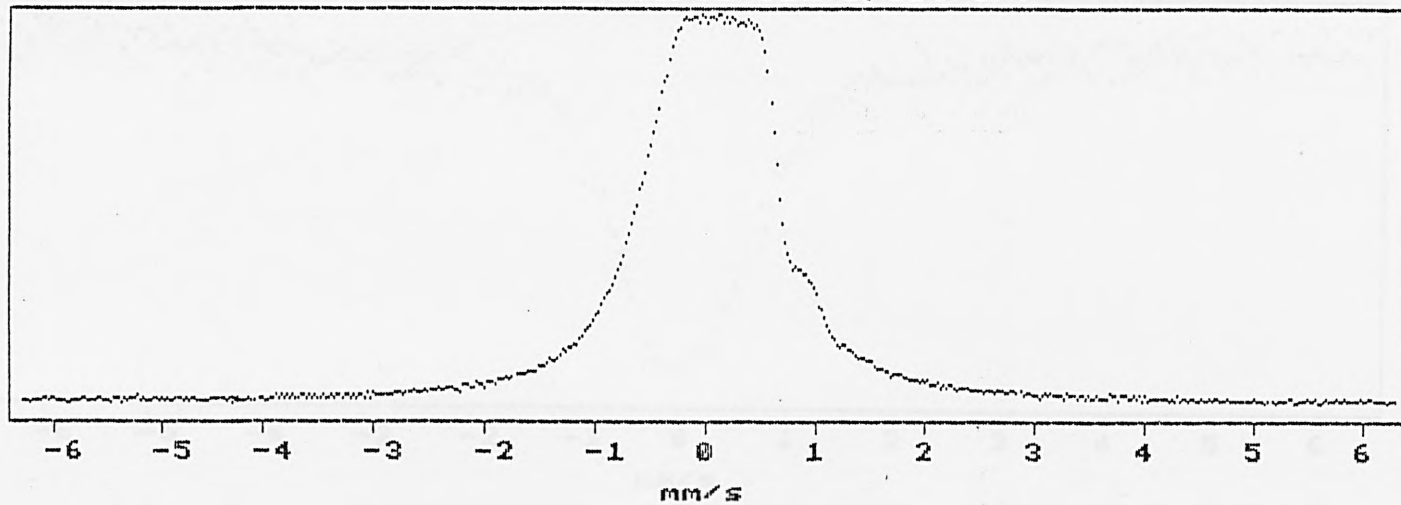


Fig.4.34

$500 \Omega/\text{cm}^2$ SnO₂ film on glass r.t.trans. spectrum

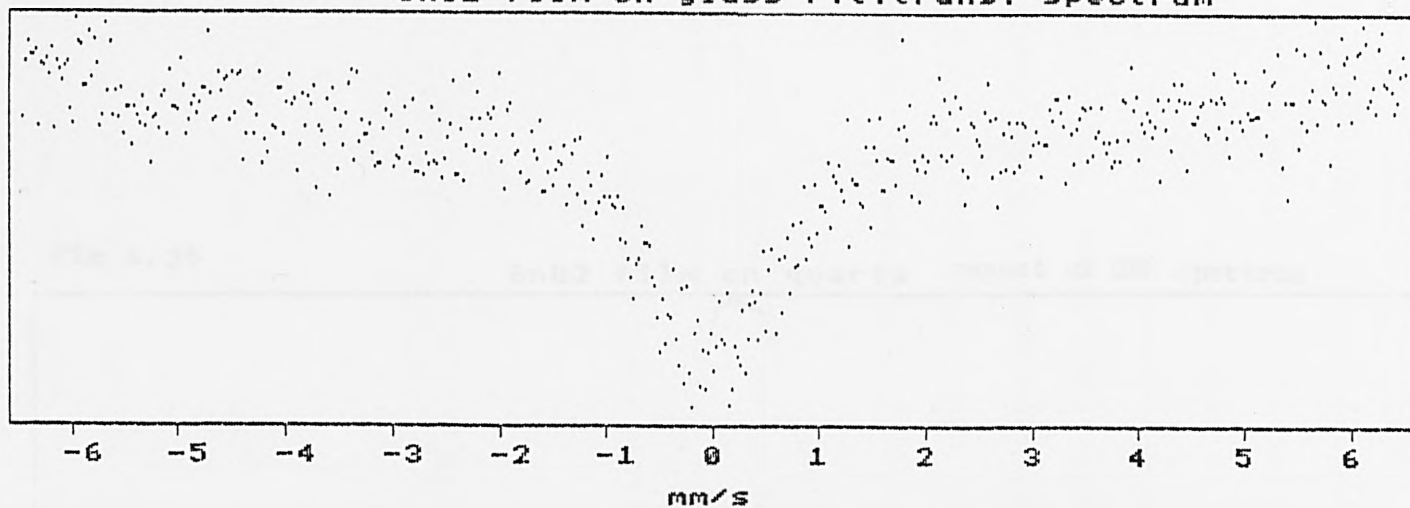


Fig.4.35

$200 \Omega/\text{cm}^2$ SnO₂ film on glass r.t.trans spectrum

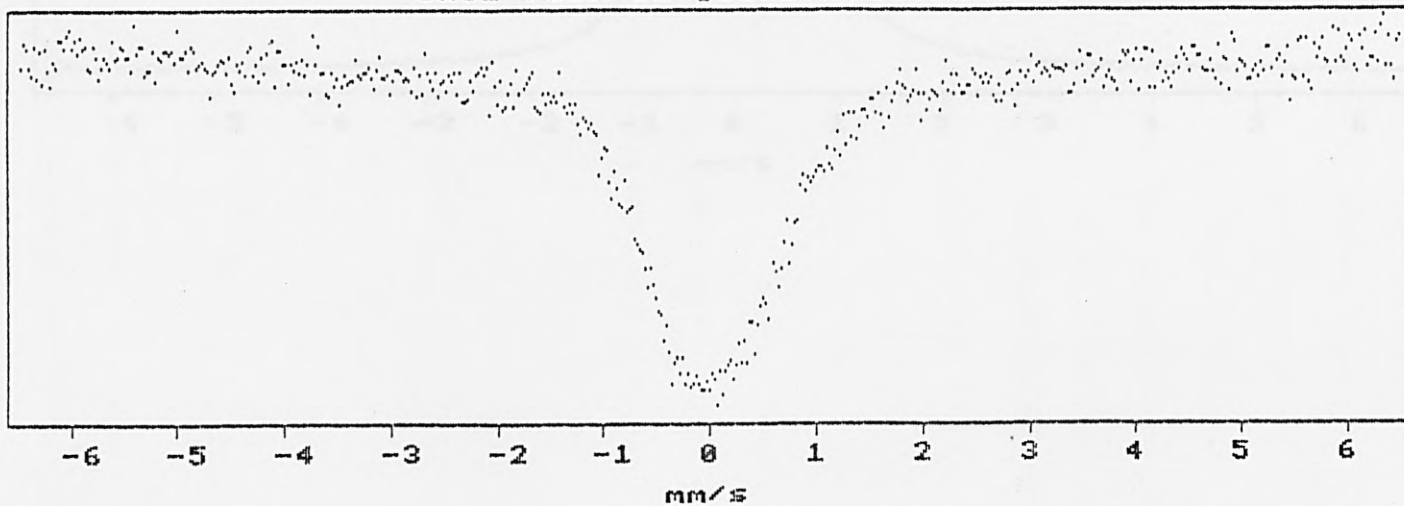
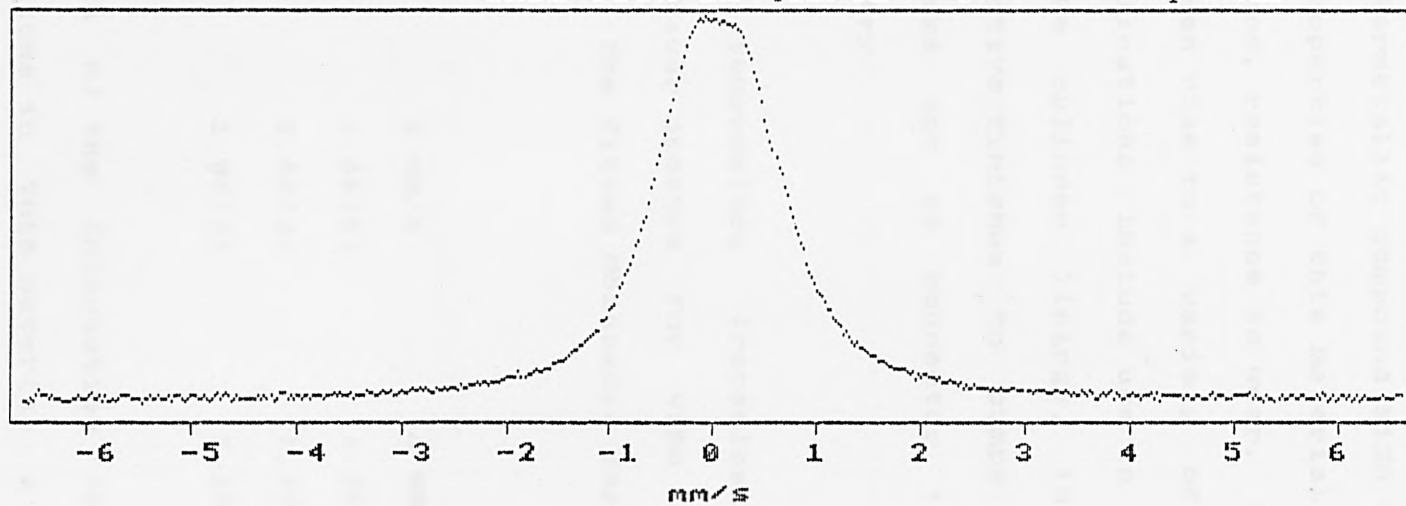


Fig.4.36

SnO₂ film on quartz repeat of CEM spectrum



(iii) An examination of NiSn alloy.

A study of the intermetallic compound NiSn was undertaken using CEMS. The properties of this material which include corrosion resistance, resistance to wear, and attractive finishing have given rise to a variety of applications [30]. These applications include use in the automobile industry as brake cylinder linings, in the brewing industry as attractive finishes to pumps, as heavy duty electrical fittings and as connector tags in the electronics industry.

The CEM, room temperature transmission and 80K transmission Mössbauer spectra for NiSn shavings are shown in fig.4.37. The fitted Mössbauer parameters are as follows:

Technique	δ mm/s	Δ mm/s
CEMS	1.84(4)	1.26(2)
R.t. trans.	1.86(2)	1.20(1)
80K trans.	1.92(2)	1.18(1)

As a consequence of the interaction between Sn and neighbouring Ni atoms in this material, a magnetic field occurs at the Sn nucleus and the resulting Mössbauer spectrum is magnetically split with a shift of 1.84(4) mm/s this compares with the figure of 1.85(2) mm/s in the CEM spectrum found by Leidheiser et al. [31]. The spectrum approximates to a doublet and was fitted as such, the

Fig.4.37a

NiSn CEM spectrum

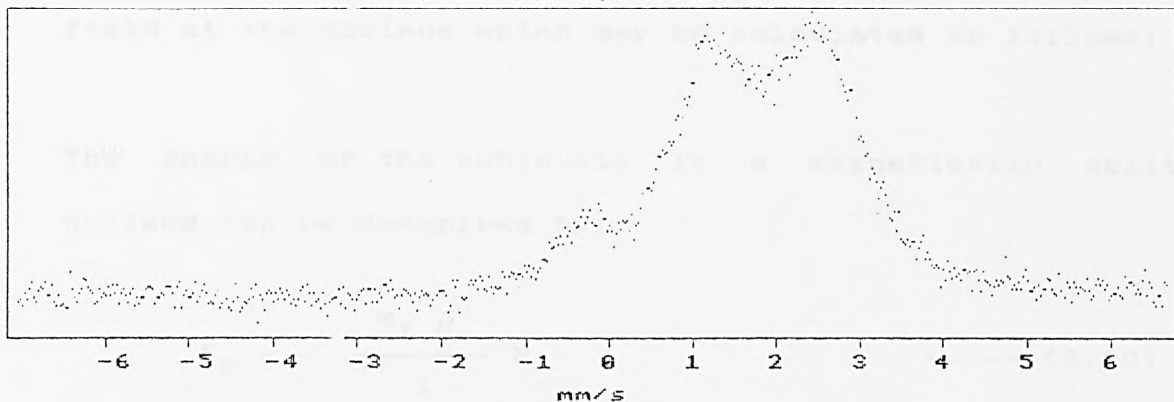


Fig.4.37b

NiSn r.t. transmission spectrum

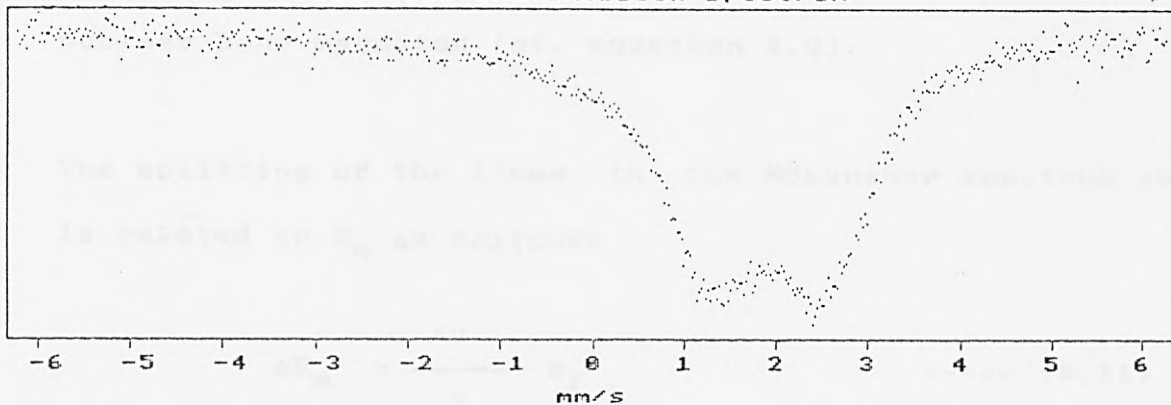
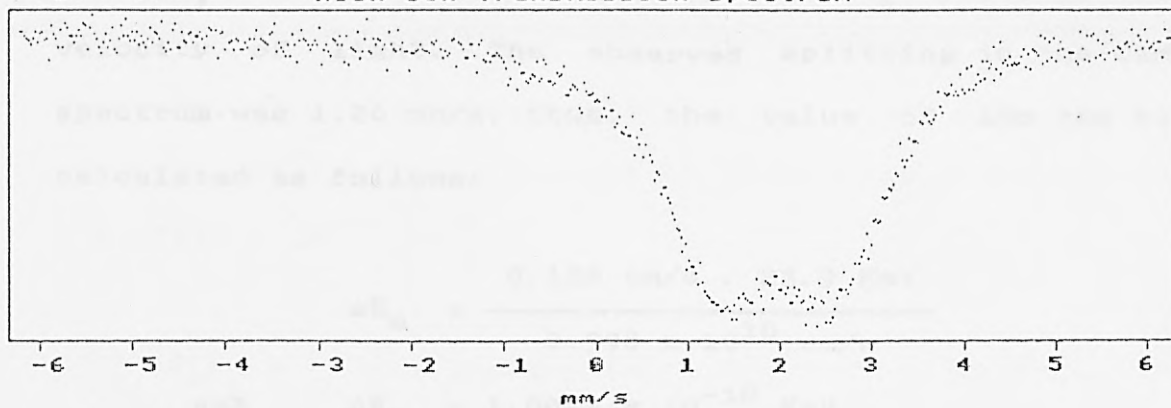


Fig.4.37c

NiSn 80K Transmission spectrum



resulting splitting is proportional to the hyperfine field at the nucleus which may be calculated as follows:

The energy of the sublevels in a magnetically split nucleus may be described by:

$$E_m = - \frac{m_I \mu}{I} H \quad \text{----- (4.10)}$$

Where m_I is the magnetic quantum number, I is the nuclear spin, H is the effective magnetic field and μ is the nuclear Bohr magneton (cf. equation 4.9).

The splitting of the lines in the Mössbauer spectrum Δv is related to E_m as follows:

$$\Delta E_m = \frac{\Delta v}{c} E_\gamma \quad \text{----- (4.11)}$$

Where E_γ is the energy of the gamma ray and c is the velocity of light. The observed splitting in the CEM spectrum was 1.26 mm/s, thus, the value of ΔE_m can be calculated as follows:

$$\begin{aligned} \Delta E_m &= \frac{0.126 \text{ cm/s} \cdot 23.9 \text{ KeV}}{2.998 \times 10^{10} \text{ cm/s}} \\ \Rightarrow \Delta E_m &= 1.0045 \times 10^{-10} \text{ KeV} \end{aligned}$$

Converting to Joules

$$\Delta E_m = 1.6093 \times 10^{-26} \text{ J}$$

Recalling equation 4.10:

$$E_m = - \frac{m_I \mu}{I} H$$

$$\Delta E_m = \left(- \frac{m_I \mu}{I} H \right)_{ex} - \left(- \frac{m_I \mu}{I} H \right)_{gs}$$

$$\Delta E_m = H \left(\left(- \frac{m_I \mu}{I} \right)_{ex} + \left(\frac{m_I \mu}{I} \right)_{gs} \right)$$

Now, the largest transition is between the $m_I = -3/2 \rightarrow m_I = -1/2$ sublevels of the excited ($I = 3/2$) and ground ($I = 1/2$) states respectively.

Thus,

$$\Delta E_m = H \left(\left(- \frac{-3/2 \mu}{3/2} \right)_{ex} + \left(\frac{-1/2 \mu}{1/2} \right)_{gs} \right)$$

$$\Rightarrow \Delta E_m = H (\mu_{ex} - \mu_{gs})$$

Now, the nuclear magnetic moments of the ground and excited states are -1.041 and $+0.67$ nm respectively ($1\text{nm} = 5.04929 \times 10^{-27} \text{JT}^{-1}$).

$$\Delta E_m = H (5.04929 \times 10^{-27} \text{JT}^{-1}) (0.67 + 1.041)$$

$$\Rightarrow \Delta E_m = H (8.6393 \times 10^{-27})$$

$$\Rightarrow H = \frac{\Delta E_m}{8.6393 \times 10^{-27}}$$

Substituting:

$$H = \frac{1.6093 \times 10^{-26} \text{ J}}{8.6393 \times 10^{-27} \text{ JT}^{-1}}$$

$$\Rightarrow H = 1.86 \text{ T}$$

Converting into KG ($T = 1 \times 10^4 \text{ G}$).

$$H = 18.6 \text{ KG}$$

In a similar way the effective fields in the other spectra may be calculated and the results are as follows:

Technique	H_{eff} KG
CEMS	18.6
R.t. trans.	17.7
80K trans.	17.4

These effective fields compare to the value of 8.00 obtained by Leidheiser et. al. [31], in a room temperature transmission experiment but the line splitting observed was considerably less than that in the present study.

The shift of NiSn increases slightly at reduced temperature. this may be explained by a localisation of electrons at lower temperatures in the metallic bonding situation.

(iv) An examination of the effects of air and light on $\text{CsSn}_3\text{Br}_{1.5}\text{F}_{5.5}$ using CEMS.

The complex $\text{CsSn}_3\text{Br}_{1.5}\text{F}_{5.5}$ undergoes a colour change when stored in atmospheric conditions. On initial preparation white crystalline needles are formed which eventually darken even when stored under nitrogen. A study was undertaken in which a sample of $\text{CsSn}_3\text{Br}_{1.5}\text{F}_{5.5}$ was divided into several parts which were then stored under various conditions, the results of which are now reported.

$\text{CsSn}_3\text{Br}_{1.5}\text{F}_{5.5}$ was prepared as described in section 2.3. The crystals were dried over silica gel and divided into several samples which were stored as follows:

- (a) In darkness under N_2 .
- (b) In light under N_2 .
- (c) In darkness and in air.
- (d) In light and in air.

The CEM spectra of the samples were recorded after approximately 2 weeks and compared with that of the fresh sample and these are shown in fig.4.38. The observed colour changes after two weeks were as follows:

Sample	Colour
Fresh	White (slightly yellow)
(a)	Yellow
(b)	Brown

- (c) Dark brown
- (d) Light brown/orange

Table 4.8 shows the fitted CEM parameters for the above samples and those of the fresh sample along with the 80K transmission Mössbauer parameters for $\text{CsSn}_3\text{Br}_{1.5}\text{F}_{5.5}$ for comparison.

It is apparent that all the CEM spectra show asymmetric doublets. The observed asymmetry is probably due to the preferential alignment of the needle-like crystallites within the sample holder. Within the limits of experimental error the Mössbauer isomer shift values are approximately 3.45mm/s although the fresh sample may genuinely have a lower shift at 3.26 mm/s. The quadrupole splitting of the fresh sample is much larger than the other samples, indicating an increase in asymmetry about the Sn atoms at the surface of the material.

The dark colouration in the samples must be due to liberation of Br_2 and the subsequent formation of a Sn(IV) species. The CEM spectrum of sample (b) does show a small peak in the Sn(0) region and refitting the data to include this line results in the following parameters:

δ_1 mm/s	δ_2 mm/s	δ_3 mm/s	Δ mm/s
-0.05(4)	2.04(6)	3.58(9)	1.22(9)

It is possible that $\text{CsSn}_3\text{Br}_{1.5}\text{F}_{5.5}$ undergoes a photolytic decomposition to give Sn(0) and SnO_2 as it is well known

Table 4.8

Fitted Mössbauer parameters
for $\text{CsSn}_3\text{Br}_{1.5}\text{F}_{5.5}$ stored
under various conditions.

Sample	Sn(IV)	Sn(II)	
	δ mm/s	δ mm/s	Δ mm/s
Fresh	0.00(5)	3.26(9)	1.77(9)
(a) Dark under N_2	-0.09(8)	3.43(6)	1.55(6)
(b) Light under N_2	-0.02(4)	3.41(8)	1.53(8)
(c) Dark in air	-0.10(4)	3.38(8)	1.57(7)
(d) Light in air	-0.10(4)	3.47(9)	1.47(8)
Fresh 80K trans.		3.50(1)	1.50(1)

Fig.4.38a Sample a (stored in darkness under N₂)

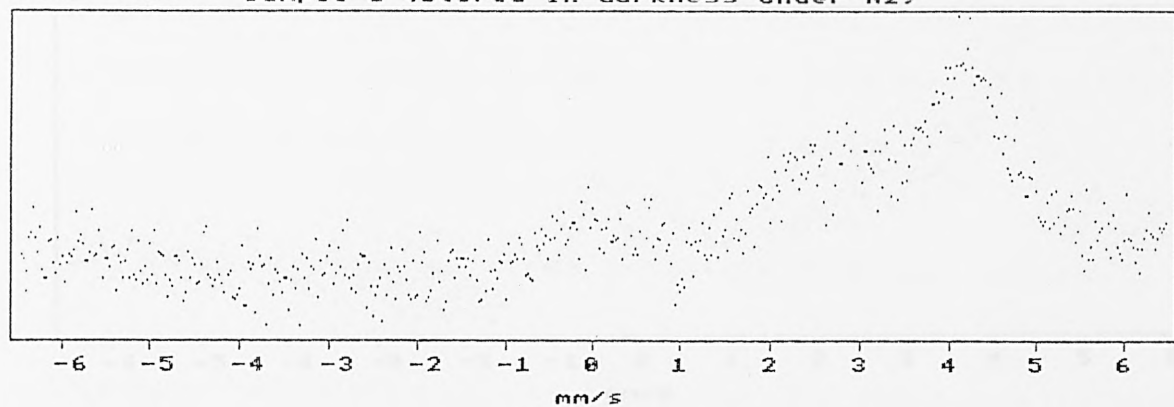


Fig.4.38b Sample b (stored in light and under N₂)

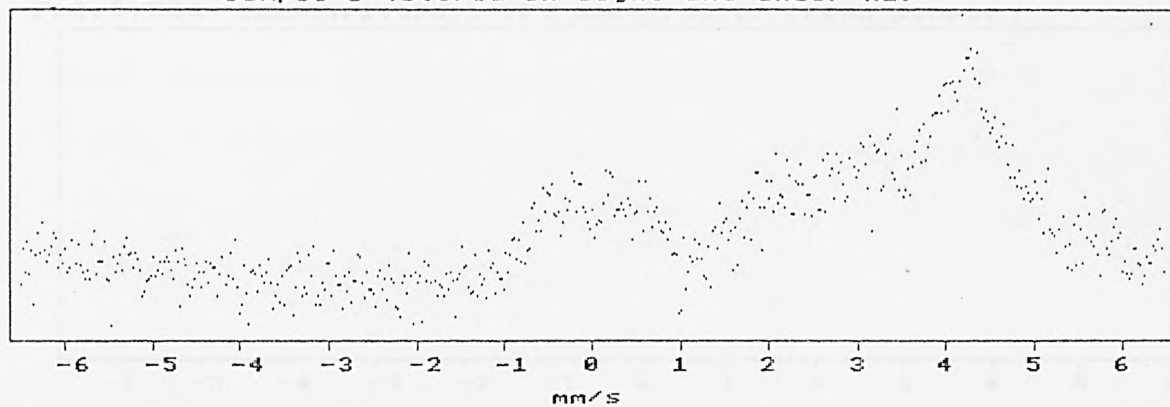


Fig.4.38c Sample c (stored in air and in darkness)

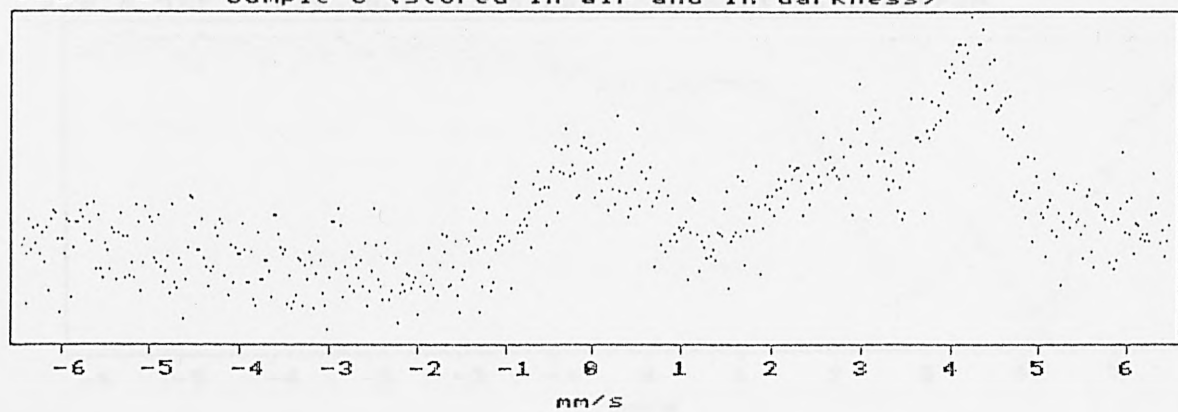


Fig.4.38d Sample d (stored in air and light)

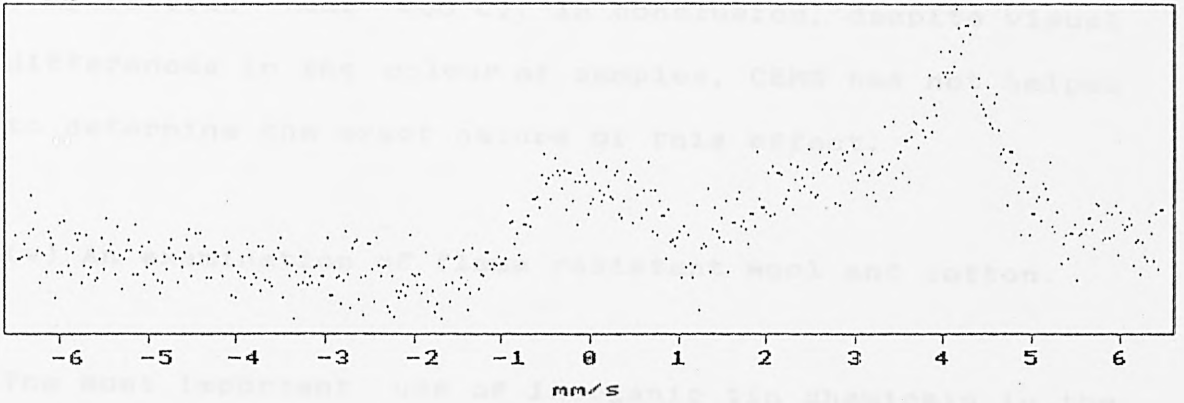


Fig.4.38e CsSn3Br1.5F5.5 CEM spectrum of fresh sample

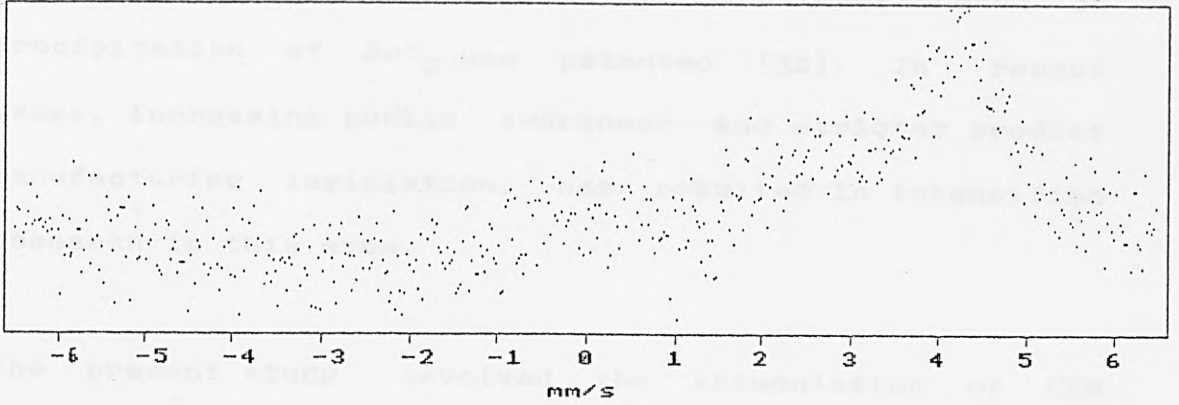
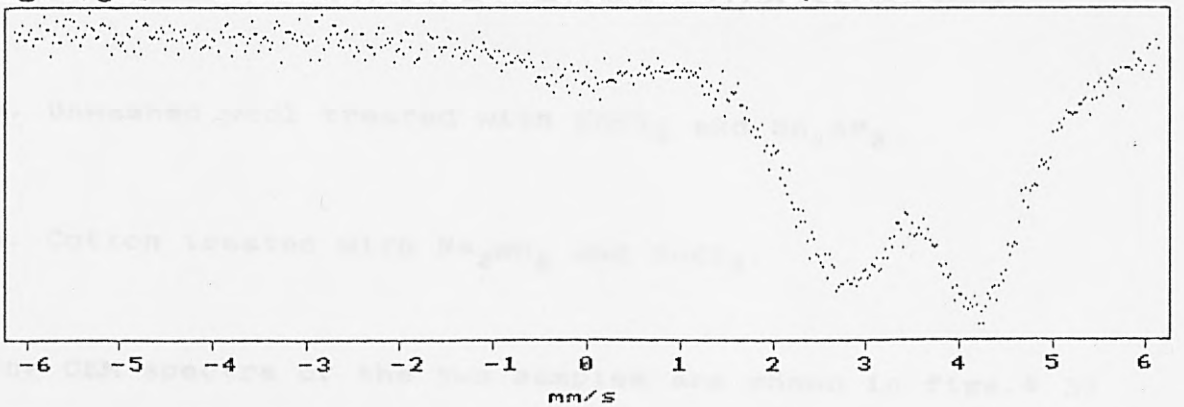


Fig.4.38f CsSn3Br1.5F5.5 86K transmission spectrum



Sample	Area	Gamma
Wood	0.1212	1.6310
Cotton	0.0212	1.4510

that SnO disproportionates to give Sn and SnO₂ at high temperatures (ca. 400 °C). In conclusion, despite visual differences in the colour of samples, CEMS has not helped to determine the exact nature of this effect.

(v) An examination of flame resistant wool and cotton.

The most important use of inorganic tin chemicals in the fabric and textile industry is as flame retardants. As early as 1859 a method of cotton treatment based on precipitation of SnO₂ was patented [32]. In recent years, increasing public awareness and stricter product manufacturing legislation, has resulted in intensified research in this area.

The present study involved the accumulation of CEM spectra on two fabric samples prepared, by P.Cusack at the International Tin Research Institute, as follows:

a. Unwashed wool treated with SnCl₄ and NH₄HF₂

b. Cotton treated with Na₂WO₄ and SnCl₄.

The CEM spectra of the two samples are shown in figs.4.39 and 4.40. the fitted data were as follows:

Sample	δ mm/s	Γ mm/s
Wool	-0.12(3)	1.48(6)
Cotton	0.02(2)	1.56(6)

Fig.4.39

Unwashed wool

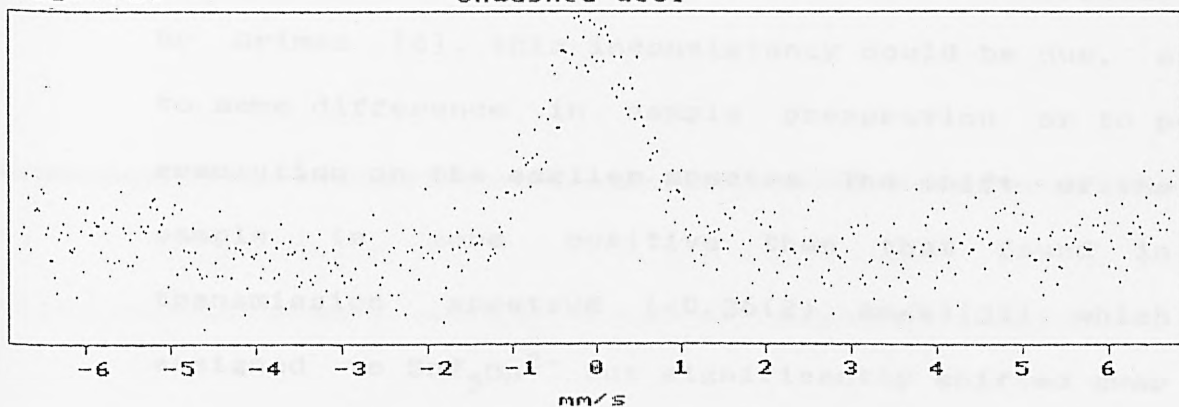
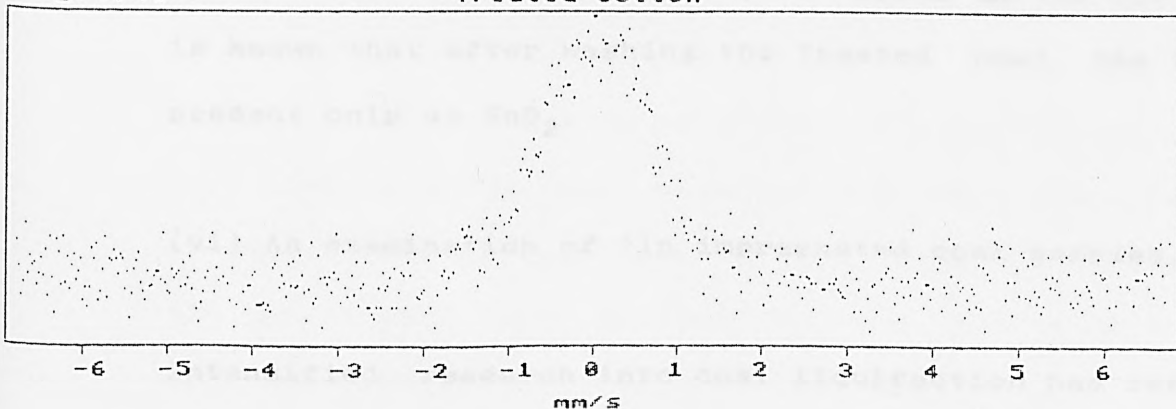


Fig.4.40

Treated cotton



It has been observed that whilst in cotton, SnO_2 is the active species, in wool, the active species in the unwashed material is $\text{SnF}_5\text{OH}^{2-}$ [33,34]. The spectrum of the cotton sample, which showed an SnO_2 singlet, verified this observation. The wool sample showed no evidence for the presence of the doublet assigned to a fluorostannate(IV) species in earlier work by Grimes [6], this inconsistency could be due, either to some difference in sample preparation or to poorer resolution on the earlier spectra. The shift of the wool sample is more positive than that found in the transmission spectrum ($-0.36(2)$ mm/s)[34] which was assigned to $\text{SnF}_5\text{OH}^{2-}$ but significantly shifted away from SnO_2 . A second wool sample that had been exposed to atmospheric conditions for some time gave a singlet with a shift of $-0.02(3)$ mm/s. This seems to indicate that if left exposed to atmospheric conditions there is a gradual change from a hydrated tin(IV) fluoride phase to SnO_2 . This may be a reaction with water vapour in the air as it is known that after washing the treated wool, the tin is present only as SnO_2 .

(vi) An examination of tin impregnated coal samples.

Intensified research into coal liquifaction has resulted in a possible use for tin catalysts. Coal impregnated with SnCl_4 was examined using CEMS. Samples were prepared by D.Searle at The International Tin Research Institute by mixing Victorian brown coal with SnCl_4 dissolved in petroleum ether, under N_2 . Several samples of tin

impregnated coal were examined and the fitted results were as follows:

%Sn	δ mm/s	Γ mm/s
19	0.15(2)	1.20(6)
17	0.15(2)	1.48(8)
13	0.10(2)	1.30(6)
10	0.08(2)	1.54(8)

CEM data for coal impregnated with SnCl_4

All spectra were singlets in the tin(IV) region near SnO_2 , suggesting that the tin is present at the surface only as SnO_2 and not as any tin chloride phase.

(vii) An examination of wood preservative

Tributyltin compounds are commonly used as wood preservatives being highly active against fungi and insects and are often applied to timber used in the construction industry.

Several samples of pine wood treated with tin-containing wood preservatives were examined and CEM spectra left to accumulate for several days. Even with relatively high tin percentages (20%) no features were visible in the CEM spectrum. The presence of a Sn(IV) species has however previously been identified in the transmission Mössbauer spectrum [35]. The absence of information in the CEM spectrum, may be accounted for by the comparatively rough surface of the wood, which meant that many of the conversion electrons were re-absorbed.

(viii) Tin(II)chloride film on white PVC

SnCl_2 is presently used to sensitise plastics prior to metal plating. It is commonly used in the automobile industry in the manufacture of chrome plated plastic trimmings. The spectrum of a sample of tin(II) chloride film on white PVC is shown in fig.4.41. the fitted results are shown below:

δ mm/s	Γ mm/s
0.09(1)	1.82(4)
3.78(6)	1.38(18)

CEM data for SnCl_2 on PVC

From the data it is apparent that oxidation occurs but this is not complete, as there is a residual tin(II) phase. The shift of the tin(II) species of 3.78 mm/s is considerably less than that of SnCl_2 at 4.21 mm/s in the CEM spectrum (see section 4.5). The lowering of shift is consistent with complex formation and could be due to the reaction of SnCl_2 with chlorine atoms on the surface of the plastic to form a trichlorostannate(II) ion which may explain how the SnCl_2 bonds to the plastic.

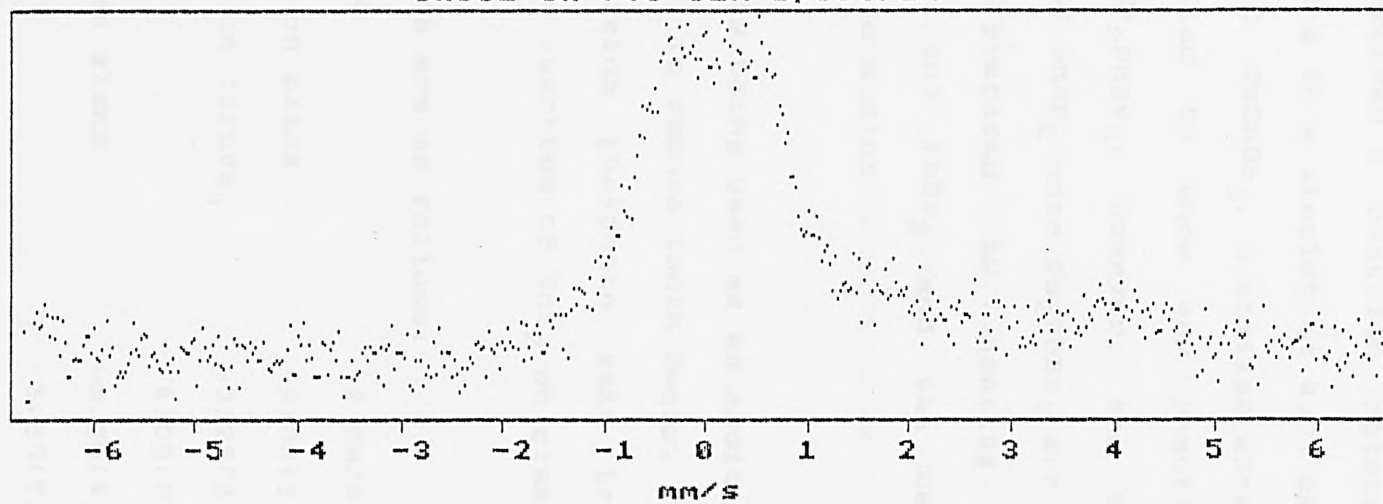
(ix) Surface reactions

Several examples of tin compounds reacting on surfaces were examined by CEMS and the results are now reported:

It is known that SnBr_2 stains glass, especially on

Fig.4.41

SnCl₂ on PUC CEM spectrum



heating. A sample of glass stained by SnBr_2 was examined by CEMS.

Franklin [36] observed a reaction between Sn vapour and Cs_4PbBr_6 resulting in a singlet at 4.08 mm/s and probably corresponding to CsSnBr_3 . A similar experiment in the current work failed to show any reaction between tin vapour and Cs_2PbBr_4 , however, the results of the volatilisation of SnBr_2 onto Cs_2PbBr_4 are reported. The CsPbBr_4 was prepared by heating the appropriate ratio of CsBr and PbBr_2 and the resulting cooled melt pressed into a disc.

SnF_2 is currently being used as an additive to tap water in certain areas to reduce tooth decay. The CEM spectrum of SnF_2 on a calcium phosphate salt is reported and compared with the spectrum of SnF_2 on glass.

The fitted results are as follows:

Sample	δ mm/s	Δ mm/s
SnBr_2 on glass	-0.02(5)	
SnBr_2 on CsPbBr_4	-0.28(8)	
	4.05(9)	
SnF_2 on glass	-0.30(4)	
	3.35(7)	2.18(4)
SnF_2 on $\text{CaH}_4(\text{PO}_4)_2$	-0.04(8)	
	3.77(6)	1.60(3)
SnF_2 (CEM)	3.33(3)	1.64(2)

The SnBr_2 stained glass spectrum shows that the staining

consists of SnO_2 with no evidence of residual bromine being present. The SnBr_2 volatilised onto a CsPbBr_4 disc shows some evidence of reaction, with a peak at 4.05(9) mm/s which compares well with Franklin's observation and is close to the shift for CsSnBr_3 at 3.97 mm/s [6]. The singlet at -0.28 mm/s indicates that there has been partial oxidation of the Sn.

The SnF_2 spectra clearly show that surface reaction has occurred on the $\text{CaH}_4(\text{PO}_4)_2$ disc. In both spectra there is evidence for Sn(IV) suggesting some of the Sn has been oxidised. On glass the oxidised species is likely to be a hydrated tin(IV) fluoride species, while on the $\text{CaH}_4(\text{PO}_4)_2$ disc, oxidation is probably to a tin(IV) phosphate species or SnO_2 . The shift in the Sn(II) region of the spectrum, being higher than that for SnF_2 or SnF_2 on glass is probably due to a surface reaction causing the tin to use its bonding electrons in a way similar to that in SnHPO_4 .

(x) An examination of tin Biocides on leaf samples.

Production of organotin biocides is one of the most important uses of organotin compounds organotin biocides are nearly all of the R_3SnX type (R= alkyl or phenyl). The alkyl or phenyl groups strongly affect the biocidal activity while the X groups mainly influence the solubility. Three popular tin biocides were examined; triphenyltin hydroxide, Ph_3SnOH , which is used as an agricultural pesticide and disinfectant; triphenyltin

acetate, $\text{Ph}_3\text{SnO.CO.Me}$, which has similar uses to the hydroxide; and tricyclohexyltin hydroxide, $(\text{cyclo-C}_6\text{H}_{11})_3\text{SnOH}$ which is used to control plant mites.

Biocides were applied as 25% slurries in ethanol, onto leaf surfaces (umberella plant). Only the data for $(\text{cyclo-C}_6\text{H}_{11})_3\text{SnOH}$ are reported as no features were visible in the CEM spectra of the other materials. The CEM and room temperature transmission spectra of $(\text{cyclo-C}_6\text{H}_{11})_3\text{SnOH}$ are shown in fig.4.42 and 4.43 and fitted results are given below:

	δ mm/s	Δ mm/s
R.T. trans	1.52(10)	3.26(10)
CEM on leaf	0.18(6)	
	1.16(9)	3.46(9)

Mössbauer data on tin biocides

The Mössbauer data show a definite difference between the CEM and transmission data. The larger quadrupole splitting in the CEM spectrum indicates a greater asymmetry around the tin nuclei located at the surface of the applied material. The decrease in shift indicates a decrease in covalency. It may be that the Sn-C bond is being broken in the R_3SnOH to give R_2Sn or RSn derivatives.

(xi) An examination of tin in coloured ceramic tiles.

There is large outlet for inorganic tin chemicals in the ceramic industry. SnO_2 -based glazes doped with metals

Fig.4.42

(cyclo-C₆H₁₁)₃SnOH on leaf CEM spectrum.

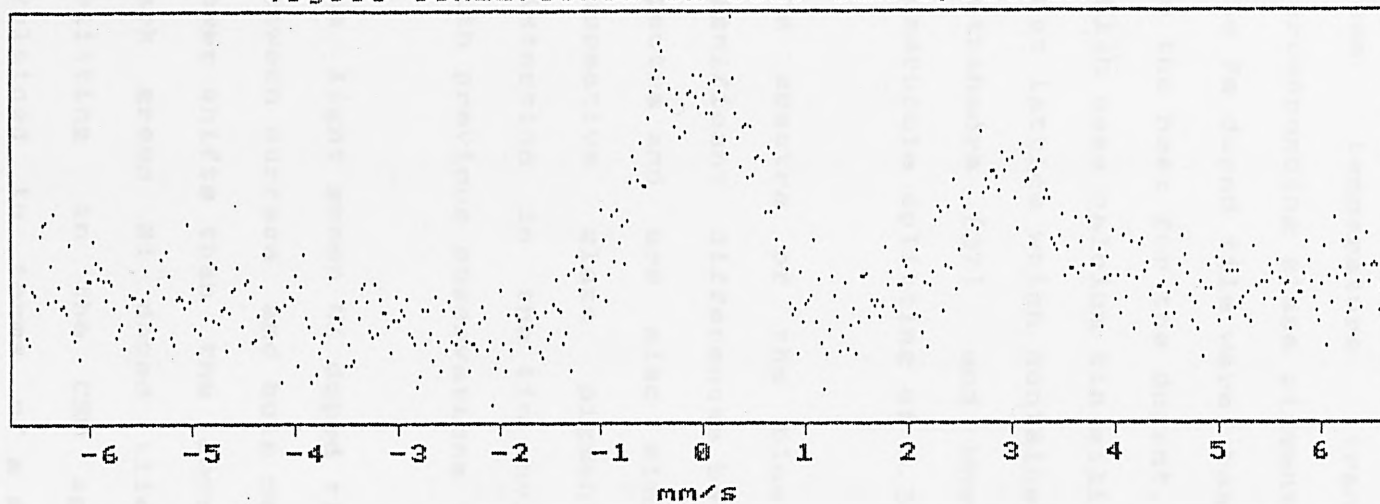
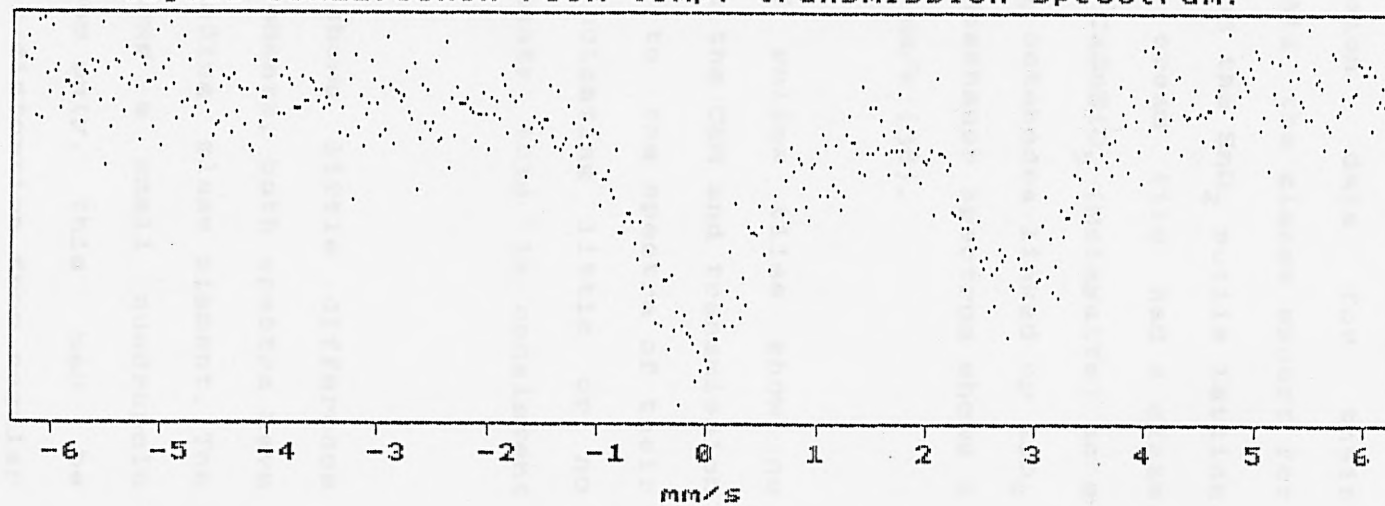


Fig.4.43

(cyclo-C₆H₁₁)₃SnOH room temp. transmission spectrum.



result in a wide variety of colourful tiles.

Several tile samples were examined by CEMS. Table 4.9 shows the fitted results for the room temperature CEM and transmission spectra of the tile samples along with room temperature transmission data for their corresponding glaze pigments. All the glazes except for the Fe doped tile were based on the SnO_2 rutile lattice as the host for the dopant. The cream tile had a glaze which uses calcium tin silicate CaSnSiO_5 (Malayaite) as a host lattice which contains SnO_6 octahedra linked by SiO_4 tetrahedra [37] and whose Mössbauer spectrum shows a quadrupole splitting of 1.32(4) mm/s [38].

The spectra of the blue and yellow tiles show no significant differences between the CEM and transmission spectra and are also similar to the spectra of their respective glaze pigments indicating little or no distortion in the tin environment; this is consistent with previous observations [38].

The light green Ni doped tile shows little difference between surface and bulk measurements, both spectra have lower shifts than the corresponding glaze pigment. The dark green Ni doped tile shows a small quadrupole splitting in the CEM spectrum only, this may be explained in terms of a slight distortion from regular octahedral geometry about the Sn atoms at the surface of the tile.

Table 4.9

Fitted CEM and transmission data for glazed tiles
and transmission data for glaze pigments.

Sample	Tile CEM data		Tile transmission data		Glaze pigment R.t.trans.data	
	δ mm/s	Δ mm/s	δ mm/s	Δ mm/s	δ mm/s	Δ mm/s
	Blue (Sb)	-0.05(4)	----	-0.07(1)	----	-0.03(1)
Yellow (V)	0.01(1)	----	-0.06(1)	----	0.01(1)	----
Dk.Green (Ni)	0.02(7)	0.44(7)	-0.09(2)	----	0.05(1)	----
Lt.Green (Ni)	-0.02(2)	----	-0.07(2)	----	0.06(1)	----
Red (Cr)	-0.01(4)	1.34(3)	-0.07(4)	1.27(3)	-0.14(1)	1.42(1)
Brown (Co)	-0.5(2)	1.7(1)	-0.10(3)	1.16(2)	-0.03(1)	----
Cream (Fe)	0.05(4)	0.85(4)	-0.08(2)	----	0.11(1)	1.47(1)

The Cr doped red tile and glaze pigment spectra all show quadrupole split doublets suggesting a significant distortion from regular octahedral geometry about the tin atoms. The shift and splitting in the glaze pigment are larger than in the tile suggesting that a higher degree of symmetry exists at the tin sites after glazing. There is no significant difference between the surface and the bulk material in the red tile.

The spectrum of the glaze pigment in the brown tile is a singlet resembling SnO_2 , in contrast to the tile spectra which both show quadrupole split doublets. Thus, there is a significant change in structure, after firing. The larger splitting in the CEM spectrum with respect to the transmission spectrum indicates a greater electronic asymmetry about the tin nuclei at the surface.

The CEM spectrum of the cream tile shows a quadrupole split doublet in contrast to the singlet shown in the transmission spectrum. This clearly indicates a breakdown of symmetry at the surface from the octahedral coordination of Sn in the bulk. The transmission spectrum of the glaze pigment shows a large quadrupole splitting and positive shift as compared with the negative shift of the undoped material ($\delta = -0.07(2)$, $\Delta = 1.32(4)$ mm/s [38]). There is, therefore, a significant change in structure in the Malayaite lattice on firing.

REFERENCES, CHAPTER FOUR

- (1) R.L.Mössbauer, Z.Phys., (1958), 151, 124.
- (2) R.L.Mössbauer, Naturwiss, (1958), 45, 538.
- (3) C.G.Davies and J.D.Donaldson, J.Chem.Soc. (A), (1968), 946.
- (4) H.Sano and K.Endo, Reviews on Silicon, Germanium, Tin and Lead Compounds, IV (3), (1980), 245-270.
- (5) M.J.Tricker, in 'Mössbauer Spectroscopy and its Chemical Applications', Advances in Chemistry, Series 194, (American Chemical Society, Washington D.C. USA), 1981, p63.
- (6) S.M.Grimes, Ph.D. Thesis, The City University, 1982.
- (7) J.S.Brooks and S.C.Thorpe, '26th meeting of the Mössbauer Spectroscopy Discussion Group - Abstracts', Royal Society of Chemistry (1985).
- (8) U.Baverstam, T.Ekdahl, C.Bohm, D.Liljequist and B.Ringstrom, Nucl.Instr.Method., (1974), 118, 313.
- (9) Ts.Bonchev, A.Minkova and M.Grozdanov, Nucl.Instr. Method., (1977), 147, 481.

- (10) M.Grozdanov, Ts.Bonchev and A.Likov, Nucl.Instr. Method., (1979), 165, 231.
- (11) Ts.Bonchev, M.Grozdanov and L.Shev, Nucl.Instr. Method., (1979), 165, 237.
- (12) J.Bainbridge, Nucl.Instr.Method., (1975), 128, 531.
- (13) R.A.Krakowski and R.B.Miller, Nucl.Instr.Method., (1972), 100, 93.
- (14) G.P.Huffmann, Nucl.Instr.Method., (1976), 137, 267.
- (15) F.Salvat and J.Parellada, Nucl.Instr.Method., B1, (1984), 70.
- (16) F.Salvat, R.Mayol, J.D.Martinez and J.Parellada, Nucl.Instr.Method., B6, (1985), 547.
- (17) F.Salvat, Private communication.
- (18) F.W.D.Woodhams and Nucl.Instr.Method., (1979), 165, 119.
- (19) F.W.D.Woodhams, Private communication.
- (20) K.Sorensen, "L.T.E. II Internal Report No.1, Laboratory of Applied Physics II ", Technical University of Denmark, Lyngby, Denmark, 1972.

(21) E.W.Müller, 'M.O.S.F.U.N. - Mössbauer Spectra Fitting Program for Universal Theories.' Institute für Anorganische Chemie und Analytische Chemie, Johannes Gutenberg-Universität, Mainz. 1980.

(22) S.Maeda, T.Asai and T.Sawairi Proceedings of the second International Tinplate Conference London 1980 286.

(23) J.S.Johannessen, A.P.Grande and T.Notevarp Proceedings of the second International Tinplate Conference London 1980 274.

(24) V.Leroy, J.P.Servais, L.Renard and J.Lempereur Proceedings of the first International Tinplate Conference London 1980 399.

(25) M.Warwick, D.Bearfield, K.Clay and B.Scott Proceedings of the Third International Tinplate Conference London 1984.

(26) A. Grobin, Plating, (1973), 60 (5), 477.

(27) G.Trumpy, E.Both, C.Djega-Mariadassou and P.Lecocq, Phys.Rev., B., 2, 3477 (1970).

(28) The Preparation, Properties and Industrial uses of Inorganic Tin Chemicals, P.A.Cusack and P.J.Smith, ITRI publication No. 604.

(29) Industrial uses of Inorganic tin chemicals,
M.J.Fuller, ITRI publication No. 499.

(30) A.H.Chapman, 'Tin and Tin-Alloy Plating -
Review', I.T.R.I. Publication No.606.

(31) H.Leidheiser Jr., I.Czako-Nagy, M.L.Varsanyi and
A.Vertes. J.Electrochem.Soc., (1979), 126, (2), 204.

(32) F.Versmann and A.Oppenheim, Eng.Patent, 2077 (1859).

(33) P.A.Cusack, P.J.Smith, J.S.Brooks and R.Smith
J.Text.Inst. (1979), 7, 308.

(34) P.A.Cusack, P.J.Smith, J.S.Brooks and R.Smith
I.T.R.I. Publication No.573.

(35) P.J.Smith, Private communication.

(36) L.E.Franklin, Unpublished work.

(37) J.B.Higgins and F.K.Ross, Cryst.Struct.Comm.,
(1977), 6, 179.

(38) D.V.Sanghani, G.R.Abrams and P.J.Smith,
Trans.J.Br.Ceram.Soc., 80, 210-214, 1981.

(39) N.N.Greenwood and T.C.Gibb 'Mössbauer Spectroscopy',
1971, Chapman and Hall, London.

(40) J.D.Donaldson and S.M.Grimes, Reviews on Silicon Germanium Tin and Lead Compounds, (1984), 8 (1), 1-132.

(41) J.D.Donaldson and A.Jelen, J.Chem.Soc. (A), (1968), 1148.

CHAPTER FIVE

STRUCTURE DETERMINATION OF TIN(II) COMPLEXES

	Page
5.1 Introduction.	249
5.2 The X-ray structure determination of RbSn ₂ Br ₅ .	250
5.3 The X-ray structure determination of CsSn ₃ Br _{1.5} F _{5.5} .	269
5.4 The X-ray structure determination of KBr.KSnBr ₂ Cl.H ₂ O.	296
5.5 A refinement of the structure of KCl.KSnCl ₃ .H ₂ O	311
5.6 A refinement of the structure of Sn ₃ BrF ₅ .	318
References.	328

CHAPTER FIVE

5.1 Introduction

The presence of stereochemically active lone pairs of electrons in tin(II) species usually results in a distorted environment around the tin atom [1,2]. The most common type of distortion found has a trigonal, pyramidal distribution of three nearest-neighbour tin-ligand bonds and three longer essentially non-bonding contacts completing a distorted octahedral geometry. The longer contacts arise because close approach of the ligands to the tin is prevented along directions in which the lone pairs point. In the less common, distorted four pyramidal environment, the tin atom usually has two short bonds to ligands and two bonds of greater length than those normally found in tin(II) compounds as nearest-neighbour contacts. Although most tin(II) compounds have low symmetry lattices, a few structures have tin in high symmetry regular octahedral sites. Such environments are usually found in compounds containing heavier halide and chalcogenide ions, in which the distorting effects of the non-bonding electron pairs, on the tin atoms, are removed by population of solid state bands arising from overlap of the empty halide or chalcogenide orbitals. Recent evidence has also shown that the direction in which the lone-pair orbitals point can lead to some delocalisation of the non-bonding electrons into cluster orbitals [3]. Several structures have been examined in the present work with two aspects in mind viz: the characterisation of the

Sn-Br bond and the extent of delocalisation of the non-bonding electron pairs on the tin atoms.

5.2 The X-ray structure determination of RbSn_2Br_5

In most cases where tin(II) forms complex ions with ligands, the triligandstannate(II) species is the stable and predominant ion. Crystal structures of a number of alkali metal trichloro- and trifluoro-stannates(II) have been determined [4]. The only other known structure of a pentahalodistannate(II) complex is that of NaSn_2F_5 [5], in which fluorine atoms bridge SnF_2 groups to form discrete $[\text{Sn}_2\text{F}_5]^-$ ions. Doubt must be cast upon the crystal structure of determination of KSn_2F_5 , which has also been reported [6], the bond lengths presented have been incorrectly calculated and also, in order to balance the molecular formula, the authors have set several of the fluorine sites to partial site occupancies, with no evidence being presented to justify the particular sites chosen. It is, however, evident that the structure of KSn_2F_5 contains bridging, ionic and terminal covalent, bonds to fluorine. There is, however, a considerable difference in the nature of bonds formed between tin and fluorine and those formed between tin and other halogen atoms [1]. RbSn_2Br_5 represents the first determination of a pentahalogenodistannate(II) complex with a halide other than fluoride.

In an attempt to prepare the complex RbSnBr_3 using the method described by Bird [7], an aqueous mixture of

RbBr and SnBr_2 in a 1:1 mole ratio resulted in the precipitation of crystals of RbSn_2Br_5 . Subsequent attempts to intentionally prepare the latter compound from a 1:2 mole ratio of starting materials, were successful, indeed the compound was also obtained from a 2:1 mole ratio indicating that it is the stable phase precipitated from this system.

(i) Preparation

The compound was prepared using the general preparative method described in section 2.2. RbBr and SnBr_2 were used in a 1:1 mole ratio and a few drops of HBr were used to suppress hydrolysis. The compound crystallised as white rhomboid plates. The material was analysed for Rb, Sn, Br and water using the methods described in section 2.2. A Mössbauer spectrum and an X-ray powder diffraction pattern of the product were also obtained using the methods described in sections 4.1 and 1.6, respectively. A single crystal was selected from the bulk material for X-ray data collection. The analytical data, Mössbauer spectrum and X-ray powder diffraction pattern are given in section 2.3.

(ii) Data collection and space group determination.

Intensity data were collected on a Philips PW1100 four circle diffractometer at Padua University, Italy, as described in section 1.7. Monochromatic $\text{MoK}\alpha$ radiation ($\lambda = 0.7107\text{\AA}$) was used throughout. Data for 365 independent

reflections, in tetragonal symmetry, were observed and of those, 284 with $I > 3 \sigma(I)$ were used in subsequent calculations. Data were corrected for Lorentz and polarisation factors but not for absorption. The crystal data are shown in table 5.1. The unit cell is tetragonal with unit cell parameter restrictions:

$$a = b = c; \quad \alpha = \beta = \gamma = 90^\circ$$

The intensity relationships for tetragonal cells are such that only a small number of unique reflections are needed to define the asymmetric unit, consequently, equivalent reflections were merged before subsequent calculations. The following systematic absences were observed in the intensity data:

$$hkl \text{ absent when } h+k+l = 2n+1$$

$$Ok1 \text{ absent when } l = 2n+1 \text{ and when } k = 2n+1$$

The first of these absences indicates a body centred cell, the second absence results from the presence of a c-glide perpendicular to b. The combination of absences excluded all but three possible tetragonal space groups, these were; $I4cm$ (no.108), $I4/mcm$ (no.140) and $I4c2$ (no.120) [8], where space group 140 is the centrosymmetric analogue of space group 108. In the initial stages the structure was determined in the non-centrosymmetric space group $I4cm$.

(iii) Location of atomic positions

A Patterson synthesis was used to locate the heavy atoms.

Table 5.1 Crystal data for RbSn_2Br_5

Morphology	White rhomboid plates
Crystal class	Tetragonal
Cell Dimensions (Å)	$a = b = 8.442(2)$ $c = 14.754(3)$ $\alpha = \beta = \gamma = 90^\circ$
Cell Volume (Å ³)	1051.48
Molecular Weight (g)	722.37
Z	4
D_c (gcm ⁻³)	4.54
D_o (gcm ⁻³)	4.44
$F(000)$	1248
$\mu(\text{MoK}\alpha)$ (cm ⁻¹)	275.31
Radiation	$\text{MoK}\alpha \lambda = 0.7107\text{Å}$

Unfortunately this system was not ideal as all the atoms are of similar atomic number.

The equivalent positions for the space group $I4cm$ are:

$x, y, z;$ $-x, -y, z;$ $x, -y, 0.5 + z;$ $-x, y, 0.5 + z;$
 $-y, x, z;$ $y, -x, z;$ $y, x, 0.5 + z;$ $-y, -x, 0.5 + z$

The corresponding Patterson vector map positions are:

$2x, 2y, 0$ $0, 2y, 0.5$ $2x, 0, 0.5$ $x+y, y-x, 0$
 $x-y, y+x, 0$ $x-y, y-x, 0.5$ $x+y, y+x, 0.5$

The highest peaks in the Patterson map are shown in table 5.2. The expected vectors can be arranged in order of peak heights based on atomic numbers as follows:

Vector	Rel.Height (%)
(1) Sn \longrightarrow Sn	100
(2) Sn \longrightarrow Rb	75
(3) Sn \longrightarrow Br	70
(4) Rb \longrightarrow Rb	55
(5) Rb \longrightarrow Br	52
(6) Br \longrightarrow Br	49

The data suggest that the atoms lie in special positions. Analysis of the map proved difficult, because no single heavy atom is distinguishable but on examining combinations of special positions it was found that vectors between sets of atoms located at the two, four fold sites, $0, 0, z$ and $0, 0, 0.25 + z$, would give rise to peaks 8 to 11 while the vectors between the atoms within individual sets would correspond to peaks 26 to 28.

A representative general heavy atom at a four-fold site

Table 5.2 Patterson map for RbSn_2Br_5 .

No.	Height	u/a	v/b	w/c	S.O.F.
1	999	0.5000	0.5000	0.5000	0.0625
2	999	0.0000	0.0000	0.0000	"
3	999	0.0000	0.0000	1.0000	"
4	410	0.5000	0.5000	0.1352	0.1250
5	"	0.5000	0.5000	0.8648	"
6	"	0.0000	0.0000	0.6352	"
7	"	0.0000	0.0000	0.3648	"
8	350	0.5000	0.5000	0.2411	"
9	"	0.5000	0.5000	0.7589	"
10	"	0.0000	0.0000	0.7411	"
11	"	0.0000	0.0000	0.2589	"
12	335	0.3389	0.0000	0.5000	0.2500
13	"	0.0000	0.3389	0.5000	"
14	"	0.5000	0.1611	0.0000	"
15	"	0.5000	0.1611	1.0000	"
16	"	0.1611	0.5000	0.0000	"
17	"	0.1611	0.5000	1.0000	"
18	221	0.3406	0.0000	0.1347	0.5000
19	"	0.0000	0.3406	0.1347	"
20	"	0.1594	0.5000	0.6347	"
21	"	0.0000	0.34066	0.8653	"
22	"	0.5000	0.1594	0.6347	"
23	"	0.3406	0.0000	0.8653	"
24	"	0.5000	0.1594	0.3653	"
25	"	0.1594	0.5000	0.3653	"

at $0,0,z$ was input into a Fourier synthesis and an electron map generated as described in section 1.8. By trial and error, based on the residual obtained, the peak was found to correspond to a set of Rb atoms. From the resultant electron density map a second four-fold site was located at $c/4$ away from Rb confirming the proposed solution of the Patterson map. This atom at $0,0,z+c/4$ was at a distance of 3.69\AA from the rubidium and was considered to be too close to be a tin atom and, therefore, to be a bromine atom and was subsequently input into a Fourier synthesis as $\text{Br}_{(i)}$. Fourier electron density maps obtained, were used to locate a second set of Br atoms, $\text{Br}_{(ii)}$, in an eight fold position at $0.34,0.16,z+0.10$. An electron density map phased on the Rb, $\text{Br}_{(i)}$ and $\text{Br}_{(ii)}$ positions located Sn in an 8 fold position $0.31,0.81,z-0.25$. The residual, at this stage, with structure factors phased on the Rb, $\text{Br}_{(i)}$, $\text{Br}_{(ii)}$ and Sn positions, was 0.38. This residual was relatively high considering the amount of electron density apparently located. Consequently, the tin atom was input alone into a Fourier synthesis and used to re-generate the other atom positions. The coordinates of the tin atom were set to $0.31,0.81,0$ with the z axis fixed at zero, having previously been left to fluctuate because there is no fixed position for the origin along the c -axis in this space group. With the tin atom, input alone, the residual was 0.53 after four cycles of least squares, as compared with 0.69 for the rubidium alone. The highest peaks in the electron density map phased on the tin position only are shown below:

No.	Height	x/a	y/b	z/c	SOF
Sn		0.1705	0.3295	0.0000	0.5000
3	316	0.5000	0.5000	0.3767	0.2500
5	311	0.5000	0.5000	0.1250	"
10	250	0.3360	0.1640	0.1364	0.5000
13	245	0.1645	0.3359	0.3653	"
14	197	0.5000	0.5000	0.0000	0.2500

An atom in the peak 10 position would be at a distance of 2.8Å from tin atom, this giving a reasonable bond distance to bromine based on previous experience [1]. Thus, with a bromine atom, Br₍₁₎, in position 10, Fourier calculations were performed again and the four fold position of 0,0,0.25 was the highest unallocated peak in the resultant electron density map. In agreement with solution of the Patterson map, rubidium was assigned to this peak. Calculations phased on Sn, Rb and Br₍₁₎ located further bromine atoms; in the four fold position 0,0,0 and in the 8 fold position, 0.156, 0.345, 0.870. With all the atoms found the residual was 0.069 and the atomic parameters were as follows:

Atom	x/a	y/b	z/c	SOF	B
Sn	0.1782	0.6782	0.0000	0.50	0.0238
Rb	0.0000	0.0000	0.0000	0.25	0.0241
Br ₍₁₎	0.0000	0.0000	0.0000	0.25	0.0182
Br ₍₂₎	0.3437	0.8437	0.8673	0.50	0.0194
Br ₍₃₎	0.3343	0.8343	0.1356	0.50	0.0212

It was now apparent that Br₍₂₎ and Br₍₃₎ were related by a center of symmetry and that the other positions would be unaffected by a solution in the centrosymmetric space group I4/mcm. The use of the higher symmetry space groups gave the slightly higher residual 0.074. Application of anisotropic thermal parameters was not initially successful, but, by applying certain constraints, on the anisotropic thermal parameters, an R factor of 0.058 was achieved. To do this all U₁₃ U₂₃ values were fixed at zero and U₁₁ and U₂₂ values were tied to a single variable; U₁₂ for Br₍₁₎ was also fixed at zero. The final refined parameters are shown in table 5.3. with bond lengths and angles in table 5.4. Structure factors are listed in Appendix 2.

(iv) Structural description and discussion

Fig.5.1 shows a projection of the unit cell contents. The arrangement of the Sn and bridging Br₍₁₎ atoms is such that they constitute a two dimensional polymeric network perpendicular to the c-axis at c = 0 and c = 1/2. The remaining Br₍₂₎ atoms lie symmetrically above and below the plane of the network, forming terminal Sn - Br bonds. The resultant layer structure, shown in fig.5.2, consists of two-dimensional polymeric [Sn₂Br₅]_nⁿ⁻ anionic layers separated by Rb cations lying symmetrically above and below Br₍₂₎ in the direction of of the c-axis. The formation of the polymeric [Sn₂Br₅]_nⁿ⁻ network is in sharp contrast to the discrete [Sn₂F₅]⁻ units found in NaSn₂F₅.

Table 5.3 Final atomic parameters for RbSn_2Br_5
with ESDs in brackets

Atom	x/a	y/b	z/c	S.O.F.
Rb	0.0	0.0	0.25	0.125
Sn	-0.3215(2)	-0.8215(2)	0.0	0.25
Br ₍₁₎	0.0	0.0	0.0	0.125
Br ₍₂₎	-0.1610(2)	-0.6610(2)	0.1341(2)	0.5

U_{11}	U_{22}	U_{33}	U_{23}	U_{13}	U_{12}
0.029(2)	0.029(2)	0.017(2)	0.0	0.0	0.006(4)
0.024(1)	0.024(1)	0.022(1)	0.0	0.0	-0.004(1)
0.013(1)	0.013(1)	0.025(2)	0.0	0.0	0.0
0.024(1)	0.024(1)	0.017(1)	-0.002(7)	-0.002(7)	0.001(1)

Table 5.4 Bond lengths (Å), angles (°) and some significant contact distances in RbSn_2Br_5 with ESDs in brackets

Sn--Br(1)	3.105(1)	Sn--Br(2)	2.755(3)
Rb..Br(1)	3.688(1)	Rb..Br(2)	3.600(1)
Br(1)..Br(2)	3.755(1)	Br(2)..Br(2)	3.844(5)
Sn..Sn	4.261(5)		
	Br(1)--Sn--Br(2)		79.0(1)
	Br(2)--Sn--Br(2)		91.8(1)
	Br(1)--Rb--Br(2)		61.6(1)
	Br(2)--Rb--Br(2)		68.0(1)
	Rb--Br(1)--Br(2)		58.0(1)
	Sn--Br(1)--Br(2)		46.4(1)
	Sn--Br(2)--Rb		97.8(1)

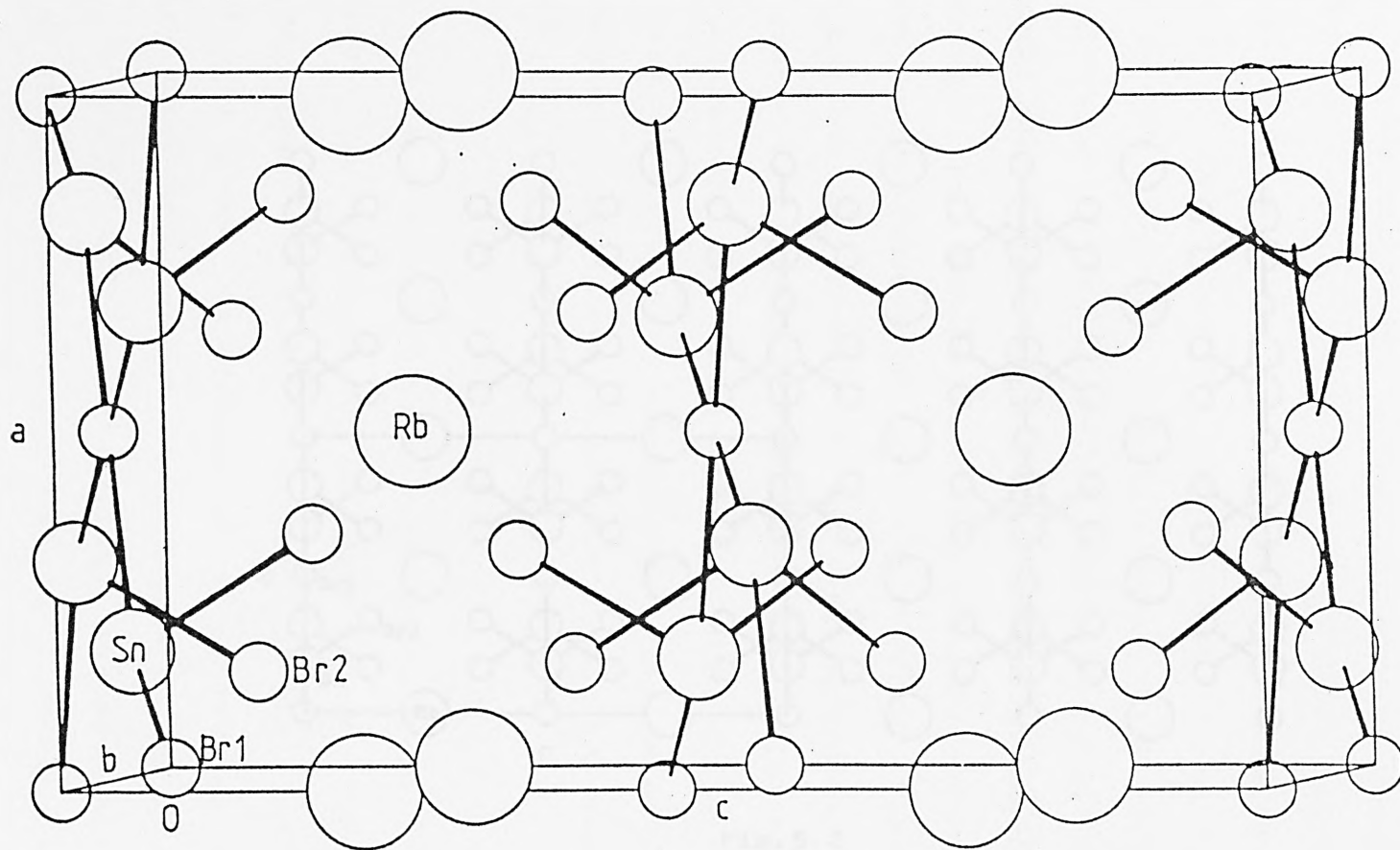


Fig. 5.1

Unit cell contents of RbSn_2Br_5

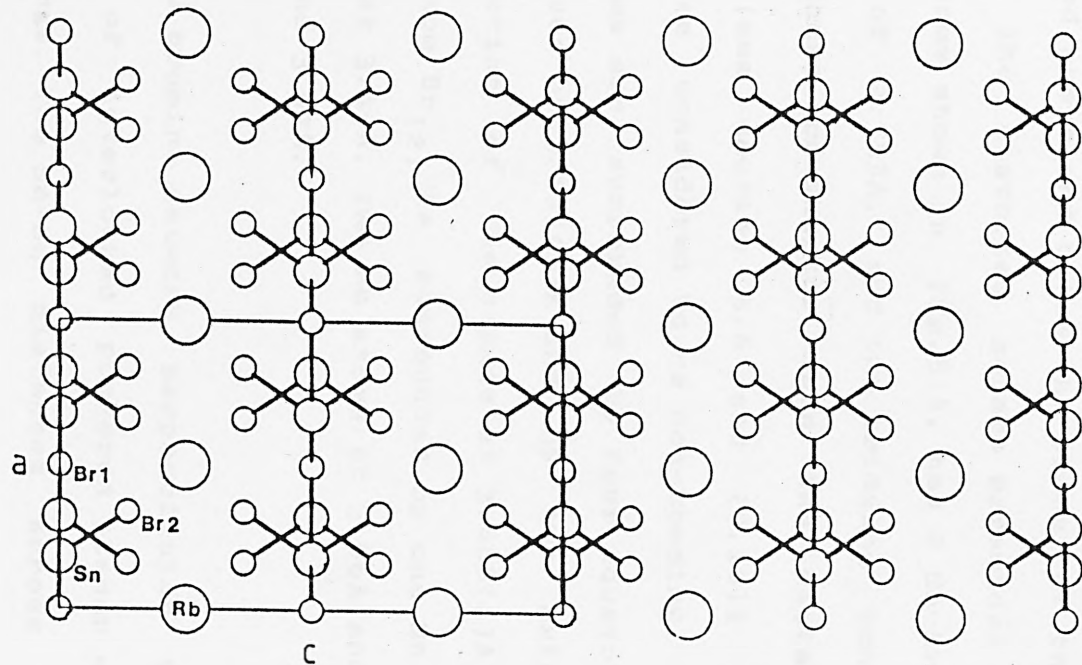


Fig. 5.2

RbSn_2Br_5 projection onto a/c showing anionic layers separated by Rb^+ cations

The Sn atoms in the structure are in distorted square pyramidal environments with two long bonds to bridging Br₍₁₎ atoms within the plane of the polymeric network and two terminal bonds to Br₍₂₎ atoms symmetrically positioned above and below the plane of the network (see fig.5.3) The distorted square pyramidal environment of the Sn atoms shown in fig.5.4, has 2 Sn-Br terminal bond lengths of 2.755Å, and two bridging bonds to Br of 3.105Å; these are shorter than the distances found in Sn₃BrF₅ (see section 5.6 and [9,10]) of 3.30-3.34Å, which were considered to be non-bonding. The bridging Br₍₁₎ atoms are surrounded by four equatorial tin atoms at distances of 3.105(1)Å and by two axial Rb atoms in the direction of the c-axis at 3.688(1)Å. The terminal bromine atom Br₍₂₎ is surrounded by one Sn at 2.75Å, two Sn atoms at 3.49Å, two Rb atoms at 3.06Å and two Br atoms at 3.84 and 3.97Å.

The tin to bromine network perpendicular to the c-axis consists of interlocked puckered planar eight membered Sn₄Br₄ rings. The Sn-Sn distances across the rings are 4.26Å and 7.68Å. The position of the terminal Br atoms causes the lone pair on the Sn atoms to lie in the plane of the ring. It is interesting to note that the lone pairs on the Sn atoms point directly towards one another across the shortest Sn-Sn distance in the ring. This distance of 4.261(5)Å is too long to permit direct interaction between the filled non-bonding orbital on one tin atom and the empty orbital on the opposite tin atom,

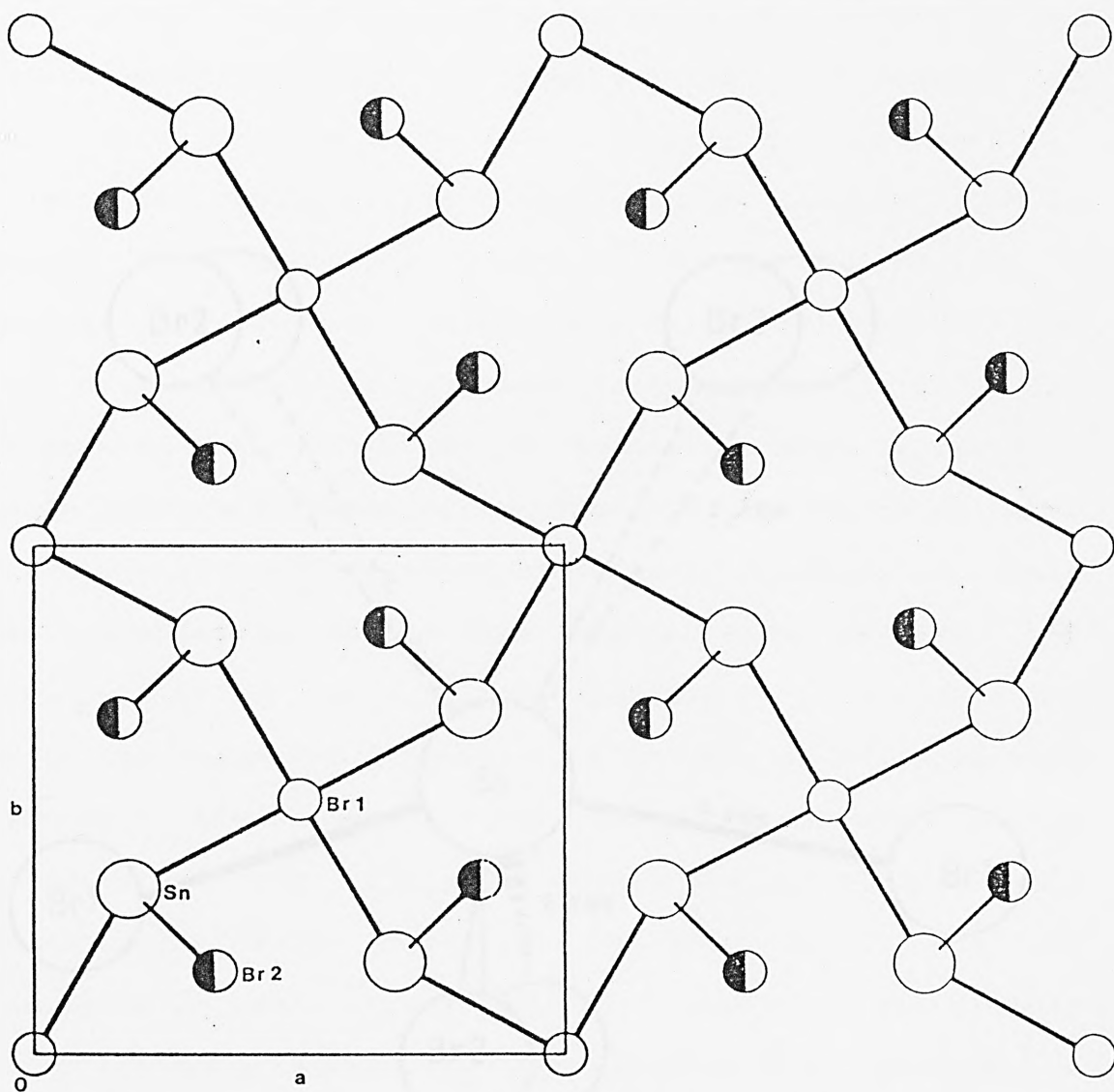


Fig.5.3

Projection of (1,1,0) layer with overlapping Br(2) atoms
above and below the network plane in RbSn_2Br_5 .

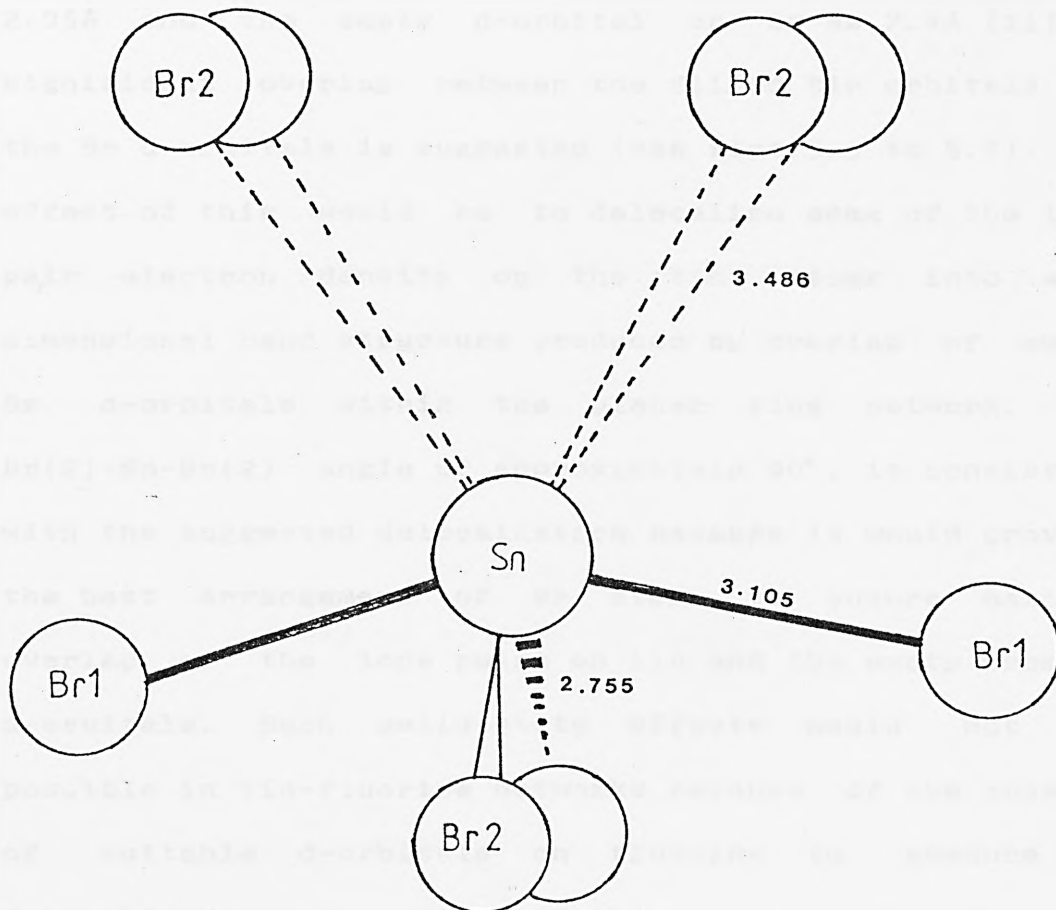


Fig.5.4

Square pyramidal tin environment in RbSn_2Br_5 .

but they are close enough to the terminal Br atoms above and below the plane, directed along the longer Sn-Sn distance of the ring, to enable interaction between the lone pair orbitals on Sn and the empty d-orbitals of Br. Taking the radius of the s-orbitals on the Sn atom as 2.05Å and the empty d-orbital on Br as 2.4Å [11], a significant overlap between the filled tin orbitals and the Br d-orbitals is suggested (see figs.5.5 to 5.7). The effect of this would be to delocalise some of the lone pair electron density on the tin atoms into a 2 dimensional band structure produced by overlap of empty Br d-orbitals within the planar ring network. The Br(2)-Sn-Br(2) angle of approximately 90°, is consistent with the suggested delocalisation because it would provide the best arrangement of Br atoms to ensure maximum overlap of the lone pairs on tin and the empty bromine d-orbitals. Such solid-state effects would not be possible in tin-fluorine networks because of the absence of suitable d-orbitals on fluorine to produce a delocalised band system and this may account for the formation of discrete $[\text{Sn}_2\text{F}_5]^-$ ions in NaSn_2F_5 rather than the polymeric network structure in RbSn_2Br_5 .

The ^{119}Sn Mössbauer shift of 3.91(6) mm/s for the complex RbSn_2Br_5 is only slightly lower than that of its parent compound SnBr_2 at 3.98 mm/s [12]. Two factors combine to reduce the shift of this material with respect to the parent compound viz: complex formation and electron delocalisation which both have the effect of

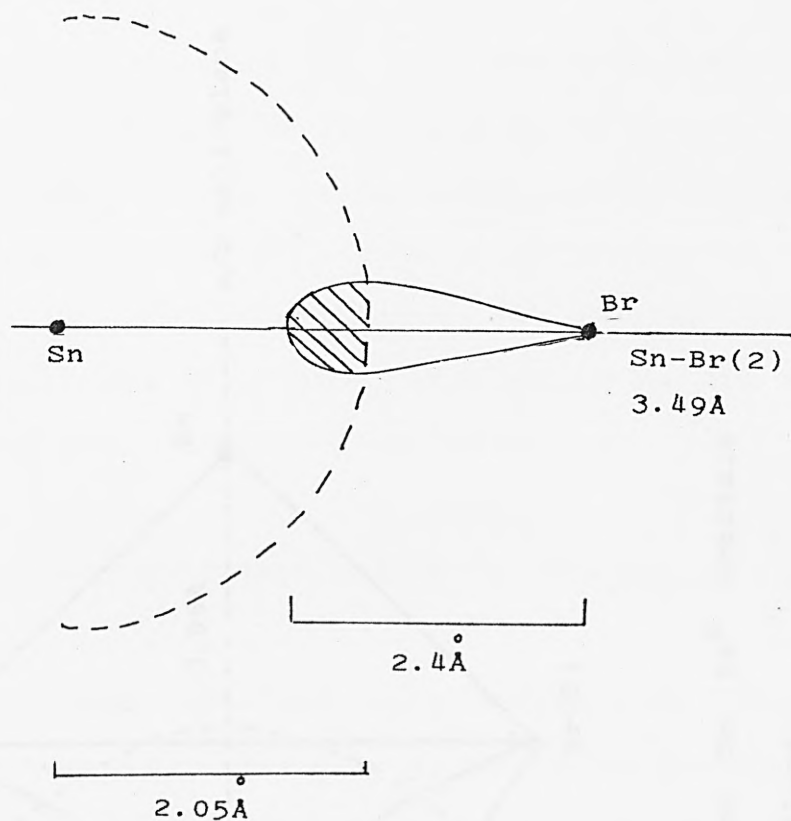


Fig.5.5

Extent of Sn $5s^2$ and Br 4d orbital overlap along Sn-Br(2)

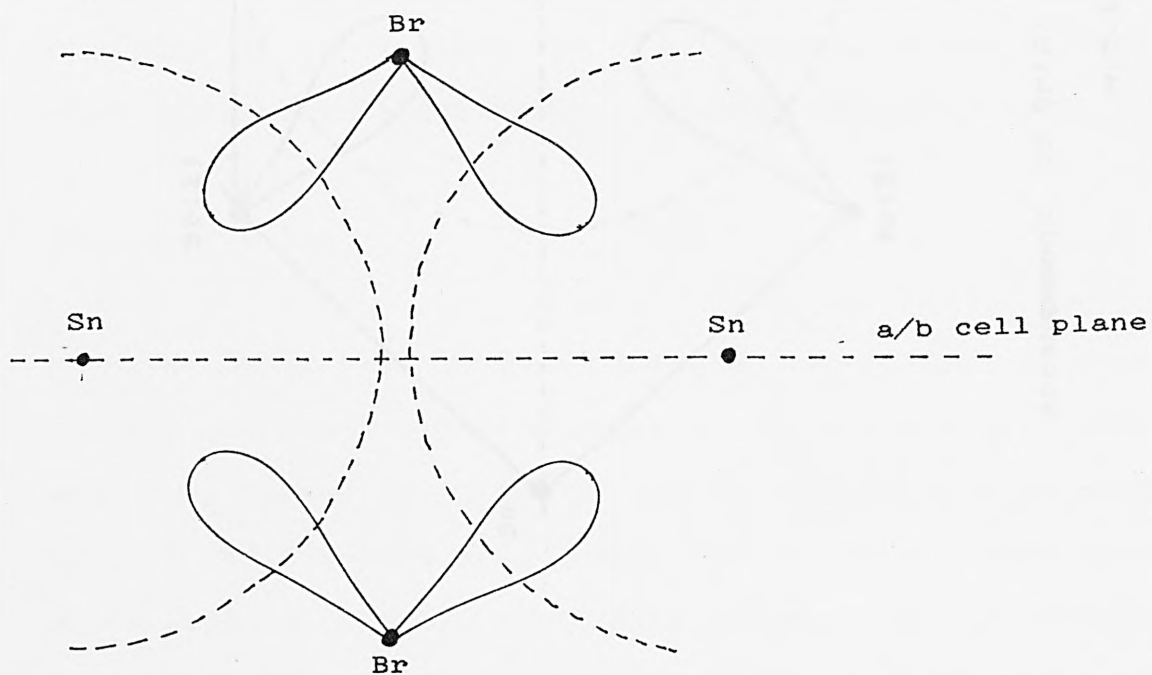


Fig.5.6

Interaction between $5s^2$ Sn orbitals via Br 4d orbitals on bromine atoms above and below a/b cell plane.

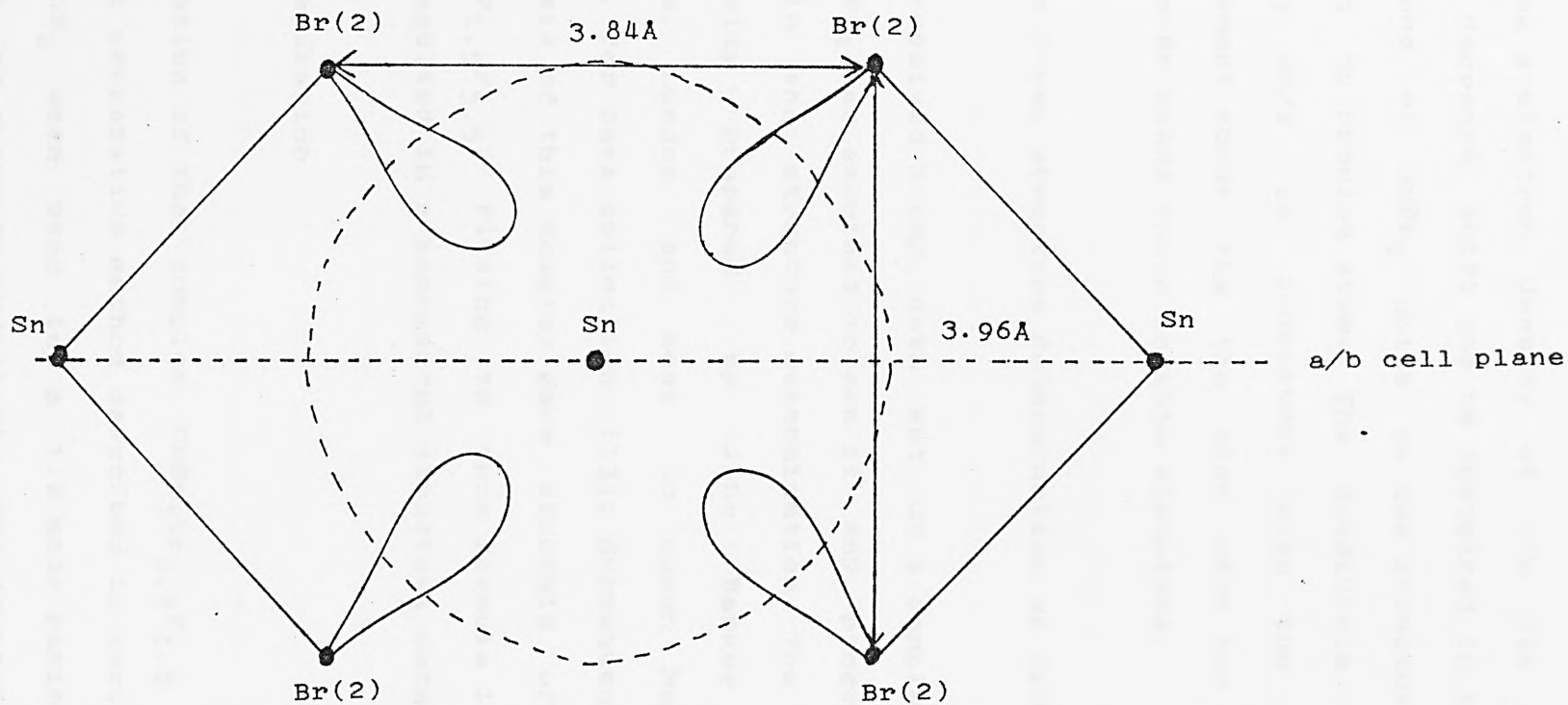


Fig. 5.7

Arrangement of Br(2) 4d orbitals and Sn 5s² orbitals
w.r.t the a/b cell plane

reducing s-electron density at the tin nucleus. This slight decrease shift can be described in terms of the existence of SnBr_2 units in the structure of RbSn_2Br_5 bridged by bromine atoms. The quadrupole splitting of 0.89(5) mm/s is consistent with the unsymmetrical arrangement about the tin atom with two short and two long Sn-Br bonds found in this structure.

5.3 The X-ray structure determination of $\text{CsSn}_3\text{Br}_{1.5}\text{F}_{5.5}$

The unresolved X-ray data set of a complex of formula $\text{CsSn}_2\text{BrF}_4$ was examined to see if any progress could be made in the structure determination. The crystals were originally prepared by John Barker at Chelsea College, London and sent to Queen Mary College, London, for data collection [13]. Subsequent attempts at synthesis of this complex gave crystals of the formula $\text{CsSn}_3\text{Br}_{1.5}\text{F}_{5.5}$. Fitting to this formula in the present work resulted in a successful structure determination.

(i) Preparation

Preparation of the complex $\text{CsSn}_3\text{Br}_{1.5}\text{F}_{5.5}$ was by the general preparative method described in section 2.2. CsBr and SnF_2 were used in a 1:2 mole ratio with no acid present to suppress hydrolysis. The crystals formed were white needles which gradually darkened in atmospheric conditions (see section 4.7(iv)). Analyses for Cs, Sn and Br were carried out using the methods described in section 2.2 The analytical data are as follows:

	Cs	Sn	Br	F
	19.4	50.1	16.5	
CsSn ₃ Br _{1.5} F _{5.5}	(18.6)	(49.9)	(16.8)	(14.7)
CsSn ₂ BrF ₄	(25.3)	(45.1)	(15.2)	(14.4)

Clearly the analytical data are closer to those of CsSn₃Br_{1.5}F_{5.5} than the formula proposed earlier. A Mössbauer spectrum and X-ray powder diffractogram were recorded as described in sections 4.1 and 1.6 respectively. The X-ray powder data are in table 5.5 and the Mössbauer spectrum in fig.5.8. A thermoanalytical trace was recorded as described in section 3.1 the results of which are discussed later.

(ii) Data collection and space group determination.

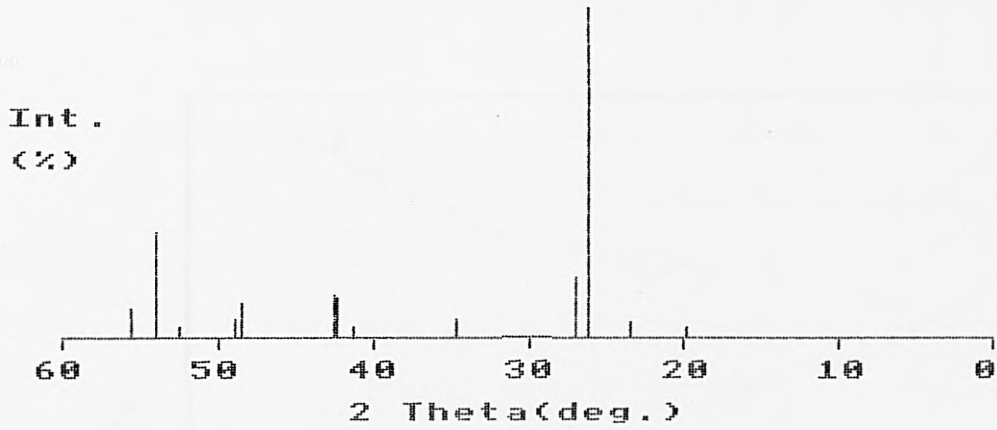
The crystal data are shown in table 5.6. Intensity data were collected, as described in section 1.7, on a Phillips PW1100 four circle diffractometer at Queen Mary College, London. Monochromatic MoK α ($\lambda = 0.7107\text{\AA}$) radiation was used throughout. Data for 660 independent reflections, in monoclinic symmetry, with $I > 3\sigma(I)$ were used in subsequent calculations. Data were corrected for Lorentz and polarisation factors but not for absorption.

The intensity data were related as follows:

$$I_{hkl} = I_{\bar{h}\bar{k}\bar{l}} = I_{\bar{h}k\bar{l}} = I_{h\bar{k}l}$$

Equivalent reflections were merged before subsequent

Table 5.5
X-ray Powder Diffraction Pattern
CsSn₃Br_{1.5}F_{5.5}



Rel. Int. (%)	d(hkl)A
4	4.484
6	3.802
100	3.401
19	3.314
6	2.578
4	2.191
13	2.132
13	2.127
11	1.877
6	1.863
4	1.743
30	1.701
33	1.698
8	1.656

Fig.5.8

80K Mössbauer spectrum of $\text{CsSn}_3\text{Br}_{1.5}\text{F}_{5.5}$

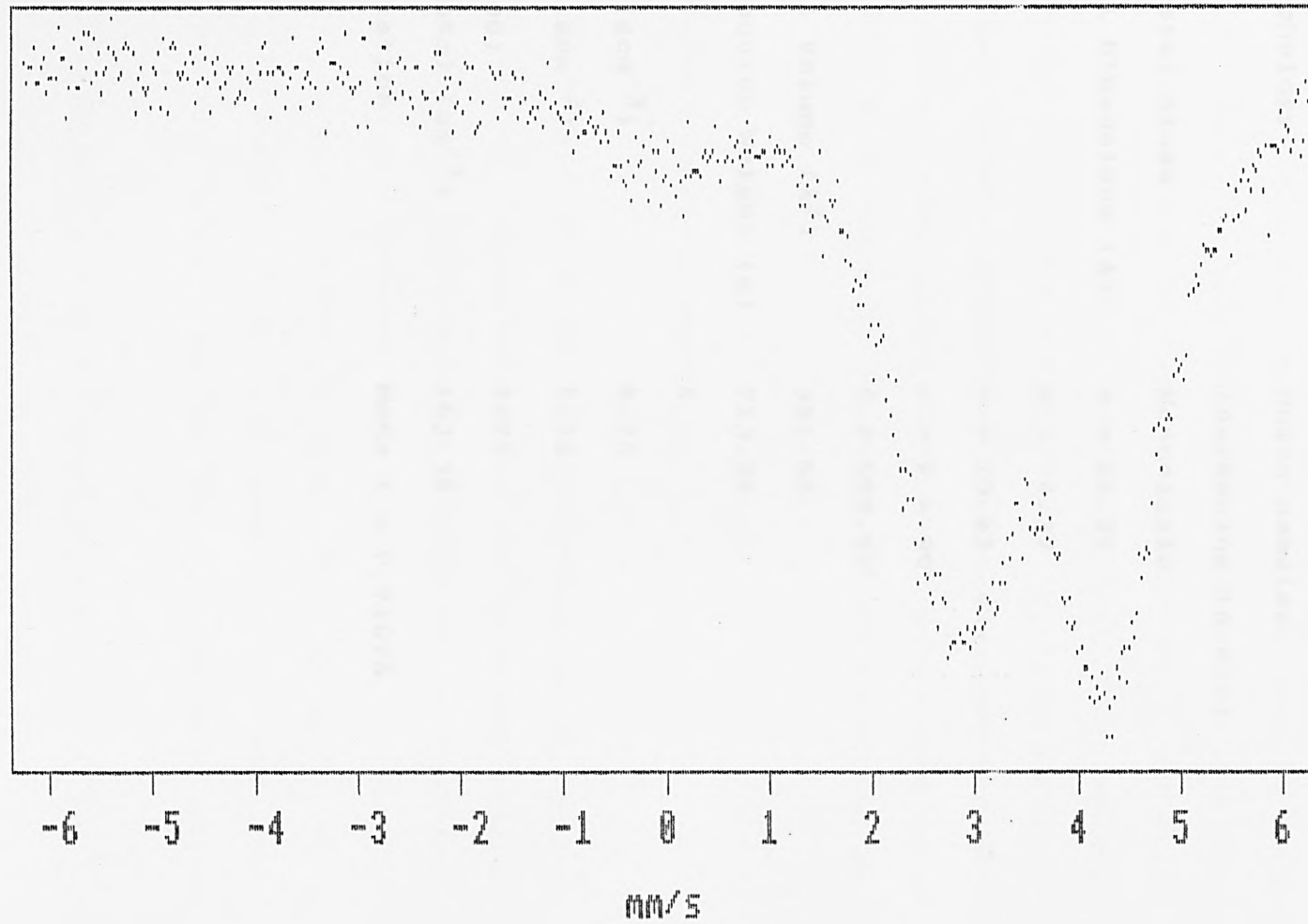


Table 5.6

Crystal data for $\text{CsSn}_3\text{Br}_{1.5}\text{F}_{5.5}$

Morphology	White needles (darkening in air)
Crystal class	Monoclinic
Cell Dimensions (Å)	a = 22.86 b = 4.37 c = 10.23 $\alpha = \gamma = 90^\circ$ $\beta = 103.94^\circ$
Cell Volume (Å ³)	991.86
Molecular Weight (g)	713.32
Z	4
D_c (gcm ⁻³)	4.78
D_o (gcm ⁻³)	4.48
$F(000)$	1228
$\mu(\text{MoK}\alpha)$ (cm ⁻¹)	163.38
Radiation	MoK α $\lambda = 0.7107\text{Å}$

calculations. The only systematic absence in the intensity data was:

$$hkl \text{ absent when } h+k = 2n+1$$

This corresponds to a C-faced centered cell. The possible space groups were therefore; C2 (no.5), Cm (no.8) and C2/m (no.12) [8] The presence of a mirror plane was excluded by examination of the Patterson map, the main peaks of which are shown in table 5.7. The complete absence in the map of any peaks of the type 0,v,0 showed that no mirror plane was present while the predominance of peaks of the type u,0,w indicated a 2 fold axis perpendicular to b. Thus the space group was confirmed as C2.

(iii) Location of atomic positions.

The relative closeness of the atomic numbers of Sn and Cs with $Z = 50$ and 55 respectively made the Patterson vector density map (table 5.7) very difficult to interpret. Consequently, direct methods were employed to locate a heavy atom. The FORTRAN program 'MULTAN-80' [14], described in section 1.9, was used to this end. The resulting electron density map had the highest peaks at:

No.	Height	x/a	y/b	z/c
1	4547	0.1104	0.5242	0.0751
2	3878	0.7672	0.5239	0.1775
3	3418	0.9866	0.5244	0.3244
4	2814	0.6553	0.5247	0.4531
5	2176	0.5000	0.5213	1.0000

Table 5.7 Patterson map for $\text{CsSn}_3\text{Br}_{1.5}\text{F}_{5.5}$

No.	Height	u/a	v/b	w/c
1	999	0.000	0.000	0.000
2	999	0.000	0.000	1.000
3	999	0.500	0.500	0.000
4	999	0.500	0.500	1.000
5	344	0.379	0.500	0.253
6	"	0.121	0.000	0.747
7	279	0.344	0.000	0.880
8	"	0.156	0.500	0.120
9	"	0.239	0.000	0.152
10	"	0.261	0.500	0.848
11	243	0.243	0.000	0.481
12	"	0.257	0.500	0.519
13	190	0.358	0.000	0.217
14	"	0.142	0.500	0.783

The positions of the two highest peaks were used in a Fourier synthesis using SHELX-76 [15] (see section 1.9). The peaks were input as two Sn atoms with the position on the y axis was fixed at zero, to define the origin. This gave an R factor of 0.53 after four cycles of least squares refinement. A third tin atom at 0.48,0,0.30 was located from the resulting electron density map.

The next highest peak on the map was at the two-fold special position 0.5,0,0. The closest contact distance to Sn from this position was 3.3Å. Although this distance is longer than the average tin to bromine bonding contact [1], the lowest residual was obtained with a bromine refined in this position. An electron density map phased on Sn and Br₍₁₎ located a full site Br at 0.36,0,0.21, which was then used to generate another electron density map, from which was located the last heavy atom Cs, at 0.34,0,0.52. The residual at this stage, with all the heavy atoms located, was 0.18.

Six fluorine sites were subsequently located from new electron density maps and refined to the following coordinates.

F ₍₁₎	0.7925,	0,	0.8184
F ₍₂₎	0.3461,	0,	0.8393
F ₍₃₎	0.2277,	0,	0.6391
F ₍₄₎	0.5869,	0.5,	0.2570

F ₍₅₎	0.4855.	0.	0.6285
F ₍₆₎	0.5567.	0.5.	0.5022

With all the fluorines at full site occupancy the molecular formula was unbalanced, with an excess of half a negative charge per formula unit. Attempts to locate half a positive charge failed and it was concluded that one of the halogen sites must be at a half site occupancy, ie ions alternating with a site vacancy. It was found that the only position that would accept half site occupancy without adverse effects on the residual was F₍₅₎.

Anisotropic thermal parameters were successfully applied to all the heavy atoms with the U₁₂ parameter of Sn₍₁₎ and the U₁₂ and U₂₃ parameters of Br₍₁₎ fixed at zero. Non unitary weights were used in the final refinement and inter-layer scale factors were calculated and refined in 1. The final residual was 0.072 and the weighted residual was 0.073. The final atomic parameters are given in table 5.8 with bond lengths and angles in tables 5.9 and 5.10. Structure factors are recorded in Appendix 2.

(iv) Structural description and discussion.

A projection of the unit cell contents is shown in fig.5.9. The arrangement of atoms in this structure is such that tin in association with bridging bromine and fluorine atoms forms polymeric chains running perpendicular to the a-c cell plane (see fig.5.10). All

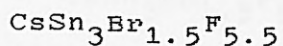
Table 5.8 Final atomic parameters

for $\text{CsSn}_3\text{Br}_{1.5}\text{F}_{5.5}$

with ESDs in brackets

Atom	x/a	y/b	z/c	S.O.F.	U_{11}	U_{22}	U_{33}	U_{23}	U_{13}	U_{12}
Cs	0.3456(1)	0	0.5388(1)	1	0.032(1)	0.023(1)	0.023(2)	-0.003(2)	0.007(1)	0.008(2)
Sn(1)	0.1081(1)	0	0.0723(1)	1	0.031(1)	0.063(1)	0.017(2)	0.009(2)	0.012(1)	0.000(0)
Sn(2)	0.7555(1)	0	0.1614(1)	1	0.040(1)	0.053(1)	0.017(1)	-0.003(2)	0.009(1)	-0.002(2)
Sn(3)	0.9881(1)	0	0.3202(1)	1	0.032(1)	0.049(1)	0.021(2)	-0.002(2)	0.009(1)	-0.002(2)
Br(1)	0.5	0	0	0.5	0.027(2)	0.029(2)	0.055(2)	0.000(0)	0.008(1)	0.000(0)
Br(2)	0.3604(1)	0	0.1958(2)	1	0.036(2)	0.038(1)	0.032(2)	-0.009(4)	0.014(1)	0.007(3)
F(1)	0.7900(7)	0	0.819(2)	1	0.070(4)					
F(2)	0.3473(6)	0	0.843(1)	1	0.053(4)					
F(3)	0.2296(5)	0	0.640(1)	1	0.042(3)					
F(4)	0.5867(5)	0.5	0.256(1)	1	0.030(3)					
F(5)	0.4842(8)	0	0.627(2)	0.5	0.012(4)					
F(6)	0.5543(5)	0.5	0.501(1)	1	0.046(3)					

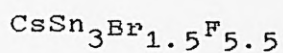
Table 5.9 Significant contact distances (Å) in



with ESDs given in brackets

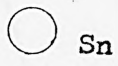
Sn(1)---Br(1)	3.248(2)	Sn(3)---F(6)	2.09(1)
Sn(1)---F(4)	2.05(2)	Sn(3)---F(5)	2.30(2)
Sn(1)---F(1)	2.33(2)	Sn(3)---F(6)'	2.26(1)
Sn(1)---F(2)	2.48(1)		
Sn(2)---Br(2)	3.200(2)	Cs-----Br(2)	3.606(2)
Sn(2)---F(3)	1.98(1)	Cs-----F(2)	3.11(1)
Sn(2)---F(1)	2.45(2)	Cs-----F(3)	3.07(1)
Sn(2)---F(2)	2.34(1)	Cs-----F(5)	3.08(2)
		Cs-----F(4)	3.16(2)
Sn(1)---Sn(2)	4.363(2)	Cs-----F(6)	3.26(2)
Sn(1)---Sn(3)	4.087(2)		

Table 5.10 Significant bond angles (°) in



with ESDs in brackets

Br(1)--Sn(1)--F(4)	82.7(4)
Br(1)--Sn(1)--F(1)	136.7(4)
F(4)-- Sn(1)--F(1)	89.7(6)
Br(1)--Sn(1)--Br(1) _(y=1)	84.6(2)
Br(2)--Sn(2)--F(3)	87.0(4)
Br(2)--Sn(2)--F(2)	136.5(4)
F(3)---Sn(2)--F(2)	86.8(6)
Br(2)--Sn(2)--Br(2) _(y=1)	86.1(2)
F(6)---Sn(3)--F(5)	72.1(7)
F(6)---Sn(3)--F(6)'	69.2(6)
F(5)---Sn(3)--F(6)'	87.6(7)



Key to figs. 5.9 to 5.14

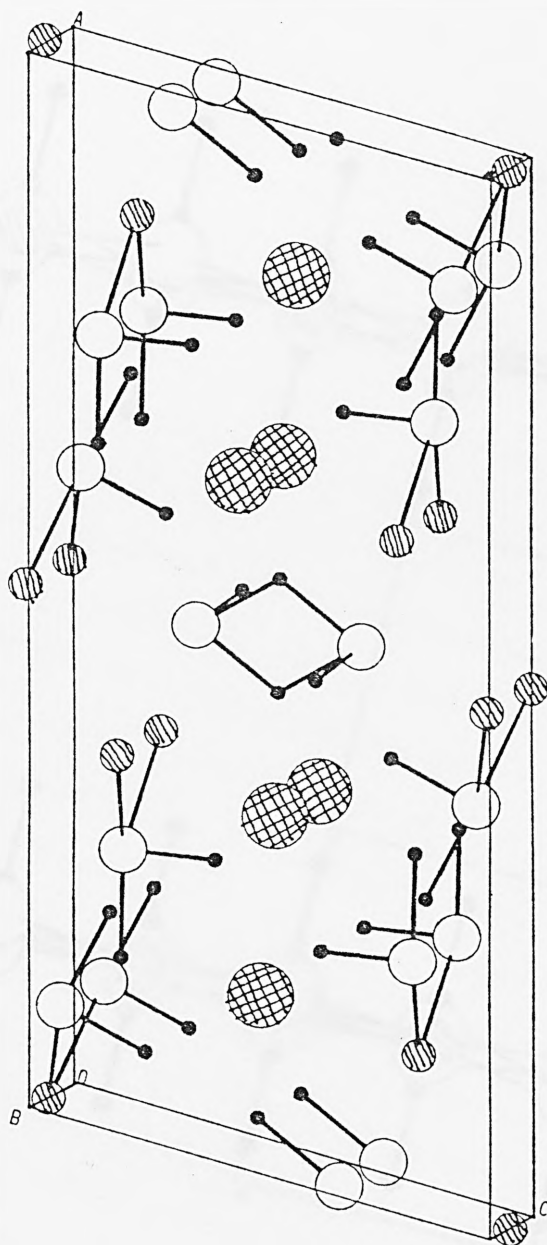


Fig.5.9
Unit cell contents of $\text{CsSn}_3\text{Br}_{1.5}\text{F}_{5.5}$

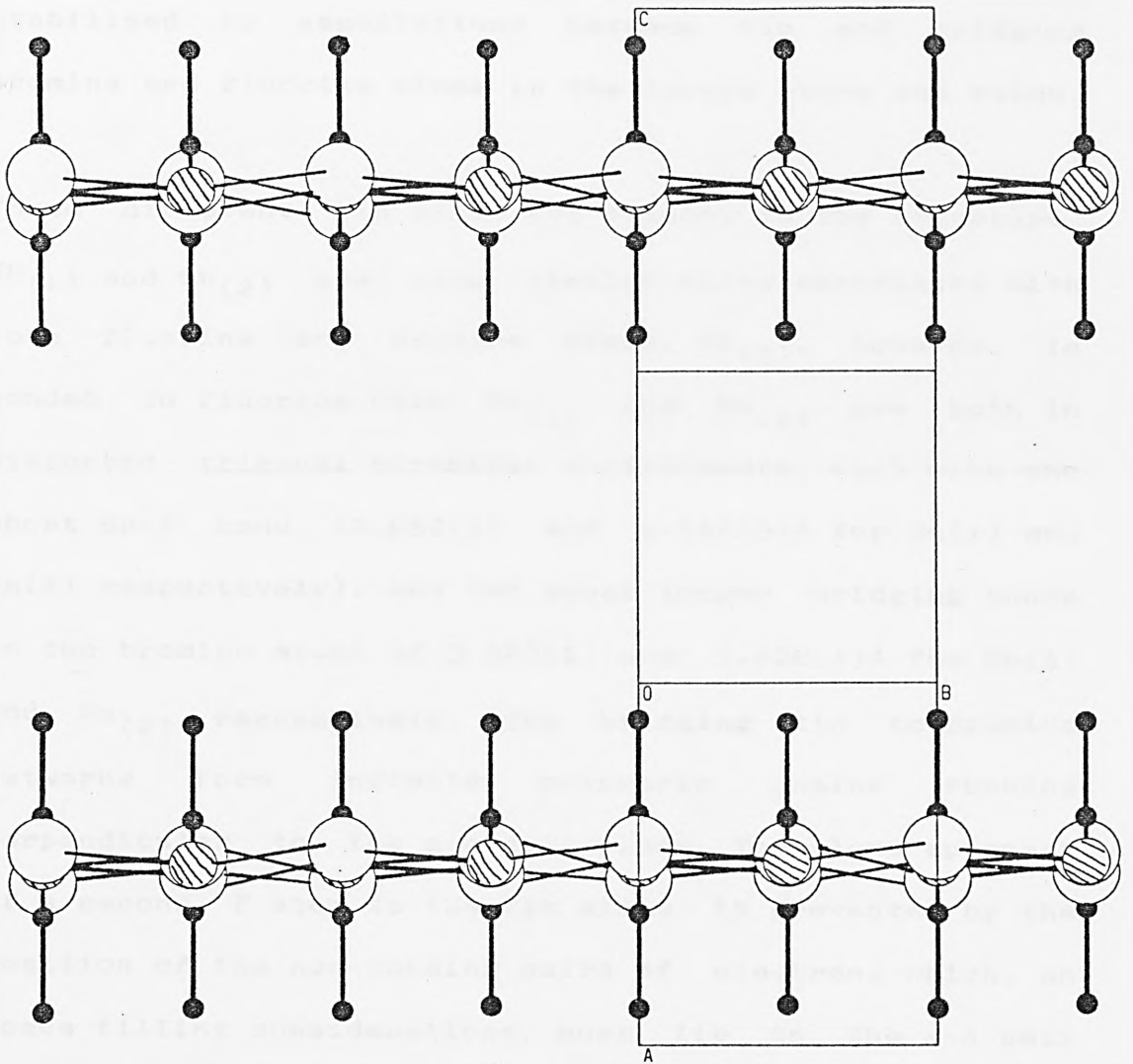


Fig.5.10.

Bridging Br networks in CsSn₃Br_{1.5}F_{5.5} running perpendicular to the a-c cell plane.

the atoms lie in planes perpendicular to the b-axis at $b = 0$ and $b = 0.5$ (see fig.5.11). This layered structure is stabilised by associations between tin and bridging bromine and fluorine atoms in the layers above and below.

Three different tin sites are present in the structure. $\text{Sn}_{(1)}$ and $\text{Sn}_{(2)}$ are very similar being associated with both fluorine and bromine atoms. $\text{Sn}_{(3)}$, however, is bonded to fluorine only. $\text{Sn}_{(1)}$ and $\text{Sn}_{(2)}$ are both in distorted trigonal pyramidal environments, each with one short Sn-F bond (2.052(5) and 1.980(5)Å for $\text{Sn}_{(1)}$ and $\text{Sn}_{(2)}$ respectively), and two equal longer bridging bonds to two bromine atoms of 3.248(1) and 3.200(1)Å for $\text{Sn}_{(1)}$ and $\text{Sn}_{(2)}$ respectively. The bridging tin to bromine networks form infinite polymeric chains running perpendicular to the a-c cell plane. The close approach of a second F atom to the tin atoms is prevented by the position of the non-bonding pairs of electrons which, on space filling considerations, must lie in the a-c cell plane. The fluorines affected by the lone pair repulsion are located at distances of 2.328(5) and 2.339(5)Å, from $\text{Sn}_{(1)}$ and $\text{Sn}_{(2)}$ respectively, and are stabilised by interactions with tin atoms in the layers above and below at distances of $\text{Sn}_{(1)}-\text{F}_{(2)} = 2.477(4)$ Å and $\text{Sn}_{(2)}-\text{F}_{(1)} = 2.449(4)$ Å, which are well within the sum of the Van der Waals radii at 3.7Å [16]. The two tin halogen polymeric chains are, therefore, interlocked at every layer giving a pair of polymeric anions of formula $[\text{SnBrF}_2]_n^{n-}$ and $[\text{Sn}_2\text{BrF}_4]_n^{n-}$ in a 2:1 ratio (see fig 5.12).

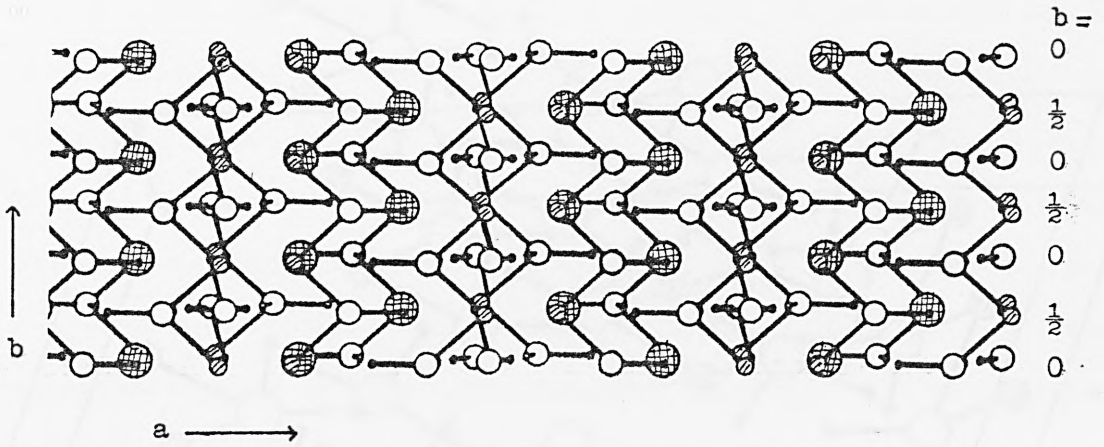


Fig.5.11.

Planes of atoms in $\text{CsSn}_3\text{Br}_{1.5}\text{F}_{5.5}$ at $b = 0$ & $b = \frac{1}{2}$.

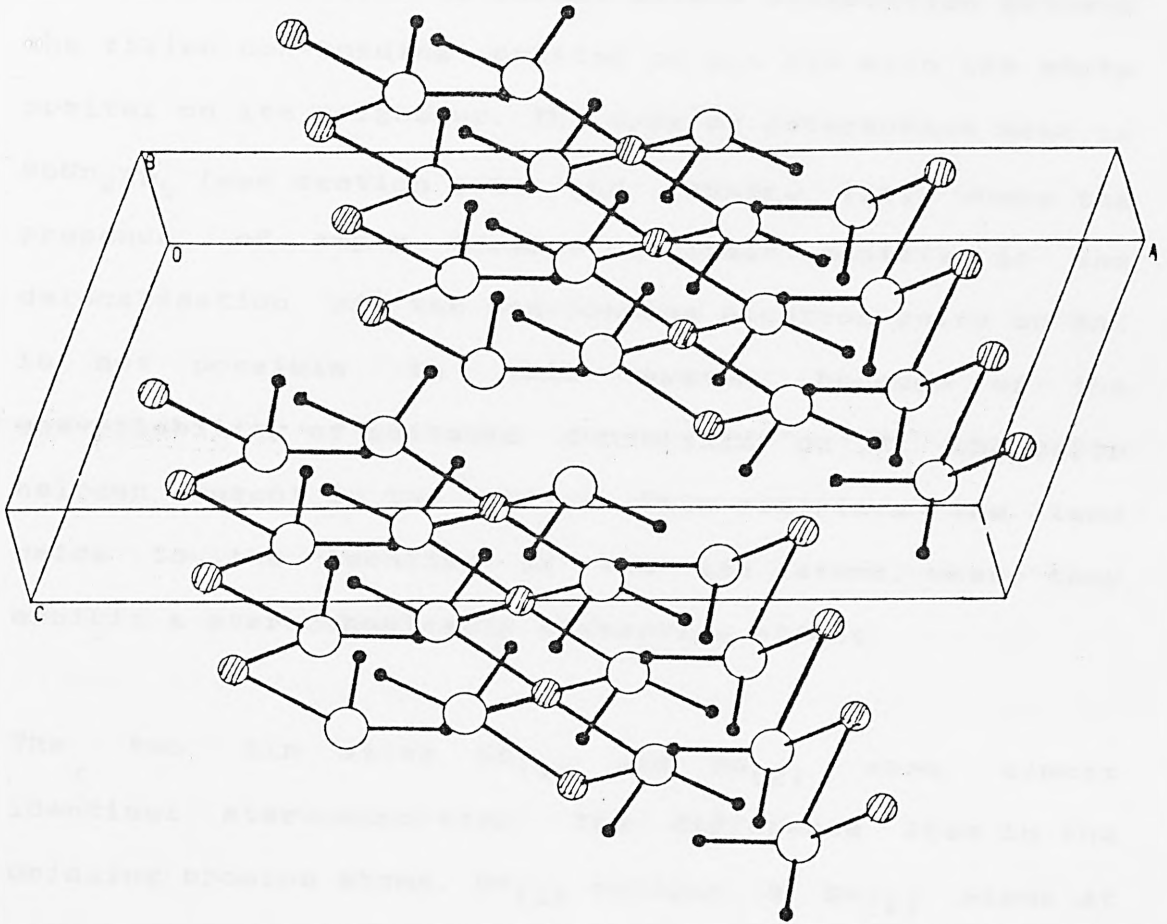


Fig.5.12

Projection of $2[\text{SnBrF}_2]_n^{n-} \cdot [\text{Sn}_2\text{BrF}_4]_n^{n-}$ interlocking
polymeric anions in $\text{CsSn}_3\text{Br}_{1.5}\text{F}_{5.5}$ which
run perpendicular to a/c

The $\text{Sn}_{(1)}\text{-Sn}_{(2)}$ distance of 4.363(4)Å is outside that normally considered to permit direct interaction between the filled non-bonding orbital on one tin with the empty orbital on its neighbour. The type of interaction seen in RbSn_2Br_5 (see section 5.2) and CsSnBr_3 [11], where the presence of empty bromine orbitals assists in the delocalisation of the non-bonding electron pairs on Sn, is not possible in this system because of the unavailability of suitable d-orbitals on F, the major halogen present in the lattice. This restricts the lone pairs to the locality of the tin atoms, where they exhibit a stereochemically distorting effect.

The two tin sites $\text{Sn}_{(1)}$ and $\text{Sn}_{(2)}$ show almost identical stereochemistry. The difference lies in the bridging bromine atoms. $\text{Br}_{(1)}$ bridges 4 $\text{Sn}_{(1)}$ atoms at equal distances of 3.248(1)Å in a square planar arrangement. Six coordinate geometry is completed with two equidistant $\text{Sn}_{(3)}$ atoms arranged axially at 4.001(1)Å. $\text{Br}_{(2)}$ bridges only two $\text{Sn}_{(2)}$ atoms in the layers above and below, at a distance of 3.200(1)Å and is seven coordinate with contacts to two $\text{Sn}_{(3)}$ atoms at 3.623(1)Å, a Cs at 3.606(2)Å and two $\text{Sn}_{(1)}$ atoms at 3.710(1)Å. The difference in the coordination of the two Br sites reflects the difference shown in the bond lengths in the two trigonal pyramidal sites at $\text{Sn}_{(1)}$ and $\text{Sn}_{(2)}$, the $\text{Sn}_{(2)}$ -site bonds being shorter than the analogous bonds around the the $\text{Sn}_{(1)}$ site.

$\text{Sn}_{(3)}$ atoms are also in trigonal pyramidal environments. Pairs of $\text{Sn}_{(3)}$ atoms at $y = 0$ and $y = 0.5$ are linked by pairs of F atoms, giving one short (2.091(1)Å) and one long (2.263(1)Å) bridging Sn-F distance to each tin atom. A pair of F atoms bridges each of the $\text{Sn}_{(3)}$ atoms in one cell with $\text{Sn}_{(3)}$ atoms in the next cell. The inter-cell bridging distances are equal (2.302(1)Å) and are responsible for the formation of a polymeric chain perpendicular to the a-c cell plane. The non-bonding electron pairs point out of the a-c plane where they prevent the close approach of any further ligands. Unlike the short bonds in the two other tin sites, the $\text{Sn}_{(3)}\text{-F}_{(6)}$ bond is non terminal and the fluorine bridges to another $\text{Sn}_{(3)}$ atom in the same plane forming a planar, four membered, ring with alternating long and short bonds. These rings are linked to others above and below the plane, by a bridging fluorine $\text{F}_{(5)}$, in a zig-zag configuration as seen in fig 5.13. The polymeric chains have 3 fluorine atoms surrounding each $\text{Sn}_{(3)}$ atom and form cationic networks $[\text{Sn}_2\text{F}_3]_n^{n+}$ running perpendicular to the a-c cell plane. Three longer tin halogen contacts complete distorted six coordinate geometry with two $\text{Br}_{(2)}$ atoms at 3.623(1) and $\text{F}_{(4)}$ at 2.495(1)Å. The environments of the three tin atoms are summarised in fig 5.14.

The Cs atoms occupy holes in the lattice and are surrounded by 7 fluorine atoms at distances ranging between 3.069 to 3.164Å and a single Br at 3.606(1)Å.

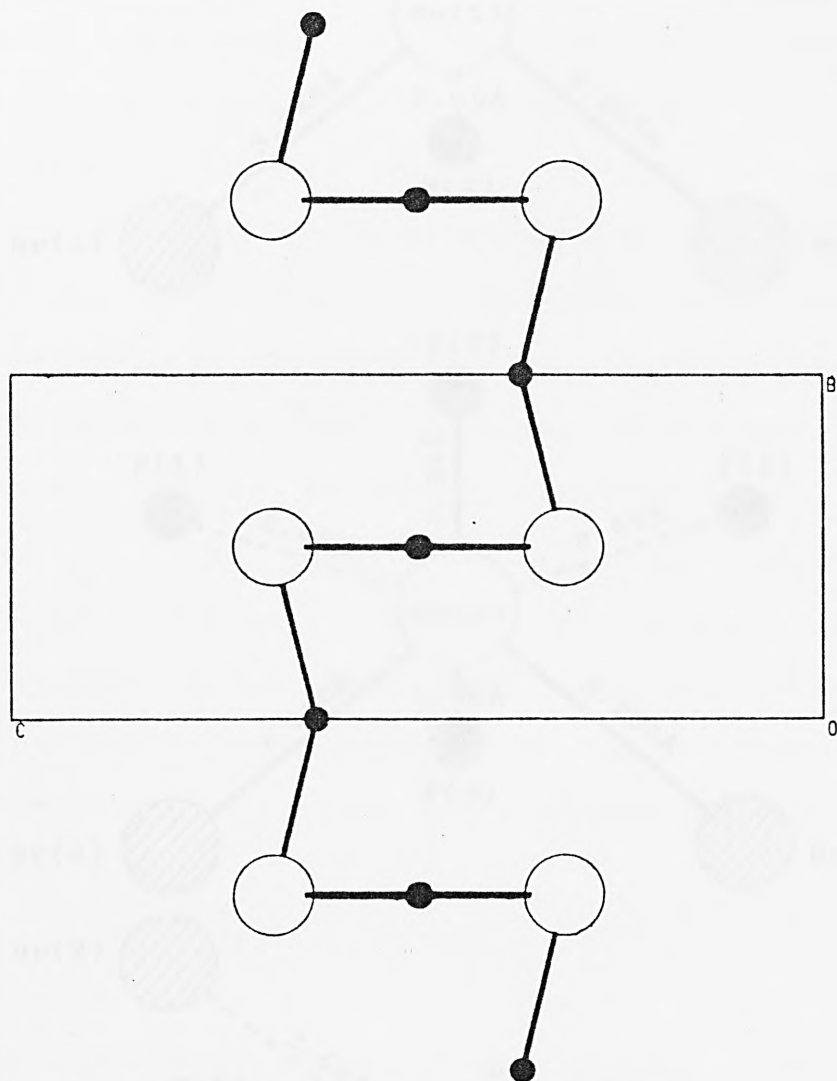


Fig.5.13

Projection of $[\text{Sn}_2\text{F}_3]_n^{n+}$ chain onto b/c in $\text{CsSn}_3\text{Br}_{1.5}\text{F}_{5.5}$ showing 'zig - zag' configuration

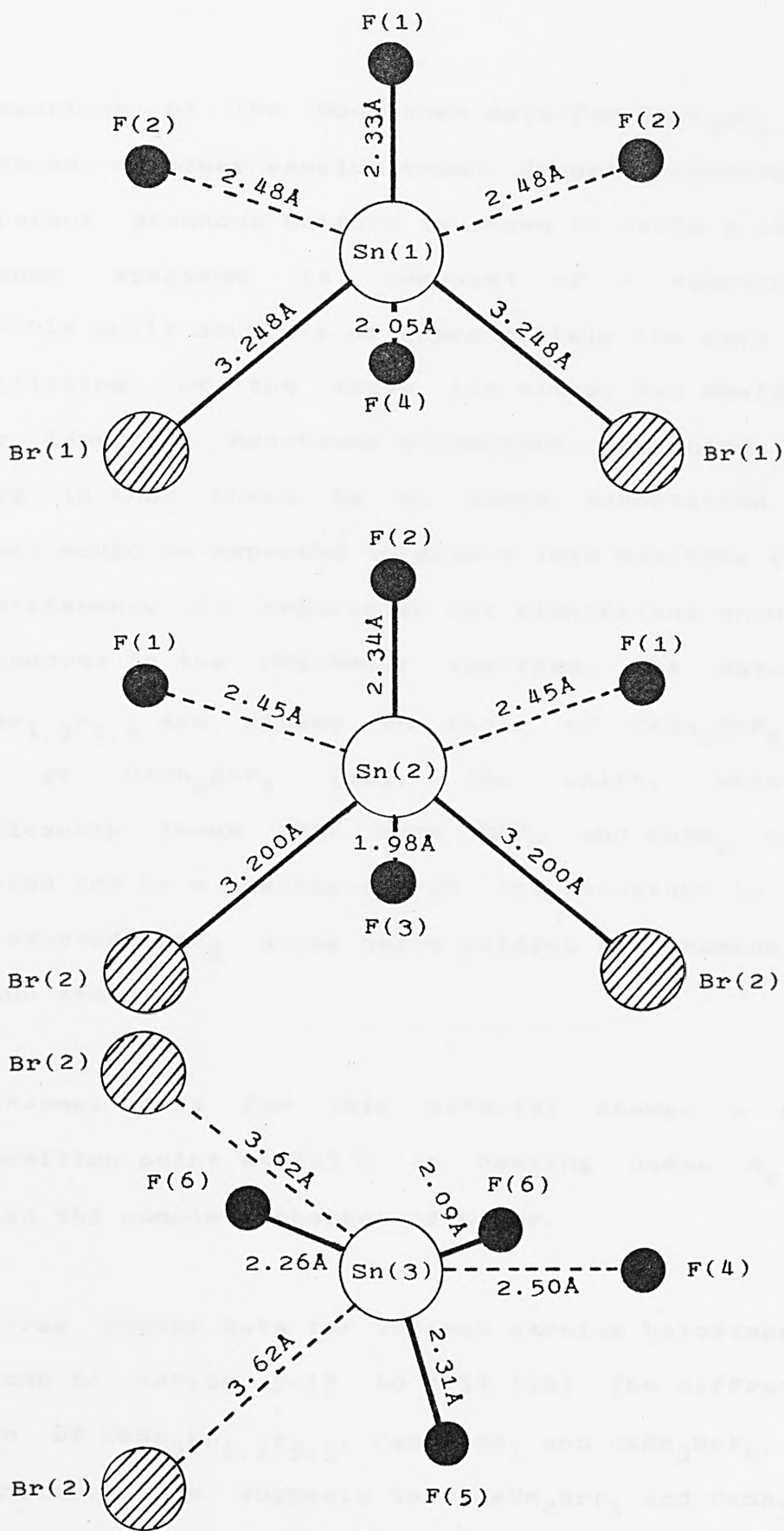


Fig. 5.14

Tin environments in CsSn₃Br_{1.5}F_{5.5}

A comparison of the Mössbauer data for $\text{CsSn}_3\text{Br}_{1.5}\text{F}_{5.5}$ with those of other caesium bromo- fluoro- stannates and the parent stannous halides is shown in table 5.11. The Mössbauer spectrum is composed of 3 superimposed quadrupole split doublets of approximately the same shift and splitting. Of the three tin sites, two would show nearly identical Mössbauer parameters, the third, which differs in that there is no close association with bromine, would be expected to show a less positive shift. This difference is apparently not significant enough to be observed in the Mössbauer spectrum. The data for $\text{CsSn}_3\text{Br}_{1.5}\text{F}_{5.5}$ are closer to those of $\text{CsSn}_3\text{BrF}_6$ than those of $\text{CsSn}_2\text{BrF}_4$ [16]. The shift, which is significantly lower than both SnF_2 and SnBr_2 , may be accounted for by a description of the structure in terms of distorted SnF_2 units being bridged by bromine and fluorine atoms.

The thermal data for this material showed a sharp decomposition point at 225 °C on heating under N_2 and verified the complete absence of water.

The X-ray powder data for various caesium halostannates are shown in tables 5.12 to 5.14 [16]. The diffraction pattern of $\text{CsSn}_3\text{Br}_{1.5}\text{F}_{5.5}$, $\text{CsSn}_2\text{BrF}_4$ and $\text{CsSn}_3\text{BrF}_6$, are all similar. This suggests that $\text{CsSn}_2\text{BrF}_4$ and $\text{CsSn}_3\text{BrF}_6$ may have structures similar to that of $\text{CsSn}_3\text{Br}_{1.5}\text{F}_{5.5}$.

Table 5.11

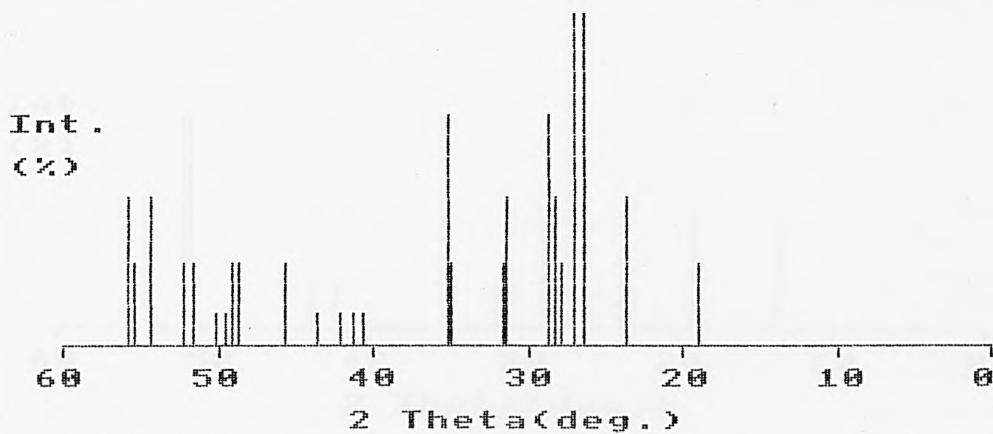
Comparison of 80K Mössbauer data for some caesium bromo-fluoro-stannates (II) and starting materials.

Formula	δ mm/s	Δ mm/s	
$\text{CsSn}_3\text{Br}_{1.5}\text{F}_{5.5}$	3.50	1.50	
$\text{CsSn}_3\text{BrF}_6$	3.46	1.53	[16]
$\text{CsSn}_2\text{BrF}_4$	3.43	1.44	[16]
$\text{CsBr} \cdot \text{CsSnBrF}_2$	2.93	1.81	[16]
SnBr_2	3.98	0.00	
SnF_2	3.65	1.80	

Note all shifts are quoted wrt to CaSnO_3 .

Table 5.12
X-ray Powder Diffraction Pattern
CsSn₃BrF₆

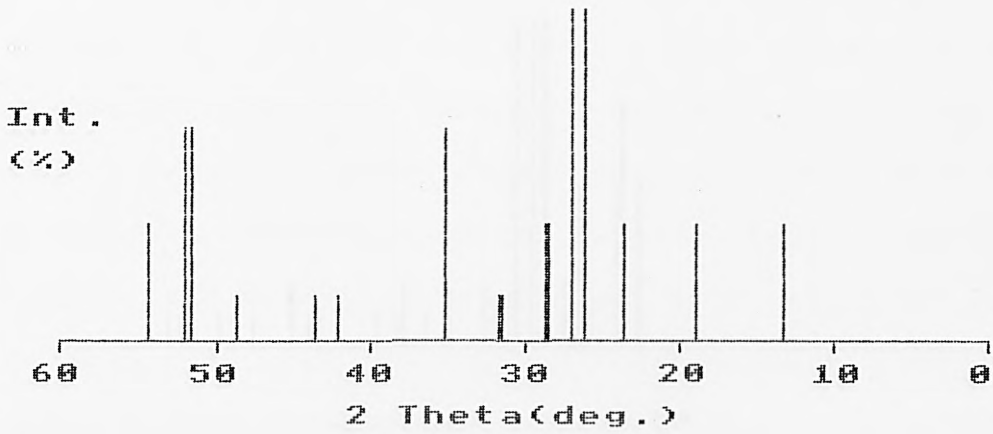
[16]



Rel. Int. (%)	d(hkl)Å
26	4.670
46	3.780
100	3.390
100	3.300
26	3.210
46	3.160
70	3.120
46	2.860
26	2.840
26	2.560
70	2.550
10	2.220
10	2.190
10	2.150
10	2.080
26	1.990
26	1.870
26	1.860
10	1.840
10	1.820
26	1.770
26	1.750
46	1.690
26	1.660
46	1.650

Table 5.13
X-ray Powder Diffraction Pattern
CsSn₂BrF₄

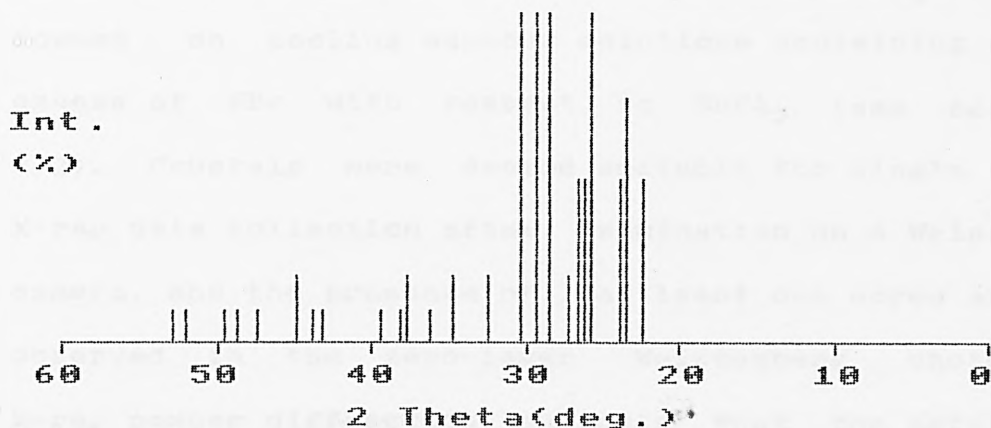
[16]



Rel. Int. (%)	d(hkl)Å
35	6.660
35	4.670
35	3.770
100	3.400
100	3.310
35	3.150
35	3.110
15	2.860
15	2.830
64	2.550
15	2.150
15	2.080
15	1.870
64	1.770
64	1.760
35	1.690

Table 5.14
X-ray Powder Diffraction Pattern
CsBr.CsSnBrF2

[16]



Rel. Int. (%)	d(hkl)A
50	3.970
76	3.820
50	3.740
100	3.460
50	3.410
50	3.360
20	3.280
100	3.150
100	3.050
100	2.940
20	2.760
20	2.580
10	2.480
20	2.390
10	2.360
10	2.360
10	2.290
10	2.100
10	2.070
20	2.020
10	1.920
10	1.870
10	1.840
10	1.760
10	1.730

5.4 The X-ray structure determination of $\text{KBr.KSnBr}_2\text{Cl.H}_2\text{O}$

Crystals of the complex salt $\text{KBr.KSnBr}_2\text{Cl.H}_2\text{O}$ are formed on cooling aqueous solutions containing a large excess of KBr with respect to SnCl_2 (see section 2.3). Crystals were deemed suitable for single crystal X-ray data collection after examination on a Weissenberg camera, and the presence of at least one screw axis was observed in the zero-layer Weissenberg photograph. X-ray powder diffraction suggests that the material is isostructural with the known structures of the all chlorine analogues $\text{KCl.KSnCl}_3.\text{H}_2\text{O}$ and $\text{NH}_4\text{Cl.NH}_4\text{SnCl}_3.\text{H}_2\text{O}$ [17,18]. The structure of this material was undertaken with three principal areas of interest; firstly is the Cl atom preferentially located, as both covalent and ionic halogen sites are known to exist in these materials; secondly to characterise the Sn-Br covalent bond in the complex $[\text{SnX}_3]^-$ anion (where $\text{X} = \text{Br}_n\text{Cl}_{3-n}$) and thirdly, to observe the extent, if any, of delocalisation of the non-bonding electrons on tin.

(i) Preparation

$\text{KBr.KSnBr}_2\text{Cl.H}_2\text{O}$ was prepared from a mixture of KBr and $\text{SnCl}_2.2\text{H}_2\text{O}$ in a 5:1 mole ratio using the general preparative method (section 2.2). A few drops of concentrated HBr were used to suppress hydrolysis. The crystals which formed on cooling were colourless rhomboid prisms. Analyses for K, Sn, Br, Cl and H_2O were carried out using the methods described in section 2.2.

The analytical data are as follows:

	K	Sn	Br	Cl	H ₂ O
KBr.KSnBr ₂ Cl.H ₂ O	18.5	22.6	47.5	7.7	5.3
Calculated	(16.0)	(24.2)	(48.9)	(7.2)	(3.6)

A Mössbauer spectrum and X-ray powder diffraction pattern were recorded as described in sections 4.1 and 1.6 respectively. The X-ray powder data and Mössbauer parameters are given in section 2.3.

(ii) Data collection and space group determination.

Intensity data were collected on a Phillips PW1100 four circle diffractometer at Queen Mary College, London as described in section 1.7. Monochromatic MoK α ($\lambda = 0.7107\text{\AA}$) radiation was used throughout. Data for 1158 unique reflections, in orthorhombic symmetry, with $I > 3 \sigma(I)$ were used in subsequent calculations. Data were corrected for Lorentz and polarisation factors but not for absorption.

The crystal data are shown in table 5.15. The crystal class is orthorhombic with unit cell parameters obeying the following restrictions:

$$a = b = c; \quad \alpha = \beta = \gamma = 90^\circ$$

The following systematic absences were observed in the intensity data:

Table 5.15

Crystal data for $\text{KBr} \cdot \text{KSnBr}_2 \cdot \text{Cl} \cdot \text{H}_2\text{O}$

Morphology	White rhomboid prisms
Crystal class	Orthorhombic
Cell Dimensions (Å)	a = 9.3830 b = 8.5824 c = 12.4937 $\alpha = \beta = \gamma = 90^\circ$
Cell Volume (Å ³)	1006.10
Molecular Weight (g)	490.03
Z	4
D_c (gcm ⁻³)	3.24
D_o (gcm ⁻³)	3.25
F(000)	756
$\nu(\text{MoK}\alpha)$ (cm ⁻¹)	111.33
Radiation	MoK α $\lambda = 0.7107\text{Å}$

The symmetry related positions for $\text{KBr} \cdot \text{KSnBr}_2 \cdot \text{Cl} \cdot \text{H}_2\text{O}$ are as follows:

(1) x, y, z

(2) -x, -y, z

(3) x, -y, -z

(4) -x, y, -z

$h00$ absent when $h = 2n + 1$

$0k0$ absent when $k = 2n + 1$

$00l$ absent when $l = 2n + 1$

$h0l$ absent when $l = 2n + 1$

$hk0$ absent when $h + k = 2n + 1$

These correspond to the symmetry operations shown below:

2_1 parallel to a

2_1 parallel to b

2_1 parallel to c

c - glide perpendicular to b

n - glide perpendicular to c

In the absence of any general systematic absences in the hkl data it was concluded that the cell was primitive. Two orthorhombic space groups are possible with the above combination of absences; $P2_1cn$ (non standard form of $Pna2_1$ no.33) and $Pmcn$ (non standard form of $Pnma$ no.62) [8]. The structure was solved in the non centrosymmetric space group $P2_1cn$.

The symmetry related positions for $P2_1cn$ are as follows:

(1) x, y, z

(2) $0.5-x, 0.5-y, 0.5+z$

(3) $0.5+x, -y, -z$

(4) $-x, 0.5+y, 0.5-z$

(iii) Location of atomic positions.

As an alternative to a Patterson vector density map, direct methods were used to locate a heavy atom using the FORTRAN program 'MULTAN-80' [14], described in section 1.9. The two highest peaks generated had the following parameters:

$$x = 0.3979, y = 0.2176, z = 0.4448$$

$$x = 0.8019, y = 0.2174, z = 0.4449$$

These two positions were input into a Fourier synthesis using SHELX-76 [15]. The peaks were initially labelled as two Sn atoms and gave an R factor of 0.53 after four cycles of least squares. A third atom was located at the top of the resulting electron density map with the following coordinates:

$$x = 0.1040, y = 0.0007, z = 0.5109$$

The distance between this position and the atom at 0.398, 0.218, 0.445 was 2.70Å which is typical of a Sn-Br covalent bond [1]. These two positions were therefore input into a Fourier synthesis as tin and bromine atoms. By trial and error, based on residuals obtained, it was found that the position found by direct methods was in fact a Br and not a Sn atom, as initially input. With two atoms located in the following positions, the residual fell to 44.3%:

Sn 0.1079, 0.0068, 0.5103

Br₍₁₎ 0.3939, 0.2113, 0.4438

The highest peak in electron density map generated using the above positions was at 0.11, 0.10, 0.76. Using this position assigned as Br₍₂₎ and the Sn and Br₍₁₎ positions the residual after 4 cycles of least squares refinement was 34.3%. At this stage the electron density peak search was expanded to cover the whole unit cell and subsequently a further two atoms were located as the highest peaks in the resulting electron density map. These positions, initially labelled Br₍₃₎ and Br₍₄₎, had the following coordinates:

Br₍₃₎ 0.3092, 0.7927, 0.5545

Br₍₄₎ 0.0869, 0.8945, 0.3044

The residual at this stage was 22.8%. Attempts to locate a Cl atom in one of the Br positions resulted in an increased residual in all but the Br₍₄₎ position, so Br₍₄₎ was re-labelled as a Cl atom. The two highest peaks in an electron density map generated using the Sn, Br and Cl atoms, were input into a Fourier synthesis as two potassium atoms and had the following coordinates:

K₍₁₎ 0.3345, 0.3665, 0.6868

K₍₂₎ 0.8705, 0.3695, 0.6842

Using these positions and those of Sn, Br and Cl to phase structure factors an oxygen atom was located in the

resulting electron density map in the following position:

0 0.0788, 0.0560, 0.0454

With all the atoms located and vibrating isotropically the residual after 4 cycles of least squares was 10.5%. Anisotropic thermal parameters were successfully applied to Sn and Br atoms. The Cl position, however, would not accept anisotropic thermal parameters; with Br substituted for Cl in this position anisotropic thermal parameters were successfully applied and was also accompanied by a relatively large drop in the residual from 9.3 to 6.3%. With the two potassium atoms also vibrating anisotropically the residual fell even further to 5.6%. The Cl atom was still unaccounted for and it was concluded that it must be sharing a site with two or more of the Br atoms. The isotropic temperature factors of the Br atoms at this stage were as follows:

Atom	B
Br ₍₁₎	0.0261
Br ₍₂₎	0.0295
Br ₍₃₎	0.0429
Br ₍₄₎	0.0482

It was noticed that the isotropic temperature factors of Br₍₃₎ and Br₍₄₎ were both higher than those of Br₍₁₎ and Br₍₂₎. With Br₍₃₎ and Br₍₄₎ set at half site occupancy, a pair of Cl atoms, also at half site occupancy, and in the same positions as Br₍₃₎ and Br₍₄₎ were added to the

atom list. Structure factor calculations phased on all of the atom positions gave a lowered residual of 3.8%. Repetition of this procedure with the other two halogen positions increased the residual. In the final refinement reflections where $2F_o < |(F_o - F_c)| > 2F_c$ were omitted from calculations, these were as follows:

h	k	l	h	k	l	h	k	l	h	k	l
11	4	1	1	0	2	9	1	3	2	9	4
3	10	5	2	7	6	8	3	8	4	8	9
1	4	11	1	6	13	3	2	14			

Attempts to fit anisotropic thermal parameters to Cl and O atoms were unsuccessful. The final residual was 3.63%. The final atomic parameters are given in table 5.16 with bond lengths and angles in tables 5.17 and 5.18. Structure factors are recorded in Appendix 2.

(iv) Structural description and discussion.

A projection of the unit cell contents is shown in fig. 5.15. The structure consists of tin atoms in trigonal pyramidal environments bonded to 3 halogen atoms constituting a $[\text{SnBr}_2\text{Cl}]^-$ anion. The remaining bromines exist as ions as do the potassiums.

Assuming a random distribution of Cl atoms four complex tin anions of the general formula $[\text{SnBr}_{1+n}\text{Cl}_{2-n}]^-$ are possible with eight possible tin environments, these are summarised in figs. 5.16 and 5.17. In all the possible

Table 5.16

Final atomic parameters for $\text{KBr.KSnBr}_2\text{Cl.H}_2\text{O}$

with ESDs in brackets

Atom	x/a	y/b	z/c	S.O.F	U_{11}	U_{22}	U_{33}	U_{23}	U_{13}	U_{12}
Sn	0.0	0.0010(1)	0.5093(1)	1.0	0.0220(4)	0.0279(5)	0.0230(4)	-0.0036(4)	-0.001(1)	0.002(1)
K(1)	0.237(1)	-0.632(1)	0.6869(8)	1.0	0.019(3)	0.037(5)	0.033(4)	-0.006(5)	-0.010(3)	-0.005(3)
K(2)	-0.221(1)	-0.633(2)	0.6834(9)	1.0	0.047(6)	0.051(7)	0.039(5)	-0.009(6)	-0.007(4)	0.005(4)
Br(1)	0.0	0.0961(2)	0.7632(1)	1.0	0.0307(8)	0.0327(8)	0.0387(8)	0.0011(7)	-0.008(2)	-0.001(3)
Br(2)	0.2991(6)	0.2131(6)	0.4428(4)	1.0	0.033(2)	0.056(3)	0.036(2)	0.002(2)	-0.008(2)	0.012(2)
Br(3)	0.207(1)	-0.213(1)	0.5537(9)	0.5	0.019(4)	0.018(4)	0.015(4)	0.001(3)	0.011(3)	0.001(3)
Br(4)	0.0	-0.110(1)	0.305(1)	0.5	0.032(3)	0.026(5)	0.015(3)	0.000(3)	0.006(4)	-0.001(4)
Cl(1)	0.0	-0.096(5)	0.305(3)	0.5	0.027(6)					
Cl(2)	0.194(3)	-0.200(3)	0.556(3)	0.5	0.043(7)					
O	-0.015(2)	0.059(1)	0.0459(9)	1.0	0.039(4)					

Table 5.17

Bond lengths (Å) and significant contact distances in $\text{KBr} \cdot \text{KSnBr}_2 \cdot \text{Cl} \cdot \text{H}_2\text{O}$ with ESDs in brackets

Sn--Br(1)	3.28(1)
Sn--Br(2)	2.70(1)
Sn--Br(3)	2.73(1)
Sn--Br(4)	2.72(1)
Sn--Cl(1)	2.68(4)
Sn--Cl(2)	2.58(2)
Sn--Sn	4.70(1)
K(1)--Br(1)	3.21(1)
K(1)--Br(2)	3.32(1)
K(1)--Br(4)	3.31(1)
K(1)--Cl(1)	3.40(5)
K(2)--Br(1)	3.27(1)
K(2)--Br(3)	3.32(1)
K(2)--Br(4)	3.31(1)
K(2)--Cl(1)	3.23(5)
K(2)--Cl(2)	3.40(4)
K(2)--O	2.66(3)

Table 5.18

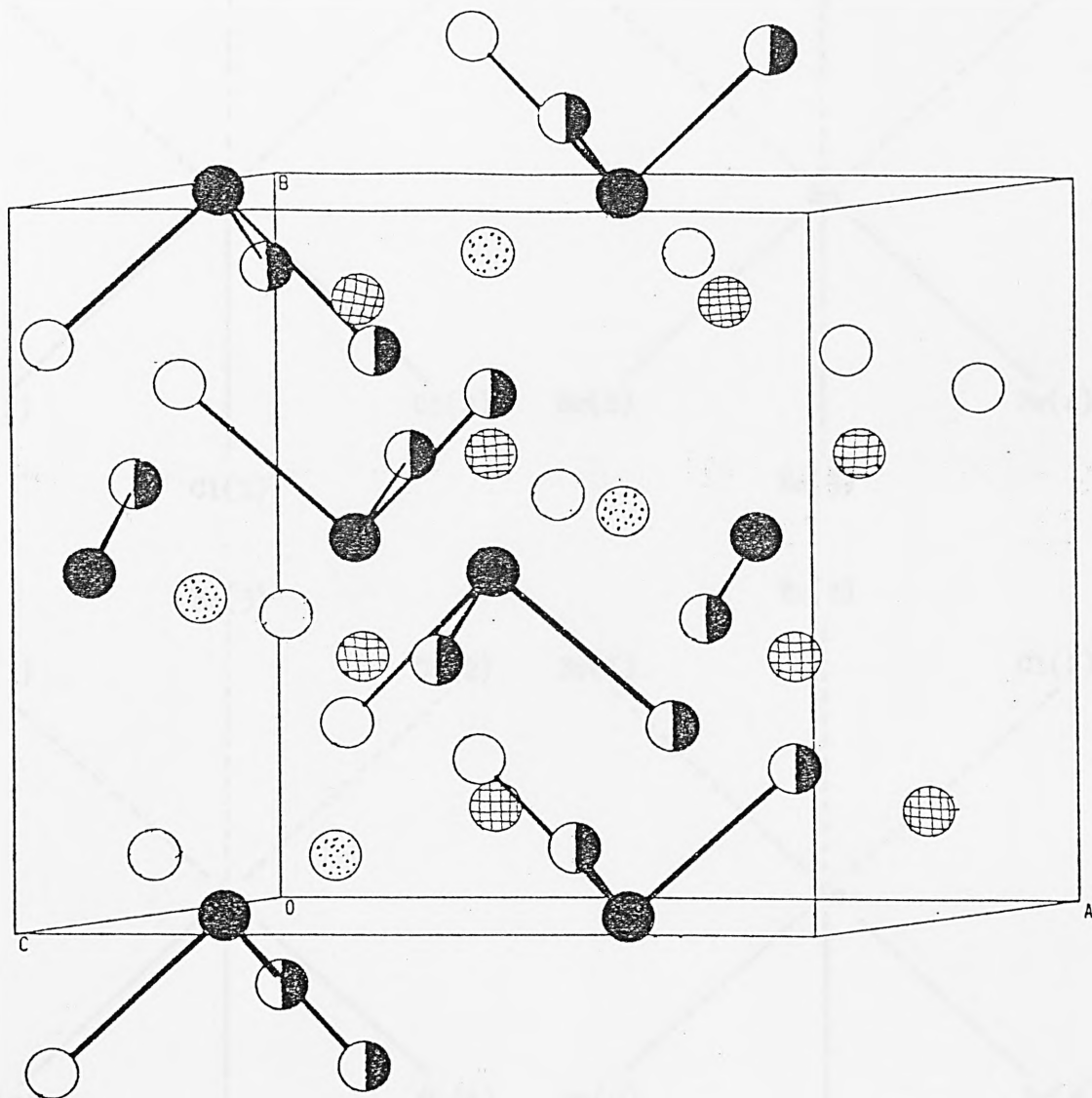
Bond angles (°) in $\text{KBr} \cdot \text{KSnBr}_2\text{Cl} \cdot \text{H}_2\text{O}$

with ESDs in brackets

Br(2)--Sn--Br(3)	89.6(0.5)
Br(2)--Sn--Br(4)	88.2(0.8)
Br(2)--Sn--Cl(1)	90.0(1.0)
Br(2)--Sn--Cl(2)	89.2(0.8)
Br(3)--Sn--Br(4)	87.3(0.3)
Br(3)--Sn--Cl(1)	89.1(0.7)
Br(4)--Sn--Cl(2)	88.7(0.8)
Cl(1)--Sn--Cl(2)	90.5(1.0)

Fig.5.15.

$\text{KBr} \cdot \text{KSnBr}_2 \text{Cl} \cdot \text{H}_2\text{O}$ and $\text{KCl} \cdot \text{KSnCl}_3 \cdot \text{H}_2\text{O}$:
Generalised Projection of Unit Cell Contents.



 Sn

 O

 K

 Br in $\text{KBr} \cdot \text{KSnBr}_2 \text{Cl} \cdot \text{H}_2\text{O}$; Cl in $\text{KCl} \cdot \text{KSnCl}_3 \cdot \text{H}_2\text{O}$

 Br/Cl in $\text{KBr} \cdot \text{KSnBr}_2 \text{Cl} \cdot \text{H}_2\text{O}$; Cl in $\text{KCl} \cdot \text{KSnCl}_3 \cdot \text{H}_2\text{O}$

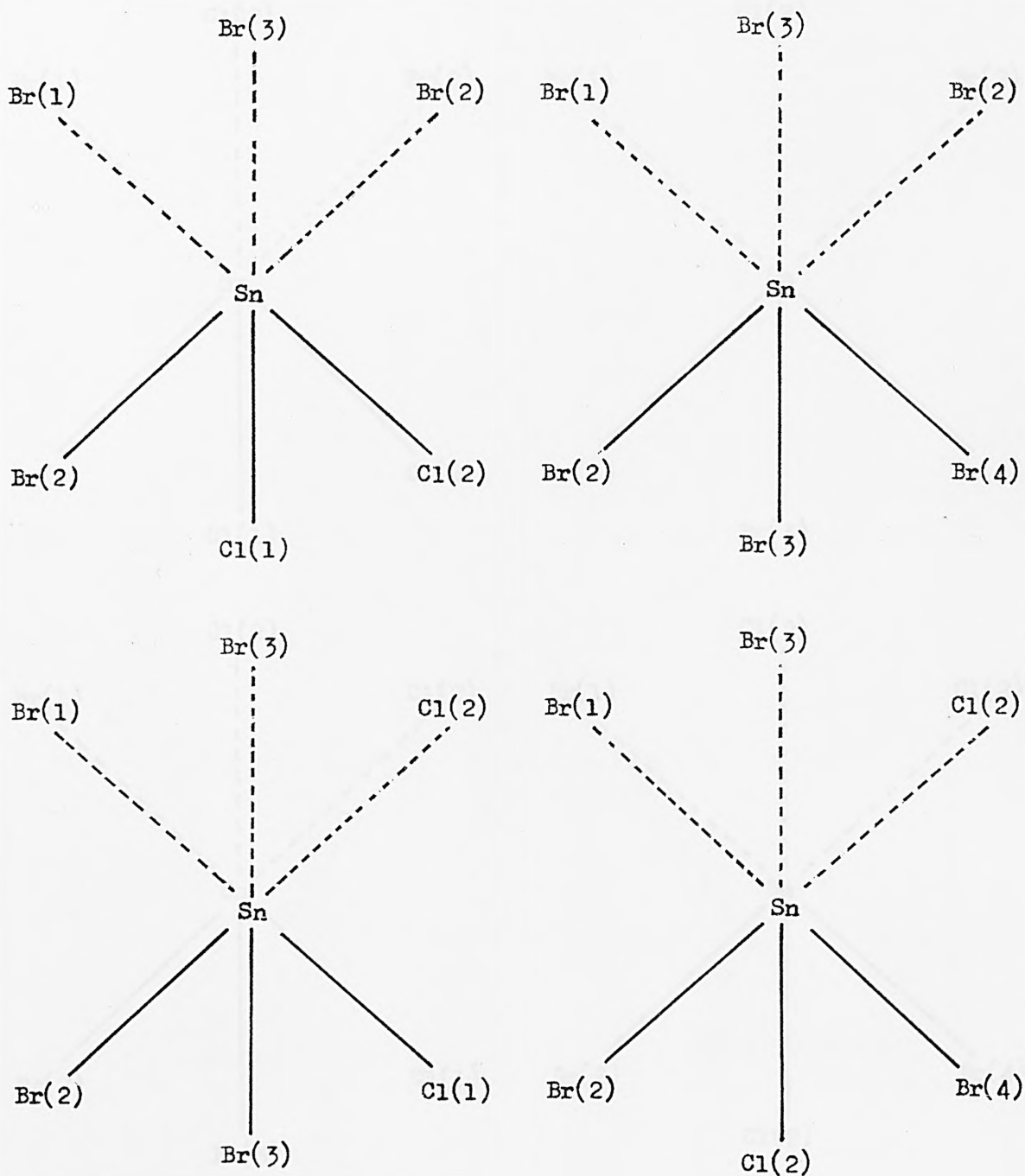


Fig.5.16a

Possible tin environments in $\text{KBr} \cdot \text{KSnBr}_2 \text{Cl} \cdot \text{H}_2\text{O}$

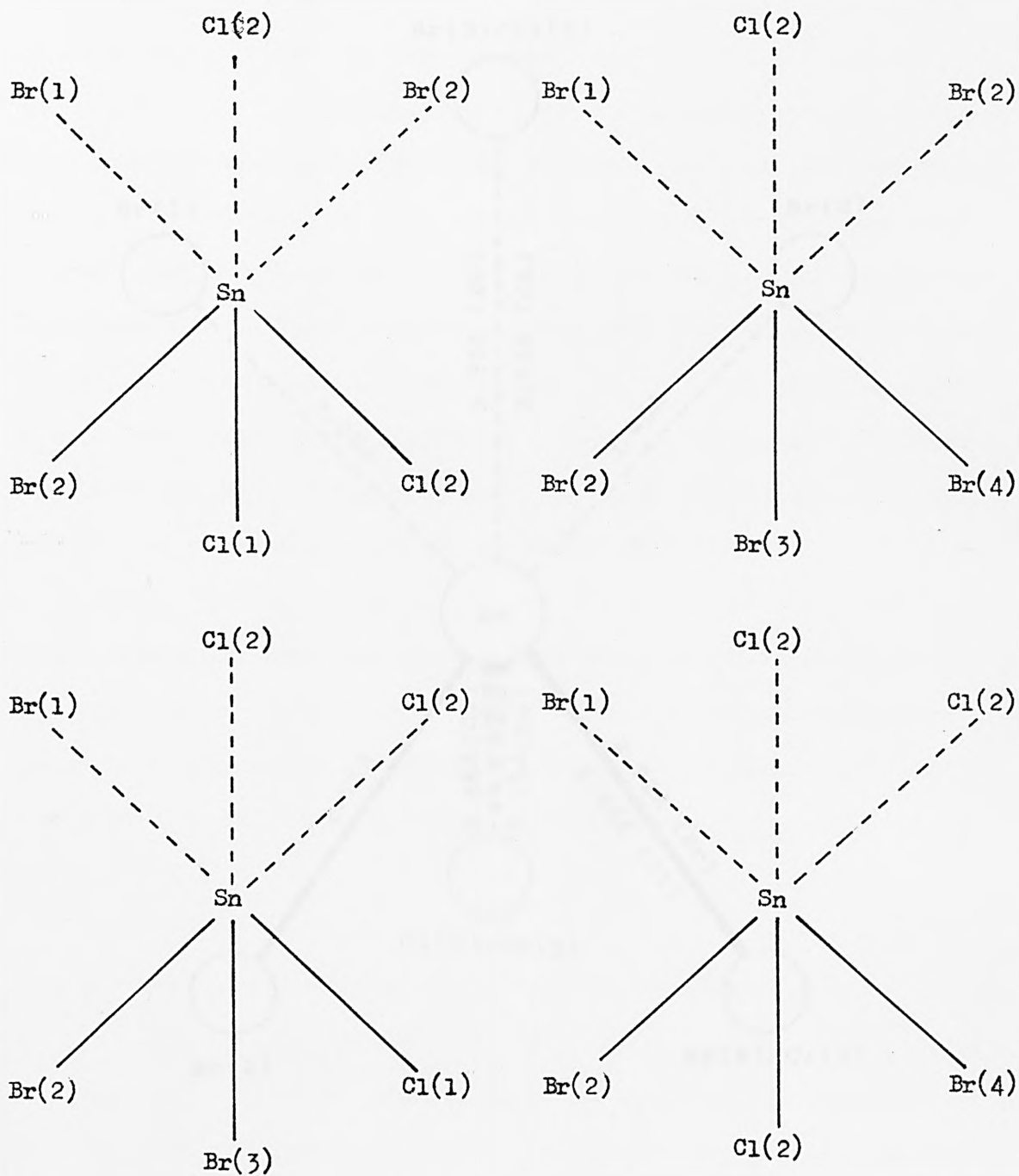


Fig.5.16b

Possible tin environments in $\text{KBr} \cdot \text{KSnBr}_2 \cdot \text{Cl} \cdot \text{H}_2\text{O}$

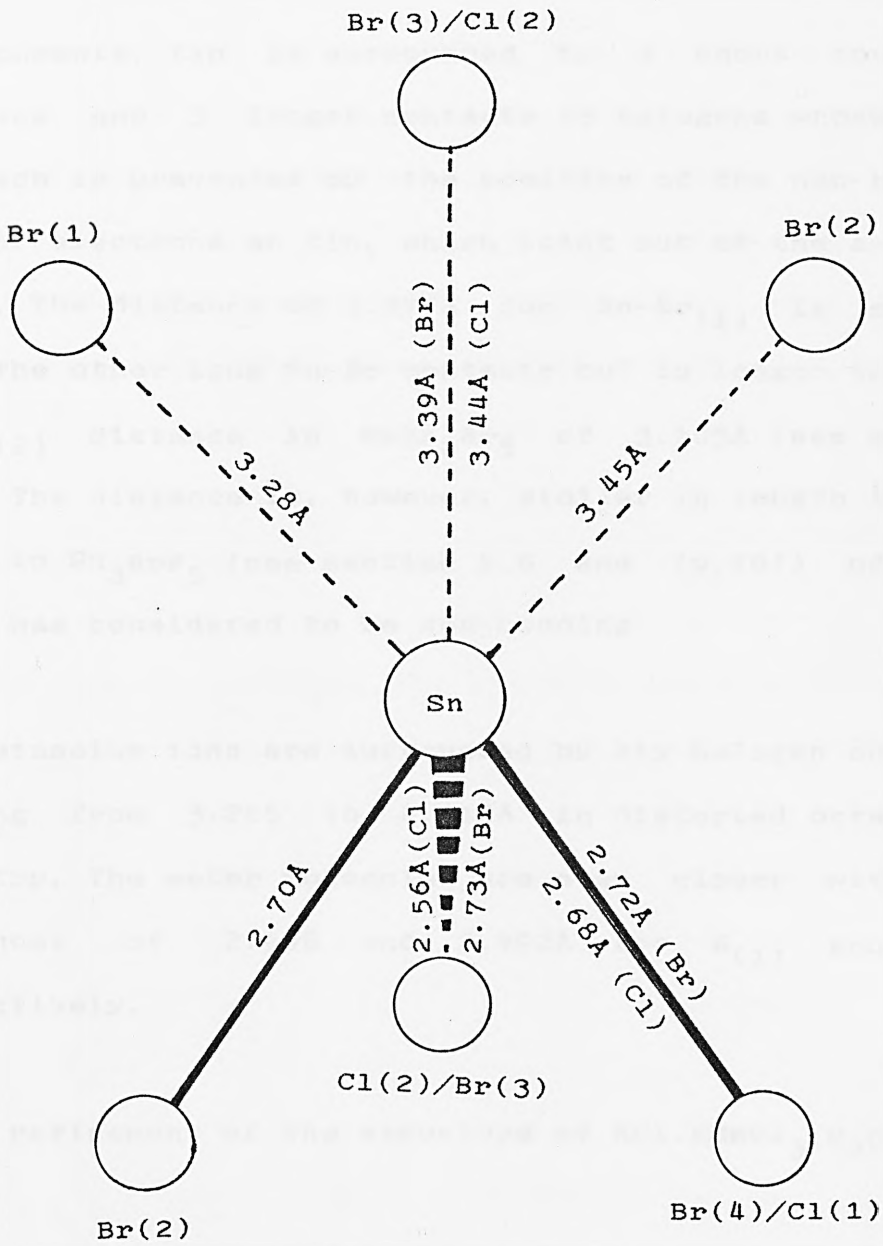


Fig.5.17

Generalised tin environment in $\text{KBr} \cdot \text{KSnBr}_2\text{Cl} \cdot \text{H}_2\text{O}$

environments, tin is surrounded by 3 short bonds to halogens and 3 longer contacts to halogens whose close approach is prevented by the position of the non-bonding pair of electrons on tin, which point out of the a-c cell plane. The distance of 3.277Å for Sn-Br₍₁₎ is shorter than the other long Sn-Br contacts but is longer than the Sn-Br₍₂₎ distance in RbSn₂Br₅ of 3.105Å (see section 5.2). The distance is, however, similar in length to that found in Sn₃BrF₅ (see section 5.6 and [9,10]) of 3.30Å which was considered to be non-bonding.

The potassium ions are surrounded by six halogen contacts ranging from 3.225 to 4.312Å in distorted octahedral geometry. The water molecules are even closer with K-O distances of 2.698 and 2.992Å for K₍₁₎ and K₍₂₎ respectively.

5.5 A refinement of the structure of KCl.KSnCl₃.H₂O

The structure of KCl.KSnCl₃.H₂O was originally determined by Kamenar and Gredenic [17] in 1962. The structure was notable in that it proved the existence of a discrete [SnCl₃]⁻ anion in the solid state. The original workers proposed a distorted trigonal pyramidal geometry in the complex anion with one long (2.63Å) and two short (2.54Å) Sn-Cl bonds. Several workers have assumed these lengths to be typical of Sn-Cl covalent bonds and have used these values in various calculations. [1,7,19]. In order to make more accurate comparisons with the structure of KBr.KSnBr₂Cl.H₂O, the data of Kamenar and Gredenic [17]

were re-examined using modern computer techniques. The original h, k, l and F_o data were typed into a 'SHELX-76' [15] input file and refined by least squares. The crystal data for $KCl.KSnCl_3.H_2O$ is given in table 5.19. The crystal class is orthorhombic and space group is the centrosymmetric Pbnm (non standard form of Pnma no.62) [8].

(i) Refinement of structure

The equivalent positions for the Pbnm space group are:

(1)	x,	y,	z
(2)	0.5+x,	0.5-y,	0.5+z
(3)	0.5-x,	0.5+y,	z
(4)	-x,	-y,	0.5+z
(5)	-x,	-y,	-z
(6)	0.5-x,	0.5+y,	0.5-z
(7)	0.5+x,	0.5-y,	-z
(8)	x,	y,	0.5-z

172 unique orthorhombic reflections were used in calculations. The original data had been collected using Ni filtered $CuK\alpha$ radiation on a Weissenberg camera and the data corrected for Lorentz and polarization factors and also for absorption.

Refining the original atom positions the residual reached 9.14% after 4 cycles of least squares as compared to a value of 12% obtained by the original workers.

Table 5.19

Crystal data for $\text{KCl.KSnCl}_3 \cdot \text{H}_2\text{O}$

Morphology	White rhomboid prisms
Crystal class	Orthorhombic
Cell Dimensions (Å)	a = 8.24 b = 12.05 c = 9.14 $\alpha = \beta = \gamma = 90^\circ$
Cell Volume (Å ³)	907.53
Molecular Weight (g)	356.68
Z	4
D_c (gcm ⁻³)	2.61
F(000)	596
$\mu(\text{MoK}\alpha)$ (cm ⁻¹)	299.68
Radiation	MoK α $\lambda = 0.7107\text{Å}$

Anisotropic thermal parameters were successfully applied to all the Cl atoms after U_{13} was fixed at zero but not the Sn and O atoms. By refining inter-layer scale factors in k and using non unitary weights a final residual of 7.36 and a weighted residual of 7.30 was obtained. The final atomic parameters are given in table 5.20. Bond lengths and angles are given in table 5.21.

(ii) Structural description and discussion

$KCl.KSnCl_3.H_2O$ is iso-structural with $KBr.KSnBr_2Cl.H_2O$ (see section 5.4) and $NH_4Cl.NH_4SnCl_3.H_2O$ [18]. Like the other materials, tin is present as the discrete complex anion $[SnX_3]^-$ ($X = Cl$). The projection of the unit cell is as for $KBr.KSnBr_2Cl.H_2O$ and is shown in fig.5.15 but it should be noted that the definition of the origin is different from that in $KBr.KSnBr_2Cl.H_2O$ and that the unit cell shown relates to the mixed halide complex. The tin environment is shown in fig.5.18 and consists of 3 short Sn-Cl bonds of 2.55, 2.55 and 2.58Å. Octahedral geometry is completed by three more chlorines at longer contacts of 3.16, 3.34 and 3.34Å, whose close approach is prevented by the non-bonding electron pair.

A comparison of bond lengths and angles in the $[SnCl_3]^-$ anion between the present work and the original reference is shown below:

Table 5.20

Final atomic parameters for $\text{KCl.KSnCl}_3 \cdot \text{H}_2\text{O}$

with ESDs given in brackets

Atom	x/a	y/b	z/c	S.O.F	U_{11}	U_{22}	U_{33}	U_{23}	U_{13}	U_{12}
Sn	-0.003(2)	-0.0094(4)	0.25	0.5	0.032(1)					
K	0.369(1)	0.1857(6)	-0.017(2)	1.0	0.045(6)	0.036(4)	0.045(7)	-0.001(6)	0.0	-0.012(4)
Cl(1)	0.107(3)	0.191(1)	0.25	0.5	0.033(9)	0.032(7)	0.05(2)	-0.03(2)	0.0	-0.005(8)
Cl(2)	0.207(1)	-0.056(7)	0.446(2)	1.0	0.035(5)	0.041(4)	0.049(8)	-0.005(7)	0.0	0.003(4)
Cl(3)	0.101(3)	0.263(1)	0.75	0.5	0.037(9)	0.041(8)	0.03(1)	0.01(8)	0.0	-0.017(8)
O	0.442(7)	0.041(3)	0.75	0.5	0.03(1)					

Table 5.21

Bond lengths (Å) and angles(°) in $\text{KCl} \cdot \text{KSnCl}_3 \cdot \text{H}_2\text{O}$

with ESDs given in brackets

Sn--Cl(1) 2.58(2)
Sn--Cl(2) 2.55(2)
Sn--Sn 4.576(1)

K--Cl(1) 3.26(2)
K--Cl(2) 3.27(2)
K--Cl(3) 3.21(2)
K--O 2.81(3)

Cl(2)--Sn--Cl(1) 88.1(5)

Cl(2)--Sn--Cl(2) 89.1(5)

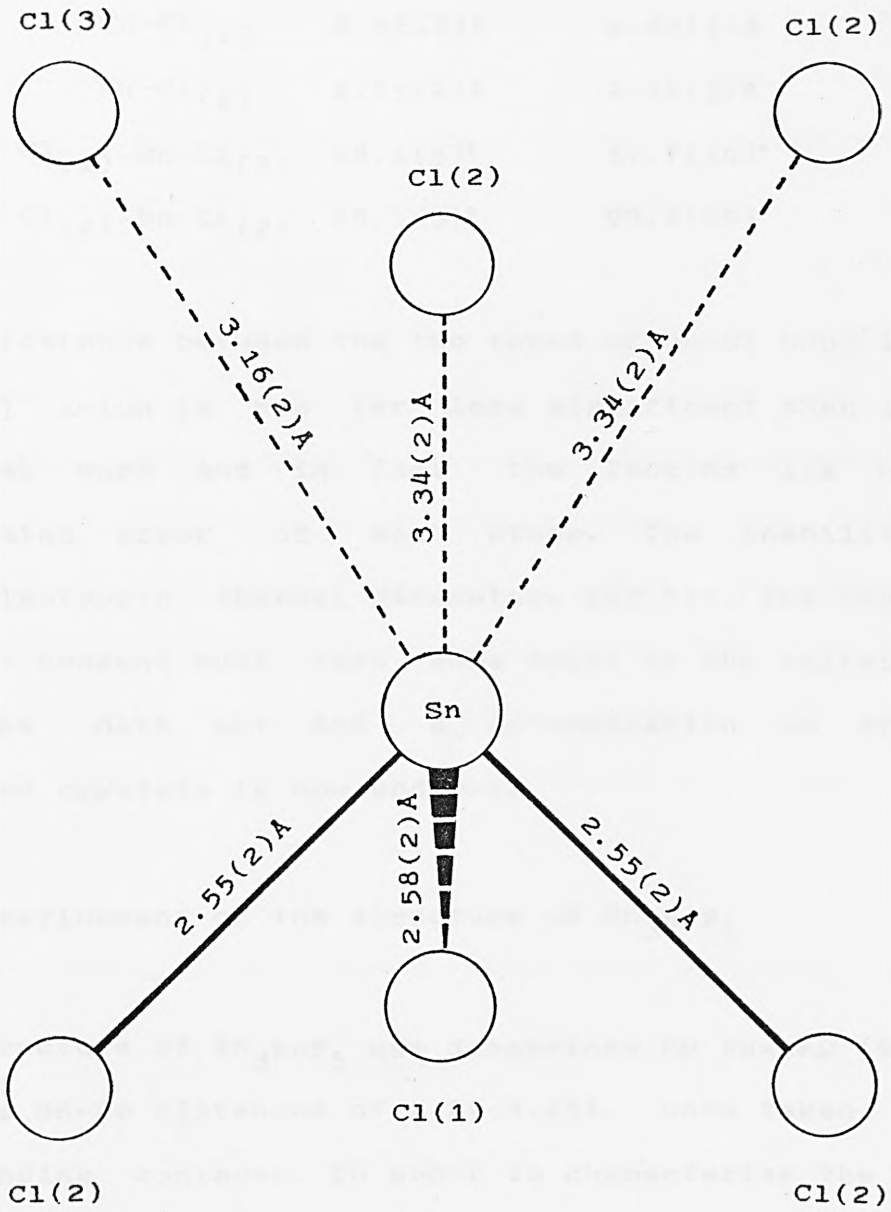


Fig. 5.18

Tin environment in $\text{KCl} \cdot \text{KSnCl}_3 \cdot \text{H}_2\text{O}$

	Refined data	Original data
Sn-Cl ₍₁₎	2.58(2)Å	2.63(3)Å
Sn-Cl ₍₂₎	2.55(2)Å	2.54(3)Å
Cl ₍₁₎ -Sn-Cl ₍₂₎	88.1(5)°	87.7(10)°
Cl ₍₂₎ -Sn-Cl ₍₂₎	89.1(5)°	90.8(10)°

The difference between the two types of Sn-Cl bond in the [SnCl₃]⁻ anion is now far less significant than in the original work and in fact the lengths lie within calculated error of each other. The inability to set anisotropic thermal parameters for tin, the heaviest element present must cast some doubt on the reliability of the data set and a determination on freshly prepared crystals is now underway.

5.6 A refinement of the structure of Sn₃BrF₅

The structure of Sn₃BrF₅ was determined by Puxley [9,10], and the Sn-Br distances of 2.29-3.25Å, were taken to be non-bonding contacts. In order to characterise the Sn-Br bond in tin(II) materials, the parameters in the original reference were refined to obtain more accurate contact distances, and to re-examine the stereochemistry around tin to see if any interaction is present between the non-bonding electron pairs and the empty Br 4d-orbitals as in the structures of CsSnBr₃ [11] and RbSn₂Br₅ (see section 5.2).

(1) Data collection and space group determination.

Data for 427 independent reflections in monoclinic symmetry were recorded by Puxley [10]. The data were initially collected on a Nonius integrating Weissenberg camera using Zn filtered $\text{MoK}\alpha$ radiation and were corrected for absorption. The final residual in the original determination was 11.3%. The crystal data are recorded in table 5.22. The unit cell parameters resemble those found in tetragonal symmetry, however, the original Weissenberg photographs failed to show the presence of a four-fold axis and it was concluded that the structure was pseudo-tetragonal. The final atomic parameters did approach tetragonal symmetry and in the present work a solution in tetragonal symmetry was attempted.

The following systematic absences were observed in the data:

$$h0l \text{ absent when } h + l = 2n + 1$$

$$0k0 \text{ absent when } k = 2n + 1$$

$$(h00 \text{ absent when } h = 2n + 1)$$

$$(00l \text{ absent when } l = 2n + 1)$$

The hkl data showed no general systematic absences. This combination is consistent with the following tetragonal space groups: $P4_2nm$ (no.102), $P4n2$ (no.118) and $P4_2/nmc$ (no.136) [8].

Table 5.22 Crystal data for Sn_3BrF_5

Morphology	White needles
Crystal class	Monoclinic (pseudo-tetragonal)
Cell Dimensions (Å)	$a = 4.27$ $b = 12.70$ $c = 12.70$ $\alpha = \beta = \gamma = 90^\circ$
Cell Volume (Å ³)	688.71
Molecular Weight (g)	530.15
Z	4
D_c (gcm ⁻³)	5.11
$F(000)$	920
$\mu(\text{MoK}\alpha)$ (cm ⁻¹)	157.44
Radiation	MoK α $\lambda = 0.7107\text{Å}$

(iii) Structural description and discussion.

The final atomic parameters approach given here were obtained by a least-squares refinement of the observed data. The final R value is 0.048. The final structure is shown in Figure 5.1. The structure is monoclinic (pseudo-tetragonal) with the following cell dimensions: $a = 4.27$, $b = 12.70$, $c = 12.70$ Å, $\alpha = \beta = \gamma = 90^\circ$. The volume of the unit cell is 688.71 Å³. The molecular weight is 530.15 g/mol. The density is 5.11 g/cm³. The number of molecules per unit cell is 4. The radiation used was MoK α with a wavelength of 0.7107 Å. The absorption coefficient is 157.44 cm⁻¹. The structure is shown in Figure 5.1.

(ii) Refinement of structure.

Attempts at solutions in tetragonal space groups failed because the tetragonal condition $0kl = 2n+1$ was not met. Consequently, as in the original work, the atomic parameters were refined in monoclinic symmetry in the space group $P2_1/n$ (non standard form of $P2_1/c$ no.14 [8]) which is consistent with the systematic absences observed. Calculations were performed using SHELX-76 [15].

The atomic parameters were refined by least squares calculations. Anisotropic thermal parameters could only be applied initially to the Br position and were only successfully applied to the tin atoms after fixing all the U_{ij} values on these atoms to 0.01. Inter-layer scale factors were calculated in k. The final residual was 9.09% after 4 cycles of least squares. The final atomic parameters are given in table 5.23 and bond lengths and angles in table 5.24. Structure factors are recorded in Appendix 2.

(iii) Structural description and discussion.

The final atomic parameters approach $4/mmm$ Laue symmetry and the inability to solve the structure in tetragonal symmetry is probably due to error in measurement of the a-cell dimension. This is supported by the fact that for all the atoms, much higher estimated standard deviations are observed in the x/a coordinates than in

Table 5.23 Final atomic parameters for Sn_3BrF_5
with ESDs in brackets

	x/a	y/b	z/c	B
Sn(1)	0.5696(12)	0.1041(4)	0.1019(4)	
Sn(2)	0.0742(13)	0.8393(5)	0.6277(5)	
Sn(3)	0.1266(12)	0.3764(5)	0.1543(4)	
Br	0.5167(18)	0.3815(8)	0.3790(7)	
F(1)	0.5425(97)	0.1049(35)	0.2701(34)	0.0151(98)
F(2)	0.5133(92)	0.2676(29)	0.1054(32)	0.0222(80)
F(3)	0.5809(106)	0.1169(45)	0.4909(37)	0.0267(108)
F(4)	0.5197(99)	0.4894(30)	0.1203(34)	0.0056(85)
F(5)	0.0084(204)	0.1431(58)	0.1533(61)	0.0674(213)

Anisotropic thermal parameters

Sn(1)	$U_{11} = U_{22} = U_{33} = U_{23} = U_{13} = U_{12} = 0.01$
Sn(2)	" " "
Sn(3)	" " "

	U_{11}	U_{22}	U_{33}	U_{23}	U_{13}
Br	0.0124(34)	0.0202(42)	0.0380(52)	-0.0081(48)	0.0099(40)
	U_{12}				
	-0.0007(53)				

Overall scale factor = 0.732(7)

Inter-layer scale factors

layer	1	2	3	4	5	6
	1.125(30)	1.095(23)	1.176(28)	1.172(27)	1.109(21)	1.197(31)

Table 5.24

Important bond lengths (Å) and angles (°) in Sn_3BrF_5
with ESDs in brackets

Sn(1)--F(1)	2.14(4)	Sn(2)--F(1)	2.21(4)
Sn(1)--F(2)	2.09(4)	Sn(2)--F(3)	2.18(4)
Sn(1)--F(5)	2.05(8)	Sn(2)--F(4)	2.19(4)
Sn(3)--F(2)	2.24(4)	Sn(1)...Br	3.34(2)
Sn(3)--F(4)	2.25(4)	Sn(2)...Br	3.30(2)
Sn(3)--F(3)	2.09(4)	Sn(3)...Br	3.31(2)

F(1)--Sn(1)--F(2) 88.2(1.6)

F(5)--Sn(1)--F(1) 74.3(2.4)

F(5)--Sn(1)--F(2) 81.9(2.3)

F(3)--Sn(2)--F(1) 79.8(1.7)

F(3)--Sn(2)--F(4) 77.8(1.7)

F(4)--Sn(2)--F(1) 77.6(1.7)

F(2)--Sn(3)--F(4) 77.9(1.2)

F(2)--Sn(3)--F(3) 79.5(1.7)

F(3)--Sn(3)--F(4) 81.5(1.7)

Sn(1)--F(1)--Sn(2) 123.3(1.8)

Sn(2)--F(3)--Sn(3) 127.9(1.9)

Sn(3)--F(2)--Sn(1) 134.6(1.8)

the other two coordinates.

In general the Sn-F bonds are within the experimental errors of those previously reported. The Sn-Br contacts are now all over 3.0Å but are still within experimental error of the previously reported values. In all cases the estimated standard deviations are lower in the refined structure.

The structure consists of infinite two dimensional fluorine bridged networks (see fig 5.19) running perpendicular to the a-axis. Three tin sites exist and are shown in fig.5.20. All of the tin atoms are in trigonal pyramidal environments. Sn₍₂₎ and Sn₍₃₎ are bonded to three bridging fluorine atoms at distances ranging between 2.09 - 2.24Å. Sn₍₁₎ is bonded to two bridging fluorines, at 2.09 and 2.14Å, and a terminal fluorine at 2.05Å.

The Sn-Br distances are longer than the longest bonding distances found in most structures. The longest bridging bonds in CsSn₃Br_{1.5}F_{5.5} were only 3.248Å whilst the ionic Sn-Br contact in KBr.KSnBr₂Cl.H₂O was 3.276Å. The distance does lie well within the sum of the Van der Waals radii of 3.95Å. Because of the trigonal pyramidal symmetry around the tin and the long distances to Br it can be concluded that these are indeed non-bonding contacts and Br exists as the anion sitting in a lattice space. Furthermore, there is no evidence from the stereochemistry of any interaction between the

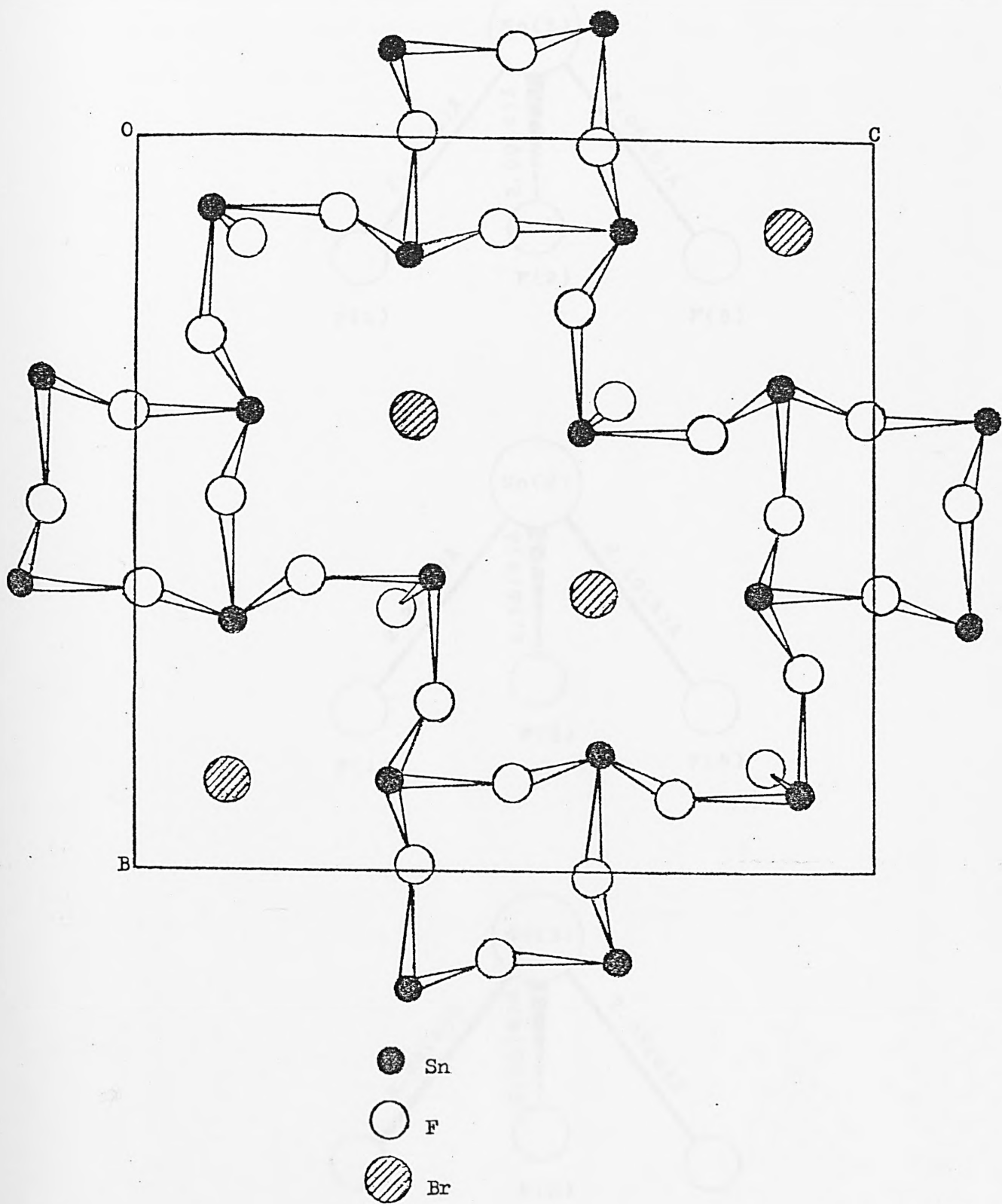


Fig.5.19: Projection onto (100) of Sn_3BrF_5

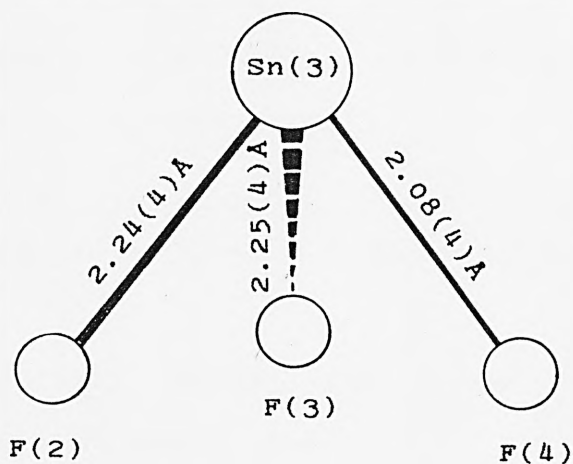
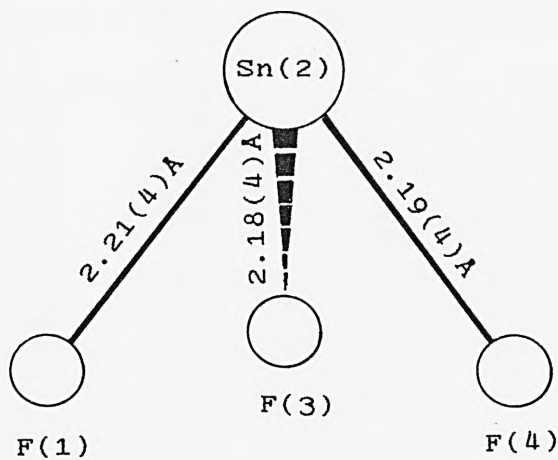
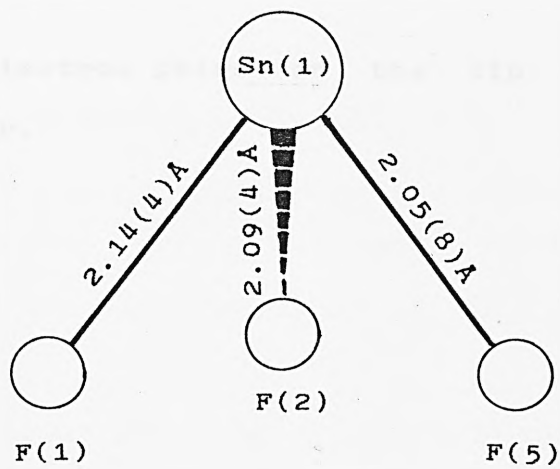


Fig. 5.20

Tin environments in Sn_3BrF_5

non-bonding electron pairs on the tin atoms and empty orbitals on Br.

(1) G.D. Donalson and D.H. Brown, Reviews on Silicon
Germanium Tin and Lead Compounds, (1961), 4 (1), 1-127.

(2) G.D. Donalson, Progress Inorganic Chem., (1967), 6,
267.

(3) G.D. Donalson and D.H. Brown, J. Chem. Soc. Dalton
Trans., (1964), 1201.

(4) F.A. Cotton, F.J. Smith, G.D. Donalson and D.H. Brown,
in Bibliography of Inorganic Chemical Structures of Tin
Compounds, I.U.C.P., publication no. 104.

(5) S.E. McDonald, G.D. Lacey and D.H. Brown, Acta Cryst.,
17 (1968), 1104.

(6) E. Villiers, G. Fares, W. Kasper, and L. Cot-
ter, Canad. Min., 17 (1969), 307.

(7) H.A. J. O'Leary, Ph.D. Thesis, London (1971).

(8) International Tables for X-ray Crystallography,
Birmingham, X-ray Press, 1962.

(9) G.D. Donalson, D.H. Laughlin and H.C. Foster,
J. Chem. Soc. Dalton Trans., (1971), 609.

REFERENCES, CHAPTER FIVE

- (1) J.D.Donaldson and S.M.Grimes, Reviews on Silicon Germanium Tin and Lead Compounds, (1984), 8 (1), 1-132.
- (2) J.D.Donaldson, Progress Inorganic Chem., (1967), 8, 287.
- (3) J.D.Donaldson and S.M.Grimes, J.Chem.Soc. Dalton Trans., (1984), 1301.
- (4) P.A.Cusack, P.J.Smith, J.D.Donaldson and S.M.Grimes, 'A Bibliography of X-ray Crystal Structures of Tin Compounds', I.T.R.I., publication No.588.
- (5) R.R.McDonald, A.C.Larson and D.T.Cromer, Acta Cryst., 17 (1984), 1104.
- (6) S.Vilminot, G.Perez, W.Granier and L.Cot. Rev.Chim.Miner., 17 (1980), 397.
- (7) S.R.A.Bird, Ph.D. Thesis, London 1971.
- (8) 'International Tables for X-ray Crystallography', Birmingham, Kynoch Press, 1962.
- (9) J.D.Donaldson, D.R.Laughlin and D.C.Puxley, J.Chem.Soc. Dalton Trans., (1977), 865.

(10) D.C.Puxley, Ph.D. Thesis, London 1972.

(11) J.D.Donaldson, J.Silver, S.Hadjiminolis and S.D.Ross, J.Chem.Soc. Dalton Trans. 15 (1975), 1500.

(12) J.Donaldson and B.J.Senior, J.Chem.Soc.(A), (1969), 2358.

(13) J.D.Donaldson, Private communication.

(14) P.Main, S.J.Fiske, S.E.Hull, L.Lessinger, G.Germain, J.P.Declercq, M.M.Woolfson, 'MULTAN-80 - A system of computer programs for the automatic solution of crystal structures from X-ray diffraction data.' 1980, Universities of York, England and Louvain, Belgium.

(15) G.M.Sheldrick, 'Program for Crystal Structure Determination', Univ of Cambridge (1975).

(16) S.M.Grimes, Ph.D. Thesis, The City University, 1982.

(17) B.Kamenar and D.Grdenic, J.Inorg.Nucl.Chem, 24 (1962), 1039.

(18) P.G.Harrison, B.J.Haylett and T.J.King, Inorg.Chim.Acta., 75 (1983), 265.

CHAPTER SIX

CONCLUSIONS.

	Page
6.1 Conclusions.	331
6.2 Recommendations for future work.	339
References.	341

CHAPTER SIX

6.1 Conclusions

Much is known about tin(II) chemistry from X-ray crystallographic and Mössbauer spectroscopic studies [1,2] which are discussed earlier (see chapters 1,4 and 5). The work in this thesis has been concerned with four aspects of the way in which tin uses its electrons in bonding viz:

(1) Studies on the effects of non-bonding electron pairs on the stereochemistry of tin-halide derivatives.

(2) Studies on the effects of the presence of more than one halide in bonding in tin(II) compounds.

(3) Studies on the nature of the tin bromine bond in various structures.

(4) Studies in the use of Mössbauer spectroscopy to provide information on the ways in which tin uses its electrons in bonding especially at the surface of tin containing materials.

Structures of tin(II) materials fall into two broad categories based on the use of the non-bonding pair of electrons on tin, viz; structures where the non-bonding electron pairs are stereochemically active and structures where partial delocalisation of the non-bonding electrons

occur. Structures from both of these categories have been examined in this work. In $\text{CsSn}_3\text{Br}_{1.5}\text{F}_{5.5} \cdot \text{KBr} \cdot \text{KSnBr}_2\text{Cl} \cdot \text{H}_2\text{O}$, $\text{KCl} \cdot \text{KSnCl}_3 \cdot \text{H}_2\text{O}$, and Sn_3BrF_5 the non bonding electron pairs are stereochemically active and no evidence is found for delocalisation. All of these structures have tin in distorted trigonal pyramidal sites. In the complexes $\text{KCl} \cdot \text{KSnCl}_3 \cdot \text{H}_2\text{O}$ and $\text{KBr} \cdot \text{KSnBr}_2\text{Cl} \cdot \text{H}_2\text{O}$ tin exists as the complex anion $[\text{SnX}_3]^-$ ($\text{X} = \text{Br}_n\text{Cl}_{3-n}$).

The stereochemistry of RbSn_2Br_5 indicates that an interaction occurs between the non-bonding electron pairs on tin and the empty 4d orbitals on Br. This is part of a range of interactions involving the non-bonding electron pairs on the tin atom. These interactions range from dimer formation in $\text{Sn}[\text{CH}(\text{SiMe}_3)_2]_2$ [3] where the stability and structure of the material arises from interactions between the lone pair on one tin atom with the empty orbital on the other tin atom in the dimer; cluster formation of tin atoms around the halogens in $\text{K}_3\text{Sn}_2(\text{SO}_4)_3\text{X}$, ($\text{X} = \text{Br}, \text{Cl}$) [4], where the distorting effects of the lone pair orbitals pointing towards the halide ions are removed by delocalisation of the tin electron density into cluster orbitals; to the population of solid state bands by non-bonding electrons that accounts for the optical and electrical properties of compounds such as CsSnBr_3 and SnO [5,6], where the non-bonding orbitals are delocalised into three dimensional and adjacent layer conduction bands respectively. This range of interactions can be expressed as follows:



Polymers can be further categorised into two and three dimensional polymers of which RbSn_2Br_5 is a two dimensional example.

In an extensive review of lone pair effects in tin(II) chemistry [2], Donaldson and Grimes were able to characterise the Sn-Cl, Sn-O and Sn-F bonds and calculate average bond distances. A gap exists in the knowledge of the nature of the Sn-Br bond, few structures have been determined which can be used to characterise this bond. All of the materials studied in the present work, except for $\text{KCl.KSnCl}_3 \cdot \text{H}_2\text{O}$ had Sn-Br contacts, enabling a comparison of these lengths to be made:

	Sn--Br A
Sn_3BrF_5	3.303, 3.305, 3.343
$\text{CsSn}_3\text{Br}_{1.5}\text{F}_{5.5}$	3.248, 3.200
RbSn_2Br_5	3.105, 2.755
$\text{KBr.KSnBr}_2\text{Cl} \cdot \text{H}_2\text{O}$	2.700, 2.722, 2.731

Donaldson and Grimes were able to calculate an average bond length for Sn-Br of 2.81Å from the few known structures containing Sn-Br contacts. The average bonding contact in the present work is 2.92Å. The average Sn-Br bond length over all the known structures containing tin to bromine bonds can now be re-calculated at 2.87Å.

Perhaps more useful than an average bonding distance for Sn-Br, is a set of bond ranges defining the nature of the tin to Br contact. Using the data in the present study these can be summarised as follows:

Covalent	2.7—2.9Å
Bridging and ionic	2.9—3.3Å
Non bonding	above 3.3Å

The average of the Sn-Cl bonds in $\text{KBr.KSnBr}_2\text{Cl.H}_2\text{O}$ and $\text{KCl.KSnCl}_3\text{.H}_2\text{O}$ is 2.59Å. This compares with the value of 2.54 quoted by Donaldson and Grimes. Similarly the average Sn-F distance was 2.18Å, compared with 2.14Å in the review article. The $[\text{SnCl}_3]^-$ anion has long been thought to have irregularity in the bond lengths between Sn and Cl. In the original structure determination of $\text{KCl.KSnCl}_3\text{.H}_2\text{O}$ [7] these lengths were 2.54 and 2.63 Å and these lengths have been assumed in various calculations of force constants and bond lengths in similar complexes [8]. In the present work atom positions in this structure have been refined and the lengths have been found to be much closer to each other than was originally reported (see fig.6.1). The situation is now much more similar to that observed in CsSnCl_3 (monoclinic) [9] where the Sn-Cl bonds range from 2.50 - 2.55Å. Because of the difference between the original and the refined bond lengths and the importance of this material in characterising the Sn-Cl covalent bond, a redetermination, using modern instrumentation is in

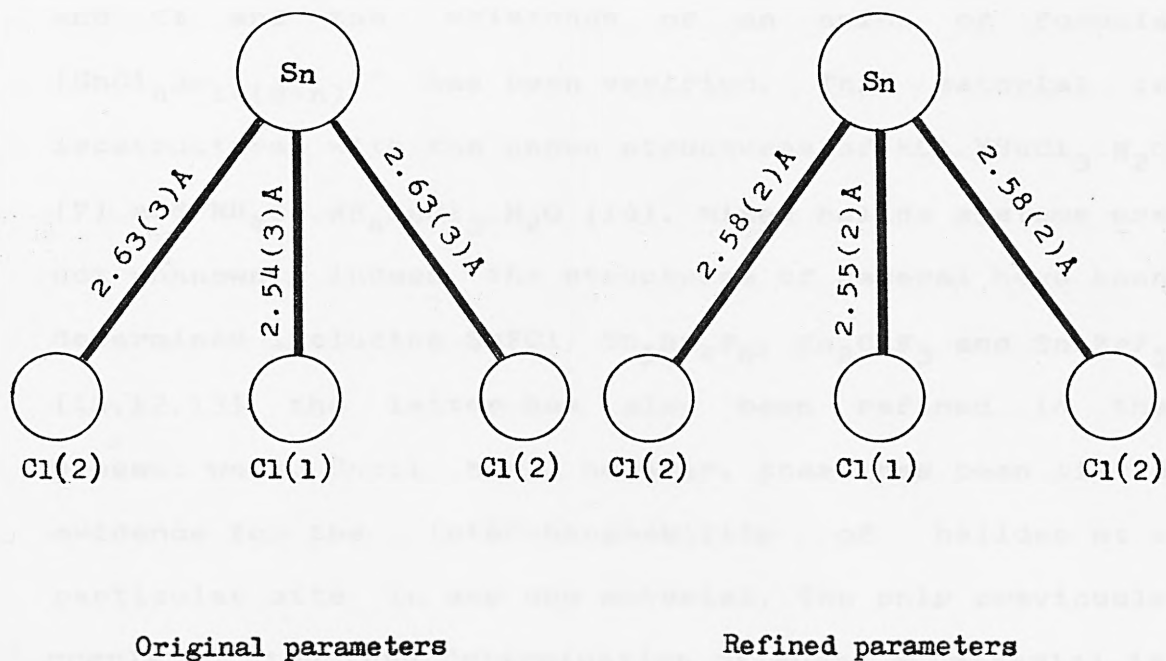


Fig.6.1

Refinement of bond lengths in the $[\text{SnCl}_3]^-$ anion

progress.

Evidence from the structure determination of $\text{KBr.KSnBr}_2\text{Cl.H}_2\text{O}$ shows that two of the sites on the trihalostannate(II) anion are interchangeable between Br and Cl and the existence of an anion of formula $[\text{SnCl}_n\text{Br}_{1+(2-n)}]^-$ has been verified. This material is isostructural with the known structures of $\text{KCl.KSnCl}_3\text{.H}_2\text{O}$ [7] and $\text{NH}_4\text{Cl.NH}_4\text{SnCl}_3\text{.H}_2\text{O}$ [10]. Mixed halide systems are not unknown, indeed the structures of several have been determined including SnFCl , $\text{Sn}_5\text{Br}_4\text{F}_6$, Sn_2ClF_3 and Sn_3BrF_5 [11,12,13] the latter has also been refined in the present work. Until now, however, there has been little evidence for the interchangeability of halides at a particular site in any one material. The only previously completed structure determination of such a material is of $\text{Sn}_2\text{Br}_{0.65}\text{Cl}_{3.35}\text{.3H}_2\text{O}$ [14] where two tin sites are in trigonal pyramidal environments and the Br and Cl sites are indistinguishable. The present work has observed interchangeability of Br and Cl in a number of materials. In the $\text{KSnBr}_n\text{Cl}_{3-n}\text{.xH}_2\text{O}$ system a range of complexes have been prepared and a correlation has been observed between the Br content and the $d_{(101)}$ lattice spacing on the powder diffraction pattern indicating a corresponding lattice expansion. This has been supported by a trend in the Mössbauer parameters ie. an increase in quadrupole splitting with increase in Cl content. This as observed for the previously known system $\text{CsSn}_2\text{Br}_n\text{Cl}_{5-n}$ [6].

Mössbauer spectroscopy has been used to give information

on the tin environments of materials studied in this work. Generally, in the present work, complex tin(II) halides have been seen to have lower shifts than the parent tin(II) halides. This can be explained by a decrease in s-electron density at the tin nucleus caused by complex formation and is due to the increased s-electron involvement in covalent bonding (see fig.6.2). Chemical shifts of tin complexes are known to decrease with increase in electronegativity of the ligands [2], but this has proved difficult to follow in the mixed halide systems because the differences in shift ranges lie within the experimental error of the measurements. Similarly as the halogen to tin ratio increases in complexes, the shift decreases as is to be expected with increasing s-electron involvement in bonding.

Conversion electron Mössbauer spectroscopy (CEMS) has been shown to be a useful tool in the study of the surface environments of tin containing materials. Differences have been found between surface and bulk measurements for several tin containing samples including many normal tin(II) compounds. In many of these materials an increase in asymmetry at the surface occurs which is characterised by an increase in quadrupole splitting.

Grimes [15] has described 2 areas of study involving CEMS:

(1) Reactions of tin compounds at matrix surfaces.

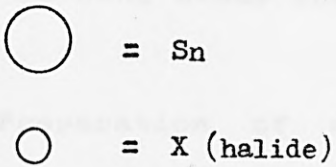
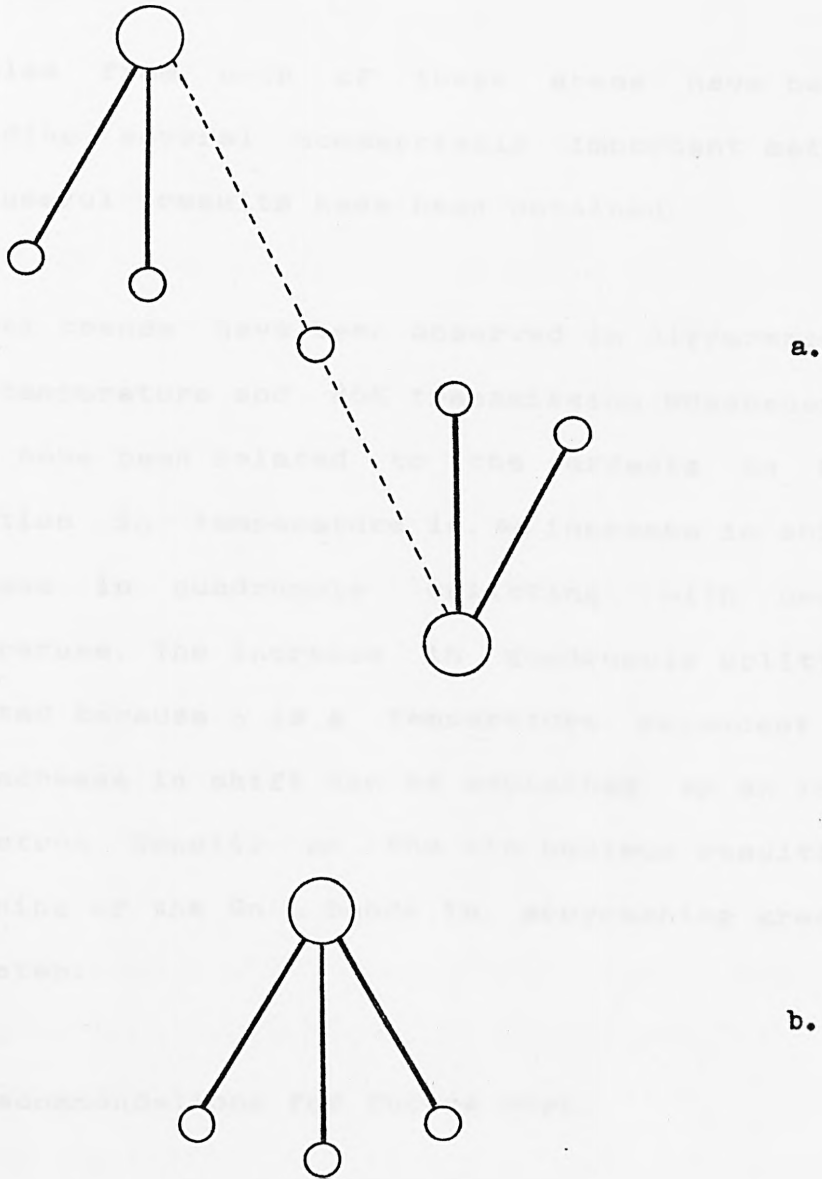


Fig.6.2

Change in Sn environment from situation in SnX_2 (a)
to complex formation in $[\text{SnX}_3]^-$ (b)

(2) Reactions at tin containing matrix surfaces.

Examples from both of these areas have been studied including several commercially important materials and some useful results have been obtained.

General trends have been observed in differences between room temperature and 80K transmission Mössbauer results. These have been related to the effects on bonding of reduction in temperature ie. an increase in shift and an increase in quadrupole splitting with decrease in temperature. The increase in quadrupole splitting is as expected because Δ is a temperature dependent quantity. The increase in shift can be explained by an increase in s-electron density at the tin nucleus resulting from a weakening of the Sn-L bonds ie. approaching greater ionic character.

6.2 Recommendations for future work.

The following areas are recommended for further study.

(1) Preparation of suitable crystals of $\text{KSnCl}_3 \cdot \text{H}_2\text{O}$, $\text{KSnBr}_3 \cdot 2\text{H}_2\text{O}$ and $\text{KSnBr}_n\text{Cl}_{3-n} \cdot \text{H}_2\text{O}$ to submit for X-ray structure determination.

(2) The redetermination of the structure of $\text{KCl} \cdot \text{KSnCl}_3 \cdot \text{H}_2\text{O}$ (in progress), to establish accurate bond lengths for the $[\text{SnCl}_3]^-$ anion.

(3) Further examination and structure determination of complexes of the type $M\text{Sn}_3\text{X}_7 \cdot x\text{H}_2\text{O}$.

(4) An examination of electrical properties of RbSn_2Br_5 and the structure determination of $\text{NH}_4\text{Sn}_2\text{Br}_4\text{Cl}$ and KSn_2Br_5 in order to see what effects the change of cation and of Cl substitution, have on the stereochemistry of these materials.

(5) An examination of the nature of sulphate incorporation into the lattice in dilute sulphuric acid solutions.

(7) Specific applications for CEMS especially with respect to industrially important materials.

(8) A detailed study of variation in shift and quadrupole splitting with temperature in various materials.

(9) The verification of differences observed between transmission and conversion electron Mössbauer spectra for normal tin(II) compounds.

REFERENCES, CHAPTER SIX

- (1) J.D.Donaldson, Progress in Inorganic Chemistry, (1967), 8, 287.
- (2) J.D.Donaldson and S.M.Grimes, Reviews on Silicon, Germanium, Tin and Lead Compounds, (1984), 8 (1), 1-132.
- (3) J.D.Cotton, P.J.Davidson, M.F.Lappert, J.D.Donaldson and J.Silver, J.Chem.Soc. Dalton Trans., (1976), 2286.
- (4) J.D.Donaldson and S.M.Grimes, J.Chem.Soc. Dalton Trans., (1984), 1301.
- (5) S.J.Clark, C.D.Flint and J.D.Donaldson, J.Phys. Chem. Solids, (1981), 42, 133.
- (6) J.D.Donaldson, J.Silver, S.Hadjiminolis and S.D.Ross, J. Chem. Soc. Dalton Trans., (1975), 1500.
- (7) B.Kamenar and D.Grdenic, J.Inorg. Nucl. Chem., (1962), 24, 1039.
- (8) S.R.A.Bird, Ph.D. Thesis, London, 1971.
- (9) F.R.Poulsen and S.E.Rasmussen, Acta. Chem. Scand., (1970), 24, 150.

(10) P.G.Harrison, B.J.Haylett and T.J.King, Inorg. Chim. Acta., (1983), 75, 265.

(11) C.Geneys, S.Vilminot and L.Cot. Acta Cryst., B32, (1976), 3199.

(12) C.Geneys and S.Vilminot, Rev. Chim. Miner., (1977), 14, 395.

(13) J.D.Donaldson, D.R.Laughlin and D.C.Puxley, J.Chem. Soc. Dalton Trans., (1977) 865.

(14) S.Vilminot, W.Granier, Z.Al Oraibi, and L.Cot, Acta Cryst., B35, (1979), 2863.

(15) S.M.Grimes, Ph.D. Thesis, The City University London, 1982.

APPENDIX ONE

COMPUTER PROGRAMS

	Page
MOLPLOT (Molecular plotting program)	344
MOL1 (Input/output routines)	346
MOL2 (Bond length & angle routines)	348
MOL3 (Plot routines)	350
MOL4 (Edit facility)	353
MOL5 (Plot options facility)	356
MOL6 (Screen dump)	358
MOL7 (symmetry generating routines)	359
TPLOT (Potentiometric halide anal. plots)	362
X-RAY (X-ray powder diffraction utility)	365

```
>LIST MOLPLOT
 10 REM MOLPLOT MkIII (DISC VERSION)
 20 REM I. Abrahams
 30 REM Original version Dec. 1984
 40 REM Last update I.A 26/11/85
 50 LOMEM=&3000
 60 H=0
 70 T%=TOP
 80 *FX6,10
 90 ONERROR CLS:REPORT:PRINT''''''"PRESS ANY KEY TO C
ONTINUE":A$=GET$:GOTO220
 100 DIMadd 40
 110 N%=100:r%=10:pr%=0:lab%=0:f=1
 120 DIMa(3,3),T$(N%),x(N%),y(N%),z(N%),X1(3),Y1(3),Z1
(3),X(N%),Y(N%),Z(N%),TY%(N%),u(8),v(8),w(8),r(r%),xs$(
16),ys$(16),zs$(16)
 130 MODE6
 140 PROCdefault
 150 PROCOVLY(1):PROCinput
 160 H=1
 170 ONERROR CLS:REPORT:PRINT''''''"PRESS ANY KEY TO C
ONTINUE":A$=GET$:GOTO220
 180 VDU3
 190 PROCOVLY(3):PROCsinangle:PROCcentre
 200 K=0
 210 IFK=80 PROCOVLY(6):PROCsetdump:VDU2:CALLdump:VDU3
 220 K=0
 225 VDU3
 230 MODE6
 240 q%=TRUE
 250 PRINTTAB(17,1)"MOLPLOT"
 260 PRINTTAB(5,3)"I ----- Input new data"
 270 PRINTTAB(5,5)"A ----- Angles between atoms"
 280 PRINTTAB(5,7)"B ----- Bond lengths"
 290 PRINTTAB(5,11)"R ----- Reset plot parameters"
 300 PRINTTAB(5,9)"G ----- Symmetry generator"
 310 PRINTTAB(5,13)"P ----- Plot"
 320 PRINTTAB(5,15)"K ----- Key plot"
 330 PRINTTAB(5,17)"U ----- Unit cell plot"
 340 PRINTTAB(5,19)"E ----- Edit data"
 350 PRINTTAB(5,21)"S ----- Save data file"
 360 in$=FNmenuin("A","B","I","R","P","K","U","E","S",
"(","*","G")
 370 IFin$="I" PROCOVLY(1):PROCinput:PROCsinangle:PROC
centre
 380 IFin$="A" PROCOVLY(2):PROCAngles
 390 IFin$="B" PROCOVLY(2):PROCBond
 400 IFin$="R" PROCOVLY(5):PROCreset
 410 IFq%=TRUE GOTO430
 420 IFq%=FALSE AND in$="P" OR in$="K" ORin$="U" :MODE
n%:PROCproc:GOTO370
 430 IFin$="P" OR in$="K" ORin$="U" PROCOVLY(3):MODEn%
:q%=FALSE:PROCproc:GOTO410
 440 IFin$="E" PROCOVLY(4):PROCCedit:PROCOVLY(3):PROCSi
nangle:PROCcentre
 450 IFin$="S" PROCOVLY(1):PROCfilesave
 460 IFin$="G" PROCOVLY(7):PROCSymgen
```

```
470 IFASC(in$)=10 PRINT"*";:INPUT""$add:X%=add MOD 2
56:Y%=add DIV 256:CLS:CALL &FFF7:A$=GET$
480 GOTO210
490 END
500 DEFPROCdefault
510 n%=4:SF%=50:cut=5:rot=10:enl=10:theta=90:psi=20:p
hi=15
520 FORI%=1TO5
530 r(I%)=(6-I%)/10
540 r(I%+5)=0.25
550 NEXT
560 ENDPROC
570 DEFFNinput(a$,b$)
580 REPEAT:Ans$=CHR$(GET AND &5F)
590 UNTILAns$=a$ OR Ans$=b$
600 =Ans$
610 DEFFNmenuin(a$,b$,c$,d$,e$,f$,g$,h$,i$,j$,k$)
620 REPEAT:in$=CHR$(GET AND &5F)
630 UNTILin$=a$ ORin$=b$ ORin$=c$ ORin$=d$ ORin$=e$
ORin$=f$ ORin$=g$ ORin$=h$ ORin$=i$ ORin$=j$ ORin$=k$
ORASC(in$)=10
640 =in$
650 DEF PROCOVLY(OV%)
660 F$="MOL"+STR$(OV%)
670 OSCLI"LOAD "+F$+" "+STR$~(T%-2)
680 ENDPROC
690 DEFPROC3Dcoords(i%)
700 xa=(x(i%)*A)+(CB*z(i%)*C)+(CG*y(i%)*B)
710 yb=y(i%)*B*SG*SA
720 zc=(z(i%)*C*SB)+(y(i%)*B*CA)
730 ENDPROC
```

```
>LIST    MOL 1
2000
2010 DEFPROCinput
2015 CLS
2020 PRINTTAB(0,5)"Do you wish to type in new data (Y/
N) ?"
2030 Ans$=FNinput("Y","N")
2040 IFAns$="Y" PROCTypedata:ENDPROC
2050 CLS
2054 *D.
2055 PRINTTAB(13,3)"DATA FILE INPUT"
2060 PRINTTAB(0,5)"Tape or Disc (T/D) ?"
2070 Ans$=FNinput("D","T")
2080 IFAns$="T" THEN *T.
2090 INPUTTAB(0,7)"Filename ? "TITL$
2100 IFTITL$<>"*." GOTO2140
2110 VDU14
2120 *.
2125 A$=GET$:CLS:GOTO2090
2130 VDU15
2140 PRINTTAB(0,10)"Searching"
2150 F=OPENIN TITL$
2160 INPUTEF,N%
2170 INPUTEF,A,B,C,alpha,beta,gamma
2180 FORI%=1TON%
2190 PRINTTAB(5,13)TITL$;TAB(15)I%
2200 INPUTEF,T$(I%),TY%(I%),x(I%),y(I%),z(I%)
2210 NEXT
2220 CLOSEEF
2225 *D.
2230 ENDPROC
2240 DEFPROCtypedata
2250 CLS
2260 INPUTTAB(0,3)"Title ? "titl$
2270 PRINTTAB(0,5)"Input a,b,c,alpha,beta,gamma"
2280 INPUTTAB(0,7)A,B,C,alpha,beta,gamma
2290 INPUTTAB(0,9)"No. of atoms in unit cell ? "N%
2300 CLS
2310 PRINTTAB(0,3)"Input Atom,type no,X,Y,Z"
2320 FORI%=1TON%
2330 INPUTTAB(0)T$(I%),TY%(I%),x(I%),y(I%),z(I%)
2340 NEXT
2345 ENDPROC
2350 DEFPROCfilesave
2355 *D.
2360 CLS
2365 PRINTTAB(13,3)"DATA FILE OUTPUT"
2370 PRINTTAB(0,5)"Tape or Disc (T/D) ?"
2380 Ans$=FNinput("D","T")
2390 IFAns$="T" THEN *T.
2410 INPUTTAB(0,7)"Filename ? "TITL$
2420 PRINT:PRINT
2430 G=OPENOUT TITL$
2440 PRINTEG,N%
2450 PRINTEG,A,B,C,alpha,beta,gamma
2460 FORI%=1TON%
```

```
2470 PRINTTAB(5,13)TITL#;TAB(15)I%  
2480 PRINTEG,T$(I%),TY%(I%),X(I%),Y(I%),Z(I%)  
2490 NEXT  
2500 CLOSEEG  
2505 *D.  
2510 ENDPROC
```

```
2520  
2530  
2540  
2550  
2560  
2570  
2580  
2590  
2600  
2610  
2620  
2630  
2640  
2650  
2660  
2670  
2680  
2690  
2700  
2710  
2720  
2730  
2740  
2750  
2760  
2770  
2780  
2790  
2800  
2810  
2820  
2830  
2840  
2850  
2860  
2870  
2880  
2890  
2900  
2910  
2920  
2930  
2940  
2950  
2960  
2970  
2980  
2990  
3000  
3010  
3020  
3030  
3040  
3050  
3060  
3070  
3080  
3090  
3100  
3110  
3120  
3130  
3140  
3150  
3160  
3170  
3180  
3190  
3200  
3210  
3220  
3230  
3240  
3250  
3260  
3270  
3280  
3290  
3300  
3310  
3320  
3330  
3340  
3350  
3360  
3370  
3380  
3390  
3400  
3410  
3420  
3430  
3440  
3450  
3460  
3470  
3480  
3490  
3500  
3510  
3520  
3530  
3540  
3550  
3560  
3570  
3580  
3590  
3600  
3610  
3620  
3630  
3640  
3650  
3660  
3670  
3680  
3690  
3700  
3710  
3720  
3730  
3740  
3750  
3760  
3770  
3780  
3790  
3800  
3810  
3820  
3830  
3840  
3850  
3860  
3870  
3880  
3890  
3900  
3910  
3920  
3930  
3940  
3950  
3960  
3970  
3980  
3990  
4000  
4010  
4020  
4030  
4040  
4050  
4060  
4070  
4080  
4090  
4100  
4110  
4120  
4130  
4140  
4150  
4160  
4170  
4180  
4190  
4200  
4210  
4220  
4230  
4240  
4250  
4260  
4270  
4280  
4290  
4300  
4310  
4320  
4330  
4340  
4350  
4360  
4370  
4380  
4390  
4400  
4410  
4420  
4430  
4440  
4450  
4460  
4470  
4480  
4490  
4500  
4510  
4520  
4530  
4540  
4550  
4560  
4570  
4580  
4590  
4600  
4610  
4620  
4630  
4640  
4650  
4660  
4670  
4680  
4690  
4700  
4710  
4720  
4730  
4740  
4750  
4760  
4770  
4780  
4790  
4800  
4810  
4820  
4830  
4840  
4850  
4860  
4870  
4880  
4890  
4900  
4910  
4920  
4930  
4940  
4950  
4960  
4970  
4980  
4990  
5000
```

```

>LIST MOL 2
2000 DEFPROCbond
2010 CLS
2020 PRINTTAB(0,3)"Do you wish to calculate specific
      bonds ?"
2030 Ans$=FNinput("Y","N")
2040 IFAns$="N" Bo%=0:GOTO2080
2050 INPUTTAB(0,7)"Input Atom from,to  "Fro$,to$
2060 PROCsinglebond
2070 GOTO2010
2080 CLS:PRINTTAB(0,5)"Do you want a copy of all the b
ond      lengths ?"
2090 Ans$=FNinput("Y","N"):IFAns$="N" ENDPROC
2100 VDU2
2110 t=15
2120 PRINTTAB(4+t)"Bonded atoms"TAB(25+t)"Distance /An
g. ""
2130 FORI%=1TON%-1
2140   @%=10
2145   PROC3Dcoords(I%)
2150   X=xa:Y=yb:Z=zc
2180   FORJ%=I%+1TON%
2185     PROC3Dcoords(J%)
2190     X2=xa:Y2=yb:Z2=zc
2220     d=SQR((X2-X)^2+(Y2-Y)^2+(Z2-Z)^2)
2230     IFd<5 @%=&2030A:PRINTTAB(0+t)T$(I%);TAB(7+t)"
-----
";T$(J%);TAB(30+t);d
2240     @%=10
2250     NEXT:NEXT
2260 VDU3
2270 ENDPROC
2280 DEFPROCangles
2290 VDU2:S=15
2300 PRINTTAB(S+8)"ATOMS"TAB(25+S)"ANGLE IN DEG.":PRIN
T
2310 FORI%=1TON%-2
2320   FORJ%=I%+1TON%-1
2330     FORK%=J%+1TON%
2340       PROC3Dcoords(I%)
2350       X=xa:Y=yb:Z=zc
2360       PROC3Dcoords(J%)
2370       X2=xa:Y2=yb:Z2=zc
2380       PROC3Dcoords(K%)
2390       X3=xa:Y3=yb:Z3=zc
2430       d=SQR((X2-X)^2+(Y2-Y)^2+(Z2-Z)^2)
2440       d1=SQR((X3-X)^2+(Y3-Y)^2+(Z3-Z)^2)
2450       d3=SQR((X3-X2)^2+(Y3-Y2)^2+(Z3-Z2)^2)
2460       angle=DEGACS((d*d+d1*d1-d3*d3)/(2*d*d1))
2470       angle2=DEGACS((d3*d3+d*d-d1*d1)/(2*d3*d))
2480       angle3=DEGACS((d1*d1+d3*d3-d*d)/(2*d1*d3))
2490       b%=29:b2%=29:b3%=29
2500       @%=&20200
2510       IFangle<100 b%=30
2520       IFangle<10 b%=31
2530       IFangle2<100 b2%=30
2540       IFangle2<10 b2%=31
2550       IFangle3<100 b3%=30
2560       IFangle3<10 b3%=31
2570       IFd<5 AND d1<5 PRINTTAB(S)T$(J%);TAB(5+S)"--
- "T$(I%);TAB(13+S)"-- "T$(K%)TAB(b%+S)angle

```

```
2580      IFd<5 ANDd3<5 PRINTTAB(S)T$(I%);TAB(5+S)"--
"T$(J%);TAB(13+S)"-- "T$(K%);TAB(b2%+S)angle2
2590      IFd1<5 AND d3<5 PRINTTAB(S)T$(I%);TAB(5+S)"
-- "T$(K%);TAB(13+S)"-- "T$(J%)TAB(b3%+S)angle3
2600      @%=10
2610      NEXT:NEXT:NEXT:VDU3
2620 ENDPROC
2630 DEFPROCsinglebond
2640 I%=0:we%=0
2650 REPEAT
2660   I%=I%+1
2670   IFFro$=T$(I%) we%=1
2680   UNTILwe%=1
2690 PROC3Dcoords(I%)
2700 X=xa:Y=yb:Z=zc
2720 J%=0:we%=0
2730 REPEAT
2740   J%=J%+1
2750   IFto$=T$(J%) we%=1
2760   UNTILwe%=1
2770 PROC3Dcoords(J%)
2780 X2=xa:Y2=yb:Z2=zc
2800 d=SQR((X2-X)^2+(Y2-Y)^2+(Z2-Z)^2)
2810 @%=&2030A
2820 PRINT''TAB(5)T$(I%);TAB(12)"----- ";T$(J%);TAB(
35);d
2830 @%=10
2840 Ans$=GET$
2850 ENDPROC
```

```
>LIST  MOL 3
 208 DEFPROCkey
 2010 *FX4,1
 2020 K=GET
 2030 *FX4,0
 2040 IFK=136 psi=psi-rot
 2050 IFK=137 psi=psi+rot
 2060 IFK=138 theta=theta+rot
 2070 IFK=139 theta=theta-rot
 2080 IFK=69 SF%=SF%+enl
 2090 IFK=82SF%=SF%-enl
 2100 IFK=80 in$="":ENDPROC
 2110 IFK=60 phi=phi+rot
 2120 IFK=62 phi=phi-rot
 2130 IFK>139 ORK<136 ANDK<>60 AND K<>62 ANDK<>80 ANDK<<
>82 ANDK<>69 in$=""
 2140 ENDPROC
 2150
 2160 DEFPROCrotationmatrix
 2170 SP=SINRADpsi
 2180 Sp=SINRADphi
 2190 ST=SINRADtheta
 2200 CP=COSRADpsi
 2210 Cp=COSRADphi
 2220 CT=COSRADtheta
 2230 a(1,1)=(Cp*CP)-(SP*Sp*ST)
 2240 a(1,2)=CT*Sp
 2250 a(1,3)=(Cp*SP)+(Sp*ST*CP)
 2260 a(2,1)=(-Sp*CP)-(SP*Cp*ST)
 2270 a(2,2)=Cp*CT
 2280 a(2,3)=(Cp*ST)-(SP*Sp)
 2290 a(3,1)=-SP*CT
 2300 a(3,2)=-ST
 2310 a(3,3)=CT*CP
 2320 ENDPROC
 2330
 2340 DEFPROCplot
 2350 VDU19,0,4;0;
 2360 FORI%=1TON%
 2370   r=r(TY%(I%))*SF%
 2380   y1=Y(I%)-r-1
 2390   REPEAT
 2400     y1=y1+1
 2410     root=(r*r)-((y1-Y(I%))^2)
 2420     IFroot<0 root=root*-1
 2430     x1=X(I%)+SQR(root)
 2440     IFy1=Y(I%)-r MOVEx1,y1
 2450     DRAWx1,y1
 2460     UNTILy1>Y(I%)+r
 2470     y1=Y(I%)-r-1
 2480     REPEAT
 2490       y1=y1+1
 2500       root=(r*r)-((y1-Y(I%))^2)
 2510       IFroot<0 root=root*-1
 2520       x1=X(I%)-SQR(root)
 2530       IFy1=Y(I%)-r MOVEx1,y1
 2540       DRAWx1,y1
 2550       UNTILy1>Y(I%)+r
 2560     NEXT
```

```
2570 ENDPROC
2580 DEFPROCcentrexyz
2590 FORI%=1TOQ%
2600   X(I%)=(X(I%)-Xc)
2610   Y(I%)=(Y(I%)-Yc)
2620   Z(I%)=(Z(I%)-Zc)
2630   NEXT
2640 ENDPROC
2650
2660 DEFPROCunitcell
2670 FORI%=1TO8
2680   IFI%MOD2 v(I%)=B ELSEv(I%)=0
2690   IFI%<5 u(I%)=0 ELSEu(I%)=A
2700   w(I%)=C:NEXT
2710 w(1)=0:w(2)=0:w(5)=0:w(8)=0
2720 Q%=8
2730 ENDPROC
2740 DEFPROCmultiply
2750 FORJ%=1TOQ%
2760   FORI%=1TO3
2770     X1(I%)=X(J%)*a(1,I%)
2780     Y1(I%)=Y(J%)*a(2,I%)
2790     Z1(I%)=Z(J%)*a(3,I%)
2800   NEXT
2810   X(J%)=(X1(1)+Y1(1)+Z1(1))*SF%+640
2820   Y(J%)=(X1(2)+Y1(2)+Z1(2))*SF%+512
2830   Z(J%)=(X1(3)+Y1(3)+Z1(3))*SF%
2840   NEXT
2850 ENDPROC
2860 DEFPROCunitcellplot
2870 VDU5
2880 MOVEX(1),Y(1):DRAWX(2),Y(2):DRAWX(4),Y(4):DRAWX(3)
),Y(3):DRAWX(1),Y(1):DRAWX(5),Y(5):DRAWX(8),Y(8):DRAWX(
2),Y(2)
2890 MOVEX(3),Y(3):DRAWX(7),Y(7):DRAWX(6),Y(6):DRAWX(4)
),Y(4):MOVEX(6),Y(6):DRAWX(8),Y(8):MOVEX(7),Y(7):DRAWX(
5),Y(5)
2900 VDU4
2910 ENDPROC
2920 DEFPROCsinangle
2930 SB=SINRADbeta
2940 SA=SINRADalpha
2950 SG=SINRADgamma
2960 CB=COSRADbeta
2970 CA=COSRADalpha
2980 CG=COSRADgamma
2982 SIA=SINRAD(180-alpha)
2983 SIB=SINRAD(180-beta)
2984 SIG=SINRAD(180-gamma)
2990 ENDPROC
3000 DEFPROCsetxyz
3010 FORI%=1TON%
3020   PROC3Dcoords(I%)
3030   X(I%)=xa:Y(I%)=yb:Z(I%)=zc
3040   NEXT
3050 ENDPROC
3060 DEFPROCcentre
3070 Xc=(A/2)+((C/2)*CB)+((B/2)*CG)
3080 Yc=(B/2)*SG*SA
```

```
3090 Zc=((C/2)*SB)+((B/2)*CA)
3100 ENDFROC
3110 DEFFROCsetunitcell
3120 FORI%=1T00%
3130   Z(I%)=(w(I%)*SB)+(v(I%)*CA)
3140   X(I%)=u(I%)+(CB*w(I%))+(v(I%)*CB)
3150   Y(I%)=v(I%)*SB*SA
3160   NEXT
3170 ENDFROC
3180 DEFFROCkeyplot
3190 VDU5
3200 FORI%=1TON%
3210   MOVEX(I%)-16,Y(I%)+16
3220   PRINTT$(I%)
3230   NEXT
3240 VDU4
3250 ENDFROC
3260 DEFFROClabel
3270 Q%=4
3280 u(1)=A/2:v(1)=-f:w(1)=-f
3290 u(2)=-f:v(2)=B/2:w(2)=-f
3300 u(3)=-f:v(3)=-f:w(3)=C/2
3310 u(4)=-f:v(4)=-f:w(4)=-f
3320 ENDFROC
3330 DEFFROCplab
3340 VDU5
3350 FORI%=1T03
3360   MOVEX(I%)-16,Y(I%)-16
3370   VDU(96+I%)
3380   NEXT
3390 MOVEX(4)-16,Y(4)-16
3400 VDU79,4
3410 ENDFROC
3420 DEFFROCproc
3430 PROCrotationmatrix
3440 PROCunitcell:PROCsetunitcell:PROCcentrexzy:PROCmulti
ltply:PROCunitcellplot
3450 IFlab%=0 GOTO3470
3460 PROClabel:PROCsetunitcell:PROCcentrexzy:PROCmulti
ply:PROCplab
3470 IFin$="U" PROCkey:ENDFROC
3480 Q%=N%:PROCsetxyz:PROCcentrexzy:PROCmultiply
3490 IFin$="K" PROCkeyplot ELSE PROCplot
3500 PROCkey
3510 ENDFROC
```

>LIST MOL 4

```
2000 DEFPROCedit:REPEAT
2010 CLS:@%=10:ed%=0
2020 PRINTTAB(13,2)"EDIT FACILITY"
2030 PRINTTAB(8,5)"E ----- Examine all data"
2040 PRINTTAB(8,7)"T ----- Change title"
2050 PRINTTAB(8,9)"S ----- Atom search"
2060 PRINTTAB(8,11)"A ----- Add to atom list"
2070 PRINTTAB(8,13)"D ----- Delete from list"
2080 PRINTTAB(8,15)"U ----- Unit cell parameters"
2090 PRINTTAB(8,17)"Q ----- Quit edit facility"
2095 PRINTTAB(8,19)"R ----- Relabel sequentially"
2100 PRINTTAB(10,21)"Please enter option"
2110 ONERRORGOTO170
2113 IFed%=1 PRINT"(C/E/T/S/A/D/U/R/Q/M)"
2115 in$=FNmenuin("A","S","E","D","U","T","Q","M",
"C","R","A")
2120 IFin$="A" GOTO2790
2130 IFin$="S" GOTO2380
2140 IFin$="E" GOTO2610
2150 IFin$="D" GOTO2980
2160 IFin$="U" GOTO2190
2170 IFin$="T" GOTO2910
2175 IFin$="M" GOTO2010
2177 IFin$="C" GOTO2570
2178 IFin$="R" PROCautorelabel
2180 UNTILin$="Q":ENDPROC
2190 @%=&20301
2200 CLS
2210 PRINTTAB(0,3)"a      ="TAB(10)A
2220 PRINTTAB(0,5)"b      ="TAB(10)B
2230 PRINTTAB(0,7)"c      ="TAB(10)C
2240 PRINTTAB(0,9)"alpha  ="TAB(10)alpha
2250 PRINTTAB(0,11)"beta   ="TAB(10)beta
2260 PRINTTAB(0,13)"gamma  ="TAB(10)gamma
2270 PRINTTAB(0,17)"Do you wish to alter any of the
above ?"
2280 Ans$=FNinput("Y","N")
2290 IFAns$="N" PROCunitcell:GOTO2010
2300 INPUTTAB(0,20)"Input parameter,new value      "p$
,NV
2310 IFp$="A" OR p$="a" A=NV
2320 IFp$="B" OR p$="b" B=NV
2330 IFp$="C" OR p$="c" C=NV
2340 IFp$="ALPHA" ORp$="alpha" alpha=NV
2350 IFp$="BETA" ORp$="beta" beta=NV
2360 IFp$="GAMMA" ORp$="gamma" gamma=NV
2370 GOTO2190
2380 CLS
2385 ed%=1
2390 PRINTTAB(0,3)"Do you wish to search for a parti
cular atom ? "
2400 Ans$=FNinput("Y","N")
2410 IFAns$="N" GOTO2010
2420 INPUTTAB(0,7)"Atom to be searched for ? "AT$
```

```
2430 VDU14
2440 FORI%=1TON%
2450 IFAT#=T$(I%) PRINT:@%=&00001:PRINTI%;TAB(3)T$(
(I%);" ";TY%(I%);:@%=&20401:PRINT" ";x(I%);" ";y(
I%);" ";z(I%)
2460 NEXT
2470 VDU15
2480 GOTO2110
2490 ONERRORGOTO170
2517 ed%=1
2570 INPUT"Which no. atom ? "at%
2580 PRINT"Input new atom,type no.,X,Y,Z"
2590 INPUTT$(at%),TY%(at%),x(at%),y(at%),z(at%)
2600 GOTO2110
2610 CLS
2615 IFed%=1GOTO2650
2617 ed%=1
2620 PRINTTAB(0,3)"Do you wish to examine all the da
ta ?"
2630 Ans$=FNinput("Y","N")
2640 IFAns$="N" GOTO2010
2650 PRINTTAB(0,3)"Would you like a hard copy ?
"
2660 Ans$=FNinput("Y","N")
2670 IFAns$="Y" VDU2:pr%=20:GOTO2710
2680 PRINTTAB(0,3)"Press ESCAPE to stop or SHIFT to
proceed"
2690 ONERRORGOTO2110
2700 VDU14
2710 FORI%=1TON%
2720 IFpr%=0 PRINT
2730 @%=&00001:PRINT'TAB(pr%)I%;TAB(3+pr%)T$(I%);T
AB(9+pr%)TY%(I%);:@%=&20401:PRINTSPC3;x(I%);SPC3;y(I%);
SPC3;z(I%)
2740 NEXT
2750 VDU3
2760 pr%=0
2770 VDU15
2780 GOTO2110
2790 IFed%=0 CLS:PRINT'
2795 ed%=1
2800 PRINT"Do you wish to add to the list ?"
2810 Ans$=FNinput("Y","N")
2820 IFAns$="N" GOTO2010
2830 PRINT"Input new atom,type no.,X,Y,Z . Put in a
negative value to stop. "
2840 I%=0:@%=10
2850 REPEAT
2860 N%=N%+1
2870 I%=I%+1
2880 @%=&00001:PRINT'I%;:@%=10:INPUTTAB(5)T$(N%),T
Y%(N%),x(N%),y(N%),z(N%)
2890 UNTIL LEFT$(T$(N%),1)="-":N%=N%-1
2900 GOTO2110
2910 CLS
2920 PRINTTAB(0,5)"Current title is ";TITL$
2930 PRINTTAB(0,9)"Do you wish to alter this ?"
```

```
2940 Ans$=FNinput("Y","N")
2950 IFAns$="N" GOTO2010
2960 PRINTTAB(0,11)"Please enter new title"
2970 INPUTTAB(0,13)TITL$
2975 GOTO2910
2980 IFed%=0 CLS:PRINT''
2985 ed%=1
2990 PRINT"Do you wish to delete any atoms ?"
3000 Ans$=FNinput("Y","N")
3010 IFAns$="N" GOTO2010
3020 INPUT'"Please input no. of atom to be deleted
"IX
3030 IFIX=N% GOTO3110
3040 FORJ%=IXTON%-1
3050 x(J%)=x(J%+1)
3060 y(J%)=y(J%+1)
3070 z(J%)=z(J%+1)
3080 TY%(J%)=TY%(J%+1)
3090 T$(J%)=T$(J%+1)
3100 NEXT
3110 N%=N%-1
3120 GOTO2110
3130 DEFPROCunitcell
3140 FORI%=1TO8
3150 IFIXMOD2 v(I%)=B ELSEv(I%)=0
3160 IFIX<5 u(I%)=0 ELSEu(I%)=A
3170 w(I%)=C:NEXT
3180 w(1)=0:w(2)=0:w(5)=0:w(8)=0
3190 Q%=8
3200 ENDPROC
3210 DEFPROCautorelabel
3220 IFed%=0 CLS
3230 INPUT'"Please input atom to be sequentially"'1
abelled "T$
3235 J=1
3240 FOR I=1TON%
3250 IFT$(I)<>T$ GOTO3270
3260 T$(I)=T$(I)+CHR$(96+J)
3265 J=J+1
3270 NEXT
3280 PRINT"Do you want to relabel any more atoms ?"
3290 Ans$=FNinput("Y","N")
3300 IFAns$="Y" GOTO3230
3310 ENDPROC
```

```
>LIST  MOL 5
2000 DEFFPROCreset
2010 REPEAT
2020   CLS
2030   @%=10
2040   PRINTTAB(13,2)"RESET FACILITY"
2050   PRINTTAB(8,5)"A ----- Atomic radii"
2060   PRINTTAB(8,7)"P ----- Plot angles"
2070   PRINTTAB(8,9)"S ----- Scale factor"
2080   PRINTTAB(8,11)"M ----- Screen mode"
2090   PRINTTAB(8,13)"D ----- Default settings"
2100   PRINTTAB(8,15)"R ----- Rotation parameters"
2110   PRINTTAB(8,17)"L ----- Label plot"
2120   PRINTTAB(8,19)"Q ----- Quit reset facility"
2130   PRINTTAB(10,22)"Please enter option"
2140   in$=FNmenuin("D","M","S","A","R","P","Q","L","A",
",","A","A")
2150   IFin$="D" PROCdefault
2160   IFin$="M" PROCmode
2170   IFin$="S" PROCsf
2180   IFin$="A" PROCradii
2190   IFin$="R" PROCrotpar
2200   IFin$="P" PROCploang
2210   IFin$="L" PROClabplot
2220   UNTILin$="Q":ENDPROC
2230 DEFFPROCmode
2240   CLS
2250   @%=&00001:PRINTTAB(0,5)"Current plot screen mode
is mode ";n%
2260   PRINTTAB(0,7)"Do you wish to alter this ?"
2270   Ans$=FNinput("Y","N")
2280   IFAns$="N" ENDFPROC
2290   PRINTTAB(0,10)"Which mode would you like ?"
2300   Ans$=GET$
2310   IFAns$<>"0" AND Ans$<>"1" AND Ans$<>"2" AND Ans$<
>"4" AND Ans$<>"5" GOTO2300
2320   n%=VAL(Ans$)
2330   GOTO2240
2340 DEFFPROCsf
2350   CLS
2360   PRINTTAB(0,9)"Current Scale Factor is ";SF%
2370   PRINTTAB(0,11)"Do you wish to alter this ?"
2380   Ans$=FNinput("Y","N")
2390   IFAns$="N" ENDFPROC
2400   INPUTTAB(0,15)"Please input new value  "SF%
2410   GOTO2350
2420 DEFFPROCradii
2430   CLS
2440   FORI%=1TOr%
2450     @%=&00001:PRINT'I% ;TAB(5)"r atom type ";I% ;TAB(
20)"=" ;:@%=&20201:PRINTTAB(25)r(I%)
2460     NEXT
2470   PRINT'"Do you wish to alter any of the above ?"
2480   Ans$=FNinput("Y","N")
2490   IFAns$="N" ENDFPROC
2500   INPUT'"Which no. radius do you wish to alter ?  "
I%
2510   PRINT
2520   INPUT"Input new value  "r(I%)
2530   GOTO2430
2540 DEFFPROCploang
2550   CLS
```

```
25 60 @%=&20202
2570 PRINTTAB(0,3)"Psi      =  ";psi;TAB(20)"degrees"
2580 PRINTTAB(0,5)"Phi      =  ";phi;TAB(20)"degrees"
2590 PRINTTAB(0,7)"Theta    =  ";theta;TAB(20)"degrees"
2600 INPUTTAB(0,9)"Do you wish to alter any of the above ?"
2610 Ans$=FNinput("Y","N")
2620 IFAns$="N" ENDFPROC
2630 PRINTTAB(0,9)"Input value to be changed,new value
"
2640 INPUTTAB(0,11)C$,NV
2650 IFLEFT$(C$,1)="T" ORLEFT$(C$,1)="t" theta=NV
2660 IFLEFT$(C$,2)="PH" ORLEFT$(C$,2)="Ph" ORLEFT$(C$,
2)="ph" ORLEFT$(C$,2)="pH" phi=NV
2670 IFLEFT$(C$,2)="PS" ORLEFT$(C$,2)="Ps" ORLEFT$(C$,
2)="ps" ORLEFT$(C$,2)="pS" psi=NV
2680 GOTO2550
2690 DEFPROCrotpar
2700 CLS
2710 @%=&20102
2720 PRINTTAB(0,4)"The rotation increment is ";rot;" d
eg."
2730 PRINTTAB(0,6)"Do you wish to alter this ?"
2740 Ans$=FNinput("Y","N")
2750 IFAns$="N" GOTO2780
2760 INPUTTAB(0,8)"Please enter new value  "rot
2770 GOTO2700
2780 PRINTTAB(0,8)"The scale increment is "enl
2790 PRINTTAB(0,10)"Do you wish to alter this?"
2800 Ans$=FNinput("Y","N")
2810 IFAns$="N" ENDFPROC
2820 INPUTTAB(0,12)"Please enter new value  "enl
2830 ENDFPROC
2840 DEFPROClabplot
2850 CLS
2860 PRINTTAB(0,3)"Do you wish to label the plot ?"
2870 Ans$=FNinput("Y","N")
2880 IFAns$="Y" lab%=1 ELSElab%=0
2890 ENDFPROC
```

>LIST MOL 6

```
2000 DEFPROCsetdump
2010 xpointlo=&70:xpointhi=&71:ypointlo=&72:ypointhi=&
73:pixelvalue=&74:printerbyte=&75:bitcount=&76:mode0=&7
7:step=&78:OSWRCH=&FFEE:OSWORD=&FFF1:OSBYTE=&FFF4
2020 DIM space% 256
2030 FOR PASS=0TO 2 STEP 2
2040   P%=space%
2050   LOFT PASS
2060   .dump LDA&FF:STAYpointlo:LDA&3:STAYpointhi
2070   LDA&0:STAmode0:LDA&4:STAstep:LDA&135:JSR0SBYTE
:TYA:BNELineGap:INCmode0:LSRstep
2080   .LineGap LDA&27:JSRPrinter:LDA&65:JSRPrinter:LD
A&8:JSRPrinter
2090   .NewLine LDA&0:STAxpointlo:STAxpointhi
2100   LDA&27:JSRPrinter:LDAmode0:BEQModeAbove0:LDA&76
:JSRPrinter:LDA&128:JSRPrinter:LDA&2:JSRPrinter:BNENewC
olumn
2110   .ModeAbove0 LDA&75:JSRPrinter:LDA&64:JSRPrinter
:LDA&1:JSRPrinter
2120   .NewColumn LDA&8:STAbitcount
2130   .ReadPixel LDX&xpointlo:LDY&0:LDA&9:JSR0SWORD
2140   CLC:LDApixelvalue:BEQSetPrinterByte:SEC
2150   .SetPrinterByte ROLprinterbyte
2160   LDAypointlo:SEC:SBC&4:STAYpointlo:BCSCheckColum
nEnd:DECypointhi
2170   .CheckColumnEnd DECbitcount:LDAbitcount:BNERead
Pixel
2180   .Print LDAprinterbyte:JSRPrinter
2190   .NextColumn CLC:LDAstep:ADCxpointlo:STAxpointlo
:BCCCheckLineEnd:INCxpointhi
2200   .CheckLineEnd LDAxpointhi:CMP&5:BEQEndLine
2210   .ColumnTop LDA&32:CLC:ADCypointlo:STAYpointlo::
BCCNewColumn:INCypointhi:BCSNewColumn
2220   .EndLine LDA&10:JSRPrinter
2230   .CheckEnd LDAypointhi:BMIEnd:JMPNewLine
2240   .End LDA&12:JSRPrinter:LDA&27:JSRPrinter:LDA&64
:JSRPrinter:RTS
2250   .Printer PHA:LDA&1:JSR&FFEE:PLA:JSR&FFEE:RTS
2260   INEXT PASS
2270 ENDPROC
```

```

MOL 7
>LIST
2000 DEFPROCsymgen
2010 centro%=FALSE
2020 cen%=FALSE
2025 PROCnormalise
2030 CLS
2040 PRINTTAB(0,7)"Is the structure centred ? "
2050 ans$=FNinput("Y","N")
2060 IFans$="N" GOTO2150
2070 cen%=TRUE
2080 INPUTTAB(0,9)"A B C or I centred ?"c$
2090 IFc$="I" xs=0.5:ys=0.5:zs=0.5:GOTO2150
2100 IFc$="A" xs=0:ys=0.5:zs=0.5:GOTO2150
2110 IFc$="B" xs=0.5:ys=0:zs=0.5:GOTO2150
2120 IFc$="C" xs=0.5:ys=0.5:zs=0:GOTO2150
2130 PRINTTAB(0,13)"Please input extra lattice point"
2140 INPUTTAB(0,15)"xs,ys,zs
2150 CLS
2160 PRINTTAB(0,5)"Is the structure centrosymmetric ?
"
2170 ans$=FNinput("Y","N")
2180 IFans$="Y" centro%=TRUE
2190 CLS
2200 PRINTTAB(0,5)"Please input symmetry relations"
2210 PRINTTAB(0,7)"Please note that X,Y,Z is assumed
and that relations generated by a centre of symmetry o
r a centred lattice need not be included"
2220 INPUTTAB(0,12)"No of unique relations ? "eq%
2225 IFeq%=0 GOTO2265
2230 FORI=2TOeq%+1
2240   @%=&000001
2250   PRINT'I-1;:INPUTTAB(5)"xs$(I),ys$(I),zs$(I)
2260   NEXT
2265   xs$(1)="X":ys$(1)="Y":zs$(1)="Z"
2267   eq%=eq%+1
2270   @%=10
2280   IFcen%=FALSE GOTO2350
2290   FORI=1TOeq%
2300     xs$(eq%+I)=xs$(I)+" "+STR$(xs)
2310     ys$(eq%+I)=ys$(I)+" "+STR$(ys)
2320     zs$(eq%+I)=zs$(I)+" "+STR$(zs)
2330     NEXT
2340   eq%=eq%*2
2350   J%=N%+1
2360   FORI=1TON%
2370     FORH=1TOeq%
2380       X=x(I):Y=y(I):Z=z(I)
2390       T$(J%)=T$(I)
2400       TY%(J%)=TY%(I)
2410       x(J%)=EVAL(xs$(H))
2420       y(J%)=EVAL(ys$(H))
2430       z(J%)=EVAL(zs$(H))
2440       PROCincell:PROCincell
2443       PROCdouble
2450       J%=J%+1
2460       NEXT:NEXT
2470   N%=J%-1
```

```
2480 IFcentro%=FALSE GOTO2585
2485 J%=N%+1
2490 FORI=1TON%
2500   T$(J%)=T$(I)
2510   TY%(J%)=TY%(I)
2520   x(J%)=1-x(I)
2530   y(J%)=1-y(I)
2540   z(J%)=1-z(I)
2550   PROCincell:PROCincell
2555   PROCdouble
2560   J%=J%+1
2570   NEXT
2580 N%=J%-1
2585 PRINT"Total no. of atoms is ";N%
2586 PRINT'"Do you wish to include atoms located"'on
the cell axes ?"
2587 Ans$=FNinput("Y","N")
2588 IFAns$="Y" PROCconaxes
2590 ENDPROC
2600 DEFPROCincell
2610 IFx(J%)>=1 x(J%)=x(J%)-1
2620 IFx(J%)<0 x(J%)=1+x(J%)
2630 IFy(J%)<0 y(J%)=1+y(J%)
2640 IFy(J%)>=1 y(J%)=y(J%)-1
2650 IFz(J%)>=1 z(J%)=z(J%)-1
2660 IFz(J%)<0 z(J%)=1+z(J%)
2670 ENDPROC
2680 DEFPROCdouble
2690 FORJ=1TOJ%-1
2700   xe$=STR$(x(J%)):xf$=STR$(x(J))
2710   ye$=STR$(y(J%)):yf$=STR$(y(J))
2720   ze$=STR$(z(J%)):zf$=STR$(z(J))
2730   IFLEFT$(xe$,6)=LEFT$(xf$,6) AND LEFT$(ye$,6)=LE
FT$(yf$,6) AND LEFT$(ze$,6)=LEFT$(zf$,6) J=J%:J%=J%-1
2745   NEXT
2750 ENDPROC
2760 DEFPROCnormalise
2770 FORI=1TON%
2780   IFx(I)<0 x(I)=1+x(I)
2790   IFy(I)<0 y(I)=1+y(I)
2800   IFz(I)<0 z(I)=1+z(I)
2802   IFx(I)>1 x(I)=x(I)-1
2804   IFy(I)>1 y(I)=y(I)-1
2806   IFz(I)>1 z(I)=z(I)-1
2810   NEXT
2820 ENDPROC
2900 DEFPROCconaxes
3000 J%=N%+1
3010 FORI=1TON%
3015   IFx(I)<>0 GOTO3110
3030   T$(J%)=T$(I)
3040   TY%(J%)=TY%(I)
3050   x(J%)=x(I)+1
3060   y(J%)=y(I)
3070   z(J%)=z(I)
3100   J%=J%+1
3110   NEXT
3120 N%=J%-1
3130 J%=N%+1
```

```
3140 FORI=1TON%
3145 IFy(I)<>0 GOTO3240
3160 T$(J%)=T$(I)
3170 TY%(J%)=TY%(I)
3180 x(J%)=x(I)
3190 y(J%)=y(I)+1
3200 z(J%)=z(I)
3230 J%=J%+1
3240 NEXT
3250 N%=J%-1
3260 J%=N%+1
3270 FORI=1TON%
3275 IFz(I)<>0 GOTO3370
3290 T$(J%)=T$(I)
3300 TY%(J%)=TY%(I)
3310 x(J%)=x(I)
3320 y(J%)=y(I)
3330 z(J%)=z(I)+1
3360 J%=J%+1
3370 NEXT
3380 N%=J%-1
3390 ENDFROC
```

```
>LIST TPL0T
  5 MODE7
 10 REM"Titration curves
 20 DIM ml(50),mv(50),d1(50),d2(50)
 30 CLS:PRINT'"Input data as titre, emf"'enter a -v
e titre to end input."
 40 I=0:@%=&2020A:REPEAT
 50 INPUTml(I),mv(I):I=I+1
 60 UNTIL ml(I-1)<0OR I=50:N%=I-2
 70 PROCedit
 80 xs%=1000/ml(N%)DIV4*4:MODE1
 90 VDU29,100;500;:PROCpldata
100 MOVE0,-400:PLOT21,0,400:MOVE0,0:PLOT21,1000,0
110 PROCderiv:PROCplder:PROCfind
120 INPUTTAB(0,2)"Do you wish to calculate percentage
s",ans$
125 IFans$="Y" MODE7:PROCF
127 IFans$="M" RUN
128 IFans$="E" MODE7:GOTO70
129 END
130
140 DEF PROCpldata
150 GCOL0,3:FOR I=0TON%
160 PLOT69,ml(I)*xs%,mv(I):NEXT
170 ENDPROC
180
190 DEF PROCderiv
200 FOR I=1TO N%:dy=mv(I)-mv(I-1)
210 dx=ml(I)-ml(I-1):d1(I)=dy/dx
220 d2(I-1)=(d1(I)-d1(I-1))/dx
230 NEXT:ENDPROC
240
250 DEF PROCplder
260 MOVE0,0:GCOL0,1
270 FOR I=1TO N%:PLOT21,ml(I)*xs%,d1(I):NEXT
280 MOVE0,0:GCOL0,2
290 FOR I=0TO N%:DRAW ml(I)*xs%,d2(I):NEXT
300 ENDPROC
310
320 DEF PROCfind
330 I=0:T%=0:GCOL3,3:MOVE4,0
340 REPEAT T%=T%+4
350 UNTIL POINT(T%,0)=2 OR T%>1000
360 IF T%>1000 VDU4:ENDPROC
370 IF POINT(T%+4,0)=2 OR POINT(T%-4,0)=2 GOTO340
380 MOVE T%,-64:DRAW T%,64
390 VDU5:MOVE T%-32,I-300:PRINT;(T%+2)/xs%;" ml s"
400 I=I-32:GOTO340
410
420 DATA 0,-100,5,-99,6,-98,7,-97,8,-95
430 DATA 9,-85,9.5,-70,9.75,-50
440 DATA 10,0,10.25,50,10.5,70,11,85
450 DATA 12,95,13,97,14,98,15,99,20,100
460 DATA-1,0
470 DATA 0,-66,1,-63,2,-61,3,-59,4,-56
480 DATA 5,-54,6,-51,7,-47,8,-43,9,-39
490 DATA 10,-33,11,-26,12,-15,13,5
```

```
500 DATA 14,179,15,248,16,265,17,275
510 DATA 18,282,19,288,20,293,-1,0
520
530 DEF PROCedit
540 VDU14,12
550 FOR I=0TO N%:PRINTI,m1(I),mv(I):NEXT
560 INPUT "Change data Y/N ",A#
570 IF A#="N" ENDPROC ELSE IF A#<>"Y" GOTO 560
580 INPUT "Point, new titre, new emf",I,m1(I),mv(I)
590 CLS:GOTO540
600
610 DEF PROCcopy
620 PROCass:VDU26,2,1,8
630 FOR I%=1TO10:VDU1,10:NEXT
640 FOR Y%=1024TO-12 STEP-28
650   FOR X%=0TO1279STEP4
660     !Xlo=X%+Y%*&10000
670     ?count7=7:CALL dump:NEXT
680   VDU1,10:NEXT
690 FOR I%=1TO20:VDU1,10:NEXT
700 VDU1,15,3:ENDPROC
710
720 DEF PROCass:DIM S% 80
730 osword=&FFF1:oswrch=&FFEE
740 Xlo=S%:Xhi=S%+1:Ylo=S%+2:Yhi=S%+3
750 value=S%+4:byte=S%+5:count7=S%+6
760 S%=S%+7:FOR O=0TO2 STEP2:P%=S%
770   LOPT 0
780   .point:LDA £9
790   LDX £Xlo MOD256:LDY £Xlo DIV256
800   JSR osword:RTS
810   .pchar:LDA £1:JSR oswrch
820   LDA byte:JSR oswrch:RTS
830   .incY:CLC:LDA Ylo:ADC £4
840   STA Ylo:BCS incYhi:RTS
850   .incYhi:INC Yhi:RTS
860   .dump:LDA £1:STA byte
870   .loop:ASL byte:JSR point
880   LDA value:BEQ goon:EOR £&FF
890   BEQ goon:INC byte
900   .goon:JSR incY:DEC count7
910   BNE loop:JSR pchar:RTS
920   JNEXT
930 ENDPROC
940
1000 DEFPROCF
1010 CLS
1020 INPUTTAB(12,2)"V(Br)= "VBr
1030 INPUTTAB(12)"V(C1)= "VC1
1040 INPUT " STANDARDISATION = "STA
1050 INPUT "Wt OF SAMPLE (g) = "Wt
1060 IFVC1<>0 VC1=VC1-VBr
1070 PBr=VBr*0.4*79.9*STA/Wt
1080 PC1=VC1*0.4*35.49*STA/Wt
1090 PBr%=PBr*1000:PC1%=PC1*1000
1100 PBr$=STR$(PBr%):PC1$=STR$(PC1%)
1110 PBr%=PBr%/10
```

```
1120 PC1%=PC1%/10
1130 IFVAL(RIGHT$(PBr$,1))>5 PBr%=PBr%+1
1140 IFVAL(RIGHT$(PC1$,1))>5 PC1%=PC1%+1
1150 PBr=PBr%/100
1160 PC1=PC1%/100
1170 PRINTTAB(7,14)"% Br is ";PBr%;"
1180 PRINTTAB(7,16)"% C1 is ";PC1%;"
1190 INPUTTAB(2,22)"Do you wish to return to the main
    programme ,continue calculating percentages
or quit (M , C OR Q)",ans$
1200 IFans$="M" CLS:RUN
1210 IFans$="C" GOTO1010
1220 ENDPROC
1225
```

```
>LIST X-RAY
 10 REM X-ray powder
 20 REM diffractogram
 30 REM interpreter
 40 REM I. Abrahams
 50 REM 12th Oct. 84
 60 *FX6,10
 70 PROCsetdump
 80 lam=1.5418
 90 @%=&201401
100 IN%=0:print$="0":ins$="0"
110 N%=50
120 DIMHT(N%),angle(N%),ht(N%),d(N%),theta(N%),int(N%
)
130 ONERROR IFGO%=1 GOTO140 ELSE RENUMBER
140 MODE6:ANS$="1":GO%=1:ans$="Y":GOTO170
150 MODE6:GO%=0:@%=10
160 PROCmenu
170 IFANS$="1" PROCwhichinput
180 PROCcalc
190 IFANS$="2" PROCprintdata:VDU1,27,1,80
200 IFANS$="3" MODE4:PROCbarchart
210 IFprint$="Y" OR print$="y" VDU2:PROCsettab:CALLdu
mp:VDU3:print$="0":VDU1,27,1,64
220 IFANS$="4" PROCsave
230 IFANS$="5" MODE6:PROCexamine
240 IFANS$="6" PROCchange
250 IFANS$="7" PROCspool
260 GOTO150
270 END
280
290
300 DEFPROCcalc
310 HTBIG=HT(1)
320 FORI%=1TON%
330 IFHT(I%)>HTBIG HTBIG=HT(I%)
340 NEXT
350 FORI%=0TON%
360 ht(I%)=HT(I%)*100/HTBIG
370 NEXT
380 FORI%=1TON%
390 d(I%)=lam/(2*SIN(RAD(angle(I%)/2)))
400 NEXT
410 ENDPROC
420
430 DEFPROCchange
440 CLS
450 PRINTTAB(9,3)"Height"TAB(19,3)"2theta"
460 VDU14
470 FORI%=1TON%
480 @%=&00902
490 PRINTTAB(0,I%+4)I%;:@%=&20205:PRINTTAB(10)HT(I%
);TAB(20)angle(I%):@%=10
500 NEXT
510 VDU15
520 PRINT:PRINT
530 PRINT"Do you want to change any values ? "
540 ans$=GET$
550 IFans$="N"ORans$="n" ENDPROC
560 IFans$<>"Y" ANDans$<>"y" GOTO 540
570 PRINT:PRINT
```

```
580 INPUT"Which value would you like to change ?"I%
590 PRINT
600 INPUT"Enter new height,2theta  "HT(I%),angle(I%)
610 IFI%>N% N%=I%
620 GOTO440
630 ENDPROC
640
650 DEFPROCprintdata
660 *FX6,10
670 M%=0
680 VDU2,1,27,1,77
690 PRINT:PRINT:PRINTTAB(M%+((96-M%)/2)-16)"X-ray Pow
der Diffraction Pattern"
700 PRINTTAB((M%+((96-M%)/2))-(LEN(tit1$)/2))tit1$
710 M%=M%+((96-M%)/2):M%=M%-48
720 PRINT:PRINT:PRINTTAB(M%+28)"Rel. Int."TAB(M%+46)"
2theta"TAB(M%+65)"d"
730 PRINT
740 FORI%=1TON%
750 ht%=ht(I%)*10
760 ht$=STR$(ht(I%))
770 ht%=ht%/10
780 IFVAL(RIGHT$(ht$,1))>=5 ht%=ht%+1
790 @%=&00303
800 PRINTTAB(M%+30)ht%,:@%=&20101:PRINTTAB(M%+47)an
gle(I%):,@%=&20301:PRINTTAB(M%+63);d(I%)
810 NEXT
820 VDU3
830 ENDPROC
840
850 DEFPROCbarchart
860 VDU19,0,4
870 CLS
880 PRINT:PRINT:PRINTTAB(4)"X-ray Powder Diffraction
Pattern"
890 PRINT:PRINTTAB(20-(LEN(tit1$)/2))tit1$
900 MOVE70,256
910 DRAW1210,256
920 FORI%=1TON%
930 int(I%)=((ht(I%)/100)*500)+256
940 theta(I%)=1210-(angle(I%)*19)
950 MOVEtheta(I%),int(I%)
960 DRAWtheta(I%),256
970 NEXT
980 @%=&000901
990 FORI%=0T06
1000 MOVE70+(I%*190),256:DRAW70+(I%*190),240
1010 PRINTTAB(37-(I%*6),25)I%*10
1020 NEXT
1030 PRINTTAB(0,13)"Int."TAB(0,15)"(%) "
1040 PRINTTAB(13,27)"2 Theta(deg.)"
1050 PRINTTAB(0,30)"Do you want a hard copy ?"
1060 print$=GET$
1070 IFprint$<>"Y" ANDprint$<>"y" ANDprint$<>"N" ANDpr
int$<>"n" GOTO 1060
1080 PRINTTAB(0,30)STRING$(27,CHR$32)
1090 VDU20
1100 ENDPROC
1110
1120 DEFPROCsetdump
```

```
1130 xpointlo=&70:xpointhi=&71:ypointlo=&72:ypointhi=&
73:pixelvalue=&74:printerbyte=&75:bitcount=&76:mode0=&7
7:step=&78:OSWRCH=&FFEE:OSWORD=&FFF1:OSBYTE=&FFF4
1140 DIM space% 256
1150 FOR PASS=0 TO 2 STEP 2
1160   F%=space%
1170   [OPT PASS
1180   .dump LDA&FF:STAYpointlo:LDA&3:STAYpointhi
1190   LDA&0:STAmode0:LDA&4:STAsstep:LDA&135:JSRROSBYTE
:TYA:BNELineGap:INCmode0:LSRstep
1200   .LineGap LDA&27:JSRPrinter:LDA&65:JSRPrinter:LD
A&8:JSRPrinter
1210   .NewLine LDA&0:STAxpointlo:STAxpointhi
1220   LDA&27:JSRPrinter:LDAmode0:BEQModeAbove0:LDA&76
:JSRPrinter:LDA&128:JSRPrinter:LDA&2:JSRPrinter:BNENewC
olumn
1230   .ModeAbove0 LDA&75:JSRPrinter:LDA&64:JSRPrinter
:LDA&1:JSRPrinter
1240   .NewColumn LDA&8:STAbitcount
1250   .ReadPixel LDX&xpointlo:LDY&0:LDA&9:JSRROSWORD
1260   CLC:LDApixelvalue:BEQSetPrinterByte:SEC
1270   .SetPrinterByte ROLprinterbyte
1280   LDAypointlo:SEC:SBC&4:STAYpointlo:BCSCheckColum
nEnd:DECypointhi
1290   .CheckColumnEnd DECbitcount:LDAbitcount:BNERead
Pixel
1300   .Print LDAprinterbyte:JSRPrinter
1310   .NextColumn CLC:LDAstep:ADCxpointlo:STAxpointlo
:BCCCheckLineEnd:INCxpointhi
1320   .CheckLineEnd LDAxpointhi:CMPE&5:BEQEndLine
1330   .ColumnTop LDA&32:CLC:ADCypointlo:STAYpointlo::
BCCNewColumn:INCypointhi:BCSNewColumn
1340   .EndLine LDA&10:JSRPrinter:LDA&9:JSRPrinter
1350   .CheckEnd LDAypointhi:BMIEnd:JMPNewLine
1360   .End LDA&12:JSRPrinter:LDA&27:JSRPrinter:LDA&64
:JSRPrinter:RTS
1370   .Printer PHA:LDA&1:JSR&FFEE:PLA:JSR&FFEE:RTS
1380   JNEXT PASS
1390 ENDPROC
1400
1410 DEFPROCmenu
1420 PRINT:PRINT:PRINTTAB(3)"X-RAY POWDER DIFFRACTION
UTILITY"
1430 PRINTTAB(10,7)"1   Input data"
1440 PRINTTAB(10,9)"2   Print data"
1450 PRINTTAB(10,11)"3   Plot data"
1460 PRINTTAB(10,13)"4   Save data"
1470 PRINTTAB(10,15)"5   Examine data"
1480 PRINTTAB(10,17)"6   Edit data"
1490 PRINTTAB(5,22)"Please select your option"
1500 ANS#=GET#
1510 IFVAL(ANS#)>7 GOTO1500
1520 VDU20
1530 ENDPROC
1540
1550 DEFPROCindata
1560 IFans#<>"Y" ANDans#<>"y" ENDPROC
1570 CLS
1580 I%=0
1590 INPUTTAB(0,2)"Title ?  "titl$
```

```
1600 PRINTTAB(0,4)"Please input Height(cm.),2theta (de
g.)"
1610 @%=&201401
1620 REPEAT
1630     I%=I%+1
1640     PRINTTAB(0,I%+6)I%;
1650     INPUTTAB(5)HT(I%),angle(I%)
1660     UNTILI%=N% OR HT(I%)=-1
1670     N%=I%-1
1680 PROCchange
1690 ENDPROC
1700
1710 DEFPROCwhichinput
1720 IFGO%=1 GOTO1810
1730 CLS
1740 PRINTTAB(0,7)"Inputing new data will destroy the
    current file."
1750 INPUTTAB(10,20)"ARE YOU SURE ?"ans$
1760 IFans$<>"Y" AND ans$<>"y" ENDPROC
1770 FORI%=1TON%+1
1780     HT(I%)=0:angle(I%)=0
1790     NEXT
1800 N%=50
1810 CLS
1820 PRINTTAB(0,7)"Do you wish to : "
1830 PRINTTAB(0,10)"(a) type in new data"
1840 PRINTTAB(0,12)"(b) load an old data file."
1850 ins$=GET$
1860 IFins$<>"A" ANDins$<>"a" ANDins$<>"B" AND ins$<>"
b" GOTO 1850
1870 IFins$="A"OR ins$="a" PROCindata:IN%=1
1880 IFins$="B"OR ins$="b" PROCinput
1890 ENDPROC
1900
1910 DEFPROCsettab
1920 VDU1,27,1,68,1,15,1,0
1930 ENDPROC
1940
1950 DEFPROCsave
1960 CLS
1970 PRINTTAB(0,3)"Tape or disc (T/D)"
1980 Ans$=GET$
1990 IFAns$="D" ORAns$="d" GOTO2020
2000 IFAns$<>"T" ANDAns$<>"t" GOTO1980
2010 *T.
2020 INPUTTAB(0,5)"Filename  ?"Fnm$
2030 G=OPENDOUT Fnm$
2040 PRINTfG,N%,titl$
2050 FORI%=1TON%
2060     PRINTTAB(5,9)Fnm$;TAB(15)I%
2070     PRINTfG,HT(I%),angle(I%)
2080     NEXT
2090 CLOSEfG
2100 *D.
2110 ENDPROC
2120
2130 DEFPROCinput
2140 CLS
2150 PRINTTAB(0,3)"Tape or disc (T/D)"
2160 Ans$=GET$
2170 IFAns$="D" ORAns$="d" GOTO2200
```

```
2180 IFAns$<>"T" ANDAns$<>"t" GOTO2160
2190 *T.
2200 INPUTTAB(0,5)"Filename ?"Fnm$
2210 G=OPENIN Fnm$
2220 INPUTfG,N%,titl$
2230 FORI%=1TON%
2240 PRINTTAB(5,9)Fnm$;TAB(15)I%
2250 INPUTfG,HT(I%),angle(I%)
2260 NEXT
2270 CLOSEfG
2280 *D.
2290 ENDPROC
2300
2310 DEFPROCexamine
2320 CLS
2330 VDU14
2340 PRINTTAB(10,2)"Height";TAB(26,2)"2 theta"
2350 FORI%=1TON%
2360 PRINT
2370 @%=&00001
2380 PRINTTAB(0)I%;:@%=&20105;PRINTTAB(10)HT(I%);:@%
=&20101;PRINTTAB(28)angle(I%)
2390 NEXT
2400 PRINT:PRINT:PRINTTAB(0)"Press any key to return t
o menu"
2410 Ans$=GET$
2420 VDU15
2430 ENDPROC
2440 DEFPROCspool
2445 ONERROROFF
2450 REM XRAY DIFFRACTION
2460 REM FILE CONVERTER
2465 CLS
2470 INPUT"TITLE ?"titl$
2480 CLS
2490 PRINT"Please insert destination disc"
2500 INPUT"Drive number ?"DN%
2505 *DRIVE0
2510 IFDN%=0 GOTO2530
2511 *DRIVE2
2530 *SPOOL VIEWIN
2540 PRINTtitl$
2550 PRINT
2560 PRINTTAB(10)"d(hk1)"TAB(26)"% Int."
2570 FOR I=1 TO N%
2580 @%=&20301;PRINTTAB(10)d(I);:@%=&00303;PRINTTAB(
28)ht(I)
2590 NEXT
2600 *SPOOL
2610 ENDPROC
```

APPENDIX TWO

CRYSTAL AND X-RAY STRUCTURE FACTOR DATA.

	Page
Table A2.1: Crystal data for $[\text{C}_6\text{H}_5.\text{CH}:\text{NH}_2]_2^+\text{SnCl}_6.\text{CH}_3\text{CO}_2\text{C}_2\text{H}_5$	371
Table A2.2: Latest atomic parameters for $[\text{C}_6\text{H}_5.\text{CH}:\text{NH}_2]_2^+\text{SnCl}_6.\text{CH}_3\text{CO}_2\text{C}_2\text{H}_5$	372
Table A2.3: Significant bond lengths and $[\text{C}_6\text{H}_5.\text{CH}:\text{NH}_2]_2^+\text{SnCl}_6.\text{CH}_3\text{CO}_2\text{C}_2\text{H}_5$	373
Observed and calculated structure factors for RbSn_2Br_5	374
Observed and calculated structure factors for $\text{CsSn}_3\text{Br}_{1.5}\text{F}_{5.5}$	376
Observed and calculated structure factors for $\text{KBr}.\text{KSnBr}_2\text{Cl}.\text{H}_2\text{O}$	379
Observed and calculated structure factors for $\text{KCl}.\text{KSnCl}_3.\text{H}_2\text{O}$	383
Observed and calculated structure factors for Sn_3BrF_5	384
Observed and calculated structure factors for $[\text{C}_6\text{H}_5.\text{CH}:\text{NH}_2]_2^+\text{SnCl}_6.\text{CH}_3\text{CO}_2\text{C}_2\text{H}_5$	386

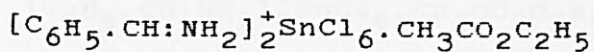
Table A2.1

Crystal data for $[\text{C}_6\text{H}_5\cdot\text{CH:NH}_2]_2^+\text{SnCl}_6\cdot\text{CH}_3\text{CO}_2\text{C}_2\text{H}_5$

Morphology	Brown needles
Crystal class	Monoclinic (or triclinic ?)
Cell Dimensions (Å)	a = 21.541 b = 16.679 c = 7.411 $\alpha = \gamma = 90^\circ$ $\beta = 99.939^\circ$
Cell Volume (Å ³)	2622.68
Molecular Weight (g)	631.8
Z	4
D_c (gcm ⁻³)	1.6
D_o (gcm ⁻³)	1.9
F(000)	1256
$\mu(\text{MoK}\alpha)$ (cm ⁻¹)	14.79
Radiation	MoK α $\lambda = 0.7107\text{Å}$

Table A2.2

Latest atomic parameters for



with ESDs in brackets

Atom	x/a	y/b	z/c	S.O.F	B
Sn	0.5	0.5	0.0	0.5	0.011(1)
Cl(1)	0.557(1)	0.422(2)	0.254(3)	1.0	0.106(7)
Cl(2)	0.581(2)	0.402(2)	0.059(5)	1.0	0.17(1)
Cl(3)	0.416(2)	0.401(2)	0.947(5)	1.0	0.17(1)
Cl(4)	0.444(1)	0.423(2)	0.736(4)	1.0	0.111(8)
Cl(5)	0.556(1)	0.423(2)	0.768(4)	1.0	0.118(8)
Cl(6)	0.443(1)	0.425(2)	0.219(4)	1.0	0.116(8)

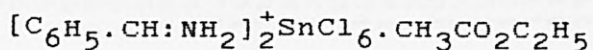
R = 35.3% after 4 cycles of least squares refinement.

Solution in Triclinic P_1 symmetry.

Overall scale factor = 2.53

Table A2.3

Significant bond lengths (Å) and angles (°) in



with ESDs in brackets

Sn--Cl(1)	2.44(2)	Sn--Cl(4)	2.48(3)
Sn--Cl(2)	2.38(4)	Sn--Cl(5)	2.60(3)
Sn--Cl(3)	2.43(4)	Sn--Cl(6)	2.53(3)

Cl(1)--Sn--Cl(2) 40.1(1.0)

Cl(1)--Sn--Cl(3) 91.5(1.0)

Cl(1)--Sn--Cl(4) 116.5(0.8)

Cl(1)--Sn--Cl(5) 91.0(0.8)

Cl(1)--Sn--Cl(6) 58.6(0.8)

Cl(2)--Sn--Cl(3) 93.4(1.2)

Cl(2)--Sn--Cl(4) 91.5(1.0)

Cl(2)--Sn--Cl(5) 51.1(1.0)

Cl(2)--Sn--Cl(6) 87.9(1.0)

Cl(3)--Sn--Cl(4) 43.1(0.9)

Cl(3)--Sn--Cl(5) 88.7(1.0)

Cl(3)--Sn--Cl(6) 48.6(1.0)

Cl(4)--Sn--Cl(5) 56.1(0.8)

Cl(4)--Sn--Cl(6) 91.4(0.8)

Cl(5)--Sn--Cl(6) 121.0(0.8)

H	K	L	10FO	10FC	H	K	L	10FO	10FC	H	K	L	10FO	10FC	H	K	L	10FO	10FC	H	K	L	10FO	10FC
1	1	0	598	496	1	3	2	1202	1002	5	5	4	585	542	4	6	6	550	-545	2	3	9	519	464
0	2	0	2027	-1809	3	3	2	2235	-1976	0	6	4	583	544	6	6	6	1477	1520	1	4	9	1199	-1147
2	2	0	4138	4281	0	4	2	459	-322	2	6	4	1447	1323	3	7	6	510	485	3	4	9	473	417
1	3	0	5031	5622	2	4	2	370	326	4	6	4	2173	2110	0	8	6	1213	-1177	4	5	9	457	-452
3	3	0	4194	-4159	1	5	2	717	-634	6	6	4	276	301	2	8	6	804	824	1	6	9	722	693
0	4	0	1183	-982	3	5	2	1606	1487	1	7	4	2030	1971	4	8	6	465	437	5	6	9	482	-487
2	4	0	3362	3109	5	5	2	809	-779	3	7	4	317	-295	6	8	6	684	-711	2	7	9	610	-660
4	4	0	2924	2673	0	6	2	1713	1533	5	7	4	1180	1183	1	9	6	633	683	4	7	9	773	823
1	5	0	365	306	2	6	2	881	-812	7	7	4	1367	1457	3	9	6	954	-1012	6	7	9	366	-426
3	5	0	4039	3982	6	6	2	983	928	0	8	4	338	273	5	9	6	672	780	1	8	9	288	79
0	6	0	5455	5901	1	7	2	229	223	2	8	4	1435	1438	1	2	7	840	-746	2	9	9	578	577
2	6	0	928	-815	7	7	2	328	317	4	8	4	900	919	2	3	7	706	664	4	9	9	540	-545
4	6	0	467	-436	0	8	2	1034	-1014	6	8	4	326	260	3	4	7	562	566	0	0	10	414	371
6	6	0	3633	3672	2	8	2	832	804	1	9	4	419	445	2	5	7	1186	-1138	0	2	10	604	-573
1	7	0	465	387	4	8	2	434	373	3	9	4	1300	1305	4	5	7	604	569	2	2	10	424	350
3	7	0	2700	2560	6	8	2	540	-579	5	9	4	792	840	1	6	7	974	957	3	3	10	347	-274
5	7	0	519	505	1	9	2	423	411	0	10	4	1766	1828	5	6	7	705	-696	0	4	10	378	386
0	8	0	684	-647	3	9	2	459	-471	2	10	4	312	216	6	7	7	470	-550	4	4	10	344	-355
2	8	0	2022	1941	5	9	2	585	657	1	2	5	3507	3464	1	8	7	844	-802	3	5	10	600	625
4	8	0	1420	1374	0	10	2	411	440	2	3	5	288	256	3	8	7	359	-298	5	5	10	458	-465
6	8	0	339	-355	1	2	3	4477	4962	1	4	5	3160	-3044	5	8	7	861	889	0	6	10	254	181
1	9	0	2056	2044	2	3	3	223	203	3	4	5	295	302	2	9	7	767	803	4	6	10	397	360
3	9	0	1351	-1335	1	4	3	4031	-4121	2	5	5	2235	2064	4	9	7	683	-720	1	7	10	399	364
5	9	0	1608	1682	3	4	3	275	274	4	5	5	1970	-1849	0	0	8	6764	7443	3	7	10	484	-489
2	10	0	1038	1036	2	5	3	3181	3012	1	6	5	429	417	1	1	8	405	380	0	8	10	560	-564
4	10	0	998	1066	4	5	3	2741	-2599	2	7	5	1782	-1718	0	2	8	1232	-1096	2	8	10	406	454
1	2	1	168	-116	1	6	3	387	350	4	7	5	1655	1667	2	2	8	3046	2938	1	2	11	3407	3255
2	3	1	855	774	5	6	3	246	-129	6	7	5	274	-330	1	3	8	3992	3880	1	4	11	3001	-2858
1	4	1	782	-701	2	7	3	2403	-2324	1	8	5	1259	1206	3	3	8	3010	-2873	2	5	11	2324	2298
3	4	1	705	649	4	7	3	2204	2171	5	8	5	783	-810	0	4	8	700	-621	4	5	11	1982	-1986
2	5	1	732	-671	6	7	3	286	-305	7	8	5	654	672	2	4	8	2410	2273	2	7	11	1733	-1769
4	5	1	229	147	1	8	3	1834	1784	2	9	5	336	275	4	4	8	2065	2023	4	7	11	1564	1644
1	6	1	1157	1063	5	8	3	1253	-1273	4	9	5	315	-361	1	5	8	335	288	1	8	11	1426	1449
5	6	1	772	-740	7	8	3	887	976	1	10	5	987	-1034	3	5	8	3022	2985	0	0	12	982	945
2	7	1	341	-299	4	9	3	336	-313	0	0	6	4153	4242	0	6	8	4346	4406	1	1	12	1604	1471
4	7	1	586	601	6	9	3	303	220	1	1	6	1032	-946	2	6	8	589	-547	0	2	12	1125	993
6	7	1	585	-600	1	10	3	1310	-1355	0	2	6	2532	-2326	4	6	8	323	-272	2	2	12	1490	1393
1	8	1	503	-509	0	0	4	1211	1120	2	2	6	1312	1194	6	6	8	2667	2832	1	3	12	794	793
3	8	1	313	-312	1	1	4	3032	2925	1	3	6	1796	1621	1	7	8	334	343	3	3	12	1400	1323
5	8	1	683	681	0	2	4	2423	2110	3	3	6	3153	-3066	3	7	8	1946	1970	0	4	12	1904	1794
2	9	1	830	848	2	2	4	2520	2355	0	4	6	1251	-1108	5	7	8	436	433	2	4	12	815	779
4	9	1	771	-772	1	3	4	1315	1139	2	4	6	711	613	0	8	8	521	-455	1	5	12	829	745
1	10	1	320	-354	3	3	4	2850	2656	4	4	6	388	374	2	8	8	1448	1524	3	5	12	1283	1331
3	10	1	259	235	0	4	4	3458	3282	1	5	6	895	-813	4	8	8	1080	1080	0	6	12	504	577
0	0	2	2896	3109	2	4	4	1341	1181	3	5	6	1802	1718	6	8	8	292	-259	2	6	12	737	727
1	1	2	651	-537	4	4	4	473	398	5	5	6	875	-860	1	9	8	1548	1595	4	6	12	1204	1242
0	2	2	2067	-1850	1	5	4	1462	1305	0	6	6	2509	2396	3	9	8	954	-991	1	7	12	1170	1203
2	2	2	1190	1059	3	5	4	2052	1956	2	6	6	1255	-1199	1	2	9	932	869	5	7	12	647	727

OBSERVED AND CALCULATED STRUCTURE FACTORS FOR RbSn₂Br₅

H	K	L	10FO	10FC	H	K	L	10FO	10FC	H	K	L	10FO	10FC	H	K	L	10FO	10FC					
2	8	12	932	982	1	1	14	843	-773	5	5	14	606	-629	4	5	15	349	440	3	5	16	1364	1418
1	2	13	1188	1111	0	2	14	1702	-1610	0	6	14	1789	1887	1	6	15	582	570	0	6	16	1880	2022
1	4	13	1129	-1123	2	2	14	775	713	2	6	14	940	-992	0	0	16	3107	3086	1	2	17	876	901
2	5	13	681	631	1	3	14	1232	1193	4	6	14	586	-660	0	2	16	372	-314	1	4	17	936	-966
4	5	13	637	-641	3	3	14	2412	-2427	3	7	14	472	547	2	2	16	1388	1342	2	5	17	430	524
2	7	13	650	-670	0	4	14	1109	-1097	1	2	15	637	-613	1	3	16	1717	1725	0	0	18	501	-503
4	7	13	677	725	2	4	14	477	458	2	3	15	431	372	3	3	16	1104	-1093	0	4	18	382	397
1	8	13	355	365	1	5	14	634	-635	3	4	15	383	324	2	4	16	1074	1071	1	2	19	1398	1480
0	0	14	3026	2889	3	5	14	1143	1137	2	5	15	811	-799	4	4	16	926	974					

H	K	L	10FO	10FC	H	K	L	10FO	10FC	H	K	L	10FO	10FC	H	K	L	10FO	10FC	H	K	L	10FO	10FC
4	0	0	148	93	-18	0	1	1375	1337	-8	2	1	536	443	0	0	2	157	159	10	2	2	591	511
6	0	0	1327	1441	-16	0	1	298	300	-6	2	1	2890	2510	2	0	2	204	178	12	2	2	1441	1556
8	0	0	3533	4923	-14	0	1	2129	2267	-4	2	1	394	288	4	0	2	3193	3573	14	2	2	59	62
10	0	0	803	819	-12	0	1	157	119	0	2	1	277	229	6	0	2	354	392	16	2	2	564	533
12	0	0	2201	2305	-8	0	1	631	633	2	2	1	385	387	8	0	2	353	388	18	2	2	754	772
14	0	0	528	548	-6	0	1	2864	3659	6	2	1	1427	1434	10	0	2	710	670	-17	3	2	259	260
16	0	0	133	114	-4	0	1	179	161	8	2	1	1646	1923	12	0	2	2022	2236	-15	3	2	1142	1055
18	0	0	316	309	-2	0	1	180	134	10	2	1	2120	2435	14	0	2	215	226	-13	3	2	1749	1518
20	0	0	2035	1853	0	0	1	630	620	12	2	1	768	767	16	0	2	687	643	-11	3	2	444	360
22	0	0	318	602	2	0	1	672	648	14	2	1	636	638	18	0	2	1054	1056	-9	3	2	530	463
1	1	0	1029	927	4	0	1	210	194	16	2	1	1597	1771	20	0	2	526	482	-7	3	2	325	356
3	1	0	2030	2803	0	0	1	1772	1956	18	2	1	1135	1111	-23	1	2	1026	1015	-5	3	2	2735	2616
5	1	0	312	252	8	0	1	2385	2832	20	2	1	277	248	-21	1	2	657	634	-3	3	2	1169	1070
7	1	0	2696	3017	10	0	1	2723	3261	-17	3	1	925	843	-17	1	2	415	438	-1	3	2	280	213
9	1	0	3270	3556	12	0	1	934	1014	-15	3	1	1351	1254	-15	1	2	1580	1571	1	3	2	1333	1256
11	1	0	1356	1406	14	0	1	740	837	-13	3	1	1275	1054	-13	1	2	2340	2486	3	3	2	1812	1707
13	1	0	1627	1605	16	0	1	2172	2198	-9	3	1	1618	1316	-11	1	2	1166	1090	5	3	2	239	250
15	1	0	1207	1135	18	0	1	1531	1510	-7	3	1	197	183	-9	1	2	469	410	7	3	2	1269	1298
17	1	0	1908	1700	20	0	1	279	244	-5	3	1	2254	2035	-7	1	2	456	468	11	3	2	1286	1292
19	1	0	353	349	22	0	1	938	844	-3	3	1	720	712	-5	1	2	4265	4881	13	3	2	1152	1246
21	1	0	304	302	-23	1	1	1285	1209	1	3	1	627	533	-3	1	2	2213	1927	15	3	2	719	771
0	2	0	4002	7010	-21	1	1	1301	1272	3	3	1	2654	2834	-1	1	2	221	182	-8	4	2	754	693
2	2	0	43	54	-19	1	1	331	296	5	3	1	265	251	1	1	2	2241	2043	-6	4	2	829	733
4	2	0	123	75	-17	1	1	1337	1366	7	3	1	431	435	3	1	2	3327	3574	-2	4	2	223	208
6	2	0	1365	1203	-15	1	1	1987	2108	9	3	1	304	335	5	1	2	750	713	0	4	2	224	297
8	2	0	3631	3449	-13	1	1	1997	2212	11	3	1	779	745	7	1	2	1907	1954	2	4	2	228	243
10	2	0	729	710	-11	1	1	435	431	13	3	1	1006	1065	9	1	2	296	253	4	4	2	1010	1106
12	2	0	1753	1765	-9	1	1	2221	2156	15	3	1	828	865	11	1	2	2382	2622	6	4	2	284	271
14	2	0	626	553	-7	1	1	585	555	-10	4	1	186	171	13	1	2	1851	2033	8	4	2	279	255
16	2	0	69	68	-5	1	1	3858	4213	-8	4	1	172	208	15	1	2	1187	1306	-22	0	3	1453	1554
18	2	0	272	243	-3	1	1	1160	973	-6	4	1	1114	1069	17	1	2	561	512	-18	0	3	755	837
20	2	0	1636	1401	-1	1	1	235	234	-4	4	1	391	373	19	1	2	1219	1174	-16	0	3	333	384
1	3	0	132	142	1	1	1	1191	990	0	4	1	152	156	21	1	2	751	775	-14	0	3	849	837
3	3	0	1645	1632	3	1	1	3880	5460	4	4	1	332	293	-20	2	2	1652	1704	-12	0	3	448	395
5	3	0	154	166	5	1	1	520	422	6	4	1	740	735	-18	2	2	1598	1586	-10	0	3	4138	5668
7	3	0	1839	1715	7	1	1	643	586	8	4	1	659	734	-16	2	2	975	998	-8	0	3	1281	1155
9	3	0	2128	1841	9	1	1	1273	1344	10	4	1	976	1232	-14	2	2	324	312	-6	0	3	895	790
11	3	0	974	824	11	1	1	1109	1239	-22	0	2	422	449	-12	2	2	2225	2078	-4	0	3	2197	1985
13	3	0	1129	1067	13	1	1	1485	1577	-20	0	2	2125	2219	-10	2	2	744	564	-2	0	3	5270	7568
15	3	0	591	617	15	1	1	1372	1428	-18	0	2	1880	1997	-8	2	2	1836	1528	0	0	3	1966	1875
17	3	0	1202	1057	17	1	1	539	467	-16	0	2	1081	1234	-6	2	2	1157	982	2	0	3	1437	1339
0	4	0	2814	3123	19	1	1	1267	1187	-14	0	2	400	396	-4	2	2	650	537	4	0	3	2351	2347
4	4	0	182	169	21	1	1	672	627	-12	0	2	2382	2648	-2	2	2	185	226	6	0	3	2816	3109
6	4	0	913	840	-20	2	1	501	541	-10	0	2	895	927	0	2	2	205	229	8	0	3	768	740
8	4	0	1665	1408	-18	2	1	1039	1011	-8	0	2	2088	2172	2	2	2	209	204	10	0	3	2816	3123
10	4	0	531	515	-16	2	1	343	328	-6	0	2	1171	1153	4	2	2	2465	2511	12	0	3	400	402
-20	0	1	454	469	-14	2	1	1660	1591	-4	0	2	961	928	6	2	2	406	355	14	0	3	158	125
-20	0	1	746	782	-10	2	1	99	79	-2	0	2	763	708	8	2	2	311	330	16	0	3	511	629

H	K	L	10FO	10FC	h	k	l	10FO	10FC	H	K	L	12FO	12FC	H	K	L	10FO	10FC	H	K	L	10FO	10FC
16	2	3	1574	1648	-3	3	3	655	637	1	1	4	2979	2982	-16	0	0	1234	1318	10	2	5	1281	1194
25	1	3	1457	1378	-1	3	3	624	556	3	1	4	829	729	-16	0	0	126	115	14	2	5	1651	652
-23	1	3	352	345	1	3	3	1834	1745	-1	1	4	363	345	-14	0	0	2568	2596	-15	3	5	1585	1477
-19	1	3	224	225	5	3	3	1187	1181	7	1	4	739	687	-12	0	0	279	287	-13	3	5	1642	1011
-17	1	3	1334	1400	5	3	3	564	631	9	1	4	1417	1480	-10	0	0	424	446	-11	3	5	421	459
-15	1	3	1498	1599	7	3	3	2022	2085	11	1	4	1658	1783	-8	0	0	397	415	-9	3	5	942	908
-13	1	3	1121	1134	9	3	3	275	257	13	1	4	1259	1243	-6	0	0	1172	1205	-7	3	5	2434	2246
-11	1	3	1880	1898	13	3	3	1230	1269	15	1	4	1458	1425	-4	0	0	145	118	-5	3	5	1586	1497
-9	1	3	2161	2128	-10	3	3	1924	1874	17	1	4	1690	1625	-4	0	0	1001	990	-5	3	5	1503	843
-7	1	3	1865	1747	-8	4	4	665	589	-20	2	4	690	663	-2	0	0	666	621	-1	3	5	1017	1004
-5	1	3	1121	1214	-6	4	4	416	406	-18	2	4	581	563	-2	0	0	3871	3938	-1	3	5	1644	1533
-3	1	3	1171	1271	-4	4	4	715	698	-16	4	4	1757	1670	4	0	0	616	541	3	3	5	235	311
-1	1	3	1340	1374	-2	4	4	2289	2310	-14	4	4	220	219	6	0	0	426	425	5	3	5	1431	1464
-1	1	3	3534	3599	0	4	4	335	340	-12	4	4	293	219	8	0	0	131	144	7	3	5	259	264
-1	1	3	2197	2107	2	4	4	365	340	-10	4	4	450	417	10	0	0	1764	1730	-4	4	5	996	905
3	1	3	667	620	0	4	4	1150	1149	-8	4	4	2074	2532	14	0	0	835	784	9	4	5	951	977
3	1	3	3331	3705	6	4	4	799	793	-4	4	4	559	400	14	0	0	739	717	-6	4	5	144	193
3	1	3	550	570	-2	4	4	339	368	-2	4	4	1341	1108	-17	1	1	517	516	-4	4	5	585	622
11	1	3	1859	1905	-16	4	4	921	891	10	2	4	236	275	-15	1	1	2223	2251	-2	4	5	144	193
15	1	3	1221	1268	-18	4	4	352	366	-13	2	4	1725	1605	-13	1	1	1968	1929	-2	4	5	585	622
17	1	3	725	715	-14	4	4	2174	2295	-11	2	4	1050	1564	-11	1	1	553	500	-2	4	5	265	266
15	1	3	241	215	-12	4	4	190	204	-9	2	4	1022	2234	-9	1	1	4012	4122	-2	4	6	1101	1135
-16	2	3	651	605	-10	4	4	569	597	10	2	4	1725	1605	-7	1	1	2726	2592	-8	4	6	218	207
-16	2	3	469	455	-8	4	4	3545	3622	14	2	4	577	605	-5	1	1	1419	1321	-16	4	6	675	580
-14	2	3	211	208	-6	4	4	211	199	16	2	4	1505	494	-3	1	1	1587	1460	-14	4	6	3417	4007
-10	2	3	949	850	-4	4	4	652	549	-1	3	4	1317	1293	-1	1	1	3410	3292	-10	4	6	997	972
-8	2	3	955	917	-2	4	4	201	1910	-15	3	4	745	656	3	1	1	591	582	-8	4	6	39	40
-6	2	3	1590	1624	0	4	4	426	400	-13	3	4	80	102	5	1	1	2221	2240	-6	4	6	2379	2344
-4	2	3	4785	5234	4	4	4	2231	2170	-1	3	4	930	874	7	1	1	511	470	-4	4	6	4253	4796
-2	2	3	1343	1327	6	4	4	2931	3078	-7	3	4	321	340	9	1	1	1756	1710	-2	4	6	1765	1698
2	2	3	1977	1900	8	4	4	1408	1343	-5	3	4	1862	1763	11	1	1	1526	1511	0	4	6	2201	2195
2	2	3	2275	2131	10	4	4	1748	1731	-3	3	4	308	338	13	1	1	1212	1260	2	4	6	1000	931
8	2	3	745	604	14	4	4	2155	2269	-1	3	4	411	457	15	1	1	265	278	4	4	6	1555	1528
8	2	3	2275	2131	16	4	4	1752	1738	1	3	4	1835	1739	-20	2	2	1033	1021	6	4	6	101	78
10	2	3	2323	2390	18	4	4	186	186	-18	2	2	493	515	-18	2	2	522	499	8	4	6	2468	2619
12	2	3	466	504	-23	1	4	591	729	-14	2	2	146	145	-14	2	2	1046	1071	10	4	6	1498	1500
16	2	3	1290	1294	-21	1	4	1154	614	-12	2	2	343	290	-12	2	2	2209	2021	12	4	6	357	321
-17	3	3	898	965	-19	1	4	2691	1223	-11	3	3	674	918	-11	4	4	347	384	14	4	6	942	966
-15	3	3	751	753	-15	1	4	1315	1350	-9	3	3	992	1054	-9	3	3	415	346	16	4	6	1058	1093
-11	3	3	1222	1205	-11	1	4	1460	1358	-8	4	4	1619	1054	-8	3	3	555	528	-21	1	6	1106	1144
-9	3	3	1114	1205	-7	1	4	3343	3567	-6	4	4	258	260	-6	2	2	949	907	-19	1	6	1289	1357
-7	3	3	1160	1257	-5	1	4	1253	1148	-4	4	4	777	782	-4	2	2	460	409	-15	1	6	1155	1175
-3	3	3	1233	1277	-3	1	4	786	642	-2	4	4	2127	2215	-2	2	2	2924	2834	-13	1	6	1046	1050
-3	3	3	787	718	-1	1	4	1162	1005	-20	4	4	597	557	-20	2	2	302	340	-11	1	6	1033	937

H	K	L	10FO	10FC	H	K	L	10FO	10FC	H	K	L	10FO	10FC	H	K	L	10FO	10FC	H	K	L	10FO	10FC
-5	1	0	440	415	-18	0	7	2223	2354	-8	2	7	457	406	-9	1	8	2337	2259	4	0	9	424	484
-3	1	0	2413	2420	-18	0	7	157	139	-6	2	7	278	302	-7	1	8	1630	1584	0	0	9	1864	1799
-1	1	0	1597	1549	-12	0	7	589	511	-4	2	7	718	729	-5	1	8	1623	1635	-15	1	9	882	927
1	1	0	2355	2300	-10	0	7	2333	2409	-2	2	7	191	200	-3	1	8	832	799	-13	1	9	107	104
3	1	0	465	510	-8	0	7	521	400	0	2	7	336	320	-1	1	8	1521	1485	-11	1	9	1077	1104
5	1	0	2901	3143	-6	0	7	290	323	2	2	7	655	722	1	1	8	406	476	-9	1	9	875	843
7	1	0	533	461	-4	0	7	1045	1064	4	2	7	2029	2061	3	1	8	1749	1780	-7	1	9	1018	1007
9	1	0	1370	1302	-2	0	7	327	375	6	2	7	559	583	5	1	8	553	574	-5	1	9	1773	1901
11	1	0	282	293	0	0	7	518	486	8	2	7	350	353	7	1	8	1551	1558	-3	1	9	650	677
13	1	0	485	464	2	0	7	882	904	-10	2	7	242	283	9	1	8	1162	1242	-1	1	9	1977	1860
15	1	0	620	595	4	0	7	2730	2711	-11	3	7	131	119	-16	2	8	922	873	1	1	9	1202	1185
-18	2	0	271	290	6	0	7	789	733	-9	3	7	1274	1212	-14	2	8	489	519	3	1	9	1350	1429
-16	2	0	425	402	8	0	7	389	391	-7	3	7	207	237	-12	2	8	328	377	5	1	9	513	457
-14	2	0	673	643	10	0	7	310	286	-5	3	7	203	222	-10	2	8	108	99	-12	2	9	543	617
-12	2	0	2972	3007	12	0	7	1666	1653	-1	3	7	1296	1279	-8	2	8	1326	1351	-10	2	9	228	298
-10	2	0	607	607	-19	1	7	1553	1534	1	3	7	440	433	-4	2	8	1082	1061	-8	2	9	1393	1381
-8	2	0	1887	1830	-17	1	7	631	795	5	3	7	248	285	-2	2	8	883	888	-6	2	9	1589	1648
-4	2	0	3512	3507	-15	1	7	270	217	-18	0	8	514	481	0	2	8	1647	1721	-4	2	9	602	586
-2	2	0	1423	1344	-13	1	7	1021	985	-1.6	0	8	1179	1121	2	2	8	612	655	-2	2	9	1403	1435
0	2	0	1020	1034	-11	1	7	87	92	-14	0	8	497	517	4	2	8	83	103	2	2	9	343	310
2	2	0	935	883	-9	1	7	2153	2149	-12	0	8	365	396	6	2	8	717	723	-14	0	10	154	131
4	2	0	1035	993	-7	1	7	227	230	-10	0	8	142	116	-7	3	8	982	997	-12	0	10	1943	1981
6	2	0	1990	2001	-5	1	7	321	312	-8	0	8	1648	1700	-5	3	8	1095	1120	-10	0	10	433	370
10	2	0	1060	1097	-3	1	7	292	335	-4	0	8	1327	1272	-3	3	8	573	564	-8	0	10	476	487
12	2	0	201	303	-1	1	7	2174	2181	-2	0	8	1085	1133	-1	3	8	685	666	-6	0	10	1265	1218
-15	3	0	767	700	1	1	7	552	531	0	0	8	2213	2292	-16	0	9	1235	1238	-4	0	10	317	330
-13	3	0	463	408	3	1	7	185	167	2	0	8	753	746	-14	0	9	2372	2483	0	0	10	582	606
-11	3	0	679	692	5	1	7	810	840	4	0	8	202	157	-12	0	9	720	770	2	0	10	2040	2013
-9	3	0	1096	1050	7	1	7	220	177	6	0	8	874	879	-10	0	9	355	357	-11	1	10	1589	1595
-3	3	0	1329	1338	9	1	7	542	491	8	0	8	1144	1155	-8	0	9	1779	1690	-9	1	10	316	305
-1	3	0	941	992	11	1	7	1164	1216	10	0	8	209	178	-6	0	9	2154	2212	-7	1	10	558	565
1	3	0	1494	1441	13	1	7	1430	1461	-19	1	8	215	277	-4	0	9	601	661	-5	1	10	368	385
3	3	0	257	258	-18	2	7	1840	1778	-17	1	8	1056	1701	-2	0	9	1703	1779	-3	1	10	1208	1194
5	3	0	1006	1053	-14	2	7	173	163	-15	1	8	1007	1899	0	0	9	192	204	-1	1	10	409	352
7	3	0	365	377	-12	2	7	347	342	-13	1	8	156	165	2	0	9	581	560	1	1	10	250	234
-20	0	7	449	472	-10	2	7	1763	1764	-11	1	8	1607	1630										

RUN COMPLETED

H	K	L	10FO	10FC	H	K	L	10FO	10FC	H	K	L	10FO	10FC	H	K	L	10FO	10FC	H	K	L	10FO	10FC
2	0	0	1336	1246	5	9	0	189	192	2	5	1	103	111	8	0	2	602	579	3	5	2	107	103
4	0	0	4203	4647	0	10	0	1065	1049	3	5	1	510	545	9	0	2	302	312	4	5	2	363	370
6	0	0	2213	2283	2	10	0	685	687	4	5	1	1305	1280	10	0	2	590	587	5	5	2	146	144
8	0	0	1351	1319	4	10	0	774	790	5	5	1	336	307	11	0	2	217	255	9	5	2	138	71
10	0	0	1652	1684	0	1	1	1858	1911	6	5	1	790	789	0	1	2	328	358	0	6	2	1431	1448
1	1	0	335	419	1	1	1	257	318	7	5	1	459	438	1	1	2	677	749	1	6	2	316	333
3	1	0	1329	1355	2	1	1	1607	1565	8	5	1	217	215	2	1	2	738	677	2	6	2	1779	1755
5	1	0	910	855	3	1	1	429	483	9	5	1	145	136	3	1	2	1161	1089	3	6	2	374	380
7	1	0	684	661	4	1	1	1348	1290	10	5	1	766	751	4	1	2	322	311	4	6	2	1339	1320
11	1	0	189	200	6	1	1	1284	1248	0	6	1	530	528	5	1	2	1380	1357	5	6	2	225	248
0	2	0	700	620	7	1	1	392	408	1	6	1	133	144	6	1	2	275	287	6	6	2	1161	1152
2	2	0	3574	3801	8	1	1	641	638	2	6	1	777	778	7	1	2	798	735	7	6	2	212	220
4	2	0	1419	1425	10	1	1	749	759	3	6	1	712	688	8	1	2	626	613	8	6	2	929	915
6	2	0	1322	1236	11	1	1	253	256	4	6	1	325	319	9	1	2	487	476	9	6	2	233	209
8	2	0	1592	1578	0	2	1	491	414	5	6	1	536	506	10	1	2	348	346	0	7	2	349	355
10	2	0	274	304	1	2	1	873	849	6	6	1	700	681	0	2	2	109	81	1	7	2	229	230
1	3	0	978	1048	2	2	1	2867	2909	7	6	1	495	481	1	2	2	233	299	3	7	2	201	176
3	3	0	703	667	3	2	1	270	301	1	7	1	292	294	2	2	2	2155	2050	4	7	2	260	274
5	3	0	1501	1484	4	2	1	627	616	2	7	1	1556	1538	3	2	2	824	838	5	7	2	200	212
7	3	0	570	577	5	2	1	1067	1022	4	7	1	409	407	4	2	2	720	718	8	7	2	127	119
9	3	0	564	529	6	2	1	1447	1389	5	7	1	476	488	5	2	2	694	693	0	8	2	101	56
11	3	0	94	73	7	2	1	343	342	6	7	1	562	565	6	2	2	551	508	1	8	2	109	86
0	4	0	88	89	8	2	1	652	644	7	7	1	188	197	7	2	2	529	505	2	8	2	720	708
2	4	0	242	261	9	2	1	434	396	8	7	1	715	711	8	2	2	980	989	4	8	2	136	150
4	4	0	254	243	10	2	1	511	524	9	7	1	267	267	9	2	2	186	175	6	8	2	433	427
6	4	0	628	604	11	2	1	133	104	0	8	1	589	583	0	3	2	1676	1624	8	8	2	245	251
8	4	0	423	405	0	3	1	578	567	1	8	1	319	314	2	3	2	678	691	0	9	2	331	313
10	4	0	440	457	1	3	1	83	101	2	8	1	699	701	3	3	2	751	784	1	9	2	257	256
1	5	0	174	145	2	3	1	1846	1811	3	8	1	295	255	4	3	2	773	737	2	9	2	330	310
3	5	0	836	819	3	3	1	168	147	4	8	1	603	599	5	3	2	312	285	4	9	2	183	180
5	5	0	323	351	4	3	1	986	977	5	8	1	565	546	6	3	2	174	191	5	9	2	259	257
7	5	0	605	607	5	3	1	114	124	6	8	1	369	361	7	3	2	487	462	0	10	2	247	271
9	5	0	151	158	6	3	1	670	639	8	8	1	504	482	9	3	2	144	118	2	10	2	208	220
0	6	0	113	76	8	3	1	1077	1059	0	9	1	1021	973	10	3	2	293	308	3	10	2	255	221
4	6	0	168	188	9	3	1	182	192	2	9	1	325	345	0	4	2	3437	3541	4	10	2	139	166
6	6	0	117	106	10	3	1	167	151	4	9	1	629	633	1	4	2	749	714	0	1	3	2047	2144
8	6	0	263	236	0	4	1	1411	1387	6	9	1	550	547	2	4	2	1309	1282	1	1	3	287	297
10	6	0	137	91	1	4	1	76	84	0	10	1	212	226	3	4	2	354	365	2	1	3	191	251
1	7	0	120	107	2	4	1	316	318	1	10	1	155	82	4	4	2	2482	2414	3	1	3	715	724
3	7	0	154	174	3	4	1	998	999	2	10	1	208	217	5	4	2	627	595	4	1	3	1530	1466
5	7	0	163	163	4	4	1	918	891	3	10	1	225	233	6	4	2	1441	1435	5	1	3	131	111
7	7	0	130	151	5	4	1	680	656	4	10	1	146	128	7	4	2	320	324	6	1	3	534	541
9	8	0	950	928	6	4	1	499	497	0	0	2	885	831	8	4	2	1026	1023	7	1	3	449	444
2	8	0	730	723	7	4	1	700	652	2	0	2	415	458	9	4	2	147	153	8	1	3	679	666
4	8	0	859	849	8	4	1	326	309	3	0	2	1622	1600	10	4	2	967	980	10	1	3	460	448
6	8	0	490	492	9	4	1	142	195	5	0	2	936	923	11	4	2	337	340	11	0	3	143	118
8	8	0	628	630	10	4	1	369	364	6	0	2	642	634	0	5	2	712	691	0	2	3	1870	1865
3	9	0	387	402	0	5	1	2279	2249	7	0	2	1135	1089	2	5	2	550	535	1	2	3	892	831

H	K	L	10FO	10FC	H	K	L	10FO	10FC	H	K	L	10FO	10FC	H	K	L	10FO	10FC	H	K	L	10FO	10FC
2	2	3	1147	1123	9	6	3	396	398	2	2	4	1991	1943	8	6	4	234	237	4	3	5	1295	1261
3	2	3	733	673	0	7	3	698	692	3	2	4	1676	1644	0	7	4	315	310	5	3	5	684	656
4	2	3	1113	1089	1	7	3	210	212	4	2	4	1430	1377	1	7	4	277	272	6	3	5	463	478
5	2	3	705	686	2	7	3	713	712	5	2	4	509	511	2	7	4	135	149	7	3	5	608	601
6	2	3	1089	1050	3	7	3	773	774	6	2	4	1168	1126	3	7	4	243	265	8	3	5	610	614
7	2	3	299	340	4	7	3	736	755	7	2	4	1014	994	4	7	4	239	239	9	3	5	184	202
8	2	3	305	315	5	7	3	111	150	8	2	4	940	948	5	7	4	129	198	10	3	5	363	381
9	2	3	547	518	6	7	3	310	317	9	2	4	117	140	6	7	4	130	124	10	4	5	1220	1202
10	2	3	653	643	7	7	3	525	514	10	2	4	536	533	7	7	4	168	175	1	4	5	478	459
0	3	3	323	313	8	7	3	635	674	0	3	4	367	408	0	8	4	599	596	2	4	5	486	483
1	3	3	92	91	0	8	3	1058	1035	1	3	4	828	836	1	8	4	189	214	3	4	5	282	262
2	3	3	2532	2466	1	8	3	185	195	2	3	4	625	594	2	8	4	663	664	4	4	5	538	527
3	3	3	915	936	3	8	3	467	482	3	3	4	577	574	3	8	4	479	493	5	4	5	408	400
4	3	3	644	644	4	8	3	599	609	4	3	4	248	224	4	8	4	521	533	6	4	5	334	333
5	3	3	538	537	5	8	3	132	81	5	3	4	712	682	6	8	4	490	494	7	4	5	179	203
6	3	3	1241	1215	6	8	3	390	391	6	3	4	197	262	7	8	4	449	453	8	4	5	140	191
7	3	3	679	693	7	8	3	356	356	7	3	4	343	339	3	9	4	162	187	10	4	5	426	454
8	3	3	757	765	0	9	3	652	653	8	3	4	609	621	4	9	4	115	94	0	5	5	770	776
9	3	3	151	148	1	9	3	132	138	9	3	4	333	324	0	10	4	647	661	2	5	5	600	610
10	3	3	458	477	3	9	3	248	238	10	3	4	331	301	1	10	4	366	408	3	5	5	907	903
11	3	3	130	152	4	9	3	431	446	0	4	4	726	690	2	10	4	590	590	4	5	5	718	724
0	4	3	93	103	5	9	3	312	304	1	4	4	112	125	0	1	5	1020	955	5	5	5	378	383
1	4	3	460	463	6	9	3	299	290	2	4	4	384	352	1	1	5	1173	1188	6	5	5	386	385
2	4	3	1446	1442	0	10	3	159	140	3	4	4	1124	1126	2	1	5	2166	2079	7	5	5	612	620
4	4	3	376	392	0	0	4	2920	3058	4	4	4	513	500	3	1	5	607	590	8	5	5	499	508
5	4	3	611	615	1	0	4	2180	2148	5	4	4	529	548	4	1	5	951	908	0	6	5	1265	1265
6	4	3	338	326	2	0	4	2433	2429	6	4	4	393	377	5	1	5	1184	1161	1	6	5	558	539
7	4	3	113	84	3	0	4	704	545	7	4	4	826	852	6	1	5	1287	1230	2	6	5	599	592
8	4	3	695	685	4	0	4	2291	2226	8	4	4	258	247	7	1	5	335	340	3	6	5	169	173
9	4	3	239	240	5	0	4	2056	1953	10	4	4	253	288	8	1	5	708	686	4	6	5	592	596
10	4	3	135	99	6	0	4	1785	1728	0	5	4	314	303	9	1	5	637	612	5	6	5	619	635
0	5	3	1591	1557	7	0	4	429	390	1	5	4	129	151	10	1	5	571	602	6	6	5	186	186
1	5	3	859	892	8	0	4	1182	1127	2	5	4	95	57	11	1	5	262	271	7	6	5	137	117
2	5	3	1191	1150	9	0	4	585	581	3	5	4	212	214	0	2	5	210	216	9	6	5	370	395
4	5	3	1090	1080	10	0	4	993	989	4	5	4	411	418	1	2	5	1076	1028	0	7	5	570	573
5	5	3	1116	1105	11	0	4	660	650	5	5	4	71	65	2	2	5	714	697	2	7	5	873	883
6	5	3	1111	1095	0	1	4	2815	2777	6	5	4	267	240	3	2	5	739	704	3	7	5	480	489
8	5	3	454	457	1	1	4	417	425	7	5	4	149	141	4	2	5	481	479	4	7	5	448	458
9	5	3	406	411	2	1	4	1856	1837	8	5	4	380	384	5	2	5	955	892	5	7	5	431	441
10	5	3	697	726	3	1	4	668	645	9	5	4	124	63	6	2	5	139	140	6	7	5	715	698
0	6	3	594	588	4	1	4	1239	1163	0	6	4	295	295	7	2	5	320	327	7	7	5	331	356
1	6	3	536	560	5	1	4	123	152	1	6	4	341	330	8	2	5	587	574	8	7	5	246	296
2	6	3	1140	1132	6	1	4	128	165	2	6	4	304	299	9	2	5	591	577	0	8	5	209	210
3	6	3	161	172	7	1	4	430	400	3	6	4	118	126	11	2	5	152	133	1	8	5	353	371
5	6	3	802	811	8	1	4	315	292	4	6	4	293	284	0	3	5	1756	1746	2	8	5	775	724
6	6	3	224	220	10	1	4	531	525	5	6	4	330	331	1	3	5	202	231	3	8	5	447	459
7	6	3	251	268	0	2	4	1612	1584	6	6	4	198	218	2	3	5	324	340	5	8	5	188	234
8	6	3	465	457	1	2	4	350	337	7	6	4	144	152	3	3	5	769	767	7	8	5	337	341

H	K	L	10FO	10FC	H	K	L	10FO	10FC	H	K	L	10FO	10FC	H	K	L	10FO	10FC	H	K	L	10FO	10FC
0	9	5	483	488	0	4	6	423	413	9	1	7	282	286	1	7	7	315	302	7	3	8	1008	1039
1	9	5	468	492	1	4	6	1131	1114	10	1	7	380	353	3	7	7	738	752	9	3	8	133	138
2	9	5	657	674	2	4	6	1761	1758	0	2	7	1191	1226	4	7	7	605	621	0	4	8	806	787
4	9	5	459	471	3	4	6	640	616	1	2	7	935	940	6	7	7	359	364	2	4	8	777	766
5	9	5	606	611	4	4	6	609	629	2	2	7	710	661	7	7	7	574	599	3	4	8	104	116
0	10	5	207	221	5	4	6	1029	1012	3	2	7	353	320	0	8	7	304	289	4	4	8	914	909
0	0	6	769	683	6	4	6	929	931	4	2	7	718	724	1	8	7	342	351	5	4	8	145	152
1	0	6	99	154	7	4	6	485	480	5	2	7	1001	996	5	8	7	438	442	6	4	8	272	275
2	0	6	844	776	8	4	6	637	632	6	2	7	144	124	0	9	7	123	96	7	4	8	155	112
3	0	6	1452	1434	9	4	6	378	381	7	2	7	134	157	1	9	7	132	49	8	4	8	781	796
4	0	6	927	895	10	4	6	386	438	8	2	7	124	126	2	9	7	521	521	1	5	8	125	107
5	0	6	868	864	0	5	6	657	637	9	2	7	493	499	3	9	7	238	215	2	5	8	137	175
6	0	6	186	167	2	5	6	456	436	0	3	7	1484	1476	4	9	7	227	221	3	5	8	325	331
7	0	6	1090	1073	4	5	6	323	329	1	3	7	608	582	0	0	8	896	878	5	5	8	335	376
8	0	6	862	831	0	6	6	1124	1092	2	3	7	706	681	1	0	8	1304	1290	7	5	8	298	288
9	0	6	269	260	1	6	6	628	616	3	3	7	789	792	2	0	8	2328	2347	8	5	8	129	91
11	0	6	146	206	2	6	6	871	872	4	3	7	974	947	3	0	8	810	756	0	6	8	535	525
0	1	6	662	672	3	6	6	677	658	5	3	7	354	361	4	0	8	120	166	2	6	8	566	565
1	1	6	348	368	4	6	6	905	887	6	3	7	868	862	5	0	8	1234	1208	4	6	8	362	388
2	1	6	797	766	5	6	6	462	469	7	3	7	487	508	6	0	8	785	764	5	6	8	153	60
3	1	6	1203	1209	6	6	6	677	690	8	3	7	305	312	7	0	8	448	450	6	6	8	493	511
4	1	6	107	116	7	6	6	362	414	9	3	7	362	367	8	0	8	769	764	7	6	8	147	69
5	1	6	267	284	8	6	6	565	555	10	3	7	622	628	9	0	8	621	592	8	6	8	179	247
6	1	6	257	272	0	7	6	253	228	10	4	7	359	331	10	0	8	132	132	0	7	8	114	144
7	1	6	876	856	1	7	6	499	501	1	4	7	219	225	0	1	8	251	203	1	7	8	420	443
8	1	6	587	590	3	7	6	487	502	2	4	7	747	741	1	1	8	873	880	3	7	8	486	511
10	1	6	428	412	4	7	6	188	190	3	4	7	861	851	2	1	8	407	397	4	7	8	128	125
11	1	6	252	250	5	7	6	374	389	5	4	7	235	206	4	1	8	95	83	5	7	8	266	256
0	2	6	1587	1571	7	7	6	345	360	6	4	7	117	150	5	1	8	1108	1080	0	8	8	280	276
2	2	6	509	513	0	8	6	825	852	7	4	7	593	610	8	1	8	222	218	1	8	8	266	267
3	2	6	1021	1002	2	8	6	285	290	8	4	7	260	260	9	1	8	311	307	2	8	8	390	386
4	2	6	995	947	4	8	6	656	679	0	5	7	123	94	10	1	8	144	129	3	8	8	216	270
5	2	6	630	619	6	8	6	309	318	1	5	7	1276	1267	0	2	8	1946	1941	4	8	8	258	225
6	2	6	823	799	0	9	6	321	330	2	5	7	1281	1240	1	2	8	602	591	5	8	8	184	207
7	2	6	692	671	1	9	6	256	229	3	5	7	570	545	3	2	8	870	850	1	9	8	235	222
8	2	6	293	292	2	9	6	267	267	4	5	7	429	417	4	2	8	1139	1116	0	1	9	539	528
10	2	6	597	595	3	9	6	275	264	5	5	7	1342	1347	5	2	8	268	265	1	1	9	1233	1206
0	3	6	1301	1275	4	9	6	228	196	6	5	7	472	470	6	2	8	790	783	2	1	9	624	595
1	3	6	955	969	5	9	6	161	169	7	5	7	256	267	7	2	8	595	594	3	1	9	1020	974
2	3	6	667	670	0	1	7	1058	1059	8	5	7	617	645	8	2	8	164	194	4	1	9	550	534
3	3	6	541	545	1	1	7	530	512	9	5	7	687	704	9	2	8	170	237	5	1	9	1054	1044
4	3	6	572	535	2	1	7	1185	1198	0	6	7	238	235	10	2	8	695	707	6	1	9	283	303
5	3	6	878	843	3	1	7	431	418	3	6	7	568	576	0	3	8	544	561	7	1	9	594	587
6	3	6	154	147	4	1	7	982	989	5	6	7	150	202	1	3	8	581	569	8	1	9	477	451
7	3	6	408	400	5	1	7	409	400	6	6	7	301	295	3	3	8	1423	1406	9	1	9	648	663
8	3	6	192	197	6	1	7	706	695	7	6	7	377	390	4	3	8	280	310	0	2	9	291	319
9	3	6	320	310	7	1	7	191	181	8	6	7	216	233	5	3	8	106	75	2	2	9	554	531
10	3	6	301	325	8	1	7	706	715	0	7	7	1034	1008	6	3	8	119	167	3	2	9	660	668

H	K	L	10FO	10FC	H	K	L	10FO	10FC	H	K	L	10FO	10FC	H	K	L	10FO	10FC	H	K	L	10FO	10FC
4	2	9	231	227	7	0	10	514	548	0	7	10	355	364	3	7	11	154	159	3	1	13	693	685
5	2	9	234	232	8	0	10	836	869	1	7	10	440	415	0	0	12	189	185	5	1	13	327	320
6	2	9	292	289	0	1	10	246	240	3	7	10	391	393	1	0	12	225	264	0	2	13	191	197
7	2	9	539	525	1	1	10	200	181	4	7	10	293	291	2	0	12	717	706	1	2	13	125	160
9	2	9	156	141	2	1	10	313	307	5	7	10	321	334	3	0	12	714	724	5	2	13	220	224
0	3	9	1316	1303	3	1	10	1097	1104	0	8	10	638	669	4	0	12	344	386	0	3	13	440	466
1	3	9	133	143	4	1	10	360	365	1	8	10	217	231	6	0	12	319	292	1	3	13	430	438
2	3	9	489	488	5	1	10	402	403	2	8	10	199	280	7	0	12	470	466	2	3	13	690	697
3	3	9	221	225	7	1	10	837	838	3	8	10	208	234	0	1	12	1219	1217	4	3	13	391	401
4	3	9	836	815	8	1	10	360	349	0	1	11	748	746	1	1	12	350	325	5	3	13	584	584
6	3	9	748	746	9	1	10	137	81	2	1	11	1487	1454	2	1	12	374	370	6	3	13	524	545
7	3	9	273	252	0	2	10	1352	1321	3	1	11	142	111	4	1	12	692	687	0	4	13	326	345
8	3	9	159	218	1	2	10	463	474	4	1	11	748	736	5	1	12	459	464	2	4	13	387	385
1	4	9	315	313	4	2	10	746	734	5	1	11	177	148	6	1	12	209	208	0	5	13	621	621
3	4	9	361	357	5	2	10	533	507	6	1	11	931	917	0	2	12	819	814	2	5	13	868	862
4	4	9	148	76	6	2	10	597	601	8	1	11	598	600	1	2	12	590	596	3	5	13	406	403
5	4	9	622	611	9	2	10	229	251	0	2	11	217	214	2	2	12	218	226	4	5	13	598	591
7	4	9	277	288	0	3	10	861	862	1	2	11	165	148	4	2	12	549	550	0	6	13	435	454
0	5	9	123	79	1	3	10	848	819	5	2	11	153	188	5	2	12	774	757	2	6	13	388	403
1	5	9	330	323	2	3	10	109	113	0	3	11	1014	1020	6	2	12	405	417	1	0	14	223	254
2	5	9	1466	1475	3	3	10	241	224	1	3	11	699	690	7	2	12	149	110	2	0	14	290	323
3	5	9	226	205	4	3	10	574	586	2	3	11	154	146	0	3	12	265	256	3	0	14	810	830
4	5	9	435	440	5	3	10	915	893	3	3	11	280	290	1	3	12	269	256	5	0	14	158	161
5	5	9	302	329	6	3	10	252	256	4	3	11	672	672	2	3	12	666	652	1	1	14	128	94
6	5	9	574	602	7	3	10	151	143	5	3	11	739	757	3	3	12	478	465	2	1	14	623	630
7	5	9	131	105	8	3	10	235	228	6	3	11	180	197	4	3	12	435	435	4	1	14	156	192
8	5	9	687	707	0	4	10	141	139	7	3	11	136	172	5	3	12	117	107	5	1	14	158	176
1	6	9	344	350	1	4	10	495	492	8	3	11	164	202	6	3	12	186	202	0	2	14	201	216
2	6	9	292	309	2	4	10	992	956	0	4	11	354	353	7	3	12	326	344	1	2	14	465	470
3	6	9	154	208	3	4	10	481	475	2	4	11	219	194	0	4	12	226	231	2	2	14	318	330
5	6	9	541	555	4	4	10	154	146	3	4	11	408	417	1	4	12	270	288	4	2	14	195	257
6	6	9	151	164	5	4	10	429	432	4	4	11	137	143	2	4	12	610	628	5	2	14	642	653
7	6	9	160	166	6	4	10	358	375	5	4	11	134	186	3	4	12	680	680	0	3	14	889	891
0	7	9	1072	1107	7	4	10	264	273	7	4	11	341	325	4	4	12	322	317	2	3	14	134	120
4	7	9	664	693	8	4	10	399	411	0	5	11	266	250	6	4	12	330	333	4	3	14	564	568
5	7	9	247	223	0	5	10	235	244	1	5	11	649	655	3	5	12	106	80	0	4	14	585	592
6	7	9	426	409	2	5	10	258	254	2	5	11	216	211	0	6	12	351	345	2	4	14	139	210
1	8	9	96	111	3	5	10	117	89	3	5	11	940	936	1	6	12	267	284	3	4	14	389	372
2	8	9	166	109	5	5	10	152	137	5	5	11	348	352	2	6	12	318	310	0	5	14	183	238
3	8	9	490	476	6	5	10	133	106	0	6	11	293	240	3	6	12	192	196	0	1	15	670	684
0	0	10	148	150	0	6	10	642	649	1	6	11	166	242	4	6	12	264	281	1	1	15	380	406
1	0	10	98	150	1	6	10	438	438	2	6	11	404	396	0	7	12	335	384	2	1	15	599	598
2	0	10	1211	1173	2	6	10	354	352	3	6	11	226	257	1	7	12	173	174	3	1	15	403	407
3	0	10	628	616	3	6	10	403	398	5	6	11	455	473	0	1	13	118	129	2	2	15	471	485
4	0	10	587	591	4	6	10	495	494	0	7	11	360	388	1	1	13	549	537	1	3	15	311	339
5	0	10	204	233	5	6	10	362	353	1	7	11	366	395	2	1	13	145	148	2	3	15	235	213
6	0	10	297	284	6	6	10	365	359	2	7	11	164	142										

H	K	L	10FO	10FC	H	K	L	10FO	10FC	H	K	L	10FO	10FC	H	K	L	10FO	10FC	H	K	L	10FO	10FC
2	0	0	1161	1171	4	4	0	986	936	4	8	0	1031	980	5	13	0	332	331	0	4	5	839	915
4	0	0	309	260	5	4	0	556	-537	6	8	0	505	459	2	14	0	194	204	0	6	5	565	651
6	0	0	628	621	6	4	0	661	611	8	8	0	323	276	3	14	0	359	334	0	8	5	627	677
8	0	0	772	778	7	4	0	304	-250	1	9	0	700	706	4	14	0	406	457	0	10	5	129	115
10	0	0	762	640	8	4	0	545	504	2	9	0	350	-328	1	15	0	350	355	0	12	5	175	189
1	1	0	1558	1699	10	4	0	441	397	3	9	0	657	678	2	15	0	157	-160	0	0	6	1410	-1435
2	1	0	404	312	1	5	0	807	867	5	9	0	267	216	0	4	1	1332	1393	0	2	6	1136	-1109
3	1	0	1062	1013	2	5	0	188	-122	6	9	0	184	203	0	6	1	429	407	0	4	6	1217	-1242
4	1	0	727	-671	3	5	0	1661	1621	7	9	0	673	659	0	8	1	849	834	0	6	6	292	-356
5	1	0	1731	1737	4	5	0	572	-512	8	9	0	111	-124	0	10	1	369	362	0	8	6	566	-638
7	1	0	439	329	5	5	0	844	872	0	10	0	516	534	0	12	1	276	281	0	10	6	203	-188
8	1	0	323	257	6	5	0	638	689	1	10	0	258	241	0	14	1	240	222	0	12	6	175	-196
9	1	0	785	650	7	5	0	441	450	2	10	0	811	814	0	0	2	1235	-1089	0	2	7	477	413
10	1	0	115	108	8	5	0	188	-139	3	10	0	470	445	0	2	2	1247	-1127	0	4	7	493	-521
0	2	0	1151	1048	9	5	0	413	401	5	10	0	266	-223	0	4	2	1584	-1922	0	6	7	292	247
1	2	0	264	-196	0	6	0	1418	1384	6	10	0	507	443	0	6	2	633	-762	0	8	7	323	-359
2	2	0	1034	938	2	6	0	1559	1347	7	10	0	350	-313	0	8	2	1587	-1632	0	10	7	369	-422
3	2	0	1034	-1138	3	6	0	848	-807	8	10	0	396	439	0	10	2	590	-603	0	12	7	175	-165
4	2	0	2464	2593	4	6	0	477	423	1	11	0	488	496	0	12	2	359	-436	0	0	8	1112	1057
5	2	0	436	426	5	6	0	312	321	3	11	0	756	784	0	14	2	221	-275	0	4	8	703	761
6	2	0	984	1043	6	6	0	721	690	4	11	0	46	53	0	2	3	791	824	0	6	8	653	699
7	2	0	345	307	7	6	0	224	146	5	11	0	194	136	0	4	3	524	-628	0	8	8	384	391
9	2	0	274	-264	8	6	0	663	687	6	11	0	194	-207	0	6	3	370	452	0	10	8	535	503
10	2	0	345	337	9	6	0	302	-284	7	11	0	212	192	0	8	3	556	-533	0	2	9	213	170
1	3	0	2170	2116	1	7	0	1014	1072	0	12	0	346	311	0	10	3	562	-576	0	4	9	157	141
2	3	0	824	811	2	7	0	857	837	1	12	0	627	-623	0	12	3	396	-378	0	6	9	205	181
3	3	0	553	528	3	7	0	1063	1059	2	12	0	498	494	0	14	3	452	-456	0	8	9	273	289
5	3	0	995	1152	4	7	0	295	-225	3	12	0	295	-274	0	0	4	3325	3363	0	0	10	844	-805
6	3	0	382	365	5	7	0	414	366	4	12	0	249	196	0	2	4	436	425	0	2	10	497	-499
7	3	0	794	776	7	7	0	719	723	5	12	0	129	136	0	4	4	1395	1562	0	4	10	514	-578
8	3	0	442	-470	9	7	0	246	181	6	12	0	240	250	0	6	4	1033	1203	0	6	10	146	-179
9	3	0	603	535	0	8	0	404	-355	1	13	0	313	328	0	10	4	525	652	0	8	10	152	-212
0	4	0	2402	2284	2	8	0	1233	1220	3	13	0	276	245	0	12	4	313	361	0	2	11	81	58
1	4	0	1909	1820	3	8	0	394	-377	4	13	0	157	162	0	2	5	598	596	0	4	11	472	-401
2	4	0	1689	1445																				

H	K	L	10FO	10FC	H	K	L	10FO	10FC	H	K	L	10FO	10FC	H	K	L	10FO	10FC	H	K	L	10FO	10FC
3	1	0	1157	1117	1	5	1	1946	2111	2	5	2	1304	-1239	-3	7	3	1116	-1116	-1	6	4	1135	-995
1	3	0	739	-568	2	5	1	1369	-1466	3	5	2	1626	-1563	-1	7	3	1828	-1666	0	6	4	624	-622
2	3	0	2021	-2149	3	5	1	657	673	1	6	2	2097	-2547	0	7	3	1259	1137	1	6	4	718	1026
3	3	0	1149	-1029	-1	6	1	588	-521	-4	7	2	1625	-1424	1	7	3	1536	-2066	-4	7	4	1493	1574
4	3	0	770	-942	0	6	1	543	-514	0	7	2	2150	2287	2	7	3	703	855	-2	7	4	2312	2314
2	4	0	1940	-1970	4	6	1	1046	799	4	7	2	1050	-819	-1	8	3	1006	-1089	-1	7	4	702	-589
4	4	0	807	862	-2	7	1	1400	-1420	-2	8	2	1348	1308	1	8	3	685	-884	1	7	4	1088	-1149
1	5	0	2169	2370	-1	7	1	1391	-1266	-3	9	2	2238	-2141	-1	9	3	1130	-957	2	7	4	1145	-1235
3	5	0	658	-459	0	7	1	1085	-1019	-1	9	2	1518	-1396	-2	9	3	1403	-1747	3	7	4	833	-959
5	5	0	1179	-934	1	7	1	1387	-1576	1	9	2	1222	1510	-2	10	3	1657	1709	-2	8	4	1303	-1226
1	6	0	1455	-1651	2	7	1	915	943	3	9	2	1555	1694	-1	10	3	658	-493	0	8	4	1703	-1832
3	6	0	1649	-1596	3	7	1	1637	-1895	-1	10	2	1055	836	0	10	3	1015	1085	-5	9	4	1704	-1737
1	7	0	921	867	4	7	1	982	1093	-4	11	2	1327	1349	-3	11	3	1118	947	-1	9	4	1444	1280
2	7	0	2120	2589	-1	8	1	1327	1215	0	11	2	1831	-1792	-1	11	3	1579	1321	0	9	4	783	697
3	7	0	907	931	0	8	1	727	-438	-3	13	2	1586	1523	-1	11	3	1109	1431	1	9	4	717	784
4	7	0	1245	1450	-4	9	1	1150	1153	-1	13	2	942	944	-1	12	3	1059	1022	-4	11	4	1449	-1341
0	8	0	2460	2875	-3	9	1	1197	1116	-1	16	2	926	-912	-2	14	3	1539	-1594	-2	11	4	1924	-1844
2	8	0	1170	976	-2	9	1	1378	1384	-3	0	3	1043	-1192	0	14	3	928	-1007	2	11	4	1013	1334
1	9	0	1415	-1761	0	9	1	1247	1229	-1	0	3	1148	-1023	-4	0	4	843	869	-1	13	4	1310	-1095
5	9	0	1447	1268	1	9	1	987	-1250	3	0	3	2135	2163	-2	0	4	2938	-3073	-1	0	5	2009	1857
0	10	0	935	715	0	10	1	1635	1589	-4	1	3	674	-768	2	0	4	1991	-2015	5	0	5	1834	-1548
2	11	0	2100	-2123	2	10	1	1006	1243	-1	1	3	658	-606	-5	1	4	1054	-1215	-2	1	5	711	680
4	11	0	1371	-1168	-1	11	1	1061	908	0	1	3	922	772	-3	1	4	1309	-1289	-1	1	5	1688	1564
1	13	0	991	1194	1	11	1	1024	1287	1	1	3	1438	1482	-2	1	4	635	-677	0	1	5	1602	-1464
0	14	0	972	-1061	3	11	1	1332	1529	3	1	3	1490	1463	-1	1	4	549	-475	1	1	5	1027	1139
2	1	1	1193	1370	-1	12	1	1920	-1982	4	1	3	1021	-887	1	1	4	910	-891	3	1	5	725	-647
-4	2	1	957	1210	-2	13	1	1120	-911	0	2	3	1301	-1041	3	1	4	937	-794	-4	2	5	991	-1277
2	2	1	1573	-1386	0	13	1	966	-845	-4	2	3	1576	1477	-3	2	4	2621	2886	-2	2	5	1957	-1995
4	2	1	1533	-1373	0	14	1	1307	-1398	-4	3	3	1337	1410	-1	2	4	1958	1872	0	2	5	1295	-1013
-3	3	1	916	966	-1	16	1	1538	1602	-2	3	3	945	724	0	2	4	481	358	2	2	5	1759	1871
-2	3	1	1229	1124	4	0	2	1189	-1145	-1	3	3	602	543	1	2	4	1271	-1413	4	2	5	1626	1538
-1	3	1	1029	933	-4	1	2	721	983	0	3	3	1516	-1116	3	2	4	1097	-986	-2	3	5	1410	-1350
0	3	1	892	722	-3	1	2	946	-1042	1	3	3	1431	1814	-3	3	4	939	898	-1	3	5	1314	1261
1	3	1	567	428	-1	1	2	968	-994	3	3	3	856	910	-2	3	4	1569	-1665	0	3	5	638	451
2	3	1	1553	-1416	2	1	2	649	576	-5	4	3	979	1128	-1	3	4	951	782	3	3	5	1418	-1520
3	3	1	1211	1224	-5	2	2	1121	-1241	-3	4	3	855	936	1	3	4	1181	1270	-2	4	5	748	-661
4	3	1	1237	-1151	-4	3	2	1363	1359	-2	4	3	705	587	2	3	4	801	742	0	4	5	1295	-1160
5	3	1	719	770	0	3	2	1357	-1335	-1	4	3	1531	1446	3	3	4	868	848	1	4	5	1275	-1428
-3	4	1	686	519	4	3	2	951	740	3	4	3	1380	-1221	-4	4	4	1000	-1011	5	4	5	1456	1408
-1	4	1	706	-650	-4	4	2	1170	-1076	-3	5	3	1145	1130	-2	4	4	1948	1876	-5	5	5	1198	1272
0	4	1	805	547	-2	4	2	2565	-2598	-1	5	3	1895	1751	1	4	4	501	686	-3	5	5	1015	951
3	4	1	638	-691	2	4	2	2075	2306	0	5	3	801	627	-2	4	4	886	727	-2	5	5	1130	969
5	4	1	1671	-1545	4	4	2	844	587	2	5	3	1624	1840	-5	5	4	1509	1536	0	5	5	2556	2878
-4	5	1	1325	-1449	-3	5	2	2211	2177	3	5	3	1289	-1178	-3	5	4	851	781	1	5	5	1259	-1523
-3	5	1	1619	-1412	-2	5	2	1106	-979	4	5	3	1406	1552	-1	5	4	1733	-1340	-3	6	5	849	696
-2	5	1	1666	-1566	-1	5	2	1841	1646	-1	6	3	771	698	0	5	4	910	-724	-2	6	5	1402	1386
-1	5	1	478	431	0	5	2	1249	-927	1	6	3	632	750	1	5	4	974	-948	0	6	5	1503	1287
0	5	1	1863	-1638	1	5	2	1445	-1424	-4	7	3	1288	-1366	-3	6	4	1807	-1747	2	6	5	840	-870

OBSERVED AND CALCULATED STRUCTURE FACTORS FOR Sn3BrF5 MONOCLINIC

PAGE 2

H	K	L	10FO	10FC	H	K	L	10FO	10FC	H	K	L	10FO	10FC	H	K	L	10FO	10FC	H	K	L	10FO	10FC
4	6	5	1107	-1009	0	5	6	1311	1020	2	5	7	1389	-1628	-2	2	9	1997	2026	3	0	11	1162	1155
-2	7	5	1314	1379	1	5	6	660	472	3	5	7	929	845	0	2	9	713	551	-3	1	11	1113	-1351
-1	7	5	616	-630	2	5	6	1248	1271	0	6	7	1190	-998	2	2	9	1402	-1491	-2	1	11	1317	1309
1	7	5	901	1087	-1	6	6	2652	2553	1	6	7	690	-907	-2	3	9	1162	1174	0	1	11	1094	1097
2	7	5	855	-967	0	6	6	1101	808	2	6	7	795	-677	-3	3	9	910	920	0	2	11	1575	-1567
-3	7	5	1664	2011	1	6	6	1127	1299	0	7	7	1167	-1098	-3	4	9	1098	-1079	-1	3	11	956	811
-3	8	5	944	-1018	-4	7	6	1416	1486	-1	8	7	1666	1584	-1	4	9	610	472	0	3	11	896	-1032
-2	8	5	973	874	-1	7	6	627	-605	-2	9	7	1039	-761	0	4	9	1060	1020	-3	4	11	1491	1563
0	8	5	1302	1196	0	7	6	1441	-1399	-2	10	7	1614	-1612	1	4	9	858	982	-1	4	11	1729	1578
1	8	5	819	822	-2	8	6	974	-868	-1	10	7	1050	1061	-1	5	9	1162	1067	-2	5	11	1445	-1403
-3	9	5	919	-950	-3	9	6	2061	2105	-1	11	7	1575	-1490	0	5	9	1927	-2117	-1	6	11	1306	1219
-2	9	5	1072	-965	-1	9	6	894	886	-1	12	7	1238	-1177	2	5	9	1227	-1358	0	6	11	1025	1036
0	9	5	1991	-2165	1	9	6	759	-940	-2	14	7	1389	1429	-3	6	9	1151	-1097	-1	7	11	1522	-1471
2	9	5	1115	-1304	3	9	6	923	-843	-2	0	8	2619	2438	-2	6	9	1563	-1556	-1	8	11	1429	-1269
0	10	5	1647	-1588	-1	10	6	953	-890	2	0	8	1262	1215	-1	6	9	745	-622	-2	9	11	1198	1108
1	11	5	742	-1202	0	10	6	788	-755	1	1	8	680	825	0	6	9	933	-785	-1	10	11	1314	-1173
-3	11	5	1386	-1714	-1	11	6	866	656	-3	2	8	2340	-2323	-1	7	9	927	869	-1	11	11	1374	1441
-3	12	5	1263	1492	0	11	6	1263	1240	-1	2	8	1065	-891	3	7	9	1077	-1282	-1	12	11	964	897
-1	12	5	1423	1514	-3	13	6	1546	-1525	-1	3	8	727	-640	-3	8	9	1285	1250	-1	1	12	1248	-1240
0	13	5	1445	1452	-3	0	7	1669	1781	1	3	8	925	-1070	0	8	9	1164	-1141	-1	3	12	1102	1032
0	14	5	1242	1240	-1	0	7	2275	2098	-2	4	8	1753	-1731	0	9	9	1666	1828	-1	0	13	1518	1361
-1	16	5	1195	-1277	1	0	7	773	-782	0	4	8	1715	-1827	0	10	9	1056	930	-1	1	13	1285	1298
-4	0	6	2197	-2274	-3	1	7	1106	1137	-5	5	8	1443	-1505	-3	12	9	1387	-1447	0	1	13	999	-837
-2	0	6	2849	-3017	-2	1	7	935	-850	-1	5	8	831	700	0	13	9	1290	-1391	-2	2	13	1864	-1841
2	0	6	1404	1267	0	1	7	1304	-1338	0	5	8	816	741	-4	0	10	1668	1595	-1	3	13	1089	1123
-3	1	6	1085	1062	3	1	7	1236	-1271	-3	6	8	1560	1411	-2	0	10	1322	1283	0	4	13	816	-851
-1	1	6	548	539	0	2	7	1867	1865	-4	7	8	1443	-1454	0	1	10	1480	1364	0	5	13	1386	1522
2	1	6	776	-713	4	2	7	1338	-1171	-2	7	8	1564	-1525	-1	2	10	1596	1477	-2	6	13	1476	1487
-5	2	6	1458	1550	-4	3	7	1297	-1288	1	7	8	932	986	0	3	10	850	806	-1	7	13	880	-816
-3	2	6	716	-650	-1	3	7	964	-923	-2	8	8	1317	1232	0	5	10	1358	-1191	0	8	13	882	1032
-4	3	6	1237	-1418	0	3	7	1366	1410	0	8	8	868	876	-1	6	10	955	-942	0	9	13	1195	-1410
0	3	6	691	532	-3	4	7	1209	-1346	-5	9	8	1640	1634	0	6	10	768	-808	0	1	14	1275	-1340
-4	4	6	1558	1530	-1	4	7	2075	-2050	0	9	8	856	-794	-1	7	10	808	694	0	3	14	883	-945
-2	4	6	2047	1980	3	4	7	1418	1440	-2	11	8	1256	1215	-1	8	10	1007	1092	0	5	14	1071	1040
0	4	6	657	-648	-3	5	7	1427	-1381	-1	0	9	1619	-1451	-1	11	10	886	-658	-1	1	16	1384	1353
2	4	6	960	-1062	-2	5	7	1082	925	-1	1	9	1585	-1533	-3	0	11	2028	-1987	-1	3	16	1116	-1133
-3	5	6	2143	-2183	-1	5	7	1037	-975	0	1	9	1212	1045	-1	0	11	2082	-1733	0	1	18	1087	1199
-1	5	6	1319	-1254	1	5	7	778	839															

H	K	L	10FO	10FC	H	K	L	10FO	10FC	H	K	L	10FO	10FC	H	K	L	10FO	10FC	H	K	L	10FO	10FC
-4	-19	0	153	205	12	-13	0	234	293	-16	-9	0	481	223	-12	-6	0	688	723	14	-4	0	910	499
-8	-18	0	373	397	14	-13	0	301	364	-14	-9	0	473	539	-10	-6	0	409	562	16	-4	0	510	508
-4	-18	0	248	297	18	-13	0	561	444	-12	-9	0	306	488	-6	-6	0	2173	2025	20	-4	0	543	348
-2	-18	0	353	176	-20	-12	0	316	357	-10	-9	0	1017	999	-4	-6	0	12332	12297	22	-4	0	425	200
-8	-18	0	255	224	-16	-12	0	257	532	-6	-9	0	733	408	-2	-6	0	1087	272	-22	-4	0	256	259
10	-18	0	401	345	-12	-12	0	257	408	-6	-9	0	733	785	0	-6	0	3587	213	-20	-3	0	304	364
-6	-17	0	214	235	-10	-12	0	390	218	-4	-9	0	482	532	2	-6	0	1302	1270	-18	-3	0	408	563
-4	-17	0	422	403	-6	-12	0	324	365	-2	-9	0	1204	667	0	-6	0	2545	1880	-16	-3	0	593	391
-2	-17	0	256	263	-4	-12	0	288	419	2	-9	0	494	398	10	-6	0	506	650	-14	-3	0	683	721
4	-17	0	528	248	2	-12	0	253	496	4	-9	0	602	747	12	-6	0	843	735	-12	-3	0	526	504
4	-17	0	227	314	-2	-12	0	1325	1152	6	-9	0	1185	386	0	-6	0	299	261	-10	-3	0	341	945
10	-17	0	227	314	-2	-12	0	1325	1152	6	-9	0	1185	386	10	-6	0	299	261	-10	-3	0	341	945
10	-17	0	227	314	-2	-12	0	1325	1152	6	-9	0	1185	386	10	-6	0	299	261	-10	-3	0	341	945
10	-17	0	227	314	-2	-12	0	1325	1152	6	-9	0	1185	386	10	-6	0	299	261	-10	-3	0	341	945
10	-17	0	227	314	-2	-12	0	1325	1152	6	-9	0	1185	386	10	-6	0	299	261	-10	-3	0	341	945
10	-17	0	227	314	-2	-12	0	1325	1152	6	-9	0	1185	386	10	-6	0	299	261	-10	-3	0	341	945
10	-17	0	227	314	-2	-12	0	1325	1152	6	-9	0	1185	386	10	-6	0	299	261	-10	-3	0	341	945
10	-17	0	227	314	-2	-12	0	1325	1152	6	-9	0	1185	386	10	-6	0	299	261	-10	-3	0	341	945
10	-17	0	227	314	-2	-12	0	1325	1152	6	-9	0	1185	386	10	-6	0	299	261	-10	-3	0	341	945
10	-17	0	227	314	-2	-12	0	1325	1152	6	-9	0	1185	386	10	-6	0	299	261	-10	-3	0	341	945
10	-17	0	227	314	-2	-12	0	1325	1152	6	-9	0	1185	386	10	-6	0	299	261	-10	-3	0	341	945
10	-17	0	227	314	-2	-12	0	1325	1152	6	-9	0	1185	386	10	-6	0	299	261	-10	-3	0	341	945
10	-17	0	227	314	-2	-12	0	1325	1152	6	-9	0	1185	386	10	-6	0	299	261	-10	-3	0	341	945
10	-17	0	227	314	-2	-12	0	1325	1152	6	-9	0	1185	386	10	-6	0	299	261	-10	-3	0	341	945
10	-17	0	227	314	-2	-12	0	1325	1152	6	-9	0	1185	386	10	-6	0	299	261	-10	-3	0	341	945
10	-17	0	227	314	-2	-12	0	1325	1152	6	-9	0	1185	386	10	-6	0	299	261	-10	-3	0	341	945
10	-17	0	227	314	-2	-12	0	1325	1152	6	-9	0	1185	386	10	-6	0	299	261	-10	-3	0	341	945
10	-17	0	227	314	-2	-12	0	1325	1152	6	-9	0	1185	386	10	-6	0	299	261	-10	-3	0	341	945
10	-17	0	227	314	-2	-12	0	1325	1152	6	-9	0	1185	386	10	-6	0	299	261	-10	-3	0	341	945
10	-17	0	227	314	-2	-12	0	1325	1152	6	-9	0	1185	386	10	-6	0	299	261	-10	-3	0	341	945
10	-17	0	227	314	-2	-12	0	1325	1152	6	-9	0	1185	386	10	-6	0	299	261	-10	-3	0	341	945
10	-17	0	227	314	-2	-12	0	1325	1152	6	-9	0	1185	386	10	-6	0	299	261	-10	-3	0	341	945
10	-17	0	227	314	-2	-12	0	1325	1152	6	-9	0	1185	386	10	-6	0	299	261	-10	-3	0	341	945
10	-17	0	227	314	-2	-12	0	1325	1152	6	-9	0	1185	386	10	-6	0	299	261	-10	-3	0	341	945
10	-17	0	227	314	-2	-12	0	1325	1152	6	-9	0	1185	386	10	-6	0	299	261	-10	-3	0	341	945
10	-17	0	227	314	-2	-12	0	1325	1152	6	-9	0	1185	386	10	-6	0	299	261	-10	-3	0	341	945
10	-17	0	227	314	-2	-12	0	1325	1152	6	-9	0	1185	386	10	-6	0	299	261	-10	-3	0	341	945
10	-17	0	227	314	-2	-12	0	1325	1152	6	-9	0	1185	386	10	-6	0	299	261	-10	-3	0	341	945
10	-17	0	227	314	-2	-12	0	1325	1152	6	-9	0	1185	386	10	-6	0	299	261	-10	-3	0	341	945
10	-17	0	227	314	-2	-12	0	1325	1152	6	-9	0	1185	386	10	-6	0	299	261	-10	-3	0	341	945
10	-17	0	227	314	-2	-12	0	1325	1152	6	-9	0	1185	386	10	-6	0	299	261	-10	-3	0	341	945
10	-17	0	227	314	-2	-12	0	1325	1152	6	-9	0	1185	386	10	-6	0	299	261	-10	-3	0	341	945
10	-17	0	227	314	-2	-12	0	1325	1152	6	-9	0	1185	386	10	-6	0	299	261	-10	-3	0	341	945
10	-17	0	227	314	-2	-12	0	1325	1152	6	-9	0	1185	386	10	-6	0	299	261	-10	-3	0	341	945
10	-17	0	227	314	-2	-12	0	1325	1152	6	-9	0	1185	386	10	-6	0	299	261	-10	-3	0	341	945
10	-17	0	227	314	-2	-12	0	1325	1152	6	-9	0	1185	386	10	-6	0	299	261	-10	-3	0	341	945
10	-17	0	227	314	-2	-12	0	1325	1152	6	-9	0	1185	386	10	-6	0	299	261	-10	-3	0	341	945
10	-17	0	227	314	-2	-12	0	1325	1152	6	-9	0	1185	386	10	-6	0	299	261	-10	-3	0	341	945
10	-17	0	227	314	-2	-12	0	1325	1152	6	-9	0	1185	386	10	-6	0	299	261	-10	-3	0	341	945
10	-17	0	227	314	-2	-12	0	1325	1152	6	-9	0	1185	386	10	-6	0	299	261	-10	-3	0	341	945
10	-17	0	227	314	-2	-12	0	1325	1152	6	-9	0	1185	386	10	-6	0	299	261	-10	-3	0	341	945
10	-17	0	227	314	-2	-12	0	1325	1152	6	-9	0	1185	386	10	-6	0	299	261	-10	-3	0	341	945
10	-17	0	227	314	-2	-12	0	1325	1152	6	-9	0	1185	386	10	-6	0	299	261	-10	-3	0	341	945
10	-17	0	227	314	-2	-12	0	1325	1152	6	-9	0	1185	386	10	-6	0	299	261	-10	-3	0	341	945
10	-17	0	227	314	-2	-12	0	1325	1152	6	-9	0	1185	386	10	-6	0	299	261	-10	-3	0	341	945
10	-17	0	227	314	-2	-12	0	1325	1152	6	-9	0	1185	386	10	-6	0	299	261	-10	-3	0	341	945
10	-17	0	227	314	-2	-12	0	1325	1152	6	-9	0	1185	386	10	-6	0	299	261	-10	-3	0	341	945
10	-17	0	227	314	-2	-12	0	1325	1152	6	-9	0	1185	386	10	-6	0	299	261	-10	-3	0	341	945
10	-17	0	227	314	-2	-12	0	1325	1152	6	-9	0	1185	386	10	-6	0	299	261	-10	-3	0	341	945
10	-17	0	227	314	-2	-12	0	1325	1152	6	-9	0	1185	386	10	-6	0	299	261	-10	-3	0	341	945
10	-17	0	227	314	-2	-12	0	1325	1152	6	-9	0	1185	386	10	-6	0	299	261	-10	-3	0	341	945
10	-17	0	227	314	-2	-12	0	1325	1152	6	-9	0	1185	386	10	-6	0	299	261	-10	-3	0	341	945
10	-17	0	227	314	-2	-12	0	1325	1152	6	-9	0	1185	386	10	-6	0	299	261	-10	-3	0	341	945
10	-17	0	227	314	-2	-12	0	1325	1152	6	-9	0	1185	386	10	-6	0	299	261	-10	-3	0	341	945
10	-17	0	227	314	-2	-12	0	1325	1152	6	-9	0	1185	386	10	-6	0	299	261	-10	-3	0	341	945
10	-17	0	227	314	-2	-12	0	1325	1152	6	-9	0	1185	386	10	-6	0	299	261	-10	-3	0	341	

H	K	L	10FO	10FC	H	K	L	10FO	10FC	H	K	L	10FO	10FC	H	K	L	10FO	10FC	H	K	L	10FO	10FC
-14	-1	0	861	922	-12	2	0	774	784	0	4	0	116	628	-4	7	0	461	472	6	10	0	607	361
-12	-1	0	702	531	-10	2	0	395	284	2	4	0	618	286	4	7	0	551	631	8	10	0	447	591
-10	-1	0	504	799	-6	2	0	1153	904	4	4	0	1592	1865	6	7	0	1976	1576	12	10	0	775	730
-8	-1	0	387	318	-4	2	0	1132	1544	6	4	0	691	972	8	7	0	395	621	14	10	0	427	298
-6	-1	0	472	345	-2	2	0	479	991	8	4	0	1941	1771	10	7	0	1290	1372	16	10	0	270	390
-4	-1	0	478	925	2	2	0	596	1059	12	4	0	628	688	14	7	0	410	449	20	10	0	282	291
4	-1	0	588	897	4	2	0	1441	1832	14	4	0	841	569	20	7	0	243	225	-14	11	0	536	431
6	-1	0	616	404	6	2	0	1534	657	16	4	0	492	574	-14	8	0	411	385	-12	11	0	295	299
8	-1	0	510	547	8	2	0	126	748	20	4	0	487	374	-12	8	0	715	730	-10	11	0	266	417
10	-1	0	650	712	10	2	0	552	475	22	4	0	393	233	-10	8	0	198	516	-4	11	0	545	411
12	-1	0	933	459	12	2	0	1089	880	-18	5	0	298	326	-8	8	0	991	1280	-2	11	0	936	1078
14	-1	0	1159	943	14	2	0	879	405	-16	5	0	304	287	-6	8	0	237	531	2	11	0	960	1062
16	-1	0	239	393	16	2	0	1109	760	-14	5	0	249	454	-4	8	0	346	792	4	11	0	619	394
18	-1	0	806	713	20	2	0	523	505	-12	5	0	466	620	-2	8	0	296	276	10	11	0	329	496
22	-1	0	393	352	22	2	0	457	321	-10	5	0	1099	1262	2	8	0	310	573	12	11	0	384	327
-20	0	0	561	559	-24	3	0	218	207	-8	5	0	337	645	4	8	0	400	908	14	11	0	716	565
-16	0	0	714	896	-22	3	0	257	302	-6	5	0	1488	2025	6	8	0	255	491	18	11	0	315	379
-12	0	0	492	908	-20	3	0	293	239	-4	5	0	732	830	8	8	0	1232	1318	-20	12	0	451	323
-8	0	0	801	285	-18	3	0	373	537	-2	5	0	264	890	10	8	0	207	581	-16	12	0	307	424
-4	0	0	1569	1410	-16	3	0	578	384	2	5	0	280	568	12	8	0	955	881	-12	12	0	217	331
4	0	0	2057	1396	-14	3	0	614	700	4	5	0	877	805	14	8	0	605	459	-10	12	0	314	211
8	0	0	1112	314	-12	3	0	492	434	6	5	0	1883	2305	-10	9	0	439	214	-6	12	0	250	306
12	0	0	690	905	-10	3	0	279	873	8	5	0	467	720	-14	9	0	286	438	-4	12	0	553	603
16	0	0	998	890	-8	3	0	717	632	10	5	0	1464	1252	-12	9	0	281	357	-2	12	0	222	494
20	0	0	822	569	-6	3	0	1044	1579	12	5	0	611	572	-10	9	0	818	881	0	12	0	1051	1155
24	0	0	336	207	-4	3	0	736	1084	14	5	0	294	506	-8	9	0	525	389	2	12	0	209	425
-22	1	0	242	345	-2	3	0	1546	1725	16	5	0	437	441	-6	9	0	554	751	4	12	0	623	640
-18	1	0	581	708	2	3	0	1825	1978	18	5	0	392	381	-4	9	0	356	415	6	12	0	275	377
-14	1	0	816	952	4	3	0	946	895	20	5	0	238	222	-2	9	0	927	881	10	12	0	388	214
-12	1	0	652	481	6	3	0	1336	1668	22	5	0	218	320	2	9	0	999	1042	12	12	0	275	405
-10	1	0	501	698	8	3	0	954	509	-18	6	0	235	208	4	9	0	404	523	16	12	0	465	528
-8	1	0	350	524	10	3	0	363	946	-12	6	0	568	725	6	9	0	679	775	20	12	0	393	362
-6	1	0	433	429	12	3	0	676	500	-10	6	0	323	647	8	9	0	674	400	-18	13	0	367	439
-4	1	0	415	882	14	3	0	843	722	-8	6	0	1755	1887	10	9	0	1066	1003	-14	13	0	296	366
4	1	0	551	948	16	3	0	788	393	-4	6	0	898	1256	12	9	0	351	492	-6	13	0	253	322
6	1	0	574	318	18	3	0	544	561	-2	6	0	245	226	14	9	0	461	540	-4	13	0	478	422
8	1	0	489	332	20	3	0	366	302	0	6	0	807	215	16	9	0	576	234	-2	13	0	976	860
10	1	0	631	813	22	3	0	404	340	2	6	0	307	303	20	9	0	231	258	2	13	0	1025	853
12	1	0	936	513	24	3	0	243	228	4	6	0	1061	1309	22	9	0	302	307	4	13	0	509	446
14	1	0	1147	915	-22	4	0	307	202	8	6	0	2255	2023	-14	10	0	278	238	0	13	0	263	385
16	1	0	242	332	-20	4	0	373	351	10	6	0	480	589	-12	10	0	572	593	12	13	0	218	245
18	1	0	860	708	-16	4	0	356	501	12	6	0	795	728	-8	10	0	352	565	14	13	0	255	439
22	1	0	377	379	-14	4	0	610	496	16	6	0	295	369	-6	10	0	517	310	18	13	0	540	494
24	1	0	170	196	-12	4	0	442	690	18	6	0	280	219	-4	10	0	492	702	-16	14	0	382	452
-22	2	0	327	276	-8	4	0	1429	1636	-14	7	0	284	373	-2	10	0	614	466	-8	14	0	130	221
-20	2	0	379	468	-6	4	0	539	989	-10	7	0	980	1266	0	10	0	968	1221	-4	14	0	338	564
-16	2	0	795	789	-4	4	0	1290	1756	-8	7	0	318	662	2	10	0	633	519	0	14	0	800	756
-14	2	0	623	493	-2	4	0	543	486	-6	7	0	1615	1515	4	10	0	556	820	4	14	0	379	604

H	K	L	10FO	10FC	H	K	L	10FO	10FC	H	K	L	10FO	10FC	H	K	L	10FO	10FC	H	K	L	10FO	10FC
6	14	0	207	362	2-15	1	526	500	7-12	1	406	323	-10	-9	1	673	567	-10	-7	1	694	506		
14	14	0	282	302	5-15	1	253	313	8-12	1	488	449	-7	-9	1	278	189	-8	-7	1	414	340		
16	14	0	583	484	6-15	1	554	527	9-12	1	142	136	-6	-9	1	795	513	-7	-7	1	411	492		
-6	15	0	418	387	13-15	1	213	217	11-12	1	384	284	-5	-9	1	149	219	-6	-7	1	932	851		
-2	15	0	430	570	-16-14	1	273	333	12-12	1	407	382	-4	-9	1	303	156	-5	-7	1	201	508		
2	15	0	430	574	-12-14	1	179	343	16-12	1	272	317	-3	-9	1	282	495	-4	-7	1	156	264		
6	15	0	516	438	-8-14	1	348	422	-14-11	1	271	397	-2	-9	1	889	875	-3	-7	1	812	497		
8	15	0	314	184	-5-14	1	381	339	-11-11	1	429	433	1	-9	1	623	615	-2	-7	1	922	652		
14	15	0	243	312	-4-14	1	574	363	-10-11	1	552	531	2	-9	1	442	643	-1	-7	1	139	317		
-4	16	0	499	432	-2-14	1	217	265	-7-11	1	252	70	3	-9	1	198	225	0	-7	1	202	344		
0	16	0	318	391	0-14	1	250	392	-6-11	1	306	365	4	-9	1	150	259	1	-7	1	636	464		
4	16	0	523	482	3-14	1	400	251	-4-11	1	325	379	5	-9	1	586	240	2	-7	1	1244	622		
6	16	0	224	299	4-14	1	675	605	-3-11	1	411	377	6	-9	1	433	359	4	-7	1	332	553		
8	16	0	188	339	7-14	1	284	352	-2-11	1	938	765	8	-9	1	164	320	5	-7	1	703	682		
-6	17	0	374	344	8-14	1	346	435	1-11	1	633	377	9	-9	1	517	284	6	-7	1	722	762		
-4	17	0	408	240	15-14	1	184	176	2-11	1	622	561	10	-9	1	748	739	7	-7	1	318	363		
-2	17	0	209	308	16-14	1	304	307	3-11	1	253	416	12	-9	1	321	254	8	-7	1	201	206		
2	17	0	177	313	-14-13	1	275	381	5-11	1	241	213	13	-9	1	365	311	9	-7	1	544	158		
4	17	0	384	264	-10-13	1	250	405	6-11	1	352	407	14	-9	1	654	478	10	-7	1	744	668		
6	17	0	457	405	-9-13	1	185	08	9-11	1	413	331	-20	-8	1	257	344	13	-7	1	292	319		
-8	18	0	294	343	-7-13	1	335	253	10-11	1	774	515	-16	-8	1	473	349	14	-7	1	673	522		
-4	18	0	214	277	-6-13	1	602	421	13-11	1	207	201	-14	-8	1	230	445	16	-7	1	141	203		
8	18	0	359	396	-3-13	1	327	252	14-11	1	270	405	-13	-8	1	299	219	18	-7	1	404	359		
-2	-19	1	294	340	-2-13	1	459	432	18-11	1	287	282	-12	-8	1	524	412	-20	-6	1	365	394		
2	-19	1	293	290	0-13	1	214	193	-20-10	1	253	282	-9	-8	1	432	239	-17	-6	1	230	325		
6	-19	1	250	235	1-13	1	315	150	-16-10	1	222	324	-8	-8	1	439	649	-16	-6	1	465	414		
-8	-18	1	153	285	2-13	1	485	540	-13-10	1	221	372	-7	-8	1	185	555	-13	-6	1	280	229		
-3	-18	1	112	206	5-13	1	432	322	-12-10	1	573	504	-5	-8	1	473	461	-12	-6	1	328	340		
4	-18	1	331	299	6-13	1	515	540	-9-10	1	327	283	-4	-8	1	726	680	-10	-6	1	165	215		
-6	-17	1	224	307	8-13	1	325	204	-8-10	1	413	479	-1	-8	1	499	515	-9	-6	1	502	579		
-3	-17	1	221	245	9-13	1	278	317	-6-10	1	137	311	0	-8	1	741	825	-8	-6	1	865	785		
-2	-17	1	299	308	10-13	1	320	342	-5-10	1	356	206	3	-8	1	558	575	-7	-6	1	189	768		
2	-17	1	331	358	14-13	1	328	296	-4-10	1	585	552	4	-8	1	753	478	-6	-6	1	231	156		
6	-17	1	360	380	18-13	1	339	309	-2-10	1	309	265	6	-8	1	320	258	-5	-6	1	767	581		
-9	-16	1	200	230	-13-12	1	238	353	-1-10	1	760	625	7	-8	1	375	273	-4	-6	1	1127	886		
-8	-16	1	403	381	-12-12	1	478	466	0-10	1	1174	919	8	-8	1	754	666	-2	-6	1	733	593		
-5	-16	1	203	307	-9-12	1	299	265	1-10	1	201	504	10	-8	1	181	311	-1	-6	1	430	392		
-4	-16	1	291	301	-8-12	1	530	400	3-10	1	418	342	11	-8	1	427	239	0	-6	1	673	375		
0	-16	1	363	339	-5-12	1	224	188	4-10	1	499	330	12	-8	1	574	647	1	-6	1	526	351		
4	-16	1	337	474	-4-12	1	401	485	7-10	1	343	253	13	-8	1	166	331	3	-6	1	880	716		
7	-16	1	274	302	-3-12	1	196	342	8-10	1	542	570	15	-8	1	399	357	4	-6	1	1313	943		
8	-16	1	344	375	-2-12	1	408	297	11-10	1	466	302	19	-8	1	264	303	5	-6	1	206	522		
-14	-15	1	253	312	-1-12	1	418	341	12-10	1	523	562	-22	-7	1	231	324	6	-6	1	337	445		
-10	-15	1	274	355	0-12	1	666	605	15-10	1	206	296	-19	-7	1	178	313	7	-6	1	736	620		
-7	-15	1	300	338	1-12	1	275	432	16-10	1	187	332	-18	-7	1	218	399	8	-6	1	916	825		
-6	-15	1	325	398	2-12	1	300	126	-15	-9	1	336	238	-15	-7	1	285	276	11	-6	1	307	162	
-3	-15	1	336	243	3-12	1	310	205	-14	-9	1	467	380	-14	-7	1	323	346	12	-6	1	554	502	
-2	-15	1	241	271	4-12	1	354	501	-11	-9	1	403	335	-11	-7	1	374	149	14	-6	1	220	286	

H	K	L	10FO	10FC	H	K	L	10FO	10FC	H	K	L	10FO	10FC	H	K	L	10FO	10FC	H	K	L	10FO	10FC
15	-6	1	403	390	11	-4	1	428	274	-8	-2	1	854	777	14	-1	1	501	492	13	1	1	750	565
16	-6	1	513	497	12	-4	1	521	379	-7	-2	1	169	343	15	-1	1	289	150	14	1	1	518	557
19	-6	1	265	304	13	-4	1	189	99	-5	-2	1	636	500	16	-1	1	239	253	15	1	1	238	162
-18	-5	1	573	474	14	-4	1	321	322	-4	-2	1	461	645	17	-1	1	223	174	16	1	1	224	302
-15	-5	1	248	292	15	-4	1	413	304	-3	-2	1	265	589	18	-1	1	313	414	17	1	1	229	213
-14	-5	1	519	326	16	-4	1	810	553	-2	-2	1	983	313	21	-1	1	230	262	18	1	1	291	387
-11	-5	1	185	222	-19	-3	1	239	245	-1	-2	1	1418	825	22	-1	1	374	379	22	1	1	366	380
-10	-5	1	336	574	-18	-3	1	456	441	0	-2	1	2092	1437	-24	0	1	227	276	-20	2	1	287	322
-7	-5	1	665	686	-14	-3	1	358	426	1	-2	1	738	1333	-21	0	1	220	194	-16	2	1	354	443
-6	-5	1	1149	978	-13	-3	1	160	189	2	-2	1	450	152	-17	0	1	174	265	-13	2	1	286	351
-5	-5	1	302	931	-11	-3	1	454	314	3	-2	1	377	388	-16	0	1	315	461	-12	2	1	594	732
-3	-5	1	597	655	-10	-3	1	820	700	4	-2	1	1137	599	-13	0	1	596	667	-11	2	1	136	350
-2	-5	1	493	570	-9	-3	1	142	298	6	-2	1	311	417	-12	0	1	710	881	-10	2	1	208	470
1	-5	1	360	747	-8	-3	1	381	363	7	-2	1	544	634	-9	0	1	372	506	-9	2	1	558	413
2	-5	1	939	560	-7	-3	1	547	552	8	-2	1	1244	801	-6	0	1	712	463	-8	2	1	575	623
4	-5	1	513	691	-6	-3	1	1049	808	9	-2	1	184	181	-5	0	1	313	484	-7	2	1	163	253
5	-5	1	946	913	-5	-3	1	203	493	10	-2	1	304	321	-4	0	1	1976	762	-5	2	1	538	216
6	-5	1	1501	1255	-4	-3	1	917	208	11	-2	1	574	595	3	0	1	1685	738	-4	2	1	416	656
9	-5	1	293	402	-3	-3	1	638	597	12	-2	1	710	572	4	0	1	647	532	-3	2	1	216	474
10	-5	1	380	505	-2	-3	1	1499	873	14	-2	1	375	312	7	0	1	626	694	-2	2	1	825	423
13	-5	1	435	241	-1	-3	1	364	807	15	-2	1	347	245	8	0	1	783	545	-1	2	1	1125	1022
14	-5	1	495	520	0	-3	1	521	285	16	-2	1	343	443	11	0	1	676	626	0	2	1	1755	1409
17	-5	1	514	354	1	-3	1	1127	795	19	-2	1	339	239	12	0	1	1244	711	1	2	1	610	1202
18	-5	1	375	433	2	-3	1	1077	904	20	-2	1	413	400	15	0	1	293	355	2	2	1	396	481
-20	-4	1	248	366	3	-3	1	724	335	23	-2	1	178	269	16	0	1	509	386	3	2	1	342	392
-17	-4	1	389	304	4	-3	1	388	269	-22	-1	1	253	259	20	0	1	442	428	4	2	1	1033	734
-16	-4	1	401	461	5	-3	1	872	578	-18	-1	1	243	303	24	0	1	314	311	6	2	1	264	313
-15	-4	1	180	248	6	-3	1	1089	969	-16	-1	1	292	169	-22	1	1	263	283	7	2	1	523	667
-14	-4	1	220	455	7	-3	1	347	599	-15	-1	1	263	505	-18	1	1	246	304	8	2	1	1144	758
-13	-4	1	215	140	8	-3	1	252	248	-14	-1	1	825	685	-16	1	1	268	120	9	2	1	134	121
-12	-4	1	467	371	9	-3	1	723	696	-12	-1	1	165	483	-15	1	1	220	434	10	2	1	315	332
-9	-4	1	440	672	10	-3	1	939	643	-11	-1	1	313	538	-14	1	1	819	677	11	2	1	566	445
-8	-4	1	1151	920	12	-3	1	423	302	-10	-1	1	891	760	-11	1	1	302	619	12	2	1	673	499
-7	-4	1	338	554	13	-3	1	315	278	-7	-1	1	330	432	-10	1	1	819	801	14	2	1	332	324
-6	-4	1	420	212	14	-3	1	429	457	-6	-1	1	459	466	-7	1	1	314	225	15	2	1	320	425
-5	-4	1	731	521	17	-3	1	423	268	-5	-1	1	119	866	-6	1	1	446	267	16	2	1	356	485
-4	-4	1	1089	793	18	-3	1	488	467	-3	-1	1	898	1081	-5	1	1	155	791	19	2	1	303	177
-3	-4	1	325	858	20	-3	1	215	226	-2	-1	1	1062	1375	-3	1	1	789	1051	20	2	1	366	364
-2	-4	1	128	315	21	-3	1	241	260	-1	-1	1	401	1471	-2	1	1	951	1538	23	2	1	257	252
-1	-4	1	356	586	-20	-2	1	347	261	0	-1	1	610	590	-1	1	1	375	1208	-22	3	1	205	264
0	-4	1	529	614	-17	-2	1	179	225	1	-1	1	830	603	0	1	1	545	435	-19	3	1	237	289
2	-4	1	552	363	-16	-2	1	357	511	2	-1	1	1546	1237	1	1	1	737	548	-18	3	1	449	451
3	-4	1	851	756	-15	-2	1	149	370	4	-1	1	279	443	2	1	1	1418	1090	-14	3	1	309	440
4	-4	1	1278	966	-13	-2	1	316	420	5	-1	1	418	375	4	1	1	201	359	-13	3	1	188	244
5	-4	1	336	434	-12	-2	1	644	602	6	-1	1	685	380	5	1	1	394	488	-11	3	1	418	301
6	-4	1	621	359	-11	-2	1	162	170	9	-1	1	791	713	6	1	1	675	546	-10	3	1	737	750
7	-4	1	1008	885	-10	-2	1	203	487	10	-1	1	665	786	9	1	1	774	665	-8	3	1	323	192
8	-4	1	838	976	-9	-2	1	610	470	13	-1	1	740	501	10	1	1	652	641	-7	3	1	465	400

H	K	L	10FO	10FC	H	K	L	10FO	10FC	H	K	L	10FO	10FC	H	K	L	10FO	10FC	H	K	L	10FO	10FC
-6	3	1	881	676	14	4	1	352	339	12	6	1	517	492	15	8	1	396	351	1	11	1	508	424
-5	3	1	142	277	15	4	1	403	365	14	6	1	229	368	19	8	1	259	315	2	11	1	524	607
-4	3	1	746	437	16	4	1	782	516	15	6	1	410	354	-15	9	1	286	194	6	11	1	295	330
-3	3	1	496	609	19	4	1	261	279	16	6	1	438	433	-14	9	1	374	371	9	11	1	346	337
-2	3	1	1197	632	20	4	1	263	325	19	6	1	242	333	-11	9	1	320	337	10	11	1	661	490
-1	3	1	271	471	-16	5	1	526	472	-22	7	1	207	267	-10	9	1	547	572	-16	12	1	114	269
0	3	1	439	384	-15	5	1	212	282	-19	7	1	218	290	-8	9	1	152	273	-13	12	1	162	336
1	3	1	883	864	-14	5	1	420	341	-16	7	1	199	332	-7	9	1	206	230	-12	12	1	433	352
2	3	1	910	939	-10	5	1	264	559	-15	7	1	260	194	-6	9	1	605	458	-9	12	1	249	294
3	3	1	614	376	-7	5	1	683	504	-14	7	1	278	358	-4	9	1	212	270	-8	12	1	408	419
4	3	1	332	133	-6	5	1	938	1144	-11	7	1	324	208	-3	9	1	165	476	-4	12	1	329	428
5	3	1	774	623	-5	5	1	229	695	-10	7	1	525	540	-2	9	1	711	894	-2	12	1	334	263
6	3	1	953	987	-3	5	1	443	501	-8	7	1	359	100	1	9	1	464	452	-1	12	1	339	275
7	3	1	313	534	-2	5	1	402	440	-7	7	1	299	352	2	9	1	365	522	0	12	1	524	615
8	3	1	295	317	1	5	1	265	700	-6	7	1	725	871	3	9	1	169	202	1	12	1	245	439
9	3	1	672	516	2	5	1	731	790	-5	7	1	553	506	4	9	1	139	335	2	12	1	231	215
10	3	1	867	562	4	5	1	421	599	-2	7	1	718	618	5	9	1	473	307	3	12	1	208	293
12	3	1	399	304	5	5	1	777	808	0	7	1	157	454	6	9	1	358	364	4	12	1	304	443
13	3	1	273	384	6	5	1	1348	1004	1	7	1	502	348	9	9	1	466	387	7	12	1	311	281
14	3	1	430	474	9	5	1	266	459	2	7	1	986	531	10	9	1	652	625	8	12	1	302	360
17	3	1	409	321	10	5	1	304	592	4	7	1	270	620	12	9	1	309	249	11	12	1	334	324
18	3	1	503	442	13	5	1	408	291	5	7	1	611	611	13	9	1	361	282	12	12	1	395	362
20	3	1	252	257	14	5	1	471	428	6	7	1	619	707	14	9	1	631	445	16	12	1	266	298
-20	4	1	273	359	17	5	1	482	303	7	7	1	279	439	21	9	1	155	263	-14	13	1	235	301
-17	4	1	349	351	18	5	1	375	439	8	7	1	148	139	-12	10	1	466	470	-10	13	1	249	322
-16	4	1	395	501	-20	6	1	261	325	9	7	1	481	290	-9	10	1	241	327	-8	13	1	186	391
-14	4	1	205	493	-17	6	1	174	314	10	7	1	637	607	-8	10	1	330	469	-7	13	1	239	243
-13	4	1	193	86	-16	6	1	409	435	13	7	1	244	279	-5	10	1	249	288	-6	13	1	439	406
-12	4	1	435	335	-13	6	1	239	98	14	7	1	619	474	-4	10	1	461	531	-3	13	1	253	201
-9	4	1	343	540	-12	6	1	286	305	18	7	1	392	327	-2	10	1	248	350	-2	13	1	329	392
-8	4	1	999	1053	-10	6	1	153	243	-16	8	1	402	294	-1	10	1	592	528	1	13	1	282	230
-7	4	1	299	673	-9	6	1	378	465	-14	8	1	196	419	0	10	1	955	893	2	13	1	418	520
-6	4	1	337	281	-8	6	1	715	931	-13	8	1	228	184	1	10	1	178	512	5	13	1	354	341
-5	4	1	571	321	-7	6	1	159	814	-12	8	1	417	472	3	10	1	318	336	6	13	1	414	440
-4	4	1	884	541	-6	6	1	180	161	-9	8	1	323	290	4	10	1	467	317	9	13	1	221	319
-3	4	1	229	658	-5	6	1	566	471	-8	8	1	327	600	7	10	1	281	260	10	13	1	271	296
-1	4	1	258	530	-4	6	1	893	748	-7	8	1	128	361	8	10	1	468	469	13	13	1	224	259
0	4	1	447	637	-2	6	1	576	604	-5	8	1	357	321	11	10	1	443	331	14	13	1	279	288
2	4	1	429	379	-1	6	1	311	316	-4	8	1	604	734	12	10	1	489	511	18	13	1	275	302
3	4	1	717	973	0	6	1	486	416	-1	8	1	364	562	16	10	1	198	314	-5	14	1	289	267
4	4	1	1118	989	1	6	1	399	408	0	8	1	575	708	20	10	1	255	249	-4	14	1	450	362
5	4	1	308	482	3	6	1	679	606	3	8	1	442	380	-14	11	1	257	360	3	14	1	343	284
6	4	1	545	251	4	6	1	1092	896	4	8	1	644	422	-11	11	1	323	363	4	14	1	545	528
7	4	1	880	678	5	6	1	132	586	6	8	1	285	391	-10	11	1	431	479	8	14	1	217	368
8	4	1	758	910	6	6	1	274	357	7	8	1	295	431	-6	11	1	263	381	-10	15	1	236	269
11	4	1	414	331	7	6	1	625	587	8	8	1	643	617	-4	11	1	239	368	-7	15	1	255	274
12	4	1	468	375	8	6	1	803	760	11	8	1	358	226	-3	11	1	314	297	-6	15	1	289	350
13	4	1	208	54	11	6	1	242	233	12	8	1	519	559	-2	11	1	719	679	-3	15	1	277	239

H	K	L	10FO	10FC	H	K	L	10FO	10FC	H	K	L	10FO	10FC	h	K	L	10FO	10FC	H	K	L	10FO	10FC
2	15	1	420	399	-4	-14	2	322	261	8	-11	2	496	418	-2	-8	2	1418	886	-20	-5	2	315	376
6	15	1	418	453	-2	-14	2	259	255	10	-11	2	695	614	0	-8	2	1906	1348	-18	-5	2	743	661
-8	16	1	272	312	2	-14	2	395	347	12	-11	2	666	398	2	-8	2	1302	814	-16	-5	2	331	618
-4	16	1	274	289	4	-14	2	559	548	14	-11	2	384	291	4	-8	2	974	604	-14	-5	2	236	268
0	16	1	286	279	6	-14	2	665	436	-16	-10	2	429	396	6	-8	2	223	542	-12	-5	2	332	276
4	16	1	299	416	8	-14	2	771	577	-14	-10	2	609	435	8	-8	2	310	388	-10	-5	2	388	529
8	16	1	275	350	10	-14	2	360	398	-12	-10	2	696	581	10	-8	2	467	354	-8	-5	2	690	620
2	17	1	253	314	12	-14	2	237	241	-10	-10	2	293	501	12	-8	2	324	471	-6	-5	2	1255	1327
6	17	1	284	342	-14	-13	2	313	361	-8	-10	2	401	390	14	-8	2	479	418	-4	-5	2	1336	909
4	18	1	270	266	-12	-13	2	421	435	-6	-10	2	714	494	16	-8	2	629	526	-2	-5	2	1155	1093
2	19	1	253	258	-10	-13	2	774	684	-4	-10	2	918	732	18	-8	2	461	389	0	-5	2	812	872
-2	-19	2	489	437	-8	-13	2	443	560	-2	-10	2	725	541	20	-8	2	308	299	2	-5	2	1906	1542
0	-19	2	291	335	-6	-13	2	418	507	0	-10	2	1092	945	-20	-7	2	344	401	4	-5	2	1383	1167
2	-19	2	327	305	2	-13	2	163	336	2	-10	2	905	533	-18	-7	2	621	639	6	-5	2	1012	1022
-4	-18	2	334	320	4	-13	2	302	425	4	-10	2	547	397	-16	-7	2	422	564	8	-5	2	386	349
-2	-18	2	253	309	6	-13	2	760	655	6	-10	2	528	407	-14	-7	2	372	335	10	-5	2	277	349
0	-18	2	427	381	8	-13	2	573	444	8	-10	2	478	526	-12	-7	2	328	383	12	-5	2	525	415
4	-18	2	301	243	10	-13	2	739	481	10	-10	2	676	425	-8	-7	2	337	472	14	-5	2	472	530
6	-18	2	224	216	12	-13	2	328	389	12	-10	2	861	538	-6	-7	2	855	824	16	-5	2	688	446
-10	-17	2	227	286	14	-13	2	193	168	14	-10	2	488	318	-4	-7	2	858	985	18	-5	2	748	563
-8	-17	2	307	270	-16	-12	2	287	259	16	-10	2	255	269	-2	-7	2	1488	1450	20	-5	2	401	322
-6	-17	2	437	334	-14	-12	2	370	360	-18	-9	2	354	390	0	-7	2	1089	973	-20	-4	2	421	416
-4	-17	2	213	309	-12	-12	2	647	598	-16	-9	2	301	373	2	-7	2	1089	1171	-18	-4	2	280	464
2	-17	2	365	330	-10	-12	2	483	544	-14	-9	2	604	511	4	-7	2	757	877	-16	-4	2	473	511
4	-17	2	400	301	-8	-12	2	496	625	-12	-9	2	518	522	6	-7	2	479	628	-14	-4	2	533	521
6	-17	2	400	315	-6	-12	2	350	527	-10	-9	2	266	399	8	-7	2	248	344	-12	-4	2	327	338
-10	-16	2	227	282	-4	-12	2	430	396	-8	-9	2	356	492	10	-7	2	245	271	-10	-4	2	560	412
-8	-16	2	532	452	-2	-12	2	324	309	-6	-9	2	530	485	12	-7	2	386	404	-8	-4	2	1016	1207
-6	-16	2	414	383	0	-12	2	390	431	-4	-9	2	1009	666	14	-7	2	814	567	-6	-4	2	1639	990
-4	-16	2	292	266	2	-12	2	310	406	-2	-9	2	1232	1245	16	-7	2	560	456	-4	-4	2	1278	1196
2	-16	2	234	305	4	-12	2	535	452	0	-9	2	875	700	18	-7	2	662	517	-2	-4	2	1067	597
4	-16	2	653	448	6	-12	2	380	394	2	-9	2	1162	797	-22	-6	2	279	290	0	-4	2	1153	1071
6	-16	2	430	331	8	-12	2	844	642	4	-9	2	866	591	-20	-6	2	592	578	2	-4	2	1360	1137
8	-16	2	428	366	10	-12	2	502	470	6	-9	2	249	388	-18	-6	2	490	561	4	-4	2	1685	1465
-10	-15	2	483	529	12	-12	2	552	378	8	-9	2	259	351	-16	-6	2	537	552	6	-4	2	1025	781
-8	-15	2	436	429	14	-12	2	329	276	10	-9	2	807	494	-8	-6	2	619	829	8	-4	2	711	802
-6	-15	2	587	463	-16	-11	2	349	261	12	-9	2	594	413	-6	-6	2	771	852	10	-4	2	558	407
-4	-15	2	349	393	-14	-11	2	666	491	14	-9	2	554	497	-4	-6	2	1255	1251	12	-4	2	640	423
0	-15	2	209	215	-12	-11	2	411	491	16	-9	2	343	344	-2	-6	2	829	923	14	-4	2	422	481
2	-15	2	370	299	-10	-11	2	582	619	18	-9	2	311	317	0	-6	2	1278	1416	16	-4	2	615	562
4	-15	2	501	407	-8	-11	2	328	535	-20	-8	2	514	471	2	-6	2	952	1147	18	-4	2	397	330
6	-15	2	637	601	-6	-11	2	585	493	-18	-8	2	288	412	4	-6	2	1267	1116	20	-4	2	428	347
8	-15	2	365	346	-4	-11	2	452	443	-16	-8	2	558	492	6	-6	2	507	644	-22	-3	2	200	251
-10	-15	2	295	303	-2	-11	2	536	640	-12	-8	2	307	386	14	-6	2	467	460	-20	-3	2	206	318
-12	-14	2	494	471	0	-11	2	375	428	-10	-8	2	407	332	16	-6	2	1051	688	-18	-3	2	256	357
-10	-14	2	478	421	2	-11	2	470	501	-8	-8	2	193	362	18	-6	2	560	413	-16	-3	2	270	486
-8	-14	2	959	656	4	-11	2	543	401	-6	-8	2	838	736	20	-6	2	475	343	-14	-3	2	562	515
-6	-14	2	421	529	6	-11	2	458	453	-4	-8	2	1290	1077	-22	-5	2	410	322	-12	-3	2	852	591

H	K	L	10FO	10FC	H	K	L	10FO	10FC	H	K	L	10FO	10FC	H	K	L	10FO	10FC	H	K	L	10FO	10FC
-10	-3	2	773	906	12	-1	2	681	772	6	2	2	793	744	18	4	2	406	370	0	7	2	775	848
-8	-3	2	976	799	14	-1	2	420	450	8	2	2	1017	1275	20	4	2	370	330	2	7	2	753	1170
-6	-3	2	1522	1311	22	-1	2	427	367	10	2	2	962	830	-22	5	2	336	299	4	7	2	601	778
-4	-3	2	1929	826	-24	0	2	250	329	12	2	2	721	778	-20	5	2	272	310	6	7	2	347	596
-2	-3	2	811	984	-16	0	2	184	327	14	2	2	367	482	-18	5	2	604	556	8	7	2	217	321
0	-3	2	1244	711	-14	0	2	542	665	20	2	2	236	258	-16	5	2	225	481	10	7	2	205	322
2	-3	2	1813	1190	-12	0	2	1360	1331	22	2	2	288	314	-14	5	2	198	225	12	7	2	307	485
4	-3	2	1859	1109	-10	0	2	1220	1091	-22	3	2	255	287	-12	5	2	210	325	14	7	2	707	542
6	-3	2	1685	1219	-8	0	2	705	1040	-18	3	2	225	320	-10	5	2	323	471	16	7	2	502	473
8	-3	2	790	561	-6	0	2	367	784	-16	3	2	229	454	-8	5	2	509	563	18	7	2	543	589
10	-3	2	1006	726	-4	0	2	916	943	-14	3	2	518	442	-6	5	2	915	998	-20	8	2	397	353
12	-3	2	779	599	-2	0	2	222	817	-12	3	2	719	536	-4	5	2	958	1034	-16	8	2	388	479
14	-3	2	583	509	0	0	2	380	1483	-10	3	2	619	761	-2	5	2	819	1047	-12	8	2	217	229
16	-3	2	318	350	2	0	2	747	1020	-8	3	2	768	785	0	5	2	594	705	-10	8	2	250	265
18	-3	2	371	354	4	0	2	689	730	-6	3	2	1232	1079	2	5	2	1441	1384	-8	8	2	195	295
20	-3	2	234	292	6	0	2	626	826	-4	3	2	1557	915	4	5	2	1080	1039	-6	8	2	588	734
-24	-2	2	339	276	8	0	2	2441	1619	-2	3	2	662	897	6	5	2	802	1168	-4	8	2	904	787
-16	-2	2	336	359	10	0	2	1244	1089	0	3	2	1024	650	8	5	2	267	341	-2	8	2	925	780
-14	-2	2	387	659	12	0	2	1159	941	2	3	2	1522	1296	10	5	2	199	358	0	8	2	1313	1300
-12	-2	2	998	1021	-16	1	2	267	409	4	3	2	1569	945	12	5	2	384	477	2	8	2	925	754
-10	-2	2	669	850	-14	1	2	725	699	6	3	2	1441	1224	14	5	2	427	572	4	8	2	747	537
-8	-2	2	983	1108	-12	1	2	844	866	8	3	2	738	584	16	5	2	660	520	8	8	2	277	371
-6	-2	2	946	894	-10	1	2	1325	1379	10	3	2	915	762	18	5	2	650	575	10	8	2	390	444
-4	-2	2	1650	1137	-8	1	2	365	937	12	3	2	740	576	20	5	2	323	321	12	8	2	285	449
-2	-2	2	489	579	-6	1	2	975	738	14	3	2	513	490	-20	6	2	433	487	14	8	2	406	425
0	-2	2	385	1088	-4	1	2	2057	872	16	3	2	224	392	-18	6	2	356	448	16	8	2	517	547
2	-2	2	2336	1035	-2	1	2	1546	1391	18	3	2	334	346	-16	6	2	377	468	18	8	2	406	397
4	-2	2	1077	1024	0	1	2	1156	793	20	3	2	252	315	-8	6	2	449	588	-18	9	2	244	331
6	-2	2	872	851	2	1	2	1697	994	22	3	2	304	272	-6	6	2	517	909	-16	9	2	242	293
8	-2	2	1065	1238	4	1	2	1085	873	-20	4	2	377	396	-4	6	2	902	1125	-14	9	2	427	442
10	-2	2	1005	758	6	1	2	790	1023	-18	4	2	231	365	-2	6	2	576	894	-12	9	2	318	334
12	-2	2	750	755	8	1	2	1290	989	-16	4	2	385	425	0	6	2	904	1223	-8	9	2	221	474
14	-2	2	385	521	10	1	2	1650	1460	-14	4	2	407	516	2	6	2	685	976	-6	9	2	363	378
-22	-1	2	155	199	12	1	2	718	795	-12	4	2	275	318	4	6	2	962	1186	-4	9	2	728	612
-16	-1	2	298	436	14	1	2	411	423	-10	4	2	402	404	6	6	2	410	582	-2	9	2	889	1032
-14	-1	2	743	760	22	1	2	330	345	-8	4	2	740	911	14	6	2	372	550	0	9	2	573	612
-12	-1	2	863	959	-24	2	2	271	316	-6	4	2	1255	900	16	6	2	876	729	2	9	2	819	601
-10	-1	2	1418	1410	-16	2	2	303	355	-4	4	2	947	1064	18	6	2	487	426	4	9	2	617	467
-8	-1	2	404	891	-14	2	2	301	583	-2	4	2	787	659	20	6	2	372	381	6	9	2	245	241
-6	-1	2	1059	757	-12	2	2	898	851	0	4	2	902	978	-20	7	2	253	342	8	9	2	214	350
-4	-1	2	2208	855	-10	2	2	549	804	2	4	2	1047	918	-18	7	2	486	555	10	9	2	625	528
-2	-1	2	1673	1497	-8	2	2	854	1108	4	4	2	1348	1548	-16	7	2	296	444	12	9	2	483	446
0	-1	2	1232	701	-6	2	2	794	931	6	4	2	866	746	-14	7	2	289	280	14	9	2	438	470
2	-1	2	1778	848	-4	2	2	1383	839	8	4	2	592	793	-12	7	2	206	270	16	9	2	328	315
4	-1	2	1130	962	-2	2	2	431	667	10	4	2	489	407	-8	7	2	253	495	-16	10	2	301	337
6	-1	2	798	1122	0	2	2	364	1321	12	4	2	549	416	-6	7	2	601	592	-14	10	2	407	292
8	-1	2	1302	983	2	2	2	2057	935	14	4	2	417	530	-4	7	2	586	992	-12	10	2	466	427
10	-1	2	1627	1360	4	2	2	965	987	16	4	2	545	561	-2	7	2	1047	1268	-8	10	2	267	313

H	A	L	10FO	10FC	H	K	L	10FO	10FC	H	K	L	10FO	10FC	H	K	L	10FO	10FC	H	K	L	10FO	10FC
-6	10	2	486	465	4	13	2	208	467	5	-16	3	231	257	-13	-11	3	553	290	-15	-8	3	313	244
-5	10	2	129	403	8	13	2	585	614	-10	-15	3	335	364	-10	-11	3	551	407	-12	-8	3	566	444
-4	10	2	566	603	8	13	2	129	403	-9	-11	3	288	315	-9	-11	3	287	295	-11	-8	3	168	229
-2	10	2	502	452	10	13	2	572	533	-6	-15	3	490	427	-5	-11	3	267	320	-10	-8	3	173	270
0	10	2	701	645	12	13	2	259	405	-2	-15	3	169	200	-2	-11	3	471	563	-7	-8	3	571	444
2	10	2	650	466	12	14	2	373	322	-1	-15	3	306	310	-1	-11	3	422	293	-0	-8	3	339	451
4	10	2	389	309	16	14	2	040	591	3	-15	3	378	329	-4	-11	3	181	390	-5	-8	3	173	419
6	10	2	360	479	16	14	2	271	428	0	-15	3	267	243	-4	-11	3	460	453	-4	-8	3	654	548
8	10	2	447	556	14	14	2	289	219	-1	-15	3	137	231	-2	-11	3	444	327	-3	-8	3	206	437
10	10	2	702	556	2	14	2	382	320	0	-14	3	447	469	0	-11	3	573	440	0	-8	3	100	374
12	10	2	392	509	4	14	2	540	427	-7	-14	3	338	314	-15	-10	3	166	319	1	-8	3	635	540
14	10	2	417	376	6	14	2	265	608	-4	-14	3	279	262	-10	-10	3	453	271	2	-8	3	259	230
14	10	2	274	473	8	14	2	265	597	0	-14	3	444	372	-7	-10	3	395	327	3	-8	3	579	485
12	10	2	376	376	10	15	2	265	412	4	-14	3	565	372	-11	-10	3	600	495	4	-8	3	416	301
10	10	2	202	361	10	15	2	239	318	5	-14	3	322	271	-8	-10	3	416	320	5	-8	3	472	489
8	10	2	414	395	12	15	2	431	446	8	-14	3	229	318	-7	-10	3	309	297	9	-8	3	372	440
6	10	2	316	507	12	15	2	239	250	12	-13	3	300	290	-3	-10	3	475	410	12	-8	3	505	273
2	10	2	553	395	14	15	2	331	350	-1	-13	3	481	435	-1	-10	3	336	474	13	-8	3	367	312
0	10	2	364	494	14	15	2	504	546	-6	-13	3	300	322	-10	-10	3	416	618	16	-8	3	350	209
0	10	2	364	429	16	15	2	370	400	-9	-13	3	253	263	-11	-10	3	874	314	16	-7	3	162	278
2	10	2	344	447	16	16	2	433	400	-4	-13	3	381	435	-14	-10	3	416	374	-17	-7	3	209	302
4	10	2	364	429	18	16	2	280	390	-10	-13	3	217	273	-16	-10	3	485	418	-16	-7	3	350	108
6	10	2	495	621	18	16	2	265	290	10	-13	3	341	276	-18	-10	3	416	320	-18	-7	3	209	302
8	10	2	378	390	18	17	2	187	201	7	-13	3	267	260	-14	-9	3	260	458	-19	-7	3	294	354
10	10	2	315	459	18	17	2	252	295	10	-13	3	504	394	-18	-9	3	260	320	-19	-7	3	294	354
12	10	2	464	459	18	17	2	263	278	7	-13	3	267	260	-14	-9	3	496	442	-19	-7	3	609	602
14	10	2	375	375	20	17	2	277	342	11	-12	3	261	300	-19	-9	3	517	382	-2	-7	3	199	512
14	10	2	315	390	20	17	2	263	278	10	-12	3	381	322	-11	-12	3	440	442	-4	-7	3	476	640
12	10	2	495	489	22	18	2	164	342	-11	-12	3	415	378	-5	-9	3	250	427	-1	-7	3	199	512
10	10	2	287	375	22	18	2	277	279	-8	-12	3	235	312	-4	-9	3	366	370	-2	-7	3	476	640
8	10	2	449	428	22	19	2	249	322	-11	-12	3	274	312	-5	-9	3	440	442	-4	-7	3	476	640
6	10	2	320	453	22	19	2	323	295	-4	-12	3	327	425	-1	-9	3	271	307	-6	-7	3	444	444
4	10	2	413	428	22	19	2	315	280	0	-12	3	309	250	-1	-9	3	271	307	-6	-7	3	444	444
2	10	2	428	453	24	18	2	249	322	-3	-12	3	288	312	-2	-9	3	271	307	-6	-7	3	444	444
0	10	2	229	428	24	18	2	164	342	-11	-12	3	415	378	-5	-9	3	250	427	-1	-7	3	476	640
0	10	2	449	428	24	19	2	249	322	-11	-12	3	274	312	-4	-9	3	440	442	-4	-7	3	444	444
2	10	2	320	453	26	18	2	323	295	-4	-12	3	327	425	-1	-9	3	271	307	-6	-7	3	444	444
4	10	2	413	428	26	18	2	315	280	0	-12	3	309	250	-1	-9	3	271	307	-6	-7	3	444	444
6	10	2	428	453	26	19	2	249	322	-3	-12	3	288	312	-2	-9	3	271	307	-6	-7	3	444	444
8	10	2	229	428	26	19	2	164	342	-11	-12	3	415	378	-5	-9	3	250	427	-1	-7	3	476	640
10	10	2	449	428	26	19	2	249	322	-11	-12	3	274	312	-4	-9	3	440	442	-4	-7	3	444	444
12	10	2	320	453	28	17	2	323	295	-4	-12	3	327	425	-1	-9	3	271	307	-6	-7	3	444	444
14	10	2	413	428	28	17	2	315	280	0	-12	3	309	250	-1	-9	3	271	307	-6	-7	3	444	444
14	10	2	428	453	28	17	2	249	322	-3	-12	3	288	312	-2	-9	3	271	307	-6	-7	3	444	444
12	10	2	188	444	28	17	2	217	217	-6	-12	3	308	280	-6	-11	3	188	212	-11	-7	3	207	245
10	10	2	454	444	28	17	2	454	444	-6	-12	3	308	280	-6	-11	3	188	212	-11	-7	3	207	245
8	10	2	264	444	28	17	2	264	444	-7	-12	3	264	444	-7	-11	3	264	444	-7	-7	3	358	353
6	10	2	274	444	28	16	2	274	444	-7	-12	3	274	444	-7	-11	3	274	444	-7	-7	3	321	311
4	10	2	294	444	28	16	2	294	444	-7	-12	3	294	444	-7	-11	3	294	444	-7	-7	3	311	285
2	10	2	261	444	28	16	2	261	444	-7	-12	3	261	444	-7	-11	3	261	444	-7	-7	3	285	44
0	10	2	281	444	28	16	2	281	444	-7	-12	3	281	444	-7	-11	3	281	444	-7	-7	3	44	44

H	K	L	10FO	10FC	H	K	L	10FO	10FC	H	K	L	10FO	10FC	H	K	L	10FO	10FC	H	K	L	10FO	10FC
-15	-6	3	245	276	-11	-4	3	227	350	11	-3	3	307	194	0	-1	3	395	187	6	1	3	1005	763
-12	-6	3	265	391	-8	-4	3	945	837	12	-3	3	291	312	1	-1	3	158	410	7	1	3	685	441
-11	-6	3	152	244	-7	-4	3	593	540	14	-3	3	519	442	2	-1	3	653	570	8	1	3	146	396
-8	-6	3	738	666	-6	-4	3	544	346	15	-3	3	299	276	3	-1	3	902	425	9	1	3	150	333
-7	-6	3	550	553	-5	-4	3	413	352	18	-3	3	372	339	5	-1	3	366	176	10	1	3	1048	612
-5	-6	3	300	333	-4	-4	3	1174	659	19	-3	3	243	264	6	-1	3	1024	606	11	1	3	516	573
-4	-6	3	774	657	-3	-4	3	469	588	-24	-2	3	166	277	7	-1	3	697	443	12	1	3	170	145
-3	-6	3	694	490	-2	-4	3	400	359	-20	-2	3	268	316	8	-1	3	177	449	14	1	3	336	415
0	-6	3	1061	693	-1	-4	3	295	374	-10	-2	3	179	294	9	-1	3	187	365	22	1	3	331	266
1	-6	3	561	567	0	-4	3	667	770	-16	-2	3	371	506	10	-1	3	1058	874	-20	2	3	282	333
2	-6	3	501	376	1	-4	3	853	479	-15	-2	3	260	441	11	-1	3	558	525	-17	2	3	122	203
4	-6	3	929	612	2	-4	3	648	335	-12	-2	3	741	564	14	-1	3	353	383	-16	2	3	343	406
5	-6	3	561	424	3	-4	3	430	345	-11	-2	3	547	453	19	-1	3	239	241	-15	2	3	241	354
6	-6	3	203	163	4	-4	3	1042	745	-10	-2	3	277	440	22	-1	3	315	263	-12	2	3	678	715
8	-6	3	242	339	5	-4	3	731	544	-8	-2	3	766	790	-24	0	3	364	313	-11	2	3	479	533
9	-6	3	217	95	8	-4	3	424	454	-7	-2	3	324	489	-16	0	3	466	512	-10	2	3	267	276
10	-6	3	235	291	9	-4	3	271	136	-6	-2	3	547	132	-15	0	3	310	493	-8	2	3	753	726
12	-6	3	552	299	12	-4	3	252	342	-5	-2	3	300	432	-12	0	3	611	763	-7	2	3	308	352
13	-6	3	416	329	13	-4	3	316	259	-4	-2	3	652	640	-11	0	3	431	563	-6	2	3	509	352
16	-6	3	571	451	16	-4	3	600	489	-3	-2	3	712	455	-8	0	3	315	609	-5	2	3	277	344
17	-6	3	334	295	17	-4	3	400	309	-2	-2	3	221	80	-7	0	3	472	416	-4	2	3	638	661
20	-6	3	234	289	20	-4	3	248	261	-1	-2	3	155	513	-4	0	3	608	846	-3	2	3	635	375
-22	-5	3	202	316	-22	-3	3	236	285	0	-2	3	1106	857	-3	0	3	393	254	-2	2	3	206	414
-21	-5	3	196	276	-18	-3	3	351	454	1	-2	3	500	541	0	0	3	639	762	-1	2	3	159	648
-18	-5	3	436	443	-17	-3	3	250	362	2	-2	3	525	400	1	0	3	463	697	0	2	3	1003	758
-17	-5	3	325	318	-14	-3	3	354	399	3	-2	3	450	110	4	0	3	891	466	1	2	3	476	542
-14	-5	3	361	333	-13	-3	3	360	345	4	-2	3	609	461	5	0	3	255	486	2	2	3	494	198
-10	-5	3	578	614	-12	-3	3	250	350	5	-2	3	661	327	6	0	3	817	919	3	2	3	402	111
-9	-5	3	422	389	-11	-3	3	184	278	6	-2	3	160	322	9	0	3	712	609	4	2	3	594	578
-6	-5	3	1084	761	-10	-3	3	862	744	7	-2	3	227	323	12	0	3	667	675	5	2	3	610	364
-5	-5	3	700	656	-9	-3	3	523	478	8	-2	3	998	754	13	0	3	446	405	6	2	3	195	466
-3	-5	3	274	167	-8	-3	3	344	255	9	-2	3	648	470	21	0	3	373	271	7	2	3	243	332
-2	-5	3	636	646	-6	-3	3	504	703	12	-2	3	543	528	-22	1	3	234	321	8	2	3	948	809
-1	-5	3	582	454	-5	-3	3	581	534	13	-2	3	352	256	-14	1	3	567	676	9	2	3	655	430
0	-5	3	433	438	-4	-3	3	222	141	17	-2	3	293	203	-13	1	3	521	556	12	2	3	529	513
2	-5	3	1160	781	-3	-3	3	119	272	20	-2	3	245	253	-12	1	3	166	447	13	2	3	342	294
3	-5	3	852	559	-2	-3	3	900	753	-22	-1	3	277	292	-10	1	3	777	717	16	2	3	242	301
4	-5	3	155	193	-1	-3	3	596	514	-14	-1	3	575	657	-9	1	3	501	525	17	2	3	314	161
6	-5	3	783	700	0	-3	3	188	275	-13	-1	3	543	484	-8	1	3	378	545	20	2	3	264	242
7	-5	3	470	360	1	-3	3	176	422	-10	-1	3	809	762	-6	1	3	1103	674	-18	3	3	334	400
11	-5	3	295	196	2	-3	3	963	729	-9	-1	3	531	611	-5	1	3	370	249	-17	3	3	228	261
14	-5	3	709	464	3	-3	3	366	413	-8	-1	3	422	516	-3	1	3	209	863	-14	3	3	353	408
15	-5	3	464	342	5	-3	3	321	365	-6	-1	3	1165	666	-2	1	3	906	980	-13	3	3	335	352
18	-5	3	414	385	6	-3	3	917	635	-5	-1	3	388	233	-1	1	3	617	612	-12	3	3	207	290
-20	-4	3	452	407	7	-3	3	736	433	-4	-1	3	117	234	0	1	3	372	326	-11	3	3	174	376
-19	-4	3	277	303	0	-3	3	343	221	-3	-1	3	228	815	2	1	3	623	436	-10	3	3	743	626
-16	-4	3	317	400	9	-3	3	224	325	-2	-1	3	974	684	3	1	3	910	413	-9	3	3	442	477
-12	-4	3	261	444	10	-3	3	733	476	-1	-1	3	660	671	5	1	3	330	210	-8	3	3	293	201

H	K	L	10FO	10FC	H	K	L	10FO	10FC	H	K	L	10FO	10FC	H	K	L	10FO	10FC	H	K	L	10FO	10FC
-6	3	3	428	778	-10	5	3	488	687	-4	7	3	189	503	2	9	3	466	546	0	13	3	172	260
-5	3	3	516	358	-9	5	3	370	438	-2	7	3	545	727	3	9	3	325	177	2	13	3	282	374
-4	3	3	266	437	-6	5	3	908	906	-1	7	3	360	308	6	9	3	363	463	3	13	3	268	330
-2	3	3	783	837	-5	5	3	549	489	2	7	3	172	332	7	9	3	189	244	6	13	3	424	416
-1	3	3	525	488	-3	5	3	236	105	2	7	3	872	846	10	9	3	307	443	7	13	3	270	240
0	3	3	145	146	-2	5	3	682	624	3	7	3	390	449	11	9	3	386	306	10	13	3	270	412
1	3	3	174	439	-1	5	3	449	366	6	7	3	406	550	14	9	3	330	332	-12	14	3	259	304
2	3	3	912	707	0	5	3	371	472	7	7	3	252	210	18	9	3	256	317	-8	14	3	350	480
3	3	3	315	435	2	5	3	981	1012	10	7	3	401	286	-10	10	3	330	386	-7	14	3	224	249
5	3	3	241	239	3	5	3	751	522	11	7	3	293	255	-12	10	3	476	506	-4	14	3	250	390
6	3	3	840	757	4	5	3	143	82	14	7	3	375	402	-11	10	3	359	269	4	14	3	400	412
7	3	3	675	420	6	5	3	697	670	15	7	3	416	294	-8	10	3	208	347	5	14	3	266	323
8	3	3	280	227	7	5	3	373	492	18	7	3	393	405	-7	10	3	193	241	8	14	3	315	361
9	3	3	212	215	11	5	3	321	262	19	7	3	190	230	-4	10	3	403	540	12	14	3	288	321
10	3	3	633	477	12	5	3	207	418	-16	8	3	324	433	-3	10	3	236	360	-6	15	3	372	446
11	3	3	320	217	14	5	3	655	429	-15	8	3	273	250	0	10	3	449	705	-2	15	3	200	259
12	3	3	289	238	15	5	3	384	318	-12	8	3	463	509	1	10	3	273	268	2	15	3	187	314
14	3	3	496	413	18	5	3	403	419	-11	8	3	171	170	4	10	3	415	339	3	15	3	316	355
15	3	3	311	223	-20	6	3	287	366	-8	8	3	442	421	8	10	3	759	542	6	15	3	301	399
18	3	3	300	305	-19	6	3	195	317	-7	8	3	267	383	9	10	3	401	377	0	16	3	243	253
-20	4	3	402	383	-16	6	3	368	457	-6	8	3	300	417	12	10	3	444	394	-4	18	3	225	287
-10	4	3	318	401	-15	6	3	230	250	-5	8	3	139	193	13	10	3	261	227	-6	-17	4	321	324
-12	4	3	244	440	-12	6	3	208	371	-4	8	3	658	689	-14	11	3	336	410	-4	-17	4	271	247
-11	4	3	199	317	-8	6	3	554	825	-3	8	3	488	429	-13	11	3	256	302	-2	-17	4	406	307
-8	4	3	788	1025	-7	6	3	409	607	-2	8	3	106	301	-10	11	3	447	457	-8	-16	4	350	351
-7	4	3	479	521	-5	6	3	244	215	0	8	3	794	798	-9	11	3	213	265	-4	-16	4	321	371
-6	4	3	480	464	-4	6	3	635	647	1	8	3	509	371	-6	11	3	144	374	0	-16	4	327	370
-5	4	3	358	199	-3	6	3	539	323	2	8	3	244	169	-5	11	3	236	223	2	-16	4	267	256
-4	4	3	1009	642	0	6	3	857	846	3	8	3	201	288	-2	11	3	539	593	4	-16	4	381	319
-3	4	3	338	397	1	6	3	460	466	4	8	3	459	580	-1	11	3	350	333	-10	-15	4	264	242
-2	4	3	371	436	2	6	3	404	254	5	8	3	373	211	2	11	3	415	433	-6	-15	4	424	446
-1	4	3	229	275	4	6	3	794	842	8	8	3	385	425	6	11	3	378	404	-2	-15	4	374	456
0	4	3	550	874	5	6	3	470	478	9	8	3	407	212	7	11	3	407	280	-2	-15	4	453	432
1	4	3	730	505	6	6	3	225	205	12	8	3	526	342	10	11	3	493	518	6	-15	4	270	215
2	4	3	581	224	8	6	3	230	403	13	8	3	300	274	11	11	3	347	332	-8	-14	4	260	316
3	4	3	366	480	9	6	3	228	103	16	8	3	385	378	-12	12	3	323	383	-4	-14	4	697	562
4	4	3	904	807	12	6	3	459	315	-18	9	3	207	326	-11	12	3	243	302	0	-14	4	766	560
5	4	3	600	554	13	6	3	389	360	-14	9	3	300	494	-8	12	3	449	457	4	-14	4	299	328
8	4	3	370	518	16	6	3	537	474	-10	9	3	225	461	-4	12	3	395	410	6	-14	4	252	191
9	4	3	245	212	17	6	3	315	317	-9	9	3	166	217	-3	12	3	246	183	-12	-13	4	267	180
12	4	3	237	320	20	6	3	271	324	-6	9	3	374	391	0	12	3	381	459	-6	-13	4	428	454
13	4	3	245	240	-18	7	3	420	401	-5	9	3	263	302	1	12	3	284	268	-4	-13	4	237	384
16	4	3	567	453	-14	7	3	329	459	-4	9	3	342	318	5	12	3	356	228	-2	-13	4	896	707
17	4	3	361	296	-13	7	3	150	179	-3	9	3	166	420	8	12	3	483	481	0	-13	4	307	423
20	4	3	222	276	-10	7	3	296	482	-2	9	3	843	831	9	12	3	243	320	2	-13	4	483	490
-18	5	3	392	460	-9	7	3	182	263	-1	9	3	539	398	-10	13	3	267	414	8	-13	4	280	206
-17	5	3	346	315	-6	7	3	506	686	0	9	3	185	178	-6	13	3	357	476	10	-13	4	185	242
-14	5	3	313	323	-5	7	3	503	558	1	9	3	230	271	-4	13	3	207	206	-16	-12	4	337	394

H	K	L	10FO	10FC	H	K	L	10FO	10FC	H	K	L	10FO	10FC	H	K	L	10FO	10FC	H	K	L	10FO	10FC
-14	-12	4	135	285	14	-9	4	255	219	2	-5	4	939	885	-14	-2	4	344	359	-14	1	4	433	420
-8	-12	4	180	281	-18	-8	4	235	167	4	-5	4	385	465	-12	-2	4	272	375	-12	1	4	186	239
-6	-12	4	507	315	-16	-8	4	374	304	6	-5	4	1453	1103	-10	-2	4	347	315	-8	1	4	696	679
-4	-12	4	722	661	-12	-8	4	936	761	10	-5	4	671	524	-8	-2	4	466	428	-6	1	4	573	605
0	-12	4	767	718	-10	-8	4	266	413	12	-5	4	595	408	-6	-2	4	293	582	-4	1	4	149	512
2	-12	4	480	413	-8	-8	4	825	719	14	-5	4	325	361	-4	-2	4	1639	1223	-2	1	4	2220	1817
8	-12	4	267	270	-4	-8	4	284	522	-22	-4	4	248	210	0	-2	4	1615	1271	0	1	4	144	650
12	-12	4	372	363	0	-8	4	220	449	-20	-4	4	287	262	2	-2	4	210	600	2	1	4	898	832
-18	-11	4	253	369	4	-8	4	901	777	-18	-4	4	284	265	4	-2	4	593	648	4	1	4	748	345
-14	-11	4	456	391	6	-8	4	464	428	-16	-4	4	286	355	6	-2	4	569	325	8	1	4	309	329
-12	-11	4	195	282	8	-8	4	1185	800	-14	-4	4	293	351	8	-2	4	299	527	10	1	4	537	638
-6	-11	4	418	300	12	-8	4	440	360	-12	-4	4	608	575	10	-2	4	461	394	12	1	4	371	353
-6	-11	4	645	466	14	-8	4	377	235	-10	-4	4	384	377	12	-2	4	666	630	14	1	4	679	638
-4	-11	4	401	311	-16	-7	4	230	341	-8	-4	4	1244	1068	14	-2	4	393	334	16	1	4	490	444
-2	-11	4	1156	819	-14	-7	4	408	505	-6	-4	4	523	534	16	-2	4	594	513	-20	2	4	317	412
0	-11	4	373	450	-10	-7	4	1185	1023	-4	-4	4	442	608	20	-2	4	315	298	-18	2	4	208	306
2	-11	4	642	501	-6	-7	4	747	663	-2	-4	4	443	369	-22	-1	4	288	364	-16	2	4	461	467
4	-11	4	504	292	-4	-7	4	317	393	0	-4	4	621	720	-18	-1	4	495	545	-14	2	4	265	291
8	-11	4	260	255	0	-7	4	273	377	2	-4	4	581	508	-16	-1	4	244	336	-12	2	4	241	292
10	-11	4	476	420	2	-7	4	732	630	4	-4	4	1406	1042	-14	-1	4	460	478	-10	2	4	324	412
12	-11	4	261	247	6	-7	4	1400	1053	6	-4	4	597	374	-10	-1	4	121	167	-8	2	4	439	481
-14	-11	4	351	324	8	-7	4	341	475	8	-4	4	703	731	-8	-1	4	743	673	-6	2	4	235	528
-16	-10	4	414	400	10	-7	4	475	577	10	-4	4	337	388	-6	-1	4	587	664	-4	2	4	1522	1053
-14	-10	4	330	321	12	-7	4	145	386	12	-4	4	393	461	-4	-1	4	208	546	0	2	4	1569	1303
-12	-10	4	380	479	14	-7	4	257	230	14	-4	4	330	309	-2	-1	4	2243	1851	2	2	4	198	463
-8	-10	4	263	384	-14	-6	4	200	435	16	-4	4	407	395	0	-1	4	193	653	4	2	4	565	524
-6	-10	4	458	287	-12	-6	4	854	795	-22	-3	4	234	286	2	-1	4	920	843	6	2	4	537	257
-4	-10	4	673	673	-10	-6	4	205	492	-20	-3	4	145	238	4	-1	4	769	466	8	2	4	272	552
0	-10	4	814	704	-8	-6	4	1313	1135	-18	-3	4	420	412	6	-1	4	136	402	10	2	4	389	342
2	-10	4	523	398	-6	-6	4	474	580	-16	-3	4	508	323	8	-1	4	301	298	12	2	4	639	595
4	-10	4	364	417	-4	-6	4	146	361	-14	-3	4	513	425	10	-1	4	537	622	14	2	4	359	294
8	-10	4	507	550	-2	-6	4	324	326	-10	-3	4	425	601	12	-1	4	401	417	16	2	4	549	494
10	-10	4	339	296	0	-6	4	224	404	-8	-3	4	506	451	14	-1	4	642	656	18	2	4	236	337
12	-10	4	354	385	2	-6	4	475	458	-6	-3	4	834	874	18	-1	4	460	439	20	2	4	346	324
-16	-9	4	349	235	4	-6	4	1410	1076	-4	-3	4	169	415	-20	0	4	466	493	-22	3	4	198	271
-14	-9	4	589	538	6	-6	4	229	482	-2	-3	4	582	922	-16	0	4	607	576	-18	3	4	358	364
-12	-9	4	144	395	8	-6	4	1063	869	2	-3	4	804	992	-12	0	4	308	286	-16	3	4	494	293
-10	-9	4	674	595	10	-6	4	234	482	4	-3	4	643	522	-8	0	4	232	116	-14	3	4	408	343
-8	-9	4	322	333	12	-6	4	289	378	6	-3	4	506	730	-4	0	4	1673	1482	-10	3	4	401	565
-6	-9	4	485	552	-18	-5	4	286	250	10	-3	4	581	550	0	0	4	1929	1634	-8	3	4	440	466
-4	-9	4	256	381	-16	-5	4	357	374	12	-3	4	726	577	4	0	4	345	291	-6	3	4	717	784
-2	-9	4	651	620	-14	-5	4	387	392	14	-3	4	574	522	8	0	4	397	536	-4	3	4	185	425
2	-9	4	565	566	-10	-5	4	1348	1096	18	-3	4	336	360	12	0	4	860	719	-2	3	4	550	844
4	-9	4	452	390	-8	-5	4	372	642	20	-3	4	298	231	16	0	4	617	553	2	3	4	812	908
6	-9	4	654	667	-6	-5	4	893	845	-24	-2	4	259	241	20	0	4	335	339	4	3	4	616	375
8	-9	4	292	352	-4	-5	4	365	346	-20	-2	4	366	417	-22	1	4	316	360	6	3	4	558	670
10	-9	4	781	569	-2	-5	4	224	252	-18	-2	4	238	270	-18	1	4	503	542	10	3	4	562	532
12	-9	4	437	284	0	-5	4	418	440	-16	-2	4	514	510	-16	1	4	286	386	12	3	4	651	330

H	K	L	10FO	10FC	H	K	L	10FO	10FC	H	K	L	10FO	10FC	H	K	L	10FO	10FC	H	K	L	10FO	10FC
14	3	4	522	484	-10	7	4	915	845	-6	11	4	438	316	-4-12	5	428	425	-8	-8	5	518	484	
18	3	4	296	367	-6	7	4	590	470	-4	11	4	275	201	-1-12	5	292	231	-5	-8	5	251	275	
20	3	4	263	249	-4	7	4	242	218	-2	11	4	861	654	0-12	5	513	402	-4	-8	5	306	410	
-18	4	4	232	199	0	7	4	181	332	0	11	4	329	275	1-12	5	148	235	-1	-8	5	308	339	
-16	4	4	238	269	2	7	4	682	528	2	11	4	456	420	2-12	5	196	210	0	-8	5	321	332	
-14	4	4	246	282	4	7	4	144	424	4	11	4	365	277	6-12	5	275	277	2	-8	5	145	312	
-12	4	4	504	511	6	7	4	1197	1017	6	11	4	231	260	-10-11	5	342	257	3	-8	5	364	189	
-10	4	4	327	220	8	7	4	241	428	10	11	4	406	405	-6-11	5	343	374	4	-8	5	529	332	
-8	4	4	1035	920	10	7	4	461	539	12	11	4	206	234	-3-11	5	343	325	7	-8	5	278	214	
-6	4	4	447	543	-16	8	4	256	227	14	11	4	277	357	-2-11	5	568	499	8	-8	5	509	512	
-4	4	4	363	572	-12	8	4	690	602	-6	12	4	372	215	0-11	5	181	229	11	-8	5	189	286	
-2	4	4	358	297	-10	8	4	266	362	-4	12	4	529	533	1-11	5	259	261	12	-8	5	253	349	
2	4	4	538	543	-8	8	4	592	588	2-11	5	539	584	2-11	5	223	286	-15	-7	5	320	132		
2	4	4	537	445	-4	8	4	236	277	0	12	4	316	334	5-11	5	253	241	-14	-7	5	307	314	
4	4	4	1232	1020	0	8	4	218	382	4	12	4	194	237	6-11	5	351	318	-11	-7	5	213	287	
6	4	4	526	317	4	8	4	719	653	12	12	4	330	382	9-11	5	244	238	-10	-7	5	691	532	
8	4	4	672	653	6	8	4	353	359	-6	13	4	245	324	10-11	5	363	338	-7	-7	5	359	346	
10	4	4	278	326	8	8	4	1020	781	-2	13	4	644	595	-10-10	5	242	270	-6	-7	5	486	483	
12	4	4	366	433	12	8	4	422	351	0	13	4	238	364	-12-10	5	358	332	-2	-7	5	315	281	
14	4	4	318	328	14	8	4	314	227	2	13	4	360	403	-8-10	5	264	305	0	-7	5	172	325	
16	4	4	393	372	-18	9	4	139	183	8	13	4	267	101	-5-10	5	265	268	1	-7	5	345	263	
18	4	4	246	219	-16	9	4	280	112	-8	14	4	194	205	-4-10	5	676	512	2	-7	5	552	379	
-18	5	4	210	162	-14	9	4	450	384	-4	14	4	490	453	-1-10	5	495	372	5	-7	5	545	232	
-16	5	4	236	292	-10	9	4	503	493	0	14	4	531	476	0-10	5	334	375	6	-7	5	442	482	
-14	5	4	379	349	-8	9	4	237	274	-6	15	4	331	312	3-10	5	181	183	9	-7	5	327	220	
-10	5	4	1083	910	-6	9	4	385	383	2	15	4	336	397	6-10	5	252	245	10	-7	5	478	435	
-8	5	4	284	426	-2	9	4	507	461	-8	16	4	224	251	7-10	5	298	261	-20	-6	5	251	242	
-6	5	4	769	745	2	9	4	364	466	-6	16	4	207	170	8-10	5	291	430	-17	-6	5	187	183	
-4	5	4	328	376	4	9	4	343	279	0	16	4	273	302	11-10	5	167	241	-16	-6	5	259	248	
-2	5	4	169	190	6	9	4	562	565	-6	17	4	274	246	-14	-9	5	403	304	-13	-6	5	199	186
0	5	4	338	412	8	9	4	200	354	2	17	4	221	272	-11	-9	5	320	246	-12	-6	5	445	432
2	5	4	815	754	10	9	4	655	573	0	-16	5	263	320	-10	-9	5	256	389	-9	-6	5	410	397
4	5	4	345	461	12	9	4	337	285	-10	-15	5	229	279	-9	-9	5	217	220	-8	-6	5	759	619
6	5	4	1313	1080	-16	10	4	313	294	-7	-15	5	267	254	-6	-9	5	238	229	-5	-6	5	224	362
8	5	4	126	320	-14	10	4	229	207	2	-15	5	350	392	-6	-9	5	423	409	-2	-6	5	145	238
10	5	4	623	449	-12	10	4	320	348	-8	-14	5	332	280	-3	-9	5	366	373	0	-6	5	408	312
12	5	4	495	421	-8	10	4	210	255	-4	-14	5	274	270	-2	-9	5	503	485	3	-6	5	576	351
14	5	4	299	366	-6	10	4	285	175	0	-14	5	245	397	1	-9	5	353	281	4	-6	5	750	553
-12	6	4	691	672	-4	10	4	495	502	3	-14	5	221	303	2	-9	5	379	229	7	-6	5	384	207
-8	6	4	1031	913	0	10	4	612	577	4	-14	5	268	361	3	-9	5	187	152	8	-6	5	443	429
-6	6	4	406	434	2	10	4	353	287	-6	-13	5	373	308	4	-9	5	354	237	12	-6	5	357	363
-2	6	4	252	261	4	10	4	313	328	-3	-13	5	249	161	5	-9	5	237	168	-19	-5	5	160	277
0	6	4	142	226	6	10	4	399	489	-2	-13	5	416	379	6	-9	5	554	414	-18	-5	5	267	263
2	6	4	403	453	10	10	4	267	284	1	-13	5	280	240	9	-9	5	313	269	-14	-5	5	310	305
4	6	4	1174	1041	12	10	4	364	414	2	-13	5	406	397	10	-9	5	390	440	-11	-5	5	415	370
6	6	4	906	825	-18	11	4	198	262	-12	-12	5	144	263	-13	-8	5	300	217	-10	-5	5	747	567
-12	6	4	281	350	-14	11	4	327	296	-6	-12	5	218	328	-12	-8	5	345	383	-7	-5	5	374	427
-14	7	4	341	409	-8	11	4	268	193	-5	-12	5	308	204	-9	-8	5	274	269	-6	-5	5	611	510

H	K	L	10FO	10FC	H	K	L	10FO	10FC	H	K	L	10FO	10FC	H	K	L	10FO	10FC	H	K	L	10FO	10FC
1	-5	5	459	303	6	-3	5	451	488	-16	0	5	442	413	15	2	5	230	189	-18	5	5	186	257
2	-5	5	626	535	9	-3	5	223	244	-12	0	5	306	343	16	2	5	301	321	-14	5	5	281	238
5	-5	5	578	387	10	-3	5	231	299	-9	0	5	252	47	-10	3	5	251	272	-11	5	5	378	392
6	-5	5	748	530	11	-3	5	242	151	-8	0	5	464	268	-16	3	5	225	271	-10	5	5	602	600
8	-5	5	279	205	12	-3	5	250	260	-5	0	5	466	478	-14	3	5	256	299	-7	5	5	338	405
9	-5	5	244	174	13	-3	5	293	222	-4	0	5	1030	747	-11	3	5	238	359	-6	5	5	535	473
14	-5	5	374	329	14	-3	5	346	352	-1	0	5	608	460	-10	3	5	497	492	1	5	5	428	369
14	-5	5	395	353	17	-3	5	216	236	0	0	5	754	785	-7	3	5	281	183	2	5	5	586	518
-20	-4	5	276	274	-21	-2	5	191	200	3	0	5	323	261	-6	3	5	483	435	5	5	5	554	358
-16	-4	5	258	283	-17	-2	5	192	313	4	0	5	414	328	-3	3	5	393	276	6	5	5	691	522
-13	-4	5	207	170	-16	-2	5	421	376	7	0	5	193	318	-2	3	5	558	497	8	5	5	241	257
-12	-4	5	454	422	-13	-2	5	260	249	8	0	5	370	386	1	3	5	389	314	9	5	5	213	224
-10	-4	5	301	246	-12	-2	5	523	361	11	0	5	453	304	2	3	5	522	489	10	5	5	329	346
-9	-4	5	424	379	-9	-2	5	244	193	12	0	5	301	343	3	3	5	152	161	14	5	5	332	324
-8	-4	5	504	519	-8	-2	5	449	376	16	0	5	264	322	4	3	5	266	308	-13	6	5	270	214
-7	-4	5	124	286	-5	-2	5	488	333	-10	1	5	311	300	5	3	5	418	353	-12	6	5	343	365
-6	-4	5	250	301	-4	-2	5	644	586	-14	1	5	476	410	6	3	5	443	477	-9	6	5	336	449
-5	-4	5	380	356	-1	-2	5	463	393	-12	1	5	206	433	9	3	5	234	278	-8	6	5	647	610
-4	-4	5	596	413	0	-2	5	784	727	-7	1	5	371	181	10	3	5	260	324	-5	6	5	216	310
-1	-4	5	411	305	2	-2	5	224	301	-6	1	5	486	492	12	3	5	327	301	0	6	5	361	330
0	-4	5	612	476	3	-2	5	392	272	-3	1	5	690	520	13	3	5	271	257	3	6	5	528	379
1	-4	5	194	263	4	-2	5	467	408	-2	1	5	1097	794	14	3	5	337	354	4	6	5	635	507
2	-4	5	252	334	6	-2	5	184	278	1	1	5	409	324	-20	4	5	291	268	7	6	5	343	248
3	-4	5	408	359	7	-2	5	445	350	2	1	5	589	524	-13	4	5	172	222	8	6	5	470	444
4	-4	5	804	600	8	-2	5	564	398	6	1	5	273	352	-12	4	5	437	405	12	6	5	307	326
5	-4	5	255	278	10	-2	5	248	295	9	1	5	439	331	-11	4	5	130	330	-15	7	5	237	100
6	-4	5	250	206	11	-2	5	356	228	10	1	5	401	384	-10	4	5	267	238	-14	7	5	284	283
7	-4	5	371	318	12	-2	5	473	304	12	1	5	230	302	-9	4	5	422	437	-11	7	5	244	313
8	-4	5	400	367	15	-2	5	244	192	13	1	5	345	221	-6	4	5	478	586	-10	7	5	609	446
10	-4	5	275	241	16	-2	5	349	343	18	1	5	280	330	-6	4	5	214	374	-7	7	5	331	384
11	-4	5	246	197	-18	-1	5	351	347	-17	2	5	209	264	-5	4	5	378	239	-6	7	5	423	463
12	-4	5	324	333	-15	-1	5	196	388	-16	2	5	406	314	-4	4	5	536	368	-3	7	5	181	238
15	-4	5	220	290	-14	-1	5	473	399	-13	2	5	292	367	-1	4	5	387	273	-2	7	5	256	267
16	-4	5	318	328	-12	-1	5	216	436	-12	2	5	464	389	0	4	5	583	447	1	7	5	339	241
-22	-3	5	259	216	-7	-1	5	338	238	-9	2	5	228	162	1	4	5	193	281	2	7	5	511	383
-18	-3	5	292	327	-6	-1	5	530	482	-8	2	5	452	356	2	4	5	217	274	5	7	5	488	309
-16	-3	5	221	278	-3	-1	5	707	501	-5	2	5	468	255	3	4	5	359	356	6	7	5	389	469
-14	-3	5	301	332	-2	-1	5	1067	670	-4	2	5	608	602	4	4	5	777	535	9	7	5	242	201
-11	-3	5	272	261	1	-1	5	411	344	-1	2	5	452	391	5	4	5	182	239	10	7	5	525	389
-10	-3	5	571	457	2	-1	5	567	519	0	2	5	762	587	6	4	5	287	278	-13	8	5	277	245
-7	-3	5	332	283	6	-1	5	293	347	2	2	5	228	246	7	4	5	363	322	-12	8	5	292	332
-6	-3	5	537	401	7	-1	5	214	169	3	2	5	377	267	8	4	5	401	409	-9	8	5	239	280
-3	-3	5	368	314	9	-1	5	395	340	4	2	5	423	451	10	4	5	287	287	-8	8	5	437	383
-2	-3	5	566	596	10	-1	5	429	378	7	2	5	420	336	11	4	5	202	237	-6	8	5	167	276
1	-3	5	388	299	13	-1	5	342	182	8	2	5	565	371	12	4	5	320	323	-5	8	5	153	351
2	-3	5	536	536	14	-1	5	238	302	10	2	5	270	288	14	4	5	171	291	-4	8	5	309	407
4	-3	5	244	304	18	-1	5	293	342	11	2	5	327	282	15	4	5	285	276	-1	8	5	221	275
5	-3	5	458	396	-17	0	5	174	355	12	2	5	437	355	-19	5	5	251	281	0	8	5	301	300

H	K	L	10FO	10FC	H	K	L	10FO	10FC	H	K	L	10FO	10FC	H	K	L	10FO	10FC	H	K	L	10FO	10FC
3	8	5	345	238	4	14	5	229	293	12	-8	6	329	376	-12	-3	6	274	271	-2	0	6	304	272
4	8	5	470	363	-10	-13	6	363	386	-18	-7	6	314	314	-10	-3	6	589	382	0	0	6	228	354
7	8	5	223	253	-6	-13	6	255	215	-8	-7	6	285	354	-8	-3	6	678	395	2	0	6	352	495
8	8	5	424	442	2	-13	6	213	332	-6	-7	6	543	483	-6	-3	6	590	371	4	0	6	354	470
-12	8	5	270	316	4	-13	6	311	322	-4	-7	6	457	449	-4	-3	6	358	326	6	0	6	626	451
-15	9	5	221	254	-12	-12	6	371	369	-2	-7	6	673	580	-2	-3	6	397	348	8	0	6	679	630
-14	9	5	385	300	-8	-12	6	303	314	0	-7	6	424	496	0	-3	6	696	370	10	0	6	321	440
-11	9	5	288	257	-4	-12	6	284	214	2	-7	6	415	373	2	-3	6	705	476	12	0	6	261	199
-6	9	5	384	354	2	-12	6	267	282	6	-7	6	169	166	4	-3	6	461	380	-16	1	6	257	188
-3	9	5	266	415	4	-12	6	261	358	12	-7	6	298	325	6	-3	6	324	420	-14	1	6	508	432
-2	9	5	423	445	6	-12	6	280	326	-10	-6	6	214	201	8	-3	6	367	331	-12	1	6	380	452
1	9	5	279	246	-14	-11	6	330	306	-8	-6	6	365	376	10	-3	6	313	296	-10	1	6	452	441
2	9	5	321	261	-10	-11	6	220	297	-6	-6	6	436	449	14	-3	6	274	260	-8	1	6	293	398
4	9	5	318	322	-8	-11	6	224	311	-4	-6	6	597	526	-16	-2	6	368	284	-6	1	6	459	356
6	9	5	480	379	-6	-11	6	239	310	-2	-6	6	452	454	-14	-2	6	423	317	-4	1	6	208	258
9	9	5	293	248	-4	-11	6	227	278	0	-6	6	702	563	-12	-2	6	395	406	-3	1	6	160	445
-10	9	5	377	383	-2	-11	6	285	322	2	-6	6	315	486	-10	-2	6	397	392	-2	1	6	251	330
-12	10	5	267	292	0	-11	6	253	297	4	-6	6	387	300	-8	-2	6	353	374	0	1	6	550	412
-8	10	5	151	229	2	-11	6	268	248	12	-6	6	303	370	-6	-2	6	579	386	2	1	6	285	366
-5	10	5	273	312	6	-11	6	359	354	-20	-5	6	203	351	-4	-2	6	335	342	4	1	6	451	391
-4	10	5	551	440	8	-11	6	304	317	-18	-5	6	286	317	-2	-2	6	230	290	6	1	6	796	599
-1	10	5	420	401	-10	-10	6	298	268	-10	-5	6	384	320	0	-2	6	507	357	8	1	6	495	480
0	10	5	337	388	-14	-10	6	285	309	-8	-5	6	468	346	2	-2	6	442	427	10	1	6	543	423
7	10	5	256	265	-8	-10	6	380	267	-6	-5	6	390	460	4	-2	6	668	493	-16	2	6	306	229
8	10	5	301	384	-6	-10	6	367	287	-4	-5	6	400	429	6	-2	6	394	392	-14	2	6	409	290
-14	11	5	268	245	-4	-10	6	544	431	-2	-5	6	532	483	8	-2	6	643	463	-12	2	6	374	434
-10	11	5	267	231	-2	-10	6	320	350	0	-5	6	292	468	10	-2	6	371	375	-10	2	6	341	391
-6	11	5	315	290	0	-10	6	456	337	2	-5	6	693	517	12	-2	6	237	241	-8	2	6	309	357
-3	11	5	296	365	8	-10	6	413	350	4	-5	6	360	369	-16	-1	6	250	221	-6	2	6	559	318
-2	11	5	450	467	10	-10	6	320	290	8	-5	6	285	259	-14	-1	6	566	463	-4	2	6	296	251
0	11	5	152	277	-14	-9	6	230	240	12	-5	6	311	299	-12	-1	6	429	451	-2	2	6	252	264
1	11	5	287	287	-12	-9	6	165	265	14	-5	6	390	409	-10	-1	6	463	400	0	2	6	545	353
6	11	5	259	257	-8	-9	6	337	304	-20	-4	6	253	284	-8	-1	6	301	408	2	2	6	449	371
10	11	5	279	312	-6	-9	6	430	407	-14	-4	6	354	221	-6	-1	6	464	380	4	2	6	688	429
-5	12	5	199	257	-4	-9	6	473	374	-12	-4	6	234	249	-4	-1	6	205	296	6	2	6	336	371
-5	12	5	296	241	-2	-9	6	643	514	-10	-4	6	284	261	-2	-1	6	300	331	8	2	6	599	507
-4	12	5	323	336	0	-9	6	384	400	-8	-4	6	629	431	0	-1	6	530	437	10	2	6	381	386
-1	12	5	166	318	2	-9	6	335	239	-6	-4	6	610	407	2	-1	6	314	402	12	2	6	167	239
0	12	5	440	400	4	-9	6	257	274	-4	-4	6	307	372	4	-1	6	408	419	-14	3	6	317	246
1	12	5	166	177	-10	-9	6	366	346	-2	-4	6	287	360	6	-1	6	769	600	-12	3	6	251	253
2	12	5	115	257	-16	-8	6	257	264	0	-4	6	655	515	8	-1	6	492	467	-10	3	6	549	384
11	12	5	216	229	-8	-8	6	271	279	2	-4	6	666	437	10	-1	6	494	400	-8	3	6	602	329
-7	13	5	207	215	-6	-8	6	439	378	4	-4	6	480	429	-16	0	6	308	279	-6	3	6	596	267
-6	13	5	289	250	-4	-8	6	636	576	6	-4	6	201	300	-14	0	6	349	359	-4	3	6	358	249
-2	13	5	323	328	-2	-8	6	471	457	8	-4	6	379	251	-12	0	6	683	548	-2	3	6	375	281
1	13	5	202	276	0	-8	6	554	437	10	-4	6	252	286	-10	0	6	202	476	0	3	6	674	317
2	13	5	310	337	2	-8	6	291	424	12	-4	6	239	308	-8	0	6	406	350	2	3	6	662	428
-8	14	5	329	239	6	-8	6	195	217	-14	-3	6	399	268	-4	0	6	357	371	4	3	6	459	321

H	K	L	10FO	10FC	H	K	L	10FO	10FC	H	K	L	10FO	10FC	H	K	L	10FO	10FC	H	K	L	10FO	10FC
6	3	6	373	399	0	8	6	471	412	2	-7	7	324	351	-6	-1	7	310	360	3	3	7	329	246
8	3	6	380	319	2	8	6	261	360	-12	-6	7	246	241	-2	-1	7	213	325	6	3	7	301	349
10	3	6	267	321	12	8	6	289	328	-3	-6	7	335	319	-1	-1	7	229	277	7	3	7	269	207
-14	3	6	228	249	-16	9	6	195	268	-7	-6	7	270	310	2	-1	7	364	251	-12	4	7	194	319
-20	4	6	314	245	-8	9	6	202	192	-4	-6	7	330	349	3	-1	7	316	280	-11	4	7	212	264
-14	4	6	336	215	-6	9	6	342	293	-3	-6	7	222	241	6	-1	7	547	434	-8	4	7	275	331
-12	4	6	229	249	-4	9	6	394	255	0	-6	7	525	435	7	-1	7	321	263	-4	4	7	238	294
-10	4	6	214	188	-2	9	6	547	461	-9	-5	7	229	301	10	-1	7	286	349	0	4	7	335	410
-8	4	6	588	355	0	9	6	303	341	-6	-5	7	381	339	-16	0	7	330	329	0	4	7	205	271
-6	4	6	559	345	2	9	6	299	205	-5	-5	7	315	259	-15	0	7	234	330	4	4	7	379	361
-4	4	6	280	263	10	9	6	275	270	-2	-5	7	451	392	-12	0	7	352	355	5	4	7	202	206
-2	4	6	261	267	-16	10	6	306	262	-1	-5	7	261	247	-11	0	7	223	260	-6	5	7	400	286
0	4	6	624	432	-8	10	6	275	205	2	-5	7	359	404	-6	0	7	244	355	-5	5	7	325	265
2	4	6	655	374	-6	10	6	287	187	-12	-4	7	215	288	-4	0	7	318	350	-2	5	7	465	379
4	4	6	449	407	-4	10	6	387	350	-8	-4	7	303	357	-3	0	7	210	246	-1	5	7	252	271
6	4	6	224	247	-2	10	6	318	243	-7	-4	7	252	276	1	0	7	302	293	2	5	7	374	412
8	4	6	400	234	0	10	6	358	294	-6	-4	7	221	341	4	0	7	437	359	-8	6	7	329	328
9	4	6	127	264	8	10	6	315	305	-4	-4	7	242	348	5	0	7	325	263	-7	6	7	223	345
12	4	6	264	315	10	10	6	284	235	-3	-4	7	170	224	8	0	7	551	467	-4	6	7	341	318
-14	4	6	325	302	-14	11	6	289	255	0	-4	7	357	394	9	0	7	265	252	-3	6	7	234	224
-10	5	6	327	248	-12	11	6	212	255	1	-4	7	214	279	-14	1	7	378	364	0	6	7	423	433
-8	5	6	428	285	-2	11	6	231	248	2	-4	7	213	227	-13	1	7	316	301	1	6	7	220	240
-6	5	6	321	405	0	11	6	224	210	4	-4	7	440	331	-10	1	7	393	344	-6	7	7	242	332
-4	5	6	341	361	6	11	6	277	301	-14	-3	7	295	258	-6	1	7	295	352	-5	7	7	279	286
-2	5	6	427	363	-12	12	6	259	300	-10	-3	7	351	359	2	1	7	325	277	-2	7	7	427	383
0	5	6	229	371	-8	12	6	208	268	-6	-3	7	317	354	3	1	7	342	280	2	7	7	354	346
2	5	6	636	490	-10	13	6	365	335	-2	-3	7	358	359	6	1	7	560	452	-7	8	7	182	340
4	5	6	288	331	4	13	6	241	246	-1	-3	7	242	250	7	1	7	330	252	-4	8	7	400	380
12	5	6	275	312	-2	-11	7	225	266	0	-3	7	223	222	10	1	7	284	352	-3	8	7	315	223
14	5	6	367	424	-12	-10	7	272	265	2	-3	7	329	323	-12	2	7	250	366	0	8	7	366	341
-6	6	6	347	270	-4	-10	7	354	320	3	-3	7	306	272	-11	2	7	157	237	-8	9	7	221	188
-6	6	6	408	407	-8	-9	7	175	204	6	-3	7	343	314	-6	2	7	344	328	-6	9	7	301	321
-4	6	6	543	456	-6	-9	7	280	292	7	-3	7	265	213	-6	2	7	236	218	-2	9	7	275	363
-2	6	6	394	373	-5	-9	7	250	286	10	-3	7	205	273	-4	2	7	331	326	2	9	7	209	235
0	6	6	605	407	-2	-9	7	329	369	-12	-2	7	272	331	-1	2	7	178	242	-4	10	7	322	344
2	6	6	270	428	-1	-9	7	234	227	-8	-2	7	360	304	0	2	7	303	295	0	10	7	177	260
4	6	6	321	294	0	-9	7	228	253	-6	-2	7	167	230	1	2	7	323	276	-8	-6	8	223	284
12	6	6	261	336	6	-9	7	209	282	-4	-2	7	264	361	4	2	7	292	379	-10	-5	8	472	386
-8	7	6	228	264	-7	-8	7	225	292	-1	-2	7	164	191	5	2	7	285	242	2	-5	8	386	390
-6	7	6	432	386	-4	-8	7	425	362	0	-2	7	291	294	8	2	7	334	381	-12	-4	8	334	308
-4	7	6	396	382	-3	-8	7	299	276	1	-2	7	315	283	-14	3	7	259	298	-8	-4	8	384	305
-2	7	6	531	503	0	-8	7	370	366	2	-2	7	216	250	-10	3	7	337	362	0	-4	8	400	310
0	7	6	385	441	-10	-7	7	228	262	4	-2	7	279	322	-9	3	7	166	231	4	-4	8	418	340
2	7	6	344	361	-9	-7	7	160	295	5	-2	7	193	250	-6	3	7	325	297	-10	-3	8	298	271
12	7	6	253	276	-6	-7	7	253	314	8	-2	7	301	374	-5	3	7	145	276	-6	-3	8	322	304
-6	8	6	324	288	-5	-7	7	275	279	-14	-1	7	384	328	-2	3	7	334	334	-2	-3	8	318	305
-4	8	6	525	477	-2	-7	7	507	407	-13	-1	7	270	295	-1	3	7	268	298	2	-3	8	352	290
-2	8	6	382	380	-1	-7	7	206	260	-10	-1	7	396	360	2	3	7	330	367	-8	-2	8	296	286

OBSERVED AND CALCULATED STRUCTURE FACTORS FOR (PHCH:NH2)2SNCL6.EtOAc

PAGE 16

H	K	L	10FO	10FC	H	K	L	10FO	10FC	H	K	L	10FO	10FC	H	K	L	10FO	10FC	H	K	L	10FO	10FC
-4	-2	8	440	412	-8	0	8	217	234	-14	2	8	187	190	-6	3	8	308	247	0	4	8	402	301
0	-2	8	289	301	-4	0	8	686	539	-4	2	8	483	400	-2	3	8	390	309	4	4	8	375	325
2	-2	8	215	248	0	0	8	364	284	0	2	8	321	311	2	3	8	401	285	-10	5	8	432	336
-6	-1	8	454	428	-6	1	8	485	387	2	2	8	201	233	-12	4	8	271	282	2	5	8	416	376
-2	-1	8	574	432	-2	1	8	569	455	-10	3	8	286	241	-8	4	8	302	261	-8	6	8	263	274